



HAL
open science

Structures biosurfactant-biopolymère auto-assemblées capables de répondre aux stimuli

Chloé Seyrig

► **To cite this version:**

Chloé Seyrig. Structures biosurfactant-biopolymère auto-assemblées capables de répondre aux stimuli. Other. Sorbonne Université, 2021. English. NNT : 2021SORUS487 . tel-03896537

HAL Id: tel-03896537

<https://theses.hal.science/tel-03896537v1>

Submitted on 13 Dec 2022

HAL is a multi-disciplinary open access archive for the deposit and dissemination of scientific research documents, whether they are published or not. The documents may come from teaching and research institutions in France or abroad, or from public or private research centers.

L'archive ouverte pluridisciplinaire **HAL**, est destinée au dépôt et à la diffusion de documents scientifiques de niveau recherche, publiés ou non, émanant des établissements d'enseignement et de recherche français ou étrangers, des laboratoires publics ou privés.



Thèse pour l'obtention du grade de Docteur en physique et chimie des matériaux (ED 397) :

STIMULI RESPONSIVE BIOSURFACTANT BIOPOLYMER SELF ASSEMBLED STRUCTURES

Présentée par Chloé SEYRIG

Thèse encadrée par Niki BACCILE

Soutenue le 7 décembre 2021 devant un jury composé de :

M. Dominique HOURDET	Professeur, Sorbonne Université	Président du jury
Mme Cosima STUBENRAUCH	Professeur, Université de Stuttgart	Rapportrice
M. Jean-Paul CHAPEL	Directeur de recherche, CNRS	Rapporteur
Mme Elmira ARAB-TEHRANY	Professeur, Université de Lorraine	Examinatrice
M. Pascal HERVE	Ingénieur de recherche, Solvay	Examineur
M. Niki BACCILE	Chargé de recherche, CNRS	Directeur de thèse

ACKNOWLEDGEMENTS

Looking back three years ago, the PhD was not an evidence for me. I have always believed in fate, and I am convinced that my desire to conduct a PhD resulted from many meetings and good circumstances combined to my interest in sciences, and especially chemistry. I had to choose between biology and chemistry during my bachelor in biomedical sciences, and I would like to thank Karin Le Barch and Sandrine Calvet-Vitale (Paris V) to have tilted the balance towards chemistry and always supported me. I also need to thank all the people I have met during my internships, especially Mélanie Etheve Quelquejeu, Nicolas Sakkas, Expédite Yen Pon and Laura Iannazo and including one of my best friends today, César (no resentment about the chemical library job :p) and all the friends who made these years of bachelor funnier and that I am happy to still be in touch today : Maxime H., Madou, Rebecca, Heltia, Léa... Master years were then very rich and I have again many people to thank: Sophie Bernard, Mathéa Pietri, Laurent Corte and Rachele Allena, as well as Wei and Stéphanie. My internships were here again a combination of exciting science and wonderful people. I have to thank Sylvie Pochet and all the Pasteur team, for all these escape games (and time records!) : Jojo, LAB, David, Dada, Glwadys, Christelle..., as well as Zacharias Amara and all his team : Bryan, Kevin, Virginie, Gauthier... At ESPCI, I would like to thank Corinne Soulie Ziakovik, Maïssa Farroux for her availability and kindness, Floflo, Antoine, Maddie, Sarah, Quentin, Phuong Anh, Alexis, Elodie, Jakob... and of course my Loulou, my best partner for a Korean diner :p.

At this point, I was shared between stopping studies and finding a job in industry and starting a PhD. However, starting a PhD was conditioned by... finding a project! I understood that finding an offer in cosmetics, my field of interest, was too restricting. And I finally found an offer entitled « Stimuli responsive biourfactant-biopolymer structures ». I did not know the lab, I did not know the supervisor, I had no expertise in the field... but it raised my curiosity, and I knew that it was this offer or nothing! So I met Niki... who immediately trusted in me (more than myself...) to pass the ED contest. Thanks for that, and many other things... Thanks for your kindness, your availability, for always raising me up and asking the best of myself, for having valorized my work in several articles, for your comprehension in some hard times I went through... I learnt a lot, even more than scientifically, while feeling as a collaborator more than as a student. Thanks for all the opportunities you gave me: spending nights in synchrotron, attending conferences, and for always guiding me towards cosmetics, a field which is not necessarily your field of predilection, by involving me in the SATT project, supporting me for the l'Oreal contest or telling me about the Cosmetic 360 congress. I wish you a lot of success and happiness to come.

I would like to thank the current directors of LCMCP, Christian Bonhomme and François Ribot, and the former one, Florence Babonneau who kindly helped me to improve my application file for the l'Oreal contest.

This lab is definitely a nice place to work thanks to all its members. Thanks to Hélène Gervais and Corinne Pozzo di Borgo which are always available and ensure the good functioning of the lab with their constant good mood. I also thank Nora Abdoul and Diana Lesueur, and the bad student I am in informatics have to address special thanks to Simon Dadoun for his help. Thanks to all the permanent members I have discussed with and/or worked with: Francisco Fernandes, Gervaise Mosser, Bernard Haye, Christophe Hélyary, Thibaud Coradin, Patrick Le Griel...

A special thank to all the members of the jury to have accepted evaluate my work and conducted interesting discussions: Dominique Hourdet, Cosima Stubenrauch, Jean-Paul Chapel, Elmira Arab-Tehrany and Pascal Hervé.

I thank all the 2021 doctors and wish them the best for the futur: Guillaume, Alexandre, Antoine, Corentin, Jérémy, Victoire, Lise, Ruhne, Yang, Thibaut, Rémi, Camille... but also the former colleagues that I always enjoy meeting again: Florian, Nadège, Tsou Hsi Camille, Marion, Laura, Ludo, Elise, Lionel... and the new ones : Viviane, Mariette, Cindy, Alexis, Igor, Daniel F., Daniel J., Cyprien, Agathe, Léna, Isabelle, Jason, Adeline, Anne, Caroline, Fernando, Hajar, Ryma, Mélissa, Fanny, Florence...

I also thank the Smiles team's members: Thierry Azaïs, Marie Alberic... the postdoctoral researchers I had the chance to work with: Silvia Alonso de Castro and Alexandre Poirier (a last run to synchrotron ??), and Korin Ozkaya, who worked very efficiently during her internship!

Thanks to my office colleagues Camila, Tristan and Vaskar, and former ones: Miléna, Kankan, Alshaba...

I also would like to particularly thank Abdellah Yousfi for discussions and support, as well as Wim Thielmans and Gertrud Kignelman for experimental help (and Belgian beer!), and Ghazi Ben Messaoud for discussions. I also thank the members of my CST, Jérôme Fresnais and Christian Serre, for their advices and helpful discussions.

A special thank to Elora: thank you for always being a listening hear and a precious help! I wish you all the happiness you deserve and a lot of corgis :p No doubt we'll keep in touch.

Maxime, my PhD would have not been the same without you, many thanks for your love and support...

Thanks to my family: Papa, Maman and Carla, in the absence of understanding what I do, you always understand and support me...

Stimuli-responsive biosurfactant-biopolymer self-assembled structures

General introduction	6
Bibliographic chapter: From surfactant-polymer to biosurfactant-biopolymer systems.....	9
0.1 Surfactant-polymer systems.....	12
0.2 Surfactant-biopolymer systems.....	17
0.3 Enhancing hydrogels functionality through Interpenetrated Networks	24
0.4 Biosurfactants: generalities, presentation, phase diagrams and applications.....	29
0.5 Biosurfactant-biopolymer systems	39
0.6 Objectives.....	43
Chapter I: pH-induced phase transitions in diluted biosurfactant-biopolymer aqueous solutions.....	45
1.1 Introduction.....	46
1.2 Experimental methods.....	49
1.3 Identification of a precise pH-range of interactions	51
1.4 Morphological and structural characterization of the mixed lipid-polymer structures.....	54
Chapter II: <i>MLWVs</i> : synthesis and applications.....	59
2.1 Introduction	60
2.2 Stability of <i>MLWVs</i> in cell culture medium.....	60
2.3 Control over the size and dispersity of <i>MLWVs</i>	61
2.4. Encapsulation of a model hydrophobic drug.....	62
Chapter III: Synthesis and characterization of biosurfactant/biopolymer hybrid gels: mechanical strength.....	65
3.1 Introduction.....	66
3.2 Experimental part.....	69
3.3 Transition diluted/concentrated systems.....	71
3.4 G-C18:1/biopolymers	84
3.5 Conclusion.....	83
Chapter IV: Synthesis and characterization of hybrid gels: pH and temperature responsiveness	85
4.1 Introduction	86

4.2. Stimuli-responsivity in G-C18:1 + biopolymer concentrated systems	87
4.3 Rheo-SAXS investigations of structural and mechanical properties of hybrid {F}G-C18:1-gelatin hydrogels.....	89
Conclusion – Perspectives	94
References	97
Résumé en français	119
Annexes	124
Annex 1: pH-resolved <i>in-situ</i> Small Angle X-Ray Scattering	124
Annex 2: Rheology	127
Annex 3: SL-C16:0 / Collagen	129
Papers	133

General introduction

Self-assembly is a spontaneous process, which drives the organization of disordered molecules into ordered structures, which can be associated to a precise function. DNA is probably the most representative example: its complex structure is a double helix resulting from the spontaneous self-assembly of four base pairs via weak interactions, e.g., hydrogen bondings. Other biomolecules undergo interesting self-assembly processes leading to a large variety of supramolecular aggregates: among them proteins or the large family of surfactants. The latter have been reported to organize into micelles, cylinders, tubes, vesicles, bilayers or fibers. Today, physico-chemical parameters such as pH, ionic strength or temperature are able to tune specific properties from chemically sophisticated surfactants.

Within the context of this thesis, we are focused on a specific type of surfactants which has gained a lot of interest over the past years: biosurfactants. Laboratoire de Chimie de la Matière Condensée de Paris, where I conducted my research, possesses an expertise concerning this fascinating class of molecules. Produced by microbial fermentation, they are entirely biosourced, biodegradable and present a large variety of interesting properties, which can be further extended by more and more structures obtained by genetic modification of the producing yeasts or chemical modifications. Especially, we will focus on two biosurfactants, which both possess a carboxylic acid function: the glucolipid G-C18:1, made of a single β -D-glucose hydrophilic headgroup and a C18:1 fatty acid tail (mono-unsaturation in position 9, 10), and SL-C18:0, composed of a sophorose (glucose β (1, 2)) headgroup and a stearic acid derivative. Their self-assembly behavior, deeply investigated at the lab, is pH-dependent. My work went further by studying their behavior in presence of pH-responsive oppositely charged biopolymers. Before envisaging potential applications, it is crucial to understand and control supramolecular assemblies of biosurfactant-biopolymer mixtures in aqueous media as a function of concentration, pH, ionic strength or temperature.

Indeed, polymer-surfactant systems, including biopolymer-surfactant systems, benefit from both theoretical and experimental knowledge. However, within the context of respecting the environment, it is of current interest to replace these petrochemistry-based surfactants by biobased, biodegradable counterparts, whose phase behavior is identified and controlled. We have the chance to work with particularly interesting molecules for this purpose: most biosurfactants, if not all, exist within several phases depending on external stimulus, especially pH. We thus expect to have access to a large variety of structures upon mixing with biopolymers, each one with its own properties and potential for different applications, only by playing with pH, e.g. the phase of the biosurfactant.

I had a lot of opportunities during these three years. First, I attended four international conferences and could present my work in front of a large audience. I had the chance to develop new skills and discover various experimental techniques while travelling: synchrotron light sources in France and United Kingdom, isothermal titration calorimetry (ITC) in Belgium... I was initiated to cell culture, even if this part of the project is the one I was the less involved in. Two papers were published and two are under preparation (these latter present raw data, conclusion and discussion are ongoing). They present different parts of my work. I have also contributed to the writing of a review about self-

assembly, interfacial properties, interactions with macromolecules and molecular modelling and simulation of biosurfactants. I have also taken part to different side projects, especially the stabilization of pH switchable pickering emulsions by polyelectrolyte biosurfactant complex coacervate colloids, in partnership with AYCC lab and supported by SATT.

This manuscript includes two published and two unpublished papers written in English, it will thus also be written in English for homogeneity purpose. It is divided into five chapters.

BIBLIOGRAPHIC CHAPTER will show how investigation and understanding of biosurfactant-biopolymer systems are quite recent fields and still deserve further highlights, whereas surfactant-polymer systems have been well known for a long time. Literature is very abundant, that's why only major trends, which will be useful to better understand our systems, will be described. Three polymers, and more precisely the three biopolymers which will be discussed in this thesis, will then be presented and their interactions with « model » chemical surfactants, in both diluted and concentrated regimes, will be detailed. In the context of concentrated regimes, classical hydrogels, interpenetrated polymer network (IPN) and low molecular weight gelator (LMWG)-based hydrogels will be presented. This chapter will then provide an overview of what are the biosurfactants and what is known about this young family of LMWG. The few knowledge available on biosurfactant-biopolymer systems will finally be discussed.

CHAPTER I will discuss the pH-dependent interactions between biopolymers and biosurfactants and the resulting structures in diluted conditions (fixed below 1wt% in the specific context of this work). For the first time, isocompositional biosurfactant-biopolymer aqueous systems are studied through a fast and continuous variation of pH, to understand the structural effect under non-equilibrium conditions applied at the micelle-vesicle and micelle-fiber phase boundaries, while literature work was more often performed under pseudo-equilibrium conditions. The two articles written based on these results are included in this manuscript (Paper I and II). Both biosurfactants within their micellar state interact with all biopolymers to form complex coacervates. Then, pH-induced phase transition triggered inside the coacervate results in two different scenarios depending on the biosurfactant involved. The biosurfactant which undergoes a micelle-to-fiber phase transition does not interact anymore with the biopolymer and both fibers and biopolymer coexist, while the vesicle-forming biosurfactant evolves into multilamellar structures, with the biopolymer « sandwiched » between biosurfactants' layers.

CHAPTER II will focus on a precise structure obtained and its possible applications. Indeed, multilamellar structures, such as the ones we obtain for given conditions are promising candidates to encapsulate compounds of interest, like curcumin, a model hydrophobic compound with promising anti-cancer properties. Strongly hydrophobic, it needs a stable amphiphilic medium to be dispersed and from which it can be released into cancer cells. Curcumin is encapsulated in multilamellar structures presented in **Chapter I**. These biosurfactant-based multilamellar structures were then found stable in cell culture media by *in-situ* SAXS measurements and polarized light microscopy, opening an alternative to classical phospholipid-based drug delivery systems. The widespread drug model curcumin was encapsulated, and the whole system remarkably exerted an enhanced therapeutic effect towards cancerous Hela cells compared to normal human dermal fibroblasts NHDF and macrophages THP-1. These results imply that side effects could be overcome in normal tissue compared to cancer cells, and that the system benefits from an increased circulation time in the bloodstream since it is not targeted by macrophages THP-1, which usually clear foreign particles *in vivo*.

This chapter will summarize the main synthesis conditions and will introduce the article including the most relevant results obtained in terms of encapsulation/cell viability (Project paper III).

CHAPTER III and IV will be devoted to the synthesis and characterization of hybrid biosurfactant/biopolymer hydrogels, the idea being to obtain a gel, which benefits from both the good mechanical properties of the polymer and the stimuli-responsiveness of the surfactant. In these chapters, only one of the two biosurfactants employed in the previous parts will be used and the concentrations are increased compared to **Chapters I and II**. Each chapter is related to an article (Project papers IV and V), focused on the mechanical reinforcement and the responsivity to external stimuli, respectively. Indeed, we were able to develop biosurfactant-biopolymer hybrid hydrogels, which not only exhibit improved mechanical properties compared to the single component's hydrogels, but also benefit from sensitivity to pH and temperature, two parameters easy to play with to control desired properties.

Bibliographic chapter: From surfactant-polymer to biosurfactant-biopolymer systems

Table of content

0.1	Surfactant-polymer systems.....	12
0.1.1	Polymer-induced surfactant aggregation.....	12
0.1.2	Phase behavior of polymer-surfactant mixtures.....	13
0.1.3	Attractive polymer-surfactant interactions depend on both polymer and surfactant	16
0.1.4	Applications of polymer-surfactant-mixtures.....	16
0.2	Surfactant-biopolymer systems	17
0.2.1	Diluted systems	19
0.2.1.1	Gelatin-surfactant mixtures.....	19
0.2.1.2	Chitosan-surfactant mixtures.....	20
0.2.1.3	Alginate-surfactant mixtures.....	22
0.2.2	Concentrated systems.....	23
0.2.2.1	Gelatin-surfactant mixtures.....	23
0.2.2.2	Chitosan-surfactant mixtures.....	23
0.2.2.3	Alginate-surfactant mixtures.....	24
0.3	Enhancing hydrogels functionality through Interpenetrated Networks	24
0.3.1	Biopolymer-lamellar systems.....	25
0.3.2	Biopolymer-vesicles systems.....	26
0.3.3	Biopolymer-fibers (SAFiN) systems.....	26
0.3.4	LMWG—(bio)polymer hydrogels: which strategies to design and fabricate mechanically strong and stimuli-responsive materials?.....	27
0.4	Biosurfactants: generalities, presentation, phase diagrams and applications.....	29

0.4.1	Self-assembly and phase diagramme.....	31
0.4.2	Stimuli-induced phase transitions	34
0.4.3	Macroscale properties and possible applications of self-assembled biosurfactants.....	36
0.4.3.1	Hydrogelling	36
0.4.3.2	Solid foams.....	37
0.4.3.3	Encapsulation	38
0.4.3.4	Mixing with surfactant and lipids	39
0.5	Biosurfactant-biopolymer systems.....	39
0.5.1	Interactions with polyelectrolytes	40
0.5.1.1	Sophorolipids, glucolipids	40
0.5.1.2	Rhamnolipids (mono- (19) , di- (18)).....	41
0.5.2	Interactions with enzymes and proteins	41
0.5.2.1	Rhamnolipids (mono- (19) , di- (18)).....	41
0.5.2.2	Sophorolipids (1-3)	42
0.5.2.3	Surfactin (20)	42
0.5.2.4	Mannosylerythritol lipids (21)	42
0.5.2.5	General comments.....	43
0.5.3	Interactions with polymers	43
0.6	Objectives	43

« L'imagination est plus importante que le savoir »

« Une personne qui n'a jamais commis d'erreurs n'a jamais tenté d'innover »

« Un problème créé ne peut être résolu en réfléchissant de la même manière qu'il a été créé »

Albert Einstein (1879-1955)

0.1 Surfactant-polymer systems

Amphiphilic molecules are omnipresent in nature and especially essential in living organisms. Bile salts solubilizing hydrophobic molecules in blood, pulmonary surfactant reducing the surface tension at the air/liquid interface in the lung, or phospholipids, constituting the outer membrane of cells, are just some crucial examples. Their interactions with polymers are the object of a large literature, this first section will thus focus on a precise family of amphiphiles, the surfactants.

Surfactants and water-soluble polymers are of great interest for many applications due to their rich underlying physicochemical mechanisms. If one has a look on the composition of diverse commercial products (cosmetics, paints, detergents, food, polymer synthesis, formulation of drugs and pesticides...), most of them contain at least one polymer combined with at least one surfactant. Their use targets specific effects, such as colloidal stability, emulsification, flocculation, structuring and suspending properties or rheology control, but sometimes they act in a synergistic way.

The present section, entirely based on a book chapter,¹ will summarize the interactions between different types of polymers, especially water-soluble homopolymers and graft copolymers, and various classes of surfactants. A comparison with other mixed solute systems will be conducted to highlight similarities/differences with surfactant-surfactant and polymer-polymer mixed solutions.

0.1.1 Polymer-induced surfactant aggregation

The main role of a surfactant is to lower the interfacial tension between two phases, often an aqueous and an apolar one. The surface tension is a parameter of importance in adsorption, wetting, catalysis, or distillation among numerous physical phenomena, with direct involvement in the conception of industrial products in coating, food, detergents, cosmetics, to cite the main ones. Surface tension is defined as the energy required to create a unit area of interphase² and surfactants are able to lower the surface tension of water at the water-air interface from about 70 mN/m to about 25 to 40 mN/m. Micromolar amounts of a surfactant in water induce that the water-air interface is occupied by surfactant monomers, pointing the hydrophilic headgroup towards water and the hydrophobic chain towards air. This phenomenon implies the reduction in surface tension and the increase in surfactant packing at the interface. The surfactant will then reach the conditions of maximum packing and will start aggregating in the bulk solution into spheroidal aggregates known as micelles. Aggregation occurs for a concentration called critical micelle concentration, commonly written CMC. It refers to CMC₁ (between 10^{-5} and 10^{-1} M, according to the molecule structure), and differs from CMC₂, the concentration value above which micellar growth is rapidly completed.³ The CMC is modified if the solution contains a polymer, especially for ionic surfactants. The effect of a polymer on the surface tension of an aqueous solution will depend on the surfactant concentration, as illustrated by the example of SDS solutions, of which surface tension was determined as a function of surfactant concentration at various concentrations of poly(vinyl pyrrolidone) (PVP).⁴ At low surfactant concentration, the surface activity of the polymer may drive the lowering of the surface tension. However, the surface tension curve shows a break and reaches a more or less constant value for some concentrations. The surface tension, γ , is then constant in a concentration region which is determined by the polymer concentration. The curve finally decreases towards the γ value reported for the polymer-free surfactant solution.

The following interpretation of the concentration dependence of γ in the presence of a polymer can be defended: there exists a concentration, known as the critical association concentration (CAC), from which the surfactant starts to associate to the polymer. This implies that the surfactant activity does not further increase and consequently that γ does not decrease anymore. The polymer being then saturated with surfactant, the surfactant concentration increases as well as its activity: γ is lowered down to the surfactant CMC. The γ value is not further modified above this concentration, and the surfactant starts to self-assemble into micelles.

Figure 1 shows a binding isotherm, which does not show any significant interaction at low surfactant concentrations. A strongly cooperative binding occurs at the CAC, above which the level reaches a plateau before the free surfactant concentration increases until the surfactant activity, or the surfactant concentration, meets the curve related to the polymer-free case. Firstly, in Figure 1, the range of concentration is close to micelle formation and then Figure 1 emphasizes a strong decrease of the CMC. A typical experiment experimental system is given by PVP associated to sodium alkyl sulfates.⁵

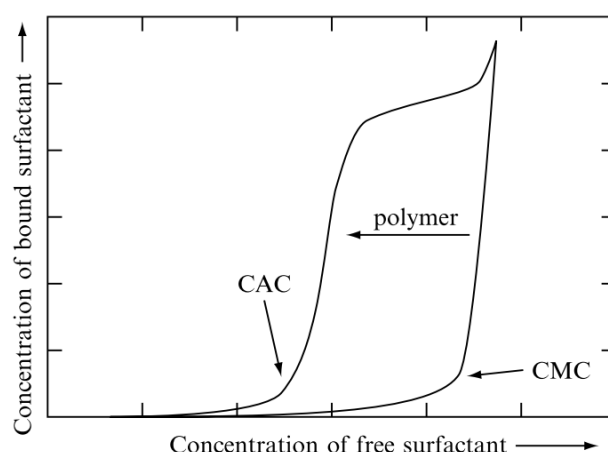


Figure 1 – “The binding isotherm of a surfactant to a polymer without distinct hydrophobic moieties, giving the concentration of bound surfactant as a function of the free surfactant concentration, can be interpreted as a lowering of the surfactant CMC by the polymer, or a strongly co-operative binding”⁴

0.1.2 Phase behavior of polymer-surfactant mixtures

0.1.2.1. General aspects

Polymer-surfactant and polymer-polymer systems display a similar behavior. Phase separation has an extent determined by the degree of polymerization of the polymer and may vary with the conditions which have an influence on the surfactant’s micelle size.

Specific interactions between the polymer and the surfactant, such as hydrophobic ones, may have different and even opposed effects on the phase behavior of polymer-surfactant systems. Indeed, phase separation will be enhanced for non-ionic systems whereas it will be decreased in the case of ionic ones. The formation of a concentrated phase containing polymer and surfactant in a charge stoichiometric ratio and a dilute phase enriched in any excess of either surfactant or polymer is expected for a mixture of oppositely charged polymer and surfactant, but a hydrophobically modified polymer will not favor this process due to its association with the micelles in the concentrated phase, whose charge stoichiometry will be disrupted, resulting in its swelling. Associative phase separation

is thus restricted to a limited concentration region for a mixture of oppositely charged hydrophobically modified polymer and surfactant.

Upon mixing two surfactants, no segregative phase separation will occur: they are likely to form mixed aggregates whose additional contribution to the entropy of mixing is high. However, an associative phase separation is generally displayed in the case of two oppositely charged surfactants.

This charge-dependent phase behavior of polymer-surfactant systems is summarized in Table 1.

Table 1 - Phase behavior of mixtures of polymer and surfactant depending on their charges. The case that has been investigated during this thesis is highlighted in orange.

Polymer charge	Surfactant charge	Phase behavior of mixtures of polymer and surfactant
+	-	Association without added electrolyte
-	+	Miscibility at intermediate electrolyte concentration Segregation at high electrolyte concentration
-	-	Segregation
+	+	
0	0	Segregation ; association may occur for less polar polymers, preferentially at high temperatures
0	+	Phase separation inhibited ; association or segregation may be induced by added salt
0	-	
+	0	
-	0	

We will comment it below, keeping in mind that if opposite and similar charges, respectively, drive attractive and repulsive electrostatic interactions between surfactants and polymers, other parameters are to be considered, including hydrophobic effects, whose strength must not be underestimated in some cases and which can even be leveraged by grafting hydrophobic groups, for instance.

0.1.2.2. Non-ionic systems

Association between the two cosolutes is largely observed for mixtures of a surfactant and an hydrophobically-modified (HM) polymer. Even if many homopolymers were found to facilitate micelle formation of an ionic surfactant, an associative interaction is not so evident since there is mostly no net attractive interaction.

Two polymers in solution in a common solvent only exhibit a weak entropic driving force of mixing, which induces segregation. Two solutions result from this process, each phase being enriched in one of the two polymers. Phase-separation is more likely observed for polymers with high molecular

weight. Micelles having also a high molecular weight, it would not be surprising that segregative phase-separation is a common phenomenon.

Two types of phase separation, either segregative or associative, can happen in the case of polymer solutions. A segregative phase separation will more likely occur in the absence of attractive interactions while a complete miscibility can be considered for a moderately strong attraction. An associative phase separation is conditioned by the presence of strong interaction between the two polymers and is characterized by a (both) polymer-rich phase and a dilute phase. The molecular weight of the polymers is in both cases a parameter which increases the degree of phase separation.

The behavior of a mixed polymer-surfactant system is very similar, except that the « degree of polymerization » of a micelle is not fixed as the one of a polymer, but is sensitive to the conditions, the temperature or the electrolyte concentration among others.

Mixtures of a non-ionic polymer and a non-ionic surfactant are not restricted to segregative phase separation but can encounter an associative phase separation for a less polar polymer, in particular at high temperatures, which favor hydrophobic association.

0.1.2.3. Introduction of charges

Phase separation can deeply be affected when charged groups are introduced in the solutes. The solubility of uncharged polymers can be significantly increased when they turn to corresponding electrolytes, mainly due to the entropy of the counterion distribution. In mixed polymer systems, there are various consequences of the electrostatic interactions. A first consequence is the low predisposition to phase separation in a mixed solution of a non-ionic and an ionic polymer, which can however be inhibited upon addition of an electrolyte, resulting in a typical incompatibility between the polymers.

Such effects are also considered in the case of mixed polymer-surfactant solutions. Introducing ionic groups, or ionic surfactants, allows to increase the charge of the polymer, or the micelles, respectively, resulting in increased polymer-surfactant miscibility. Addition of electrolytes also cancel these charge effects. If the polymer bears the same charge, there is no improvement compared to the parent non-ionic mixture and incompatibility remains.

0.1.2.4. Mixed ionic systems

A strong association behavior, causing phase separation, occurs in mixtures of two polyelectrolytes with opposed charges, as well as mixtures of oppositely charged polyelectrolyte and surfactant.

The CMC is decreased by orders of magnitude for surfactants with a long chain, which undergo a strong associative phase separation. The phase separation of an aqueous mixture of oppositely charged polyelectrolyte and surfactant results in a dilute phase which coexists with a highly viscous phase concentrated in both polymer and surfactant.

The surfactant alkyl chain length and the polymer molecular weight drive the extent of phase separation.

The Coulombic attraction enriches the surface of highly charged micelles and polyelectrolyte molecules with counterions. The association triggers a transfer of the counterions of both cosolutes

into the bulk; there is an entropy gain which explains a preferred associative phase separation without salt.

0.1.3 Attractive polymer-surfactant interactions depend on both polymer and surfactant

There exists two descriptions of mixed polymer-surfactant solutions. The first description is the one of an interaction based on a (strongly cooperative) association, or binding, of the surfactant to the polymer, whereas the second one supports a micellization of surfactant on, or in the vicinity of, the polymer chain. Even if both are useful and are widely overlapping, the binding approach will be preferred for polymers with hydrophobic groups, whereas the micelle formation description is more accurate for hydrophilic homopolymers.

Concerning the aggregation behavior of these systems and the resulting structures, one is commonly preferred in the case of mixed solutions of ionic surfactants and homopolymers: the « pearl-necklace » model, which describes the formation of discrete surfactant micellar-like clusters along the polymer chain. The micelles' size is not influenced by the presence of the polymer and the aggregation numbers can be slightly lower when micelles form in presence of a polymer.

With respect to variation in surfactant alkyl chain length, solubilization, micelle structure and dynamics essentially, the micellization is not so different from the one of the lone surfactant. The free energy of association should be led by the contribution of the hydrophobic effect between the alkyl chains, which will be however sensitive to mainly two factors described in the following lines.

If the surfactant and the polymer both contain a charge, electrostatic interactions will obviously occur; a quite strong association can even be expected if they are oppositely charged, but will coexist with the repulsive interactions already present between charged polymer molecules or between charged surfactant molecules. In particular, an increased concentration of counterions at the aggregate surface to the detriment of the bulk triggers an entropy loss which unfavors self-assembly and induces ionic surfactants to have CMCs orders-of-magnitude higher than non-ionic ones.

These arguments suggest that ionic surfactants interact with many water-soluble polymers. This is particularly true for anionic surfactants, as the higher degree of counterion binding of cationic ones limits interactions which are significantly weaker in this case. Concerning non-ionic surfactants, they are not expected to interact with hydrophilic homopolymers, since no further stabilization of micelles is possible, but will spontaneously associate to hydrophobic polymers by the hydrophobic effect.

0.1.4 Applications of polymer-surfactant-mixtures

Using a combination of a polymer and a surfactant may target different goals: they can together control phase behavior, interfacial properties or the formation of networks because of association. A major, well studied and now understood use of this kind of combination is to perform an accurate rheology, especially thickening or gelation effects. The design of stimuli-responsive systems based on hydrophobically modified water-soluble polymers or homopolymers can be envisaged, for example a system whose gelation is induced upon increasing the temperature.

An example of phase behavior effect is the solubilization of water-insoluble polymers, such as the increased of the cloud point of a polymer solution when an ionic surfactant is added. The polymer-induced micellization reduces the surfactant concentration and thus decreases its activity, a point to keep in mind to achieve elimination of a surfactant-induced irritation.

Suspensions can be stabilized for example, taking advantage of the interfacial behavior of surfactant-polymer mixtures, which depends on how different pair interactions interplay. Removing the surfactant from a surface and enhancing its adsorption are two opposite effects which can however both be achieved by addition of a polymer, and vice versa. The final effect will depend on how polymer-surfactant complexes behave in solution and at the interface, and on its relative stability.

Surfactant's self-assembly combined to the complexation properties of polyelectrolytes lead to a wide class of colloidal systems: polyelectrolyte-surfactant complexes (PESCs), with applications in food science, tissue engineering, drug and gene delivery, cosmetics or water treatment, among others.⁶ Their driving force is mainly electrostatic attraction between oppositely-charged surfactants and polyelectrolytes, but other parameters, like the packing parameter of the surfactant, rigidity of the polyelectrolyte, charge density, ionic strength or pH, may have a non-negligible influence. Polyelectrolyte-coated dense aggregates of spheroidal micelles can be found as a solid-liquid, or liquid-liquid, phase separation and in the latter case one refers to as complex coacervates.⁷ Other morphologies can however be observed, such as pearl-necklace or multilamellar wall vesicles.^{6,8,9} Complex coacervation, or coacervation between two macromolecules or between a macromolecule and a colloid, is a specific case of PESCs which remains among the more mysterious systems in colloid chemistry, even suspected to be at the origin of life on Earth.¹⁰ It occurs in water under relatively mild conditions of pH and temperature¹¹ (eco-friendly process) and does not require neither a special device nor extensive production steps. An increasing interest is since devoted to their preparation for applications in food,¹² tissue engineering,^{13,14} drug delivery,¹⁵ underwater adhesives,^{16,17} porous materials¹⁸ or even water treatment^{19,20} among many others.

0.2 Surfactant-biopolymer systems

After this general introduction, the following part will detail the interactions experimentally reported between the three main biopolymers studied during this thesis (gelatin, chitosan and alginate) and common « model » chemical surfactants (we will note that biopolymers here interact with micelles). This part does not aim to be exhaustive; literature provides many examples among which some significant ones were chosen to feed this section. This later is divided into three subparts, one for each biopolymer, of various lengths depending on the relevance of related data available.

Figure 2 well illustrates why these biopolymers were chosen: gelatin is a protein which can be positively charged below its isoelectric point (the value of this latter depends on gelatin's sourcing) and negatively charged above, chitosan is a polysaccharide positively charged below its pK_a (neutral above) and alginate is also a polysaccharide but negatively charged above its pK_a (neutral below). They thus cover a nice variety of cases.



Figure 2 – Summary of the state of charge (+ : positive; - : negative; N : neutral) of gelatin, chitosan and alginate in function of pH

Table 2 summarizes the effects/interactions engaged between gelatin, chitosan or alginate with positively-charged, neutral or negatively-charged surfactants. It is in agreement with the charge behavior of each biopolymer in function of pH reminded by Figure 2 and the theory about surfactant-polymer interactions presented in the first part of this bibliographic chapter.

Table 2 – Summary of the trends observed between biopolymers and positively-charged, neutral or negatively charged surfactants

surfactant biopolymer	+	0	-
Gelatin	hydrophobic	hydrophobic	electrostatic
Chitosan	hydrophobic	hydrophobic	electrostatic
Alginate	electrostatic	hydrophobic	hydrophobic

Literature provides interesting studies of interaction between these biopolymers and common « model » chemical surfactants. We were interested in three cases : equality of charges, unequality of charges and no charges, first in diluted conditions (0.1-1wt%, summarized in Table 3) and then in concentrated conditions, especially in the case of hydrogels' formation (1-10wt%, summarized in Table 4).

Table 3 - Example of studies of interactions between gelatin, chitosan or alginate and anionic, non-ionic and cationic surfactants

Surfactant	Anionic surfactant	Non-ionic surfactant	Cationic surfactant
Biopolymer			
Gelatin	SDS ²¹	TX-100 ²¹	CTAB ²¹
Chitosan	<i>Strong</i> : SDS ^{22,23} <i>Weak</i> : fatty acids, alkyl oligooxyethylene carboxylic acids ²²	C ₁₂ E ₈ , non-ionic sorbitan esters ²²	CTAB, LAE ²²
Alginate	SDS ^{24,25,26,27}	Tween 20 ²⁸ Brij 35 ²⁷	DTAC, ²⁴ CTAC ²⁴ LAE29, DTA+ and TTA+ ³⁰ , CTAB ³¹ CTAB and gemini ²⁷

Table 4 – Examples of studies of gelatin-, chitosan- or alginate-based hydrogels supplemented with anionic, non-ionic or cationic surfactant

Surfactant	Anionic surfactant	Non-ionic surfactant	Cationic surfactant
Biopolymer			
Gelatin	AOS ³²	TX-100 ³²	CTAB ³²
Chitosan	SDS ³³	TX-100 ³³	HTAB ³³
Alginate	SDS ^{34,35}	Brij 35 ³⁴ Pluronic® F68 ³⁶	CTAB and gemini homologue ³⁷

Note - **SDS** : sodium dodecyl sulfate ; **TX-100** : triton X-100 ; **CTAB** : cetyl trimethyl ammonium bromide ; **C₁₂E₈** : octaethyleneoxide n-dodecyl ether ; **DTAC** : dodecyl trimethyl ammonium chloride ; **CTAC** : cetyl trimethyl ammonium chloride ; **LAE** : lauric arginate ethyl ester hydrochloride ; **DTA⁺** : dodecyltrimethylammonium ; **TTA⁺** : tetradecyltrimethylammonium ; **AOS** : alpha olefin sulfonate ; **HTAB** : hexadecyltrimethylammonium bromide

0.2.1 Diluted systems

0.2.1.1. Gelatin-surfactant mixtures

Gelatin is obtained by the denaturation of collagen protein and has many potential applications due to its ability to stabilize colloids and its gelation below 30°C, whence it results in the formation of a physical gel, *via* the formation of inter-molecular, triple-helical structures.³⁸ Gelatin and other proteins commonly interact with anionic surfactants. Below its isoelectric point (7<IP<9), gelatin is positively charged and its interaction with a negatively charged surfactant results in the precipitation of polymer-surfactant complexes.³⁹⁻⁴¹

A typical example is illustrated by Saxena *et al.*²¹ (Table 3), who investigated the binding of three surfactants (SDS, TX-100 and CTAB, respectively anionic, non-ionic and cationic) to gelatin chains (0.5% w/v) in aqueous buffer (pH= 7) at T= 30°C by dynamic light scattering. For surfactant concentrations ranging from 0 to 100 mM, SDS electrostatically binds to the charged groups of the polymer chains, resulting in a significant decrease of the hydrodynamic radius (R_h) of gelatin up to the CAC. Above this value, an equilibrium state is established between coexisting SDS micelles and SDS-gelatin complexes. The opposite effect was reported using CTAB: the size of gelatin chains slightly increases up to the CAC, beyond which the gelatin-CTAB complexes grow significantly and establish an equilibrium with CTAB micelles. In the case of TX-100, no electrostatic but only little hydrophobic binding to gelatin occurs and the size of gelatin remains unchanged. Micellar shapes are different (near-spherical SDS micelles vs. oblate ellipsoidal CTAB micelles) and results were rationalized using the common necklace-bead model of polymer-surfactant interactions.

0.2.1.2. Chitosan-surfactant mixtures

Chitosan results from the deacetylation of chitin, the second most widespread natural polysaccharide, through employing concentrated sodium hydroxide or enzymatically via the action of chitin deacetylase. The final structure is a mixture of N-acetylglucosamine and glucosamine, linked together into linear chains through β -(1-4) connections.⁴² Among many advantages which make it attractive for different applications, chitosan is biocompatible, biodegradable, exhibits anti-microbial activity, or promotes wound healing. Its structure also approaches the one of the glycosaminoglycans, main constituents of the natural extracellular matrix, an advantage for tissue engineering applications.⁴³ Chitosan is positively charged below its pKa (≈ 6.5) and neutral above.

The following Table 5, extracted from ref.²², lists interesting chitosan-based systems, which take advantage from their high biocompatibility. The variation of formulation properties or the introduction of desired functionality such as the ability to incorporate hydrophobic compounds for drug delivery purposes or extractions of hydrophobic contaminants, can be achieved by the choice of a suitable surfactant to mix with.

Table 5 - References and details about most relevant studies involving chitosan/surfactant systems. Extracted and adapted from Ref.²²

Molecular weight	DA	Surfactant	Exp. techniques	Topic	Ref.
Unkn. Mw = 190–400 kDa	ca. 0.2 0.08–0.24	Sodium dodecyl sulfate	ITC, SSE, Turbidity SSE	Effect of ionic strength and pH on the binding process Study of DA on binding isotherm	[67] [38]
Mw = 195 kDa Mw = 120 kDa	0.12 0.15	Sodium dodecyl sulfate Sodium lauryl ether sulfate	Optical microscopy, SAXS Optical and electron microscopy, UV-Vis	Capsule formation and internal structure Microcapsule formation and their Cu(II) uptake ability	[75] [76]
Unkn. Mw = 296 kDa	0.15 Unkn.	Sulfonated dyes 1-butyl-3-methylimidazolium octylsulfate	UV-Vis Tensiometry, conductimetry, turbidimetry, DLS	Chitosan-dye interaction and effects on wool dyeing Study on the binding of [C ₄ mim][C ₈ OSO ₃] to chitosan	[77] [78]
Mw = 250 kDa Unkn.	ca. 0.2 ≤ 0.25	Sodium taurocholate Sodium taurodeoxycholate	ITC SAXS	Thermodynamics of binding Structure formation at chitosan-surfactant solution interfaces	[79] [80]
Mw = 600 kDa Mv = 0.6–1.1 MDa	Unkn. 0.0–0.2	Sodium bis(2-ethylhexyl)sulfosuccinate Undecylenic acid	Capsule formation UV-vis, DLS, electron microscopy	Visual observation Behavior of chitosan-undecylenic acid mixtures.	[81] [82–84]
Mw = 3.5–270 kDa	0.16–0.22	Stearic acid	Langmuir balance, AFM	Chitosan-stearic acid interactions at the air-water interphase.	[71]
Mw = 330 kDa	0.3	Unsaturated fatty acids	Langmuir balance	Chitosan interaction with different fatty acids at the air-water interphase.	[72]
Mw = 300 kDa	0.2	Ammonium phosphatidic fatty acids	SEM, interfacial shear rheology	Formation of chitosan coated phosphatidic fatty acids droplets and their decoration with polystyrene particles	[85]

Chitosan strongly interacts and forms water-insoluble and structured complexes over a wide range of concentrations and mixing ratios with strong anionic surfactants (sulfated for the most part) including SDS, according to a cooperative process described with the Satake -Yang model,^{44,45} which is a reliable approximation of the adsorption process quantifying the extent of binding in terms of the binding constant K and the cooperativity parameter u, with C_f being the free surfactant concentration and s the equilibrium constant (**Eq. 1**):

$$\theta = \frac{1}{2} \left[1 + \frac{KuC_f - 1}{\sqrt{(1s - KuC_f)^2 + 4KC_f}} \right] \quad (\text{Eq. 1})$$

This model describes the polymer chain as a linear array of binding sites, which can be free, non-cooperatively occupied or cooperatively occupied (when at the least two consecutive sites are occupied). Interactions between surfactant and polymer imply “vertical” (mainly electrostatic, but including also hydrophobic forces and hydrogen bonding, between surfactant and polymer) and “horizontal” (hydrophobic and dispersion forces among the surfactant tails) forces. Based on this description, Wei and Hudson⁴⁶ concluded that increasing the degree of acetylation of chitosan lowers the cooperativity of the binding process to SDS due to the increased spacing among the surfactant tails, but has no effect on the non-cooperative binding constant, i.e. the “vertical” surfactant/glucosammonium interaction. An increased ionic strength decreases the binding constant K without changing the cooperativity of the process, evidencing the electrostatic nature of the “vertical” interaction and the hydrophobic origin of the cooperativity, supported by calorimetric and potentiometric titrations. A stoichiometric insoluble SDS-chitosan complex is formed, with a strength of interaction depending on the ionic strength and an ionic strength-independent SDS content in the complex. These results suggest that the hydrophobic “horizontal” interactions among the surfactant alkyl chains mainly drive the cooperativity of the process and that strong electrostatic “vertical” interactions are at stake between the glucosammonium units and the sulfated and sulfonated headgroups, a conclusion further confirmed using a short-chain surfactant. The low solubility of chitosan/sulfated surfactant complexes however restricts their use. The case of complex coacervation was more investigated by Onesi *et al.*²³ who used surface tension measurements, turbidity, zeta potential measurements and ITC to optimize ionic ratio and propose a system potentially eligible as wall material for capsules using the coacervation process.

Weak anionic surfactants' category includes fatty acids and alkyl oligoethylene carboxylic acids. The behavior of chitosan-alkyl carboxylic acid mixtures depends on pH and on hydrophobicity of the fatty acid. It is admitted that chitosan acts as a “supramolecular glue”, providing an extended network for the assembly of the surfactant aggregates. There is no supramolecular ordering when chitosan is mixed with short-chain carboxylic acids ($n(C) \leq 5$), as the hydrophobic cooperative interactions among the aliphatic chains are not sufficient.⁴⁷ Differently, using (un)protonated long-chain fatty acids ($n(C) \geq 16$), which form self-emulsified droplets, or intermediate-chain fatty acids, stable μ -meter sized emulsions⁴⁸ and well-defined nanometer sized micelles are formed in acidic medium. These latter have a low solubility and complex, stable aggregates are formed in a narrow pH and alkyl chain length range.⁴⁹⁻⁵¹ Mixtures of alkyl oligoethylene oxide acids and chitosan give rise to supramolecular structures which depend on mixing ratio, pH and on the packing parameter, which imposes the surfactant aggregate shape.⁵² They exhibit higher solubility than their analogues alkyl sulfates or carboxylic acids. The local organization of the surfactant is explained by its natural tendency for self-assembly and the supramolecular structure retains the type of aggregate formed in the pure surfactant solution (spherical micelle, vesicle, etc.).

Despite their weakness, interactions of chitosan with non-ionic surfactants do exist. At a pH low enough to solubilize chitosan, no precipitate is expected to form. If no large supramolecular aggregates result from the self-assembly of chitosan and octaethyleneoxide *n*-dodecyl ether $C_{12}E_8$, a strong effect on the viscosity time-dependence is due to their interaction and triggers a viscosity drop over time.^{53,54} This effect is observed only above the CMC, unchanged in presence of polymer, and may be due to a modification of the polymer conformation in presence of surfactant micelles.

No strong synergistic interaction is expected between a cationic surfactant and chitosan: electrostatic repulsions do not drive a significant complex formation. For example, adding chitosan to a CTAB solution do not change its solubilization power.⁵⁵ Repulsive interactions between chitosan and lauric arginate ethyl ester hydrochloride prevent the formation of supramolecular aggregates but create an excluded volume effect at the origin of the decrease of the surfactant's CMC.²⁹

0.2.1.3. Alginate-surfactant mixtures

Alginates are naturally derived polysaccharide block copolymers composed of regions of sequential β -D- mannuronic acid monomers (M-blocks), regions of α -L- guluronic acid (G-blocks), and regions of interspersed M and G units. Their source determine the length of the M- and G- blocks and sequential distribution along the polymer chain.⁵⁶ Alginates undergo reversible gelation in aqueous solution under mild conditions through interaction with divalent cations, mainly Ca^{2+} , whose cooperative binding between the G-blocks of adjacent alginate chains create ionic interchain bridges.⁵⁷

Alginate, a polyelectrolyte bearing negative charges on its main chain above $\text{pH} \approx 4$ ($3.38 < \text{p}K_a < 3.65$), is not expected to associate to anionic surfactants. Neumann *et al.*²⁴ used pyrene fluorescence to measure SDS-alginate interactions. A small and slow decrease of the intensity ratio is reported for SDS concentrations up to 2 mM and is attributed to the attraction of the hydrophilic sulfonate groups towards the microdomains formed by the hydroxyl groups on the polyelectrolyte chain. A hydrophobic effect between the alkyl chain on the surfactant and the hydrophobic backbone of alginate is discarded as a small influence is assigned to this effect using a cationic surfactant with equivalent chain length. Same effects occur between SDS and poly(styrene sulfonate) PSS copolymerized with an hydrophobic monomer. For larger surfactant amount, normal micelles form around the critical micellar concentration, as for cationic surfactants. Further microcalorimetric measurements²⁵ establish a pH-dependence of the SDS-alginate interactions. From pH 7 to 6, NaAlg polymers act as a simple salt with regards to the CMC of SDS: electrostatic repulsion between SDS and alginate avoids any association. However, upon further decrease of the pH from 5 to 3, hydrophobic effect prevails and drives aggregation.

Oppositely charged to alginate when $\text{pH} \approx 4$, cationic surfactants are the most studied case. According to turbidity and SANS results of Bu *et al.*,²⁷ hexadecyltrimethylammonium bromide (CTAB) and Gemini induce the formation of large inhomogeneous structures in pure alginate solution. Yang *et al.* also studied the effect of pH using CTAB, with viscosity measurements this time.³¹ The rheological response of diluted alginate solutions is sensitive to acidity change in the low pH range. The steady shear and intrinsic viscosity measurements suggest a strong association between alginate and CTAB by electrostatic attraction above pH 5.0, supplemented by significant hydrophobic effect below this value. Hayakawa *et al.*³⁰ reported binding isotherms for dodecyl- and tetradecyltrimethylammonium (DTA^+ and TTA^+) ion binding to alginate using a potentiometric technique based on surfactant cation selective solid-state membrane electrodes. Their results reveal a highly cooperative binding process. TTA^+ exhibits a larger cooperative binding constant (K_u). The difference between DTA^+ and TTA^+ in the free energy of surfactant binding ($2.50 kT$ for alginate) can be compared to the free energy of transfer of two methylene groups from water to a hydrocarbon medium or to a micelle. Finally, the fluorescence study of Neumann *et al.*²⁴ evidenced that alkyltrimethylammonium surfactants associate to alginate. DTAC and CTAC form induced micelles at concentrations smaller than those needed to form micelles in aqueous solution. The main initial

interaction between alginate and oppositely charged surfactant is certainly electrostatically established between the charged centers on the macromolecular chain and the charged heads of the surfactant. These aggregates form less hydrophobic microenvironments than free micelles. At larger surfactant concentrations, normal micelles are formed for a higher CMC value compared to aqueous solution conditions. Hydrophobic effect is not the main driving force in these systems, but it was interestingly observed that the strength of interactions increases for surfactants with longer chains. Its contribution is not excluded on the interactions between alginate and anionic surfactants.

0.2.2 Concentrated systems

This section has the goal of showing the existence of a specific literature on the interaction between biopolymers in their hydrogel state and surfactants *via* selected examples.

0.2.2.1. Gelatin-surfactant mixtures

Abed *et al.*³² studied the effect of binding of three surfactants, alpha olefin sulfonate (AOS, anionic), Triton-X100 (TX-100, non-ionic) and cetyl trimethyl ammonium bromide (CTAB, cationic), to hydrogels of gelatin at room temperature (25 °C) by dynamic light scattering and oscillatory rheology with larger surfactant concentrations (20–100 mM) than their critical micellar concentrations (CMC). They concluded that micelles gradually change significantly the structural properties of gelatin hydrogels. The cross-over point is defined for a physically distinguishable surfactant concentration around 55 mM. For lower surfactant concentrations, the hydrogen bonded triple helix physical network dominates. The formation of transient micellar bridges occurs starting from a 25 mM surfactant concentration but triple helices are still present enough inside the gel structure to provide it rigidity. Above the cross-over concentration, an exponential increase of the density of micellar crosslinks is related with a softening-like behavior of the gel phase. The storage modulus G' has been seen as a measure of crosslink density. Since the rigidity of the gel is due to the existence of intermolecular hydrogen bonds between peptide linkages of adjacent helix units, the loss of these linkages and the consequent gain in micelle-ridged linkages triggers the loss of rigidity (G'), whose severity depends on the surfactant: this loss is more pronounced for AOS, then CTAB and finally TX-100.

0.2.2.2. Chitosan-surfactant mixtures

Bamgbose *et al.*³³ were interested in the swelling equilibrium of Chitosan and sodium tripolyphosphate (NaTPP) cross-linked chitosan hydrogels in aqueous solutions of surfactants of different structure, charge and hydrophobicity at 25°C. The anionic surfactant sodium dodecylsulfate (SDS), the cationic surfactant hexadecyltrimethylammonium bromide (HTAB) and neutral surfactants Triton X-100 all induced abrupt change in the gel volume. The equilibrium swelling ratio first decreased sharply as the concentration of the surfactant increased, then reaches a plateau around the critical micelles concentration (CMC) of the surfactants and finally increased again as the concentration increased beyond the CMC of the surfactant. The equilibrium volume change of hydrogel was significantly increased from HTAB > Triton X-100 > SDS > the mixed SDS/Triton X100 system. A decrease in equilibrium swelling ratio of the gel in SDS/TX-100 mixtures was observed with an increase in the mole ratio of SDS. This swelling study provides keys to understand the equilibrium swelling of chitosan gel which depends on cross-linking density, surfactant type, and their respective concentrations.

0.2.2.3. Alginate-surfactant mixtures

The interaction of cetyltrimethylammonium bromide (CTAB) and its gemini homologue (butanediyl-1,4-bis (dimethylcetylammmonium bromide), 16-4-16 with biocompatible polymer sodium alginate (SA) has been investigated in aqueous medium by Jabeen *et al.*³⁷ Rheological investigations revealed that the viscosity of sodium alginate first decreases and then increases with increase in CTAB/16-4-16 concentration. The viscosity drop upon addition of the surfactant is more in gemini containing alginate system than that of CTAB one, attributed to more charge density of former, which leads to more screening of interpolymer association. Moreover, the viscosity of the SA+CTAB or SA+16-4-16 system is greatly affected upon the addition of salt to the extent that the relative magnitude gets reversed due to more interpolymer association in the SA+CTAB system. The addition of the two surfactants affects the alginate gel differently, gemini improves drug encapsulation and loading but doesn't improve release behavior whereas addition of CTAB reduces the encapsulation and loading capacity but improves the release behavior compared to alginate gel without surfactant. Therefore, this study highlights the importance of amphiphile chemical structure on gelation characteristics of sodium alginate and encourages the use of wide range of amphiphiles to optimize the alginate gels for desired applications like high encapsulation and delayed release of poorly soluble hydrophobic drugs.

0.3 Enhancing hydrogels functionality through Interpenetrated Networks

Mixed polymer-surfactant systems have been massively investigated over the last decades, with a main focus on interactions involving surfactants in a particular aggregation state, the micellar one. Major phase behaviors, driving forces and structural/rheological effects of these systems were elucidated and are now well known. Polymer-fibers⁵⁸ or polymer-vesicles⁶² systems, on the other hand, have received much less attention from a physico-chemical perspective but a few studies were reported. According to them, the same forces mainly drive interactions between polymer and surfactant vesicles or polymer and lipid vesicles and polymer-surfactant, polymer-polymer and surfactant-surfactant interactions.

Hydrogelation is a property commonly displayed in more concentrated systems (>1wt%). Different aspects of hydrogels will be discussed in the next section, from their classical definition to the more recent strategies employed to optimize these fascinating materials.

Hydrogels are often defined as water-swollen hydrophilic polymer 3D networks. They benefit from tunable properties and are able to reproduce aspects of native tissues. Traditional hydrogels are attractive materials for biomedical applications which may however suffer from some drawbacks. Main disadvantages are relatively "weak" mechanics, static properties or only partial replication of essential aspects of the cellular microenvironment.

Apart from synthetic polymers, biopolymers derived from tissues [hyaluronic acid (HA), chondroitin sulfate, collagen, gelatin...] or from natural materials (chitosan, alginate, cellulose...) are getting increasing interest for hydrogel formation. Biopolymer hydrogels are formed either by leveraging the biopolymers native intermolecular interactions or by crosslinking through chemical modifications. Biopolymers possess advantageous inherent properties such as bioactivity, degradability or biocompatibility. For example, HA is a non-sulfated glycosaminoglycan with unique viscoelastic properties, whose interactions with specific chemical receptors are crucial to regulate cell adhesion and tissue morphogenesis. Although biopolymers possess many promising advantages for their use in

hydrogel design, some drawbacks are to be deplored : they generally exhibit weak mechanical properties, wide distributions in molecular weights, undefined chemical compositions and may trigger immune responses depending on their sourcing.⁶¹

Introducing some hydrogel crosslinking chemistries to biopolymers has largely widened the range of attainable biopolymer hydrogel properties but however, they still do not meet all the conditions for many biomedical applications.⁶² Modulations in terms of hydrogel physical properties have been achieved by polymer blends and composite hydrogel formulations.⁶³ These latter however suffer major drawbacks : negative effects over encapsulated cells were reported and they often undergo a phase separation at the origin of the fast degradation of the hydrogel properties.

To go further and improve the attainable and desired properties of biopolymer hydrogels in an efficient and sustainable way, an emerging strategy is to design complex multicomponent (bio)polymer systems and incorporate either a second interpenetrating polymer network, referring to a combination of independent, interdigitating polymer networks at the molecular scale, or another phase.

Secondary networks provide to interpenetrated polymers network (IPN) hydrogels improved mechanical properties, stimuli-responsiveness and the capacity to very satisfyingly mimic complex cell-material interactions for targeted applications in drug delivery, tissue engineering, *in vitro* disease modeling or biofabrication. Many IPN hydrogels rely on synthetic polymer network, but the fabrication and use of IPN hydrogels that only consist of at least one biopolymer network do exist. The functionality of hydrogels can also be enhanced by the use of a secondary polymer rather than a network; this is the case for semi-IPN hydrogels.

The addition of another phase, may it be micelles, vesicles or fibers, is also of interest, for release purposes using the vesicular phase or depollution application using the micellar phase for instance.

The objective of this section is to highlight the main trends on the enhanced functionality resulting from the incorporation of a second component into classical biopolymer-based gels, including mechanical reinforcement, « smart » systems sensitive to external stimuli or the ability to tune cell-material interactions.

Two aspects have been highlighted by this PhD project work e.g., the two articles included in **Chapters III** and **IV**: first the mechanical reinforcement through interpenetrating networks and secondly the stimuli-responsiveness through interpenetrating networks hydrogels. Bibliography related to these topics is included in the articles and will not be discussed here. However, this bibliography mainly concerns two polymers networks. Synthesis and characteristics of the IPN hydrogel composed of chitosan and polyallylamine were for example reported.⁶⁴ The following lines will rather present the work achieved involving polymer combined to another family of molecules.

0.3.1. Biopolymer-lamellar systems

Lamellar hydrogels⁶⁵ made of a phospholipid L_{α} phase stabilized by a polymer-grafted lipid were the first example of an elastic 2D self-assembled material at concentration below 10 wt%. Since their discovery by Safinya and Davidson in 1996, lamellar hydrogels were obtained by polymer-stabilization,⁶⁶ or by combining a lamellar lyotropic phase (> 50 wt%) with a gelator.⁶⁷⁻⁷³ If lamellar hydrogels are complex elastic fluids generated by defects⁶⁵ whose mechanical properties are hard to control, this unique feature is also an opportunity for the emergence of new materials.⁷⁴

0.3.2. Biopolymer-vesicles systems

Some vesicles-loaded biopolymer systems were reported, with specific interactions engaged or not.⁶³ For example, Dowling *et al.* designed pH-responsive gelatin gels containing fatty acid vesicles. They do not evoke any interaction but evidenced that the vesicle-to-micelle transition releases hydrophobic solutes encapsulated within the vesicles into the bulk gel. On the other hand, Chiappisi *et al.* worked on the self-assembly of alkyl ethylene oxide carboxylates and the biopolymer chitosan into supra-molecular structures with various shapes⁷⁵ at pH 4.0, where the chitosan is almost fully charged and the surfactants are partially deprotonated. Changes in the alkyl chain length and the number of ethylene oxide units result in very different water-soluble complexes, ranging from globular micelles incorporated in a chitosan network to formation of ordered multiwalled vesicles.

0.3.3. Biopolymer-fibers (SAFiN) systems

Molecular hydrogels are obtained by the self-assembly of low molecular weight gelators (LMWG) into a Self-Assembled Fibrillar Network (SAFiN).⁷⁶ These soft materials are highly promising due to their reversible gelation (possible because of their stimuli-responsiveness towards pH, T, ionic force, light...), an advantage compared to polymer hydrogels for biomedical applications. Nonetheless, SAFiN suffer from poorer mechanical properties compared to polymer hydrogels: SAFiN stands on weak intermolecular forces (H-bonding, hydrophobic...) instead of covalent bonds in polymer hydrogels.






Nandi and co-workers stabilized LMWG gels by adding the biopolymer chitosan to a folic acid gel, and suggested hydrogen bond interactions between chitosan and folic acid occur.⁷⁷ As expected, increased branching enhanced mechanical strength. The gels could also adsorb dyes and heavy metal ions from water, a promising result for water purification applications – an active area in gel technology. Adams and co-workers hypothesized that polymers can have viscosity-induced effects on the properties of LMWG gels, and added dextran biopolymers to pH-dependent naphthalene-dipeptide hydrogels.⁷⁸



Yang and co-workers added hyaluronic acid (HA) polymer to a LMWG hydrogel based on succinated taxol.⁷⁹ They evidenced that the presence of the polymer favors the hydrogel fibers to bundle, and not only slightly enhance the mechanical properties of the gel but also boosts the anticancer activity of the nanofibers at high HA concentrations. This is a nice example of how polymeric additives may impact rheology and nanostructure of LMWG hydrogels, and simultaneously introduce their own functionality. The presence of these protein clusters further influenced the self-assembly of the peptide gelator, resulting in a material with new unique mechanical and morphological properties. These effects result from cooperative interactions between both systems, and illustrate how LMWG materials can be relevant in the evolution and control of biological systems. The presence of polymers in the solution phase drives LMWG self-assembly either by interactions with the gel fibers or through viscosity effects. Small amounts of polymeric additive are thus a cheap and simple method to largely change LMWG nanoscale morphology and rheology, a point of significant importance for industrial considerations.

0.3.4. LMWG—(bio)polymer hydrogels: which strategies to design and fabricate mechanically strong and stimuli-responsive materials?

Low molecular weight gelators (LMWGs) and polymers have been combined since quite recently, but the field gained interest over the last years and its potential for further exploitation results in its fast expansion. This paragraph aims at summarizing the state-of-the-art and provide an overview of the new technologies that might be explored. LMWG–polymer systems are divided into five categories: (i) polymerisation of self-assembled LMWG fibers, (ii) capture of LMWG fibers in a polymer matrix, (iii) addition of non-gelling polymer solutions to LMWGs, (iv) systems with directed interactions between polymers and LMWGs, and (v) hybrid gels containing both LMWGs and polymer gels (PGs),⁸⁰ illustrated by Table 6 with corresponding references. Polymers can deeply modify the nanoscale morphology and materials performance of LMWGs, while LMWGs can have a significant impact on the rheological properties of polymers and provide a stimuli-responsiveness. The combination of different types of gelation system is a strategy to benefit from both LMWGs and PGs advantages (essentially stimuli-responsiveness and good mechanical properties, respectively), whilst overcoming their drawbacks. Bringing both technologies together not only enhances materials performance, which is useful for common applications, but it may also lead to major advances in environmental remediation, drug delivery, microfluidics and tissue engineering, among other high-tech areas.

Table 6 - Illustrations of the five main types of LMWG-polymer combinations ; *illustrations and reference numbers are from ref.⁸⁰*

(i)	 <p>Polymerisation of LMWG fibres Via polymerisable groups in gelator molecule</p>	<u>references 9 to 20</u>
(ii)	 <p>Capture of LMWG fibres in polymer matrix Fluid monomer phase polymerised around self-assembled network</p>	<u>references 21 to 36</u>
(iii)	 <p>Addition of non-gelling polymer to LMWG gel Can directly or indirectly influence LMWG network</p>	<u>references 43 to 55</u>
(iv)	 <p>Directed interactions between LMWG and polymer Via a recognition motif of controlled supramolecular interactions</p>	<u>references 56 to 61</u>
(v)	 <p>Hybrid gel combining LMWG and PG networks Multi-component system utilising properties of both networks</p>	<u>references 62 to 75</u>

Key:  = LMWG fibre  = Polymer

The fifth category is the one closest to the gels prepared and presented in the experimental part of this thesis. Hybrid hydrogels contain two gelators bringing each its own properties and are particularly interesting smart multifunctional materials for biomedical applications, from tissue engineering to drug delivery. In an approach close to the one of IPN described above, using a polymer gelator is expected to reinforce a mechanically weak LMWG network, while LMWGs are rather employed to induce directed interactions with tissue or drugs and to have a control over growth factors drug release rates for instance, through their stimuli-responsiveness. In 2009, Yang and co-workers were the first to report this kind of material.⁸¹ They obtained two-component hybrid gels with enhanced strength by combining Fmoc-peptide-based LMWG (H-lysine(Fmoc)-OH with one of three Fmoc-peptides) with agarose (the polymer gelator which provides mechanical strength). It is possible to incorporate additional components within these gels, such as Congo red, which was used as a model drug and was found to interact with the LMWG nanofibers. The choice of the LMWG is determinant to control its rate of release. The same team evidenced the potential of such gels for environmental concerns using a similar hybrid hydrogel, more efficient in the extraction of methyl violet from aqueous solutions than each of its individual components gels.⁸²

There exists a class of LMWG of particular interest: the large family of biosurfactants include many promising compounds. They are produced by microbial fermentation and are fully biodegradable, nice advantages considering that an emerging challenge in our current societies is to find an

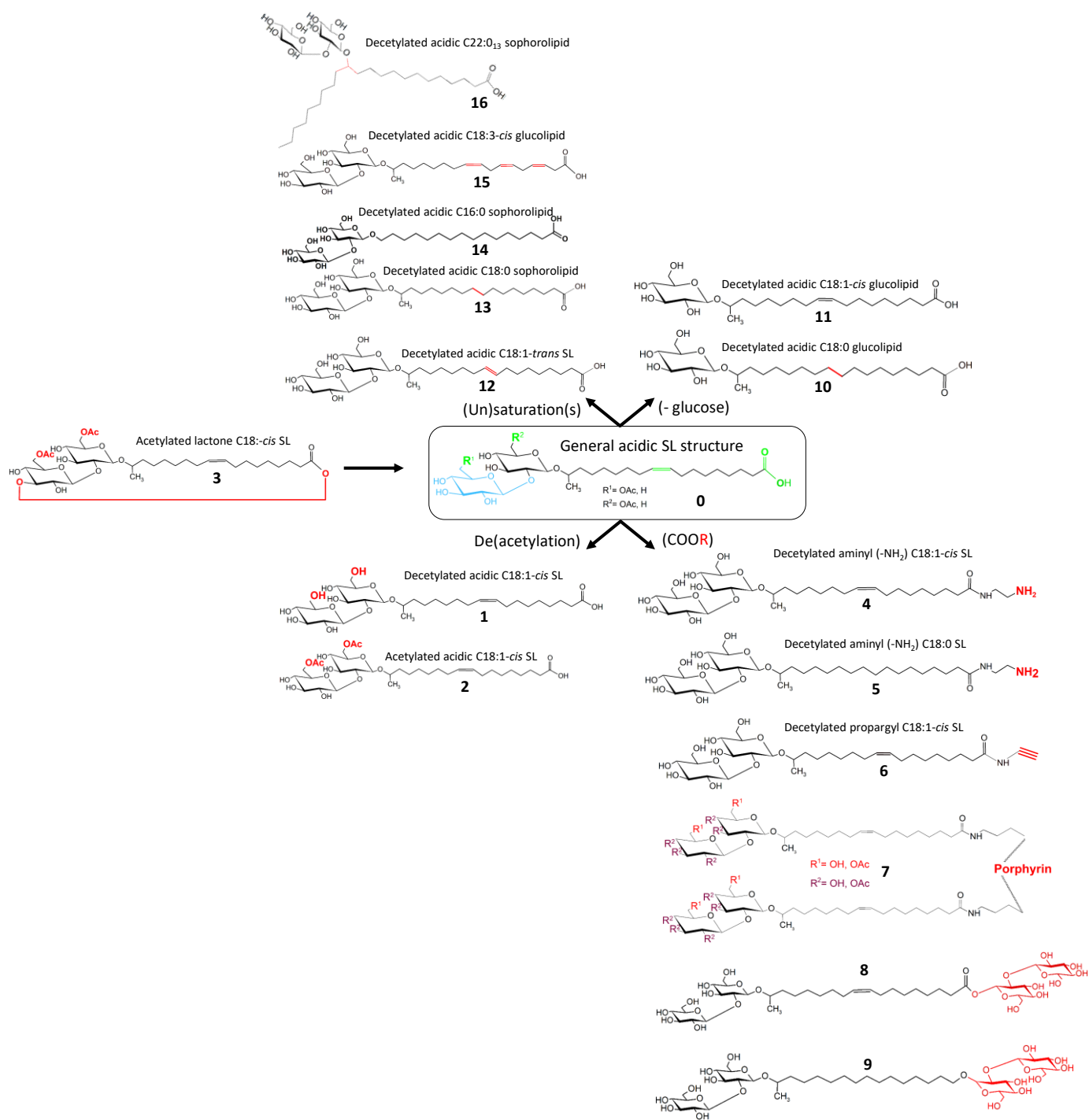
alternative to the chemical surfactants which are produced by oil industry, first for environmental concerns but also to extend their applications to the biomedical field. In addition, they allow to answer interesting questions due to their unique ability to switch from one phase to another upon application of an external stimulus, and thus fill a large gap in literature: what is the influence of a non-equilibrium phase transition triggered at phase boundaries on a (bio)polymer-(bio)surfactant system?

Next section will thus be devoted to biosurfactants : largely inspired by a review we wrote during the confinement and recently published,⁸³ it will present in details the richness of this family of molecules and their main characteristics.

0.4 Biosurfactants: generalities, presentation, phase diagrams and applications

Biosurfactants, or microbial surfactants, result from the fermentation process of yeasts, fungi and bacteria. These natural compounds are mostly produced by the wild type from a culture medium rich in glucose and vegetable oil. Properties and, hence, application potential, can be directly monitored by the structures of the biosurfactants. The molecular portfolio can be extended by the use of modified strains or chemical modifications of given biosurfactants. Biosurfactants are targeted by a large number of reviews which especially describe their origin, their producing strains and conditions as well as the main widely accepted categories.⁸⁴⁻⁹⁸ One can also refer to a review we recently published in order to build « a crossroad between communities, by merging the science and technology of soft colloids with biosurfactants science and giving new perspectives in terms of applications ».⁸³

The main existing biosurfactants are given in Figure 3. Compounds from **1** to **16** reflect the wide variety of sophorolipids (SL) and their derivatives. Besides SL, cellobioselipids (CL) in their hydrolyzed form (**17**), rhamnolipids (RL), both di- (**18**) and mono- (**19**), surfactin (**20**) and MELs (**21**) also exist and deserve consideration. MELs are commonly further divided into four sub-compounds (MEL-A, MEL-B, MEL-C and MEL-D) discriminated by different acetylation degrees (**21A-D**, R¹=H, Ac; R²= H, Ac).



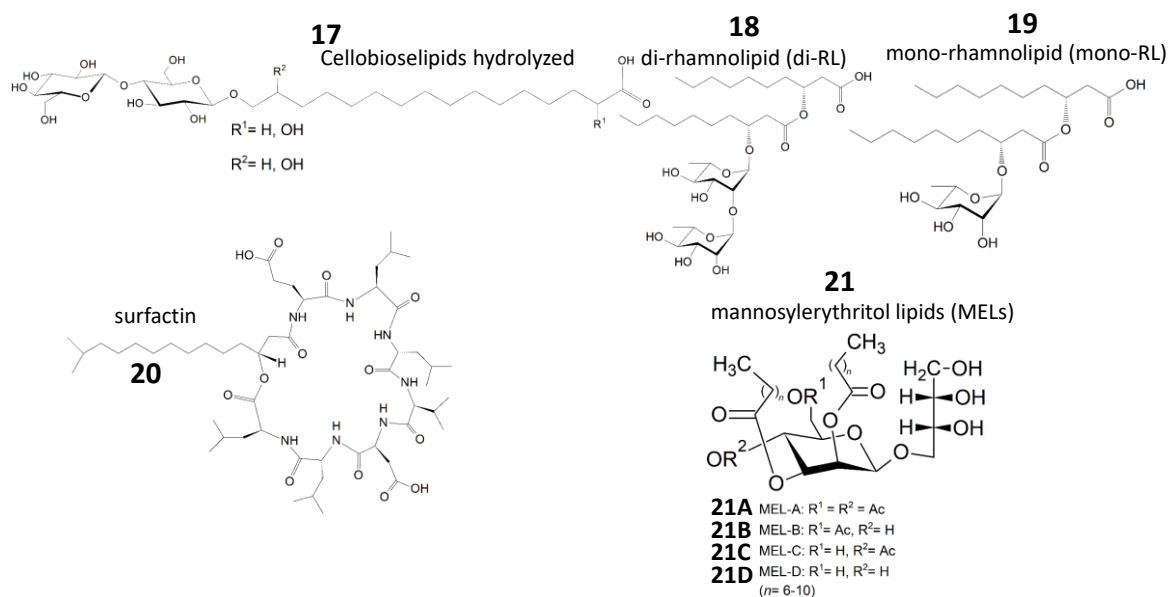


Figure 3 - Chemical structure of the main biosurfactant molecules (reproduced from ref.⁸³)

Biosurfactants can be primarily characterized in solution through the same generic approaches than surfactants, especially surface tension and CMC which are largely referenced in the biosurfactants' literature since decades. As deployed for standard surfactants, these parameters are however insufficient to understand and establish a right prediction of self-assembly or stimuli-responsivity of biosurfactants. The self-assembly/physicochemical properties of biosurfactants,^{99–101} rhamnolipids,^{92,102} mannosylerythritol lipids⁸⁸ or surfactin¹⁰³ are discussed in existing reviews which are however neither comprehensive nor do they propose a critical analysis of the biosurfactants' behavior with regards to the general concepts of surfactants assembly. Biosurfactants are furthermore characterized by a unique interesting complex phase behavior driven by external stimuli like pH, temperature or ionic strength, which is however rarely emphasized. Such a rich, dynamic, phase behavior in water at low concentrations is not only an attractive advantage for many applications^{104–108} but a unique opportunity for fundamental understanding of the self-assembly process of natural compounds, often under nonequilibrium conditions.

Classical parameters crucial in surfactant's science (HLB, surface tension and CMC) are reported for biosurfactants but will not be detailed here. The complex self-assembly properties of biosurfactants in water, including stimuli-responsivity, within and beyond the limits of the packing parameter approach, will be briefly presented before describing the relationship between self-assembly and macroscopic behavior, like hydrogel formation.

0.4.1. Self-assembly and phase diagramme




Biosurfactants' self-assembly was first explored in 1987 and focused on the pH-dependence of the aggregation of RL.¹⁰⁹ The first study of surfactin self-assembly dates back to 1995, of MEL to 2000,¹¹⁰ of sophorolipids (SL) to 2004¹¹¹ and cellobioselipids (CL) to 2012.¹¹² The self-assembly properties of lipids and surfactants are studied since the 50's and were rationalized in the 70's by Tanford¹¹³ and Israelachvili and coworkers.^{114,115} This comparison evidences a gap of several decades between the surfactants' science and biosurfactants communities in terms of mutual interests, a gap that can be explained by different reasons.





The main one deals with the chemical structure of biosurfactants. Indeed, it is more complex than common head-tail surfactants; biosurfactants are often bolaform and many of them bear ionizable chemical groups such as carboxylic acids in the case of glycolipids or lipopeptides. These chargeable groups induce that external stimuli like pH, ionic strength or temperature are particularly affecting biosurfactants' phase behavior. Considering the importance of additional weak interactions in the self-assembly process, such as hydrogen bond or π - π stacking at the same time as ionic, steric, van der Waals and entropic forces, the morphology of biosurfactants' aggregates and phase behavior in water are hardly predictable. Biosurfactants' aggregation can sometimes be explained by the packing parameter theory based on molecular shape, but the classical theory is not accurate for this class of functional compounds, as the distinction between hydrophilic and hydrophobic regions is sometimes challenging, as clearly stated for surfactin.¹¹⁶ The aqueous self-assembly and phase behavior of biosurfactants presented in Figure 3 are described in ref.⁸³ The following lines detail the cases of the biosurfactants studied during this PhD project: SL-C18:0 (**13**) and G-C18:1-*cis* (**11**).

The sphorolipid **SL-C18:0 (13)** forms spherical, ellipsoidal micelles (L_1) above pH 7.5. A minor phase of nanoplatelets may be observed at pH > 8. When $7.5 > \text{pH} > 3$, this compound self-assembles into fibers.

The same micellar phase is reported for the glucolipid **G-C18:1 (11)** at pH > 7.5 (bilayer fragments exist in minority above pH 8). At neutral pH ($7.5 > \text{pH} > 6.5$), the spherical, ellipsoidal micelles rather adopt a cylindrical, wormlike conformation. When $7.5 > \text{pH} > 4.5$, unilamellar vesicles are formed. In these pH conditions, a flat lamellar phase is observed only if $T < T_m$. A flat lamellar phase (condensed) is observed below pH 4 in all cases. An astonishing behavior associated to this molecule is the lamellar-to-multilamellar vesicle phase transition triggered by an increase from pH 3 to pH 6, and the micelle-to-fiber transition above pH 7, under study. These phases are summarized in the following Table 7 with the corresponding references:

Table 7 - Summary of the self-assembly and phase behavior in water of SL-C18:0 and G-C18:18-*cis*, adapted from table 5 of our review.⁸³

Biosurfactant N°	Biosurfactant name	Conditions	Ref.
Diluted (> CMC or CAC), < 0.1-1 wt% (often up to 5-10 wt%)			
Major phase			
 Micellar (spherical, ellipsoidal)			
<i>Sphorolipids and derivatives of SL</i>			
13	Acidic sphorolipids (C18:0)	Basic (pH > 7.5)	78
<i>Glucolipids</i>			
11	Acidic glucolipids (C18:1- <i>cis</i>)	Basic (pH > 7.5)	117,121
 Micellar (cylindrical, wormlike)			
<i>Glucolipids</i>			
11	Acidic glucolipids (C18:1- <i>cis</i>)	Neutral (6.5-7.5)	117,121
 Unilamellar vesicle			
<i>Glucolipids</i>			
11	Acidic glucolipids (C18:1- <i>cis</i>)	Acidic (7 < pH < 4.5)	117,121

 Multilamellar vesicle (MLV)			
<i>Glucolipids</i>			
11	Acidic glucolipids (C18:1- <i>cis</i>)	(pH 3 →) pH 6	122
 Flat lamellar			
<i>Glucolipids</i>			
11	Acidic glucolipids (C18:1- <i>cis</i>)	Acidic (7 < pH < 4.5), T < T _m	117,121
 Flat lamellar (condensed)			
11	Acidic glucolipids (C18:1- <i>cis</i>)	pH < 4	117,121
 Fiber			
<i>Sophorolipids</i>			
13	Acidic sophorolipids (C18:0)	Neutral/acidic 7.5 < pH < 3	78,84–86
11	Acidic glucolipids (C18:1- <i>cis</i>)	pH > 7, Ca ²⁺	126

It worthes adding some comments about the different phases presented.

Micelles: Most of classical head-tail surfactants under dilute conditions spontaneously self assemble into micelles above pH 7. The packing parameter associated to this morphology is $0 < P < 0.33$ for spherical micelles and $0.33 < P < 0.5$ for elongated, rod- until worm-like micelles.

Fibers: Fibrillation of lipids and proteins is an important crystallization phenomenon largely observed in soft matter and involved in many living processes, like bacterial motility or neuronal degeneration respectively conditioned by fibrillation of actin¹²⁷ and protein Tau. Low-molecular weight bolaamphiphile^{128–130} and peptides-based¹³¹ surfactants have the ability to make fibrils, and similar processes have been reported for biosurfactants.^{132,111,117–119,123,125,133–135} A unitary packing parameter for flat fibers or contained between 0.3 and 0.5 for cylindrical fibers could have been expected, but the packing parameter description is not accurate to discuss crystalline objects, because the theory behind the *PP* relies on a liquid hydrocarbon core that crystalline objects do not possess.

Vesicles: Vesicles are appreciated for being a metastable phase made of unique objects possessing a strong potential to encapsulate, transport and deliver a cargo (hydrophobic drugs, macromolecules, nanoparticles), which are interesting features in many domains from medicine to cosmetics. The packing parameter for vesicles is $0.5 < PP < 1$. Vesicle-forming biosurfactants are reported.^{117,121,122}

Lamellar phase: Lamellar phases play a major role in living organisms. Especially, biological membranes are mainly composed of phospholipids, not discussed in this context. Biosurfactants may form lamellar phases.^{117,121}

Concentration is a common parameter in evaluating the phase diagram of surfactants. Most studies related to biosurfactants, discussed above, have been performed under dilute to semi dilute conditions, rarely above 10 wt%, probably due to the lack of large amounts of matter having an acceptable molecular uniformity. Few studies do report on the self-assembly properties of biosurfactants at large volume fractions in water.

There exists even more phases observed for other biosurfactants,⁸³ but they will not be discussed in this manuscript (*Cylindrical/wormlike micelles, Ill-defined large-scale structures, Nanoplatelets, Columnar phase, Coacervate/L₃ phase*).

0.4.2. Stimuli-induced phase transitions

Most of the biosurfactants undergo a pH-responsive phase transition. The structures are most of the time studied *ex situ* at a precise pH, but the detailed mechanism of the morphological transition is being clarified by advanced pH-resolved *in situ* SAXS studies. Table 8 summarizes the main data about the pH-driven phases reported for biosurfactants while Figure 4 highlights some selected examples concerning acidic C18:1-*cis*, C18:0 sophoro- and glucolipids. Phases given in italic in Table 8 refer to a minor fraction whereas the most plausible morphology is written in brackets.

The effect of temperature is also not negligible, although only a few biosurfactants have been studied in relation with this parameter up to now. Table 9 reports the main biosurfactant systems where temperature-induced transitions have been investigated.

Finally, literature provides an example of light-responsive biosurfactant,¹³⁶ whose chemical stability once irradiated, resulting phase and mechanism of fluorescence emission remain however uncertain.

Table 8 - pH-driven phase transitions in biosurfactants (N° given in Figure 3). *: in brackets is given the most plausible morphology; §: in italic it is given the minority phase. †: The micelle phase is favored by a spurious (< 5%) amount of C18:2, C16:0, C18:0 sophorolipid congeners while the ribbon phase is favored by an excess amount (> 10-15%) of C18:0 SL congeners in the batch.

BS	Type	N°	Structure				Met hod	Ref
			Basic pH > 8-7	Neutral 8 < pH < 7	Acidic 7 < pH < 4	Strongly acidic pH < 4		
RL	Mono	19	Planar (vesicle) (> 20 mM) Micelles (< 20 mM)	Unknown	<i>Bilayer</i> (vesicle)*	-	<i>Ex situ</i>	109,137-139
RL	Di	18	Micelles	Unknown	<i>Bilayer</i> (vesicle)*	-	<i>Ex situ</i>	109,137-139
SL	C18:1- <i>cis</i>	1	Micelles <i>/Platelets</i> §	Micelles	Micelles	Micelles/ <i>Ribbons</i> †	<i>In situ</i>	111,117,123,124,140,141
SL	-NH ₂ C18:1- <i>cis</i>	4	Micelles	Micelles	Micelles <i>/Platelets</i> §	-	<i>Ex situ</i>	134
SL	C18:1- <i>trans</i>	12	Micelles <i>/Ribbons</i> §	Micelles	Ribbons	Ribbons	<i>In situ</i>	118,123
SL	C18:0	13	Micelles <i>/Platelets</i> §	None	Ribbons	Ribbons	<i>In situ</i>	117,125
SL	-NH ₂ C18:0	5	Ribbons	None	Micelles <i>/Platelets</i> §	-	<i>Ex situ</i>	134
SL	C18:3	15	-	Unknown	Vesicle	-	<i>Ex situ</i>	142

SL	C22:0 ₁₃	16	Micelles /Vesicles [§]	Undetermined	Vesicle	multilamellar	<i>In situ</i>	120
GL	C18:1- <i>cis</i>	11	Micelles /Lamellar [§]	Cylinders- wormlike	Vesicle/ MLV	multilamellar	<i>In situ</i>	117,121,122
GL	C18:0	10	Micelles /Lamellar [§]	None	<i>P_β</i> (Lamellar)	multilamellar	<i>In situ</i>	117,121
CL	Hydrolyzed	17	Filaments	Unknown	Ribbons	-	<i>Ex situ</i>	117
Surf	Cyclic	20	Micelles /Other	Unknown	Bilayer (Vesicle)	-	<i>Ex situ</i>	116,143–146

Table 9 - Temperature-driven phase transitions in biosurfactants (*N*° given in Figure 3).

BS	Type	N°	Structure		Transition Temperature	Ref
			Low T	High T		
SS	Symmetric C16:0	9	Ribbons	Micelles	28°C	117
SL	Phorphyrin- derivatives	7	Columnar or micelles	Monomers	34-37°C	147
GL	C18:1- <i>cis</i>	11	Lamellar	Vesicle	Below RT	117
GL	C18:0	10	Lamellar	Vesicle	Above RT	117
MEL	Mel-A (<~57 wt%)	21A	Coacervate (<i>L₃</i>)	Isotropic	~63°C	148
MEL	MEL-B (<~60 wt%)	21B	MLV	MLV	-	149

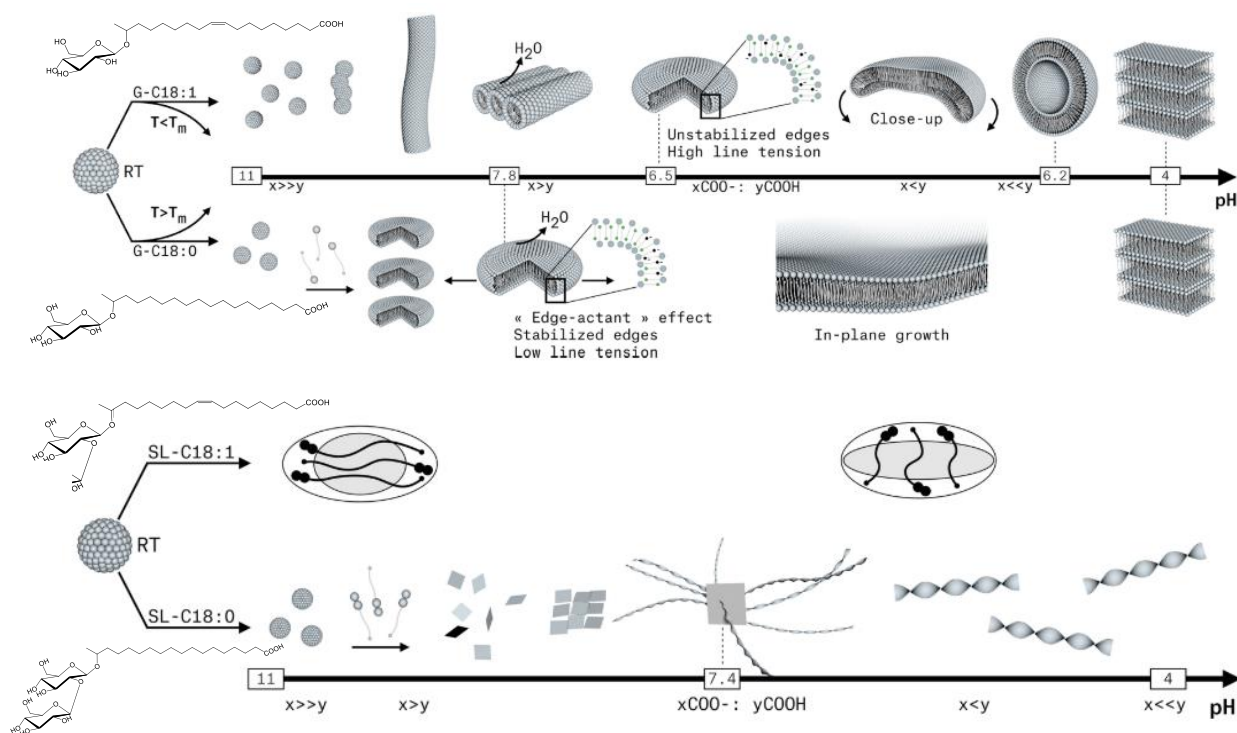


Figure 4 - pH-dependent phase transitions for nonacetylated acidic C18:1-cis (**1**), C18:0 sophoro (**13**) and glucolipids (**10**)¹²¹, adapted from our review⁸³

0.4.3. Macroscale properties and possible applications of self-assembled biosurfactants

One can find old and more recent reviews which discuss the physicochemical properties of biosurfactants^{88,99–101} serving several examples of application as antimicrobial, antiviral, gene delivery¹⁵⁰ molecules or as components in cosmetic formulations.^{97,99,151} Precise control over the self-assembly is even opening the door to promising opportunities in the fields of physics, chemistry, colloids and materials science: amphiphiles are able to stabilize interfaces, an interesting feature to develop biobased emulsions; lamellar objects are promising tools to encapsulate and release colloids and molecules; fibers can be considered to modulate viscosity or to template chiral inorganic materials for enantioselective catalysis, among other examples. Biosurfactants systems (and eventually formulations with other surfactants or lipids) can lead to innovative systems presented below, thus broadening the application potential of these compounds into new fields.¹⁵² All these examples cover a large range of application domains and prove that the knowledge generated from the study of the biosurfactants' self-assembly properties still deserve further investigation.

0.4.3.1. Hydrogelling

Hydrogels can be based on colloids, polymers and low molecular weight gelators (LMWG). Biosurfactants are simple adjuvants to other gelling systems, like polymers, but behave as LMWG.^{60,153–156} According to the strong knowledge available about LMWG, these molecules self-assemble into fibers upon cooling and so drive the stabilization of a solvent into a gel.

Table 10 summarizes the results reported up to now.

Table 10 - Additive-free biosurfactants hydrogels and related stimuli-responsivity and mechanical performances. *= Mechanical properties strongly vary with pH change rate; the value reported is obtained with homogeneous pH variation with glucono- δ -lactone. §= Elastic properties depend on rate of temperature variation. Slow temperature variation could improve G' of a factor 10. #= At RT, elastic properties strongly depend on a combination of pH, ionic strength and time. For a given time, pH and temperature, ionic strength strongly improves the elastic properties.

BS	Type	N°	Gel	G' / kPa $\nu = 1 \text{ Hz}$ linear domain	C / wt%	pH	T / °C	Stimuli	Ref
SL*	C18:0	13	Fibrous	Up to 10	3	< 7	25	pH	157
SS§	C16:0 symmetric	9	Fibrous	1	3	neutral	25	T	158
CL	Sodium salt	17	Fibrous	0.01- 0.03	2	neutral	25	T	112
GL#	C18:0	10	Lamellar	10-100	3	< 7	25	pH, T, ionic strength, time	159,160

0.4.3.2. Solid foams

Freeze-casting (or ice-templating, e.g. the directional freezing of water) and freeze-drying (water removal), have processed fibrillar and lamellar sophoro- and glucolipid hydrogels into soft condensed macroporous materials.¹⁶¹⁻¹⁶⁴ Both hydrogels exhibiting close elastic properties (Figure 5a) were frozen at rates up to 10°C/min keeping their nanostructure, as supported by temperature-responsive *in situ* SAXS and electron microscopy experiments.¹⁶⁵ Dried fibrous foams benefit from a preferential orientation of the macropores along the freezing axis, their axial Young modulus is about 20 times higher than the transversal modulus (anisotropic mechanical properties). They hardly support weights 100 times heavier than them. On the contrary, lamellar-based material reach a Young modulus in the order of 20-30 kPa in both directions (isotropic orientation of the macropores) and can withstand up to 1000 times their own weight (Figure 5b). These unexpected results highlight different properties of the self-assembled lamellar and fibrous structures, the ones of lamellar structures being greater.

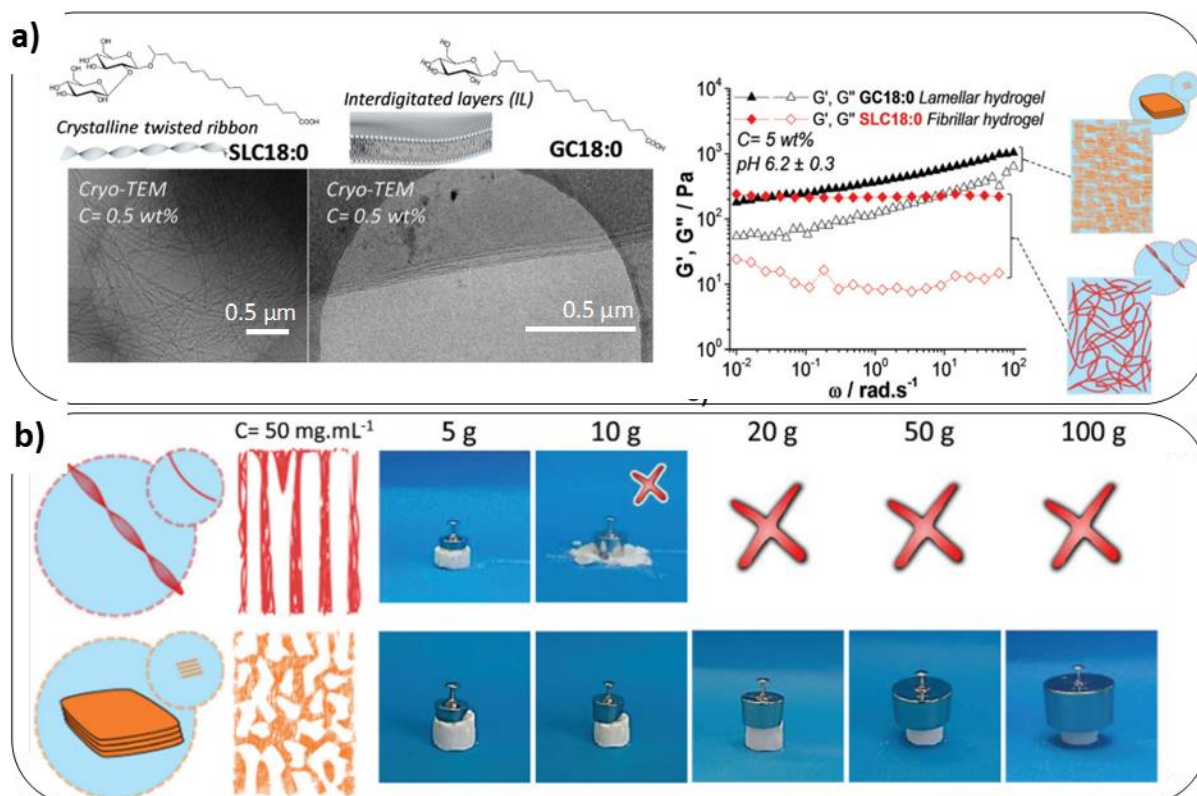


Figure 5 - a) Comparison of frequency-dependent G' , G'' between fibrillar and lamellar hydrogels respectively obtained from C18:0 sophoro and glucolipids at acidic pH.^{157,160,165} b) Comparison of the axial compression applied to solid foams prepared from fibrillar and lamellar hydrogels using the ice-templating process.¹⁶⁵ Image adapted from cited references.

0.4.3.3. Encapsulation

Encapsulation and release of hydrophobic compounds within amphiphilic carriers is a common application in medicine and undergoes increasing demand. It is essentially based on the self-assembly properties of the amphiphile in solution. Current encapsulation processes mainly rely on phospholipid liposomes although several tests have been reported in the fields of drug and gene delivery with biosurfactants in formulations with phospholipid liposomes. Devices based exclusively on biosurfactants is quite a new field of research, probably because the phase diagrams of biosurfactants do not benefit yet from the decades of studies worldwide devoted to phospholipids, which provided a strong knowledge and consequently a control over their phase diagrams.

Among the few studies reported,¹³⁸ a recent work has evidenced the dynamic encapsulation properties of deacetylated acidic C18:1-*cis* (**11**) glucolipids-based vesicles. The lamellar-to-MLV phase transition from acidic to neutral pH at RT of this biosurfactant was leveraged to encapsulate systems unstable in water, such as uncoated magnetic iron oxide (Figure 6a) or hydrophobic luminescent up-converting nanoparticles (Figure 6b), but also stable ferritin nanocages (Figure 6c)¹²² among various colloids.

Direct and reverse micellization processes respectively exploit the solubilization potential of hydrophobic molecules by micelles in water and hydrophilic molecules in organic solvents. They are now well understood and widely employed. The use of sophorolipids in order to solubilize molecules

of biomedical interest, antibiotics or antioxidants, is a valuable strategy according to a series of work, curcumin for example, a powerful antioxidant with promising anticancer properties whose solubilisation in water remains challenging.^{166,167,168} This set of studies shows an efficient solubilization of curcumin and promising effects, but do not clarify the nature of the SL self-assembled form. Another question concerns the spectroscopic FT-IR signature of curcumin, which is not observed in the SL-curcumin systems. These structural and spectroscopic aspects still deserve further investigations. A similar approach allowed to solubilize antibiotics using SL.^{169,170}

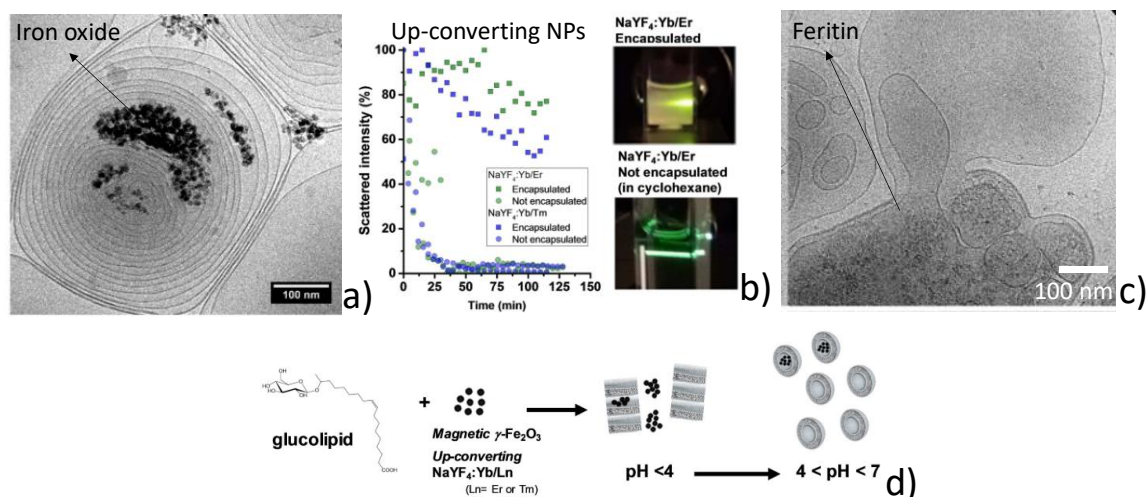


Figure 6 - Encapsulation of a,b) unstable (uncoated iron oxide, hydrophobic NaYF₄:Yb/Er) and c) stable (ferritin) nanocolloids within multilamellar vesicles prepared through d) a phase-change (lamellar-to-vesicle) process using deacetylated a cidiic C18:1-*cis* glucolipids.¹²²

0.4.3.4. Mixing with surfactant and lipids

Increasing interest is devoted to the topic of interactions between biosurfactants and other surfactants and lipids. These latter however increase the complexity of the interactions whose understanding goes beyond the understanding of biosurfactants' self-assembly. These systems will not be detailed here but are however promising and deserve interest : mixed BS/surfactants and BS/lipid systems are studied either to formulate greener detergents^{141,171,172} or to develop more efficient gene transfection and drug carriers^{88,150,173-186} but also to determine which is the impact of BS on lipid membranes, in order to know more about their interactions with living organisms.^{173-178,186}

0.5 Biosurfactant-biopolymer systems

The goal of this thesis is now to design and fabricate fully biobased systems with valuable properties, leveraging the huge potential and our knowledge on biosurfactants. We are indeed convinced that a molecule (a biosurfactant) existing within at least three phases, each one responding to a precise stimulus, in combination with a biopolymer will provide new fascinating materials. This section will present the few examples of biosurfactant-biopolymer systems available in the literature and highlight the importance of this thesis work to fill this gap.

Hybrid hydrogels can be designed according to a safe-by-design approach, involving the selection of only biodegradable and biocompatible individual molecules. The optimization of such systems requires the preliminary understanding of the interactions between biosurfactants and biopolymers .

This section will thus highlight the main features concerning the behavior of biosurfactants with macromolecules: polymers, biopolymers, as well as proteins or enzymes, and establish to which extent behaviors of biosurfactant-biopolymer and surfactant-biopolymer can be compared. We will present a first set of biosurfactant-polymer systems relying on mutual interactions, such as hydrophobic effect or electrostatic, and a second one where biosurfactant and biopolymers coexist without any specific interaction.

0.5.1. Interactions with polyelectrolytes

0.5.1.1. Sophorolipids, glucolipids

The most relevant study to cite here and to detail is the one which established the ground for the work of this thesis, that is to say the complex coacervation of natural sophorolipid bolaamphiphile micelles with cationic polyelectrolytes by G. Ben Messaoud.¹⁸⁷ To be precise, this work concerns complex coacervation of micelles from a bolaform sophorolipid biosurfactant with oppositely charged cationic polyelectrolytes (i.e., chitosan oligosaccharide lactate, poly (L-lysine) and poly(allylamine)).

Biobased sophorolipid bolaform biosurfactant micelles were found able to form complex coacervates with the cationic polyelectrolytes employed. The coacervation process is mainly driven by pH and turbidimetric titration revealed that the coacervates can be formed in the large 5-9 pH range as a function of the cationic polyelectrolyte type and concentration (Figure 7a). The charge-pairing mechanism is confirmed by quantitative NMR analysis, which also reveals that 25% of the initial SL – polyelectrolyte concentration is involved in the coacervates. The coacervation structure investigated by cryo-TEM (Figure 7b) and SAXS indicates the coexistence of polymer and micelles upon coacervate formation and the presence of well-defined coacervates in their stability region. The description here proposed for complex coacervate formation between a chargeable bolaform surfactant and chargeable polyelectrolytes is in agreement with the knowledge concerning classical ionic surfactants-polyelectrolyte systems.

This study calls to further investigate the binding behavior of such bolaamphiphiles to macromolecules and valorizes their potential for the preparation of future functional soft materials. It also proposes new prospects for the use of bolaform sophorolipid micelles to prepare complex coacervates that could be imagined to be used for pollutant and dye removal or like an encapsulation matrix for drug delivery applications.

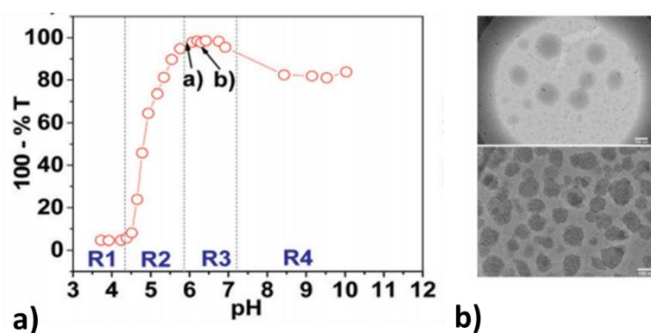


Figure 7 - a) pH-dependent turbidimetric profile and b) Cryo-TEM images (top: pH 5.94, bottom: pH 6.33) of acidic C18:1-cis sophorolipid(1)-chitosan complex coacervates (Reproduced from ref.¹⁸⁷ with permission of The Royal Society of Chemistry)

0.5.1.2. Rhamnolipids (mono-(**19**), di-(**18**))

Efforts were devoted to systems involving rhamnolipids. Antimicrobial rhamnolipid-rich chitosan nanoparticles were designed based on electrostatic interactions between chitosan and a polyphosphate (TPP), while rhamnolipids are associated to the system as an adjuvant improving stability of chitosan nanoparticles.¹⁸⁸ Replacing petrochemical surfactants in hair-washing formulations motivated Fernández-Peña *et al.*¹⁸⁹ who recently focused on the capability of rhamnolipids (mono-RL(C10), mono-RL(C14), di-RL(C10), di-RL(C14)) to substitute sodium laureth sulfate (SLES) in binary mixtures with a cationic polyelectrolyte (PDADMAC, poly(diallyl-dimethylammonium chloride)).

0.5.2. Interactions with enzymes and proteins

Interactions between surfactants and proteins, or enzymes, is a rich and fascinating important topic benefiting from a huge potential for applications from medical to environmental science. There exists specific reviews dedicated to this topic.^{190,191} A number of parameters are of equal importance to draw a tendency, complexifying this field: the intrinsic value of surfactant's CMC as well as its shift in the presence of proteins, the isoelectric point (Ip) of proteins and its shift in the presence of surfactants, the eventual charge of surfactants and its nature, the chemical nature of the charged group, the size of the protein, the solution pH and ionic strength, the type of counterion... are the main ones. According to a general trend, valid for classical surfactants like SDS, there exists strong surfactant-protein interactions below the CMC, with possible stimulation of β -sheet formation and fibrillation. This effect would be triggered by both non-specific (hydrophobic effect) and specific (electrostatic) interactions. Above the CMC, on the contrary, surfactant micelles denature the protein, resulting in protein-decorated micelles, or bead-necklace, structures.^{190,191} The study of biosurfactant-protein interaction have only generated a reduced amount of work, although some have been performed recently.¹⁷⁴ Here is discussed a broad set of data investigating the interactions between biosurfactants and proteins, or enzymes, which will be correlated to the broader literature of surfactant-protein interactions.

0.5.2.1. Rhamnolipids (mono-(**19**), di-(**18**))

First studies on the effect of biosurfactants on proteins stability date back to 2008. Ortiz *et al.* were interested by the effect of RLs^{192,193} and reported thermodynamic and structural changes associated with the interaction of di-RL with bovine serum albumin (BSA).¹⁹² Since 2014, the group of Otzen *et al.* largely studied RLs-protein interactions,^{194,195} the interactions between RL (1:0.35 mono-RL (**19**): di-RL (**18**)) and two model proteins, α -lactalbumin (α LA) and myoglobin (Mb) in buffer at pH 7.¹⁹⁴ RLs denature α LA below the CMC and Mb above the CMC by increasing α -helicity.

Otzen's group was also interested by interactions between RLs and enzymes. The impact of RL (1:0.35 mono-RL: di-RL) against three industrially-relevant enzymes (cellulase Carezyme® (CZ), the phospholipase Lecitase Ultra® (LT) and the α -amylase Stainzyme® (SZ)) was studied at pH 8 and compared to SDS.¹⁹⁶ RL display little, or no, binding against all enzymes, except CZ, and did not affect the structural integrity nor the activity of any enzyme, contrary to SDS.

0.5.2.2. Sphorolipids (1-3)

Otzen *et al.* have studied both the interactions between SLs or RLs and proteins and enzymes. Their conclusions exhibit only minor differences. They reported a similar stoichiometry (at saturation) of 29 SL (**1**) molecules per apo-Ala when nonacetylated acidic C18:1-cis SL (**1**) are used instead of RLs.¹⁹⁷ SLs have an even gentler interaction with apo-aLA than RLs. Globally, acidic SL start denaturing apo-aLA with slow kinetics compared to, e.g., SDS, and only in the proximity of their CMC, while RLs show some interactions below the CMC.

Silk fibroin (SF) extracted from *Bombix mori* is a protein benefiting from well-known hydrogelation properties.^{198–202} However, its clinical applications are limited considering its quite long process of hydrogelation (from 10–16 hours below the isoelectric pH to a few days or even weeks slightly above the isoelectric pH),²⁰³ what can be overcome by cationic, anionic and non-ionic surfactants, able to faster the gelation process.^{204,205} However, chemical and non-biodegradable additives are not accurate to synthesize biologically relevant hydrogels. Dubey and co-workers explored the possibility to use nonacetylated C18:1-cissphorolipids (nonacetylated acidic, ASL (**1**), diacetylated lactonic, LSL (**3**), or 1:3 mixture of them, MSL) as SDS analogues and used them as initiators for the hydrogelation of SF.^{153,154,156} Their experiments evidenced a behavior close to the one of SDS or other surfactants which can reduce the gelation time to less than the hour.^{204,205} gelation times were improved from the order of weeks to hours.

0.5.2.3. Surfactin (20)

Interactions between surfactin and BSA were studied by Zou *et al.* in buffer at pH 7.2.²⁰⁶, related data mostly corroborate previous works studying the interactions between biosurfactants and proteins. In particular, the CMC of surfactin increases from 0.15 μM to 0.33 μM , the number of surfactin molecules per BSA is evaluated between 7.5 and 17.6, according to the BSA concentration in solution and, finally, the structure of BSA is only affected by surfactin above its CMC and in a gentle way, as shown by the moderate evolution of circular dichroism data. The micellization process of surfactin and its influence on the aggregation behavior of A β (1-40) peptide into fibrils, identified as a key pathological process at the heart of Alzheimer disease, were investigated and found efficient to stimulate fibrillation in the vicinity of surfactin's CMC and prevent it above CMC.²⁰⁷

0.5.2.4. Mannosylerythritol lipids (21)

Fan *et al.* reported several studies probing the influence of MEL-A (21A) on the structure and properties of β -glucosidase and β -lactoglobulin (β -lg):^{208,209} MEL-A (**21A**) modifies the secondary structure and physicochemical properties of β -glucosidase,²⁰⁸ of which the activity is enhanced at MEL-A (**21A**) concentration in the vicinity or lower than the CMC ($\sim 20.0 \mu\text{M}$) but also increases its thermal stability.

Some years ago, Kitamoto and co-workers reported the spontaneous formation of giant MEL-based vesicles at pH 7.0 and 25 °C.¹¹⁰ Their surface is rich in the mannopyranoside residues, the sugar constituting the carbohydrate part of MELs, and to which mannose-binding proteins like concanavalin A (ConA) are expected to bind easily. ConA-mannose interaction was only reported for MEL-B (**21B**) and MEL-C (**21C**)-based vesicles, which bear a free OH group at C-4' or C-6' position of mannose and known as a preferential ConA binding site.²¹⁰ It supports the hypothesis of a specific binding behavior on the vesicular surface.

0.5.2.5. General comments

- In agreement with the body of work on general protein-surfactant interactions,^{174,190,191} the non-specific hydrophobic effect would be the driving force for biosurfactant-protein interactions. However, the stability, activity, binding affinity and molecules-per-protein of a protein is also influenced by other specific interactions, which depend on the specific nature of the protein, biosurfactant but also pH and ionic strength.
- Biosurfactants have milder interactions with proteins for several reasons. This is probably first due to the softer carboxylate groups, which exhibit less affinity than classical sulfate groups for oppositely-charged binding sites on the protein. The bolaform or branched structure of biosurfactants but also their lower charge density distribution also certainly contribute to reduce the strength of the interactions.
- The affinity of biosurfactants towards proteins is generally observed around and above the corresponding CMC, rather than in their monomeric state below the CMC, as classically found for SDS. ITC data recorded on several systems support the hypothesis of negligible interactions below the biosurfactant's CMC.
- As a consequence, low amounts of biosurfactants do not exert any influence on the proteins' structure. However, at higher biosurfactant concentrations, proteins can be inserted into the biosurfactant's hydrophilic shell, inducing deep structural changes through the increase in β -sheets content.
- It results from the above that fibrillation of specific proteins (e.g., α -synuclein, FapC or silk fibroin) can be induced and/or accelerated by the presence of biosurfactants above their CMC. This contrasts with reported data for SDS-protein interactions, where fibrillation is generally induced below the CMC of SDS, denaturation even generally occurs above its CMC.

0.5.3. Interactions with polymers

Mannosylerythritol lipids (21)

Park *et al.*²¹¹ prepared polymeric nanoparticles employing poly(ethylene oxide)-b-poly(ϵ -caprolactone) copolymers (PEO-b-PCL) and cell-penetrating TAT peptides. They have shown that use of MELs (without mentioning which type) covalently modified with a maleimide peptide linker results in a more flexible polymer core, thus promoting the formation of smaller particles of a factor two and formation of a soft gel. The YGRKKRRQRRR-cysteamine peptide-linked maleimide achieved improvements in cellular uptake by human skin fibroblasts.

0.6 Objectives

Interactions between biosurfactants and macromolecules (proteins, enzymes, polymers...) generally benefit from a large literature, which however suffers from some drawbacks. Factually, there is first a number of biosurfactants which are not the object of any study, including SL-C18:0 and G-C18:1, the two biosurfactants employed in this work. Secondly, proteins or enzymes are more documented than (bio)polymers. Then, from a physico-chemical point of view, authors mainly describe interactions between macromolecules and biosurfactants within a static state (often micellar or vesicular). Many questions remain regarding the induction of phase transitions: do they generate a new phase? Do they involve interactions and if yes, of which nature? Biosurfactants are molecules of

choice to answer these questions due to their unique ability to switch from one phase to another, of which classical surfactants are not able.

All the work of this thesis is first devoted to the understanding of biosurfactant-biopolymers interactions for selected systems under such non-equilibrium conditions, poorly explored up to now, and their potential applications. A second part deals with the design of hybrid materials with valuable properties based on this knowledge. The whole of results is presented in this manuscript.

More precisely, we first want to clearly establish which structures result from the self-assembly of a set of biosurfactants and biopolymers in each pH conditions and clarify the influence of each biosurfactants' phase transition on these structures. These points are addressed in **Chapter I**. This latter presents multilamellar structures among others, particularly interesting for encapsulation of compounds; this applicative point will be discussed in **Chapter II**.

The second objective is to combine biosurfactant and biopolymer in a hybrid material, whose new mechanical properties are expected to be improved compared to biosurfactant or biopolymer hydrogel, with an additional functionality regarding pH and/or temperature. These aspects will be respectively detailed in **Chapters III** and **IV**.

CHAPTER I: pH-induced phase transitions in diluted biosurfactant-biopolymer aqueous solutions

Table of contents

1.1	Introduction	46
1.2	Experimental methods.....	49
1.2.1	Chemicals.....	49
1.2.2	Preparation of stock solutions	50
1.2.3	Preparation of samples.....	50
1.3	Identification of a precise pH-range of interactions.....	51
1.4	Morphological and structural characterization of the mixed lipid-polymer structures.....	54

1.1 Introduction

As discussed in the **bibliographic chapter**, biosurfactants remain rarely studied in the presence of other macromolecules, while their interactions constitute a large and fascinating area of investigations with many potential applications. As a short summary, reported studies mainly concern rhamnolipids and mannosylerythritol lipids, in the presence of proteins or enzymes.^{192–195,196,208,209} The goal of this PhD project was thus to fill this gap and to address the following questions: do biosurfactants interact with macromolecules? If so, which is the nature of the interaction? Under which physicochemical conditions? Do such interactions generate new phases?

This work was motivated and based on the results obtained at LCMCP by Ghazi Ben Messaoud²¹² using the sophorolipid SL-C18:1 (Figure 3, **Chapter I**, p.38) and cationic polyelectrolytes (chitosan oligosaccharide lactate, poly(L-lysine) and poly(allylamine)). A commercial source of SL-C18:1 forms a micellar phase in a broad pH range and he demonstrated the formation of complex coacervates in a pH range where micelles are negatively-charged and polyelectrolytes positively-charged. These structures result from the process of complex coacervation, during which a homogeneous macromolecular aqueous solution undergoes an associative liquid-liquid phase separation.²¹³ Contrary to simple coacervation, it involves more than one macromolecular component^{214,215} and can occur between polyelectrolytes and oppositely charged polyelectrolytes,^{216–221} proteins,^{12,222,223} dendrimers²²⁴ or micelles.^{225–230} Surfactant-polymer coacervation is commonly observed between a nonionic surfactant and a nonionic polymer or polyelectrolyte, or between an ionic surfactant and nonionic polymer or polyelectrolyte.²³¹ In the case of complex coacervation between oppositely charged surfactants and polymers, the strength of electrostatic binding must be high enough to induce coacervation, but not too much to avoid precipitation.²³¹ As stated in the objectives of this thesis, biosurfactants behavior is mainly, if not always, studied under pseudo-equilibrium conditions, in a micellar or vesicular state most of the time. It is the case for SL-C18:1, which self-assembles into micelles over the whole pH range. However, there is a lot to explore under non-equilibrium conditions and at phase boundaries, some biosurfactants being characterized by several pH-dependent phase transitions. For this reason, my work goes further by repeating these experiments using two glycolipids, which exhibit a more complex phase behavior: SL-C18:0 (SL: sophorolipid, D-glucose (1, 2) β (1, 2)) and G-C18:1 (GC: glucolipid, β -D glucose), of which the structures, given in Figure 8, are close as their differences are only a sugar moiety and an unsaturation.

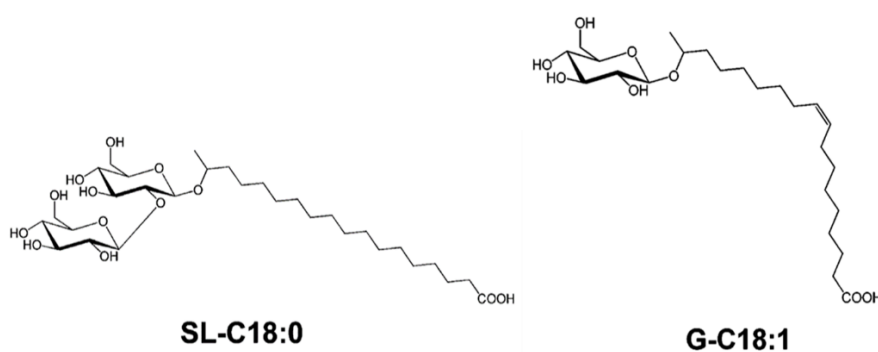


Figure 8 – Chemical structures of glycolipids employed: SL-C18:0 (left) and G-C18:1 (right) (pH-dependant COOH/COO⁻ group)

The phase behavior of microbial surfactants has been deeply investigated at LCMCP under diluted conditions (< 1 wt%). Figure 9 provides a schematic view of the phase behaviors of SL-C18:0 and G-C18:1 respectively.

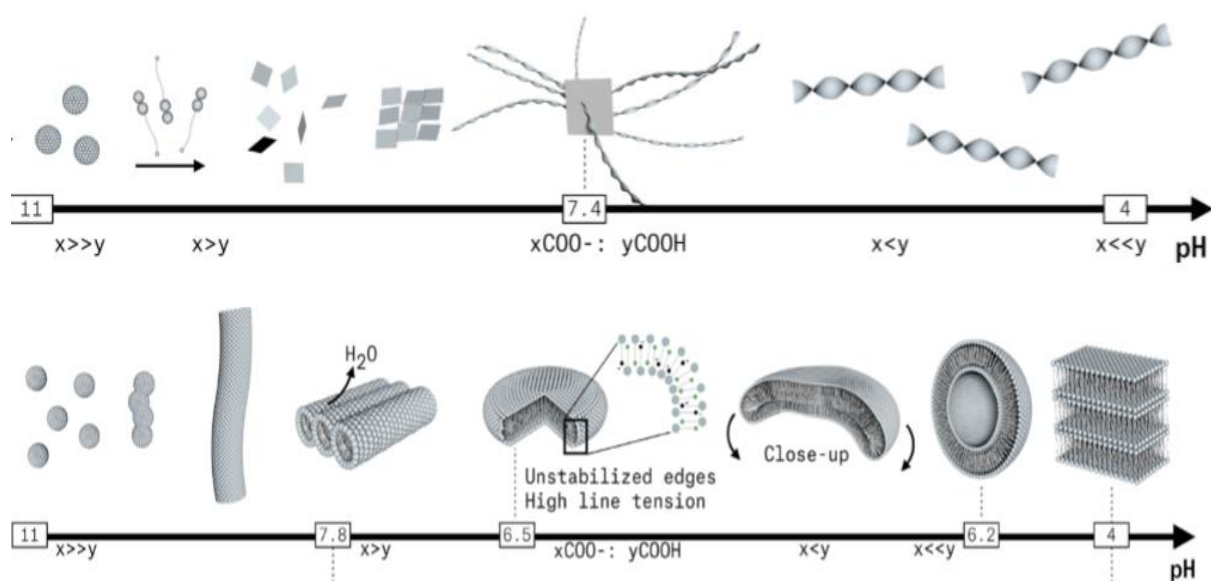


Figure 9 - Phase diagrams in function of pH of SL-C18:0 (upper part) and G-C18:1 (lower part) in water and at room temperature (0.5wt%)¹²¹

In a few words, both systems form micelles at basic pH, like SL-C18:1. SL-C18:0 micelles then rearrange into fibers below pH 7.4, while G-C18:1 micelles progressively self-assemble into vesicles below pH=6.5 and precipitate into a lamellar phase below pH 4. Both systems are of interest for different reasons: fibers can form self-assembled fibrillar networks (SAFiN) gels, while vesicles can be rather interesting for encapsulation purposes.

Their phase diagrams at room temperature in water at low concentration (0.5 wt%) are well-known, but were never investigated in presence of a macromolecule. This presents a real interest first for the biosurfactants' field. Indeed, the richness of their phase diagrams opens the door to a wide range of interactions and potential new structures in presence of a polymer, especially if this latter is oppositely charged. In this case, we expect to form complex coacervates in the micellar phase of the biosurfactants and will then explore phase transitions triggered inside the self-assembled structure. This work will thus be devoted to the comprehension of the interactions between biosurfactants and macromolecules, and more specifically biobased and synthetic polyelectrolytes, in function of pH, e.g. their state of charge, at low concentrations. Secondly, it more largely deserves attention in colloids science, phase transitions triggered inside complex coacervates being never explored for the reason that phase transitions for classical surfactants are usually concentration dependent.²³²

Complexation of surfactant and polyelectrolytes is a wide field of research on its own. The type of polyelectrolyte-surfactant complex formed (PESC) depends on the surfactant's phase.²³³ Complex coacervation commonly occurs when this latter is micellar. Morphologies are however different and more complex using lipids. Typical surfactant-polyelectrolyte complexes reported in the literature involve a surfactant, of which the charge is generally not sensitive to pH and its assembled state is always micellar, and neutral or oppositely charged polyelectrolytes, of which the charge may, or may not, be pH-dependent.^{7,230,234} SL-C18:0 and G-C18:1 give, in addition, the opportunity to modulate

the charge of both compounds in an opposite way playing with pH, which also induce a change in their self-assembled form (Figure 9). In such a system, we expect the electrostatically-induced formation of complex coacervates, when the biosurfactant (under its micellar state) and the polyelectrolyte are oppositely charged. Otherwise, when the biosurfactant adopts another conformation, both species may still interact or coexist without any specific interactions, but the role of hydrophobic effects is not negligible in the formation of polyelectrolyte-surfactant complexes (PESCs).⁶ The pH-dependent phase diagrams of biosurfactants allow to go even a step further by triggering phase transitions directly inside the complex coacervate, an aspect never explored up to now.

For this work, we used four polyelectrolytes, previously studied by Ben Messaoud *et al.*:²¹² chitosan oligosaccharide lactate (CHL, $pK_a \sim 6.5$)²³⁵, poly(L-lysine) (PLL, $pK_a \sim 10-10.5$)²³⁶, polyethylenimine (PEI, $pK_a \sim 8$)²³⁷ and poly(allylamine) (PAA, $pK_a \sim 9.5$)²³⁶, all chosen because they undergo a neutral-positive transition with pH. Therefore, it exists a pH range where they are oppositely-charged to the biosurfactants. CHL is a biobased water soluble model molecule derived from chitosan (high molecular weight, HMW, which will be discussed later). Among many advantages which make it attractive for different applications, chitosan is widely available, biocompatible, biodegradable and poorly toxic,²³⁸ exhibits anti-microbial activity, or promotes wound healing. Its structure also approaches the one of the glycosaminoglycans, main constituents of the natural extracellular matrix. It was thus seriously considered in tissue engineering applications.⁴³ PLL, PAA and PEI are synthetic polymers with a model chemical structure. PLL, although synthetic, is a polyaminoacid commonly used for biomedical applications.²³⁹ They all extend the study to a larger set of polyamines. Their respective chemical structures are given in Figure 10.

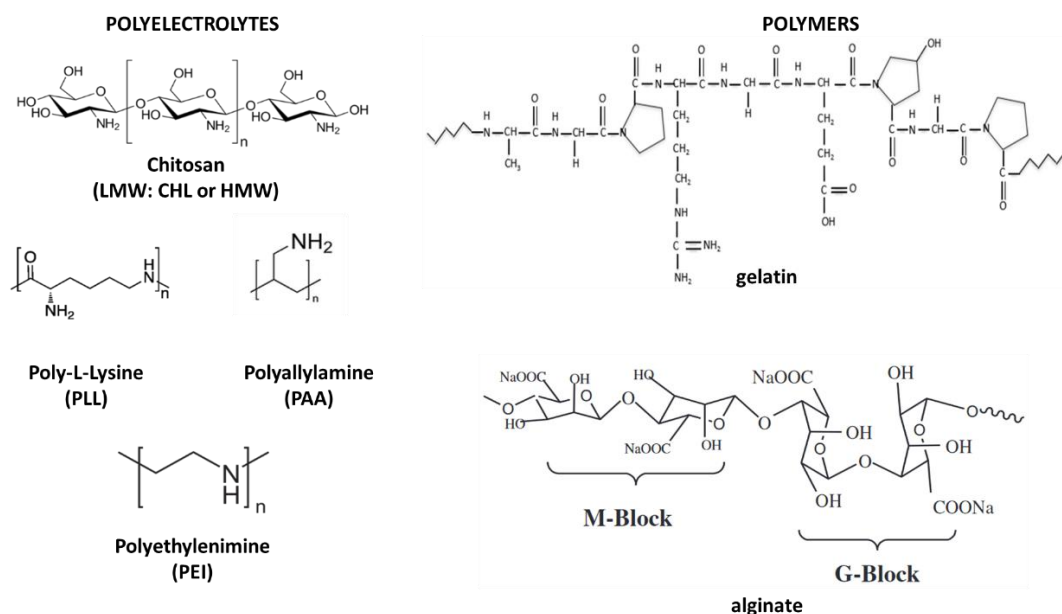


Figure 10 – Chemical structures of polyelectrolytes and biopolymers employed

Other biopolymers were selected not to be oppositely charged to biosurfactants and to provide “control” systems. They were also chosen for their biobased origin in view to be used at higher concentrations at a second stage of this work: gelatin ($7 < IP < 9$), chitosan (high molecular weight, $pK_a = 6.5$) and alginate ($pK_a = 4$), of which the structures are given in Figure 10. Gelatin, derived from the collagen protein denaturation, has many potential applications due to its ability to stabilize

colloids, which has been exploited ever since the classical experiments of Faraday. Its gelation occurs below 30°, whence it results in the formation of a physical gel, *via* the formation of inter-molecular, triple-helical structures.³⁸ Gelatin and other proteins are known to interact with anionic surfactants. Below its isoelectric point, gelatin is positively charged and its interaction with a negatively charged surfactant leads to the precipitation of polymer-surfactant complexes.³⁹⁻⁴¹

Alginates are naturally derived polysaccharide block copolymers composed of regions of sequential β -D-mannuronic acid monomers (M-blocks), regions of α -L-guluronic acid (G-blocks), and regions of interspersed M and G units. The source of the alginate determines the length of the M- and G- blocks and sequential distribution along the polymer chain.⁵⁶ Alginates undergo reversible gelation in aqueous solution under mild conditions through interaction with divalent cations, mainly Ca^{2+} , whose cooperative binding between the G-blocks of adjacent alginate chains create ionic interchain bridges.⁵⁷

Chitosan is a cationic polysaccharide resulting from deacetylation of chitin, the second most widespread natural polysaccharide and main structural polysaccharide of insects and crustaceans' shells, through employing concentrated sodium hydroxide or enzymatically via the action of chitin deacetylase. The final structure comprises a mixture of N-acetylglucosamine and glucosamine, linked together into linear chains through β -(1-4) connections.⁴² Chitosan (high molecular weight) was also employed to validate the reproducibility of experiments compared to CHL.

The following experiments and discussions will thus investigate the interactions between biosurfactants and biobased or synthetic polyelectrolytes/polymers, in function of pH, e.g. their state of charge (Figure 11), at low concentrations and answer the questions: what is the influence of these species on the phase behavior of the biosurfactant? Which interactions occur and in which conditions?

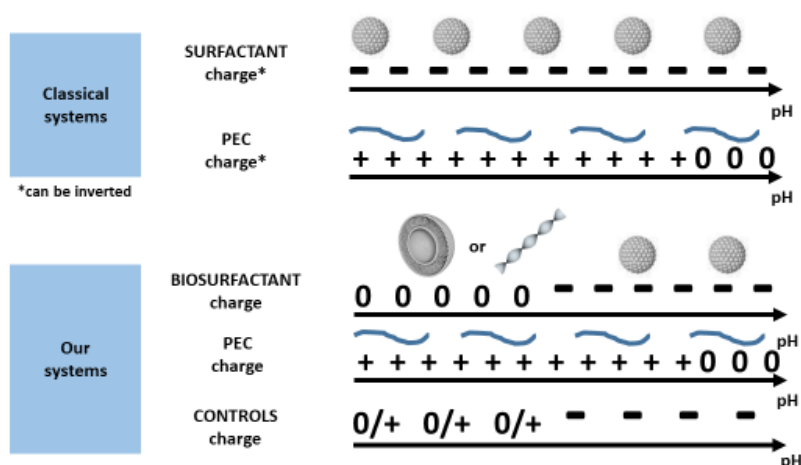


Figure 11 – Schematic representation of the state of charge of surfactant and PEC systems commonly used (top) we used (bottom)

1.2 Experimental methods

1.2.1 Chemicals

In this work we use glycolipids G-C18:1 ($M_w = 460 \text{ g mol}^{-1}$), made of a single β -D-glucose hydrophilic headgroup and a C18 fatty acid tail (monounsaturations in position 9,10), and SL-C18:0

($M_w = 620 \text{ g}\cdot\text{mol}^{-1}$), composed of a sophorose headgroup and a stearic acid derivative. From alkaline to acidic pH, the former undergoes a micelle-to-vesicle phase transition¹²¹ while the latter undergoes a micelle-to-fiber phase transition (Figure 9).¹²⁵ The syntheses of sophorolipid SL-C18:0 and glucolipid G-C18:1 are respectively described in Ref ¹²⁵ and ¹¹⁷, where the typical ¹H NMR spectra and HPLC chromatograms are also given. The compounds used in this work have a molecular purity of more than 95%.

The cationic polyelectrolytes (PEC) used in this work are chitosan, obtained from the deacetylation of chitin from crusteans' shells, poly-L-lysine, widely used in biomedical field, poly(allylamine) and polyethylenimine. Chitosan oligosaccharide lactate (CHL) ($M_w \approx 5 \text{ kDa}$, $pK_a \sim 6.5$)²³⁵ with a deacetylation degree >90%, (PLL) hydrobromide ($M_w \approx 1\text{-}5 \text{ kDa}$, $pK_a \sim 10\text{-}10.5$)²³⁶, poly(allylamine) (PAA) ($M_w \approx 17.5 \text{ kDa}$, $pK_a \sim 9.5$)²³⁶ and polyethylenimine (PEI) hydrochloride (linear, $M_w \approx 4 \text{ kDa}$, $pK_a \sim 8$)²³⁷ are purchased from Sigma-Aldrich. The three polymers used in this work, gelatin (type A, from porcine skin, $M_w \approx 50\text{-}100 \text{ kDa}$, isoelectric point 7–9), alginate (from brown algae, medium viscosity, $M_w \approx 20\text{-}240 \text{ kDa}$, $pK_a \approx 4$) and chitosan (high molecular weight, HMW, from shrimp shell, practical grade, $M_w \approx 190\text{-}375 \text{ kDa}$, $pK_a \approx 6.5$) with a deacetylation degree >75%, are purchased from Sigma Aldrich. All other chemicals are of reagent grade and are used without further purification.

1.2.2 Preparation of stock solutions

SL-C18:0 ($C = 5 \text{ mg}\cdot\text{mL}^{-1}$), G-C18:1 ($C = 5 \text{ mg}\cdot\text{mL}^{-1}$, $C = 20 \text{ mg}\cdot\text{mL}^{-1}$), CHL ($C = 2 \text{ mg}\cdot\text{mL}^{-1}$), PLL ($C = 5 \text{ mg}\cdot\text{mL}^{-1}$, $C = 20 \text{ mg}\cdot\text{mL}^{-1}$), PEI ($C = 5 \text{ mg}\cdot\text{mL}^{-1}$), PAA ($C = 5 \text{ mg}\cdot\text{mL}^{-1}$), gelatin ($C = 5 \text{ mg}\cdot\text{mL}^{-1}$), alginate ($C = 5 \text{ mg}\cdot\text{mL}^{-1}$) and chitosan HMW ($C = 5 \text{ mg}\cdot\text{mL}^{-1}$) stock solutions are prepared by dispersing the appropriate amount of each compound in the corresponding amount of Milli-Q-grade water. The solutions are stirred at room temperature ($T = 23 \pm 2 \text{ }^\circ\text{C}$) and the final pH is increased to 11 by adding a few μL of NaOH ($C = 0.5 \text{ M}$ or $C = 1 \text{ M}$).

1.2.3 Preparation of samples

Samples are prepared at room temperature ($T = 23 \pm 2 \text{ }^\circ\text{C}$) by mixing appropriate volume ratios of the lipid (SL-C18:0 or G-C18:1) stock solutions at pH 11 and cationic polyelectrolyte or polymer stock solutions (PEC), as defined in Table 11. The final total volume is generally set to $V = 1 \text{ mL}$ or $V = 2 \text{ mL}$, the solution pH is about 11 and the final concentrations are given in Table 11. The pH of the mixed solution is eventually decreased by the addition of 1-10 μL of a HCl solution at $C = 0.5 \text{ M}$ or $C = 1 \text{ M}$. pH has been changed by hand and by mean of a push-syringe device. The rate at which pH is changed is generally not controlled although it is in the order of several $\mu\text{L}\cdot\text{min}^{-1}$. Differently than in other systems,^{157,240} we did not observe unexpected effects on the PESC structure to justify a tight control over the pH change rate.

Table 11 – Relative volumes of lipid and cationic polyelectrolyte (PEC) solutions to mix to obtain given concentrations

Volume			Concentration ($\sim 0.25\text{-}1 \text{ wt}\%$)	
Lipid stock solution / mL	PEC stock solution / mL	Water / mL	$C_{\text{Lipid}} / \text{mg}\cdot\text{mL}^{-1}$	$C_{\text{PEC}} / \text{mg}\cdot\text{mL}^{-1}$
0.5	0.5	0	2.5 or 10	2.5 or 10
	0.25	0.25	2.5	1.25
	0.125	0.375	2.5	0.625

Further experimental and technical details are provided in the Experimental part of **Paper I** and **Paper II** associated to this chapter.

1.3 Identification of a precise pH-range of interactions

Turbidimetry is a classical method to investigate the formation of coacervates, characterized by an increase of the turbidity of an initially transparent solution. Figure 12 presents the results of Ben Messaoud *et al.*:²¹²

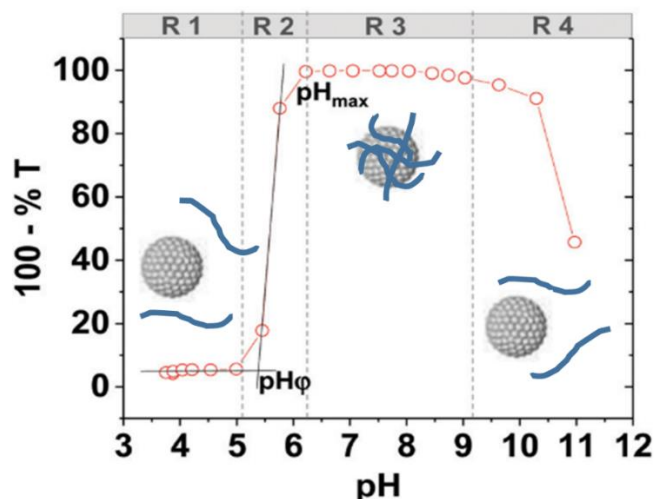


Figure 12 - Turbidity (100 - %T) as a function of pH for a SL-PAA mixture. [SL] = 5 mg mL⁻¹; [PAA] = 0.75 mg mL⁻¹. R stands for Region. (Reproduced from ref. ²¹²)

Coacervation process as a function of pH can be described in terms of a set of specific pH values delimiting four different regions. Below pH 5, a first region, where the solution is clear and the turbidity is constant and not so high, can be identified. Region 2 is characterized by a strong increase in turbidity from a starting pH, noticed pH_{ϕ} , and reflects the cloudy aspect of the solution. Starting from pH_{max} , the turbidity profile reaches a maximum and constant plateau and the solution has an opalescent aspect all over the region 3. In the region 4 the turbidity decreases until the solution is transparent. As a general remark, the transparency in Region 1 and that in Region 4 strongly depend on the solubility of each component.

Preliminary turbidimetry experiments were conducted at a constant concentration of SL-C18:0, or G-C18:1, with different concentrations of PLL. Starting from high pH, where both compounds form negatively-charged micelles, acidification induces modifications of the carboxylic/ate and amine/ammonium groups and thus drive the presence, or lack, of electrostatic interactions. The sense of pH change (basic to acid) is different from the work discussed in Figure 12 (acid to basic), and our compounds display phase changes, from non-scattering micelles to fibers or vesicles which are highly scattering objects.

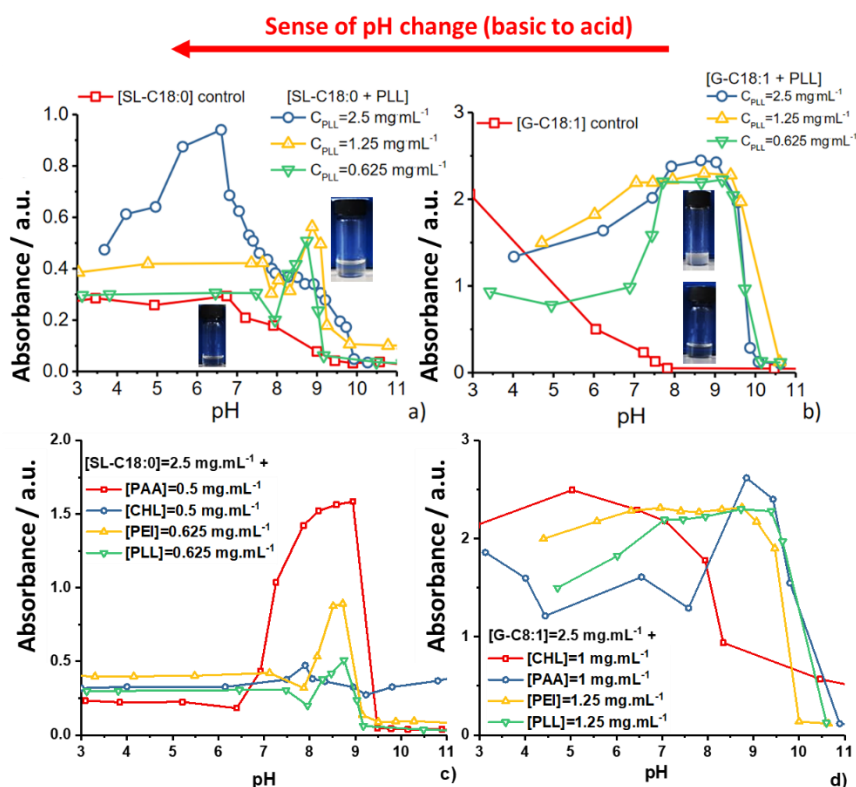


Figure 13 - Turbidimetric profiles of a) SL-C18:0 and b) G-C18:1 alone (2.5 mg.mL^{-1} , red profile), or in combination with different concentrations of PLL (2.5 mg.mL^{-1} : blue profile, 1.25 mg.mL^{-1} : yellow profile, 0.625 mg.mL^{-1} : green profile). Profiles c and d respectively show the absorbance of SL-C18:0 and G-C18:1 with the different polyelectrolytes tested.

Red squares in Figure 13a and b refer to the control lipid solutions, which display a similar behavior: the micellar region at alkaline pH exhibits poor scattering, while the intensity increases at acidic pH, in the respective fibrillar and vesicular regions of SL-C18:0 and G-C18:1. When mixed with different concentrations of PLL, scattering profiles all show a common bell-like shape, with an enhanced signal between pH 7 and 10. Indeed, blue, yellow and green curves, respectively standing for concentration of PLL of 2.5 mg.mL^{-1} , 1.25 mg.mL^{-1} and 0.625 mg.mL^{-1} , present an intensity peak in the slight pH 8.5 – 9 range. These behaviors are classically-observed in oppositely charged PECs, like chitosan with Arabic gum,²¹⁷ or with hyaluronic acid²¹⁶ and for PEC-protein systems, like poly-(dimethyl-diallylammonium chloride) with bovine serum albumin,²⁴¹ Arabic gum with whey protein²⁴² or with β -lactoglobulin.²⁴³ A similar phenomenon is partially described for some micelles-PEC systems, including polyacrylic acid with mixed micelles of n-hexadecyl trimethyl ammonium chloride and n-dodecyl hexaoxyethylene glycol monoether.²⁴⁴ The precise identification of a preferred pH range of interaction between lipids and PLL, precisely from pH 7 to pH 9, is thus possible.

As shown in Figure 13c and d, similar results were obtained for all polyelectrolytes tested in addition to PLL: CHL (chitosan lactate), polyallylamine (PAA) and polyethylenimine (PEI) and are the starting point of a large range of experiments detailed here after.

Interpretation of the results however requires caution and complementary data from other techniques are necessary.

DLS experiments, widely used to estimate the size of colloids in solution, were tentatively performed on the [SL-C18:0 + PAA] and [G-C18:1 + PAA] mixtures from basic to acidic pH, knowing in which pH

range they are expected to form coacervates according to turbidimetry experiments (Figure 13). Comparison with the size of biosurfactant alone self-assembled structure was recorded while lowering the pH. Results concerning [SL-C18:0 + PAA] mixture (Figure 14) suggest a size of about 200 nm at pH 12.15 with a moderate polydispersity (about 0.3). This profile is close to the one of SL-C18:0 micelles alone, indicating that free micelles coexist with PAA at this high pH.

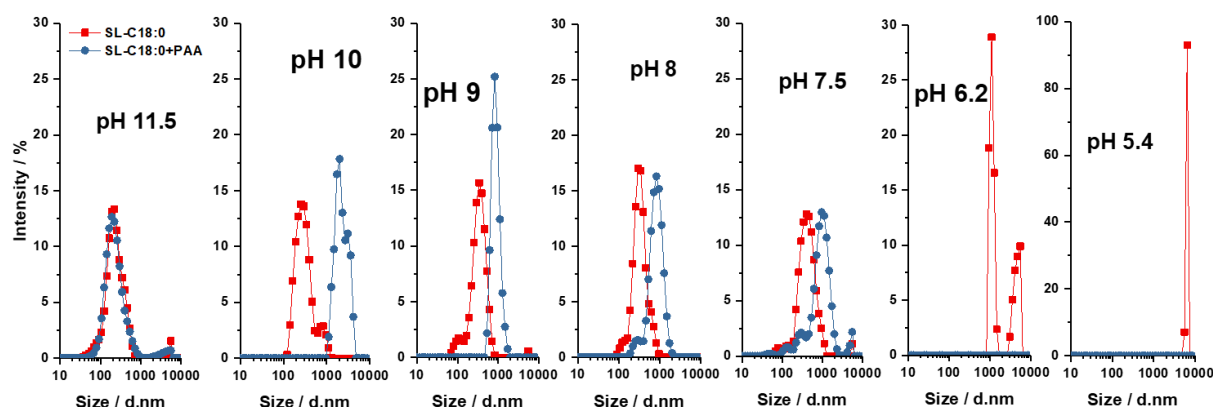


Figure 14- DLS curve of SL-C18:0 and SL-C18:0 + PAA mixture upon decreasing pH.

Size of [SL-C18:0 + PAA] structure increases upon decreasing the pH and polydispersity remains low. Size and polydispersity both increase upon further lowering of the pH. Polydispersity is the highest around pH 7.5, a transition area characterized by reorganization/dissociation of the SL-C18:0.¹²⁵ At lower pH, correlation is no longer satisfying and [SL-C18:0 + PAA] structure does not exhibit any signal.

Coming to the [G-C18:1 + PAA] system, the particle size distributions of both G-C18:1 and [G-C18:1 + PAA] are perfectly superimposed, as shown by Figure 15 and centered around 350 nm at pH 12.80, with a good polydispersity of 0.1, suggesting that free micelles coexist with PAA. Upon decreasing the pH, the signal of [G-C18:1 + PAA] does not significantly change, the peak appears a bit larger and flatten, suggesting an inhomogeneous distribution.

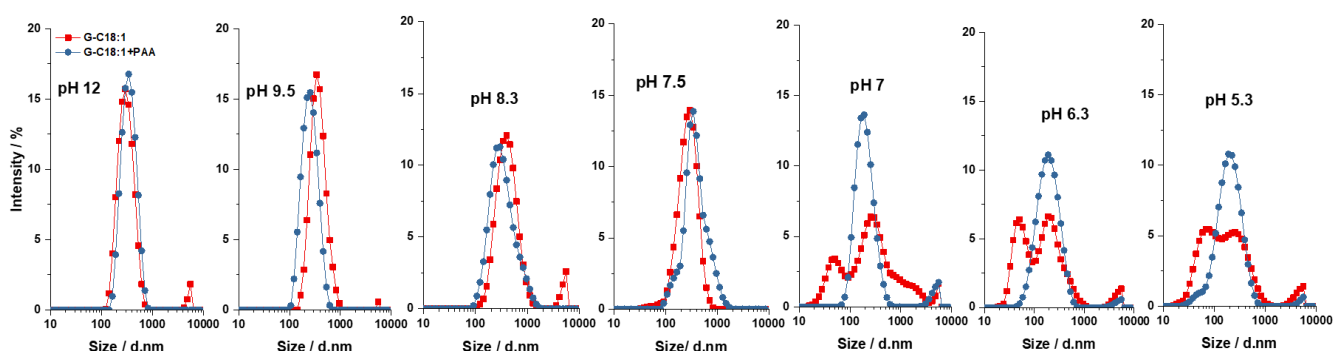


Figure 15 - DLS curve of G-C18:1 and G-C18:1 + PAA mixture mixture upon decreasing pH.

All in all, DLS is an interesting but not really accurate technique to study these dynamic systems. The presence of large objects (in the 100-1000 nm range) with different scattering profiles than controls can be verified, but coacervates cannot be distinguished from micelles and the signal can involve many components, including free micelles, fibers or vesicles. It was thus not employed with all the polyelectrolytes.

More suitable techniques were then used to describe the structures formed under each pH condition at these low concentrations (<1wt%). These latter have been observed in the direct space by cryo-TEM and further investigated in the indirect space by Small Angle X-Ray Scattering. A detailed cryo-TEM/SAXS crossed analysis is proposed. Additional quantification experiments are also described and interpreted (ITC and ^1H solution NMR). The next section briefly presents these data, which can be found in the joint publications.

1.4 Morphological and structural characterization of the mixed lipid-polymer structures

Cryo-TEM allows observing frozen structures, which do not suffer from any drying process. A selection of pictures is shown on the left part of Figure 16 and Figure 17. At basic pH, both SL-C18:0 and G-C18:1 form spherical structures comparable to complex coacervates reported in the literature,^{212,245} of which shape/appearance depend on the stage of coacervation with all polyelectrolytes tested. At acidic pH, characteristic fibers of SL-C18:0 are visible,¹²⁵ which suggest that they do not interact anymore with polyelectrolyte chains, whereas astonishing multilamellar structures, never observed for this compound, are obtained with G-C18:1. However, cryo-TEM, like any microscopy technique, is characterized by poor statistics despite the useful morphological information. For this reason, cryo-TEM data can be cross-checked with SAXS analysis to deeply investigate the structures. pH-resolved *in-situ* SAXS analysis have been performed using a unique home-made set up described in **Annex 1**. By crossing both techniques analysis, robust conclusions can be proposed. The SAXS data we obtained, shown on the right part of Figure 16 and Figure 17, nicely agree with the hypothesis raised from cryo-TEM pictures: at basic pH, scattering profiles exhibit oscillations, different from the profiles of each components, indicating interactions between them. Upon lowering pH, scattering profiles of systems involving SL-C18:0 are identical to the one of this molecule alone, with a peak centered at the $q = 0.24 \text{ \AA}^{-1}$ value related to the inter-molecular distance inside ribbons.¹²⁵ Concerning G-C18:1 (Figure 17), scattering profiles at acidic pH show two peaks characteristic of a multilamellar structures, such as the ones described by cryo-TEM. All these pictures and profiles are presented and discussed in **Paper I** and **Paper II**. Additional quantification experiments (ITC and ^1H NMR) are also described and interpreted in **Paper I**. ITC and ^1H NMR respectively give access to the $[\text{COO}^-]/[\text{NH}_3^+]$ molar ratio and thermodynamic parameters of the interaction.

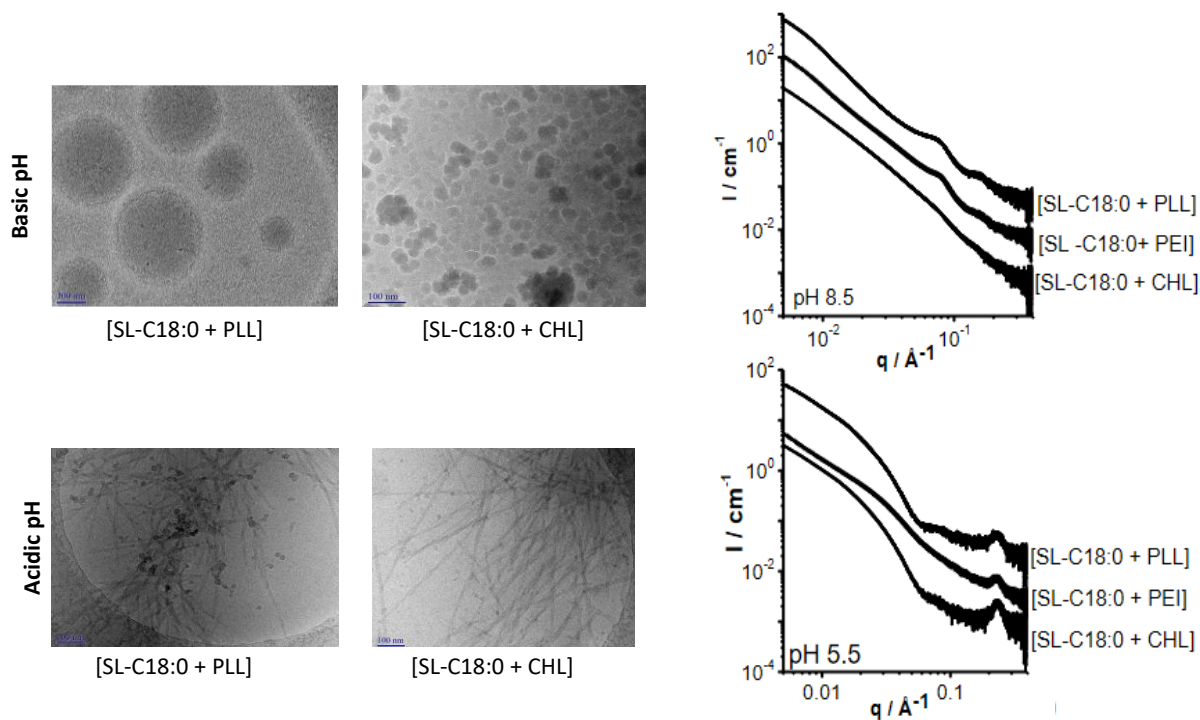


Figure 16 – Cryo-TEM pictures and SAXS profiles of [SL-C18:0+PEC] at basic (top) and acidic (bottom) pH. Cryo-TEM pictures of [SL-C18:0+PEI] and SAXS profiles of [SL-C18:0+PAA] are missing.

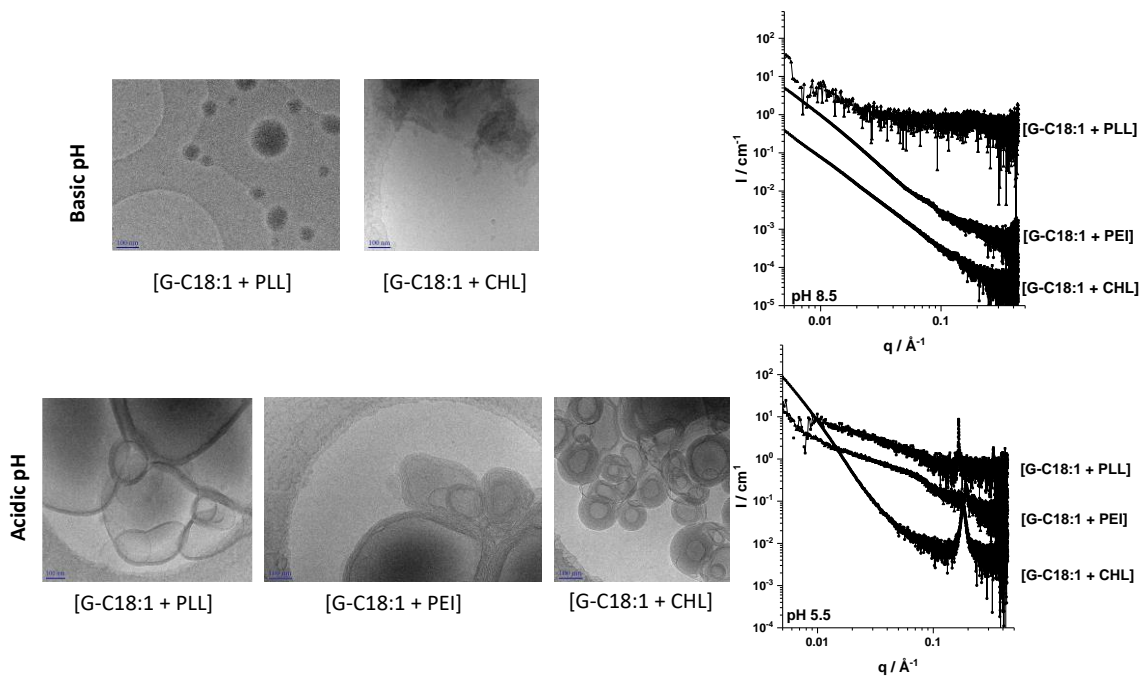


Figure 17 - Cryo-TEM pictures and SAXS profiles of [G-C18:0+PEC] at basic (top) and acidic (bottom) pH. Cryo-TEM pictures of [SL-C18:0+PEI] and SAXS profiles of [SL-C18:0+PAA] are missing.

Similar experiments were performed with chitosan HMW. Chitosan HMW ($190 < M_w < 375$ kDa) is an approximately 50 times heavier analogue of CHL ($M_w \approx 5$ kDa). Keeping G-C18:1 concentration constant, a concentration of $0.044 \text{ mg}\cdot\text{mL}^{-1}$ of chitosan HMW (calculated according to CHL and chitosan HMW molecular weights to keep the same molar ratio) is hardly usable. We then chose to

keep the same mass ratio than with CHL. SAXS experiments (Figure 18) were performed with 2.5 mg.mL⁻¹ of chitosan HMW : the signal of coacervates is not well-defined (left) and the signal obtained at pH 5.5 (right) shows a peak at $q=0.18 \text{ \AA}^{-1}$ even if we do not really distinguish a second harmonic which would be the proof of multilamellar structures. We exclude the G-C18:1 lamellar phase, which is usually displayed at lower pH. Our hypothesis is that the structures are formed as for CHL, but are less defined (further confirmed by optical microscopy under crossed polarizers).

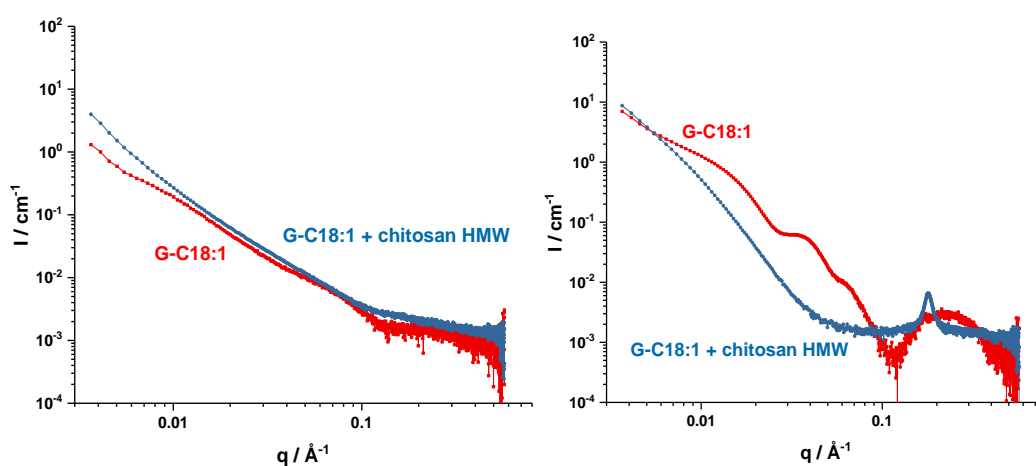


Figure 18 - SAXS profiles of G-C18:1, and G-C18:1-chitosan HMW mixture at pH 8 (left profile) and pH 5.5 (right profile)

To conclude this part, these results demonstrate the interest to study biosurfactant's phase diagram in presence of biopolymers under non-equilibrium conditions. Although each biosurfactant's phase diagram was precisely known, their becoming in presence of a polymer (summarized in Figure 19) was not predictable. Both SL-C18:0 and G-C18:1 form complex coacervates in their micellar domain in presence of an oppositely charged polymer. When SL-C18:0 undergoes its micelle-to-fiber phase transition, complex coacervates dissociate and fibers coexist with polymer chains at acidic pH. In the case of G-C18:1 vesicles, they were found forming astonishing multilamellar structures. Although such structures were more or less described, the pH-induced phase transition process we employed results in particularly well ordered structures composed of well-defined layers which were rigorously characterized. More generally, this work supports the use of microbial glycolipid biosurfactants in the development of sustainable polyelectrolyte-surfactant complexes, including biobased multilamellar walls vesicles, promising soft colloids with applications in the field of personal care, cosmetics, or pharmaceuticals, to cite the main ones.

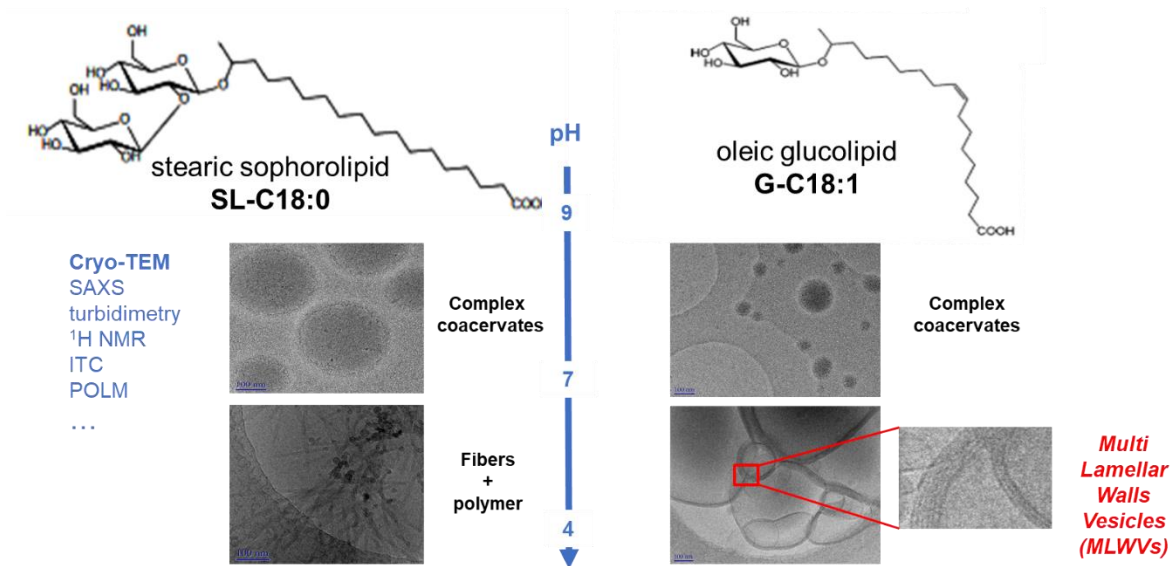


Figure 19 – Summary of crossed cryo-TEM/SAXS analysis on SL-C18:0 (left) and G-C18:1 (right) combined with oppositely charged polyelectrolytes

The experimental part is detailed in the *Material and Methods* section of **Paper I** and **Paper II** which summarize and discuss the main results.

Study of controls

Electrostatic interactions driving the formation of MLWVs, the following SAXS experiments were performed with the idea to use gelatin and alginate as counterexamples, as their charge do not fill the requirements to complex with biosurfactants.

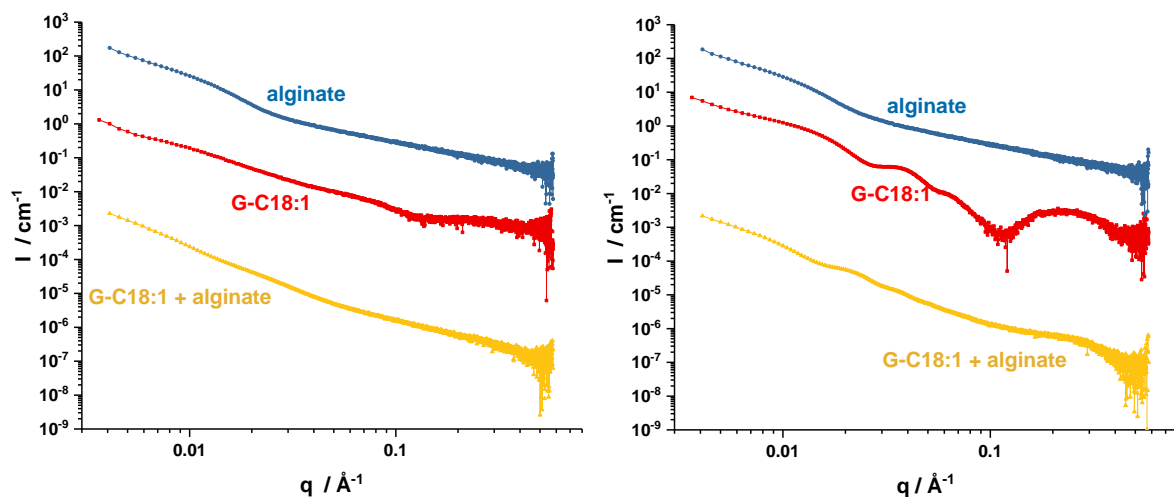


Figure 20 - SAXS profiles of G-C18:1, alginate, and G-C18:1-alginate mixture at pH 8 (left profile) and pH 5.5 (right profile) (artificial offset performed)

The coacervate and consequently the MLWV scattering profiles described in the **Paper I** are not found in SAXS experiments (Figure 20, pH 8 and 5.5 on the left and the right part respectively) using alginate: yellow profiles do not exhibit any oscillation/peak, suggesting an absence of interactions with G-C18:1. This result was expected considering that both molecules are negatively charged at this pH.

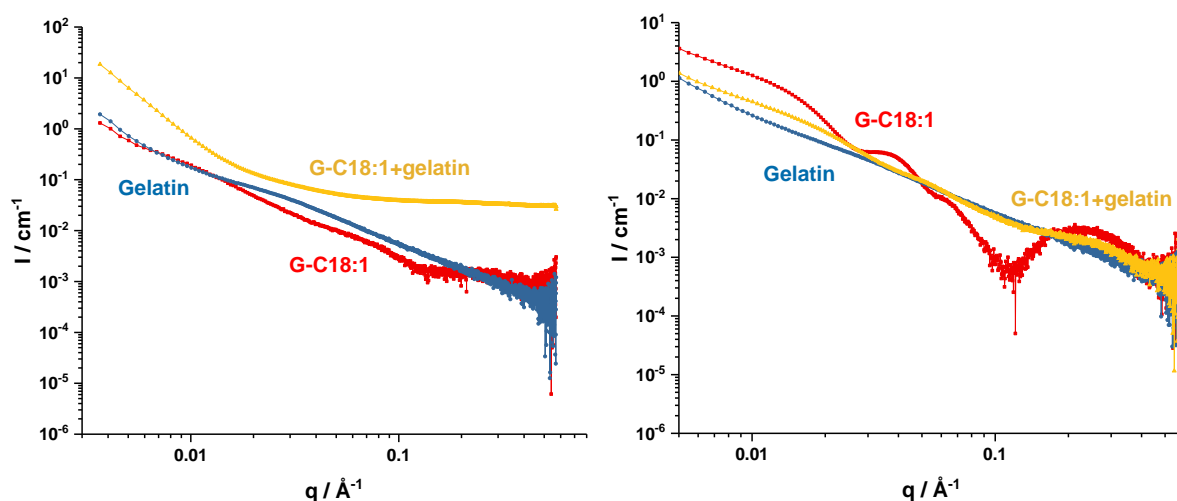


Figure 21 - SAXS profiles of G-C18:1, gelatin, and G-C18:1-gelatin mixture at pH 8 (left profile) and pH 5.5 (right profile)

Gelatin was also employed. SAXS profiles obtained do not exhibit the characteristic peak of coacervates (Figure 21, left part) and in absence of coacervates, *MLWV* do not form as discussed in **Paper II** (Figure 21, right part). Despite an expected positive charge density of this polymer whose isoelectric point is comprised between 7.0 and 9.0, these results suggest that its charge density is however too low to interact with negatively charged G-C18:1 micelles.

These two examples prove the key role of both electrostatic interactions and density of charge in the formation of complex coacervates and *MLWV*. Indeed, electroneutrality, e.g. perfect compensation of negative/positive charges, is often described as a main factor governing coacervation.²²⁵ Coacervation is thus conditioned by the opposition of charges and the use of concentrations allowing charge compensation.

In conclusion, interactions between G-C18:1 and oppositely charged polymers are maintained from basic to acidic pH, while self-assembly of SL-C18:1 and oppositely charged polymers proceeds from an orthogonal process at acidic pH. No interaction occur between G-C18:1 and similarly charged alginate and gelatin.

All the work presented in this chapter has been divided into two parts and is more largely described and discussed in **Papers I and II**.

CHAPTER II: *MLWVs*: synthesis and applications

Table of content

2.1	Introduction	60
2.2	Stability of <i>MLWVs</i> in cell culture medium	60
2.3	Control over the size and dispersity of <i>MLWVs</i>	61
2.4	Encapsulation of a model hydrophobic drug.....	62

2.1. Introduction

MLWVs, obtained through a pH-induced micelle-to-vesicle phase transition of G-C18 :1 from a complex biosurfactant-biopolymer coacervate, were presented in the previous chapter, and in more details in the publication titled *Synthesis of multilamellar walls vesicles polyelectrolyte-surfactant complexes from pH-stimulated phase transition using microbial biosurfactants*. We have established a robust method, illustrated by Figure 22, based on biosurfactant's pH-induced phase transition to obtain multilamellar vesicular structures. Such objects have been reported upon mixing chitosan and large surfactant vesicles with a number of layers directly controlled by the mixing ratio,^{75,233} but colloidal stability and possible control over the size are more complicated.

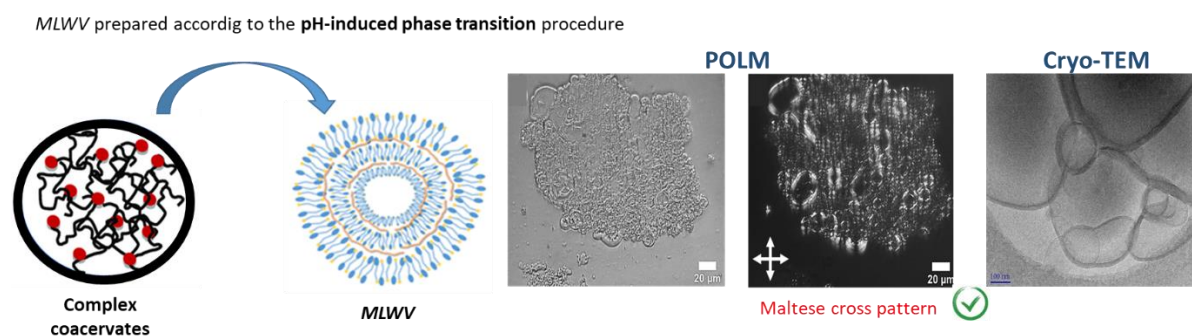


Figure 22 – The strategy employed to obtain multilamellar vesicles from biosurfactants: pH-induced phase transition from complex coacervates to *MLWV*

In the field of biosurfactants, self-assembly into multilamellar vesicles of some molecules was proposed, especially for rhamnolipids and mannosylerythritol lipids,⁸³ but the structures are generally poorly characterized and loosely studied. Further work is then motivated by the great interest of multilamellar structures to encapsulate many compounds, especially hydrophobic ones, for drug delivery applications.²⁴⁶ We thus addressed the question of the legitimacy of *MLWV* as efficient drug delivery carriers.

Drug delivery systems are engineered technologies for the protection of bioactive compounds and their targeted and/or controlled release. The main challenges that they overcome are related to the administration of pharmaceutical molecules, including side effects, low drug solubility, poor stability in biological conditions, clearance or non-specific delivery.²⁴⁷ A lot of systems, mainly based on lipids, exist to reach this goal and Doxil or Amphotec are just two examples among the commercialized ones.^{248,249} In this context, biosurfactants were only used as adjuvants up to now: rhamnolipids, mainly, were inserted in liposomes, of which the membrane properties result modified.²⁵⁰ No system fully based on biosurfactant, without the presence of phospholipids, has been reported so far. This argument motivated the work presented in this chapter.

2.2. Stability of *MLWVs* in cell culture medium

The starting point of such project was to verify that formation of *MLWVs* can occur in cell culture medium, a key point for the use of these latter for biomedical applications. Gibco Dulbecco's Modified Eagle Medium (DMEM) is a widely used basal medium for supporting the growth of many different mammalian cells. *MLWVs* were prepared according to the procedure described in **Chapter I**,^{251,252} water being replaced by DMEM cell culture medium supplemented with 10% FBS. To verify

that the *MLWV* structures form in DMEM, we employ SAXS and chose the [G-C18:1+PLL] based *MLWVs* because this is the system we best characterized and that PLL is already widely used for biomedical applications:²³⁹ it is easy to check if the SAXS profile displays the double peak attributed to *MLWVs* in previous work.^{251,252}

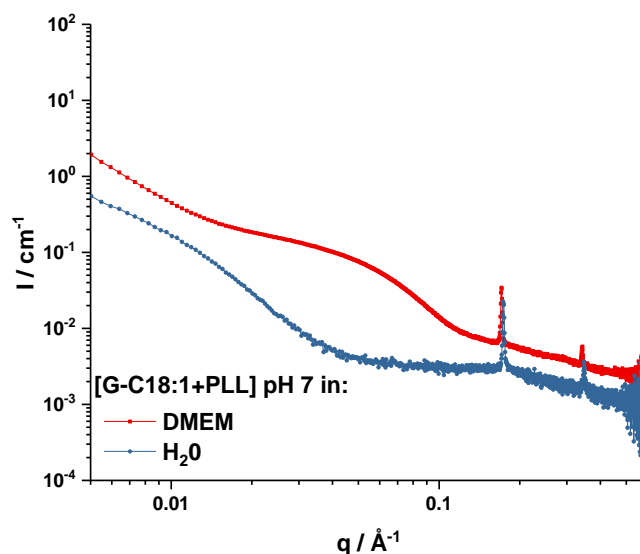


Figure 23 - SAXS profile of GC18:1 + PLL in DMEM (2.5 mg.mL⁻¹) and in water (10 mg.mL⁻¹) at pH 7 (pH decreased from 10)

According to SAXS experiments, the [G-C18:1+PLL] profile in DMEM (in red, Figure 23) exhibits a double peak perfectly superimposed to the one attributed to *MLWVs* in water^{251,252} (Figure 10 in **Chapter 1**, reminded in blue in Figure 23) of which the peaks, centered around $q_1 = 0.17 \text{ \AA}^{-1}$ and $q_2 = 0.34 \text{ \AA}^{-1}$, are attributed to the (001) and (002) reflection of a lamellar order.^{251,252} [G-C18:1+PLL] based *MLWVs* form and are stable in DMEM at physiological pH: this is an encouraging result to then explore biomedical applications, starting with investigation of cell viability in presence of *MLWV*. We cannot however compare both profiles below $q < 0.1 \text{ \AA}^{-1}$. The complexity of DMEM composition results in the coexistence of various structures, and the likely presence of free micelles in DMEM can be at the origin of the broad oscillation observed for $0.01 < q < 0.1 \text{ \AA}^{-1}$ in the red profile.¹²¹ For this reason, *MLWVs* in DMEM were always centrifuged before further use.

2.3. Control over the size and dispersity of *MLWVs*

Control over the size of *MLWVs*, and vesicular objects in general, is another aspect which can be important for further applications. Two classical methods were employed, filtration (solution passed through a 0.45 μm pore diameter filter with a push syringe) and ultrasounds, to try to control their size both in water and DMEM. Results presenting the average hydrodynamic diameter (nm) determined by DLS are summarized in Figure 24. Non-treated *MLWVs* are slightly smaller in DMEM than in water (around 400 vs 900 nm), maybe due to the presence of all the components of the medium, especially salts. As discussed in the joined **Project paper III**, coacervate-to-*MLWV* phase transition occurs at higher pH in DMEM than in water and is thus maybe not completely achieved in the aqueous system at pH 7. The size can be further decreased by using filtration in both media: it is decreased from 900 to 500 nm and 400 to 200 nm respectively in water and in DMEM, but dispersity increases. Ultrasounds (US) are on the contrary able to reduce the size from around 700 to 150-200 nm compared to non-treated *MLWVs*, independently of the mixing time, at least on the investigated time range. However, the quantity of matter remaining after an US treatment of 1'30'' seems not to

be sufficient to conduct cell viability experiments (no cytotoxicity observed, data not shown). This loss of matter probably disturbs MLWV's formation, which explains such poor performances. Untreated MLWVs were thus still employed.

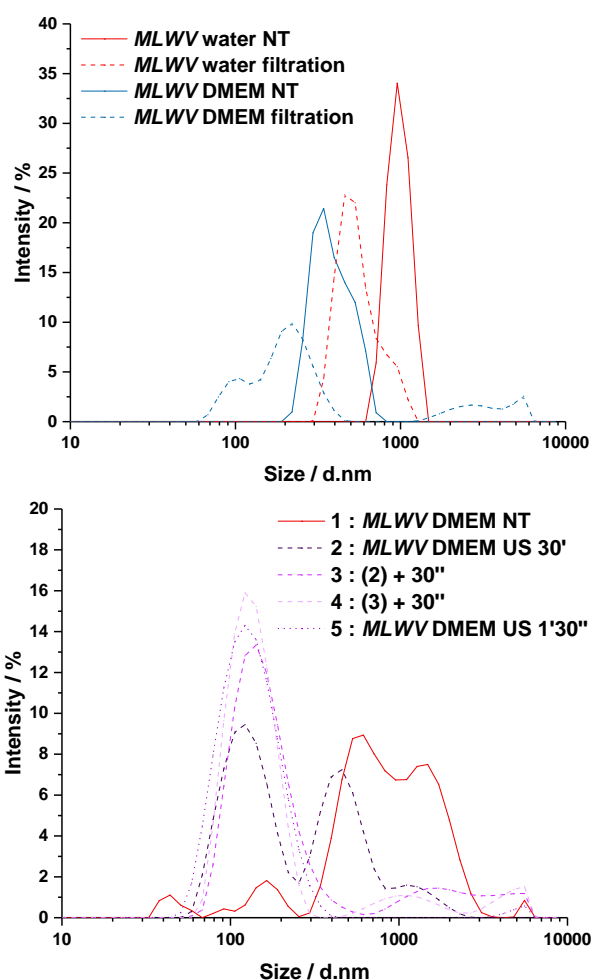


Figure 24 - Size of non-treated (NT) and filtered G-C18:1-PLL MLWVs in water and DMEM (left) ; Size of non-treated and ultrasounds (US) treated G-C18:1-PLL MLWVs in DMEM (right)

2.4. Encapsulation of a model hydrophobic drug

The next step was the choice of the molecule to encapsulate. We defined several criteria: interesting therapeutic properties, biobased, widely available at low-cost, hydrophobic and, ideally (and for practical reasons), fluorescent. Hydrophobic and fluorescent,²⁵³ curcumin, the active component of *Curcuma longa* plant (Figure 25), appeared as a first molecule of choice to fill all these requirements, keeping in mind that the strategy can be later extended to other hydrophobic drugs.



Figure 25 - *Curcuma rhizome* cross section, commercial curcuminoid powder (*Curcuma longa*) and chemical structure (Adapted and reproduced from ref.²⁵⁴)

Curcumin has indeed common applications like coloring and antioxidant agent as food additives, but displays also a broad range of favorable biological functions, such as anti-inflammatory, anti-microbial, and anti-diabetic activities.^{255,256} Anti-cancer activities of curcumin were also largely evidenced and support its potential use in chemoprevention and treatment of a wide variety of tumors including breast,²⁵⁷ gastrointestinal,^{258,259} melanoma²⁶⁰ and sarcoma.²⁶¹ However, this promising molecule suffers from some limitations, especially short shelf life or low bioavailability, respectively due to its poor chemical stability and its poor absorption, low water solubility, rapid metabolism and rapid systemic elimination.²⁶² Nanoencapsulation has been addressed as an innovative and emerging technology for resolving these shortcomings. Rafiee *et al.* recently summarized the different delivery systems used for loading of curcumin, including lipid-based, chemical polymer and biopolymer-based, nature-inspired, special equipment-based and surfactant-based techniques,²⁶³ briefly presented here after with a non-exhaustive number of references.

First, there exists widely used lipid-based techniques to achieve curcumin's encapsulation: nanoemulsions, nanoliposomes and lipid nanoparticles loaded with curcumin. Liposomes are the most commonly encountered, but however suffer from some drawbacks, including the reticuloendothelial clearance and/or immune response.²⁶⁴ A few years ago, Arab-Tehrany *et al.* for example reported that chitosan-coating enhanced the stability of nanoliposomes and slowed the release of encapsulated curcumin in the simulated gastrointestinal environment.²⁶⁵ Polymer-based techniques were also shown to be efficient for nanoencapsulation of curcumin, comprising chemical polymer-based techniques,^{266,267} biopolymer-based techniques and dendrimers. Biopolymer-based techniques include themselves several strategies: single biopolymer nanoparticles,²⁶⁸ complexation of biopolymers²⁶⁹ (including coacervation)²⁷⁰ and hydrogels.²⁷¹ Nanoencapsulation of curcumin was also achieved based on nature-inspired techniques: unique structural and functional properties of caseins (major protein in cow's milk) and cyclodextrins (cyclic polymers – ring structure - produced from starch by enzymatic conversion) make these two natural molecules promising nanocarriers for curcumin in pharmaceutical and food industries. Synthesis of new water soluble β -Cyclodextrin@Curcumin conjugates and *in vitro* safety evaluation in primary cultures of rat cortical neurons has for example been described by Arab-Tehrany *et al.*²⁷² Some techniques for nanoencapsulation of curcumin require special equipment: electrohydrodynamic processes^{273,274} or nanospray dryer²⁷⁵ for instance. A last category of surfactant-based techniques has been reported for nanoencapsulation of curcumin, which use niosomes²⁷⁶ and cubosomes.²⁷⁷

I was partially involved in the work presented in this chapter: I synthesized the *MLWV*, worked on the control of their dispersity and verified their viability in cell culture medium. I collaborated

then with a postdoctoral researcher, Silvia Alonso de Castro, who had a strong background in biology and initiated me to cell culture to conduct cell viability experiments. She was in charge of the encapsulation of curcumin and received the help of the intern Korin Ozkaya. They went further by investigating the curcumin loaded *MLWVs* uptake in different cell lines, by conducting a mechanistic study to explain the cytotoxic effects observed and by encapsulating other molecules. All results are presented and discussed in **Project paper III**.

CHAPTER III: Synthesis and characterization of hybrid gels: mechanical strength

Table of content

3.1	Introduction	66
3.2	Experimental part	69
3.2.1	Chemicals	69
3.2.2	Preparation of the hydrogels	69
3.3	Transition diluted/concentrated systems	71
3.4	G-C18:1/biopolymers	72
3.4.1	G-C18:1/gelatin	73
3.4.1.1	Gelatin + {M}G-C18:1	73
3.4.1.2	Gelatin + {V}G-C18:1	74
3.4.1.3	Gelatin + {F}G-C18:1	75
3.4.1.4	Influence of Ca ²⁺ addition rate	78
3.4.1.5	Influence of the anion	79
3.4.2	G-C18:1/Collagen	80
3.4.3	G-C18:1/Alginate	82
3.4.4	G-C18:1/chitosan HMW	82
3.4.5	General remarks	83
3.5	Conclusion	84

3.1 Introduction

The work presented up to now was performed under diluted conditions for both biopolymer and biosurfactant (< 1 wt %). **Chapter I** focused on the interactions between biosurfactants and polyelectrolytes as function of the pH. At basic pH, their opposite charges result in the formation of complex coacervates. The unique pH-triggered phase behavior of biosurfactants allowed us to explore the effect of amphiphile phase transitions within complex coacervates, a particularly interesting topic also for the field of colloid sciences. In the case of *micelle-to-fiber* phase transition, biosurfactant fibers and polyelectrolyte chains display orthogonal behaviors and finally coexist in solution, while the *micelle-to-vesicle* phase transition was found particularly efficient to synthesize well-defined multilamellar walls vesicles (*MLWVs*), of which the biocompatibility and potential to encapsulate hydrophobic drugs are explored in **Chapter II**. One could then wonder what happens upon increasing concentrations of both biosurfactants and macromolecules.

Using the PEC employed in **Chapter I** raises some issues at higher concentrations (> 1 wt%), especially PLL which is an expensive chemical. We then decided to keep working with the natural, readily available, macromolecules, gelatin, chitosan and alginate. They are well-known to display hydrogelation properties at sufficiently high concentrations and under optimized conditions of temperature, pH or type of counterion. Concerning biosurfactants, there exists studies presenting hydrogels with unique properties at concentrations > 1 wt%.^{119,157,160,165} Concentrated fibers of SL-C18:0 were reported to form self-assembled fibrillar networks (SAFIN)¹⁵⁷ while concentrated G-C18:1 vesicles do not seem to form hydrogels, even if vesicular hydrogels are reported for other compounds.²⁷⁸

Naturally coming questions related to the work presented in **Chapter I** are: what happens upon mixing concentrated biopolymer (> 1 wt%) with fibers or vesicles? Will they behave in an orthogonal way, as observed combining G-C18:1 and SL-C18:0 with alginate or gelatin under dilute conditions? (see **Chapter I**) Are phase transitions possible in a concentrated system? Which are the consequences on the gel properties? This introduces to the notion of polymer hydrogels and hybrid hydrogels, a specific class of which is known in the literature as interpenetrated polymer networks, IPN, when two or more polymers are mixed together.⁶¹

Hydrogels are often composed of a 3D network of a hydrophilic polymer, formed through cross-linking or entanglement of polymer chains, able to swell in an aqueous environment. There exists a variety of mechanisms leading to gelation, either physical or chemical as illustrated by Figure 26.

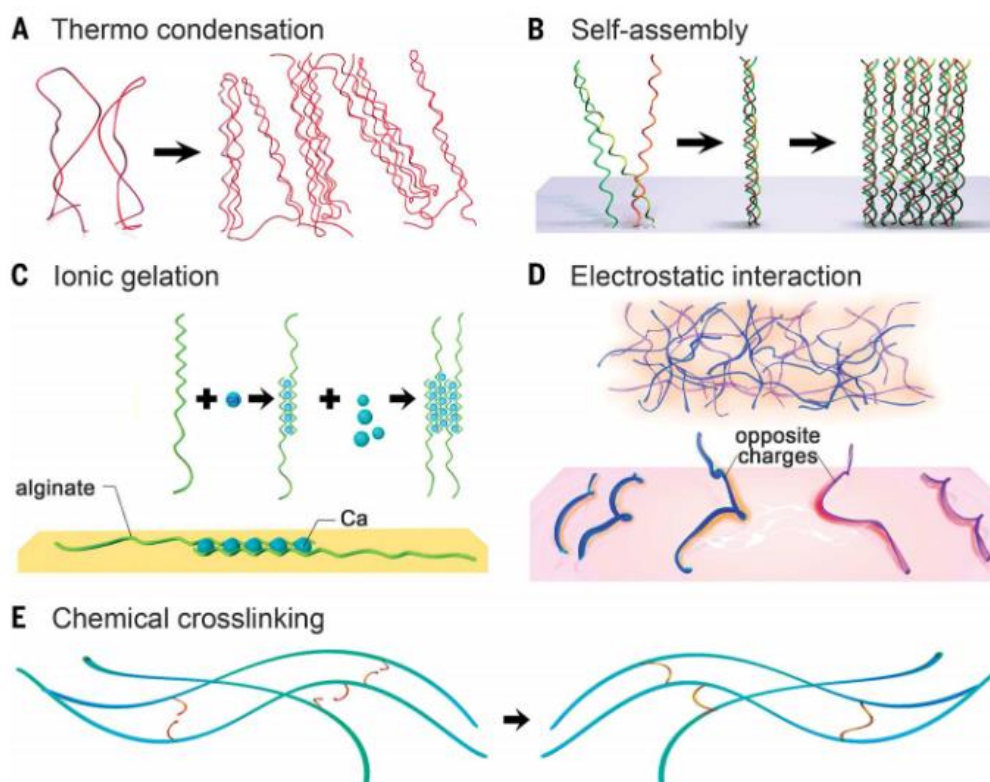


Figure 26 - Cross-linking of hydrogels. (A to D) Physical cross-linking. (A) Thermally induced entanglement of polymer chains. (B) Molecular self-assembly. (C) Ionic gelation. (D) Electrostatic interaction. (E) Chemical cross-linking (Reproduced from ref.²⁷⁹)

Their high content in water makes them suitable and interesting for a wide range of applications, from tissue engineering, drug delivery or soft electronics to actuators.²⁷⁹ Classical hydrogels commonly suffer from limited mechanical strength and undergo permanent breakage. The lack of desired dynamic and structural complexity within the hydrogels are other drawbacks limiting their functions. Advanced engineering of parameters such as mechanics and spatially/temporally controlled release of (bio)active moieties, as well as manipulation of multiscale shape, structure, and architecture, could significantly widen the applications of hydrogels.

One strategy increasingly employed to address such challenges is the incorporation of a second polymeric network, resulting in IPN hydrogels displaying both networks' properties.⁶¹ Both physical and covalent crosslinking chemistries have been used for the formation of IPN hydrogels that have been explored for *in vivo* applications.⁶¹ For example, ionic physical crosslinking between alginate and poly(γ -glutamic acid) crosslinked by lysine results in an IPN hydrogel, which has been used for full-thickness cartilage defect in the trochlear grooves of rabbit femurs and was well integrated between the neo-subchondral bone and the surrounding host bone.²⁸⁰ On the other hand, covalent crosslinking based on Schiff-base reaction between glycol chitosan and dibenzaldehyde functionalized PEG, and alginate forms a IPN hydrogel which was subcutaneously injected into mouse model and induced slight inflammation and local production of GAG at the site of implantation.²⁸¹

The idea in this and the next chapters is to synthesize and characterize an IPN-like hydrogel, whereas one polymeric component is constituted by a biopolymer (gelatin, chitosan HMW, alginate...) but where the second polymer is substituted by a self-assembled biosurfactant. The role of the biopolymer is then essentially to generate a mechanically strong scaffold, the properties of which

may be stimuli-dependent (pH, ion, T). The impact of the known phases of the biosurfactants on the biopolymer hydrogels will then be evaluated (**Chapter III**). The interesting aspect of this approach is that the phase behavior of the surfactant can also be externally triggered, in principle modifying the properties of the hybrid network (**Chapter IV**). One should also note that the stimuli may not be the same for the biosurfactant and the biopolymer, thus making the hybrid system potentially responsive to a multitude of stimuli at once.

In the specific case of the fiber phase, the biopolymer and biosurfactant could form an interpenetrated hybrid network, having a certain analogy with an IPN (but not being an IPN). Gelification of the biopolymer and biosurfactant generally occurs separately, either sequentially or simultaneously. This implies the notions of orthogonality and self-sorting, intimately linked but with some subtleties.²⁸² A typical orthogonal self-assembly process relies on multiple reversible interactions that are orthogonal to each other,^{283,284} whereas self-sorting efficiently uses the encoded information in individual components to provide a « clean » mixture by « recognizing self from non-self ». ^{285–288} Würthner *et al.*²⁸⁵ pointed out five molecular codes driving self-sorting: size and shape,^{289–305} steric effects,^{306–310} coordination sphere,^{311–318} charge transfer^{319–322} and complementary hydrogen bondings.^{323–331} Reversible interactions and intrinsic information are of course both involved in multicomponent systems.²⁸²

The biosurfactants used here are in principle the same as the ones used in **Chapter I**, namely SL-C18:0 and G-C18:1 (Figure 8, **Chapter I**, page 44). Their stable phases at room temperature are micellar (basic pH), vesicular (G-C18:1 only, acidic pH) and fibrillar (SL-C18:1 only, acidic pH). Unfortunately, we encountered several issues with the fibrillar phase generated by SL-C18:0 which was then no further used. First, the molecule was not available in sufficient quantities. Then, this molecule systematically displays a pH-induced *micelle-to-fiber* phase transition¹²⁵, but this is more capricious regarding the formation of SAFiN hydrogels.¹⁵⁷ Due to solubility and diffusion issues, the rate of acidification controls the fiber homogeneity, resulting either in spherulites (precipitate in solution) or in homogeneous fibers (which form hydrogels). Reproducibility would have thus been a challenge using this compound in a viscous medium. By chance, a colleague at our lab (A. Poirier, postdoc) observed fibrillation and gelation of G-C18:1 itself, when calcium ions are added to its micellar phase above pH about 7. His work puts in evidence a systematic homogeneous fiber phase under both diluted and concentrated conditions, studied by rheology, small angle X-ray scattering and rheo-SAXS. Reproducibility was also very good and stability was high up to 50°C.¹²⁶ This fibrillar phase of G-C18:1 will be referred to as {F}G-C18:1.

The unexpected fibrillation of G-C18:1 opens very interesting opportunities, because one can then employ one single molecule to form three phases, as illustrated by Figure 27. This aspect is important, as it excludes possible molecule-specific effects. Three cases can now be distinguished. The first one consists in mixing biopolymer and micelles. The second one consists in mixing biopolymer and vesicles, following the work of Dowling *et al.*, for example. Sodium oleate (NaOA) vesicles were added to a gelatin gel and the whole system exhibited efficiency in encapsulating and releasing calcein dye.³³² The last case, which generates increasing interest in classical gels science,⁸⁰ consists in mixing a biopolymer and self-assembled fibers.

The influence of each phase on the mechanical properties of the hybrid gels will be investigated and external stimuli will be triggered on these latter to evaluate their functionality. Mechanical strength and stimuli-responsivity will be discussed separately, in **chapters III** and **IV**,

respectively. **Chapter III** will be divided into three main subsections, one for each biopolymer. The first one, related to gelatin, will detail the influence of each G-C18:1 phase on the hybrid gel's mechanical properties. Details will be given in the joined article for other biopolymers, and additional experiments, specific to each biopolymer, will be presented in the corresponding subsection **{M}G-C18:1**

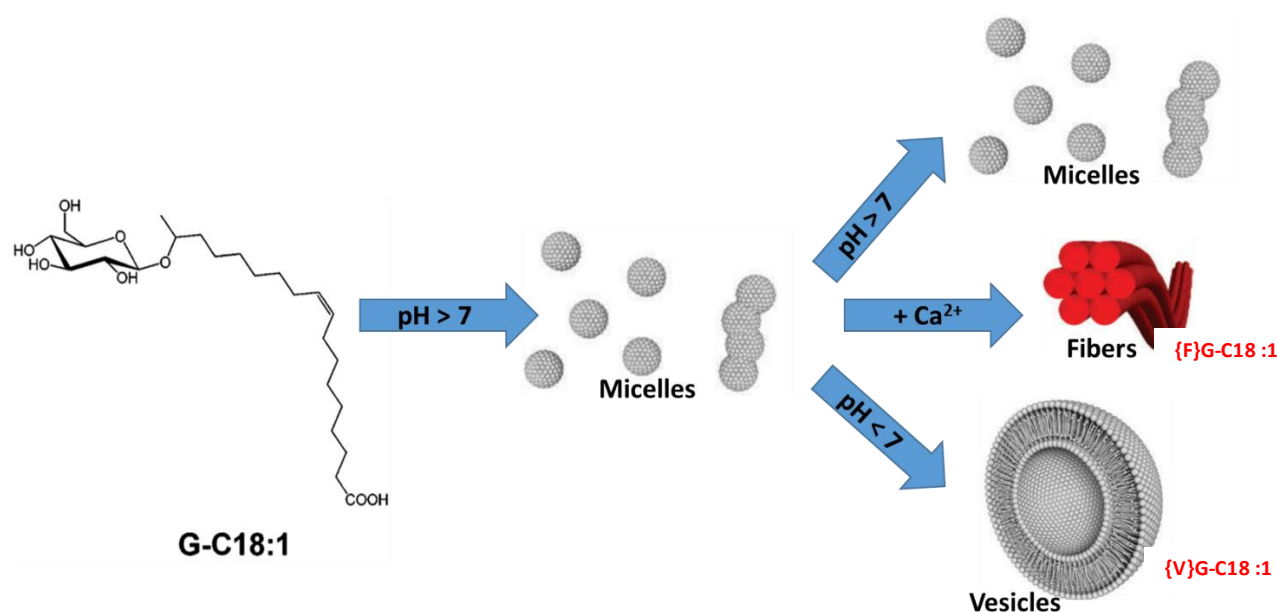


Figure 27 - Summary of the three stimuli-responsive phases obtained in water from the G-C18:1 molecule at concentrations >1 wt% (< 10 wt%). $\{V\}G-C18:1$ refers to the unilamellar Vesicle phase of G-C18:1 ($pH < 7$), $\{M\}G-C18:1$ refers to the Micellar phase ($pH > 7$) and $\{F\}G-C18:1$ to its Fiber phase ($pH > 7 + Ca^{2+}$).

3.2 Experimental part

3.2.1 Chemicals

In this work, we employ the same microbial glycolipid G-C18:1 than in **Chapter I** and **Chapter II**, of which the structure and phases above 1 wt% are reminded in Figure 27. The three polymers used in this work, gelatin (type A, from porcine skin, $M_w \approx 50\text{--}100$ kDa, isoelectric point 7–9), alginate (from brown algae, medium viscosity, $M_w \approx 20\text{--}240$ kDa, $pK_a \approx 4$) and chitosan (high molecular weight, HMW, from shrimp shell, practical grade, $M_w \approx 190\text{--}375$ kDa, $pK_a \approx 6.5$) with a deacetylation degree $>75\%$, are purchased from Sigma Aldrich. Collagen is also tested and it is extracted from rat tail following a well-mastered procedure at Laboratoire de Chimie de la Matière Condensée de Paris.³³³

3.2.2 Preparation of the hydrogels

Stock solutions. The G-C18:1 stock solution at concentration, $C_{G-C18:1} = 40$ mg/mL, is prepared by dissolving the G-C18:1 powder in the appropriate volume of milli-Q grade water at $pH = 6$ or 8 , adjusted with a few μL of NaOH 5 or 1 M solution. The stock solutions for each biopolymer are prepared as follows.

Gelatin: 80 mg of gelatin powder is dispersed in 2 mL of milli-Q water, for a concentration of $C_{\text{gelatin}} = 40$ mg/mL. The gelatin stock solution is vortexed and set in the oven at 50°C . Once the solution is homogeneous, pH is increased up to $pH 6$ or 8 with $1\text{--}5 \mu\text{L}$ of a 0.5 M - 1 M NaOH solution. **Chitosan:** 100 mg of chitosan dispersed in 10 mL of 0.1 M acetic acid aqueous solution for a concentration $C = 10$ mg/mL. For an optimal solubilization, the chitosan stock solution is stirred during one day before

use. *Alginate*: 100 mg of alginate powder is dispersed in 10 mL of Milli-q water for a concentration $C = 10$ mg/mL and stirred until complete solubilization. The magnetic stirrer usually sticks upon water addition; in this case, a manual help may be required to improve stirring. For a typical volume of 10 mL, pH is then increased to 6 or 8 with 1-10 μL of a 5 M or 1 M NaOH solution under stirring. Stirring and vortexing are eventually necessary to obtain a homogeneous alginate solution. *Collagen*: A 0.54wt% solution in 17 mM acetic acid was provided by a colleague and stored at 4°C. For a typical volume of 1 mL, pH is then increased to 6 or 8 with 1-10 μL of a 5 M or 1 M NaOH.

Preparation of the hybrid gels

{F}G-C18:1 fibrillar gels (no biopolymer). For a 1 mL sample, one increases the pH of 1 mL of the G-C18:1 stock solution up to ≈ 8 using 2-5 μL of a 5 M or 1 M NaOH solution. CaCl_2 solution (1 M, $V_{\text{CaCl}_2} = 33.5$ μL , $[\text{CaCl}_2] = 33.5$ mM) is manually added for a total $[\text{CaCl}_2] : [\text{G-C18:1}] = 1 : 1.3$ molar ratio. The final solution is stirred and a gel is obtained after few minutes at room temperature.

{X}G-C18:1/biopolymer gels (X= V, M or F). A volume of 500 μL of the biopolymer stock solution is mixed with 500 μL of G-C18:1 stock solution (sample) at the same pH (6 or 8) to prepare either vesicle-containing (*{V}G-C18:1/biopolymer*, pH 6) or micelle-containing (*{M}G-C18:1/biopolymer*, pH 8) hydrogels. For the controls, 500 μL of the biopolymer stock solution and 500 μL of G-C18:1 stock solution are each mixed with 500 μL of water. For the fiber-containing gels, in a typical volume of 1 mL, a CaCl_2 solution (1 M, $V_{\text{CaCl}_2} = 33.5$ μL , $[\text{CaCl}_2] = 33.5$ mM) is eventually manually added to form *{F}G-C18:1/biopolymer* gels, for a total $[\text{CaCl}_2] : [\text{G-C18:1}] = 1 : 1.3$ molar ratio. This procedure is the same for gelatin, collagen and chitosan at pH 8. In the case of alginate at pH 8, a volume of $V_{\text{CaCl}_2} = 50$ μL of a CaCl_2 solution ($[\text{CaCl}_2] = 1$ M) is added, for a final CaCl_2 concentration of 50 mM and $[\text{CaCl}_2] : [\text{G-C18:1}] = 1 : 0.86$ molar ratio and $[\text{CaCl}_2] : [\text{alginate}] \approx 1 : 0.0015$ molar ratio. The final solution is stirred and a gel is obtained after resting a few hours at room temperature.

{F}G-C18:1/chitosan gels. A second, specific procedure, was tested to prepare only fibrillary *{F}G-C18:1/chitosan* gels, because the procedure above resulted in a heterogeneous medium. Both will be commented in the results section. 1 mL of the acidic chitosan stock solution is mixed with either 1 mL 0.1 M acetic acid aqueous solution to prepare a control or with 1 mL of G-C18:1 solution, to prepare the final sample. The pH of the mixture is acidic and not adjusted further. The sample is vortexed and eventually a volume of $V_{\text{CaCl}_2} = 67$ μL of a CaCl_2 solution ($[\text{CaCl}_2] = 1$ M) are added, followed by further mixing, for a final concentration of CaCl_2 in the sample of 33.5 mM and a $[\text{CaCl}_2] : [\text{G-C18:1}] = 1 : 1.3$ molar ratio. The sample is then poured in a 35 mm \varnothing petri dish. The opened dish is localized under a glass bell containing a 1 M ammonia solution. A homogeneous gel, of which the pH is estimated to $\text{pH} \approx 10$ according to pH paper, is obtained after 3 h. The pH is then eventually decreased down to 8 or 6 by successive washes with milliQ water.

Table 12 summarizes the reference, sample and stock solution concentrations in wt% employed throughout this study.

Table 12 – Concentration of stock solutions, volumes from stock solutions and final concentration in the samples. *: concentrations are given in molar, M or millimolar, mM.

	G-C18:1 (pH 6 or 8)	Gelatin (pH 6 or 8)	Alginate (pH 6 or 8)	Chitosan (pH 6 or 8)	Collagen (pH 6 or 8)	CaCl_2
Stock solution concentration	4	4	2	2	0.54	1 M*

(wt%)						
V (mL)	0.5 (1 for the second procedure with chitosan)	0.5	0.5	0.5/1 (first/second procedure)	0.5	0.0335/0.05 (alginate)
Reference and sample concentration (wt%)	2	2	1	1	0.27	33.5 mM/50 mM*(alginate)

3.3 Transition diluted/concentrated systems

We worked in **Chapter I** with a 2.5-2.5 mg.mL⁻¹ optimized amount of G-C18:1-macromolecule in G-C18:1/PEC systems ($M_{w\text{ PEC}} \approx 5$ kDa) regarding the G-C18:1/PEC charge ratio, where the PEC was the cationic polyelectrolyte (Figure 10, **Chapter I**, page 46). When employing an approximately 50times heavier compound such as high molecular weight (HMW) chitosan ($M_w \approx 282.5$ kDa), we thought to adapt the amount of HMW chitosan with respect to the content of G-C18:1. To keep an optimal charge ratio while keeping the G-C18:1 concentration constant, we should thus divide by 50 (this corresponds to the mass ratio between HMW chitosan and chitosan lactate CHL, being 5 kDa; see **Chapter I**) the amount of HMW chitosan. We explored this route by recalling the properties of the G-C18:1/CHL system, studied in **Chapter I**. In an optimal charge ratio, they form MLWVs at neutral/acidic pH. MLWVs can be easily detected by optical microscopy under crossed polarizers, due to the birefringence of the multilamellar walls. Birefringence of supposed MLWVs was checked for a system composed of 2.5 mg.mL⁻¹ of G-C18:1 and (2.5/50)=0.044 mg.mL⁻¹ of chitosan. However, we could not find any significant birefringent colloid. We then decide to optimize the G-C18:1-to-chitosan ratio. We multiply by 100 the quantity of chitosan keeping the same amount of G-C18:1 (2.5 mg.mL⁻¹): birefringence was observed for 2.5-4.4 mg.mL⁻¹. We also multiplied by 50 the amount of initial content of G-C18:1, for a 10 mg.mL⁻¹ concentration of chitosan. In this case, the mixture is viscous, opaque, and hardly usable. Eventually, if we keep the mass ratio equivalent, birefringence is also observed for both 2.5-2.5 and 10-10 mg.mL⁻¹ G-C18:1-chitosan solutions. We thus chose this mass ratio of 1, which probably does not reflect exactly the negative-to-positive charge ratio, but 1) it shows the presence of MLWVs, thus indicating that the charge ratio is not too far off; 2) it is highly convenient to work with; 3) it allows formation of chitosan hydrogel. In the absence of MLWVs formation with gelatin and alginate, their final concentrations were rather retained to be comparable with HMW chitosan. This discrepancy between theoretical and experimental chitosan amount can be explained by the different degrees of deacetylation between CHL (>90%) and HMW chitosan (> 75%) and thus a different number of free amine groups.

For the final systems, we retain a G-C18:1/gelatin or alginate (2 wt%-2 wt%) and G-C18:1/chitosan HMW (2 wt%-1 wt%). For example, it is required to prepare a 2 wt% chitosan HMW stock solution to get a final concentration of 1 wt%, and a higher amount makes the compound difficult to manipulate for the procedure we follow (described in the related papers).

All gels were mainly characterized through their loss and storage moduli, determined by rheology, a technique widely used to follow sol-gel transition and understand structural features involved in gel formation (**Annex 2**).

For the method of analysis, two options were explored. Either the heated G-C18:1/biopolymer mixture was deposited in its sol state on the plate (the sol-gel transition occurs *in-situ*) and mechanical properties were followed over time at fixed shear strain and frequency, or the sample was deposited in its gel state and mechanical properties were followed over time at fixed shear strain and frequency as well. Preliminary experiments performed with gelatin according to the first option (data not reported) show that the mechanical properties reach a plateau once the sol-gel transition is crossed. However, further, sudden increase in the elastic modulus was spuriously observed after an uncontrolled amount of time (minutes to ten of minutes). We found out that such increase was not real and it was most likely explained by evaporation and drying phenomenon at the plate-plate junction (1 mm), rather than to a real increase of the properties. Similar effects were also observed in a couette cell environment. This approach was no more investigated and following experiments were performed according to the second option, once gelification is done out of the rheometer.

Throughout this chapter, we perform oscillatory rheology and record the mechanical properties of gels over a 5 min time range. This requires a preliminary study to identify the linear viscoelastic domain (LVER): all samples were initially analyzed in function of frequency and shear strain to determine LVER and typical experiments are shown in Figure 28. Once the frequency (1 Hz) and the shear strain (0.1%) are fixed (average value of the linear domain chosen), experiments are performed in function of time to evaluate G' and G'' : a gel is usually called so when $G' \geq 10G''$. The structure of the gels was then assessed by means of SAXS experiments, performed on the Swing beamline at Soleil Synchrotron. Experiments were performed using standard *ex situ* borosilicate capillaries (1.5 mm)

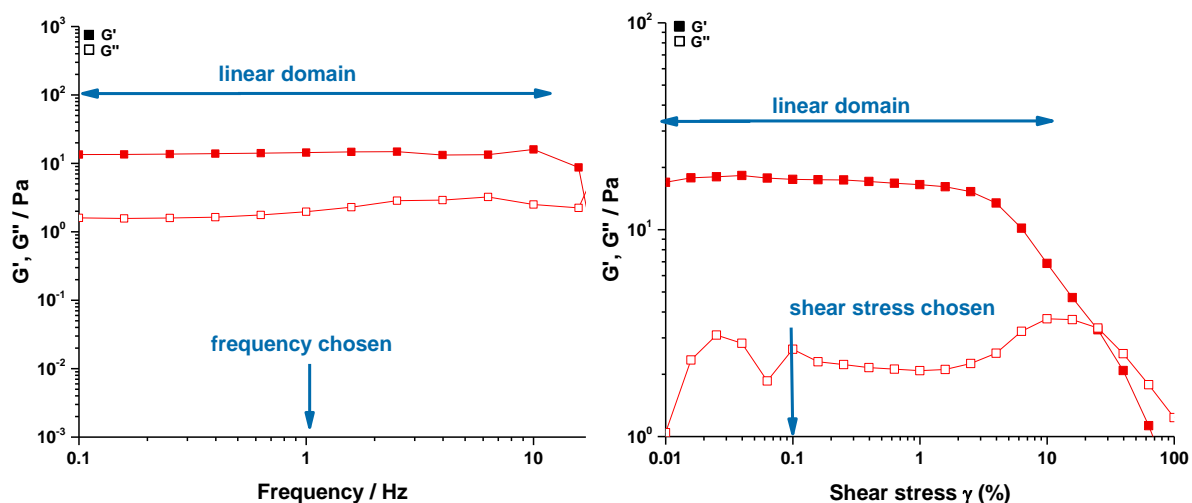


Figure 28 – Rheological experiments performed on a {F}G-C18 :1 (2wt%, pH 8) gel in function of frequency (left) and shear stress (right) to determine the linear domain for further experiments in function of time.

3.4 G-C18:1/biopolymers

The present work consists in mixing each of the three G-C18:1 phases presented in Figure 27 with an aqueous biopolymer solution in the concentration range discussed above. Biopolymers tested are the following ones: gelatin (which does not interact with G-C18:1, **Chapter I**), collagen (of which the

composition is the same than gelatin, but with an enhanced biological interest in tissue engineering), alginate (which exhibits calcium dependent gelation properties), and chitosan.

The entire approach as well as additional experiments will be detailed for gelatin, preliminary results obtained with collagen will be presented as they are not included in the related **Project paper III**, motivations for the choice of alginate and chitosan will be discussed but the reader is addressed to **Project paper III** for experimental results and comments.

3.4.1. G-C18:1/gelatin

According to experiments presented in **Chapter I**, gelatin does not interact with G-C18:1 under diluted conditions. As shown in Figure 27, **Chapter III**, G-C18:1 forms three different structures and each one will be tested with gelatin. We expect either vesicles or micelles loaded gelatin gels or orthogonal gels combining fibers and polymer networks. For the latter case, we have verified in a control experiment that 33.5 mM calcium (Table 12) have no influence on the mechanical properties of gelatin (data not shown).

3.4.1.1. Gelatin + {M}G-C18:1

Micellar solutions of G-C18:1, having the notation {M}G-C18:1, at 2 wt%, are liquids, with obviously no measurable elastic properties. The storage modulus of a 2 wt% gelatin gel, recorded within about 5 min from loading the gel onto the rheometer, is about 50 Pa (Figure 29, right, yellow).

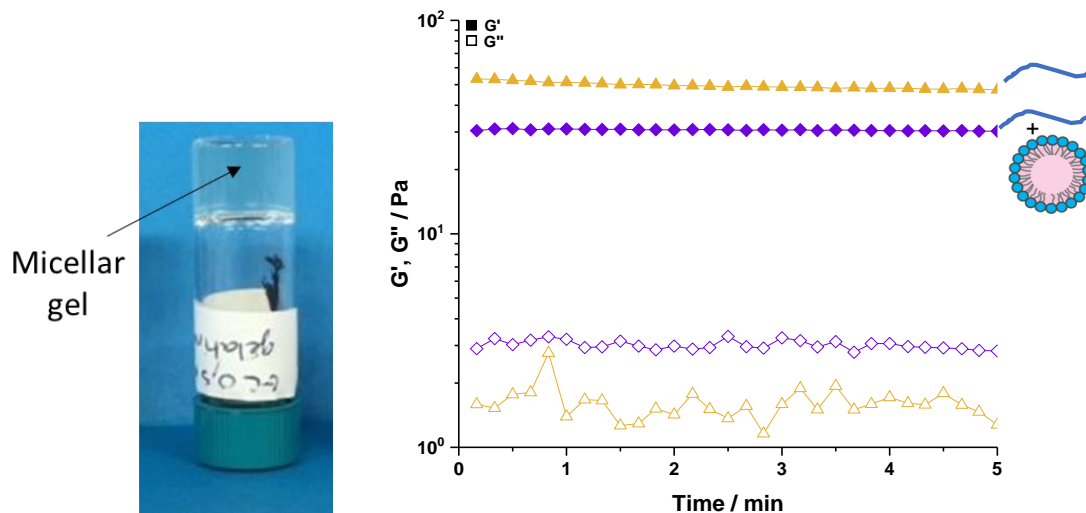


Figure 29 - G-C18:1 micelles loaded gelatin gel (left) - Loss and storage modulus in function of time of gelatin (2 wt%, yellow triangles) and G-C18:1 (2 wt%) micelles loaded gelatin (2 wt%) gel (purple diamonds)

Macroscopically, a micelles loaded gelatin gel (Figure 29, left) looks very close to a pure gelatin gel. This qualitative result is supported by quantitative rheology experiments. The influence of micelles insertion on gelatin's mechanical properties is shown by Figure 29, right: storage modulus although undergoing a decrease from about 50 Pa to 30 Pa, is still quite comparable with the G' of gelatin only. The qualitative structural study is performed by SAXS. Related SAXS profiles are given in Figure 30: the red profile of {M}G-C18:1 is the one expected from micelles¹²¹ while the yellow one of gelatin is typical of a polymer chain in a good solvent. The blue profile probes the sample constituted by the mixture of {M}G-C18:1 and gelatin. This profile is superimposable to the arithmetical sum of red and yellow profiles, which confirms the absence of interactions and coexistence of two networks.

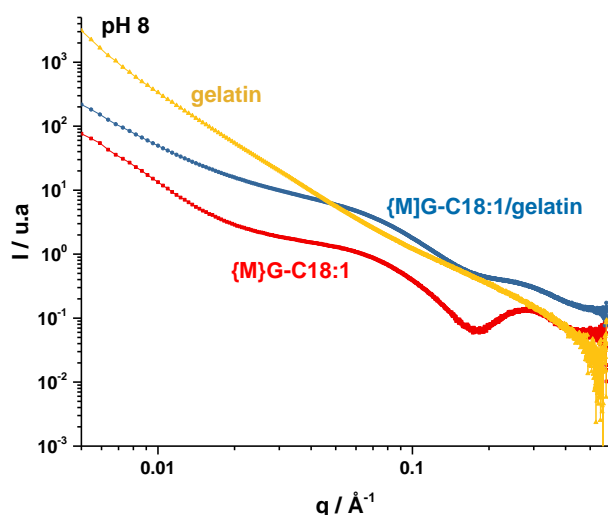


Figure 30 – SAXS profiles of {M}G-C18:1 (2 wt%), gelatin (2 wt%) and {M}G-C18:1/gelatin (2-2 wt%) mixture at pH 8

Conclusions are first that a colloidal solution of micelles dilute the gelatin gel and slightly decrease its elastic modulus, and secondly that the resulting gel formed through an orthogonal process.

3.4.1.2. Gelatin + {V}G-C18:1

Vesicular solutions of G-C18:1, {V}G-C18:1, at 2 wt%, are liquid, with obviously no measurable elastic properties. The storage modulus of a 2 wt% gelatin gel, recorded within about 5 min from loading the gel onto the rheometer, is about 50 Pa (Figure 31, right, yellow).

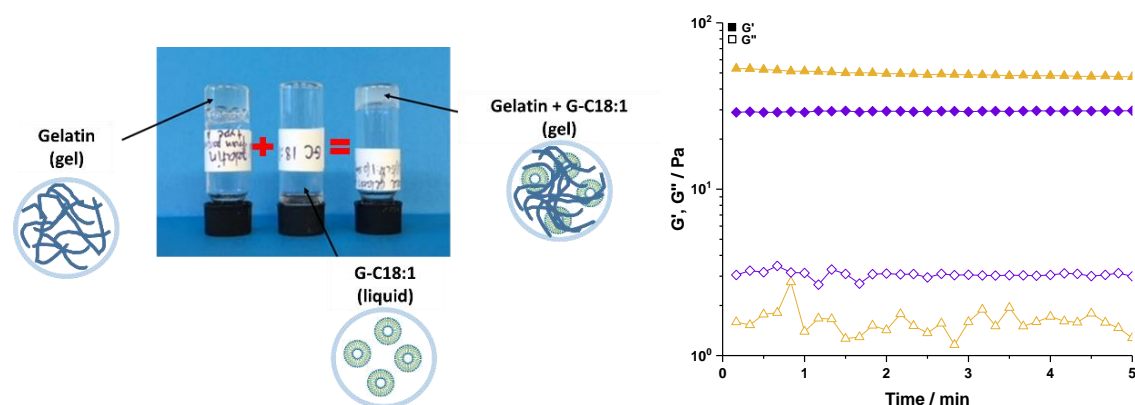


Figure 31 – Gelatin (5wt%) gel, {V}G-C18:1 (0.5 wt%) solution and {V}G-C18:1 (0.5 wt%)-loaded gelatin (5 wt%) gel (left) - Loss and storage modulus in function of time of gelatin (2 wt%, yellow triangles) and {V}G-C18:1 (2 wt%)/gelatin (2 wt%) gel (purple diamonds) (right)

As illustrated by Figure 31, left, the addition of vesicles inside a gelatin gel has a macroscopic consequence: a transparent gelatin gel combined to a liquid vesicular solution results in a gel with enhanced turbidity. This qualitative result is supported by quantitative rheology experiments. Concerning the mechanical properties, vesicles do not provide any additional strength to a gelatin gel and even decrease its storage modulus value from 50 Pa to 30 Pa, as shown by Figure 31, right, displaying a similar effect as in the {M}G-C18:1/gelatin system discussed above. Related SAXS profiles are given in Figure 32: the red profile of {V}G-C18:1 is the one expected from vesicles¹²¹ while the yellow one of gelatin is typical of a polymer chain in a good solvent. The blue profile probes the sample constituted by the mixture of {V}G-C18:1 and gelatin. This profile is superimposable to the

arithmetical sum of red and yellow profiles, which confirms the absence of interactions and coexistence of two networks.

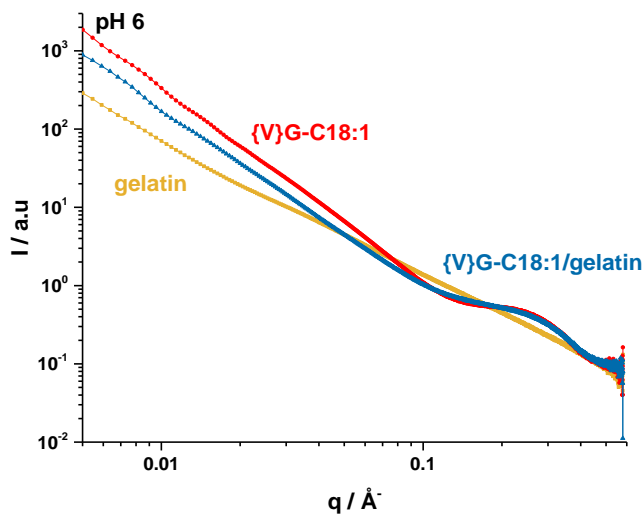


Figure 32 - SAXS profiles of {V}G-C18:1 (2 wt%), gelatin (2 wt%) and {V}G-C18:1/gelatin (2-2 wt%) mixture at pH 6

Conclusions are first that a colloidal solution of vesicles dilute the gelatin gel and slightly decrease its mechanical properties, as similarly observed for micelles, and secondly that the resulting gel formed through an orthogonal process. All in all, for a constant concentration of gelatin (2 wt%), colloidal solutions of either micelles or vesicles dilute the gelatin gel, which loses few decades of Pa in terms of its elastic modulus. If we think in terms of quantity of matter, the decrease is even more drastic, the mechanical properties of a 4 wt% gelatin gel being expected in the 100 Pa range. We chose to perform experiments at a fixed gelatin concentration, but the point quantity of gelatin vs. quantity of matter will be commented later.

3.4.1.3. Gelatin + {F}G-C18:1

If G-C18:1 micelles and vesicles are not able to gelify, G-C18:1 in its fiber form obtained in presence of calcium¹²⁶ do possess gelation properties. The gel obtained is opaque as shown in Figure 33, left.

A typical {F}G-C18:1 fiber gel (2 wt% + 33.5 mM CaCl₂) has a storage modulus in the 10 Pa range (Figure 33, right, red squares). This value is increased in presence of gelatin up to 100 Pa, as illustrated by Figure 33 (right, purple squares), right, and even exceeds the storage modulus value of gelatin gel (with calcium) which is around 50 Pa (Figure 33, right, yellow squares). Macroscopically, the hybrid gel looks like a gel composed of {F}G-C18:1 alone (Figure 33, left).

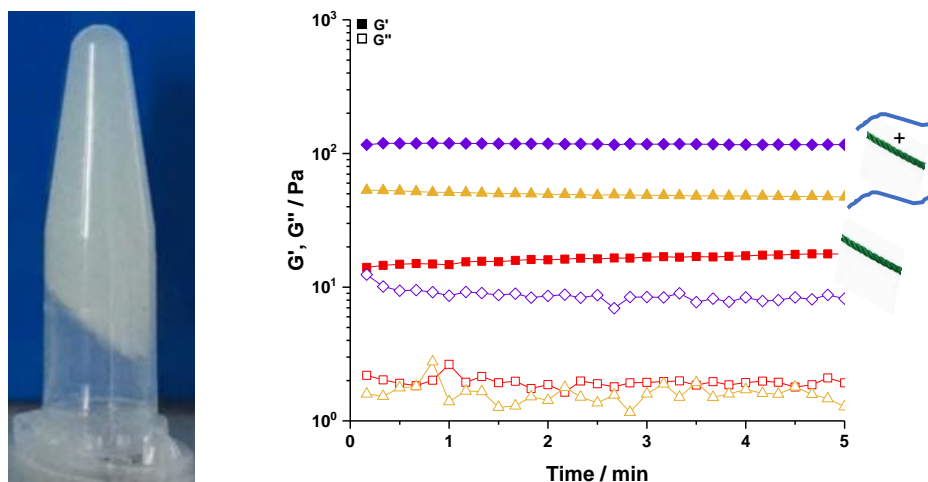


Figure 33 – Gel of {F}G-C18:1 (left) - Loss and storage modulus in function of time of {F}G-C18:1 (2 wt% + 33.5 mM CaCl₂, red squares), gelatin (2 wt% + 33.5 mM CaCl₂, yellow triangles) and {F}G-C18:1 (2 wt%, 33.5 mM CaCl₂) + gelatin (2 wt%)(purple diamonds) (right)

Related SAXS profiles are shown in Figure 34: {F}G-C18:1 profile (red) is typical of fibers due to the q^{-2} dependence at low q and exhibits three peaks which suggest a crystalline structure at high q . Indeed, these three peaks are respectively centered at $q_1=0.24 \text{ \AA}^{-1}$, $q_2=0.3 \text{ \AA}^{-1}$ and $q_3=0.47 \text{ \AA}^{-1}$, and their ratio are $q_2/q_1 = 1.25$ and $q_3/q_1 \approx 2$. The former does not correspond to a hexagonal packing ($q_2/q_1 = \sqrt{2}$) and fibers being anisotropic, cubic phases are discarded. However, a tetragonal structure is likely formed.¹²⁶ The yellow profile of gelatin with calcium is strictly the same than without calcium. Finally, for the blue one associated to the mixture, the structural signature of fibers is present and the profile corresponds to the sum of both individual components.

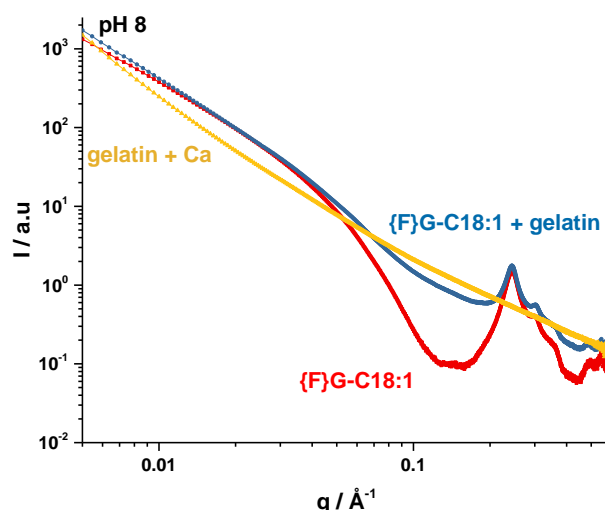


Figure 34 - SAXS profiles of {F}G-C18 :1 (2 wt%), gelatin (2 wt% + 33.5 mM CaCl₂) and {F}G-C18:/gelatin (2-2 wt%) mixture at pH 8

Concerning the gels composed of G-C18:1 fibers only, their mechanical properties increase with increasing G-C18:1 concentration.¹²⁶ For a constant concentration of G-C18:1 fixed at 2wt%, an increasing concentration of gelatin (2 to 6 wt%) enhances the mechanical properties of the hybrid gel as well (from 80 Pa to about 1000 Pa, Figure 35). Increasing the concentration of G-C18:1, keeping the gelatin concentration constant, has not been explored, yet (for lack of time, but it will be done

for the oral defense): the strength is expected to come mainly from the biopolymer and our goal is to test the effect of each phase while using a reasonable G-C18:1 amount.

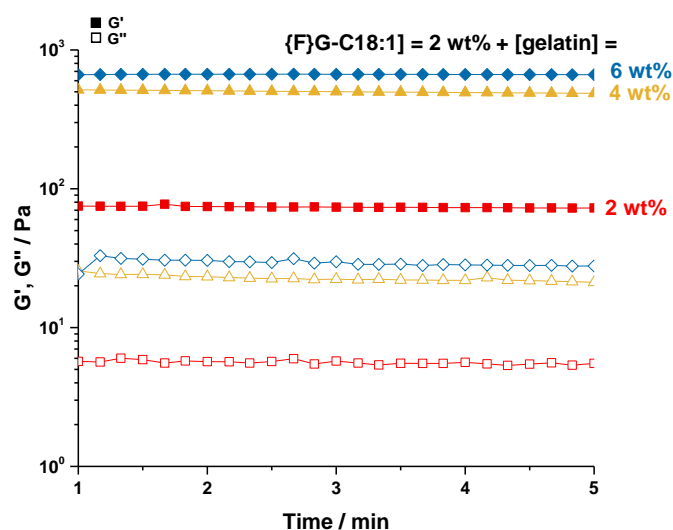


Figure 35 – Mechanical properties in function of gelatin concentration for a fixed {F}G-C18:1 concentration

Conclusions regarding the fiber phase are first that it enhances the mechanical properties of gelatin hydrogels for a constant concentration of gelatin, which was not the case with micelles and vesicles, and secondly that the mechanical properties reached at 4 wt% of total matter are comparable with a 4 wt% gelatin gel. Finally, the hybrid gel result from an orthogonal self-assembly process, in agreement with results in **Chapter I** and literature.

The overall conclusions regarding the influence of G-C18:1 in its micelles, vesicles or fibers form on gelatin hydrogels are summarized on Figure 36: neither micelles nor vesicles in a colloidal solution form but only fibers provide an enhanced mechanical strength to gelatin hydrogels for a constant gelatin concentration (2 wt%) and reinforce them up to the properties expected for a more concentrated gelatin gel (4 wt%). These conclusions are in agreement with data presented in **Bibliographic chapter** regarding the effect of micelles and vesicles or fibers on gels, respectively discussed pages 22 and 26.

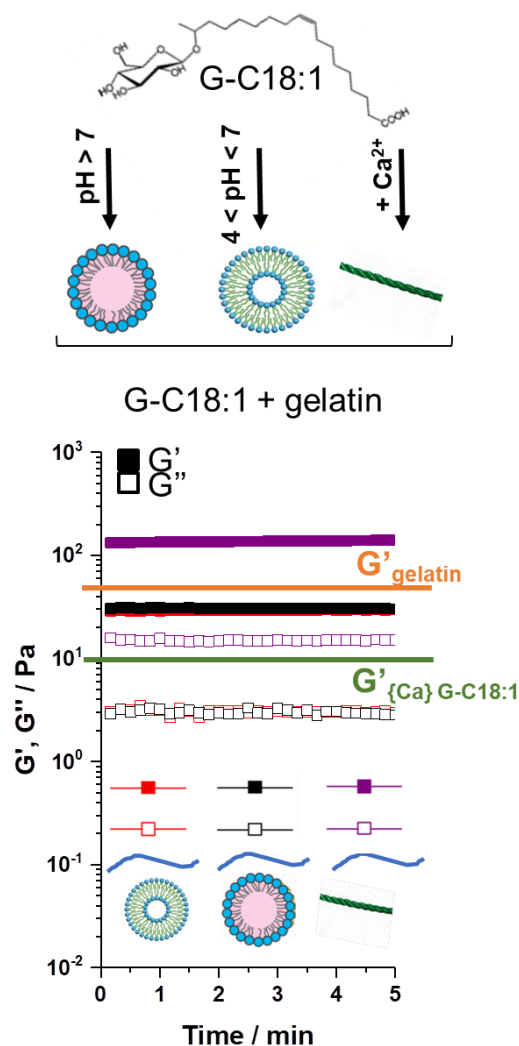


Figure 36 - Summary of storage and loss modulus of {M}G-C18/gelatin (2-2wt%, black squares), {V}G-C18:1-/ gelatin (2-2wt%, red squares) and {F}G-C18:1/gelatin gels (2-2wt%, purple squares) – Control G' of gelatin (2 wt%, pH 8) and {F}G-C18:1 (2 wt%, pH 8) are respectively reminded by orange and green lines.

3.4.1.4. Influence of Ca^{2+} addition rate

If the presence of calcium is essential for G-C18:1 gelification and enhancement of hybrid gel's mechanical properties, the influence of its rate of addition raises questions which involve kinetics and thermodynamic aspects, already reported to be determinant for the final mechanical properties of a sophorolipid gel.¹⁵⁷ We thus compared the mechanical properties obtained after addition of the total volume manually in one shot (Figure 37, red squares) with controlled addition of calcium using a push syringe delivering calcium at a predetermined rate. According to Figure 37, all gels exhibit G' in the 100 Pa range, with only slight differences. The trend seems to be in favor of a fast calcium addition ($G' > 100$ Pa for addition in one shot, red squares on Figure 37, vs. $G' < 100$ Pa for slow rates, blue and yellow squares on Figure 37). Changes of the rate of calcium addition however always results in a quite tough gel and is thus not as much important as the rate of acidification of self-assembled fibers for instance, for which a too fast acidification results in liquid dispersion of spherulites.¹⁵⁷ Eventually, the calcium's addition rate does not seem to be a crucial parameter to control the resulting mechanical properties of the {F}G-C18:1/gelatin gel.

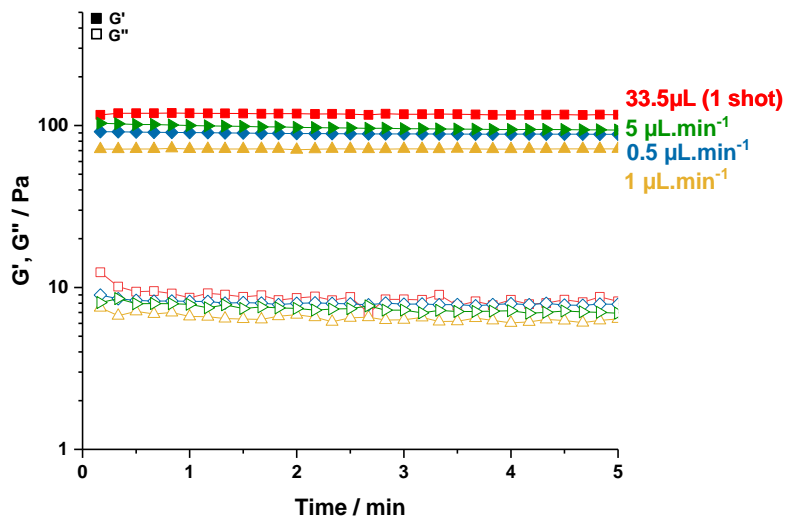


Figure 37 – Loss and storage modulus of {F}G-C18:1 + gelatin gels in function of calcium addition rate.

3.4.1.5. Influence of the anion

Gels were formed using CaCl_2 as a source of calcium according to an optimized G-C18:1/ Ca^{2+} molar ratio.¹²⁶ My colleague A. Poirier evidenced an influence of the divalent cation nature. The question here addressed is to know whether or not the anion associated to Ca^{2+} has an influence on the gelification process of the {F}G-C18:1/gelatin system. We have tested the different salts available at the lab and the results are summarized in the following Table 13:

Table 13 - Effect of the calcium's counterion on gelification of {F}G-C18:1/gelatin mixtures and resulting mechanical properties. In parentheses: G'

CaCl_2	CaF_2	CaCO_3	CaHPO_3	Ca(OH)_2
Gel ($\approx 50\text{Pa}$)	Gel ($\approx 30\text{Pa}$)	Gel ($\approx 40\text{Pa}$)	Gel ($\approx 45\text{Pa}$)	Gel ($\approx 20\text{Pa}$)

The mechanical properties were determined for each case and are compared in Figure 38:

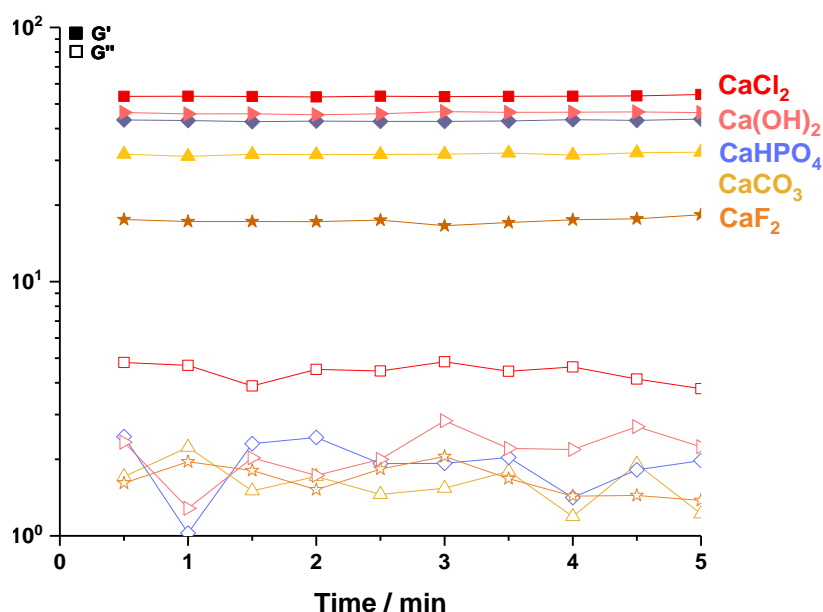


Figure 38 – Loss and storage modulus of {F}G-C18:1/gelatin gels obtained using different sources of calcium, e.g. different counterions.

Most of the resulting properties are in the same order of magnitude, suggesting that the counterion involved, whatever their size and valency, has not so much influence on the gelation process and that interaction with calcium is not disturbed. Fluorine ions are a bit apart and display lower mechanical properties, a likely hypothesis to explain such results are related to the electronegativity of fluorine ions. In addition, they are heading the Hofmeister series, or lyotropic series,³³⁴ which classifies a series of salts displaying consistent effects on the solubility of proteins and on the stability of their secondary and tertiary structure. Fluorine ions are classified as kosmotropic (or water-structure maker),³³⁵ which means that they tend to be hydrated and contribute to the stability and structure of water-water interactions. They cause water molecules to favorably interact, which results in the stabilization of intramolecular interactions in macromolecules, especially proteins.³³⁶ It would be thus envisaged that self-assembly of {F}G-C18:1 fibers is disturbed. Considering the above, CaCl₂ has been used for the rest of the work.

3.4.2. G-C18:1/Collagen

Satisfying results obtained upon mixing G-C18:1 fibers with gelatin motivated preliminary investigations with its parent molecule, collagen, an interesting compound for biomedical applications.^{337,338} If gelatin and collagen exhibit identical molecular compositions, gelation proceeds from distinct mechanisms and results in different types of molecular assemblies.³³⁹ Collagen is the most represented protein in human body (≈ 6 wt%) : it exists within 16 forms and is the main component of the extracellular matrix ; it provides resistance to stretching to tissues. The protein is made of three associated α -polypeptides chains, composed of 1055 amino acids each, and linked through hydrogen bonds between hydroxylysine and hydroxyproline, and covalent bonds. Each combination defines a type of collagen with its unique structure and specific localization within organs. For instance, type I collagen plays a role in the formation of the skin, tendons, bones, and cornea, while type III collagen is rather found in the cardiovascular system. In addition, fresh collagen solutions are prepared and available at our laboratory within the framework of a number of ongoing

projects. They were used as such (0.54 wt%, diluted to 0.27 wt%), without further treatment. Isoelectric point is $\text{pH} \approx 4.7$.³⁴⁰

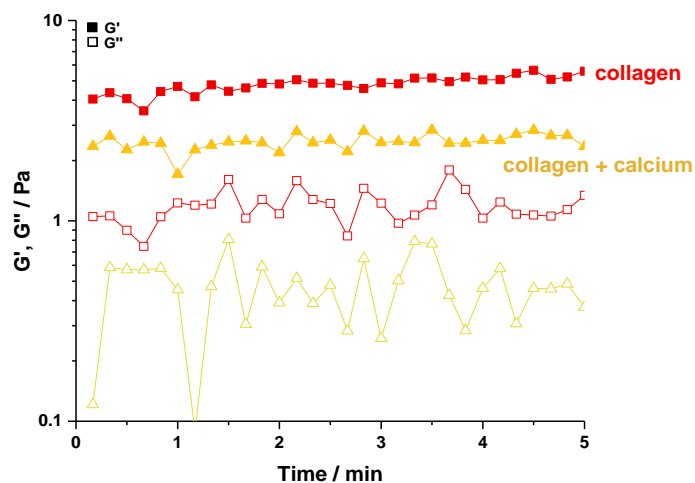


Figure 39 – Effect of calcium on collagen (0.27 wt%, pH 8 – red squares; 0.27 wt%, pH 8, + 33.5 mM CaCl_2 – yellow triangles)

As a control, we added calcium to a collagen solution: according to Figure 39, collagen’s mechanical properties, as the ones of gelatin, are not particularly sensitive to the presence of calcium and remain in the 2-5 Pa range. We are now sure that any effect observed later is not due to the coexistence of these two compounds.

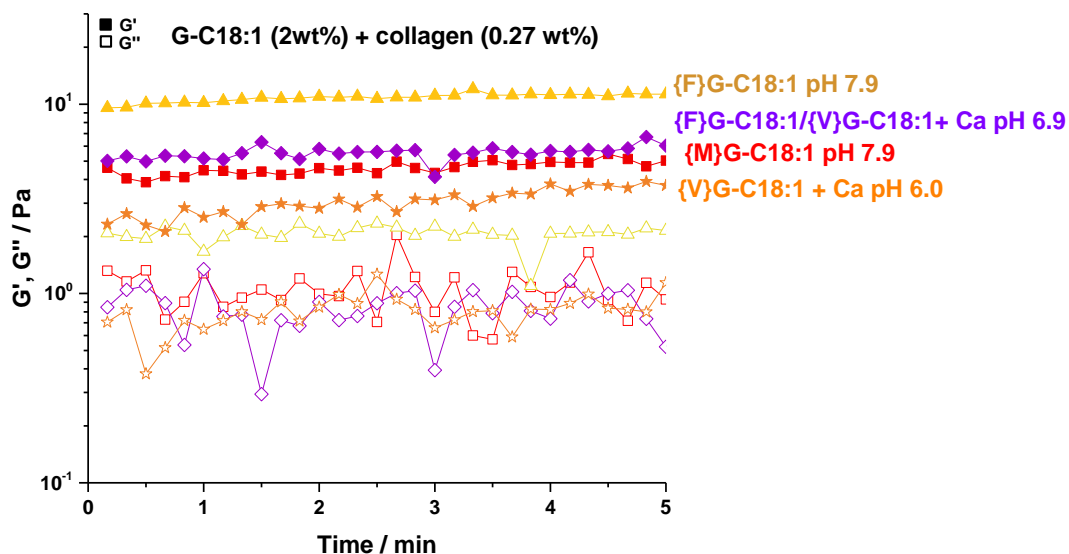


Figure 40 - Influence of calcium addition on G-C18:1/collagen mixture and effect of pH on mechanical properties

Collagen was first mixed with {M}G-C18:1 at pH 7.9: the solution displays poor viscoelastic properties (≈ 4 Pa, red squares, Figure 40). This performance is enhanced up to 10 Pa upon calcium addition and formation of {F}G-C18:1 fibers (yellow triangles, Figure 40). If pH is then decreased to 6.9, in fiber-to-vesicle transition area, properties go back to the initial level without calcium (purple squares, Figure 40). Upon further decrease of pH down to 6, properties keep decreasing around 2 Pa in the vesicular domain of G-C18:1 (orange stars, Figure 40). These results are in agreement with the key role of {F}G-C18:1 phase in the enhancement of gelatin hydrogels properties discussed above and generalize this conclusion to collagen.

Collagen was also studied in combination with another biosurfactant, a C16:0 derivative of sophorolipids. Motivations and results are given in **Annex 3**.

The structure of collagen and {F}G-C18:1 could not be studied so far, but a synchrotron run in November 2021 should allow us to confirm, or infirm, the orthogonal coexistence of collagen and fibers. If successful, results will be presented at the oral defense.

3.4.3. G-C18:1/Alginate

Alginate is negatively charged and is not expected to interact with G-C18:1 as described in **Chapter I** and known for similarly charged polymers and surfactants (**bibliographic chapter**), but it also needs calcium to gelify, thus competing with gelification of G-C18:1.⁵⁷ Similarly to the work on gelatin, alginate solutions will be mixed to the three phases of G-C18:1. However, alginate is particularly interesting to combine with {F}G-C18:1. We supposed that the amount of calcium had to be adapted for the alginate-containing system, as both components need a specific amount of calcium to gelify: do we need the sum of individual calcium amounts? Less? More? Several conditions were tested to identify the right amount of calcium to add to a G-C18:1/alginate mixture at pH 8 to obtain a homogeneous gel, the following Table 14 indicates which conditions succeeded:

Table 14 - Effect of calcium concentration on the gelification of alginate and {F}G-C18:1/alginate mixture

CaCl ₂ (mM)	25	50	75	100	200
Alginate 1wt%	YES	NO	NO	NO	NO
{Ca}GC-18:1 2wt% + Alginate 1wt%	YES	YES	NO	NO	NO

In the conditions for which the table indicates « NO », gelation partially occurred: a part of the mixture formed a gel but another significant part remained liquid, even after 24h. Rheological properties were then determined for the fully gelled systems: alginate alone (25 mM CaCl₂) is the reference, while increased properties for the hybrid gel containing 50 mM CaCl₂ compared to 25 mM CaCl₂ were recorded (data not shown).

Does G-C18:1 or alginate gelify first in presence of calcium? This is an interesting question from a physico-chemical point of view. We provide an answer in **Project paper IV** (joint hereafter) based on rheological measurements performed on {F}G-C18:1/alginate systems with different calcium quantities, and supported by Isothermal Titration Calorimetry (ITC) experiments, which provide thermodynamic parameters of G-C18:1/calcium interaction, that we compared to existing literature about alginate.

Concerning the G-C18:1 micellar, vesicular and fibrillary phases combined to alginate, results are similar to those obtained with gelatin and are detailed in **Project paper IV**.

3.4.4. G-C18:1/chitosan HMW

We used the same approach described so far using chitosan, but we encountered some issues related to its gelation properties. Indeed, we tested two procedures to prepare gels (described in *experimental part 3.2.2*, page 68, and illustrated by Figure 41) and we are aware of their respective defects, even if we could not find a more reliable way to perform the experiment. The first one consists in increasing the pH of an acidic chitosan solution (chitosan solubilized in 0.1 M acetic acid

aqueous solution), which does not result in a homogeneous gel, as gelatin or alginate, but in a biphasic system. The contribution of {F}G-C18:1 makes the aqueous part gelify, but the result is more a composite hydrogel than an hybrid one: the medium is gelified but without apparent intimate interpenetration. We thus tested a second approach, based on a mixture of both components at acidic pH and using the diffusion of ammonia to increase the pH, which allows to prepare a more homogeneous media, but we realized that we do not control if the presence of calcium at acidic pH has the effects expected at basic pH, especially the formation of fibers was not ensured considering that calcium is usually added to a micellar phase and not of a vesicular one. In addition, the control of the pH after successive washings was not precise enough using pH-paper and maybe we finally compare identical gels.

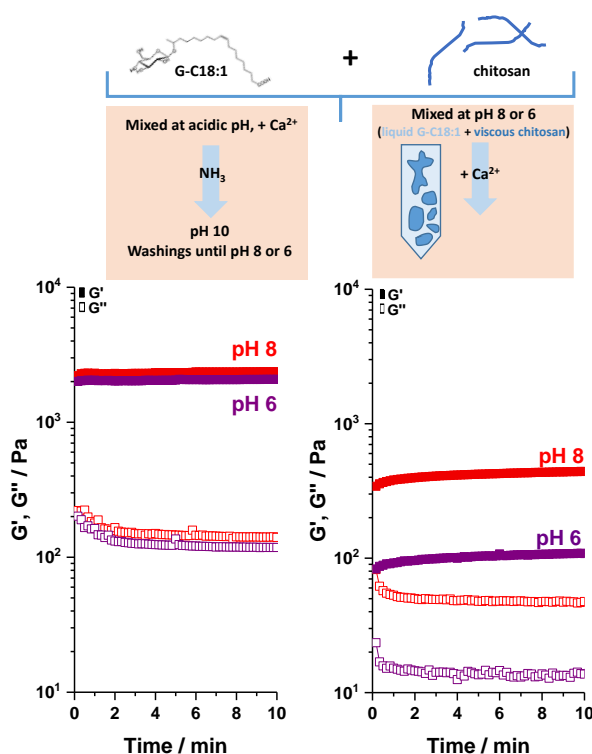


Figure 41 – Two procedures employed to synthesize chitosan-based hydrogels and resulting mechanical properties

Same conclusions regarding the influence of the three G-C18:1 phases on chitosan HMW gels mechanical properties were obtained; experiments are detailed in **Project paper IV**.

3.4.5. General remarks

1) All rheological measurements were performed after gelification *ex situ* and can thus be compared. Indeed, a colleague and I noticed that mechanical properties of a given gel can differ depending on the gelification conditions: *in-situ* or *ex-situ*. We neither have a clear explanation neither have further investigated this point but it was significant enough to be mentioned.

2) It is important to consider the procedure employed to prepare the gel. Indeed, we employed a procedure and obtained gels with given mechanical properties. One has to be aware that it is not excluded that employing another procedure would have an influence on the mechanical properties of the gel, even if quantities and pH are the same. The effect of assembling the molecules under different conditions, i.e. the self-assembly process, is not harmless, and there is sufficient literature

reporting that how the molecules are assembled can have a significant effect on the properties of the resulting gels.³⁴¹ For example, the acidification method was shown to induce different kinetics of gelification and consequently different mechanical properties in SL-C18:0 biosurfactant gel.¹⁵⁷ The impact of the process will be briefly commented in **Chapter IV**.

3.5 Conclusion

The present data assess the feasibility of hybrid G-C18:1/biopolymer hydrogels and the general enhancement of mechanical properties observed for all biopolymers tested compared to lonely components' hydrogels. The phase of the biosurfactant is important and drives the resulting mechanical properties, which remain at the same level with micelles or vesicles but are significantly enhanced with fibers of {F}G-C18:1. In our systems, each network gelifies in response to external stimuli which generate reversible interactions, our systems would thus be categorized as orthogonal hydrogels. This point can however be discussed for alginate-based hydrogels: calcium addition being irreversible, self-sorting terminology may be more accurate.

At the light of these results, preliminary experiments were also conducted on other systems, first combining G-C18:1 with collagen, a molecule of choice for biomedical applications. Same trends seem valid for this system. Interesting results were obtained mixing collagen with a new biosurfactant, SL-C16:0, both molecules having opposite pH-dependent viscoelastic behaviors: their synergy provides mechanical strength to the hybrid gel over a wider pH-range.

Main results concerning {F}G-C18:1/gelatin, chitosan HMW or alginate hydrogels are presented and discussed in the project paper entitled *Mechanical reinforcement of biosurfactant/biopolymer hydrogels through interpenetrating networks*. Supported by additional experiments described in this chapter, they emphasize the potential of biosurfactants to overcome the mechanical strength issues encountered in common hydrogels.

CHAPTER IV: Synthesis and characterization of hybrid gels: pH and temperature responsiveness

Table of content

4.1	Introduction	86
4.2	Stimuli-responsivity in G-C18:1 + biopolymer concentrated systems ...	87
4.3	Rheo-SAXS investigations of structural and mechanical properties of hybrid {F}G-C18:1-gelatin hydrogels	89
4.3.1	PH effect	89
4.3.2	Temperature effect.....	93

4.1 Introduction

As a short summary of **Chapter I**, micelle-to-fiber and micelle-to-vesicle phase transitions triggered inside biosurfactant-PEC complex coacervates result in the orthogonal behavior of fibers and polymer chains and in the formation of *MLWVs*, respectively. These latter are further described in **Chapter II** which emphasizes their poor cytotoxicity, their efficiency to encapsulate curcumin and release it in cancer cells. Orthogonal systems are however interesting in other conditions: **Chapter III** focuses on their hydrogelation properties; the synthesis and the characterization of hydrogels possessing enhanced mechanical properties are described. The fibrillar phase formed by G-C18:1 (in the presence of calcium ions) was found to be the key to reinforce the mechanical properties of a wide range of biopolymer-based hydrogels, contrary to micelles or vesicles.

Polymeric hydrogels are generally stable in time, but external stimuli (temperature or pH, Table 15 and Table 16) or interpenetration with a second polymer network can modify and control their mechanical properties for a wide number of applications as in textile development or drug delivery.

Table 15 – The chemical nature and biomedical applications of thermoresponsive hydrogels (Extracted from ref.³⁴²; number of references corresponds to the book's one)

Chemical constituents of thermoresponsive hydrogel	Biomedical application of thermoresponsive hydrogel	References
pNIPAAm, butyl methacrylate	Drug delivery application	[76]
NIPAAm, propylacrylic acid	Drug delivery application	[77]
pNIPAAm, polyurethane, chitosan	Textile application (antibacterial)	[84]
PF127, glycol chitosan	Drug delivery application	[89]
PF127, hyaluronic acid	Drug delivery application	[90]
PF127, carboxymethyl cellulose sodium	Textile application (drug delivery and moisture management)	[94, 95]

Table 16 - The chemical nature and biomedical applications of pH-responsive hydrogels (Extracted from ref.³⁴²; number of references corresponds to the book's one)

Chemical constituents of pH-responsive hydrogels	Charge of pH-responsive hydrogel	Biomedical application of pH-responsive hydrogel	References
PAA, poly(l-glutamic acid)	Anionic	Drug delivery application	[114]
PAA, polyvinyl acetate	Anionic	Textile application (wound healing monitoring)	[115]
Albumin	Anionic	Drug delivery application	[116]
BSA, methacrylate	Anionic	Drug delivery application	[117]
BSA	Anionic	Textile application (medical textiles)	[118]

Both physical (temperature, light, shear/strain) and chemical (pH, ionic strength, redox, enzymes) stimuli may control the hydrogel properties. Although responsive single network hydrogels can be designed, the secondary network provided by IPN hydrogels allows to better modulate

individual network mesh sizes and trigger selective network degradation to drive hydrogel features (drug delivery among others, as illustrated by Figure 42).³⁴³

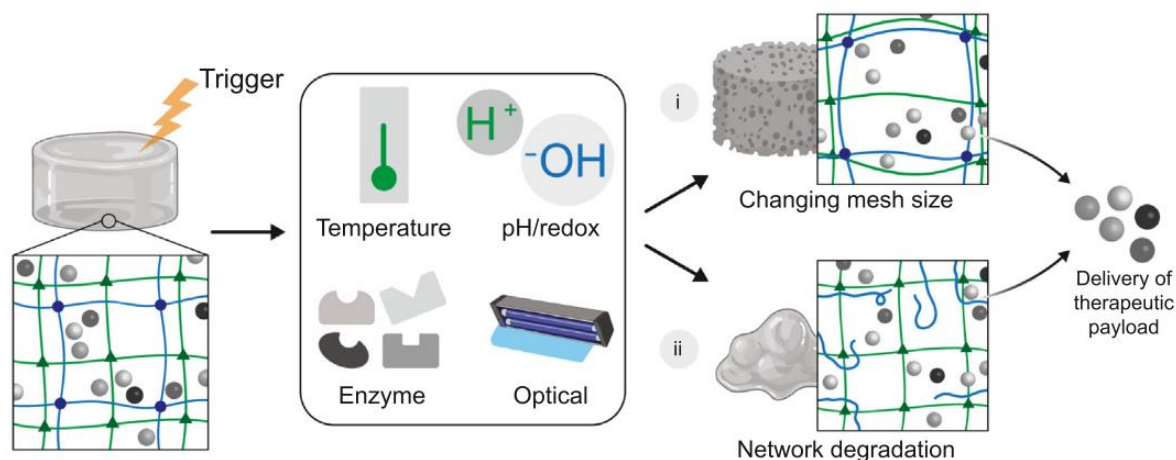


Figure 42 – Schematic representation of stimuli responsive hydrogels for drug delivery applications (reproduced from ref.³⁴⁴)

As discussed in the bibliographic chapter, biosurfactants are highly sensitive to external stimuli, mainly pH but also temperature or light. As G-C18:1 does not interact with the biopolymers tested neither under diluted (**Chapter I**) nor concentrated (**Chapter III**) conditions, we can expect that it keeps its stimuli-responsivity even in presence of a biopolymer, and, in the best-case scenario, the biosurfactant's responsivity to an external stimulus affects the overall mechanical properties.

4.2. Stimuli-responsivity in G-C18:1 + biopolymer concentrated systems

In **Chapter III**, we studied mixtures of biopolymer with different phases at thermodynamic equilibrium. The present chapter will be devoted to explore the effect of stimuli in complex medium, knowing that G-C18:1 responds to pH,¹¹⁷ to calcium and temperature (may it be in the fibrillar¹²⁶ or vesicular phase¹²¹ for the latter parameter), while the biopolymers are sensitive to pH (chitosan), salt (alginate) and temperature (gelatin).

The goal is to evaluate the effect of pH and temperature over the mechanical properties of the hydrogel. There exists a cutting-edge method for this purpose, which allow to follow *in situ* the viscoelastic properties of the gels: rheo-SAXS. (Both were performed in parallel in **Chapter III**, they are here simultaneously performed on the same sample). Rheo-SAXS can be used for temperature-dependency studies. Unfortunately, this experimental setup is not adapted to study the effect of calcium diffusion or its manual addition. However, pH effects are relatively easy to study. We discuss below four possible methods, which could be employed to adapt pH variations studies to the rheo-SAXS environment (couette cell).

1. An external buffer solution can be used, as described in the work of Dowling *et al.*³³² and shown in Figure 43, left: pH 10 buffer solution is put in contact with a G-C18:1 vesicles loaded gelatin gel, and the vesicle-to-micelle phase transition can be macroscopically followed. Vesicular environment is more turbid than micellar one, and this loss of turbidity can be estimated over time, as shown by Figure 43, right. The vesicular (h) and micellar (h') fronts, evolve in an opposite way and are totally reversed within 24h. This experiment validates that phase transitions can occur in these concentration conditions and in this complex medium.

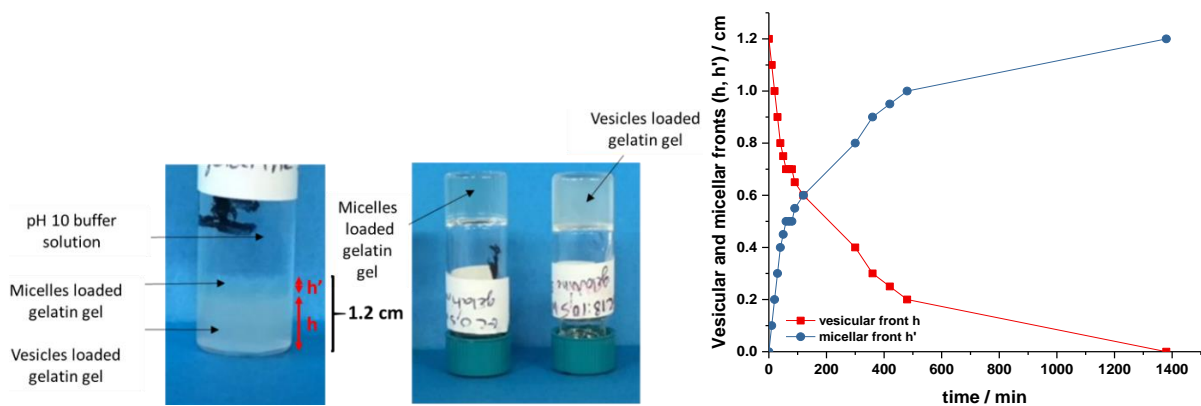


Figure 43 – pH-induced vesicle-to-micelle G-C18:1 phase transition triggered inside the gelatin/G-C18:1 gel (left); Evolution of vesicular front h and micellar gel front h' in function of time (right)

Interestingly, the contrary was not observed using a pH 4 buffer solution. A likely hypothesis, discussed by Dowling *et al.* for their own system,³³² is related to the mesh size of the gel: this latter retains the vesicles, which are large enough to be trapped within the gel, whereas micelles can escape from the gel into the surrounding buffer, the gel being consequently depleted in micelles. Dowling *et al.* did not characterize their NaOA vesicles-loaded gelatin gels in terms of mechanical properties, but we have shown in previous chapter that micelles and vesicles do not enhance the mechanical properties of the biopolymer-based gel. The functionality is however different, they performed for example controlled release of calcein from vesicle-loaded gels, an unexplored point concerning our systems but which deserves further investigations. This approach is visual and practical, but hardly adaptable to *in situ* rheo-SAXS experiments. In addition, it only seems accurate to increase the pH, but not to decrease it, while our work first targets the basic-to-acidic pH-induced phase transitions.

2. A second approach is to trigger basification/acidification by diffusion of a volatile base/acid (NH_3 , acetic acid, HCl...) but this method is also hard to put to practice for an *in situ* rheo-SAXS study.
3. It is also possible to change pH manually by addition of base/acid using a micropipette (and a pH-meter). This method was efficient to work at the lab and also nicely adaptable to *in situ* SAXS under diluted conditions, as shown in the experiments presented in **Paper I, Chapter I**. However, it cannot be adapted neither to a classical rheology nor to a rheo-SAXS environment.
4. A last approach is to employ the low-molecular weight sugar GDL (glucono- δ -lactone),³⁴⁵ widely used as a straightforward, economic, and smart method to reduce the pH in an homogeneous, although uncontrolled, manner inside both liquid and viscous solutions. GDL spontaneously hydrolyzes into gluconic acid and is commonly used to prepare strong low-molecular weight gels by homogeneously decreasing pH without interfering with the self-assembly process.³⁴⁶ The kinetics and final pH are poorly controlled but this method allows to efficiently follow our system's behavior, we thus selected it to perform rheology, SAXS and rheo-SAXS: after GDL insertion, the sample is splitted into two, half being deposited on the rheometer and half being in a vial, in which the pH-meter is dipped. Both experiments are then started with about 2 min delay. Gels are prepared according to the experimental part of **Chapter III**, with the only differences being the pH which is specifically increased up to 10 for

these pH-resolved experiments, and the concentrations which are divided by two for a better dispersion of GDL powder.

We focused on the functionality of gels involving the fibrillar phase, which has improved elastic properties with respect to gels involving micellar or vesicular phases, as concluded from **Chapter III**. We conduct a systematic study presented in this new chapter, which addresses the influence of phase transitions triggered in more concentrated systems and investigates *in situ* the responsivity of hybrid nanofibers/biopolymer hydrogels to external stimuli, the nanofibers being composed of G-C18:1 containing calcium, as described in **Chapter III** ({F}G-C18:1). The present work combines rheology with small angle X-ray scattering (SAXS), rheo-SAXS, to correlate, *in situ*, the structural and mechanical properties of hybrid {F}G-C18:1-biopolymer hydrogels upon application of two different stimuli: pH and temperature. Experiments were run at the Swing beamline of Soleil synchrotron (Saint-Aubin, France) using the in house Anton Paar rheometer, equipped with a couette cell. Further technical details are given in the joint publication.

4.3 Rheo-SAXS investigations of structural and mechanical properties of hybrid {F}G-C18:1-gelatin hydrogels

This chapter is structured as **Chapter III**: only experiments regarding gelatin, our reference system, are shown and discussed. They are reproduced using alginate and chitosan, related conclusions are integrated in **Project paper V**.

4.3.1 PH effect

First, rheology and SAXS control experiments (not performed *in situ*) regarding gelatin are presented in Figure 44, left and right respectively. Mechanical properties of gelatin at a concentration of 2 wt% are slightly higher at pH 8 than pH 6 (50 vs. 20 Pa, Figure 44, left), while its structure is not significantly changed according to Figure 44, right: the slope of SAXS profiles is different at pH 6 and pH 8 (higher at pH 8 than at pH 6, red vs. blue profile), meaning that the radius of gyration (extracted from the Guinier law, **Eq.2**), reflecting polymer-polymer interactions, is different.³⁴⁷ This is due to a different aggregation state of the polymer, which is explained by a different charge density: at pH 8, gelatin is closer to its isoelectric point than at pH 6, charge density is thus decreased as well as repulsive interactions, which results in a more compacted structure and so a lower radius of gyration.

$$\begin{aligned}
 P(Q) &= \frac{1}{N^2} \sum_{i=1}^N \sum_{j=1}^N \left[1 - \frac{(QR_{ij})^2}{3!} + \dots \right] \\
 &= 1 - \frac{(QR_g)^2}{3} + \dots \approx \exp\left(-\frac{Q^2 \langle R_g^2 \rangle}{3}\right)
 \end{aligned}
 \tag{Eq. 2}$$

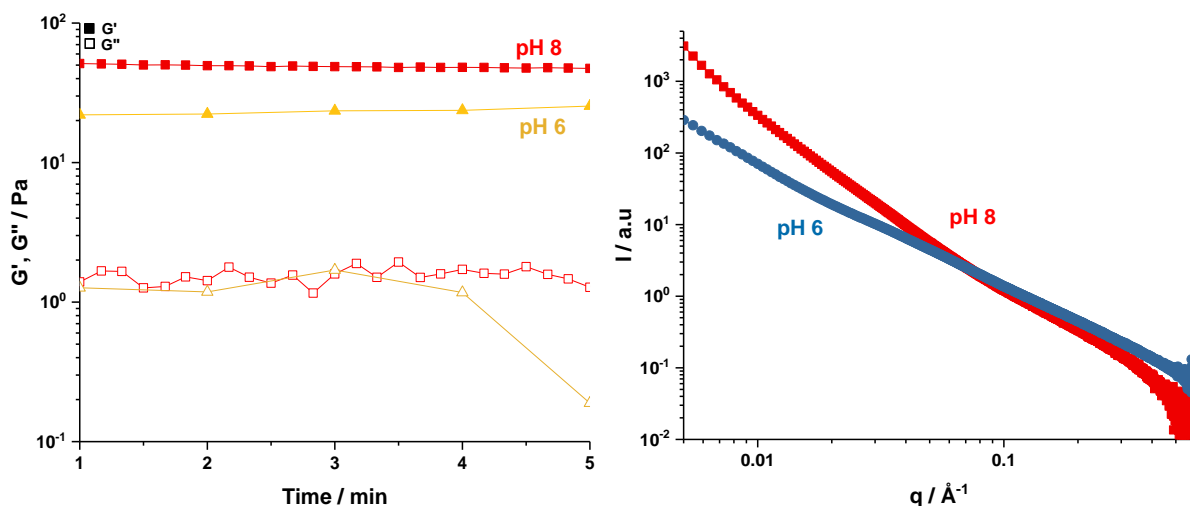


Figure 44 – Rheology (left) and SAXS (right) profiles of gelatin (2 wt%) recorded at pH 6 and 8

Mechanical properties and structural data of {F}G-C18:1 at pH 8 are respectively known from Figure 33 and Figure 34 in **Chapter III** (page 75). No data are available at pH 6 as the fibers disassemble below pH 7: calcium induces precipitation of G-C18:1 under acidic conditions, probably due to the formation of a lamellar structure.¹²⁶

In order to study the effect of phase transitions in the {F}G-C 18:1/gelatin hydrogel induced by GDL in an *in situ* rheo-SAXS environment, we needed to perform some preliminary optimization tests. First, the GDL quantity employed (quantities were calculated in equivalent regarding G-C18:1), and then adapting concentrations for a better GDL dispersion.

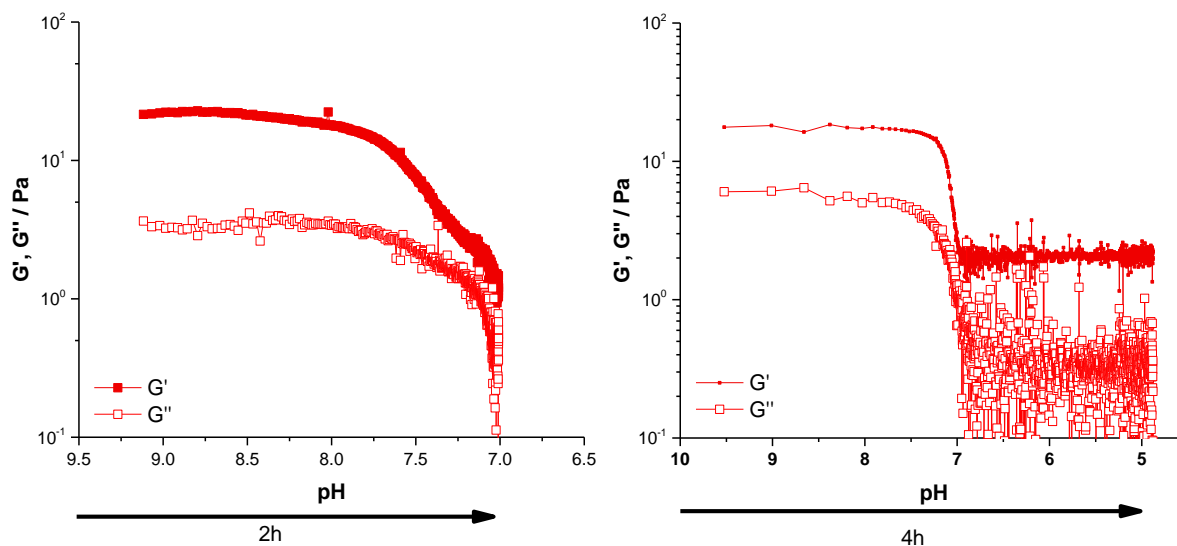


Figure 45 – *In situ* acidification of {F}G-C18:1/gelatin gels (2-2 wt%) using (1 eq) 7.7 mg.mL⁻¹ GDL (left) or (2 eq) 15.4 mg.mL⁻¹ GDL (right)

According to Figure 45, left, 7.7 mg.mL⁻¹ of GDL (for 2 wt% {F}G-C18 :1) is not a sufficient quantity to explore properties below pH 7. Increasing GDL quantity up to 15.4 mg.mL⁻¹ for the same lipid content allows to overcome this point, but we encountered reproducibility issues, which we attributed to the high viscosity of the medium, causing poor homogeneity during GDL dispersion. To solve this

problem, we decided to work with diluted solutions (factor 2) of {F}G-C18:1 and gelatin, and we adapted the quantity of GDL employed to 10 mg.mL⁻¹. Results are shown in Figure 46, left.

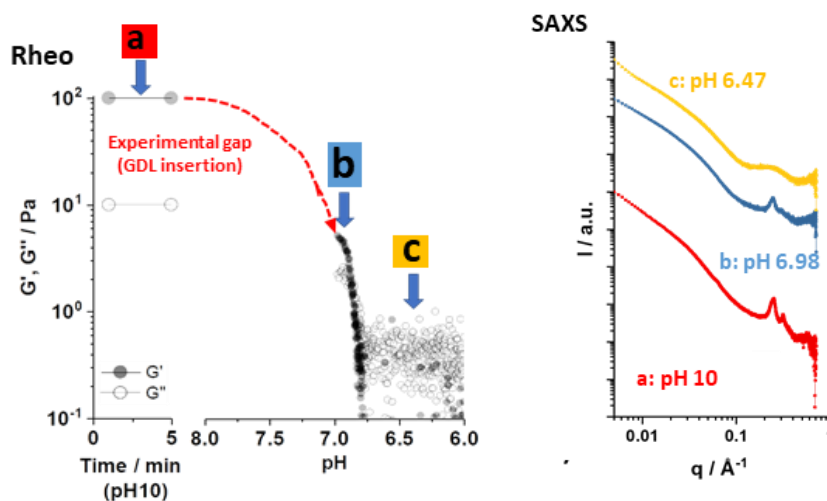


Figure 46 – pH effects on {F}G-C18:1-gelatin hydrogels' mechanical properties (left) and corresponding SAXS profiles (right) at pH 10 (a), pH 6.98 (b) and pH 6.47 (c).

Rheological data show that pH lowering triggers a loss of mechanical properties from 100 Pa to below 1 Pa, associated to a loss of structure according to the disappearance of the fiber structural peaks ($q_1=0.24 \text{ \AA}^{-1}$, $q_2=0.3 \text{ \AA}^{-1}$ and $q_3=0.47 \text{ \AA}^{-1}$)¹²⁶ by SAXS from pH 10 (a) to 6.47 (c) (Figure 46-right).

Does the way phase transitions are triggered impact the resulting mechanical properties?

We have just concluded that {F}G-C18:1/gelatin gels lose their viscoelastic properties at pH 6, but it is legitimate to wonder if this effect is real, as we obtained not so bad {V}G-C18:1/ gelatin gels in **Chapter III**. However, the experiments were repeated at least three times on the rheometer with a plate-plate geometry (normal force fixed to 0) and at synchrotron using a couette cell, the only hypothesis is that there is an influence of the way phase transitions are triggered. Experiments were performed to test this hypothesis and related results are given in Figure 47. Two procedures are opposed to prepare gels: the first one is closely related to the work performed under diluted conditions and consists in mixing both polymer and surfactant at pH \approx 8 before lowering the pH down to 6 (red squares), while the second one simply consists in mixing both solutions directly at pH 6 (blue squares). According to Figure 47, the final properties are decreased when the procedure with pH change was used, but in both cases the gel is quite strong at pH 6. These results seem in contradiction with the loss of elastic properties displayed at pH 6 in Figure 46, but we identified an effect of time on the elastic properties: when a sample typically prepared by *in situ* acidification as in Figure 46 was left overnight, it partially recovered its elasticity the day after.

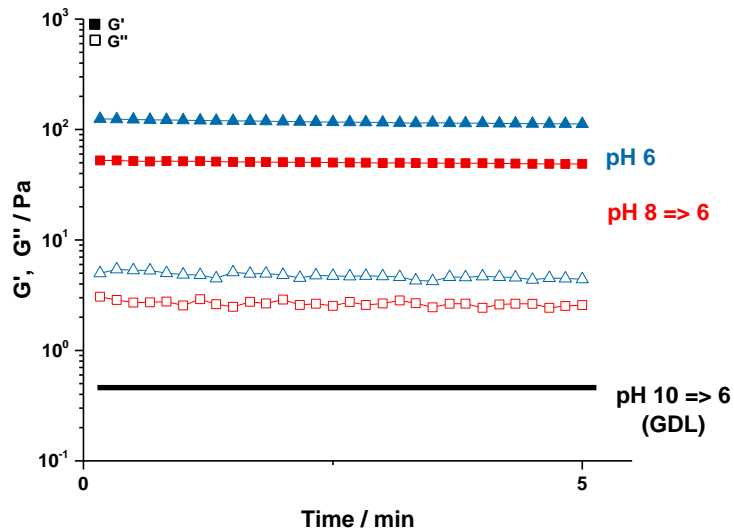


Figure 47 – Loss and storage modulus of {Ca}G-C18:1 + gelatin gels prepared either directly at pH 6 (blue triangles) either through a pH 8 -> 6 change (red squares) (black lines reminds the mechanical properties at pH 6 following GDL-induced acidification)

This qualitative argument is supported by the experiment shown in Figure 48. A hybrid {F}G-C18:1 + gelatin (2-2wt%, pH 8) sample is prepared and split in two separate vials. Both vials are left at rest during 2h30. The first vial is then analyzed during 15 min (Figure 48, left) and the elastic modulus reaches a pseudo-plateau at about 100 Pa. At this moment, the pH of the second vial is decreased to 6 and its properties are rapidly recorded over time. Indeed, the elastic modulus of the gel of which the pH is decreased to 6 is weaker by about one order of magnitude than the initial gel at pH 8, although it is still a gel and not a sol, as observed during the *in situ*, GDL-induced, decrease of pH (Figure 46, left). As hypothesized, when the gel at pH 6 is left at rest in the rheometer, its elastic modulus slowly increases over time (Figure 7, right). The abrupt increase in the elastic modulus above 4000 s (Figure 48, right) shows the effect of drying on the gel and it validates, again, our methodological choices to work.

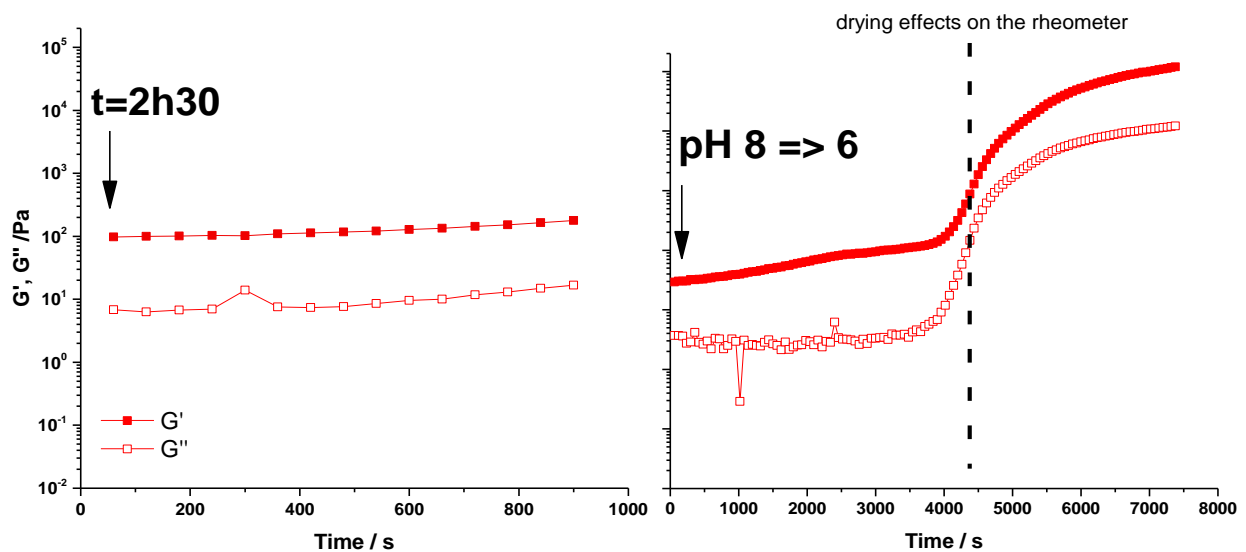


Figure 48 – Mechanical properties of {Ca}G-C18:1 + gelatin (2-2wt%, pH 8) gel recorded 2h after sample preparation (left), and after the pH is decreased to 6. Sudden increase in G' after 4000 s is due to drying.

4.3.2 Temperature effect

The same approach was used to investigate the effect of temperature at fixed pH by programming a heating/cooling temperature gradient from 20 to 50°C on the rheometer. If the results are given and commented in **Project paper V**, we show hereafter the approach to select the rate of temperature variation (eventually, 1°C.min⁻¹).

We mentioned in **Chapter III** that resulting mechanical properties of the gels do not depend on the calcium addition rate. The influence of the pH change rate was not investigated because it does not seem to play an important role for {F}G-C18:1. On the contrary, we do test the rate of temperature change, known to have an effect on the fibrillation of SAFIN.^{348,349}

Temperature of the {F}G-C18:1/gelatin hybrid gel has been changed at two different rates (1 and 10°C.min⁻¹, from 20 to 50°C, Figure 49 – Mechanical properties of a {Ca}G-C18:1 gel in function of temperature at to different heating/cooling rates). The initial G' at $t = 0$ ($T = 20^\circ\text{C}$) are slightly different due to different aging of the samples. This aspect is not relevant for the present experiment. The expected gel-sol transition occurs around 45°C in both cases because of the known temperature-dependent network softening of both gelatin and {F}G-C18:1 (the latter studied in parallel by A. Poirier at LCMCP). Upon cooling, both experiments show recovery of mechanical properties around 40°C. This is interesting because it shows that the material does not have a « heat » memory and its properties do not depend on its previous heating-cooling cycle.

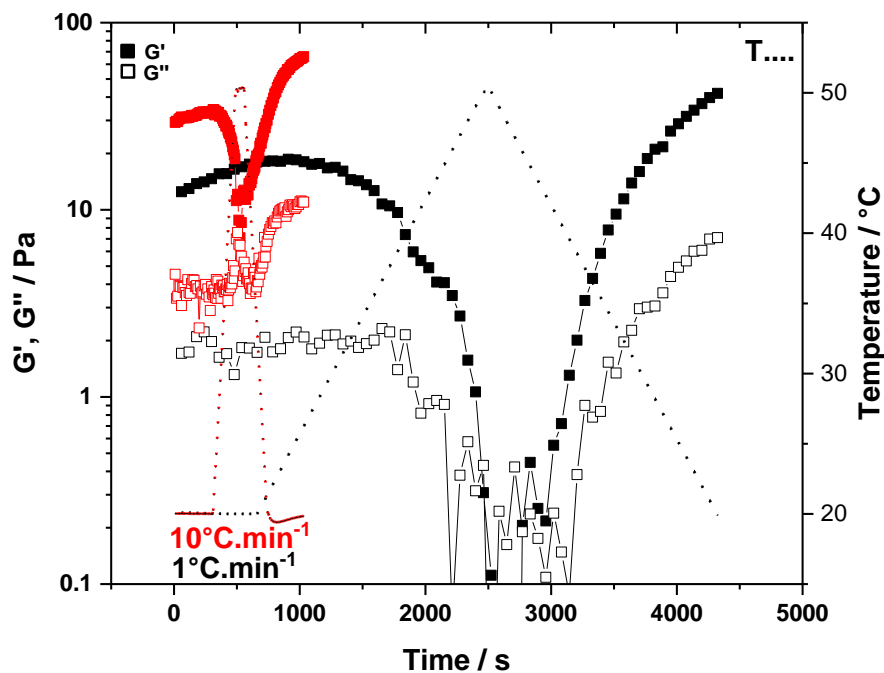


Figure 49 – Mechanical properties of a {Ca}G-C18:1 gel in function of temperature at to different heating/cooling rates

Same approaches were used with other biopolymers (alginate and chitosan), related results are presented in the following paper.

CONCLUSION – PERSPECTIVES

This section not only aims at summarizing the main results presented in this manuscript but will more largely try to replace them in the existing literature and highlight the most significant perspectives. The field of biosurfactants is quite young, but benefits from a solid specific knowledge acquired at the Laboratoire de Chimie de la Matière Condensée, which has inspired the work of this PhD project, which finally adds some new aspects to this growing literature. It is worth noticing that due to the double identity of biosurfactants (surfactants and lipids), this work does not only complete literature related to (bio)surfactants, but more largely the one of bioamphiphiles.

First, we evidenced in **Chapter I** the formation of complex coacervates, generalized between biosurfactants and oppositely charged polyelectrolytes in alkaline pH conditions. This was already widely reported for chemical surfactants, especially by Dubin *et al.*^{7,226,228,234,350–352} However, it is quite rare to propose a crossed SAXS/cryo-TEM analysis, which allows us to draw clear and robust conclusions. An unprecedented aspect of our work is also to study the complexes' phase diagrams under nonequilibrium conditions. This is possible due to the ability of biosurfactants to switch from one phase to another upon pH change, while studies were rather performed under pseudo equilibrium conditions up to now, often inside the micellar or vesicular region of surfactants' phase diagrams. The becoming of complex coacervates when the pH is lowered only depends on the biosurfactant: if this latter undergoes a micelle-to-fiber phase transition, fibers coexist with the biopolymer, while a vesicle-forming biosurfactant is still intimately interacting with the polymer within multilamellar structures. This kind of structures was already reported but never as the result of a micelle-to-vesicle phase transition from a complex coacervate, a process that we found crucial to obtain precise structures with well-defined layers and large lumen. A control over their size is possible through classical methods such as filtration or ultrasounds. All these results enrich the young literature about biosurfactants which attracts increasing interest, and especially the literature related to biosurfactant-polymer interactions, still quite poor according to our review.⁸³ In addition, most of the reported studies present systems with novel properties where biosurfactant and biopolymers coexist without any specific interaction, but not relying on mutual interactions, such as hydrophobic or electrostatic.

We also report in **Chapter II** a simple method to encapsulate curcumin within these multilamellar structures and the whole system was found to disturb cancer cells' (HeLa) viability but not fibroblasts' one *via* a precise mechanism of membrane fusion and curcumin release. The procedure was extended to other hydrophobic drugs. In this context of drug release, recent works developed rhamnolipids-based nanostructured lipid carriers whose stability and crystallinity can be controlled,³⁵³ or stable vesicles self-assembled from phospholipid and mannosylerythritol lipid for anthocyanins encapsulation.³⁵⁴

In the field of biosurfactants, hydrogelation has been reported only recently and for a limited number of molecules. This is among the first reports of the combination of a biosurfactant with gelling polymers for this purpose and is so a first step towards further investigations and discoveries, playing on the biosurfactant and/or the biopolymer among other parameters. Surfactin-reinforced gelatin methacrylate hydrogel were for example recently synthesized and was found to accelerate

diabetic wound healing by regulating the macrophage polarization and promoting angiogenesis³⁵⁵ (We note that it requires a step of functionalization of gelatin).

There exists a large literature related to mechanical reinforcement or stimuli-responsivity of polymer hydrogels. We prepared fully biobased hydrogels exhibiting both properties: they do not only exhibit enhanced mechanical properties, discussed in **Chapter III**, but a multi stimuli responsivity, which is the object of **Chapter IV**. Gelatin-based hybrid hydrogels involve gelatin which brings temperature-responsivity and G-C18:1, which is pH-responsive and whose phase behavior drives the mechanical properties. Within its fibrillary state, in presence of calcium, it increases the mechanical properties of the hybrid gel. Mechanical reinforcement is also displayed using alginate or chitosan. pH sensitivity is also true for alginate and chitosan-based gels, but temperature does not have any effect on these gels. Compared to literature, the synthesis of biosurfactant-biopolymer hybrid networks is very simple: components are mixed in water with minimum constraints, the synthesis is performed in mild conditions and does not require any crosslinker neither organic chemistry reaction. They also open the door to more biomedical applications due to their biological origin. The most recent reviews about hybrid polymer hydrogels highlight how they have revolutionized the field of hydrogels, especially how they have enhanced the functionality of biopolymer hydrogels, but also point some remaining lacks, including hybrid polymer hydrogels mechanical properties and structure. For example, mimicking anisotropy or tension-compression linearity, important for load-bearing tissues, remains challenging. Incorporation of 3D bioprinted or woven fibers into hybrid polymer hydrogels is expected to provide control over internal architecture and mechanical properties at multiple length scales and one can think about further studies to tune the fiber arrangement to replicate the native organization of collagen fibers within load bearing tissues. There is no argument against the potential use of {F}G-C18:1 fibers for this project.

The availability and cost of biosurfactants could be discussed and partly restrain the « biosurfactants revolution » and the complete replacement of petrochemical surfactants by biosurfactant, but we can hope that an increasing demand triggers an increasing production and decreasing prices, in parallel with an increasing understanding of their properties in solution for an optimal use.

References

- (1) Holmberg, K.; Jönsson, B.; Kronberg, B.; Lindman, B. Ch. 13 Surfactant-Polymer Systems. *Surfactants Polym. Aqueous Solut.* **2002**, 277–303.
- (2) Navascues, G. Liquid Surfaces: Theory of Surface Tension. *Reports Prog. Phys.* **1979**, 42, 1131–1186.
- (3) Bergström, L. M. A Theoretical Investigation of the Influence of the Second Critical Micelle Concentration on the Solubilization Capacity of Surfactant Micelles. *AIP Adv.* **2018**, 8, 055136.
- (4) Breuer, M. M.; Robb, I. D. Interactions between Macro-Molecules and Detergent. *Chem. Ind.* **1972**, 530–535.
- (5) Lange, H. Interaction between Sodium Alkyl Sulfates and Polyvinylpyrrolidone in Aqueous Solutions. *Kolloid-Z. Z. Polym.* **1971**, 243, 101.
- (6) Gradzielski, M.; Hoffmann, I. Polyelectrolyte-Surfactant Complexes (PESCs) Composed of Oppositely Charged Components. *Curr. Opin. Colloid Interface Sci.* **2018**, 35, 124–141.
- (7) Kizilay, E.; Kayitmazer, A. B.; Dubin, P. L. Complexation and Coacervation of Polyelectrolytes with Oppositely Charged Colloids. *Adv. Colloid Interface Sci.* **2011**, 167, 24–37.
- (8) Ferreira, G. A.; Loh, W. Liquid Crystalline Nanoparticles Formed by Oppositely Charged Surfactant-Polyelectrolyte Complexes. *Curr. Opin. Colloid Interface Sci.* **2017**, 32, 11–22.
- (9) Lindman, B.; Antunes, F.; Aidarova, S.; Miguel, M.; Nylander, T. Polyelectrolyte-Surfactant Association—from Fundamentals to Applications. *Colloid J.* **2014**, 76, 585–594.
- (10) Oparin, a I. The Origin of Life. *Nord. Med.* **1961**, 65, 693–697.
- (11) Fukuoka, T.; Morita, T.; Konishi, M.; Imura, T.; Sakai, H.; Kitamoto, D. Structural Characterization and Surface-Active Properties of a New Glycolipid Biosurfactant, Mono-Acylated Mannosylerythritol Lipid, Produced from Glucose by *Pseudozyma Antarctica*. *Appl. Microbiol. Biotechnol.* **2007**, 76, 801–810.
- (12) Schmitt, C.; Turgeon, S. L. Protein/Polysaccharide Complexes and Coacervates in Food Systems. *Adv. Colloid Interface Sci.* **2011**, 167, 63–70.
- (13) Winslow, B. D.; Shao, H.; Stewart, R. J.; Tresco, P. A. Biocompatibility of Adhesive Complex Coacervates Modeled after the Sandcastle Glue of *P. Californica* for Craniofacial Reconstruction. *Biomaterials* **2010**, 31, 9373–9381.
- (14) Chu, H.; Gao, J.; Chen, C.-W.; Huard, J.; Wang, Y. Injectable Fibroblast Growth Factor-2 Coacervate for Persistent Angiogenesis. *Proc. Natl. Acad. Sci.* **2011**, 108, 13444–13449.
- (15) Johnson, N. R.; Wang, Y. Coacervate Delivery Systems for Proteins and Small Molecule Drugs. *Expert Opin. Drug Deliv.* **2014**, 11, 1829–1832.
- (16) Hwang, D. S.; Zeng, H.; Srivastava, A.; Krogstad, D. V.; Tirrell, M.; Israelachvili, J. N.; Waite, J. H. Viscosity and Interfacial Properties in a Mussel-Inspired Adhesive Coacervate. *Soft Matter* **2010**, 6, 3232–3236.
- (17) Kim, S.; Yoo, H. Y.; Huang, J.; Lee, Y.; Park, S.; Park, Y.; Jin, S.; Jung, Y. M.; Zeng, H.; Hwang, D. S.; et al. Salt Triggers the Simple Coacervation of an Underwater Adhesive When Cations Meet Aromatic π Electrons in Seawater. *ACS Nano* **2017**, 11, 6764–6772.

- (18) Baccile, N.; Reboul, J.; Blanc, B.; Coq, B.; Lacroix-Desmazes, P.; In, M.; Gérardin, C. Ecodesign of Ordered Mesoporous Materials Obtained with Switchable Micellar Assemblies. *Angew. Chemie - Int. Ed.* **2008**, *47*, 8433–8437.
- (19) Chiappisi, L.; Simon, M.; Gradzielski, M. Toward Bioderived Intelligent Nanocarriers for Controlled Pollutant Recovery and PH-Sensitive Binding. *ACS Appl. Mater. Interfaces* **2015**, *7*, 6139–6145.
- (20) Zhao, W.; Fan, Y.; Wang, H.; Wang, Y. Coacervate of Polyacrylamide and Cationic Gemini Surfactant for the Extraction of Methyl Orange from Aqueous Solution. *Langmuir* **2017**, *33*, 6846–6856.
- (21) Saxena, A.; Antony, T.; Bohidar, H. B. Dynamic Light Scattering Study of Gelatin-Surfactant Interactions. *J. Phys. Chem. B* **1998**, *102*, 5063–5068.
- (22) Chiappisi, L.; Gradzielski, M. Co-Assembly in Chitosan-Surfactant Mixtures: Thermodynamics, Structures, Interfacial Properties and Applications. *Adv. Colloid Interface Sci.* **2015**, *220*, 92–107.
- (23) Onesippe, C.; Lagerge, S. Study of the Complex Formation between Sodium Dodecyl Sulfate and Chitosan. *Colloids Surfaces A Physicochem. Eng. Asp.* **2008**, *317*, 100–108.
- (24) Neumann, M. G.; Schmitt, C. C.; Iamazaki, E. T. A Fluorescence Study of the Interactions between Sodium Alginate and Surfactants. *Carbohydr. Res.* **2003**, *338*, 1109–1113.
- (25) Yang, J.; Zhao, J.; Fang, Y. Calorimetric Studies of the Interaction between Sodium Alginate and Sodium Dodecyl Sulfate in Dilute Solutions at Different PH Values. *Carbohydr. Res.* **2008**, *343*, 719–725.
- (26) Bu, H.; Kjøniksen, A. L.; Elgsaeter, A.; Nyström, B. Interaction of Unmodified and Hydrophobically Modified Alginate with Sodium Dodecyl Sulfate in Dilute Aqueous Solution: Calorimetric, Rheological, and Turbidity Studies. *Colloids Surfaces A Physicochem. Eng. Asp.* **2006**, *278*, 166–174.
- (27) Bu, H.; Kjøniksen, A. L.; Knudsen, K. D.; Nyström, B. Characterization of Interactions in Aqueous Mixtures of Hydrophobically Modified Alginate and Different Types of Surfactant. *Colloids Surfaces A Physicochem. Eng. Asp.* **2007**, *293*, 105–113.
- (28) Li, Y.; McClements, D. J. Influence of Non-Ionic Surfactant on Electrostatic Complexation of Protein-Coated Oil Droplets and Ionic Biopolymers (Alginate and Chitosan). *Food Hydrocoll.* **2013**, *33*, 368–375.
- (29) Bonnaud, M.; Weiss, J.; McClements, D. J. Interaction of a Food-Grade Cationic Surfactant (Lauric Arginate) with Food-Grade Biopolymers (Pectin, Carrageenan, Xanthan, Alginate, Dextran, and Chitosan). *J. Agric. Food Chem.* **2010**, *58*, 9770–9777.
- (30) Hayakawa, K.; Santerre, J. P.; Kwak, J. C. T. Study of Surfactant-Polyelectrolyte Interactions. Binding of Dodecyl- and Tetradecyltrimethylammonium Bromide by Some Carboxylic Polyelectrolytes. *Macromolecules* **1983**, *16*, 1642–1645.
- (31) Yang, J.; Chen, S.; Fang, Y. Viscosity Study of Interactions between Sodium Alginate and CTAB in Dilute Solutions at Different PH Values. *Carbohydr. Polym.* **2009**, *75*, 333–337.
- (32) Abed, M. A.; Bohidar, H. B. Surfactant Induced Softening in Gelatin Hydrogels. *Eur. Polym. J.* **2005**, *41*, 2395–2405.
- (33) Bamgbose, J. T.; Nkiko, M. O.; Bamigbade, A. A.; Dare, E. O. Interactions of Cross-Linked and Uncross-Linked Chitosan Hydrogels with Surfactants for Biomedical Applications. *Ife J. Sci.*

- 2014**, *16*, 341-351–351.
- (34) Kaygusuz, H.; Evingür, G. A.; Pekcan, Ö.; von Klitzing, R.; Erim, F. B. Surfactant and Metal Ion Effects on the Mechanical Properties of Alginate Hydrogels. *Int. J. Biol. Macromol.* **2016**, *92*, 220–224.
 - (35) Kahya, N.; Erim, F. B. Surfactant Modified Alginate Composite Gels for Controlled Release of Protein Drug. *Carbohydr. Polym.* **2019**, *224*, 115165.
 - (36) Stoppel, W. L.; White, J. C.; Horava, S. D.; Bhatia, S. R.; Roberts, S. C. Transport of Biological Molecules in Surfactant-Alginate Composite Hydrogels. *Acta Biomater.* **2011**, *7*, 3988–3998.
 - (37) Jabeen, S.; Chat, O. A.; Maswal, M.; Ashraf, U.; Rather, G. M.; Dar, A. A. Hydrogels of Sodium Alginate in Cationic Surfactants: Surfactant Dependent Modulation of Encapsulation/Release toward Ibuprofen. *Carbohydr. Polym.* **2015**, *133*, 144–153.
 - (38) Djabourov, M. Architecture of Gelatin Gels. *Contemp. Phys.* **1988**, *29*, 273.
 - (39) Pankhurst, K. G. A.; Smith, R. C. M. The Adsorption of Paraffin-Chain Salts to Proteins. Part I. Some Factors Influencing the Formation and Separation of Complexes between Gelatin and Dodecyl Sodium Sulfate. *Trans. Faraday Soc.* **1944**, *40*, 465.
 - (40) Tamaki, K.; Tamamushi, B. The Interaction of Gelatin Molecule with Surface Active Ions. *Bull. Chem. Soc. Jpn.* **1955**, *28*, 555.
 - (41) Know, W. J.; Wright, J. F. The Interaction of Sodium Dodecyl Sulfate with Gelatin. *J. Colloid Sci.* **1965**, *20*, 177.
 - (42) Zargar, V.; Asghari, M.; Dashti, A. A Review on Chitin and Chitosan Polymers : Structures, Chemistry, Solubility, Derivatives, and Applications. *Chem. Bio. Eng. Rev.* **2015**, *2*, 204–226.
 - (43) Ullah, S.; Zainol, I.; Idrus, R. H. Incorporation of Zinc Oxide Nanoparticles into Chitosan-Collagen 3D Porous Scaffolds : Effect on Morphology, Mechanical Properties and Cytocompatibility of 3D Porous Scaffolds. *Int. J. Biol. Macromol.* **2017**, *104*, 1020–1029.
 - (44) Schwarz, G. Cooperative Binding to Linear Biopolymers. 1. Fundamental Static and Dynamic Properties. *Eur. J. Biochem.* **1970**, *12*, 442–453.
 - (45) Satake, I.; Yang, J. T. Interaction of Sodium Decyl Sulfate with Poly(L-ornithine) and Poly(L-lysine) in Aqueous Solution. *Biopolymers* **1976**, *15*, 2263–2275.
 - (46) Wei, Y.; Hudson, S. Binding of Sodium Dodecyl Sulfate to a Polyelectrolyte Based on Chitosan. *Macromolecules* **1993**, *26*, 4151–4154.
 - (47) Demarger-André, S.; Domard, A. Chitosan Carboxylic Acid Salts in Solution and in the Solid State. *Carbohydr. Polym.* **1994**, *23*, 211–219.
 - (48) Bonferoni, M. C.; Sandri, G.; Dellera, E.; Rossi, S.; Ferrari, F.; Mori, M. Ionic Polymeric Micelles Based on Chitosan and Fatty Acids and Intended for Wound Healing. Comparison of Linoleic and Oleic Acid. *Eur. J. Pharm. Biopharm.* **2014**, *87*, 101–106.
 - (49) Demarger-André, S.; Domard, A. Chitosan Behaviours in a Dispersion of Undecylenic Acid. *Carbohydr. Polym.* **1993**, *22*, 117–126.
 - (50) Demarger-André, S.; Domard, A. Chitosan Behaviours in a Dispersion of Undecylenic Acid. Structural Parameters. *Carbohydr. Polym.* **1994**, *24*, 177–184.
 - (51) Demarger-André, S.; Domard, A. Chitosan Behaviours in a Dispersion of Undecylenic Acid. Morphological Aspects. *Carbohydr. Polym.* **1995**, *27*, 101–107.

- (52) Chiappisi, L.; Prévost, S.; Gradzielski, M. Chitosan/Alkylethoxy Carboxylates: A Surprising Variety of Structures. *Langmuir* **2014**, *30*, 1778–1787.
- (53) Jovic, D.; Julià, M. R.; Erra, P. The Time-Dependence of Chitosan/Nonionic Surfactant Solution Viscosity. *Colloid Polym. Sci.* **1996**, *274*, 375–383.
- (54) Jovic, D.; Julià, M. R.; Erra, P.; Jovic, D.; Julih, M. R. Application of a Chitosan/Nonionic Surfactant Mixture to Wool Assessed by Dyeing with a Reactive Dye. *J. Soc. Dye. Colour* **2008**, *113*, 25–31.
- (55) Chatterjee, S.; Chatterjee, T.; Woo, S. H. Effect of Chitosan Addition on Phenanthrene Solubilization in Anionic or Cationic Surfactant Solutions. *Desalin Water Treat* **2012**, *37*, 253–258.
- (56) Martinsen, A.; Skjaak-Braek, G.; Smidsroed, O. Alginate as Immobilization Material : I. Correlation between Chemical and Physical Properties of Alginate Gel Be ads. *Biotechnol. Bioeng.* **1989**, *33*, 79–89.
- (57) Rowley, J. A.; Madlambayan, G.; Mooney, D. J. Alginate Hydrogels as Synthetic Extracellular Matrix Materials. *Biomaterials* **1999**, *20*, 45–53.
- (58) Fleischfresser, B. E. The Interaction of Positively Charged Polymer Particles with Wool Fibers. *Text. Res. J.* **1982**, *52*, 328–334.
- (59) Antunes, F. E.; Marques, E. F.; Miguel, M. G.; Lindman, B. Polymer-Vesicle Association. *Adv. Colloid Interface Sci.* **2009**, *147–148*, 18–35.
- (60) Lee, J. H.; Gustin, J. P.; Chen, T.; Payne, G. F.; Raghavan, S. R. Vesicle-Biopolymer Gels: Networks of Surfactant Vesicles Connected by Associating Biopolymers. *Langmuir* **2005**, *21*, 26–33.
- (61) Dhand, A. P.; Galarraga, J. H.; Burdick, J. A. Enhancing Biopolymer Hydrogel Functionality through Interpenetrating Networks. *Trends Biotechnol.* **2021**, *39*, 519–538.
- (62) Zhang, Y. S.; Khademhosseini, A. Advances in Engineering Hydrogels. *Science* **2017**, *356*, 3627.
- (63) Neves, S. C. Leveling up Hydrogels : Hybrid Systems in Tissue Engineering. *Trends Biotechnol.* **2020**, *38*, 292–315.
- (64) Shin, M. S.; Kim, S. J.; Park, S. J.; Lee, Y. H.; Kim, S. I. Synthesis and Characteristics of the Interpenetrating Polymer Network Hydrogel Composed of Chitosan and Polyallylamine. *J. Appl. Polym. Sci.* **2002**, *86*, 498–503.
- (65) Warriner, H. E.; Idziak, S. H.; Slack, N. L.; Davidson, P.; Safinya, C. R. Lamellar Biogels: Fluid-Membrane-Based Hydrogels Containing Polymer Lipids. *Science* **1996**, *271*, 969–973.
- (66) Ilyas, M.; Haque, M. A.; Yue, Y.; Kurokawa, T.; Nakajima, T.; Nonoyama, T.; Gong, J. P. Water-Triggered Ductile–Brittle Transition of Anisotropic Lamellar Hydrogels and Effect of Confinement on Polymer Dynamics. *Macromolecules* **2017**, *50*, 8169–8177.
- (67) Steck, K.; Esch, J. H. Van; Smith, D. K.; Stubenrauch, C. Tuning Gelled Lyotropic Liquid Crystals (LLCs) – Probing the Influence of Different Low Molecular Weight Gelators on the Phase Diagram of the System H₂O/NaCl–Genapol LA070. *Soft Matter* **2019**, *15*, 3111–3121.
- (68) Koitani, S.; Dieterich, S.; Preisig, N.; Aramaki, K.; Stubenrauch, C. Gelling Lamellar Phases of the Binary System Water-Didodecyldimethylammonium Bromide with an Organogelator. *Langmuir* **2017**, *33*, 12171–12179.
- (69) Steck, K.; Preisig, N.; Stubenrauch, C. Gelling Lyotropic Liquid Crystals with the Organogelator

- 1,3:2,4-Dibenzylidene-d-Sorbitol Part II: Microstructure. *Langmuir* **2019**, *35*, 17142–17149.
- (70) Steck, K.; Stubenrauch, C. Gelling Lyotropic Liquid Crystals with the Organogelator 1,3:2,4-Dibenzylidene-d-Sorbitol Part I: Phase Studies and Sol-Gel Transitions. *Langmuir* **2019**, *35*, 17132–17141.
- (71) Dieterich, S.; Prévost, S.; Dargel, C.; Sottmann, T.; Giesselmann, F. Synergistic Structures in Lyotropic Lamellar Gels. *Soft Matter* **2020**, *16*, 10268–10279.
- (72) Dieterich, S.; Sottmann, T.; Giesselmann, F. Gelation of Lyotropic Liquid-Crystal Phases-The Interplay between Liquid Crystalline Order and Physical Gel Formation. *Langmuir* **2019**, *35*, 16793–16802.
- (73) Dieterich, S.; Stemmler, F.; Preisig, N.; Giesselmann, F. Micellar Lyotropic Nematic Gels. *Adv. Mater.* **2021**, *33*.
- (74) Stubenrauch, C.; Gießelmann, F. Gelled Complex Fluids: Combining Unique Structures with Mechanical Stability. *Angew. Chem. Int. Ed.* **2016**, *55*, 3268–3275.
- (75) Chiappisi, L.; Prévost, S.; Grillo, I.; Gradzielski, M. From Crab Shells to Smart Systems: Chitosan-Alkylethoxy Carboxylate Complexes. *Langmuir* **2014**, *30*, 10615–10616.
- (76) Weiss, R. G. The Past, Present, and Future of Molecular Gels. What Is the Status of the Field, and Where Is It Going? *Journal of the American Chemical Society*. 2014.
- (77) Chakraborty, P.; Roy, B.; Bairi, P.; Nandi, A. K. Improved Mechanical and Photophysical Properties of Chitosan Incorporated Folic Acid Gel Possessing the Characteristics of Dye and Metal Ion Absorption. *J. Mater. Chem* **2012**, *22*, 20291–20298.
- (78) Chen, L.; Revel, S.; Morris, K.; Spiller, D. G.; Serpell, L. C.; Adams, D. J. Low Molecular Weight Gelator–Dextran Composites. *Chem. Commun.* **2010**, *46*, 6738–6740.
- (79) Yang, C.; Bian, M.; Yang, Z. A Polymer Additive Boosts the Anti-Cancer Efficacy of Supramolecular Nanofibers of Taxol. *Biomater. Sci.* **2014**, *2*, 651–654.
- (80) Cornwell, D. J.; Smith, D. K. Expanding the Scope of Gels - Combining Polymers with Low-Molecular-Weight Gelators to Yield Modified Self-Assembling Smart Materials with High-Tech Applications. *Materials Horizons*. 2015.
- (81) Wang, J.; Wang, Z.; Gao, J.; Wang, L.; Yang, Z.; Kong, D.; Yang, Z. Incorporation of Supramolecular Hydrogels into Agarose Hydrogels - A Potential Drug Delivery Carrier. *J. Mater. Chem.* **2009**, *19*, 7892–7896.
- (82) Wang, J.; Wang, H.; Song, Z.; Kong, D.; Chen, X.; Yang, Z. A Hybrid Hydrogel for Efficient Removal of Methyl Violet from Aqueous Solutions. *Colloids Surf., B.* **2010**, *80*, 155–160.
- (83) Baccile, N.; Seyrig, C.; Poirier, A.; Castro, S. A.; Roelants, S. L. K. W.; Abel, S. Self-Assembly, Interfacial Properties, Interactions with Macromolecules and Numerical Modelling of Microbial Bio-Based Amphiphiles (Biosurfactants). A Tutorial Review. *Green Chem.* **2021**, *23*, 3842–3944.
- (84) Desai, J. D.; Banat, I. M. Microbial Production of Surfactants and Their Commercial Potential. *Microbiol. Mol. Biol. Rev.* **1997**, *61*, 47–64.
- (85) Cameotra, S. S.; Makkar, R. S.; Kaur, J.; Mehta, S. K. Synthesis of Biosurfactants and Their Advantages to Microorganisms and Mankind. *Adv. Exp. Med. Biol.* **2010**, *672*, 261–280.
- (86) Delbeke, E. I. P.; Movsisyan, M.; Van Geem, K. M.; Stevens, C. V. Chemical and Enzymatic Modification of Sophorolipids. *Green Chem.* **2016**, *18*, 76–104.

- (87) Mnif, I.; Ellouz-Chaabouni, S.; Ghribi, D. Glycolipid Biosurfactants, Main Classes, Functional Properties and Related Potential Applications in Environmental Biotechnology. *J. Polym. Environ.* **2018**, *26*, 2192–2206.
- (88) Coelho, A. L. S.; Feuser, P. E.; Carciofi, B. A. M.; de Andrade, C. J.; de Oliveira, D. Mannosylerythritol Lipids: Antimicrobial and Biomedical Properties. *Appl. Microbiol. Biotechnol.* **2020**, *104*, 2297–2318.
- (89) Van Bogaert, I. N. A.; Saerens, K.; De Muynck, C.; Develter, D.; Soetaert, W.; Vandamme, E. J. Microbial Production and Application of Sophorolipids. *Appl. Microbiol. Biotechnol.* **2007**, *76*, 23–34.
- (90) Lang, S. Biological Amphiphiles (Microbial Biosurfactants). *Curr. Opin. Colloid Interface Sci.* **2002**, *7*, 12–20.
- (91) Mukherjee, A. K.; Das, K. Microbial Surfactants and Their Potential Applications: An Overview. *Adv. Exp. Med. Biol.* **2010**, *672*, 54–64.
- (92) Benincasa, M.; Marqués, A.; Pinazo, A.; Manresa, A. Rhamnolipid Surfactants: Alternative Substrates, New Strategies. *Adv. Exp. Med. Biol.* **2010**, *672*, 170–184.
- (93) Marchant, R.; Banat, I. M. Microbial Biosurfactants: Challenges and Opportunities for Future Exploitation. *Trends in Biotechnology*. 2012.
- (94) Makkar, R. S.; Cameotra, S. S.; Banat, I. M. Advances in Utilization of Renewable Substrates for Biosurfactant Production. *AMB Express* **2011**, *1*, 5.
- (95) De, S.; Malik, S.; Ghosh, A.; Saha, R.; Saha, B. A Review on Natural Surfactants. *RSC Adv.* **2015**, *5*, 65757–65767.
- (96) Rodrigues, L. R. Microbial Surfactants: Fundamentals and Applicability in the Formulation of Nano-Sized Drug Delivery Vectors. *J. Colloid Interface Sci.* **2015**, *449*, 304–316.
- (97) Morita, T.; Fukuoka, T.; Imura, T.; Kitamoto, D. Mannosylerythritol Lipids: Production and Applications. *J. Oleo Sci.* **2015**, *64*, 133–141.
- (98) Paulino, B. N.; Pessôa, M. G.; Mano, M. C. R.; Molina, G.; Neri-Numa, I. A.; Pastore, G. M. Current Status in Biotechnological Production and Applications of Glycolipid Biosurfactants. *Appl. Microbiol. Biotechnol.* **2016**, *100*, 10265–10293.
- (99) Kitamoto, D.; Morita, T.; Fukuoka, T.; Konishi, M.; Imura, T. Self-Assembling Properties of Glycolipid Biosurfactants and Their Potential Applications. *Curr. Op. Coll. Interf. Sci.* **2009**, *14*, 315–328.
- (100) Dhasaiyan, P.; Prasad, B. L. V. Self-Assembly of Bolaamphiphilic Molecules. *Chem. Rec.* **2017**, *17*, 597–610.
- (101) Jahan, R.; Bodratti, A. M.; Tsianou, M.; Alexandridis, P. Biosurfactants, Natural Alternatives to Synthetic Surfactants: Physicochemical Properties and Applications. *Adv. Colloid Interface Sci.* **2020**, *275*, 102061.
- (102) Irfan-Maqsood, M.; Seddiq-Shams, M. Rhamnolipids: Well-Characterized Glycolipids with Potential Broad Applicability as Biosurfactants. *Ind. Biotechnol.* **2014**, *10*, 285–291.
- (103) Chen, W. C.; Juang, R. S.; Wei, Y. H. Applications of a Lipopeptide Biosurfactant, Surfactin, Produced by Microorganisms. *Biochem. Eng. J.* **2015**, *103*, 158–169.
- (104) Yamamoto, S.; Morita, T.; Fukuoka, T.; Imura, T.; Yanagidani, S.; Sogabe, A.; Kitamoto, D.; Kitagawa, M. The Moisturizing Effects of Glycolipid Biosurfactants, Mannosylerythritol Lipids,

- on Human Skin. *J. Oleo Sci.* **2012**, *61*, 407–412.
- (105) Rodrigues, L. R.; Teixeira, J. A. Biomedical and Therapeutic Applications of Biosurfactants. *Adv. Exp. Med. Biol.* **2010**, *672*, 75–87.
- (106) Garidel, P.; Kaconis, Y.; Heinbockel, L.; Wulf, M.; Gerber, S.; Munk, A.; Vill, V.; Brandenburg, K. Self-Organisation, Thermotropic and Lyotropic Properties of Glycolipids Related to Their Biological Implications. *Open Biochem. J.* **2015**, *9*, 49–72.
- (107) Mo, J.; Milleret, G.; Nagaraj, M. Liquid Crystal Nanoparticles for Commercial Drug Delivery. *Liq. Cryst. Rev.* **2017**, *5*, 69–85.
- (108) Mezzenga, R.; Seddon, J. M.; Drummond, C. J.; Boyd, B. J.; Schröder-Turk, G. E.; Sagalowicz, L. Nature-Inspired Design and Application of Lipidic Lyotropic Liquid Crystals. *Adv. Mater.* **2019**, *31*.
- (109) Ishigami, Y.; Gama, Y.; Nagahora, H.; Yamaguchi, M.; Nakahara, H.; Kamata, T. The PH-Sensitive Conversion of Molecular Aggregates of Rhamnolipid Biosurfactant. *Chem. Lett.* **1987**, *16*, 763–766.
- (110) Kitamoto, D.; Ghosh, S.; Ourisson, G.; Nakatani, Y. Formation of Giant Vesicles from Diacylmannosylerythritols, and Their Binding to Concanavalin A. *Chem. Commun.* **2000**, No. 10, 861–862.
- (111) Zhou, S.; Xu, C.; Wang, J.; Gao, W.; Akhverdiyeva, R.; Shah, V.; Gross, R. Supramolecular Assemblies of a Naturally Derived Sophorolipid. *Langmuir* **2004**, *20*, 7926–7932.
- (112) Imura, T.; Kawamura, D.; Ishibashi, Y.; Morita, T.; Sato, S.; Fukuoka, T.; Kikkawa, Y.; Kitamoto, D. Low Molecular Weight Gelators Based on Biosurfactants, Cellobiose Lipids by *Cryptococcus humicola*. *J. Oleo Sci.* **2012**, *61*, 659–664.
- (113) Tanford, C. *The Hydrophobic Effect: Formation of Micelles and Biological Membranes*; Wiley-Interscience, 1973.
- (114) Israelachvili, J. N.; Mitchell, D. J.; Ninham, B. W. Theory of Self-Assembly of Hydrocarbon Amphiphiles into Micelles and Bilayers. *J. Chem. Soc. Faraday Trans. 2* **1976**, *72*, 1525.
- (115) Israelachvili, J. N.; Ninham, B. W.; Mitchell, D. J. Theory of Self-Assembly of Lipids and Vesicles. *Biochim. Biophys. Acta* **1977**, *470*, 185–201.
- (116) Shen, H. H.; Thomas, R. K.; Chen, C. Y.; Darton, R. C.; Baker, S. C.; Penfold, J. Aggregation of the Naturally Occurring Lipopeptide, Surfactin, at Interfaces and in Solution: An Unusual Type of Surfactant? *Langmuir* **2009**, *25*, 4211–4218.
- (117) Baccile, N.; Selmane, M.; Le Griel, P.; Prévost, S.; Perez, J.; Stevens, C. V.; Delbeke, E.; Zibek, S.; Guenther, M.; Soetaert, W.; et al. PH-Driven Self-Assembly of Acidic Microbial Glycolipids. *Langmuir* **2016**.
- (118) Dhasaiyan, P.; Prévost, S.; Baccile, N.; Prasad, B. L. V. PH- and Time-Resolved in-Situ SAXS Study of Self-Assembled Twisted Ribbons Formed by Elaidic Acid Sophorolipids. *Langmuir* **2018**, *34*, 2121–2131.
- (119) Baccile, N.; Messaoud, G. Ben; Griel, P. Le; Cowieson, N.; Perez, J.; Geys, R.; Graeve, M. De; Roelants, S. L. K. W.; Soetaert, W. Palmitic Acid Sophorolipid Biosurfactant: From Self-Assembled Fibrillar Network (SAFin) To Hydrogels with Fast Recovery. *Philos. Trans. A* **2021**, *10.1098/rsta.2020.0343*.
- (120) Baccile, N.; LeGriel, P.; Prévost, S.; Everaert, B.; VanBogaert, I. N. A.; Roelants, S.; Soetaert, W.

Glucosomes: Glycosylated Vesicle-in-Vesicle Aggregates in Water from PH-Responsive Microbial Glycolipid. *ChemistryOpen* **2017**.

- (121) Baccile, N.; Cuvier, A.-S.; Prévost, S.; Stevens, C. V.; Delbeke, E.; Berton, J.; Soetaert, W.; Van Bogaert, I. N. A.; Roelants, S. Self-Assembly Mechanism of PH-Responsive Glycolipids: Micelles, Fibers, Vesicles, and Bilayers. *Langmuir* **2016**, *32*, 10881–10894.
- (122) Renterghem, L. Van; Guzzetta, F.; Le Griel, P.; Selmane, M.; Messaoud, G. Ben; Teng, T. T. S.; Lim, S.; Soetaert, W.; Roelants, S.; Julián-López, B.; et al. Easy Formation of Functional Liposomes in Water Using a PH-Responsive Microbial Glycolipid: Encapsulation of Magnetic and Upconverting Nanoparticles. *ChemNanoMat* **2019**, *5*, 1188–1201.
- (123) Dhasaiyan, P.; Banerjee, A.; Visaveliya, N.; Prasad, B. L. V. Influence of the Sophorolipid Molecular Geometry on Their Self-Assembled Structures. *Chem. Asian J.* **2013**, *8*, 369–372.
- (124) Cuvier, A. S.; Babonneau, F.; Berton, J.; Stevens, C. V.; Fadda, G. C.; Péhau-Arnaudet, G.; Le Griel, P.; Prévost, S.; Perez, J.; Baccile, N. Nanoscale Platelet Formation by Monounsaturated and Saturated Sophorolipids under Basic PH Conditions. *Chem. - A Eur. J.* **2015**, *21*, 19265–19277.
- (125) Cuvier, A. S.; Berton, J.; Stevens, C. V.; Fadda, G. C.; Babonneau, F.; Van Bogaert, I. N. A.; Soetaert, W.; Pehau-Arnaudet, G.; Baccile, N. PH-Triggered Formation of Nanoribbons from Yeast-Derived Glycolipid Biosurfactants. *Soft Matter* **2014**, *10*, 3950–3959.
- (126) Poirier, A. et al. *In preparation*.
- (127) Uhde, J.; Keller, M.; Sackmann, E.; Parmeggiani, A.; Frey, E. Internal Motility in Stiffening Actin-Myosin Networks. *Phys. Rev. Lett.* **2004**, *93*, 1–4.
- (128) Fuhrhop, J.-H.; Wang, T. Bolaamphiphiles. *Chem. Rev.* **2004**, *104*, 2901–2937.
- (129) Iwaura, R.; Yoshida, K.; Masuda, M.; Yase, K.; Shimizu, T. Spontaneous Fiber Formation and Hydrogelation of Nucleotide Bolaamphiphiles. *Chem. Mater.* **2002**, *14*, 3047–3053.
- (130) Graf, G.; Drescher, S.; Meister, A.; Dobner, B.; Blume, A. Self-Assembled Bolaamphiphile Fibers Have Intermediate Properties between Crystalline Nanofibers and Wormlike Micelles: Formation of Viscoelastic Hydrogels Switchable by Changes in PH and Salinity. *J. Phys. Chem. B* **2011**, *115*, 10478–10487.
- (131) Oliveira, I. S.; Lo, M.; Araújo, M. J.; Marques, E. F. Temperature-Responsive Self-Assembled Nanostructures from Lysine-Based Surfactants with High Chain Length Asymmetry: From Tubules and Helical Ribbons to Micelles and Vesicles. *Soft Matter* **2019**, *15*, 3700–3711.
- (132) Baccile, N.; Van Renterghem, L.; Le Griel, P.; Ducouret, G.; Brennich, M.; Cristiglio, V.; Roelants, S. L. K. W.; Soetaert, W. Bio-Based Glyco-Bolaamphiphile Forms a Temperature-Responsive Hydrogel with Tunable Elastic Properties. *Soft Matter* **2018**, *14*, 7859–7872.
- (133) Dhasaiyan, P.; Le Griel, P.; Roelants, S.; Redant, E.; Van Bogaert, I. N. A.; Prévost, S.; Prasad, B. L. V.; Baccile, N. Micelles versus Ribbons: How Congeners Drive the Self-Assembly of Acidic Sophorolipid Biosurfactants. *ChemPhysChem* **2017**, *18*, 643–652.
- (134) Ba, A. A.; Everaert, J.; Poirier, A.; Griel, P. Le; Soetaert, W.; Roelants, S. L. K. W.; Hermida-Merino, D.; Stevens, C. V.; Baccile, N. Synthesis and Self-Assembly of Aminyl and Alkynyl Substituted Sophorolipids. *Green Chem.* **2020**, *22*, 8323–8336.
- (135) Manet, S.; Cuvier, A. S.; Valotteau, C.; Fadda, G. C.; Perez, J.; Karakas, E.; Abel, S.; Baccile, N. Structure of Bolaamphiphile Sophorolipid Micelles Characterized with SAXS, SANS, and MD Simulations. *J. Phys. Chem. B* **2015**, *119*, 13113–13133.

- (136) Singh, P. K.; Mukherji, R.; Joshi-Navare, K.; Banerjee, A.; Gokhale, R.; Nagane, S.; Prabhune, A.; Ogale, S. Fluorescent Sophorolipid Molecular Assembly and Its Magnetic Nanoparticle Loading: A Pulsed Laser Process. *Green Chem.* **2013**, *15*, 943–953.
- (137) Champion, J. T.; Gilkey, J. C.; Lamparski, H.; Retterer, J.; Miller, R. M. Electron Microscopy of Rhamnolipid Morphology. *J. Colloid Interface Sci.* **1995**, *170*, 569–574.
- (138) Pornsunthorntawe, O.; Chavadej, S.; Rujiravanit, R. Solution Properties and Vesicle Formation of Rhamnolipid Biosurfactants Produced by *Pseudomonas Aeruginosa* SP4. *Colloids Surfaces B Biointerfaces* **2009**, *72*, 6–15.
- (139) Chen, M. L.; Penfold, J.; Thomas, R. K.; Smyth, T. J. P.; Perfumo, A.; Marchant, R.; Banat, I. M.; Stevenson, P.; Parry, A.; Tucker, I.; et al. Solution Self-Assembly and Adsorption at the Air-Water Interface of the Monorhamnolipid and Dirhamnolipid Rhamnolipids and Their Mixtures. *Langmuir* **2010**, *26*, 18281–18292.
- (140) Baccile, N.; Babonneau, F.; Jestin, J.; Pehau-Arnaudet, G.; Van Bogaert, I. Unusual, PH-Induced, Self-Assembly of Sophorolipid Biosurfactants. *ACS Nano* **2012**, *6*, 4763–4776.
- (141) Penfold, J.; Chen, M.; Thomas, R. K.; Dong, C.; Smyth, T. J. P.; Perfumo, A.; Marchant, R.; Banat, I. M.; Stevenson, P.; Parry, A.; et al. Solution Self-Assembly of the Sophorolipid Biosurfactant and Its Mixture with Anionic Surfactant Sodium Dodecyl Benzene Sulfonate. *Langmuir* **2011**, *27*, 8867–8877.
- (142) Dhasaiyan, P.; Pandey, P. R.; Visaveliya, N.; Roy, S.; Prasad, B. L. V. Vesicle Structures from Bolaamphiphilic Biosurfactants: Experimental and Molecular Dynamics Simulation Studies on the Effect of Unsaturation on Sophorolipid Self-Assemblies. *Chem. - A Eur. J.* **2014**, *20*, 6246–6250.
- (143) Imura, T.; Ikeda, S.; Aburai, K.; Taira, T.; Kitamoto, D. Interdigitated Lamella and Bicontinuous Cubic Phases Formation from Natural Cyclic Surfactin and Its Linear Derivative. *J. Oleo Sci.* **2013**, *62*, 499–503.
- (144) Déjugnat, C.; Diat, O.; Zemb, T. Surfactin Self-Assembles into Direct and Reverse Aggregates in Equilibrium and Performs Selective Metal Cation Extraction. *ChemPhysChem* **2011**, *12*, 2138–2144.
- (145) Sánchez, M.; Aranda, F. J.; Espuny, M. J.; Marqués, A.; Teruel, J. A.; Manresa, Á.; Ortiz, A. Aggregation Behaviour of a Dirhamnolipid Biosurfactant Secreted by *Pseudomonas Aeruginosa* in Aqueous Media. *J. Colloid Interface Sci.* **2007**, *307*, 246–253.
- (146) Shen, H. H.; Lin, T. W.; Thomas, R. K.; Taylor, D. J. F.; Penfold, J. Surfactin Structures at Interfaces and in Solution: The Effect of PH and Cations. *J. Phys. Chem. B* **2011**, *115*, 4427–4435.
- (147) Peters, K. C.; Mekala, S.; Gross, R. A.; Singer, K. D. Cooperative Self-Assembly of Helical Exciton-Coupled Biosurfactant-Functionalized Porphyrin Chromophores. *ACS Appl. Bio Mater.* **2019**, *2*, 1703–1713.
- (148) Imura, T.; Hikosaka, Y.; Worakitkanchanakul, W.; Sakai, H.; Abe, M.; Konishi, M.; Minamikawa, H.; Kitamoto, D. Aqueous-Phase Behavior of Natural Glycolipid Biosurfactant Mannosylerythritol Lipid A: Sponge, Cubic, and Lamellar Phases. *Langmuir* **2007**, *23*, 1659–1663.
- (149) Worakitkanchanakul, W.; Imura, T.; Fukuoka, T.; Morita, T.; Sakai, H.; Abe, M.; Rujiravanit, R.; Chavadej, S.; Minamikawa, H.; Kitamoto, D. Aqueous-Phase Behavior and Vesicle Formation of Natural Glycolipid Biosurfactant, Mannosylerythritol Lipid-B. *Colloids Surfaces B Biointerfaces*

- 2008**, *65*, 106–112.
- (150) Inoh, Y.; Furuno, T.; Hirashima, N.; Kitamoto, D.; Nakanishi, M. Synergistic Effect of a Biosurfactant and Protamine on Gene Transfection Efficiency. *Eur. J. Pharm. Sci.* **2013**, *49*, 1–9.
- (151) Kitamoto, D.; Isoda, H.; Nakahara, T. Functions and Potential Applications of Glycolipid Biosurfactants--from Energy-Saving Materials to Gene Delivery Carriers. *J. Biosci. Bioeng.* **2002**, *94*, 187–201.
- (152) Du, X.; Zhou, J.; Shi, J.; Xu, B. Supramolecular Hydrogelators and Hydrogels: From Soft Matter to Molecular Biomaterials. *Chem. Rev.* **2015**, *115*, 13165–13307.
- (153) Dubey, P.; Nawale, L.; Sarkar, D.; Nisal, A.; Prabhune, A. Sophorolipid Assisted Tunable and Rapid Gelation of Silk Fibroin to Form Porous Biomedical Scaffolds. *RSC Adv.* **2015**, *5*, 33955–33962.
- (154) Dubey, P.; Kumar, S.; Ravindranathan, S.; Vasudevan, S.; Aswal, V. K.; Rajamohanam, P. R.; Nisal, A.; Prabhune, A. PH Dependent Sophorolipid Assemblies and Their Influence on Gelation of Silk Fibroin Protein. *Mater. Chem. Phys.* **2018**, *203*, 9–16.
- (155) Pingali, S.; Benhur, A. M.; Amin, S. Engineering Rheological Response in Chitosan–Sophorolipid Systems through Controlled Interactions. *Int. J. Cosmet. Sci.* **2020**, *42*, 407–414.
- (156) Dubey, P.; Kumar, S.; Aswal, V. K.; Ravindranathan, S.; Rajamohanam, P. R.; Prabhune, A.; Nisal, A. Silk Fibroin-Sophorolipid Gelation: Deciphering the Underlying Mechanism. *Biomacromolecules* **2016**, *17*, 3318–3327.
- (157) Ben Messaoud, G.; Griel, P. Le; Merino, D. H.; Roelants, S. L. K. W.; Stevens, C. V.; Baccile, N. PH-Controlled Self-Assembled Fibrillar Network (SAFiN) Hydrogels: Evidence of a Kinetic Control of the Mechanical Properties. *Chem. Mater.* **2019**, *31*, 4817–4830.
- (158) Baccile, N.; Renterghem, L. Van; Ducouret, G.; Brennich, M.; Cristiglio, V.; Roelants, S.; Soetaert, W. *New-to-Nature Glyco-Bolaamphiphile Forms a Temperature-Responsive Hydrogel with Tunable Elastic Properties.*
- (159) Ben Messaoud, G.; Griel, P. Le; Merino, D. H.; Baccile, N. Effect of PH, Temperature and Shear on the Structure-Property Relationship of Lamellar Hydrogels from Microbial Glycolipid Probed by in-Situ Rheo-SAXS. *Soft Matter* **2020**, *16*, 2540–2551.
- (160) Ben Messaoud, G.; Le Griel, P.; Prévost, S.; Hermida-Merino, D.; Soetaert, W.; Roelants, S. L. K. W.; Stevens, C. V.; Baccile, N. Single-Molecule Lamellar Hydrogels from Bolaform Microbial Glucolipids. *Soft Matter* **2020**, *16*, 2528–2539.
- (161) Ferrer, M. L.; Esquembre, R.; Ortega, I.; Mateo, C. R.; Monte, F. Freezing of Binary Colloidal Systems for the Formation of Hierarchy Assemblies. *Chem. Mater.* **2006**, *18*, 554–559.
- (162) Deville, S. Freeze-Casting of Porous Ceramics: A Review of Current Achievements and Issues. *Adv. Eng. Mater.* **2008**, *10*, 155–169.
- (163) Deville, S. Ice-Templating, Freeze Casting: Beyond Materials Processing. *J. Mater. Res.* **2013**, *28*, 2202–2219.
- (164) Deville, S. *Freezing Colloids: Observations, Principles, Control, and Use*; Springer Nature: Manchester, 2017.
- (165) Baccile, N.; Ben Messaoud, G.; Zinn, T.; Fernandes, F. M. Soft Lamellar Solid Foams from Ice-Templating of Self-Assembled Lipid Hydrogels: Organization Drives the Mechanical Properties.

Mater. Horizons **2019**, *6*, 2073–2086.

- (166) Singh, P. K.; Wani, K.; Kaul-Ghanekar, R.; Prabhune, A.; Ogale, S. From Micron to Nano-Curcumin by Sophorolipid Co-Processing: Highly Enhanced Bioavailability, Fluorescence, and Anti-Cancer Efficacy. *RSC Adv.* **2014**, *4*, 60334–60341.
- (167) Vasudevan, S.; Prabhune, A. A. Photophysical Studies on Curcumin-Sophorolipid Nanostructures: Applications in Quorum Quenching and Imaging. *R. Soc. Open Sci.* **2018**, *5*, 170865.
- (168) Darne, P. A.; Mehta, M. R.; Agawane, S. B.; Prabhune, A. A. Bioavailability Studies of Curcumin-Sophorolipid Nano-Conjugates in the Aqueous Phase: Role in the Synthesis of Uniform Gold Nanoparticles. *RSC Adv.* **2016**, *6*, 68504–68514.
- (169) Chuo, S. C.; Abd-Talib, N.; Mohd-Setapar, S. H.; Hassan, H.; Nasir, H. M.; Ahmad, A.; Lokhat, D.; Ashraf, G. M. Reverse Micelle Extraction of Antibiotics Using an Eco-Friendly Sophorolipids Biosurfactant. *Sci. Rep.* **2018**, *8*, 1–13.
- (170) Joshi-Navare, K.; Prabhune, A. A Biosurfactant-Sophorolipid Acts in Synergy with Antibiotics to Enhance Their Efficiency. *Biomed Res. Int.* **2013**, *2013*, 1–8.
- (171) Chen, M.; Dong, C.; Penfold, J.; Thomas, R. K.; Smyth, T. J. P.; Perfumo, A.; Marchant, R.; Banat, I. M.; Stevenson, P.; Parry, A.; et al. Influence of Calcium Ions on Rhamnolipid and Rhamnolipid/Anionic Surfactant Adsorption and Self-Assembly. *Langmuir* **2013**, *29*, 3912–3923.
- (172) Liley, J. R.; Penfold, J.; Thomas, R. K.; Tucker, I. M.; Petkov, J. T.; Stevenson, P. S.; Banat, I. M.; Marchant, R.; Rudden, M.; Terry, A.; et al. Self-Assembly in Dilute Mixtures of Non-Ionic and Anionic Surfactants and Rhamnolipid Biosurfactants. *J. Colloid Interface Sci.* **2017**, *487*, 493–503.
- (173) Monnier, N.; Furlan, A. L.; Buchoux, S.; Deleu, M.; Dauchez, M.; Rippa, S.; Sarazin, C. Exploring the Dual Interaction of Natural Rhamnolipids with Plant and Fungal Biomimetic Plasma Membranes through Biophysical Studies. *Int. J. Mol. Sci.* **2019**, *20*, 1009.
- (174) Otzen, D. E. Biosurfactants and Surfactants Interacting with Membranes and Proteins: Same but Different? *Biochimica et Biophysica Acta - Biomembranes*. Elsevier B.V. April 2017, pp 639–649.
- (175) Ortiz, A.; Teruel, J. A.; Manresa, Á.; Espuny, M. J.; Marqués, A.; Aranda, F. J. Effects of a Bacterial Trehalose Lipid on Phosphatidylglycerol Membranes. *Biochim. Biophys. Acta - Biomembr.* **2011**, *1808*, 2067–2072.
- (176) Ortiz, A.; Aranda, F. J.; Teruel, J. A. Interaction of Dirhamnolipid Biosurfactants with Phospholipid Membranes: A Molecular Level Study. *Adv. Exp. Med. Biol.* **2010**, *672*, 42–53.
- (177) Ortiz, A.; Teruel, J. A.; Espuny, M. J.; Marqués, A.; Manresa, Á.; Aranda, F. J. Interactions of a Bacterial Biosurfactant Trehalose Lipid with Phosphatidylserine Membranes. *Chem. Phys. Lipids* **2009**, *158*, 46–53.
- (178) Ortiz, A.; Teruel, J. A.; Espuny, M. J.; Marqués, A.; Manresa, Á.; Aranda, F. J. Effects of Dirhamnolipid on the Structural Properties of Phosphatidylcholine Membranes. *Int. J. Pharm.* **2006**, *325*, 99–107.
- (179) Moussa, Z.; Chebl, M.; Patra, D. Interaction of Curcumin with 1,2-Dioctadecanoyl-Sn-Glycero-3-Phosphocholine Liposomes: Intercalation of Rhamnolipids Enhances Membrane Fluidity, Permeability and Stability of Drug Molecule. *Colloids Surfaces B Biointerfaces* **2017**, *149*, 30–

37.

- (180) Inoh, Y.; Kitamoto, D.; Hirashima, N.; Nakanishi, M. Biosurfactants of MEL-A Increase Gene Transfection Mediated by Cationic Liposomes. *Biochem. Biophys. Res. Commun.* **2001**, *289*, 57–61.
- (181) Inoh, Y.; Kitamoto, D.; Hirashima, N.; Nakanishi, M. Biosurfactant MEL-A Dramatically Increases Gene Transfection via Membrane Fusion. *J. Control. Release* **2004**, *94*, 423–431.
- (182) Nakanishi, M.; Inoh, Y.; Kitamoto, D.; Furuno, T. Nano Vectors with a Biosurfactant for Gene Transfection and Drug Delivery. *J. Drug Deliv. Sci. Technol.* **2009**, *19*, 165–169.
- (183) Delbeke, E. I. P.; Lozach, O.; Le Gall, T.; Berchel, M.; Montier, T.; Jaffrès, P. -A.; Van Geem, K. M.; Stevens, C. V. Evaluation of the Transfection Efficacies of Quaternary Ammonium Salts Prepared from Sophorolipids. *Org. Biomol. Chem.* **2016**, *14*, 3744–3751.
- (184) Delbeke, E. I. P.; Everaert, J.; Lozach, O.; Le Gall, T.; Berchel, M.; Montier, T.; Jaffrès, P. A.; Rigole, P.; Coenye, T.; Brennich, M.; et al. Synthesis and Biological Evaluation of Bolaamphiphilic Sophorolipids. *ACS Sustain. Chem. Eng.* **2018**, *6*, 8992–9005.
- (185) Delbeke, E. I. P.; Everaert, J.; Lozach, O.; Gall, T. Le; Berchel, M.; Montier, T.; Jaffrès, P. -A.; Rigole, P.; Coenye, T.; Brennich, M.; et al. Lipid-Based Quaternary Ammonium Sophorolipid Amphiphiles with Antimicrobial and Transfection Activities. *ChemSusChem* **2019**, *12*, 3642–3653.
- (186) Singh, P. K.; Bohr, S. S. R.; Hatzakis, N. S. Direct Observation of Sophorolipid Micelle Docking in Model Membranes and Cells by Single Particle Studies Reveals Optimal Fusion Conditions. *Biomolecules* **2020**, *10*, 1–16.
- (187) Ben Messaoud, G.; Promeneur, L.; Brennich, M.; Roelants, S. L. K. W.; Le Griel, P.; Baccile, N. Complex Coacervation of Natural Sophorolipid Bolaamphiphile Micelles with Cationic Polyelectrolytes. *Green Chem.* **2018**, *20*, 3371–3385.
- (188) Marangon, C. A.; Martins, V. C. A.; Ling, M. H.; Melo, C. C.; Plepis, A. M. G.; Meyer, R. L.; Nitschke, M. Combination of Rhamnolipid and Chitosan in Nanoparticles Boosts Their Antimicrobial Efficacy. *ACS Appl. Mater. Interfaces* **2020**, *12*, 5488–5499.
- (189) Fernández-Peña, L.; Guzmán, E.; Leonforte, F.; Serrano-Pueyo, A.; Regulski, K.; Tournier-Couturier, L.; Ortega, F.; Rubio, R. G.; Luengo, G. S. Effect of Molecular Structure of Eco-Friendly Glycolipid Biosurfactants on the Adsorption of Hair-Care Conditioning Polymers. *Colloids Surfaces B Biointerfaces* **2020**, *185*, 110578.
- (190) Otzen, D. Protein-Surfactant Interactions: A Tale of Many States. *Biochim. Biophys. Acta - Proteins Proteomics* **2011**, *1814*, 562–591.
- (191) Otzen, D. E. Amyloid Formation in Surfactants and Alcohols: Membrane Mimetics or Structural Switchers? *Curr. Protein Pept. Sci.* **2010**, *11*, 355–371.
- (192) Sánchez, M.; Aranda, F. J.; Espuny, M. J.; Marqués, A.; Teruel, J. A.; Manresa, Á.; Ortiz, A. Thermodynamic and Structural Changes Associated with the Interaction of a Dirhamnolipid Biosurfactant with Bovine Serum Albumin. *Langmuir* **2008**, *24*, 6487–6495.
- (193) Zaragoza, A.; Teruel, J. A.; Aranda, F. J.; Marqués, A.; Espuny, M. J.; Manresa, Á.; Ortiz, A. Interaction of a Rhodococcus Sp. Trehalose Lipid Biosurfactant with Model Proteins: Thermodynamic and Structural Changes. *Langmuir* **2012**, *28*, 1381–1390.
- (194) Andersen, K. K.; Otzen, D. E. Denaturation of α -Lactalbumin and Myoglobin by the Anionic Biosurfactant Rhamnolipid. *Biochim. Biophys. Acta - Proteins Proteomics* **2014**, *1844*, 2338–

2345.

- (195) Andersen, K. K.; Otzen, D. E. Folding of Outer Membrane Protein A in the Anionic Biosurfactant Rhamnolipid. *FEBS Lett.* **2014**, *588*, 1955–1960.
- (196) Madsen, J. K.; Pihl, R.; Møller, A. H.; Madsen, A. T.; Otzen, D. E.; Andersen, K. K. The Anionic Biosurfactant Rhamnolipid Does Not Denature Industrial Enzymes. *Front. Microbiol.* **2015**, *6*, 1–13.
- (197) Andersen, K. K.; Vad, B. S.; Roelants, S.; van Bogaert, I. N. A.; Otzen, D. E. Weak and Saturable Protein-Surfactant Interactions in the Denaturation of Apo-a-Lactalbumin by Acidic and Lactonic Sophorolipid. *Front. Microbiol.* **2016**, *7*, 1–9.
- (198) Wang, L.; Wang, Y.; Qu, J.; Hu, Y.; You, R.; Li, M. The Cytocompatibility of Genipin-Crosslinked Silk Fibroin Films. *J. Biomater. Nanobiotechnol.* **2013**, *04*, 213–221.
- (199) Yucel, T.; Cebe, P.; Kaplan, D. L. Vortex-Induced Injectable Silk Fibroin Hydrogels. *Biophys. J.* **2009**, *97*, 2044–2050.
- (200) Wang, X.; Kluge, J. A.; Leisk, G. G.; Kaplan, D. L. Sonication-Induced Gelation of Silk Fibroin for Cell Encapsulation. *Biomaterials* **2008**, *29*, 1054–1064.
- (201) Leisk, G. G.; Lo, T. J.; Yucel, T.; Lu, Q.; Kaplan, D. L. Electrogelation for Protein Adhesives. *Adv. Mater.* **2010**, *22*, 711–715.
- (202) Yucel, T.; Kojic, N.; Leisk, G. G.; Lo, T. J.; Kaplan, D. L. Non-Equilibrium Silk Fibroin Adhesives. *J. Struct. Biol.* **2010**, *170*, 406–412.
- (203) Matsumoto, A.; Chen, J.; Collette, A. L.; Kim, U. J.; Altman, G. H.; Cebe, P.; Kaplan, D. L. Mechanisms of Silk Fibroin Sol-Gel Transitions. *J. Phys. Chem. B* **2006**, *110*, 21630–21638.
- (204) Wu, X.; Hou, J.; Li, M.; Wang, J.; Kaplan, D. L.; Lu, S. Sodium Dodecyl Sulfate-Induced Rapid Gelation of Silk Fibroin. *Acta Biomater.* **2012**, *8*, 2185–2192.
- (205) Park, J. H.; Kim, M. H.; Jeong, L.; Cho, D.; Kwon, O. H.; Park, W. H. Effect of Surfactants on Sol-Gel Transition of Silk Fibroin. *J. Sol-Gel Sci. Technol.* **2014**, *71*, 364–371.
- (206) Zou, A.; Liu, J.; Jin, Y.; Liu, F.; Mu, B. Interaction Between Surfactin and Bovine Serum Albumin. *J. Dispers. Sci. Technol.* **2014**, *35*, 48–55.
- (207) Han, Y.; Huang, X.; Cao, M.; Wang, Y. Micellization of Surfactin and Its Effect on the Aggregate Conformation of Amyloid β (1-40). *J. Phys. Chem. B* **2008**, *112*, 15195–15201.
- (208) Fan, L.; Xie, P.; Wang, Y.; Huang, Z.; Zhou, J. Biosurfactant-Protein Interaction: Influences of Mannosylerythritol Lipids-A on β -Glucosidase. *J. Agric. Food Chem.* **2018**, *66*, 238–246.
- (209) Fan, L.; Xie, P.; Wang, Y.; Liu, X.; Li, Y.; Zhou, J. Influences of Mannosylerythritol Lipid-A on the Self-Assembling Structure Formation and Functional Properties of Heat-Induced β -Lactoglobulin Aggregates. *Food Hydrocoll.* **2019**, *96*, 310–321.
- (210) Naismith, J. H.; Field, R. A. Structural Basis of Trimannoside Recognition by Concanavalin A. *J. Biol. Chem.* **1996**, *271*, 972–976.
- (211) Park, D.; Lee, J. Y.; Cho, H. K.; Hong, W. J.; Kim, J.; Seo, H.; Choi, I.; Lee, Y.; Kim, J.; Min, S. J.; et al. Cell-Penetrating Peptide-Patchy Deformable Polymeric Nanovehicles with Enhanced Cellular Uptake and Transdermal Delivery. *Biomacromolecules* **2018**, *19*, 2682–2690.
- (212) Ben Messaoud, G.; Promeneur, L.; Brennich, M.; Roelants, S. L. K. W.; Le Griel, P.; Baccile, N. Complex Coacervation of Natural Sophorolipid Bolaamphiphile Micelles with Cationic

- Polyelectrolytes. *Green Chem.* **2018**, *20*, 3371–3385.
- (213) Bungenberg de Jong, H. G.; Kruyt, H. R. Coacervation (Partial Miscibility in Colloid Systems). *Proc. Natl. Acad. Sci. Amsterdam* **1929**, *32*, 849–856.
- (214) Wang, M.; Fan, Y.; Han, Y.; Nie, Z.; Wang, Y. Coacervation of Cationic Gemini Surfactant with N-Benzoylglutamic Acid in Aqueous Solution. *Langmuir* **2013**, *29*, 14839–14847.
- (215) Khaledi, M. G.; Jenkins, S. I.; Liang, S. Perfluorinated Alcohols and Acids Induce Coacervation in Aqueous Solutions of Amphiphiles. *Langmuir* **2013**, *29*, 2458–2464.
- (216) Kayitmazer, A. B.; Koksal, A. F.; Kilic Iyilik, E. Complex Coacervation of Hyaluronic Acid and Chitosan: Effects of PH, Ionic Strength, Charge Density, Chain Length and the Charge Ratio. *Soft Matter* **2015**, *11*, 8605–8612.
- (217) Espinosa-Andrews, H.; Báez-González, J. G.; Cruz-Sosa, F.; Vernon-Carter, E. J. Gum Arabic-Chitosan Complex Coacervation. *Biomacromolecules* **2007**, *8*, 1313–1318.
- (218) Wang, Q.; Schlenoff, J. B. The Polyelectrolyte Complex/Coacervate Continuum. *Macromolecules* **2014**, *47*, 3108–3116.
- (219) Boudier, A.; Aubert-Pouëssel, A.; Gérardin, C.; Devoisselle, J. M.; Bégu, S. PH-Sensitive Double-Hydrophilic Block Copolymer Micelles for Biological Applications. *Int. J. Pharm.* **2009**, *379*, 212–217.
- (220) Warnant, J.; Marcotte, N.; Reboul, J.; Layrac, G.; Aqil, A.; Jérôme, C.; Lerner, D. A.; Gérardin, C. Physicochemical Properties of PH-Controlled Polyion Complex (PIC) Micelles of Poly(Acrylic Acid)-Based Double Hydrophilic Block Copolymers and Various Polyamines. *Anal. Bioanal. Chem.* **2012**, *403*, 1395–1404.
- (221) Reboul, J.; Nugay, T.; Anik, N.; Cottet, H.; Ponsinet, V.; In, M.; Lacroix-Desmazes, P.; Gérardin, C. Synthesis of Double Hydrophilic Block Copolymers and Induced Assembly with Oligochitosan for the Preparation of Polyion Complex Micelles. *Soft Matter* **2011**, *7*, 5836–5846.
- (222) De Kruif, C. G.; Weinbreck, F.; De Vries, R. Complex Coacervation of Proteins and Anionic Polysaccharides. *Curr. Opin. Colloid Interface Sci.* **2004**, *9*, 340–349.
- (223) Aberkane, L.; Jasniewski, J.; Gaiani, C.; Scher, J.; Sanchez, C. Thermodynamic Characterization of Acacia Gum- β -Lactoglobulin Complex Coacervation. *Langmuir* **2010**, *26*, 12523–12533.
- (224) Leisner, D.; Imae, T. Interpolyelectrolyte Complex and Coacervate Formation of Poly(Glutamic Acid) with a Dendrimer Studied by Light Scattering and SAXS [†]. *J. Phys. Chem. B* **2003**, *107*, 8078–8087.
- (225) Wang, Y.; Kimura, K.; Huang, Q.; Dubin, P. L. Effects of Salt on Poly Electrolyte-Micelle Coacervation. *Macromolecules* **1999**, *32*, 7128–7134.
- (226) Wang, Y.; Kimura, K.; Dubin, P. L.; Jaeger, W. Polyelectrolyte-Micelle Coacervation: Effects of Micelle Surface Charge Density, Polymer Molecular Weight, and Polymer/Surfactant Ratio. *Macromolecules* **2000**, *33*, 3324–3331.
- (227) Mukherjee, S.; Dan, A.; Bhattacharya, S. C.; Panda, A. K.; Moulik, S. P. Physicochemistry of Interaction between the Cationic Polymer Poly(Diallyldimethylammonium Chloride) and the Anionic Surfactants Sodium Dodecyl Sulfate, Sodium Dodecylbenzenesulfonate, and Sodium N-Dodecanoylsarcosinate in Water and Isopropyl Alcohol-Wate. *Langmuir* **2011**, *27*, 5222–5233.

- (228) Li, Y.; Xia, J.; Dubin, P. L. Complex Formation between Polyelectrolyte and Oppositely Charged Mixed Micelles: Static and Dynamic Light Scattering Study of the Effect of Polyelectrolyte Molecular Weight and Concentration. *Macromolecules* **1994**, *27*, 7049–7055.
- (229) Li, Y.; Dubin, P. L.; Dautzenberg, H.; Lück, U.; Hartmann, J.; Tuzar, Z. Dependence of Structure of Polyelectrolyte/Micelle Complexes upon Polyelectrolyte Chain Length and Micelle Size. *Macromolecules* **1995**, *28*, 6795–6798.
- (230) Dubin, P. L.; Davis, D. Stoichiometry and Coacervation of Complexes Formed between Polyelectrolytes and Mixed Micelles. *Colloids and Surfaces* **1985**, *13*, 113–124.
- (231) Zhao, W.; Wang, Y. Coacervation with Surfactants: From Single-Chain Surfactants to Gemini Surfactants. *Adv. Colloid Interface Sci.* **2017**, *239*, 199–212.
- (232) Kronberg, B.; Holmberg, K.; Lindman, B. Surfactant Self-Assembly. *Surf. Chem. Surfactants Polym.* **2014**, 75–94.
- (233) Gradzielski, M.; Hoffmann, I. Polyelectrolyte-Surfactant Complexes (PESCs) Composed of Oppositely Charged Components. *Curr. Opin. Colloid Interface Sci.* **2018**, *35*, 124–141.
- (234) Dubin, P. L.; Chew, C. H.; Gan, L. M. Complex Formation between Anionic Polyelectrolytes and Cationic/Nonionic Mixed Micelles. *J. Colloid Interface Sci.* **1989**, *128*, 566–576.
- (235) Liu, W.; Sun, S.; Cao, Z.; Zhang, X.; Yao, K.; Lu, W. W.; Luk, K. D. K. An Investigation on the Physicochemical Properties of Chitosan/DNA Polyelectrolyte Complexes. *Biomaterials* **2005**, *26*, 2705–2711.
- (236) Lewis, S. R.; Datta, S.; Gui, M.; Coker, E. L.; Huggins, F. E.; Daunert, S.; Bachas, L.; Bhattacharyya, D. Reactive Nanostructured Membranes for Water Purification. *Proc. Natl. Acad. Sci. U. S. A.* **2011**, *108*, 8577–8582.
- (237) Mady, M. M.; Mohammed, W. A.; El-Guendy, N. M.; Elsayed, A. A. Effect of Polymer Molecular Weight on the Dna/Pei Polyplexes Properties. *J. Biophys* **2011**, *21*, 151–165.
- (238) Pillai, C. K. S.; Paul, W.; Sharma, C. P. Chitin and Chitosan Polymers: Chemistry, Solubility and Fiber Formation. *Prog. Polym. Sci.* **2009**, *34*, 641–678.
- (239) Samal, S. K.; Dash, M.; Vlierberghe, S. Van; Kaplan, D. L.; Chiellini, E.; Blitterswijk, C. van; Moroni, L.; Dubruel, P. Cationic Polymers and Their Therapeutic Potential. *Chem. Soc. Rev.* **2012**, *41*, 7147–7194.
- (240) Hayward, D. W.; Chiappisi, L.; Teo, J. H.; Prévost, S.; Schweins, R.; Gradzielski, M. Neutralisation Rate Controls the Self-Assembly of PH-Sensitive Surfactants. *Soft Matter* **2019**, *15*, 8611–8620.
- (241) Kaibara, K.; Okazaki, T.; Bohidar, H. B.; Dubin, P. L. PH-Induced Coacervation in Complexes of Bovine Serum Albumin and Cationic Polyelectrolytes. *Biomacromolecules* **2000**, *1*, 100–107.
- (242) Weinbreck, F.; Vries, R. De; Schrooyen, P.; Kruif, C. G. De. Complex Coacervation of Whey Proteins and Gum Arabic. *Biomacromolecules* **2003**, *4*, 293–303.
- (243) Sanchez, C.; Mekhloufi, G.; Renard, D. Complex Coacervation between β -Lactoglobulin and Acacia Gum: A Nucleation and Growth Mechanism. *J. Colloid Interface Sci.* **2006**, *299*, 867–873.
- (244) Yoshida, K.; Dubin, P. L. Colloids Surfaces A. *Physicochem. Eng. Asp.* **1999**, *147*, 161–167.
- (245) Koga, S.; Williams, D. S.; Perriman, A. W.; Mann, S. Peptide-Nucleotide Microdroplets as a Step towards a Membrane-Free Protocell Model. *Nat. Chem.* **2011**, *3*, 720–724.

- (246) Betageri, G. V.; Parsons, D. L. Drug Encapsulation and Release from Multilamellar and Unilamellar Liposomes. *Int. J. Pharm.* **1992**, *81*, 235–241.
- (247) Majumder, J.; Minko, T. Multifunctional and Stimuli-Responsive Nanocarriers for Targeted Therapeutic Delivery. *Expert Opin. Drug Deliv.* **2021**, *18*, 205–227.
- (248) Vargason, A. M.; Anselmo, A. C.; Mitragotri, S. The Evolution of Commercial Drug Delivery Technologies. *Nat. Biomed. Eng.* **2021**.
- (249) Liu, D.; Yang, F.; Xiong, F.; Gu, N. The Smart Drug Delivery System and Its Clinical Potential. *Theranostics* **2016**, *6*, 1306–1323.
- (250) Sanches, B. C. P.; Rocha, C. A.; Bedoya, J. G. M.; Da Silva, V. L.; Da Silva, P. B.; Fusco-Almeida, A. M.; Chorilli, M.; Contiero, J.; Crusca, E.; Marchetto, R. Rhamnolipid-Based Liposomes as Promising Nano-Carriers for Enhancing the Antibacterial Activity of Peptides Derived from Bacterial Toxin-Antitoxin Systems. *Int. J. Nanomedicine* **2021**, *16*, 925–939.
- (251) Seyrig, C.; Kignelman, G.; Thielemans, W.; Le Griel, P.; Cowieson, N.; Perez, J.; Baccile, N. Stimuli-Induced Nonequilibrium Phase Transitions in Polyelectrolyte-Surfactant Complex Coacervates. *Langmuir* **2020**, *36*, 8839–8857.
- (252) Seyrig, C.; Le Griel, P.; Cowieson, N.; Perez, J.; Baccile, N. Synthesis of Multilamellar Walls Vesicles Polyelectrolyte-Surfactant Complexes from PH-Stimulated Phase Transition Using Microbial Biosurfactants. *J. Colloid Interface Sci.* **2020**, *580*, 493–502.
- (253) Chignell, C. F.; Bilski, P.; Reszka, K. J.; Motten, A. G.; Sik, R. H.; Dahl, T. A. Spectral and Photochemical Properties of Curcumin. *Photochem. Photobiol.* **1994**, *59*, 295–302.
- (254) Stanić, Z. Curcumin, a Compound from Natural Sources, a True Scientific Challenge – A Review. *Plant Foods Hum. Nutr.* **2017**, *72*.
- (255) Tomeh, M. A.; Hadianamrei, R.; Zhao, X. A Review of Curcumin and Its Derivative as Anticancer Agents. *Int. J. Mol. Sci.* **2020**, *20*.
- (256) Goel, A.; Kunnumakkara, A. B.; Aggarwal, B. B. Curcumin as “Curecumin”: From Kitchen to Clinic. *Biochem. Pharmacol.* **2008**, *75*, 787–809.
- (257) Liu, H.-T.; Ho, Y.-S. Anticancer Effect of Curcumin on Breast Cancer and Stem Cells. *Food Sci. Hum. Wellness* **2018**, *7*, 134–137.
- (258) Jakubek, M.; Kejik, Z.; Kaplánek, R.; Hromádka, R.; Šandriková, V.; Sýkora, D.; Král, V. Strategy for Improved Therapeutic Efficiency of Curcumin in the Treatment of Gastric Cancer. *Biomed. Pharmacother.* **2019**, *118*, 109278.
- (259) Rajasekaran, S. A. Therapeutic Potential of Curcumin in Gastrointestinal Diseases. *World J. Gastrointest. Pathophysiol.* **2011**, *2*, 1.
- (260) Wang, B.; Liu, X.; Teng, Y.; Yu, T.; Chen, J.; Hu, Y.; Shen, Y. Improving Anti-Melanoma Effect of Curcumin by Biodegradable Nanoparticles. *Oncotarget* **2017**, *8*, 108624–108642.
- (261) Singh, M.; Pandey, A.; Karikari, C. A.; Singh, G.; Rakheja, D. Cell Cycle Inhibition and Apoptosis Induced by Curcumin in Ewing Sarcoma Cell Line SK-NEP-1. *Med. Oncol.* **2010**, *27*, 1096–1101.
- (262) Anand, P.; Kunnumakkara, A. .; Newman, R. A.; Aggarwal, B. B. Bioavailability of Curcumin: Problems and Promises. *Mol. Pharm.* **2007**, *4*, 807–818.
- (263) Rafiee, Z.; Nejatian, M.; Daeihamed, M.; Jafari, S. M. Application of Different Nanocarriers for Encapsulation of Curcumin. *Crit. Rev. Food Sci. Nutr.* **2019**, *59*, 3468–3497.

- (264) Sercombe, L. Advances and Challenges of Liposome Assisted Drug Delivery. *Front. Pharmacol.* **2015**, *6*, 286.
- (265) Hasan, M.; Elkhoury, K.; Kahn, C. J. F.; Arab-tehrany, E.; Linder, M. Preparation, Characterization, and Release Kinetics of Chitosan-Coated Nanoliposomes Encapsulating Curcumin in Simulated Environments. *Molecules* **2019**, *24*, 1–14.
- (266) Mulik, R.; Mahadik, K.; Paradkar, A. Development of Curcuminoids Loaded Poly(Butyl) Cyanoacrylate Nanoparticles: Physicochemical Characterization and Stability Study. *Eur. J. Pharm. Sci.* **2009**, *37*, 395–404.
- (267) Sahu, A.; Kasoju, N.; Goswami, P.; Bora, U. Encapsulation of Curcumin in Pluronic Block Copolymer Micelles for Drug Delivery Applications. *J. Biomater. Appl.* **2011**, *25*, 619–639.
- (268) Yadav, A.; Lomash, V.; Samim, M.; Flora, S. J. S. Curcumin Encapsulated in Chitosan Nanoparticles: A Novel Strategy for the Treatment of Arsenic Toxicity. *Chem. Biol. Interact.* **2012**, *199*, 49–61.
- (269) Zheng, Z.; Zhang, X.; Carbo, D.; Clark, C.; Nathan, C.-A.; Lvov, Y. Sonication-Assisted Synthesis of Polyelectrolyte-Coated Curcumin Nanoparticles. *Langmuir* **2010**, *26*, 7679–7681.
- (270) Anitha, A.; Deepagan, V. G.; Rani, V. V. D.; Menon, D.; Nair, S. V.; Jayakumar, R. Preparation, Characterization, in Vitro Drug Release and Biological Studies of Curcumin Loaded Dextran Sulphate–Chitosan Nanoparticles. *Carbohydr. Polym.* **2011**, *84*, 1158–1164.
- (271) Chuah, L. H.; Roberts, C. J.; Billa, N.; Abdullah, S.; Rosli, R. Cellular Uptake and Anticancer Effects of Mucoadhesive Curcumin-Containing Chitosan Nanoparticles. *Colloids Surfaces B Biointerfaces* **2014**, *116*, 228–236.
- (272) Mihoub, A. Ben; Acherar, S.; Frochot, C.; Malaplate, C.; Yen, F. T.; Arab-Tehrany, E. Synthesis of New Water Soluble β -Cyclodextrin@curcumin Conjugates and in Vitro Safety Evaluation in Primary Cultures of Rat Cortical Neurons. *Int. J. Mol. Sci.* **2021**, *22*.
- (273) Chakraborty, S.; Liao, I.-C.; Adler, A.; Leong, K. W. Electrohydrodynamics: A Facile Technique to Fabricate Drug Delivery Systems. *Adv. Drug Deliv. Rev.* **2009**, *61*, 1043–1054.
- (274) Jiang, H.; Wang, L.; Zhu, K. Coaxial Electrospinning for Encapsulation and Controlled Release of Fragile Water-Soluble Bioactive Agents. *J. Control. Release* **2014**, *193*, 296–303.
- (275) Jafari, S. M. Chapter 10- Nanocapsules Formation by Nano Spray Drying. Nanoencapsulation Technologies for the Food and Nutraceutical Industries. In *Academic Press*; 2017.
- (276) Mandal, S.; Banerjee, C.; Ghosh, S.; Kuchlyan, J.; Sarkar, N. Modulation of the Photophysical Properties of Curcumin in Nonionic Surfactant (Tween-20) Forming Micelles and Niosomes: A Comparative Study of Different Microenvironments. *J. Phys. Chem. B* **2013**, *117*, 6957–6968.
- (277) Esposito, E.; Ravani, L.; Mariani, P.; Contado, C.; Drechsler, M.; Puglia, C.; Cortesi, R. Curcumin Containing Monoolein Aqueous Dispersions: A Preformulative Study. *Mater. Sci. Eng. C* **2013**, *33*, 4923–4934.
- (278) Review, T.; Gradzielski, M. Vesicles and Vesicle Gels — Structure and Dynamics Of. *Rev. Lit. Arts Am.* **2003**, *15*.
- (279) Zhang, Y. S.; Khademhosseini, A. Advances in Engineering Hydrogels. *Science* **2017**, *356*, 3627.
- (280) Zhu, X. Biomimetic Bacterial Cellulose-Enhanced Double-Network Hydrogel with Excellent Mechanical Properties Applied for the Osteochondral Defect Repair. *ACS Biomater. Sci. Eng.* **2018**, *4*, 3534–3544.

- (281) Yan, Y. Construction of Injectable Double-Network Hydrogels for Cell Delivery. *Biomacromolecules* **2017**, *18*, 2128–2138.
- (282) Wang, W.; Zhang, Y.; Sun, B.; Chen, L. J.; Xu, X. D.; Wang, M.; Li, X.; Yu, Y.; Jiang, W.; Yang, H. B. The Construction of Complex Multicomponent Supramolecular Systems via the Combination of Orthogonal Self-Assembly and the Self-Sorting Approach. *Chem. Sci.* **2014**, *5*, 4554–4560.
- (283) Ho Wong, C.; Zimmerman, S. C. Orthogonality in Organic, Polymer, and Supramolecular Chemistry: From Merrifield to Click Chemistry. *Chem. Commun.* **2013**, *49*, 1679–1695.
- (284) Saha, M. L.; De, S.; Pramanik, S.; Schmittel, M. Orthogonality in Discrete Self-Assembly – Survey of Current Concepts. *Chem. Soc. Rev.* **2013**, *42*, 6860–6909.
- (285) Safont-Sempere, M. M.; Fernández, G.; Würthner, F. Self-Sorting Phenomena in Complex Supramolecular Systems. *Chem. Rev.* **2011**, *111*, 5784–5814.
- (286) Lal Saha, M.; Schmittel, M. Degree of Molecular Self-Sorting in Multicomponent Systems. *Org. Biomol. Chem.* **2012**, *10*, 4651–4684.
- (287) Osowka, K.; Miljanic, O. S. Kinetic and Thermodynamic Self-Sorting in Synthetic Systems. *Synlett* **2011**, *12*, 1643.
- (288) Rest, C.; Mayoral, M. J.; Fernández, G. Aqueous Self-Sorting in Extended Supramolecular Aggregates. *Int. J. Mol. Sci.* **2013**, *14*, 1541–1565.
- (289) Kramer, R.; Lehn, J.; Bel, I. Le; Pasteur, U. L.; Marquis-rigault, A. Self-Recognition in Helicate Self-Assembly: Spontaneous Formation of Helical Metal Complexes from Mixtures of Ligands and Metal Ions. *Proc. Natl. Acad. Sci. USA* **1993**, *90*, 5394–5398.
- (290) Caulder, D. L.; Raymond, K. N. Supramolecular Self-Recognition and Self-Assembly in Gallium(III) Catecholamide Triple Helices. *Angew. Chem. Int. Ed. Engl.* **1997**, No. 13/14, 1440.
- (291) Hutin, M.; Frantz, R.; Nitschke, J. R. A Dynamic Tricopper Double Helicate. *Chem. - A Eur. J.* **2006**, *12*, 4077–4082.
- (292) Nitschke, J. R. Construction, Substitution, and Sorting of Metallo-Organic Structures via Subcomponent Self-Assembly. *Acc. Chem. Res.* **2007**, *40*, 103–112.
- (293) Acharyya, K.; Mukherjee, P. S. Hydrogen-Bond-Driven Controlled Molecular Marriage in Covalent Cages. *Chem. - A Eur. J.* **2014**, *20*, 1646–1657.
- (294) Jiménez, A.; Bilbeisi, R. A.; Ronson, T. K.; Zarra, S.; Woodhead, C.; Nitschke, J. R. Selective Encapsulation and Sequential Release of Guests within a Self-Sorting Mixture of Three Tetrahedral Cages. *Angew. Chemie - Int. Ed.* **2014**, *53*, 4556–4560.
- (295) Huang, Z.; Yang, L.; Liu, Y.; Wang, Z.; Scherman, O. A.; Zhang, X. Supramolecular Polymerization Promoted and Controlled through Self-Sorting. *Angew. Chemie - Int. Ed.* **2014**, *53*, 5351–5355.
- (296) Ayme, J. F.; Beves, J. E.; Campbell, C. J.; Leigh, D. A. The Self-Sorting Behavior of Circular Helicates and Molecular Knots and Links. *Angew. Chemie - Int. Ed.* **2014**, *53*, 7823–7827.
- (297) Wang, M.; Wang, C.; Hao, X. Q.; Li, X.; Vaughn, T. J.; Zhang, Y. Y.; Yu, Y.; Li, Z. Y.; Song, M. P.; Yang, H. B.; et al. From Trigonal Bipyramidal to Platonic Solids: Self-Assembly and Self-Sorting Study of Terpyridine-Based 3d Architectures. *J. Am. Chem. Soc.* **2014**, *136*, 10499–10507.
- (298) Enemark, E. J.; Stack, T. D. P. Stereospecificity and Self-Selectivity in the Generation of a Chiral Molecular Tetrahedron by Metal-Assisted Self-Assembly. *Angew. Chem. Int. Ed.* **1998**, *37*,

932–935.

- (299) Stiller, R.; Lehn, J. M. Synthesis and Properties of Silver(I) and Copper(I) Helicates with Imine-Bridged Oligobipyridine Ligands. *Eur. J. Inorg. Chem.* **1998**, No. 7, 977–982.
- (300) Taylor, P. N.; Anderson, H. L. Cooperative Self-Assembly of Double-Strand Conjugated Porphyrin Ladders. *J. Am. Chem. Soc.* **1999**, *121*, 11538–11545.
- (301) Albrecht, M.; Schneider, M. Formation of Helicate-Type Complexes. *Angew. Chem. Int. Ed.* **1999**, *38*, 557–559.
- (302) Kondo, T.; Oyama, K. I.; Yoshida, K. Chiral Molecular Recognition on Formation of a Metalloanthocyanin: A Supramolecular Metal Complex Pigment from Blue Flowers of *Salvia patens*. *Angew. Chemie - Int. Ed.* **2001**, *40*, 894–897.
- (303) Kobayashi, K.; Yamada, Y.; Yamanaka, M.; Sei, Y.; Yamaguchi, K. Complete Selection of a Self-Assembling Homo- or Hetero-Cavitand Cage via Metal Coordination Based on Ligand Tuning. *J. Am. Chem. Soc.* **2004**, *126*, 13896–13897.
- (304) Chi, K. W.; Addicott, C.; Arif, A. M.; Stang, P. J. Ambidentate Pyridyl-Carboxylate Ligands in the Coordination-Driven Self-Assembly of 2D Pt Macrocycles: Self-Selection for a Single Isomer. *J. Am. Chem. Soc.* **2004**, *126*, 16569–16574.
- (305) Schultz, D.; Nitschke, J. R. Choices of Iron and Copper: Cooperative Selection during Self-Assembly. *Angew. Chemie - Int. Ed.* **2006**, *45*, 2453–2456.
- (306) Ma, Y.; Kolotuchin, S. V.; Zimmerman, S. C. Supramolecular Polymer Chemistry: Self-Assembling Dendrimers Using the DDA·AAD (GC-like) Hydrogen Bonding Motif. *J. Am. Chem. Soc.* **2002**, *124*, 13757–13769.
- (307) Yoshizawa, M.; Nagao, M.; Kumazawa, K.; Fujita, M. Side Chain-Directed Complementary Cis-Coordination of Two Pyridines on Pd(II): Selective Multicomponent Assembly of Square-, Rectangular-, and Trigonal Prism-Shaped Molecules. *J. Organomet. Chem.* **2005**, *690*, 5383–5388.
- (308) Braekers, D.; Peters, C.; Bogdan, A.; Rudzevich, Y.; Böhmer, V.; Desreux, J. F. Self-Sorting Dimerization of Tetraurea Calix[4]Arenes. *J. Org. Chem.* **2008**, *73*, 701–706.
- (309) Rudzevich, Y.; Rudzevich, V.; Klautzsch, F.; Schalley, C. A.; Böhmer, V. A Self-Sorting Scheme Based on Tetra-Urea Calix[4]Arenes. *Angew. Chemie - Int. Ed.* **2009**, *48*, 3867–3871.
- (310) Rudzevich, Y.; Rudzevich, V.; Böhmer, V. Fine-Tuning the Dimerization of Tetraureacalix[4]Arenes. *Chem. - A Eur. J.* **2010**, *16*, 4541–4549.
- (311) Schmittel, M.; Kalsani, V.; Fenske, D.; Wiegrefe, A. Self-Assembly of Heteroleptic [2x2] and [2x3] Nanogrids. *Chem. Commun.* **2004**, 490–491.
- (312) Mahata, K.; Schmittel, M. From 2-Fold Complementary to Integrative Self-Sorting: A Five-Component Supramolecular Trapezoid. *J. Am. Chem. Soc.* **2009**, *131*, 16544–16554.
- (313) Schmittel, M.; Mahata, K. A Fully Dynamic Five-Component Triangle via Self-Sorting. *Chem. Commun.* **2010**, *46*, 4163–4165.
- (314) Mahata, K.; Saha, M. L.; Schmittel, M. From an Eight-Component Self-Sorting Algorithm to a Trisheterometallic Scalene Triangle. *J. Am. Chem. Soc.* **2010**, *132*, 15933–15935.
- (315) Saha, M. L.; Bats, J. W.; Schmittel, M. Merging Strong and Weak Coordination Motifs in the Integrative Self-Sorting of a 5-Component Trapezoid and Scalene Triangle. *Org. Biomol. Chem.* **2013**, *11*, 5592–5595.

- (316) Saha, M. L.; Schmittel, M. From 3-Fold Complete Self-Sorting of a Nine-Component Library to a Seven-Component Scalene Quadrilateral. *J. Am. Chem. Soc.* **2013**, *135*, 17743–17746.
- (317) De, S.; Mahata, K.; Schmittel, M. Metal-Coordination-Driven Dynamic Heteroleptic Architectures. *Chem. Soc. Rev.* **2010**, *39*, 1555–1575.
- (318) Saha, M. L.; Neogi, S.; Schmittel, M. Dynamic Heteroleptic Metal-Phenanthroline Complexes: From Structure to Function. *Dalt. Trans.* **2014**, *43*, 3815–3834.
- (319) Yoshizawa, M.; Nakagawa, J.; Kumazawa, K.; Nagao, M.; Kawano, M.; Ozeki, T.; Fujita, M. Discrete Stacking of Large Aromatic Molecules within Organic-Pillared Coordination Cages. *Angew. Chemie - Int. Ed.* **2005**, *44*, 1810–1813.
- (320) Yamauchi, Y.; Yoshizawa, M.; Akita, M.; Fujita, M. Engineering Double to Quintuple Stacks of a Polarized Aromatic in Confined Cavities. *J. Am. Chem. Soc.* **2010**, *132*, 960–966.
- (321) Murase, T.; Otsuka, K.; Fujita, M. Pairwise Selective Formation of Aromatic Stacks in a Coordination Cage. *J. Am. Chem. Soc.* **2010**, *132*, 7864–7865.
- (322) Sugiyasu, K.; Kawano, S.; Fujita, N.; Shinkai, S. Self-Sorting Organogels with p - n Heterojunction Points. *Chem. Mater.* **2008**, *20*, 2863–2865.
- (323) Jolliffe, K. A.; Timmerman, P.; Reinhoudt, D. N. Noncovalent Assembly of a Fifteen -Component Hydrogen-Bonded Nanostructure. *Angew. Chemie - Int. Ed.* **1999**, *38*, 933–937.
- (324) Cai, M.; Shi, X.; Sidorov, V.; Fabris, D.; Lam, Y. F.; Davis, J. T. Cation-Directed Self-Assembly of Lipophilic Nucleosides: The Cation's Central Role in the Structure and Dynamics of a Hydrogen-Bonded Assembly. *Tetrahedron* **2002**, *58*, 661–671.
- (325) Corbin, P. S.; Lawless, L. J.; Li, Z.; Ma, Y.; Witmer, M. J.; Zimmerman, S. C. Discrete and Polymeric Self-Assembled Dendrimers: Hydrogen Bond-Mediated Assembly with High Stability and High Fidelity. *Proc. Natl. Acad. Sci. U. S. A.* **2002**, *99*, 5099–5104.
- (326) Wu, A.; Chakraborty, A.; Fettingter, J. C.; Flowers, R. A.; Isaacs, L. Molecular Clips That Undergo Heterochiral Aggregation and Self-Sorting. *Angew. Chemie - Int. Ed.* **2002**, *41*, 4028–4031.
- (327) Zhao, X.; Wang, X. Z.; Jiang, X. K.; Chen, Y. Q.; Li, Z. T.; Chen, G. J. Hydrazide-Based Quadruply Hydrogen-Bonded Heterodimers. Structure, Assembling Selectivity, and Supramolecular Substitution. *J. Am. Chem. Soc.* **2003**, *125*, 15128–15139.
- (328) Lighthart, G. B. W. L.; Ohkawa, H.; Sijbesma, R. P.; Meijer, E. W. Complementary Quadruple Hydrogen Bonding in Supramolecular Copolymers. *J. Am. Chem. Soc.* **2005**, *127*, 810–811.
- (329) Maeda, T.; Furusho, Y.; Sakurai, S. I.; Kumaki, J.; Okoshi, K.; Yashima, E. Double -Stranded Helical Polymers Consisting of Complementary Homopolymers. *J. Am. Chem. Soc.* **2008**, *130*, 7938–7945.
- (330) Ajami, D.; Hou, J.; Dale, T. J.; Barrett, E.; Rebek, J. Disproportionation and Self-Sorting in Molecular Encapsulation Dariushin Molecular Encapsulation. *PNAS* **2009**, *106*, 10430–10434.
- (331) Pellizzaro, M. L.; Houton, K. A.; Wilson, A. J. Sequential and Phototriggered Supramolecular Self-Sorting Cascades Using Hydrogen-Bonded Motifs. *Chem. Sci.* **2013**, *4*, 1825–1829.
- (332) Dowling, M. B.; Lee, J. H.; Raghavan, S. R. PH-Responsive Jello: Gelatin Gels Containing Fatty Acid Vesicles. *Langmuir* **2009**, *25*, 8519–8525.
- (333) Helary, C.; Foucault-Bertaud, A.; Godeau, G.; Coulomb, B.; Giraud Guille, M. M. Fibroblast Populated Dense Collagen Matrices: Cell Migration, Cell Density and Metalloproteinases Expression. *Biomaterials* **2005**, *26*, 1533–1543.

- (334) Salis, A.; Ninham, B. W. Models and Mechanisms of Hofmeister Effects in Electrolyte Solutions, and Colloid and Protein Systems Revisited. *Chem. Soc. Rev.* **2014**, *43*, 7358–7377.
- (335) Collins, K. D. Charge Density-Dependent Strength of Hydration and Biological Structure. *Biophys. J.* **1997**, *72*, 65–76.
- (336) Moelbert, S.; Normand, B.; Rios, P. D. L. Kosmotropes and Chaotropes: Modelling Preferential Exclusion, Binding and Aggregate Stability. *Biophys. Chem.* **2004**, *112*, 45–57.
- (337) Lee, C. H.; Singla, A.; Lee, Y. *Biomedical Applications of Collagen*; 2001; Vol. 221.
- (338) Rezvani Ghomi, E.; Nourbakhsh, N.; Akbari Kenari, M.; Zare, M.; Ramakrishna, S. Collagen-Based Biomaterials for Biomedical Applications. *Journal of Biomedical Materials Research - Part B Applied Biomaterials*. John Wiley and Sons Inc December 1, 2021, pp 1986–1999.
- (339) Djabourov, M.; Lechaire, J.-P.; Gaill, F. Structure and Rheology of Gelatin and Collagen Gels. *Biorheology* **1993**, *30*, 191–205.
- (340) Thomas, A. W.; Kelly, M. W. The Iso-Electric Point of Collagen. *J. Am. Chem. Soc.* **1922**, *44*, 195–201.
- (341) Raeburn, J.; Cardoso, A. Z.; Adams, D. J. The Importance of the Self-Assembly Process to Control Mechanical Properties of Low Molecular Weight Hydrogels. *Chem. Soc. Rev.* **2013**, *42*, 5143–5156.
- (342) Chatterjee, S.; Hui, P. C. L. Stimuli-Responsive Hydrogels: An Interdisciplinary Overview. In *Hydrogels - Smart materials for biomedical applications - chapter 2*; 2018.
- (343) Censi, R. Interpenetrating Hydrogel Networks Enhance Mechanical Stability, Rheological Properties, Release Behavior and Adhesiveness of Platelet-Rich Plasma. *Int. J. Biol. Sci.* **2020**, No. 21, 1399.
- (344) Dhand, A. P.; Galarraga, J. H.; Burdick, J. A. Enhancing Biopolymer Hydrogel Functionality through Interpenetrating Networks. *Trends Biotechnol.* **2021**, *39*, 519–538.
- (345) Pocker, Y.; Green, E. Hydrolysis of D-Glucono-. Delta.-Lactone. I. General Acid-Base Catalysis, Solvent Deuterium Isotope Effects, and Transition State Characterization. *J. Am. Chem. Soc.* **1973**, *95*.
- (346) Adams, D. J.; Butler, M. F.; Frith, W. J.; Kirkland, M.; Mullen, L.; P., S. A New Method for Maintaining Homogeneity during Liquid–Hydrogel Transitions Using Low Molecular Weight Hydrogelators. *Soft Matter* **2009**, *5*.
- (347) Wei, Y.; Hore, M. J. A. Characterizing Polymer Structure with Small-Angle Neutron Scattering: A Tutorial. *J. Appl. Phys.* **2021**, *129*.
- (348) Wang, R.; Liu, X.-Y.; Xiong, J.; Li, J. Real-Time Observation of Fiber Network Formation in Molecular Organel: Supersaturation- Dependent Microstructure and Its Related Rheological Property. *J. Phys. Chem. B.* **2006**, *110*, 7275.
- (349) Yu, R.; Lin, N.; Yu, W.; Liu, X. Y. Crystal Networks in Supramolecular Gels: Formation Kinetics and Mesoscopic Engineering Principles. *CrystEngComm* **2015**, *17*, 7986–8010.
- (350) Kizilay, E.; Dinsmore, A. D.; Hoagland, D. A.; Sun, L.; Dubin, P. L. Evolution of Hierarchical Structures in Polyelectrolyte-Micelle Coacervates. *Soft Matter* **2013**, *9*, 7320–7332.
- (351) Swanson-Vethamuthu, M.; Dubin, P. L.; Almgren, M.; Yingjie, L. Cryo-TEM of Polyelectrolyte–Micelle Complexes. *J. Colloid Interface Sci.* **1997**, *186*, 414–419.

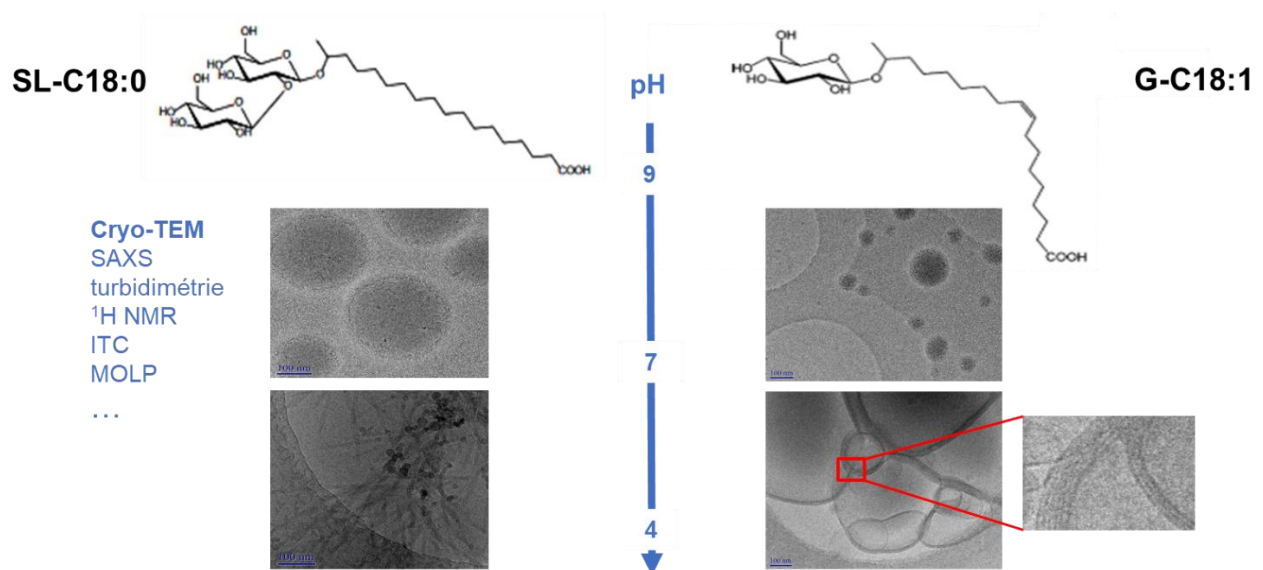
- (352) Wang, Y. Effects of Salt on Poly Electrolyte-Micelle Coacervation. *Macromolecules* **1999**, *32*, 7128–7134.
- (353) Azevedo, M. A.; Cerqueira, M. A.; Fuciños, P.; Silva, B. F. B.; Teixeira, J. A.; Pastrana, L. Rhamnolipids-Based Nanostructured Lipid Carriers: Effect of Lipid Phase on Physicochemical Properties and Stability. *Food Chem.* **2021**, *344*.
- (354) Fan, L.; Chen, Q.; Mairiyangu, Y.; Wang, Y.; Liu, X. Stable Vesicle Self-Assembled from Phospholipid and Mannosylerythritol Lipid and Its Application in Encapsulating Anthocyanins. *Food Chem.* **2021**, *344*, 128649.
- (355) Yan, L.; Han, K.; Pang, B.; Jin, H.; Zhao, X.; Xu, X.; Jiang, C.; Cui, N.; Lu, T.; Shi, J. Surfactin-Reinforced Gelatin Methacrylate Hydrogel Accelerates Diabetic Wound Healing by Regulating the Macrophage Polarization and Promoting Angiogenesis. *Chem. Eng. J.* **2021**, *414*, 128836.

Résumé en français

Systèmes biosurfactant-biopolymère sensibles au pH : de la formation de multiples structures à la synthèse d'hydrogels

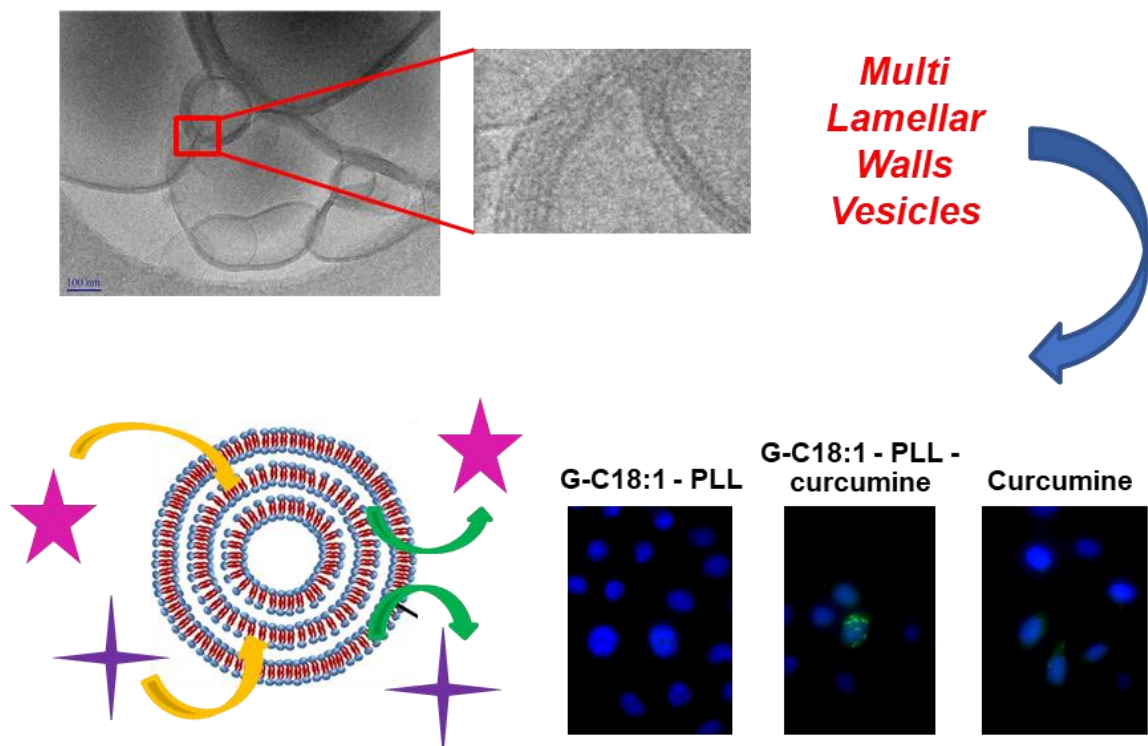
Les surfactants (ou tensioactifs), ces molécules amphiphiles qui, placées en solution diluée dans l'eau, abaissent sa tension superficielle, sont omniprésents dans les produits du quotidien (shampoings ou détergents, par exemple). Ils constituent une science à part entière et leur production atteint les 20 millions de tonnes par an. Ils représentent un marché estimé à 43,7 milliards de dollars, qui pourrait atteindre 66,4 milliards de dollars en 2025. Cependant, leur origine pétrochimique est aujourd'hui controversée par les préoccupations environnementales de notre société. En plus de leur production polluante, ils sont associés à des complications dermatologiques. De nombreux produits ont été retirés du marché ces 30 dernières années et d'autres suivront probablement. Dans ce contexte de recherche active d'alternatives biosourcées, ils pourraient être remplacés par des composés très prometteurs : les biosurfactants. Ce terme désigne une vaste famille de molécules biosourcées produites par fermentation microbienne, extraction de plantes ou biocatalyse, dont le potentiel est encore limité par leur faible production, leur coût élevé, mais aussi par un manque de connaissances, et donc l'absence de maîtrise, de leurs propriétés en solution. Les surfactants entièrement biosourcés ne représentent aujourd'hui que 4% de la production totale. La recherche dans le domaine des biosurfactants se développe depuis les années 60, mais a pris une envergure significative depuis une vingtaine d'années, comme en témoigne le nombre croissant d'articles publiés à ce sujet. Cependant, la grande majorité de ces publications s'intéresse à la classification des biosurfactants, à leurs stratégies de synthèse, dont les modifications génétiques et les nombreux dérivés rendus possibles, à leurs propriétés antibactériennes et à leurs applications dans des domaines divers et variés. Le Laboratoire de Chimie de la Matière Condensée de Paris, où j'ai effectué ma thèse, possède une expertise dans le domaine des biosurfactants et a acquis de solides connaissances concernant leurs propriétés physicochimiques en solution aqueuse, aux interfaces et en présence de macromolécules. Celles-ci sont en effet essentielles avant d'envisager toute application. L'expertise du laboratoire est particulièrement portée sur la catégorie des biosurfactants produits par fermentation microbienne, qui inclue les glycolipides, les lipopeptides, les phospholipides, les lipides neutres et les biosurfactants microbiens polymériques. Mes travaux de thèse ont porté sur deux glycolipides en particulier, dont les structures chimiques sont très proches puisqu'elles ne diffèrent que d'une insaturation et d'une unité glycosidique : G-C18:1 et SL-C18:0 sont respectivement composés d'une (ou deux) unité(s) glycosidique(s), d'une chaîne carbonée de 18 atomes (mono)insaturée et d'une fonction acide carboxylique terminale. Cette dernière leur confère une propriété intéressante : le pH va modifier l'état de charge de ce groupe fonctionnel, un état de charge qui va lui-même dicter le comportement de la molécule en solution. Le diagramme de phase en fonction du pH de ces deux glycolipides a été précisément étudié au laboratoire par de multiples techniques. La cryo-microscopie électronique et la diffusion de rayons X aux petits angles ont notamment mis en évidence la formation de micelles à pH basique. Chaque glycolipide forme des micelles avec ses caractéristiques propres, ces résultats ont été publiés mais ces différences n'auront aucune importance pour la suite de ces travaux. A pH acide, le comportement de chaque glycolipide en solution est très différent : SL-C18:0 s'organise en structures fibrillaires tandis que G-C18:1

s'auto-assemble sous forme de vésicules. Le point de départ de mes travaux de thèse est la formation de coacervats complexes mise en évidence par un collègue lorsque à pH basique SL-C18:1, qui forme lui aussi des micelles, est en présence d'un polyélectrolyte dont la charge est opposée. J'ai donc dans un premier temps démontré que le phénomène de coacervation complexe est aussi observé entre les micelles de G-C18:1 ou SL-C18:0 et différents polyélectrolytes (PEC) de charge opposée (polyallylamine, poly-L-lysine, polyéthylèneimine, chitosan lactate). Si les biosurfactants ont souvent été étudiés dans une région précise de leur diagramme de phase, je me suis intéressée aux transitions de phase, et particulièrement aux transitions micelle-fibre et micelle-vésicule provoquées à l'intérieur même de coacervats complexes. L'évolution des interactions biosurfactant-polyélectrolyte a pu être suivie par SAXS *in-situ* grâce à une procédure bien particulière faisant intervenir une pompe péristaltique, un pousse seringue et un pH-mètre interfacé. Les interprétations qui en découlent ont été confrontées aux clichés obtenus par cryo-TEM. Il en résulte que l'interaction SL-C18:0-PEC n'est pas maintenue à pH acide, où les fibres coexistent avec le polyélectrolyte, tandis que G-C18:1 interagit toujours étroitement avec le polyélectrolyte. En effet, dans ce dernier cas, le coacervat se réorganise en une structure multilamellaire, composée d'une alternance de couches de polyélectrolytes et de couches de biosurfactant. Des études quantitatives ont été menées par ¹H RMN et ITC afin de quantifier l'interaction G-C18:1/PLL. Elles ont notamment mis en avant la contribution d'interactions spécifiques (électrostatiques) mais aussi une contribution non négligeable d'interactions non-spécifiques (effet hydrophobe).



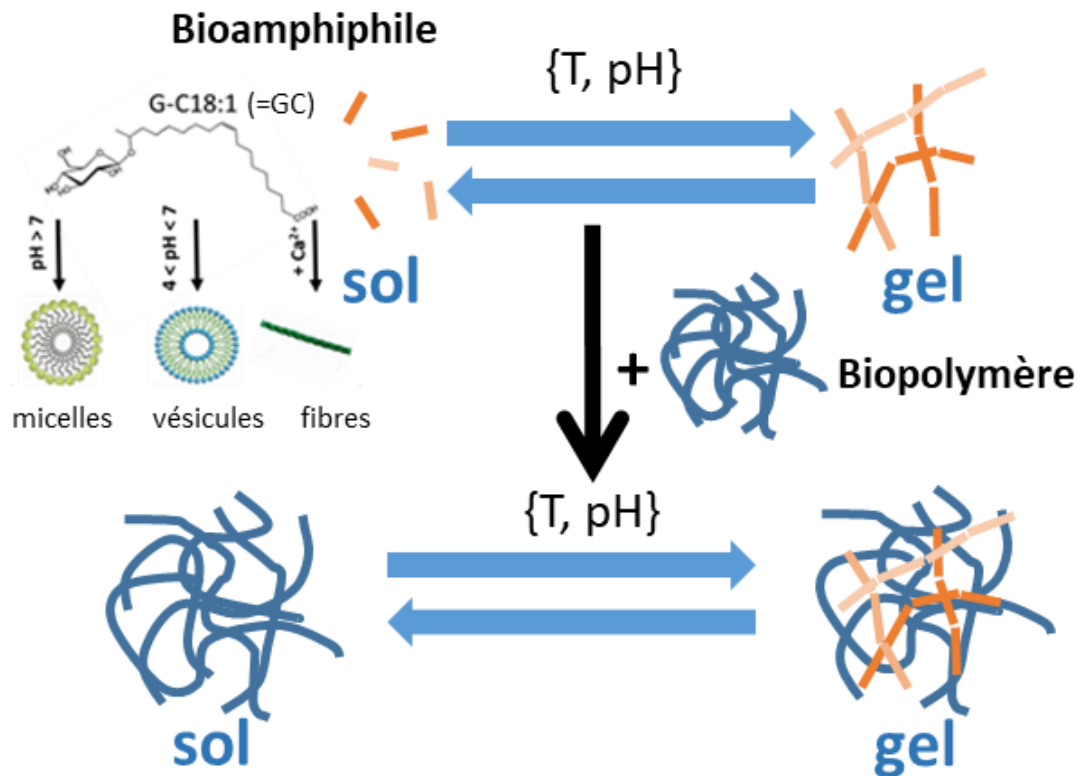
Ces résultats ont donné lieu à la publication de deux articles, un premier présentant la globalité de ces données, et un second exclusivement consacré à l'étude de ces curieuses structures multilamellaires. Il a été montré que l'obtention de ces dernières est strictement conditionnée par la transition de phase à partir du coacervat : mélanger des vésicules de G-C18:1 et un polyélectrolyte ne permet pas d'obtenir une structure multilamellaire bien définie, avec des couches bien ordonnées, mais une structure plus grossière et désorganisée. Un travail a été consacré à l'optimisation du contrôle de leur taille par des méthodes classiques telles que la filtration ou la sonication. De telles structures possèdent un réel potentiel pour l'encapsulation de composés d'intérêt, une série d'expériences a donc été menée dans ce sens. Le premier point qui a été vérifié est la formation de ces structures multilamellaires dans un milieu de culture cellulaire, le DMEM, et la viabilité de différentes lignées cellulaires en leur présence. Les résultats sont encourageants

puisque le milieu de culture cellulaire s'avère propice à la formation de ces structures multilamellaires. De plus, deux lignées cellulaires différentes ont été cultivées en leur présence : Normal Human Dermal Fibroblast (NHDF) and HeLa cells, et leur devenir n'est pas le même. En effet, les fibroblastes survivent et se développent, ce qui n'est pas le cas pour les cellules cancéreuses. La curcumine a ensuite été choisie comme composé à encapsuler ; il s'agit d'un puissant antioxydant et anticancéreux dont l'encapsulation est essentielle à l'exercice de ces activités. Un protocole robuste a été mis en place afin d'encapsuler efficacement la curcumine à l'intérieur des structures multilamellaires. Les résultats obtenus précédemment concernant la viabilité des cellules en présence des structures multilamellaires sont valables quand ces dernières contiennent de la curcumine.



Cette partie plus biologique est celle dans laquelle j'ai été le moins impliquée, les résultats obtenus seront néanmoins prochainement publiés. L'ensemble des résultats obtenus jusque-là en conditions diluées permettent de mieux connaître et maîtriser le comportement des biosurfactants en solution d'un point de vue physicochimique, mais ouvrent des pistes également d'un point de vue applicatif.

Les biosurfactants sont aussi intéressants à étudier dans des conditions très différentes puisque à plus forte concentration, certains possèdent des propriétés d'hydrogélification. Le design et la synthèse d'hydrogels entièrement biosourcés sont des enjeux majeurs pour toutes sortes d'applications biomédicales. Je les étudie toujours en présence de biopolymères, les hydrogels synthétisés pourront donc bénéficier des propriétés et avantages de deux réseaux interpénétrés. Ce type de gel peut se présenter sous différentes formes : les deux réseaux peuvent interagir ou gélifier chacun indépendamment, la présence simultanée de deux réseaux peut perturber le comportement de l'un des deux réseaux ou non... Nous nous attendons notamment à ce que le polymère assure de bonnes propriétés mécaniques à l'ensemble du gel, et à ce que le biopolymère permette lui de moduler ces propriétés en fonction de stimuli tels que le pH.



Un premier résultat concerne la gélification du biosurfactant G-C18 :1, qui s’opère en présence de calcium à pH≈8. Une nouvelle phase a été mis en évidence par cryo-TEM et caractérisée par SAXS, une phase fibrillaire. C’est un gel qui atteint des propriétés mécaniques de l’ordre de la centaine de Pa pour une concentration de 2wt%. Il est sensible à la température mais la transition sol-gel est réversible, et ce sur plusieurs cycles de température. Le coût des polyélectrolytes utilisés précédemment ne permettait pas de travailler avec à plus forte concentration, d’autres biopolymères ont donc été choisis pour cette partie du projet : la gélatine, l’alginate et le chitosan (haut poids moléculaire). Quelques expériences préliminaires ont également été réalisés avec du collagène, une molécule très proche de la gélatine dont l’intérêt est considérable dans le domaine biomédical. Plusieurs tendances ont été observées et ont fait l’objet de deux publications distinctes, d’une part une amélioration des propriétés mécaniques du gel hybride par rapport aux gels de chacun des composés, et d’autre part une capacité à répondre à deux stimuli extérieurs, le pH et la température. Le G-C18 :1 existe sous différentes formes comme évoqué précédemment, et cette phase s’est révélée déterminante pour les propriétés mécaniques du gel hybride. En effet, l’ajout de micelles, équivalent à l’ajout de vésicules, n’a que peu d’effet sur les propriétés mécaniques du gel de biopolymère, tandis que l’ajout de fibres obtenues en présence de calcium permet d’augmenter significativement les propriétés mécaniques du gel de l’ensemble des biopolymères testés. Les données SAXS obtenues suggèrent que ces gels hybrides sont basés sur la coexistence de deux réseaux indépendants et que la somme de leurs propriétés mécaniques respectives résulte en un gel hybride plus fort. Cet effet d’amélioration des propriétés mécaniques dépendant de la phase de G-C18 :1 impliquée est valable pour tous les biopolymères testés. D’autres séries d’expériences ont été consacrées aux éventuelles fonctionnalités de ces gels hybrides. L’influence d’un premier stimulus a été étudiée, celle du pH. Elle a été étudiée en suivant les propriétés mécaniques d’un gel à pH basique lors de son acidification *in-situ* par hydrolyse de la delta gluconolactone (GDL). La tendance

observée est la même pour tous les biopolymères étudiés : les propriétés mécaniques du gel hybride diminuent avec le pH, mais cet effet est plus ou moins prononcé en fonction du biopolymère. En effet, la perte des propriétés mécaniques est plus marquée pour les gels comprenant de la gélatine que ceux à base de chitosan ou d'alginate. L'étude SAXS couplée à la rhéologie a mis en évidence une perte de structure associée à la perte des propriétés mécaniques. L'effet de la température (étudié jusqu'à 50°C), lui, n'est pas généralisable. Un gel de G-C18 :1 seul perd ses propriétés mécaniques de manière réversible : la transition sol-gel s'opère de nouveau en revenant à température ambiante. Cette propriété va être transmise à un gel hybride G-C18 :1-gélatine, ce qui est intéressant si on considère qu'un gel de gélatine seule, lui aussi sensible à la température, ne se reforme pas sur le même intervalle de temps. De plus, cette réversibilité intervient sur plusieurs cycles de température. En ce qui concerne l'alginate et le chitosan, les propriétés mécaniques des gels de chacun de ces deux biopolymères ne sont pas influencées par la température ($20^{\circ}\text{C} < T < 50^{\circ}\text{C}$), leur présence confère donc au gel hybride une meilleure résistance à la température. Tous les gels hybrides possèdent cependant un point commun : la température n'a pas d'effet sur la structure du gel. Le renforcement des propriétés mécaniques par les gels hybrides a fait l'objet d'un premier papier, un second est lui plutôt consacré à la fonctionnalité apportée vis-à-vis du pH et de la température. Ces gels hybrides entièrement biosourcés sont très novateurs, et largement valorisables pour des applications dans le domaine biomédical, particulièrement friand d'hydrogels fonctionnels biocompatibles. Quelques expériences préliminaires ont été menées avec du collagène ou d'autres biosurfactants.

L'ensemble de ces travaux de thèse a contribué à enrichir la connaissance des biosurfactants, aussi bien d'un point de vue physicochimique que d'un point de vue applicatif, ce qui ne fait qu'accroître leur intérêt et encourage à de futures découvertes, rendant progressivement possible le remplacement des surfactants pétrochimiques par une alternative plus respectueuse de l'environnement et moins susceptible de rencontrer des problèmes de biocompatibilité.

ANNEX 1: pH-resolved *in-situ* Small Angle X-Ray Scattering

Small angle X-ray scattering (SAXS) is a small-angle scattering technique able to quantify differences in electron density at the Å scale in a sample through the interactions between photons and the electrons cloud of atoms. It provides the size, shape and polydispersity of colloids in the Å-150 nm range (nanoparticles, micelles...). These data result from the analysis of the elastic scattering behavior of X-rays when crossing the material, recording their scattering at small angles (typically in the 10^{-3} - 1 Å^{-1} range). Contrary to small-angle neutron scattering, SAXS is typically performed using hard X-rays whose wavelength is comprised between 0.07 – 0.2 nm. Depending on the angular range in which a clear scattering signal can be recorded, SAXS provides structural information of dimensions between 1 and 100 nm, and of repeat distances in partially ordered systems of up to 150 nm. The smaller the recorded angle, the larger the object dimensions that are probed.

Concerning proteins or other biological macromolecules, the advantage of SAXS over crystallography is that no crystalline sample is mandatory. Furthermore, the properties of SAXS allow investigation of conformational diversity in these molecules, while nuclear magnetic resonance spectroscopy methods hardly serve for macromolecules of higher molecular mass (> 30–40 kDa). However, owing to the random orientation of dissolved or partially ordered molecules, the spatial averaging induces a loss of information in SAXS not observed using crystallography.

The method is accurate, generally non-destructive (denaturation of proteins can occur) and generally requires a minimal sample preparation for very broad applications. It includes various colloids, metals, cement, oil, polymers, plastics, proteins, foods and pharmaceuticals and can be leveraged in research as well as in quality control. X-rays can come from a laboratory source or a higher X-ray flux can be provided by synchrotron light.

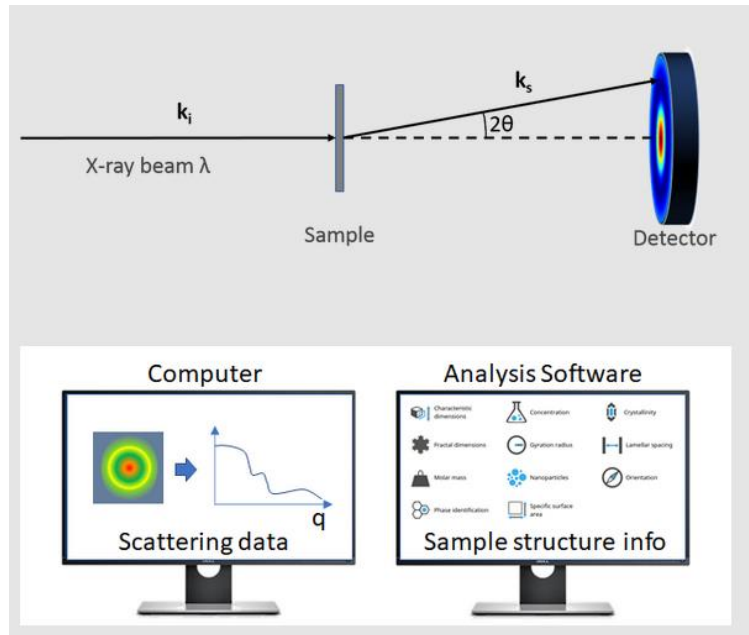


Figure 51 – Schematic representation of a SAXS setup (<https://www.xenocs.com/knowledge-base/saxs>)

In a typical experiment, a highly collimated beam of monochromatic X-rays (incident monochromatic radiation of wave vector k_i) passes through the sample (on the order of 1 mm in thickness). The scattered X-rays are collected on a 2-dimensional area detector azimuthally in 360° at a continuous range of scattering angles which deviate from the direct, transmitted beam as a function of the scattering angle θ , defined by convention as 2θ , and which defines a “probe length” expressed as $D = 2\pi/q$, where $q = 4\pi \frac{\sin(\theta)}{\lambda}$, in which λ is the wavelength of the X-rays (typically 0.154 nm for the Cu X-ray source).

Elastic interactions are characterized by zero energy transfer so that the modulus of the scattered wave vector k_f is equal to the modulus of the incident wave vector $|k_i| = |k_f|$. The scattered

intensity is a function of the scattering vector $q = |k_i| - |k_f|$ defined by :

$$q = \frac{4\pi}{\lambda} \sin \frac{\theta}{2} q = \frac{4\pi}{\lambda} \sin \frac{\theta}{2}$$

with θ the scattering angle and λ the wavelength of the incident beam. The scattered intensity $I(q)$ is measured at very small angles which allows the study of characteristic sizes ranging from crystallographic distances (a few angstroms) to colloidal distances (0.1 micron).

The intensity of a solution of particles $I(q) = \Delta\rho^2 \phi_v V_p P(q) S(q)$ where $\Delta\rho^2$ is the contrast, ϕ_v is the volume fraction of the particles and V_p the volume of a dry particle. $P(q)$ is the form factor of the particle and depends only on its geometry. $S(q)$ is the structure factor and describes the correlations between particles; this term occurs when the molecules are ordered for example.

In this work, we used three different set up.

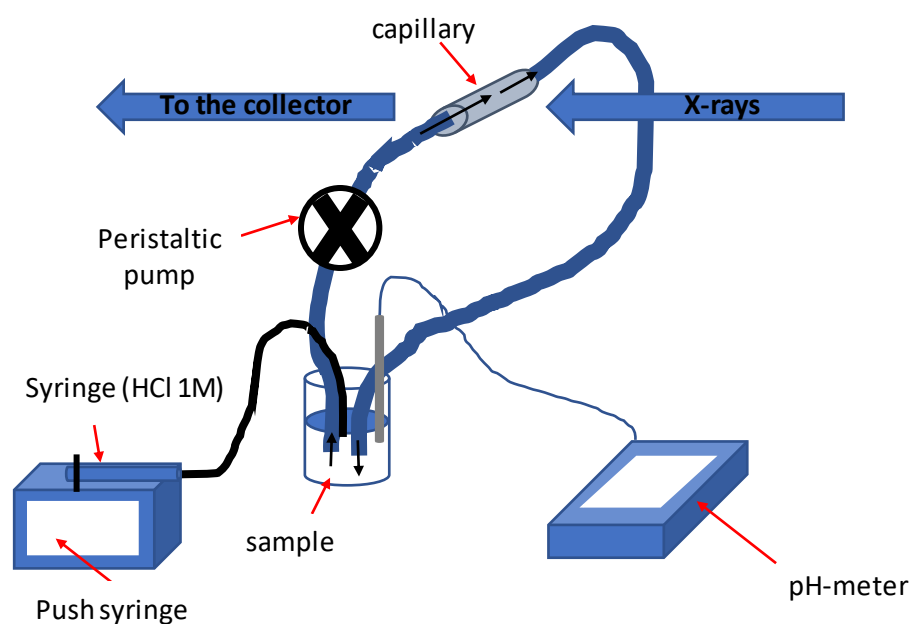


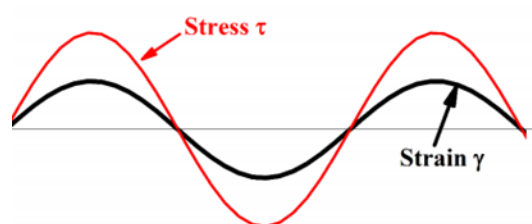
Figure 52 – Scheme of the experimental setup used for time resolved in-situ SAXS experiments.

The first set up (pH-resolved *in situ* SAXS, used to study diluted systems in **Chapters I and II**), illustrated by Figure 52, aims to simultaneously record SAXS data and pH of the solution to attribute a structure to a pH: an eppendorf is filled with sample which circulates through the capillary by the use of a peristaltic pump while it is acidified by a HCl 1M solution contained in a syringe at a precise rate and the pH is recorded by a pH-meter. A difficulty encountered during the first runs was to manually record the pH (seen through a camera on the pH-meter) at a fast rate, but was overcome by the acquisition of an interfaced apparatus and a software recording automatically the pH at a predetermined rate.

To study gels in **Chapters III and IV**, we rather used either capillaries or rheo-SAXS set up.

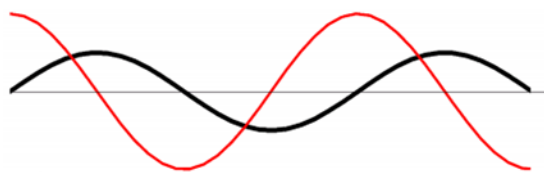
Annex 2: Rheology

Small amplitude oscillatory rheology is able to determine the viscoelastic response of gels to dynamic shear stress, allowing multiple measurements without sample destruction due to small deformations. Another advantage comes from the possible comparison of values obtained from different studies regardless of the instrumentation used. A substance under an imposed stress is typically either ideal solid or ideal liquid. The energy transferred to an ideal solid (Hookean) will be totally and reversibly stored, stress and strain are in phase :



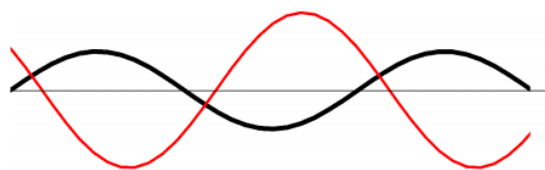
Phase angle = 0

On the contrary, an ideal liquid (Newtonian) will fully convert irreversibly the transferred energy into internal energy *via* dissipative effects; stress and strain are thus out of phase by 90° :



Phase angle: 90°

Gels exhibit both solid-like (elastic) and a liquid-like (viscous) behaviors simultaneously: stress and strain are not in phase :



$0 < \text{phase angle} < 90^\circ$

The relative contributions of the elastic and viscous components, among other significant information, can be determined using the phase lag.

The dynamic shear stress response to small amplitude oscillation is described by two moduli. The elastic modulus (G') is related to the energy reversibly stored during deformation, whereas the viscous modulus (G'') is linked to the energy dissipated as heat/internal energy due to sample viscosity. The loss tangent ($\tan \delta$) is calculated by the ratio G''/G' and reflects the phase angle between stress and strain; its value suggests liquid-like properties if greater than 1, whereas it indicates solid-like properties if lower than 1. For a specific gel, magnitudes of G' and G'' are measurement frequency, temperature and strain dependent. In the linear regime, both values are independent of strain (or stress). Gels commonly undergo four types of dynamic tests to investigate their properties:^{1,2}

Strain sweep is performed at a constant frequency and temperature, and determines the linear response range of a network to increasing strain (or stress) amplitude. In the linear viscoelastic range, stress evolves linearly with strain, resulting in constant values of G' and G'' .

Frequency sweep determines G' and G'' as functions of frequency at a fixed temperature and strain amplitude. There exists four types of material based on the mechanical spectra: diluted solution (e.g. fruit juice), entangled solution (e.g. semi-dilute chitosan solution), strong gel (e.g. jelly) and weak gel (e.g. ketchup) [124,125]. For strong gels, $G' \approx 10G''$ throughout the frequency range, and G' and G'' are almost independent of frequency, whereas for weak gels, both moduli depend on frequency and their values are less different.

Temperature sweep is useful to investigate some temperature-related processes, such as the gelation of heated dispersion during cooling, starch gelatinization during heating and protein aggregates and gel formation. G' and G'' are determined as functions of temperature at fixed frequency and strain.

Time sweep is used to study the structure development of gels, during which G' and G'' are measured as functions of time at fixed frequency, strain and temperature. Additional information on the gelation and melting phenomena can be obtained with time and temperature sweeps by calculating the structure development rates (dG'/dt or dG'/dT) or structure loss rates ($-dG'/dt$ or $-dG'/dT$). The gel point marks the phase transition of polymer solution from liquid to a soft viscoelastic solid during gelation. The gel point can be given as a precise time or as a specific temperature.³ The transition is triggered by the increasing connectivity in the material. The zero-shear viscosity increases and diverges as the connectivity increases when approaching the gel point. At the gel point, the viscosity diverges to infinity but the equilibrium modulus is still zero. Beyond the gel point, the equilibrium modulus starts to increase.⁴⁻⁷

REFERENCES

- (1) Rao, M. A. Measurement of Flow and Viscoelastic Properties. In *Rheology of Fluid and Semisolid Foods: Principles and Applications*, Springer US: Boston, MA; 2007; pp 59–151.
- (2) Kasapis, S.; Bannikova, A. Chapter 2 - Rheology and Food Microstructure. In *J. Ahmed, P. Ptaszek, S. Basu (Eds.), Advances in food rheology and its applications*, Woodhead Publishing; 2017; pp 7–46.
- (3) Lopes da Silva, J. A.; Rao, M. A. Rheological Behavior of Food Gels. In *Rheology of Fluid and Semisolid Foods: Principles and Applications*, Springer US: Boston, MA; 2007; pp 339–401.
- (4) Winter, H. H.; Mours, M. Rheology of Polymers Near Liquid-Solid Transitions. In *Neutron Spin Echo Spectroscopy Viscoelasticity Rheology*, Springer Berlin Heidelberg: Berlin, Heidelberg; 1997; pp 165–234.
- (5) Grillet, A. M.; Gloe, L. M.; Wyatt, N. B. Polymer gel rheology and adhesion. *Rheology* **2012**
- (6) Henning Winter, H. Gel Point. In *Encyclopedia of Polymer Science and Technology*, John Wiley & Sons, Inc.; 2002.
- (7) Winter, H. H.; Morganelli, P.; Chambon, F. Stoichiometry effects on rheology of model polyurethanes at the gel point. *Macromolecules* **1988**, *21*, 532–535

Annex 3: SL-C16:0 / Collagen

In **Chapter III**, collagen's hydrogels mechanical properties were found enhanced in presence of G-C18:1 fibrillar phase (pH 8). Knowing that viscosity of collagen increases with pH and that the biosurfactant SL-C16:0 (structure given in Figure 53) exhibits the opposite behavior,¹ the idea to combine collagen with SL-C16:0 came up, in view to obtain a tough hydrogel over the whole pH range.

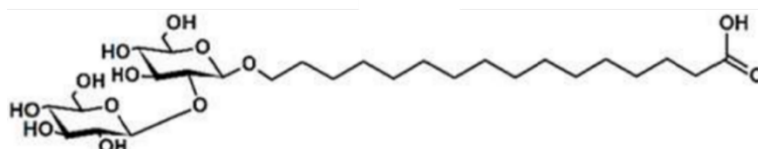


Figure 53 – Chemical structure of SL-C16:0

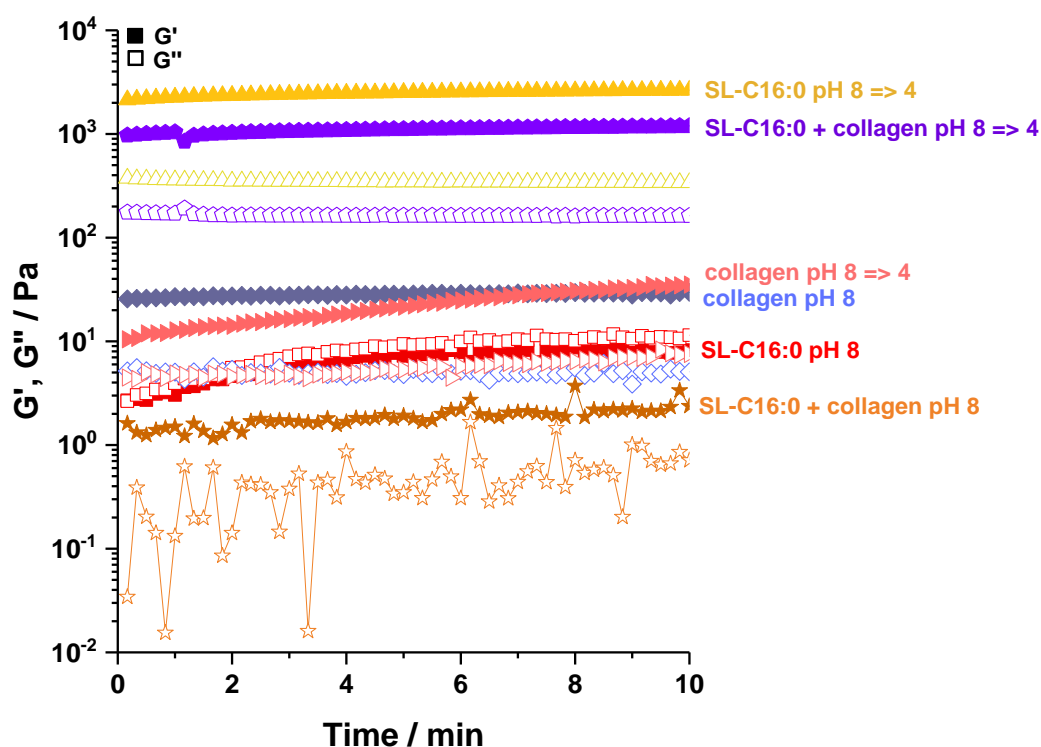


Figure 54 – Storage and loss modulus of SL-C16:0, collagen and mix of both at pH 8 and pH 8 decreased down to 4

As shown by Figure 54, collagen alone displays poor mechanical properties, at both pH 8 and 4, due to the concentration employed (0.27 wt%). Mechanical strength is enhanced ($\times 100$) upon addition of SL-C16:0 (SL-C16:0/collagen: 2/0.27 wt%) at pH 8 decreased to 4, up to the mechanical properties exhibited by SL-C16:0 alone at pH 4 (liquid at pH 8).

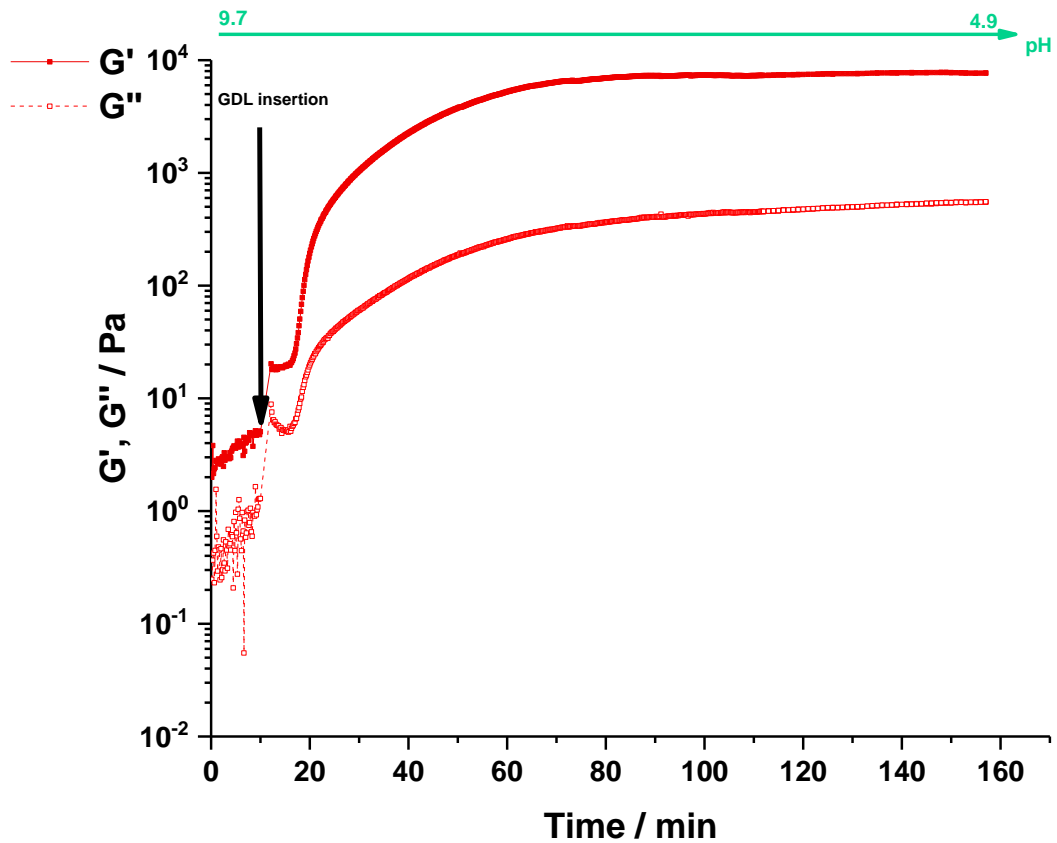


Figure 55 – Evolution of storage and loss modulus of a SL-C16:0/collagen gel (1/0.135wt%) upon GDL hydrolysis

We then employed the same approach than in **Chapter IV** to follow the mechanical properties of a SL-C16:0/collagen gel upon lowering the pH. As expected, acidification triggered by GDL hydrolysis results in a huge increase of the mechanical properties, from a few Pa to 10^4 Pa (Figure 55). We are further interested in performing the same experiment at higher collagen contents, e.g. at a higher initial G' , keeping constant the sophorolipid amount.

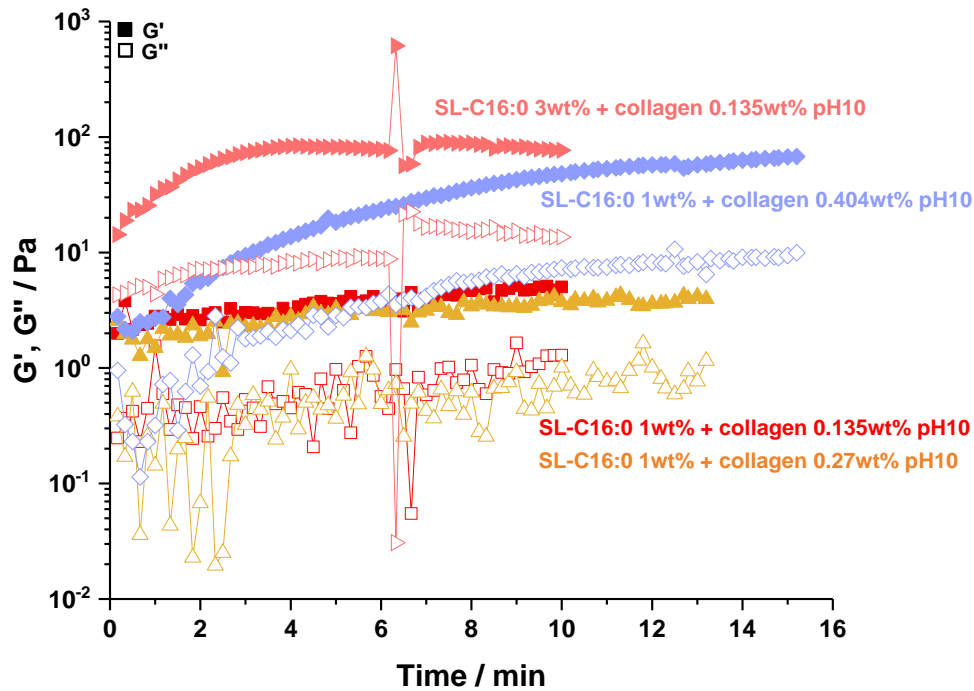


Figure 56 – Influence of increased SL-C16:0 or collagen concentration over the resulting mechanical properties of the hybrid gel

Rheological measurements shown in Figure 56 suggest that for a fixed concentration of SL-C16:0 (1wt%, red, yellow and purple curves), increasing the collagen concentration allows to enhance the mechanical properties of the hybrid gel, starting from a threshold: below 0.404wt%, comparable properties have been measured. The contrary does also occur: for a fixed concentration of collagen (0.135wt%, red and pink curves), increasing the SL-C16:0 concentration allows to enhance the mechanical properties of the hybrid gel. If we compare pink (more SL-C16:0, less collagen) and purple curves (less SL-C16:0, more collagen), both samples reach a plateau at comparable mechanical properties at about $t = 10$ min, suggesting that SL-C16:0 and collagen amounts can both be balanced to reach the same properties.

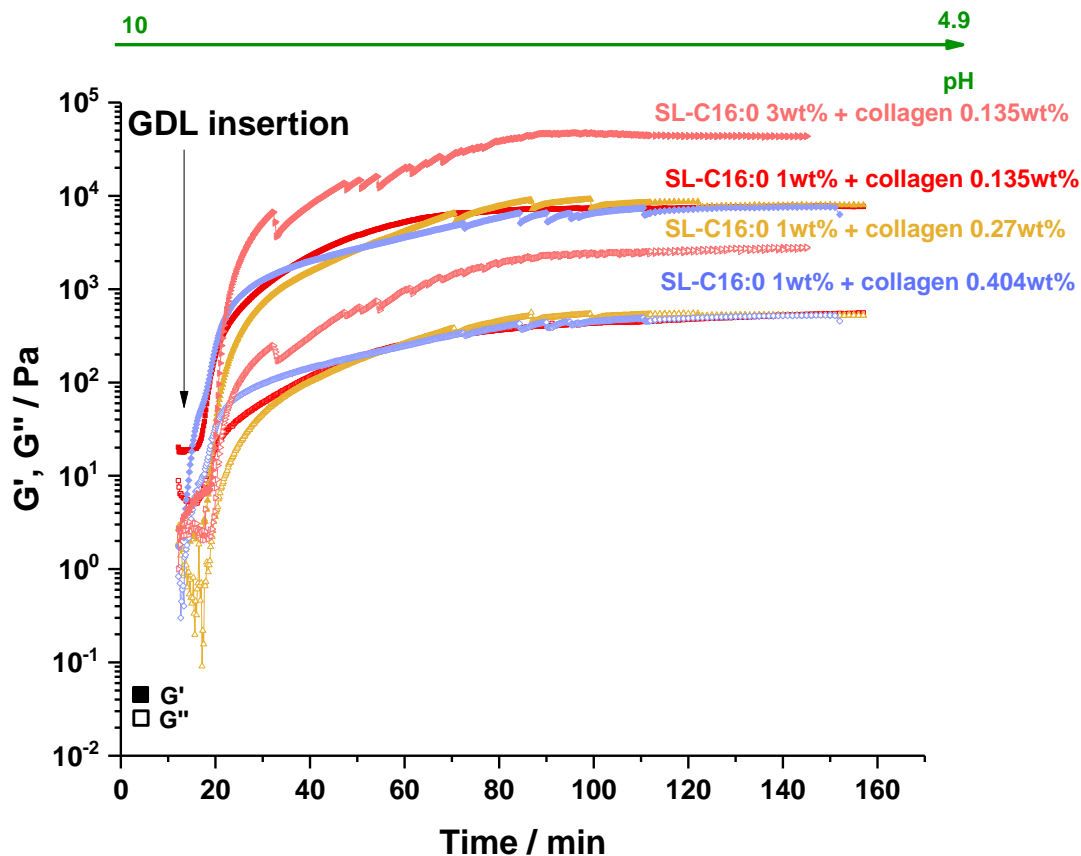


Figure 57 - Evolution of storage and loss modulus of a SL-C16:0/collagen gel (1-3/0.135-0.404wt%) upon GDL hydrolysis

Upon GDL hydrolysis and consequent pH decrease, rheological measurements shown in Figure 57 suggest that for a fixed concentration of SL-C16:0 (1wt%, red, yellow and purple curves), increasing the collagen concentration does not increase the final mechanical properties at acidic pH. On the contrary, for a fixed concentration of collagen (0.135wt%, red and pink curves), increasing the SL-C16:0 concentration allows to significantly enhance the final mechanical properties of the hybrid gel at acidic pH.

Reference

- (1) Baccile, N.; Messaoud, G. Ben; Griel, P. Le; Cowieson, N.; Perez, J.; Geys, R.; Graeve, M. De; Roelants, S. L. K. W.; Soetaert, W. Palmitic Acid Sophorolipid Biosurfactant: From Self-Assembled Fibrillar Network (SAFiN) To Hydrogels with Fast Recovery. *Philos. Trans. A* **2021**, 10.1098/rsta.2020.0343.

Paper I: Stimuli-Induced Nonequilibrium Phase Transitions in Polyelectrolyte-Surfactant Complex Coacervates

This paper presents results supporting the generalization of complex coacervates' formation for all biosurfactants and polyelectrolytes tested in the micellar region of each biosurfactant's phase diagram when oppositely charged. The influence of pH-induced phase transitions of the biosurfactant triggered inside a complex coacervate is then investigated. The *micelle-to-fiber* transition results in the dissociation of the complex and the coexistence of SL-C18:0 fibers and polyelectrolyte chains in solution without any interaction, while the *micelle-to-vesicle* transition exhibits a clear continuity between the complex coacervate and a multilamellar walled vesicle obtained in the vesicular domain of G-C18:1 after progressive reorganization of the coacervate.

Paper II: Synthesis of multilamellar walls vesicles polyelectrolyte-surfactant complexes from pH-stimulated phase transition using microbial biosurfactants

This paper focuses on the multilamellar walled vesicles presented in the first article and details a robust method leveraging the *micelle-to-vesicle* phase transition for the preparation of multilamellar structures exhibiting more order than structures obtained using classical methods, emphasizing that the self-assembly resulting structures can also depend on the procedure employed in an oppositely charged biosurfactant-biopolymer system.

Project paper III: Glycolipid Biosurfactants as Multilamellar Vesicular Drug Carriers

This study acts as a proof of concept which assesses the stability of [G-C18:1+PLL] based *MLWV* in culture medium at physiological pH according to advanced pH-resolved *in situ* small angle X-ray scattering (SAXS) using synchrotron radiation arguments. Once these systems were found suitable to work under biological conditions, their cytotoxicity towards mouse fibroblasts L929, normal human dermal fibroblasts NHDF, macrophages derived THP-1 and human cervical carcinoma HeLa was addressed. Below 250 $\mu\text{g}/\text{mL}$, the nanocarriers did not present any cytotoxicity on cells. Curcumin was encapsulated as model drug to evaluate if [G-C18:1+PLL] based *MLWV* could be efficient novel drug delivery systems to specifically target cancer cells. The curcumin loaded *MLWVs* are more uptaken in HeLa cells (50%) than in NHDF (35%) and THP-1 derived macrophages (20%), which is correlated to a large amount of curcumin released within the cytoplasm and associated to a cytotoxic effect for the dose 250 $\mu\text{g}/\text{mL}$. No significant cytotoxic effect is recorded on NHDF and macrophages. According to a unique mechanistic study, this cytotoxic effect results from *MLWV* fusion with the cell membrane and the consequent release of curcumin within cells. Curcumin or other hydrophobic drugs' therapeutic effects could thus be enhanced by *MLWVs*, an alternative composition of current drug delivery systems.

Project paper IV: Mechanical reinforcement of biosurfactant/biopolymer hydrogels through interpenetrating networks

This project paper describes the synthesis of hybrid G-C18:1/biopolymer (gelatin, chitosan HMW and gelatin) hydrogels and discuss their rheological behaviors. Mechanical properties of such hybrid gels were found enhanced compared to G-C18:1 or biopolymer hydrogels when the biosurfactant is within its fibrillary state due to the presence of calcium. The addition of G-C18:1 micelles or vesicles do not have a significant effect on the mechanical properties of biopolymers' hydrogels.

Project paper V: pH and temperature responsivity of biosurfactant/biopolymer interpenetrated networks

This project paper reports the functionality of fully biobased IPN hydrogels resulting from the combination of a biosurfactant and a biopolymer regarding two external stimuli: pH and temperature. Rheo-SAXS studies allow to associate a viscoelastic behavior to a structure (structure-property relationship). Both stimuli are more or less efficient depending on the biopolymer involved, with a more pronounced effect using gelatin than alginate or chitosan. These results are particularly encouraging for drug delivery applications knowing that acidity conditions depend on the body tissue. Biosurfactants, never reported in such systems up to now, are molecules of choice to design hybrid biopolymers IPNs with responsiveness to stimuli, especially pH, knowing their rich pH-dependent phase diagrams.



HAL
open science

Stimuli-induced non-equilibrium phase transitions in polyelectrolyte-surfactant complex coacervates

Chloé Seyrig, Gertrude Kignelman, Wim Thielemans, Patrick Le Griel,
Nathan Cowieson, Javier Perez, Niki Baccile

► **To cite this version:**

Chloé Seyrig, Gertrude Kignelman, Wim Thielemans, Patrick Le Griel, Nathan Cowieson, et al.. Stimuli-induced non-equilibrium phase transitions in polyelectrolyte-surfactant complex coacervates. Langmuir, American Chemical Society, In press, 10.1021/acs.langmuir.0c01177 . hal-02905979

HAL Id: hal-02905979

<https://hal.archives-ouvertes.fr/hal-02905979>

Submitted on 24 Jul 2020

HAL is a multi-disciplinary open access archive for the deposit and dissemination of scientific research documents, whether they are published or not. The documents may come from teaching and research institutions in France or abroad, or from public or private research centers.

L'archive ouverte pluridisciplinaire **HAL**, est destinée au dépôt et à la diffusion de documents scientifiques de niveau recherche, publiés ou non, émanant des établissements d'enseignement et de recherche français ou étrangers, des laboratoires publics ou privés.

Stimuli-induced non-equilibrium phase transitions in polyelectrolyte-surfactant complex coacervates

Chloé Seyrig,^a Gertrude Kignelman,^b Wim Thielemans,^b Patrick Le Griel,^a Nathan Cowieson,^c Javier Perez,^d Niki Baccile^{a,*}

^a Sorbonne Université, Centre National de la Recherche Scientifique, Laboratoire de Chimie de la Matière Condensée de Paris, LCMCP, F-75005 Paris, France

^b Sustainable Materials Lab, Department of Chemical Engineering, KU Leuven, campus Kulak Kortrijk, Etienne Sabbelaan 53, 8500 Kortrijk, Belgium

^c Diamond Light Source Ltd, Harwell Science and Innovation Campus, Didcot, OX11 0QX, U.K.

^d SWING, Synchrotron Soleil, BP 48, 91192 Gif-sur-Yvette, France

* Corresponding author: niki.baccile@sorbonne-universite.fr

Abstract

Polyelectrolyte-surfactant complexes (PESCs) are important soft colloids with applications in the field of personal care, cosmetics, pharmaceuticals and much more. If their phase diagrams have long been studied under pseudo-equilibrium conditions, and often inside the micellar or vesicular regions, understanding the effect of non-equilibrium conditions, applied at phase boundaries, on the structure of PESCs generates an increasing interest. In this work we cross the micelle-vesicle and micelle-fiber phase boundaries in an isocompositional surfactant-polyelectrolyte aqueous system through a continuous and rapid variation of pH. We employ two microbial glycolipid biosurfactants in the presence of polyamines, both systems being characterized by their responsiveness to pH. We show that complex coacervates (*Co*) are always formed in the micellar region of both glycolipids' phase diagram and that their phase behaviour drives the PESCs stability and structure. However, for glycolipid forming single-wall vesicles, we observe an isostructural and isodimensional transition between complex coacervates and a multilamellar walls vesicle (*MLWV*) phase. For the fiber-forming glycolipid, on the contrary, the complex coacervate disassembles into free polyelectrolyte coexisting with the equilibrium fiber phase. Last but not least, this work also demonstrates the use of microbial glycolipid biosurfactants in the development of sustainable PESCs.

Keywords. Polyelectrolyte-Surfactant Complex (PESC), complex coacervates, biosurfactants, polyelectrolytes, multilamellar walls vesicles

Introduction

Polyelectrolyte-surfactant complexes (PESCs) are a wide class of colloidal systems where surfactant's self-assembly is combined to the complexation properties of polyelectrolytes.¹⁻⁷ In the past three decades a large number of works has shown the interest of a wide community of scientists towards these systems for the broad set of applications in food science,⁸ tissue engineering,⁹ drug and gene delivery,^{2,10} underwater adhesives conception,¹¹ structuring agents,¹² water treatment,¹³ but also personal care, cosmetics,¹⁴ food, pharmaceutical science¹⁵⁻¹⁷ and much other.⁵⁻⁷

The structure of PESCs depend on many parameters, including the intrinsic packing parameter of the surfactant,¹⁸ rigidity of the polyelectrolyte, charge density and distribution on both surfactant and polyelectrolyte, ionic strength and pH, just to cite the main ones.^{3,4,6,7,19,20} Supramicellar aggregates are the most common structures when the surfactant is in the micellar region of its phase diagram. They can be found as polyelectrolyte-coated dense aggregates of spheroidal micelles, which can undergo either a solid-liquid,^{3,7} or liquid-liquid,^{3,21} phase separation. In the latter case, they are referred to as complex coacervates.^{21,22} Supramicellar colloids can also be found in the form of pearl-necklace or cylindrical morphologies.^{3,4} The micellar morphology and structure are generally not affected by complexation,^{3,7,21,23} however, phase transitions can occur inside the supramicellar complexes due to the local rise in concentration.^{3,4,7,24} Multilamellar PESCs, of both flat or vesicular morphologies, have also been explored from a fundamental point of view^{3,5,7,19,25} for their interest in gene delivery applications, as described for DNA-complexed phospholipids, known as lipoplexes.^{2,19}

Considering the importance of PESCs, the study of their phase diagrams started long ago for a wide range of surfactants complexed by polymers or block copolymers. The complexity of this task is high due to multidimensionality, where effects of ionic strength, cosolvent, cosurfactants and charge could be taken into account.^{5,6,19,20,24-26} Even if the debate about whether PESCs are at equilibrium or not is still open,³ the study of their phase diagram has long been addressed using a classical thermodynamic approach, involving a systematic parametric study and equilibration times. However, more recent trends consider the importance of crossing phase boundaries under non-equilibrium conditions.^{3,4} This is motivated by both practical considerations on applications and fundamental questioning.³ If non-equilibrium transitions are a recent concern in PESCs³, they are in fact a major concern in the broader field

of macromolecular complexation,^{27–29} and complex coacervation in particular, as shown by recent works, concerned by selective control of interactions between polyelectrolytes and lipids.^{30,31} Molecular dynamics and diffusion-limited processes open again, under a new perspective, old questions such as possible shift of the surfactant's phase boundary, promotion of a new surfactant's phase but also PESC disassembling, promotion of a new PESC phase or coexistence between surfactant and polyelectrolyte phases.

The micelle-to-vesicle transition is particularly interesting because, while being classical in lyotropic surfactant and lipid phases,^{25,32} it could be exploited in delivery applications under non-equilibrium conditions. Interestingly, non-equilibrium micelle-to-vesicle transitions are well-known,³³ however, to the best of our knowledge, they were rarely investigated in PESC, even under pseudo-equilibrium conditions. The equilibrium phase diagram of ethoxy fatty acids in aqueous solutions displayed a pH-dependent micelle-to-vesicle transition,³⁴ but the same transition was not observed in the presence of polyelectrolytes,³⁵ thus confirming the yet unpredictable effect of polyelectrolytes on surfactants' phase diagram. This is particularly true in the case of lipid bilayer membranes, of which the physical properties, including the local composition, defects, segregation and bending energy depend on the polyion.^{25,36–39} Even if the complexity of the interactions between polyelectrolytes and (soft) interfaces has been addressed for decades,^{39–41} predicting the equilibrium curvature in PESC³ is still a challenge,^{42,43} and this is a matter of utmost importance for more advanced applications of PESC.^{30,31}

Fibrillation of low-molecular weight compounds is also another important field of research, from both applicative (hydrogelation)⁴⁴ and fundamental (non-equilibrium phase transitions)⁴⁵ perspectives. Development of PESC from low-molecular weight gelators is still a virgin field of research and questioning the interactions between polyelectrolytes and self-assembled fibers has only started with recent works.⁴⁶

In a series of recent communications, many authors have addressed the solution self-assembly of microbial glycolipid biosurfactants.^{47–49} These molecules have a multiple interest in the field of PESC: they are biobased and biodegradable amphiphiles⁵⁰ with a rich phase diagram and stimuli responsiveness. For these reasons they are highly prompt for the development of biocompatible PESC but also for the study of non-equilibrium phase transitions in complex systems, both aspects generating an increasing interest in the community.^{3,7} In particular, we have shown that acidic C18:1 sophorolipids, which form a stable micellar phase in a broad pH range,^{49,51,52} also form pH-responsive complex coacervates in the presence of both synthetic and natural polyamines.⁵³ Interestingly, sophorolipid

analogues have a richer, pH-stimulated, phase diagram including micelle-to-vesicle, micelle-to-fiber and micelle-to-lamellar transitions.^{49,52,54}

In this work, we explore the stability of a polyelectrolyte-surfactant complex coacervate at two distinct iso-compositional phase boundaries, micelle-vesicle and micelle-fiber, where phase transition is triggered by pH. To do so, we use two microbial glycolipid biosurfactants in the presence of three cationic polyelectrolytes (PEC). Turbidimetric analysis, cryogenic transmission electron microscopy (cryo-TEM) and pH-resolved *in situ* small angle X-ray scattering (SAXS) using synchrotron radiation experiments show that complex coacervates are only stable in the micellar region of both glycolipids' phase diagram. However, if the lipid undergoes a micelle-to-vesicle transition, we observe a complex coacervate (*Co*) to multilamellar walls vesicles (*MLWV*) (*Co*-to-*MLWV*) phase transition. *MLWV* are composed of PEC entrapped between single lipid layers, of which the mutual interactions are quantified by nuclear magnetic resonance (NMR) and isothermal titration calorimetry (ITC). If the lipid undergoes a micelle-to-fiber transition, on the contrary, the coacervate disassembles and the glycolipid's fiber phase coexists with the polyelectrolyte, with no apparent interactions, against the literature's expectations.⁴⁶ Finally, this work demonstrates the use of biobased surfactants for the development of sustainable PESCs.

Experimental section

Chemicals

Glycolipids G-C18:1 ($M_w = 460 \text{ g mol}^{-1}$), made of a single β -D-glucose hydrophilic headgroup and a C18:1 fatty acid tail (monounsaturated in position 9,10), and SL-C18:0 ($M_w = 624 \text{ g mol}^{-1}$), composed of a sophorose headgroup and a stearic acid derivative. From alkaline to acidic pH, the former undergoes a micelle-to-vesicle phase transition⁴⁹ while the latter undergoes a micelle-to-fiber phase transition.⁵⁵ The syntheses of sophorolipid SL-C18:0 and glucolipid G-C18:1 are respectively described in Ref ⁵⁵ and ⁵⁴, where the typical ¹H NMR spectra and HPLC chromatograms are also given. The compounds used in this work have a molecular purity of more than 95%.

The cationic polyelectrolytes (PEC) used in this work are chitosan, obtained from the deacetylation of chitin from crustaceans' shells, poly-L-lysine, widely used in biomedical field, and polyethylenimine. Chitosan oligosaccharide lactate (CHL) ($M_w \approx 5 \text{ kDa}$, $pK_a \sim 6.5$)⁵⁶ with a deacetylation degree >90%, poly-L-lysine (PLL) hydrobromide ($M_w \approx 1-5 \text{ kDa}$, $pK_a \sim 10-10.5$)⁵⁷ and polyethylenimine (PEI) hydrochloride (linear, $M_w \approx 4 \text{ kDa}$, $pK_a \sim 8$)⁵⁸ are purchased from

Sigma-Aldrich. All other chemicals are of reagent grade and are used without further purification.

Preparation of stock solutions

SL-C18:0 ($C = 5 \text{ mg}\cdot\text{mL}^{-1}$), G-C18:1 ($C = 5 \text{ mg}\cdot\text{mL}^{-1}$, $C = 20 \text{ mg}\cdot\text{mL}^{-1}$), CHL ($C = 2 \text{ mg}\cdot\text{mL}^{-1}$), PLL ($C = 5 \text{ mg}\cdot\text{mL}^{-1}$, $C = 20 \text{ mg}\cdot\text{mL}^{-1}$), and PEI ($C = 5 \text{ mg}\cdot\text{mL}^{-1}$) stock solutions ($V = 10 \text{ mL}$) are prepared by dispersing the appropriate amount of each compound in the corresponding amount of Milli-Q-grade water. The solutions are stirred at room temperature ($T = 23 \pm 2 \text{ }^\circ\text{C}$) and the final pH is increased to 11 by adding a few μL of NaOH ($C = 0.5 \text{ M}$ or $C = 1 \text{ M}$).

Preparation of samples

Samples are prepared at room temperature ($T = 23 \pm 2 \text{ }^\circ\text{C}$) by mixing appropriate volume ratios of the lipid (SL-C18:0 or G-C18:1) stock solutions at pH 11 and cationic polyelectrolyte stock solutions (PEC), as defined in Table 1. The final total volume is generally set to $V = 1 \text{ mL}$ or $V = 2 \text{ mL}$, the solution pH is about 11 and the final concentrations are given in Table 1. The pH of the mixed lipid-PEC solution is eventually decreased by the addition of 1-10 μL of a HCl solution at $C = 0.5 \text{ M}$ or $C = 1 \text{ M}$. pH has been changed by hand and by mean of a push-syringe device. The rate at which pH is changed is generally not controlled although it is in the order of several $\mu\text{L}\cdot\text{min}^{-1}$. Differently than in other systems,^{34,59} we did not observe unexpected effects on the PESC structure to justify a tight control over the pH change rate.

Table 1 – Relative volumes of lipid and cationic polyelectrolyte (PEC) solutions to mix to obtain given concentrations

Volume			Concentration	
Lipid stock solution / mL	PEC stock solution / mL	Water / mL	$C_{\text{Lipid}} / \text{mg}\cdot\text{mL}^{-1}$	$C_{\text{PEC}} / \text{mg}\cdot\text{mL}^{-1}$
0.5	0.5	0	2.5 or 10	2.5 or 10
	0.25	0.25	2.5	1.25
	0.125	0.375	2.5	0.625

Turbidimetric titration using UV-Vis spectroscopy

The influence of pH and concentration of PEC on the formation of coacervate droplets is investigated by measuring the absorbance at a wavelength of $\lambda = 450$ nm. Data are recorded at room temperature ($T = 23 \pm 2$ °C) using a UV/Vis spectrophotometer (UVIKON XL, BioTek). Preparation of the samples for these experiments is the same as described above, however, the final concentration of the lipid is systematically set at $C = 2.5$ mg·mL⁻¹, while the final concentrations of the PEC range between $0.25 < C / \text{mg}\cdot\text{mL}^{-1} < 1$ for CHL and $0.63 < C / \text{mg}\cdot\text{mL}^{-1} < 2.5$ for PLL and PEI. The titrated volume is systematically $V = 1$ mL. The pH of each lipid-PEC mixed solution is decreased progressively by the manual addition of small amounts ($V < 10$ μL) of HCl = 0.1 M. The turbidity curves are recorded after each pH variation. Each solution is stirred before analysis, which is however performed at rest under static conditions, thus favoring sedimentation during the measurement. The turbidity curve of control lipid and PEC solutions is also measured as a function of pH.

Turbidimetric titration using Light Scattering (LS) and ζ -potential

To avoid sedimentation, we have repeated the turbidimetric titration experiment on selected samples using the automatic titration unit MPT-2 of a Malvern Zetasizer Nano ZS90 (Malvern Instruments Ltd, Worcestershire, UK) instrument, equipped with a 4 mW He-Ne laser at a wavelength of $\lambda = 633$ nm, measuring angle, $\theta = 90^\circ$, temperature, $T = 25^\circ\text{C}$, and the signal is never attenuated throughout the entire experiment. The sample solution ($V = 7$ mL) is contained in an external beaker and pumped with a peristaltic pump through the ζ -potential cuvette cell located in the instrument for analysis. pH is adjusted in the beaker by adding aliquots of $V = 6$ μL of a HCl solution at $C = 0.5$ M and controlled by the MPT-2 Zetasizer software. The beaker undergoes gentle stirring to avoid the formation of air bubbles in the flow-through tubing system and, consequently, in the ζ -potential cuvette. Avoiding air bubbles in the cuvette is crucial and accurately inspected throughout the experiment. Light scattering and ζ -potential are simultaneously recorded between each pH variation while the sample solution is continuously pumped through the cuvette. The latter action guarantees that sedimentation occurs neither in the cuvette nor in the external beaker.

pH-resolved in situ Small angle X-ray scattering (SAXS)

In situ SAXS experiments during pH variation are performed at room temperature on two different beamlines. The B21 beamline at Diamond Light Source Synchrotron (Harwell, England) is employed using an energy of $E = 13.1$ keV and a fixed sample-to-detector (Eiger X 4M) distance of 2.69 m. The Swing beamline at Soleil Synchrotron (Saint-Aubin, France) is

employed using an energy of $E= 12$ keV and a fixed sample-to-detector (Eiger X 4M) distance of 1.995 m. For all experiments: the q -range is calibrated to be contained between $\sim 5 \cdot 10^{-3} < q/\text{\AA}^{-1} < \sim 4.5 \cdot 10^{-1}$; raw data collected on the 2D detector are integrated azimuthally using the in-house software provided at the beamline and so to obtain the typical scattered intensity $I(q)$ profile, with q being the wavevector ($q = 4\pi \sin \theta / \lambda$, where 2θ is the scattering angle and λ is the wavelength). Defective pixels and beam stop shadow are systematically masked before azimuthal integration. Absolute intensity units are determined by measuring the scattering signal of water ($I_{q=0} = 0.0163 \text{ cm}^{-1}$). SAXS profiles are treated with SasView software, version 3.1.2, available at the developer's website (sasview.org).

The same sample experimental setup is employed on both beamlines: the sample solution ($V= 1$ mL) with the lipid and PEC at their final concentration and pH ~ 11 is contained in an external beaker under stirring at room temperature ($T= 23 \pm 2^\circ\text{C}$). The solution is continuously flushed through a 1 mm glass capillary using an external peristaltic pump. The pH of the solution in the beaker is changed using an interfaced push syringe, injecting microliter amounts of a 0.5 M HCl solution. pH is measured using a micro electrode (Mettler-Toledo) and the value of pH is monitored live and manually recorded from the control room via a network camera pointing at the pH-meter located next to the beaker in the experimental hutch. Considering the fast pH change kinetics, the error on the pH value is ± 0.2 .

Cryogenic transmission electron microscopy (cryo-TEM)

Cryo-TEM experiments are carried out on an FEI Tecnai 120 twin microscope operated at 120 kV and equipped with a Gatan Orius CCD numeric camera. The sample holder is a Gatan Cryoholder (Gatan 626DH, Gatan). Digital Micrograph software is used for image acquisition. Cryofixation is done using a homemade cryofixation device. The solutions are deposited on a glow-discharged holey carbon coated TEM copper grid (Quantifoil R2/2, Germany). Excess solution is removed and the grid is immediately plunged into liquid ethane at -180°C before transferring them into liquid nitrogen. All grids are kept at liquid nitrogen temperature throughout all experimentation. Cryo-TEM images have been treated and analyzed using Fiji software, available free of charge at the developer's website.⁶⁰

^1H solution Nuclear Magnetic Resonance (NMR)

^1H solution NMR experiments are performed on a Bruker Avance III 300 spectrometer using a 5 mm 1H-X BBFO probe. The number of transients is 32 with 7.3 s recycling delay, an

acquisition time of 2.73 s and a receiver gain of 322. We have employed a 5 mm NMR tube containing 500 μL of solution. The latter is obtained upon solubilization of a dried pellet in MeOD, also containing 3-(Trimethylsilyl) propionic-2,2,3,3- d_4 acid sodium salt (TMSP- d_4) at $1 \text{ mg}\cdot\text{mL}^{-1}$ (5.8 mM). The pellet is obtained by centrifugation of a solution at final pH of 5 containing the lipid and the polyelectrolyte and prepared according to the method described in the “Preparation of samples” paragraph in this section. After centrifugation, the supernatant is removed and the pellet is dried in an oven at 40°C for 2 days. These conditions have been kept constant throughout all experiments.

Isothermal Titration Calorimetry (ITC)

ITC experiments were performed using a TAM III isothermal calorimeter from TA Instruments. All the solutions (buffer pH 5.8, PLL 2 mM, G-C18:1 2 mM, and G-C18:1 4 mM) were degassed by 15 min sonication under vacuum. ITC experiments employ phosphate buffer solutions ($\text{NaH}_2\text{PO}_4/\text{Na}_2\text{HPO}_4$, 10 mM) at pH 5.8. The titration experiments between PLL and G-C18:1 were performed with PLL 2 mM in the calorimetric cell and G-C18:1 (2 or 4 mM) solution in the syringe. Preliminary experiments (not shown) showed that high stirring rates (120 rpm) result in an unstable stable calorimetric trace most likely due to the foaming of the G-C18:1 despite the degassing step. This was also confirmed by visual inspection of the retracted measurement cell. For this reason, the experiments are conducted at a lower stirring speed of 30 rpm and with the G-C18:1 solution in the syringe. Prior to the start of the titrations, the system was equilibrated at 25°C until baseline variation was less than 50 nW/h. After calibration (dynamic and gain), 20 injections of $10\mu\text{L}$ each of G-C18:1 (2 or 4 mM) were successively added at 20 min intervals into the cell containing 0.8 mL of PLL 2 mM. A blank titration experiment to estimate the heat of dilution was also performed under the same conditions by injecting the buffer solution into PLL 2 mM. The calorimetric results were corrected for the heat of dilution by subtracting the blank experiment from the actual experiments. The data was fitted with a multi site model using NanoAnalyse data analysis software (TA Instruments) in order to determine the thermodynamic as well as the reaction parameters of the interaction between PLL and G-C18:1. From the enthalpy (ΔH) and the binding constant (K_a) of the reaction, the entropy (ΔS) and the Gibbs free energy (ΔG) of reaction were calculated using the following equation:

$$\Delta G = \Delta H - T\Delta S = -RT\ln(K_a)$$

Results

Deacetylated acidic sophorolipid SL-C18:0 (saturated) and glucolipid G-C18:1 (monounsaturated) are two microbial glycolipid biosurfactants used in this work and both containing a free carboxylic acid chemical function (Figure 1). Alkaline solutions of SL-C18:0 and G-C18:1 at room temperature and concentrations below 10 wt% are characterized by a major micellar phase. At $\text{pH} < 7.4$, SL-C18:0 self-assembles into crystalline twisted ribbons, while at $\text{pH} < 6.2$ G-C18:1 self-assembles into vesicles.^{49,54,55}

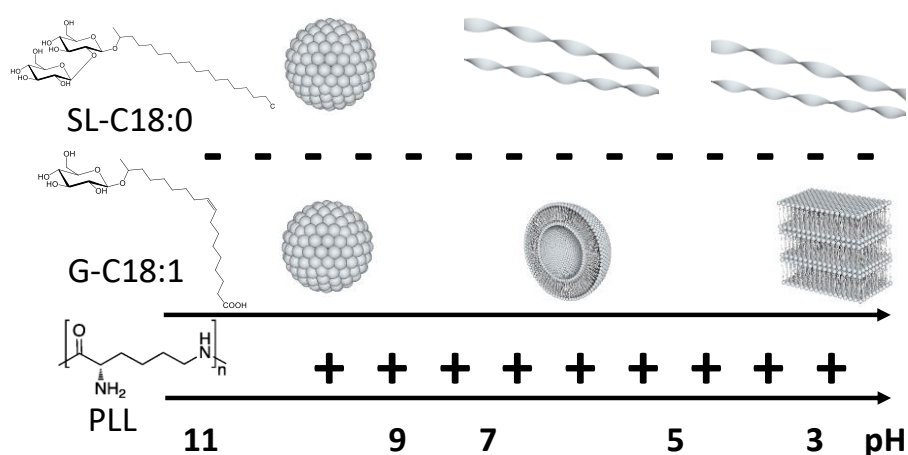


Figure 1 – pH-dependent phase and (negative) charge diagram for SL-C18:0 and G-C18:1 microbial glycolipids biosurfactants at $C < 10$ wt% and room temperature. The (positive) charge of PLL polyelectrolyte is also indicated as a function of pH

Figure 1 summarizes the pH-dependent phase and charge diagram of SL-C18:0 and G-C18:1 glycolipids, which are negatively charged above $\text{pH} \sim 4.5$, due to their carboxylate function. PLL polyelectrolyte is on the contrary positively charged below $\text{pH} 10$, water-soluble and it adopts a random coil conformation. The other PEC employed in this work, CHL and PEI, have a similar behavior, except for their $\text{p}K_a$ values, which are respectively 6.5 and 8. The charge complementarity between the glycolipids and PEC in a given pH range leads to an expected electrostatic interaction, and which was shown to form glycolipid-PEC complex coacervates, when acidic deacetylated monounsaturated sophorolipids (SL-C18:1) were employed.⁵³ To explore whether SL-C18:0 and G-C18:1 glycolipids form complex coacervates, and whether their pH-induced phase transition has a potential impact on the coacervate structure, we perform a series of pH-stimulated experiments on mixtures of each glycolipid and PEC. The main body of this work summarizes the results obtained with PLL, while the data

collected on CHL and PEI are only briefly discussed and presented as supporting information, as they support the main conclusions obtained with PLL.

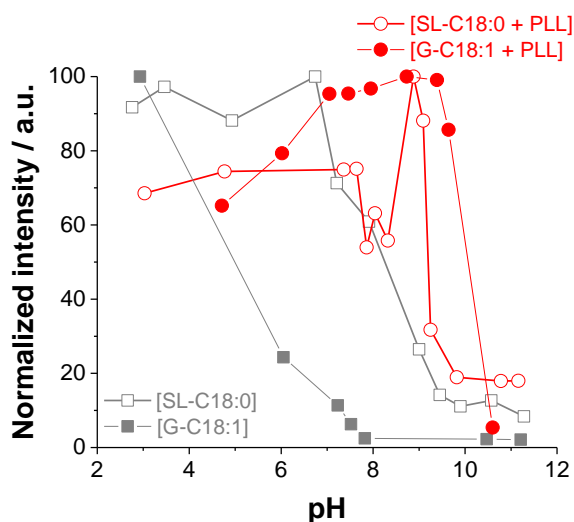


Figure 2 – Room temperature turbidimetric analysis performed by UV-Vis spectroscopy of SL-C18:0 and G-C18:1 glycolipid solutions with and without PLL as a function of pH. The typical sample preparation is described in the materials and method section. The final lipid and PEC concentrations are $C_{G-C18:1} = C_{SL-C18:0} = 2.5 \text{ mg mL}^{-1}$, $C_{PLL} = 1.25 \text{ mg mL}^{-1}$. pH is decreased from 11 to 3.

Figure 2 presents the pH-resolved turbidimetric analysis on control lipid ([SL-C18:0] and [G-C18:1]) solutions (grey symbols) and mixtures of lipids with PLL (red symbols). As a general result, control solutions display poor scattering (micellar phase) above pH ~ 8 and ~ 9 for, respectively, G-C18:1 and SL-C18:0; on the contrary, scattering is maximized below pH ~ 6 and ~ 7 for, respectively, G-C18:1 and SL-C18:0. These results are in agreement with their respective micelle-to-vesicle⁴⁹ and micelle-to-fiber⁵⁵ phase transitions. One must notice that scattering of SL-C18:0 fibers below pH 7 is weaker than what it should be⁵⁵ and this is due to sedimentation issues during the experiment. A specific comment on this aspect is associated to Figure S 1 in the Supporting Information and where pH-resolved experiments are performed *in situ* in the light scattering apparatus. Finally, scattering of PLL alone is negligible on the entire pH range and for this reason it is not displayed in Figure 2. Mixtures of SL-C18:0, or G-C18:1, and PLL highlight a region of strong scattering (red symbols) already at $9 < \text{pH} < 10$, that is at least two to three orders of pH higher than the controls, and indicating that both glycolipids preferentially interact with PLL under these pH conditions, according to the likely hypothesis of charge matching schematized in Figure 1. The data in Figure 2, reported for final concentrations of lipid and PLL of, respectively, 2.5 mg mL^{-1} and 1.25 mg mL^{-1} , are quite robust and reproducible for a broader range of lipid-to-PLL mass ratios, as shown in Figure S 2.

Similar results were also reported for SL-C18:1 sophorolipids and PEC solutions⁵³ and for a broad range of micelle-polyelectrolyte complex coacervates.²¹ pH-resolved *in situ* ζ -potential measurements are employed to show mutual interactions by charge-matching (Figure S 3). The lipid control solutions display the presence of negatively-charged colloids between pH 10 and 4, while lipid and PLL mixed solutions show an overall charge neutralization process occurring since pH 10, indirectly demonstrating the interaction between the lipid and polyelectrolyte, supported by both NMR and ITC presented later in the manuscript.

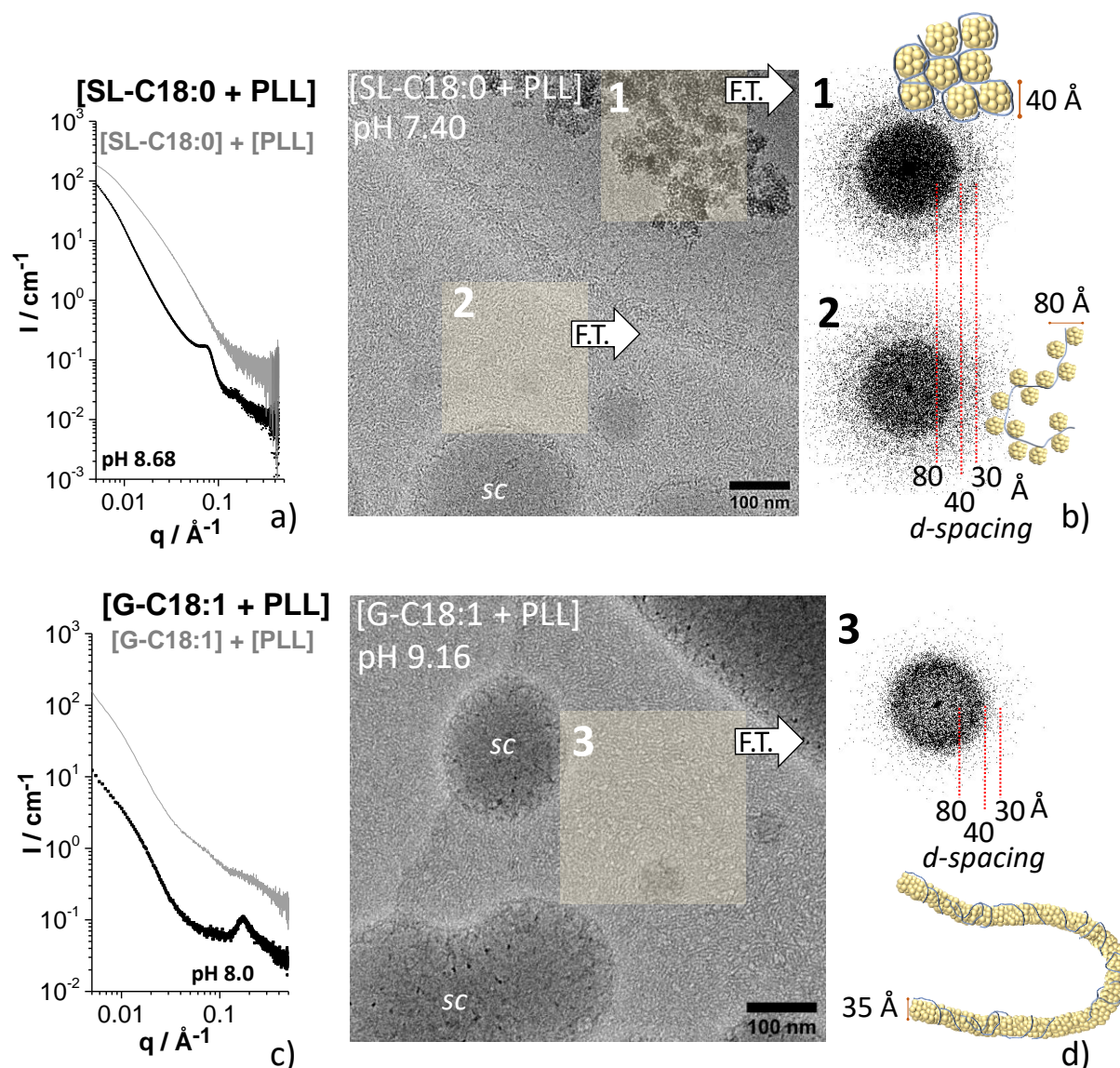


Figure 3 – a) SAXS profile recorded for a co-assembled mixture of [SL-C18:0 + PLL] (black curve) at pH 8.68. Grey curve: arithmetical summation of the SAXS profiles each recorded individually on the control solutions of [SL-C18:0] and [PLL] at pH 8.68. An artificial offset has been added for sake of clarity. Concentrations: $C_{\text{SL-C18:0}} = C_{\text{PLL}} = 2.5 \text{ mg mL}^{-1}$. **b)** Cryo-TEM image of the co-assembled [SL-C18:0 + PLL] solution at pH 7.40. Concentrations: $C_{\text{SL-C18:0}} = 2.5 \text{ mg mL}^{-1}$, $C_{\text{PLL}} = 1.25 \text{ mg mL}^{-1}$. Panels 1 and 2 identify regions where Fourier Transform (F.T.) is performed. F.T. images are indicated by the arrows on the right-

hand side of each cryo-TEM image. c) SAXS profile recorded for a co-assembled mixture of [G-C18:1 + PLL] (black curve) at pH 8.0. Grey curve: arithmetical summation of the SAXS profiles each recorded individually on the control solutions of [G-C18:1] and [PLL] at pH 8.0. An artificial offset has been added for sake of clarity. Concentrations: $C_{G-C18:1} = C_{PLL} = 10 \text{ mg mL}^{-1}$. d) Cryo-TEM image of the co-assembled [G-C18:1 + PLL] solution at pH 9.16. Concentrations: $C_{G-C18:1} = 2.5 \text{ mg mL}^{-1}$ and $C_{PLL} = 1.25 \text{ mg mL}^{-1}$. The F.T. of panel 3 is shown on the right-hand side. Images have been analyzed using Fiji software.⁶⁰

A combination of SAXS and cryo-TEM experiments (Figure 3 and Figure 4) is used to study the structure of SL-C18:0 and G-C18:1 with PLL in the regions of strong light scattering and below pH 7 (Figure 2). The SAXS profiles show the signals recorded at basic (Figure 3a,c) and acidic (Figure 4a,c) pH, where black curves labelled [SL-C18:0 + PLL] and [G-C18:1 + PLL] correspond to co-assembled lipid:PLL PESC solutions. Grey curves labelled [SL-C18:0] + [PLL] and [G-C18:1] + [PLL] correspond to the arithmetic sum of the SAXS profiles recorded on the individual lipid and PLL controls solutions separately. Figure S 4 illustrates the SAXS profiles of the individual SL-C18:0 (blue symbols) and PLL (red symbols) control solutions recorded at pH 5.50 and 8.68 as well as their arithmetic sum (grey symbols). The difference in concentration between the G-C18:1 system at pH 8.0 ($C = 10 \text{ mg mL}^{-1}$) and the rest ($C = 2.5 \text{ mg mL}^{-1}$) is simply a matter of signal-to-noise ratio. The corresponding SAXS profile collected at $C_{G-C18:1} = C_{PLL} = 2.5 \text{ mg mL}^{-1}$ and pH 8.0 is given in Figure S 5 and it indeed shows a similar profile but with a poorer signal-to-noise, probably due to a combination of poor contrast and low concentration.

Study of the complex coacervate (Co) phase

In the micellar region of the phase diagram (pH > 8), both glycolipids in their mixture with PLL have SAXS profiles characterized by a strong low- q scattering and a broad peak (black curves in Figure 3a,c). The peak is centered at $q = 0.078 \text{ \AA}^{-1}$ ($d = 80.5 \text{ \AA}$) while a second peak can be observed at $q = 0.15 \text{ \AA}^{-1}$ ($d = 41.8 \text{ \AA}$) for SL-C18:0 and at $q = 0.174 \text{ \AA}^{-1}$ ($d = 36.1 \text{ \AA}$) for G-C18:1. Comparison between the co-assembled lipid and PLL solution (black curves) with the corresponding controls (grey curves in Figure 3a,c above pH 8) at basic pH shows that, if low- q scattering is generally comparable, the correlation peak is unique only in the co-assembled solutions and never observed for the pure glycolipids. The presence of a correlation peak is actually general and not only observed with PLL. For instance, SL-C18:0 (at basic pH) systematically shows two broad correlation peaks centered at $q = 0.078 \pm 0.002 \text{ \AA}^{-1}$ and at $q = 0.15 \pm 0.10 \text{ \AA}^{-1}$ when it is co-assembled with PLL, PEI or CHL (Figure S 6a). These peaks, common in scattering experiments of micelle-polyelectrolyte complex coacervates,²¹ are

generally associated to the structure of the co-assembled lipid with PEC. To better understand the origin of the peak at basic pH in the SAXS experiments, we study the structure of [SL-C18:0 + PLL] and [G-C18:1 + PLL] using cryo-TEM.

The typical cryo-TEM images of [SL-C18:0 + PLL] and [G-C18:1 + PLL] at basic pH are shown in Figure 3, while additional images are given in Figure S 7. All samples, irrespective of the pH value, are characterized of large spherical colloidal (*sc*) structures, of diameter larger than 1000 Å, embedded in a medium, which often displays a fingerprint-like texture (panels 2 and 3 in Figure 3, Figure S 7a,d,e). Regions of much smoother, untextured, background are however observed, as well (Figure S 7b,c). *sc* display as dense, untextured, more contrasted, objects. One can occasionally observe, mainly in [SL-C18:0 + PLL] systems, a third type of component, constituted of agglomerated, highly contrasted, particles of typical primary size contained between 20 nm and 50 nm (panel 1 in Figure 3, Figure S 7b). Both aggregated particles and *sc* of similar texture, size, morphology and contrast were largely documented using cryo-TEM by us⁵³ and by others^{23,61,62} in polyelectrolyte-surfactant complex coacervates.

The entire set of cryo-TEM images that we have recorded on glycolipids SL-C18:0 and G-C18:1 co-assembled with PLL or PEI at basic pH show the same type of structures as presented in Figure 3 and Figure S 7. From a macroscopic point of view, all samples form a stable suspension of liquid spherical droplets similarly to our previous results,⁵³ rather than a solid precipitate. The combination of these pieces of evidence³ indicate that complex coacervation systematically occurs in the micellar region of the glycolipids phase diagram. Concerning CHL, we cannot draw a clear-cut conclusion due to the fact that this compound precipitates above pH 7⁶³ and its interactions with glycolipids in the alkaline region are at the moment unclear. The SAXS data corresponding to [SL-C18:0 + CHL] shown in Figure S 6 confirm this assumption: the typical correlation peaks, clearly observed in the PLL and PEI systems, can be hardly identified. However, complementary data recorded on the [G-C18:1 + CHL] system, and presented elsewhere,⁶⁴ still suggest the formation of complex coacervates.

Agglomerated, highly contrasted, particles (e.g., panel 1 in Figure 3) are generally attributed to dehydrated complex coacervates driven by microscopic electroneutrality^{23,53} on the coacervation plateau, while *sc* structures surrounded by a textured background (e. g., panel 2 and 3 in Figure 3) are attributed to sections of 3D hydrated complex coacervates structures at the point of macroscopic coacervation.⁶² Dense structures are always superimposed to a clear background, as described by Dubin *et al.*,²³ while the fingerprint-like background is systematically associated to *sc* structures, independently of the glycolipid employed. This is nicely shown for [SL-C18:0 + PLL] in Figure 3b, where a clear-cut frontier delimitates dense

coacervates on top from *sc* on the bottom, the former being embedded in a smooth background while the latter embedded in a fingerprint-like background. In line with Dubin *et al.*,⁶² we speculate that the composition of the fingerprint-like background is rich in glycolipid, while *sc* are rather rich in PEC. Probably due to the kinetic control of coacervation process, we are unable to establish the physicochemical conditions that could favor either dense aggregates or *sc* regions, as we observe both of them irrespectively of the pH value (Figure S 7a-c), or even coexisting at the same pH (Figure 3b). Nonetheless, we propose a structural interpretation through a crossed SAXS-cryo-TEM analysis of both [SL-C18:0 + PLL] and [G-C18:1 + PLL] systems.

The Fourier Transform (F.T.) of the fingerprint-like region in the [SL-C18:0 + PLL] system (panel 2 in Figure 3b) provides a broad ring corresponding to *d*-spacing between 80 Å and 40 Å, while the dense coacervate region, panel 1 in Figure 3b, provides an additional ring of *d*-spacing between 30 Å and 40 Å. Comparison between the *d*-spacing values estimated from cryo-TEM with *d*-spacing obtained by SAXS ($d= 80.5$ Å and $d= 41.8$ Å, Figure 3a) confirms the hypothesis according to which the correlation peak in SAXS is reasonably associated to the structure of complex coacervates. Interestingly, the *q*-values are in a 1:2 ratio, generally found in lamellar stacking but excluded in this system by cryo-TEM arguments. Correlation peaks with *q*-values in 1:2 ratio were observed before in β -lactoglobulin(β LgA)-pectin complex coacervates⁶⁵ and were attributed to the presence of β LgA clusters coexisting with ordered protein-to-protein correlations observed inside the clusters. In the present case, the *d*-spacing at $d= 41.8$ Å can be reasonably attributed to the dense aggregates (panel 1 in Figure 3b), most likely composed of tightly packed SL-C18:0 micelles embedded in the polyelectrolyte matrix adopting a globular conformation (Figure 3b).²³ This hypothesis is also in agreement with the typical cross-sectional diameter of SL-C18:0 micelles (~ 35 Å)⁴⁹ and with the previously-proposed colloid cluster model in complex coacervates.²¹ However, the colloid cluster model unfortunately explains neither larger *d*-spacing values nor the fingerprint-like textured background. The only way to explain a *d*-spacing value corresponding to approximately twice the size of a SL-C18:0 molecule is by considering a “pearl-necklace”-like structure, proposed long time ago for polyelectrolyte-micelles complexes,^{4,7,35,66} and adapted to the present (Figure 3b) to account for the larger experimental *d*-spacing.

The Fourier Transform (F.T.) of the fingerprint-like region, panel 3 in Figure 3d, in the [G-C18:1 + PLL] system, also shows a broad ring with *d*-spacing values contained between 40 Å and 60 Å, a range which is overestimated by at least a factor 1.5 with respect to the *d*-spacing value measured by SAXS ($d= 36.1$ Å). Despite such a discrepancy, the lack of other organized

structures in cryo-TEM and the lack of other correlation peaks in SAXS suggest that the correlation peak should be attributed to the textured background identified in panel 3 in Figure 3d. However, a spontaneous question arises: why is the d -spacing value associated to the textured region in the [G-C18:1 + PLL] system correlated to the size of a single G-C18:1 molecule^{49,54} and not to twice its size, as found for [SL-C18:0 + PLL]? The only reasonable answer that we can propose is the possibly different packing of G-C18:1 around the polyelectrolyte: instead of the expected micellar packing, G-C18:1 could form interdigitated wormlike micelles stabilized by the polyelectrolyte (scheme in Figure 3d), as also discussed for other polyelectrolyte-micelle complexes.^{3,4,20,67} This hypothesis is not outrageous because wormlike micelles are experimentally found as a transitory phase during the micelle-to-vesicle transition in the PEC-free G-C18:1 aqueous system.⁴⁹ Analysis of the slope in, or even modelling of, SAXS profiles could certainly help to corroborate the hypotheses of “pearl-necklace” (Figure 3b) and wormlike (Figure 3d) models, as proposed by other authors.^{35,68} However, any tentative analysis of our SAXS data in the log-log scale provide a dependence of the intensity on q around -3 , which is typically found for fractal structures but which, unfortunately, does not bring any additional structural information on the present system. Cryo-TEM experiments show a multiphasic medium with coexistence of more than one structural intermediate, thus making a clear-cut interpretation of the SAXS profile very hard, if not impossible.

In the rest of the manuscript, the term *Co* phase will broadly refer to the complex medium in the basic pH region composed of aggregated structures (panel 1 in Figure 3), PEC-rich *sc* (Figure 3) and glycolipid-rich textured (panel 2,3 in Figure 3) regions.

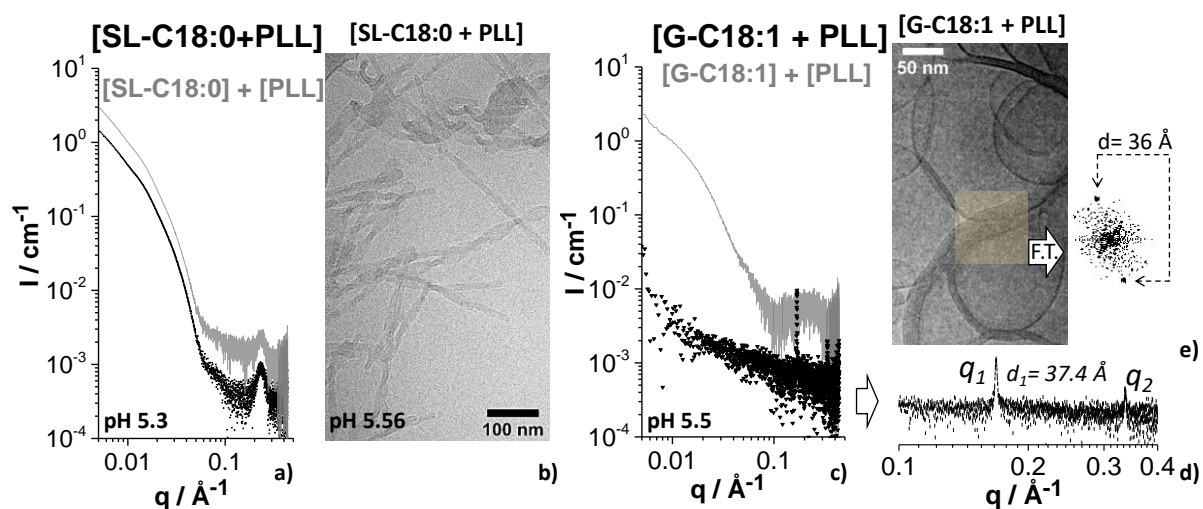


Figure 4 – a) SAXS profile recorded for a co-assembled mixture of [SL-C18:0 + PLL] at pH 5.30. Grey curve: arithmetical summation of the SAXS profiles each recorded individually on the control solutions of [SL-C18:0] and [PLL] at pH 5.30. An artificial offset has been added for sake of clarity. b) Cryo-TEM image of the co-assembled [SL-C18:0 + PLL] solution at pH 5.56. Concentrations in a-b) are $C_{\text{SL-C18:0}} = C_{\text{PLL}} = 2.5 \text{ mg}\cdot\text{mL}^{-1}$. c) SAXS profile recorded for a co-assembled mixture of [G-C18:1 + PLL] (black curves) at pH 5.50. Grey curve: arithmetical summation of the SAXS profiles each recorded individually on the control solutions of [G-C18:1] and [PLL] at pH 5.50. An artificial offset has been added for sake of clarity. d) Highlighted high- q region of [G-C18:1 + PLL] at pH= 5.50. e) Cryo-TEM image of the co-assembled [G-C18:1 + PLL] solution at pH 4.70. Concentrations in c-e) are $C_{\text{G-C18:1}} = C_{\text{PLL}} = 2.5 \text{ mg}\cdot\text{mL}^{-1}$. Images has been analyzed using Fiji software.⁶⁰

In situ study of the lipid-PLL system below neutral pH

pH-resolved *in situ* SAXS is employed to study the lipid-PLL phase behavior below neutral pH. Experiments performed at acidic pH are shown in Figure 4a,b (SAXS: black curve, pH 5.30; cryo-TEM: pH 5.56) for the [SL-C18:0 + PLL] mixture and in Figure 4c-e (SAXS: black curve, pH 5.50; cryo-TEM: pH 4.70) for the [G-C18:1 + PLL] mixture. In the SL-C18:0 system, SAXS shows a strong low- q scattering and a diffraction peak at $q = 0.24 \text{ \AA}^{-1}$. The same exact profile is observed for the [SL-C18:0] + [PLL] control signal (grey curve, pH 5.30, Figure 4a) and reported for a typical aqueous solution of SL-C18:0 twisted ribbons, the peak being attributed to the repeating inter-lipid layer distance within each ribbon.⁵⁵ Twisted ribbons of similar size (cross section $\sim 150 \text{ \AA}$) and morphology compared to the previous findings of pure SL-C18:0 system at acidic pH are actually observed in the corresponding cryo-TEM images (Figure 4b). Knowing that SL-C18:0 assembles into a fibrillar phase at acidic pH, one can reasonably suppose that SL-C18:0 does not interact with PLL under these conditions and the micelle-to-fiber self-assembly process (Figure 1) occurs independently whether SL-C18:0 is in a free micellar^{49,55} or in PESC's complex coacervates. At the moment, we do not have evidence, both by SAXS and cryo-TEM, later on confirmed by NMR arguments, that SL-C18:0 fibers interact in any way with PEC, differently than what was reported for the fibrillation of bile salts complexed with block copolymers.⁴⁶ We could explain this evidence by the fact that self-assembled fibers are only composed of the COOH form of SL-C18:0 and they are thus neutral objects, which do not interact with PEC. This statement seems to be in contrast with ζ -potential experiments performed on the SL-C18:0 system below pH 7 (Figure S 3) and showing an overall negative charge. However, one should be aware that ζ -potential experiments are not structure-selective and we have no direct proof that the global negative charge is specifically associated to fibrillar structures rather than to a set of coexisting colloids composed of fibers

and residual micelles. If fibers are actually negatively charged, one should also not exclude the possibility that the charge density is too low to drive complexation with PEC.

The SAXS profile of the [G-C18:1 + PLL] at pH 5.50 (black curve, Figure 4c,d) is on the contrary very different than the corresponding [G-C18:1] + [PLL] control signal (grey curve, pH 5.50, Figure 4c): the mixture displays two sharp peaks at $q_1 = 0.17 \text{ \AA}^{-1}$ and $q_2 = 0.34 \text{ \AA}^{-1}$ (Figure 4d), referring to the (100) and (200) reflection of a lamellar order, while the control signal has the typical profile of single-wall vesicles, expected for G-C18:1 in water at concentration below 10 wt% and $\text{pH} < 7$.^{49,54} The $q_1:q_2 = 0.5$ and the sharpness of the peaks ($\Delta q = 1.4 \cdot 10^{-3} \text{ \AA}^{-1}$) strongly suggest the presence of extended lamellar domains, never observed for this compound alone prepared under the same conditions. The corresponding cryo-TEM image in Figure 4e interestingly shows the systematic massive presence of vesicular objects having a thick lamellar wall (white arrows in Figure 4e), as similarly found in lipoplex systems,^{2,19} and other multilamellar walls vesicle PESC_s,⁴ where the lipid walls (here G-C18:1) are held together by the sandwiched polyelectrolyte (here PLL). Cryo-TEM excludes the presence of a flat lamellar phase, or condensed platelets. A more detailed electron microscopy study of the [G-C18:1 + PLL] material under acidic pH conditions are reported elsewhere.⁶⁴

To better understand the phase transition from alkaline to acidic pH, Figure 5 shows the full range of the pH-resolved *in situ* SAXS experiment, presented as 2D contour plots.

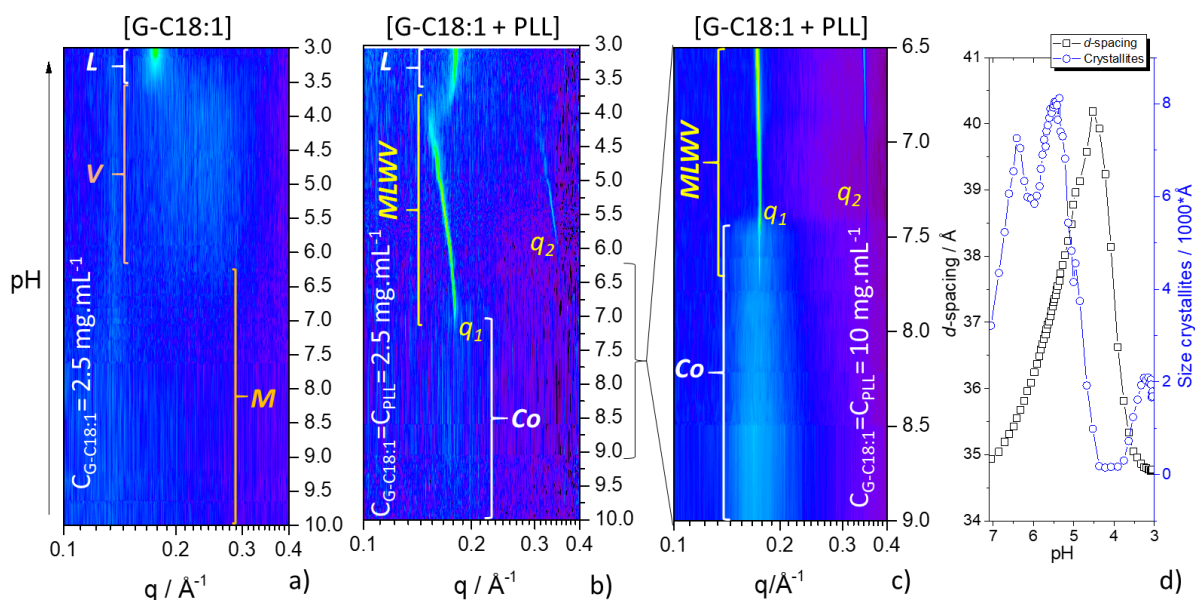


Figure 5 – pH-resolved (pH is changed from alkaline to acidic) *in situ* SAXS 2D contour plots of a) G-C18:1 control solution ($C = 2.5 \text{ mg mL}^{-1}$), b) [G-C18:1 + PLL] sample at $C_{\text{G-C18:1}} = C_{\text{PLL}} = 2.5 \text{ mg mL}^{-1}$ and c) [G-C18:1 + PLL] sample at $C_{\text{G-C18:1}} = C_{\text{PLL}} = 10 \text{ mg mL}^{-1}$. *M*: Micellar phase; *V*: Vesicles phase; *L*: Lamellar phase; *MLWV*: Multilamellar wall vesicle phase; *Co*: Complex coacervate phase. d) Evolution of *d*-spacing

and size of crystallites at pH < 7 for experiment in b). d -spacing is obtained from $6.28/q_1$ while size of crystallites is obtained using the Scherrer formula $(0.9 \cdot 6.28)/FWHM$, where $FWHM$ is the full width at half maximum of peak q_1 given in \AA^{-1} units. q_1 and $FWHM$ have been obtained by mean of a Lorentzian peak fitting procedure.

The contour plot ($0.1 < q / \text{\AA}^{-1} < 0.4$) concerning the pH dependency of G-C18:1 control sample solution is shown in Figure 5a. The pH region between pH 10 and ~6.5 is characterized by no distinct signal in the contour plot representation, as expected, because G-C18:1 forms a micellar, M , phase in this pH range.^{49,54} Below pH ~6.5 and until pH ~3.5, the contour plot shows a broad signal, characterizing the vesicle, V , phase and corresponding to the oscillation of the vesicle membrane form factor (grey profile, pH 5.5, Figure 4c) and largely documented in Ref. ^{49,54}. Below pH ~3.5, two sharp diffraction peaks at $q = 0.176 \text{\AA}^{-1}$ and $q = 0.352 \text{\AA}^{-1}$ (Figure S 8) refer to the (100) and (200) reflections of a lamellar order and characterize a lamellar phase, L , precipitate in solution.⁴⁹ In summary, the control G-C18:1 solution displays a micelle-to-vesicle-to-lamellar phase transition in agreement with our previous results.⁴⁹

The contour plot for the [G-C18:1 + PLL] PESC at $C = 2.5 \text{ mg mL}^{-1}$ is shown in Figure 5b. From pH 10 to about pH 7.5, the plot shows the dim signal of the broad ($\Delta q = 0.06 \text{\AA}^{-1}$) correlation peak at $q = 0.171 \text{\AA}^{-1}$ attributed to the Co phase, of which the composition is defined earlier in the manuscript. Figure S 5 better highlights the peak, which is hardly observable in the contour plot due to a simple matter of plotting levels. The signal of the same phase is more intense and better identified at higher lipid and PLL concentration, as highlighted by the Co phase region between pH 9 and 7.5 in Figure 5c and Figure S 5. Below pH ~7.5, two sharp diffraction peaks of full width at half maximum $\Delta q = 0.0015 \text{\AA}^{-1}$, respectively corresponding to the first and second order reflections, q_1 and q_2 , of the multilamellar walls vesicle, $MLWV$, phase in Figure 4d,e, are observed until pH 4. Figure 5b shows that the position of q_1 (and q_2) varies continuously from $q_1 = 0.178 \text{\AA}^{-1}$ at pH 7.5 to $q_1 = 0.157 \text{\AA}^{-1}$ at pH 4, corresponding to a variation in d -spacing of 5\AA , between 35\AA to 40\AA (black squares in Figure 5d). Below pH 4, the contour plot is characterized by an abrupt jump in the q -value from 0.157\AA^{-1} back to 0.176\AA^{-1} , immediately stabilizing itself at 0.181\AA^{-1} , and corresponding to a similar decrease in d -spacing of 5\AA , from 40\AA back to 35\AA .

The q_1 peak below pH 4 has the same features (position, invariance of the position towards pH, appearance in the same pH range) as the peak characterizing the L phase of the control G-C18:1 solution (Figure 5a). We then reasonably attribute it to the precipitation of the lipid L phase, probably without PLL, which is most likely expelled in the surrounding solution.

This assumption will be discussed in more detail in the next paragraphs. All in all, the G-C18:1 lipid undergoes a pH-driven *Co*-to-*MLWV*-to-*L* phase transition when mixed with PLL. In fact, this result is more general and not restricted to PLL only: we find similar results for all other PEC tested in this study and discussed elsewhere.⁶⁴

In comparison to G-C18:1, SL-C18:0-based PESCs behave in a completely different manner, because they are characterized by a straight micelle-to-fiber phase transition around pH 7. No structural or morphological continuity in the micelle-to-fiber phase transition is ever observed for this system, where micelles are more thought to play a reservoir role rather than a nucleation site.^{49,59} Interestingly, when SL-C18:0 is mixed with PLL, we also observe a systematic direct coacervate-to-fiber phase transition (Figure S 9), where the coacervate signal ($q = 0.078 \text{ \AA}^{-1}$; $q = 0.15 \text{ \AA}^{-1}$) at basic pH fades away until the appearance of the typical fiber structural peak at $q = 0.229 \text{ \AA}^{-1}$ below pH 7.⁴⁹ This behavior follows the direct micelle-to-fiber phase transition observed for the SL-C18:0 control and we could reproduce it with all PEC employed in this work when they are mixed with this lipid.

Complex coacervate-to-Multilamellar wall vesicles (Co-to-MLWV) phase transition

The pH-resolved *in situ* SAXS experiments show a remarkably different behaviour of the G-C18:1 lipid in the presence of PLL with respect to the control. The latter undergoes a micelle-to-vesicle phase transition, driven by the carboxylate-to-carboxylic acid reaction upon lowering the pH and inducing a conformational change of the lipid. Low curvature membrane (Figure 6b) morphologies are then favoured over high curvature micelles (Figure 6a), due to the progressive disappearance of repulsive electrostatic interactions, which indirectly impact the packing parameter of the lipid.^{18,69} Our data show that the same phenomenon occurs in the presence of PLL, when the lipid micelles are engaged in the formation of complex coacervates (Figure 6c). Upon lowering the pH, micelle-to-vesicle phase transition always occurs despite the presence of PLL; however, instead of forming single-wall vesicles, classically found in the control,⁵⁴ we observe a *Co*-to-*MLWV* phase transition (Figure 6d).

The continuity in the phase transition and the isostructural and isodimensional correlations between the coacervate and *MLWV* phases is explicit in the 2D SAXS experiment at $C_{G-C18:1} = 10 \text{ mg mL}^{-1}$ (Figure 5c): the broad correlation peak of the *Co* phase at $q = 0.171 \text{ \AA}^{-1}$ fades away between pH 7.7 and 7.5 and it overlaps to the sharp diffraction peak of the *MLWV* phase at $q_1 = 0.179 \text{ \AA}^{-1}$. Their position only shifts in $|q - q_1| = 0.007 \text{ \AA}^{-1}$ (1.6 \AA) strongly suggesting an internal, progressive, restructuring of the coacervates into *MLWV* (Figure 6c,d). The average *d*-spacing associated to the *q* range contained between 0.171 \AA^{-1} and 0.179 \AA^{-1} is

$d = 35.9 \text{ \AA}$, in agreement with both the typical diameter of a G-C18:1 micelle and the thickness of its corresponding membrane,⁴⁹ but also to the length of a single lipid molecule, estimated to be about 25 \AA using the Tanford relationship.^{54,70} G-C18:1 is a bolaform amphiphile and we have previously shown that its micellar structure is not a classical core-shell spheroid, where the diameter roughly corresponds to twice the size of the molecule,⁷¹ but rather to a core-shell ellipsoid, where the diameter matches the size of each single lipid, a typical behavior in bolaamphiphiles (Figure 6a,c).^{49,71,72} In the meanwhile, we have also shown that, differently than bilayer-forming lipids, G-C18:1 forms vesicles with an interdigitated lipid layer (IL), of which the thickness corresponds to the size of a single molecule (Figure 6b,d).^{49,54,71,72} In light of these observations, the most reasonable hypothesis explaining the *Co*-to-*MLWV* transition is a local decrease in curvature due to the micelle-to-IL transition (Figure 6c,d) of G-C18:1. The driving force is the screening of electrostatic repulsions between adjacent carboxylate groups due to progressive acidification (Figure 6a,b). The residual negative charges in the membrane guarantee a charge density high enough to promote electrostatic attraction with the positively-charged PLL contained between two G-C18:1 IL, as theoretically predicted and experimentally observed in polyelectrolyte systems at charged interfaces.^{41,73,74}

The equilibrium curvature in lipid-polyelectrolyte complexes depends on a subtle force balance between the bending modulus and electrostatic energy, which can be comparable.^{38,39,75} Polymers can have a significant impact on the bending energy of lipid bilayers in the case of strong adsorption and large polymer volume fractions.³⁶ For charged systems in particular, the interplay between the bending stiffness of the lipid bilayer and the charge density of both the lipid bilayer and polyelectrolyte govern the overall free energy of the complex.^{4,25,38,39,75} As a consequence, it is not obvious to predict the equilibrium curvature in a complex polyelectrolyte-bilayer system at equilibrium,^{42,43} and this task becomes even harder, if not impossible, in non-equilibrium systems with variable surface charge density.

Micelles have a high charge density and a higher spontaneous curvature compared to vesicles. When the decrease in pH reduces the charge density inducing the micelle-to-vesicle phase transition, the PESC undergoes the *Co*-to-*MLWV* phase transition, meaning a decrease in spontaneous curvature. Interestingly, the pH region where this phenomenon occurs is the same in the control and in the complex, thus meaning that the contribution of the membrane bending energy prevails over the electrostatic energy contribution.³⁸ It is also interesting to note that [G-C18:1 + PLL] PESC form vesicular (*MLWV*), and not flat, multilamellar objects. This is also not an obvious result and it can also be explained by the subtle interplay between the electrostatic and bending energies.^{37,39} The former is not large enough to counterbalance the

membrane spontaneous tendency to bend; on the contrary, the magnitude of the latter, being proportional to the membrane bending rigidity,⁷⁶ is not high enough to drive the complex towards an infinitely small curvature, characterizing a flat structure.

In the description proposed by Brooks *et al.*³⁶, the effective bending energy can significantly vary in the case of strong adsorption and large volume fraction of the polymer, meaning that, in principle, the polymer could flatten the membrane. Other authors point at the importance of the charge ratio, Z , between the polyelectrolyte and the lipid but also at the persistence length, that is the rigidity, of the polymer:⁷ for small Z and flexible polymers, supramicellar aggregates like complex coacervates are favoured, while for high Z and rigid polymers, micellar rods or flat bilayers might be favoured. In the present work we observe the same phase *Co*-to-*MLWV* transition, whichever the polymer employed, may it be PLL or chitosan, the latter being considered as rigid.⁷ The ionic strength is not controlled but the pH change process generates salt concentrations generally below 50 mM, which are generally enough to keep the rigidity properties of the polyelectrolyte.⁷ A specific comment on the ionic strength will be given at the end of the manuscript. The actual value of Z for our systems is harder to determine. A mere calculation based on the lipid and PEC concentrations and respective molecular weight indicates $Z < 1$, which is compatible, according to ref. ⁷, with the existence of complex coacervates. However, in these systems Z increases during pH variation because of the carboxylate-to-carboxylic reaction and in fact we are not able to quantify Z at a given pH simply because we cannot measure the actual surface charge density and distribution in PESCs. On the basis of these considerations, we conclude that the impact of polymer adsorption (including strength, quantity, rigidity and screening) is not strong enough to prevent the micelle-to-vesicle transition and to counterbalance the bending energy of the surfactant in the vesicle phase. For this reason, the stable phase is vesicular and not flat lamellar, as found at lower pH values.

In the *MLWV* phase, between pH 7.5 and 4, the d -spacing of the lamellar wall progressively increases from $d = 34.9 \text{ \AA}$ ($q_l = 0.180 \text{ \AA}^{-1}$) to $d = 40.2 \text{ \AA}$ ($q_l = 0.156 \text{ \AA}^{-1}$), before precipitation of the *L* phase below pH 4 with $d = 34.8 \text{ \AA}$ ($q = 0.181 \text{ \AA}^{-1}$) measured at pH 3 (Figure 5d). At the moment of formation, *MLWV* have the same d -spacing value as in the *L* phase and this value is less than 1 \AA shorter compared to the lamellar period in the G-C18:1 *L* phase control ($d = 35.7 \text{ \AA}$). The fact that the shortest d -spacing in the *MLWV* is comparable to the control is counterintuitive, because the interlamellar volume in the *MLWV* must accommodate PLL chains, which occupy a given volume. However, from the theory of polyelectrolyte adsorption on surfaces of opposite charges and from many experimental works, it is well-known

that polyelectrolytes can form a flat 2D layer.^{74,77} In this case, the thickness of the polyelectrolyte layer corresponds to its molecular cross-section. The cross-sectional diameter of PLL is reasonably expected to be contained between 1 Å and 8 Å, the former being the lower limit found in many polymeric systems⁷⁸ and the latter estimated in bilayer/PLL multilayers at pH below 7.⁷⁹ The thickness of the G-C18:1 interdigitated layer can be calculated to be about 25 Å by applying the Tanford formula ($L = 1.54 + 1.265 * n$, L being the length of the aliphatic chain and n the number of methylene groups)⁷⁰ to an effective C16 aliphatic chain (considering the 120° of the double bond in G-C18:1) and taking 8 Å as the size of a single glucose molecule.⁸⁰ Experimentally, we have estimated the thickness of the G-C18:1 membrane to be contained between 28 Å (pH 7) and 30 Å (pH 6) by modelling SAXS data (Figure S 4 in Ref. ⁴⁹), with an error due to fitting process of at least ±10 %. To account for the experimental d -spacing values, one has to consider a hydration interlamellar layer between 5.7 and 7.7 Å in the PLL-free control system, which can be classically found in lipid lamellar phases.^{81,82} At the moment of formation of the *MLWV* at pH 7 ($d = 34.9$ Å), one can otherwise estimate the contribution of PLL to the interlamellar layer to be contained between 4.9 Å and 6.9 Å, the latter being in better agreement with what it was experimentally reported in ref. ⁷⁹ and taking into account a thickness of the IL of 28 Å.

Several points should be highlighted from the above:

- Considering the thickness of the lipid membrane, the resulting interlamellar space is compatible with the diameter of PLL. In other words, a single PLL layer accommodates in between G-C18:1 interdigitated layers during the formation of *MLWV* in agreement with the dilute and semidilute regimes described in ref. ⁷⁴.
- Considering the fact that the interlamellar distance is practically equivalent to the expected diameter of PLL, one does not expect a significant content of hydration water and counterions in the proximity of PLL. This is consistent with the entropic gain of releasing water molecule and counterions during the formation of PESCes,^{4,25} verified and quantified below by ITC experiments. However, hydration water and counterions can fill the space between adjacent polyelectrolyte molecules, as also implied by the semidilute regimes described in ref. ⁷⁴.
- At the moment of *MLWV* formation and after precipitation of the *L* phase below pH 4, the thickness of the interlamellar space is the same and it is comparable with the interlamellar thickness in the PLL-free control. This fact shows that PLL can partly replace hydration water, confirming the assumptions above.
- Considering that d -spacing is the same at the moment of *MLWV* formation at pH 7 and after precipitation of the *L* phase below pH 4, one could formulate the hypothesis that PLL is trapped

in the *L* phase. Our data cannot directly prove this assumption, but we will provide more insights on this point in the following paragraphs, suggesting that this is not the case.

- Increase of the *d*-spacing in the *MLWV* between pH 7 and pH 4 is certainly related to the protonation of G-C18:1, an analogous, although opposite, mechanism described for systems composed of lipid membrane with constant charge density and pH-reactive polyelectrolytes.²⁰ A more detailed explanation of the pH-dependent evolution profiles of both *d*-spacing and size of lamellar crystallites (Figure 5d) is given below.

- Reversibility of the *Co*-to-*MLWV* to *MLWV*-to-*Co* phase transitions is addressed on Figure S 10, of which a)-panel focuses on the alkaline-to-acidic *Co*-to-*MLWV* transition ($C = 10 \text{ mg mL}^{-1}$), discussed above, and b)-panel highlights the reversed acidic-to-alkaline pH variation performed on the same sample. Figure S 10b shows the lamellar peak of the *Co*-to-*MLWV* phase but it does not show any evidence of the correlation peak typical of the *Co* phase, indicating that the *Co*-to-*MLWV* phase transition is not reversible. This could be due to a number of reasons among which the screening effect of salt generated during the pH variation process, known to have a strong impact on the phase diagram.²⁵

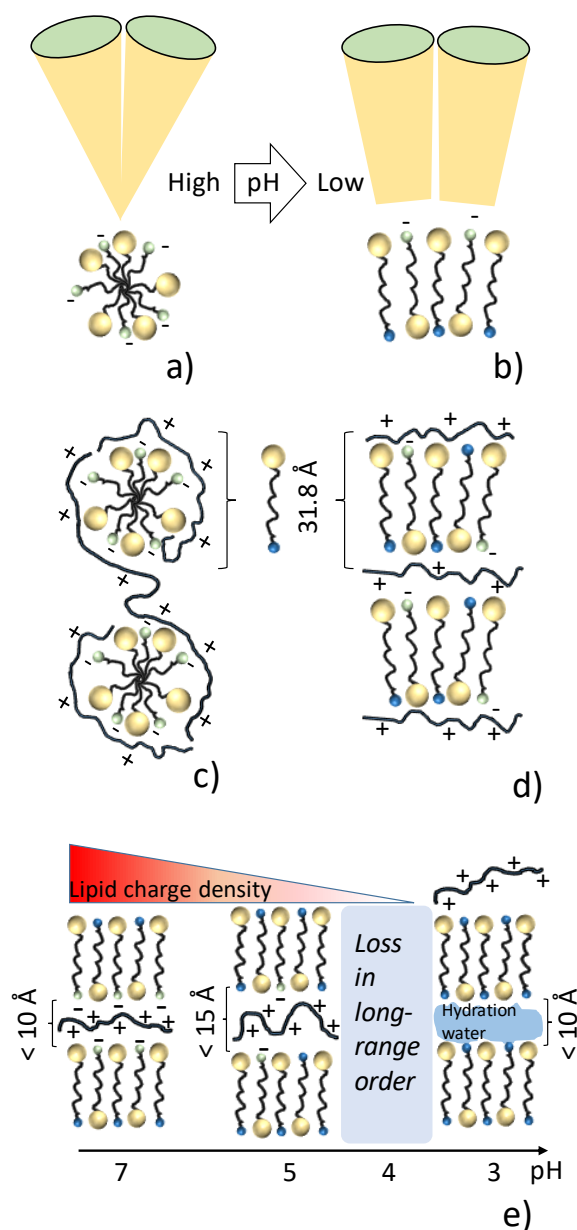


Figure 6 – Schematic view of the pH-driven transition between (a) micelles and (b) interdigitated membrane composed solely of G-C18:1. In the presence of PLL, the transition between the (a) complex coacervate and (b) the multi-lamellar wall in the *MLWV* occurs via a morphology change (micelle-to-vesicle) but a structural continuity (micelle-diameter \approx membrane thickness). e) Insight on the evolution of the pH-dependent interlamellar spacing inside the multi-lamellar walls of *MLWV*: upon decrease in the membrane charge density, PLL expands and it applies a repulsive pressure to the lipid membranes. When the membrane is close to neutrality, long-range order is lost, *MLWV* disassemble, PLL is expelled and G-C18:1 precipitates into a hydrated lamellar phase.

The pH-dependent d -spacing evolution is explained by looking at the intermolecular forces equilibrating in the interlamellar space. In a polymer-free lipid bilayer system, attractive Van der Waals interaction counterbalances two short-range ($< 30 \text{ \AA}$), steric and hydration, and

two long-range ($> 30 \text{ \AA}$ up to hundred of nanometers) repulsive interactions, electrostatic and thermal undulation.⁸³⁻⁸⁵ For interlamellar spacing below 30 \AA , which is the case here, electrostatic and undulation are generally neglected. In the case of a polyelectrolyte contained between membranes with variable charge density, which is the case in this work, one should consider additional terms in the energy balance like a repulsive free polymer term, including chain elasticity and excluded-volume terms, an entropic contribution of the small ions, an electrostatic contribution, containing the polyelectrolyte-surface attractive and inter-chain repulsive interaction.^{40,41,73,74,86,87} Under the conditions of *MLWV* formation, around pH 7, the negatively-charged G-C18:1 membrane undergoes strong electrostatic attraction with PLL, largely-documented in both theoretical and experimental works on polyelectrolytes at charged interfaces.^{41,73,74,87-89} When pH decreases, the carboxylate to carboxylic acid reaction reduces the number of negative charges and, consequently, it lowers the charge density of the lipid membrane. Since the attractive electrostatic component in the lipid-polyelectrolyte complex depends on the lipid charge density, lowering pH will reduce its contribution to the free energy. The consequence will be an increased volume occupied by the polyelectrolyte,⁷⁴ which will cause an increase in the repulsive osmotic pressure^{40,41} with consequent swelling of the membranes, experimentally shown in Figure 5b,d and schematized in Figure 6e.

Below pH 4, the *MLWV* peak disappears until pH ~ 3 , when the signal of the *L* phase at $d = 34.8 \text{ \AA}$ appears again. Interestingly, this value is practically the same one observed at the moment of the *MLWV* formation at pH 7 and actually 0.9 \AA smaller than the *d*-spacing found in the G-C18:1 control at the same pH value. Such an observation could induce to formulate the hypothesis that in the *MLWV*-to-*L* phase transition below pH 4, PLL is confined in between the lamellae. In fact, we believe that this is not the case for several reasons. It is well-known that at low hydration and in the absence of specific attraction interactions, large polymers segregate outside the lipid interlamellar space.⁹⁰ However, the polymer cannot be reasonably expelled from a dense, closed, multilamellar object. The evolution of the crystallite size with pH in Figure 5d helps understanding the mechanism of expulsion. Between pH 5 and 4, *d*-spacing is still increasing, testifying of the expansion of the lamellae due to the repulsive pressure applied by PLL. In the meanwhile, the peak becomes broader, with consequent drop in the crystallite size. At pH 4, the peak becomes so large that the crystallite size has dropped from several thousand of \AA to only few \AA , while *d*-spacing drops back to 34.7 \AA . Below pH 5, the repulsive pressure exerted by PLL becomes so strong that the long-range order in the *MLWV* is lost. Complete disruption of the multilamellar walls occurs below pH 4, when PLL could eventually be expelled in the surrounding aqueous solution. Upon expulsion

of PLL, G-C18:1 precipitates in its thermodynamically favorable *L* phase, the same as found in the control lipid solution. This mechanism is summarized in Figure 6e at pH below 5.

Study of the interactions between glycolipids and PLL

To confirm and quantify the interactions between G-C18:1 and PLL in the *MLWV* phase, as hypothesized in Figure 6, and to prove that SL-C18:0 fibrils do not contain PLL, we run a combination of solution NMR and ITC experiments. ^1H NMR is employed to prove the presence (or absence) of PLL at pH 5, either in the fiber or *MLWV* phase. From ^1H NMR experiments, it is also possible to estimate the efficiency of the assembly process and the [COOH]-to-[NH₂] molar ratio. *MLWV* and fibers formed at pH 5 are centrifuged out of their parent solution, dried, dissolved in MeOD-d₄ and analyzed by ^1H NMR employing an internal reference (0 ppm, TMS-*d*₄, C = 5.8 mM). The lipids are characterized by a well-defined triplet around 2.18 - 2.20 ppm (RCH₂C=O) while PLL is characterized by a broad signal at 2.92 ppm [(RCH₂NH₂)_{*x*} (*x* ~ 20)].

In the [SL-C18:0 + PLL] system, only the peaks of SL-C18:0 are observed while the characteristic peak of PLL at $\delta = 2.92$ ppm is not detected in any of the samples initially prepared at various SL-C18:0-to-PLL ratios (Figure S 11c,d). If SAXS and cryo-TEM data (Figure 4a,b) show the formation of twisted ribbons, NMR shows that their composition is only constituted by SL-C18:0, demonstrating, within the NMR sensitivity, that they do not contain PLL, thus confirming the absence of specific interactions between SL-C18:0 and PLL.

The characteristic peaks of both G-C18:1 ($\delta = 2.20$ ppm) and PLL ($\delta = 2.92$ ppm) are on the contrary observed in the *MLWV* phase (Figure S 11a,b), showing the simultaneous presence of both G-C18:1 and PLL, thus supporting the hypothesis of strong interactions between these compounds.

Table 2 shows the quantitative analysis of the NMR data (full integration data are given in Table S 1). The initial $\frac{[\text{G-C18:1}]_{In}}{[\text{PLL}]_{In}}$ molar ratio corresponds to the initial solution (exact concentrations are given in Table S 1), while $\frac{[\text{G-C18:1}]_F}{[\text{PLL}]_F}$ corresponds to the final ratio found in the *MLWV* phase. The former, also known as *r* in the literature,²¹ is generally different than the latter, known as *r**.²¹ This behaviour is expected and often reported for complex coacervate systems, which follow their own stoichiometry even if the initial ratio is not optimized.²¹ $\frac{[\text{G-C18:1}]_F}{[\text{PLL}]_F}$ ranges between roughly 100 and 200, where the large discrepancy is in fact not so

surprising and probably due to the crude method to prepare the sample (centrifugation, redispersion) prior to NMR analysis.

From the above, one can estimate the final monomer ratio $\frac{[COOH]_F}{[NH_2]_F}$ in the *MLWV* phase and varying between 5 and 10. These numbers should be taken with caution for two reasons: 1) the large uncertainty on the M_w of PLL, here taken as 2.5 kDa but actually varying between 1 kDa and 5 kDa; 2) the uncertainty on the integral of PLL, which, being a high-molecular weight compound, may not be quantitatively probed by solution NMR due to long T2 relaxation times. Despite the uncertainty on the signal of PLL, $\frac{[COOH]_F}{[NH_2]_F}$ seems to show that interactions between G-C18:1 and PLL occur with an excess of carboxylic acids. In fact, simple considerations based on pKa and pH at which experiments are performed show that the actual charged monomer ratio, $\frac{[COO^-]_F}{[NH_3^+]_F}$, is in fact much closer to unity, as one would expect on the hypothesis of charge neutralization between G-C18:1 and PLL and in agreement with ζ -potential experiments (Figure S 3). *MLWV* are initially prepared at pH 5, where all amine are essentially protonated into NH_3^+ (pKa ~10-10.5).⁵⁷ The pKa of the oleic acid moiety of G-C18:1 could be considered of about 7, a classical value found for oleic acid in water.^{91,92} Then, the actual COO^- content at pH 5 could reasonably be estimated between 10% and 30%, for which $\frac{[COO^-]_F}{[NH_3^+]_F}$ now varies respectively between 0.7 and 2 (Table 2).

Within the hypothesis of a contained ionic strength (this point will be discussed at the end of the manuscript), the formation of *MLWV* occurs just above pH 7, in the proximity of, or slightly above, the pKa of oleic acid, with a $\frac{[COO^-]_F}{[NH_3^+]_F}$ content ranging between 2 and 5. *MLWV* are then stable until pH 4, when $\frac{[COO^-]_F}{[NH_3^+]_F}$ falls below the range 0.5 – 1. Finally, in terms of amount of lipid and PLL consumed, NMR shows that an average of about 70% of the initial content of G-C18:1 is employed to form *MLWV* in spite of less than 10% of the initial PLL content. Variations in the initial $\frac{[G-C18:1]_{In}}{[PLL]_{In}}$ do not seem to have any particular influence on the amount of consumed reactants.

Table 2 – Quantitative evaluation of G-C18:1 and PLL in *MLWV* by 1H solution NMR. The NMR spectra and full list of parameters are respectively given in Figure S 11 and Table S 1. In brief: the molar ratio column gives the G-C18:1-to-PLL molar ratio (square brackets identify molar concentrations) in the initial solution ($\frac{[G-C18:1]_{In}}{[PLL]_{In}}$) and in the *MLWV* phase ($\frac{[G-C18:1]_F}{[PLL]_F}$). The monomer ratio column identifies the ratio

between the neutral $\frac{[COOH]_F}{[NH_2]_F}$ and charged $\frac{[COO^-]_F}{[NH_3^+]_F}$ functional groups in the *MLWV*. $\frac{[COO^-]_F}{[NH_3^+]_F}$ is calculated from $\frac{[COOH]_F}{[NH_2]_F}$ assuming that the interaction occurs at pH 5, with 100 % of NH_3^+ and two values of COO^- (10% and 30%), estimated at the same pH for a pKa of about 7. The % consumed column identifies the molar percentage of consumed G-C18:1 and PLL during formation of *MLWV* (subscript *F*) with respect to their initial concentration (subscript *In*) in solution.

Molar ratio		Monomer ratio in <i>MLWV</i>			% consumed reactants in <i>MLWV</i>	
$\frac{[G - C18:1]_{In}}{[PLL]_{In}}$ (in solution)	$\frac{[G - C18:1]_F}{[PLL]_F}$ (in <i>MLWV</i>)	$\frac{[COOH]_F}{[NH_2]_F}$	$\frac{[COO^-]_F}{[NH_3^+]_F}$		$\frac{[G - C18:1]_F}{[G - C18:1]_{In}}$	$\frac{[PLL]_F}{[PLL]_{In}}$
			(10% COO^-)	(30% COO^-)		
5.4	92 ± 22	4.6 ± 1.1	0.5 ± 0.1	1.4 ± 0.3	63 ± 11	3.7 ± 0.6
10.8	192 ± 46	9.6 ± 2.3	1.0 ± 0.2	2.9 ± 0.7	69 ± 12	3.9 ± 0.7
21.6	144 ± 35	7.2 ± 1.7	0.7 ± 0.2	2.2 ± 0.5	47 ± 8	7.0 ± 1.2
2.75	113 ± 27	5.7 ± 1.4	0.6 ± 0.1	1.7 ± 0.4	94 ± 16	2.3 ± 0.4

To confirm and strengthen the NMR data, ITC experiments are performed in the *MLWV* phase region. In particular, ITC provides a direct proof of the specificity of the interaction between G-C18:1 and PLL and it quantifies its thermodynamic parameters. Figure 7a shows the heat rate profile upon controlled injections of buffer (phosphate) and G-C18:1 solutions into a PLL solution. The negative peaks identify an exothermic process, while the rapid loss in the heat rate intensity, compared to the buffer injection, shows that PLL binding sites are rapidly saturated with G-C18:1. Typically, data obtained by ITC for the adsorption of surfactant on polyelectrolytes are interpreted by using the Satake-Yang binding isotherm,⁹³ but more recent multiple site binding models have appeared in the literature^{94,95} and are provided by the Nanoanalyze software,⁹⁶ allowing a handy way to extract thermodynamic parameters and to compare them across studies.^{97,98} The “independent model” considers the interaction of “n” ligands with a macromolecule that has one binding site (or multiple equivalent binding sites);^{99,100,101} the “multiple site” model allows for fitting to two independent sites, each with a unique association constant, k_a , stoichiometry, n , and enthalpy change, ΔH ; the “sequential (two sites)” model considers two binding sites where the first is populated before the second accepts a ligand.

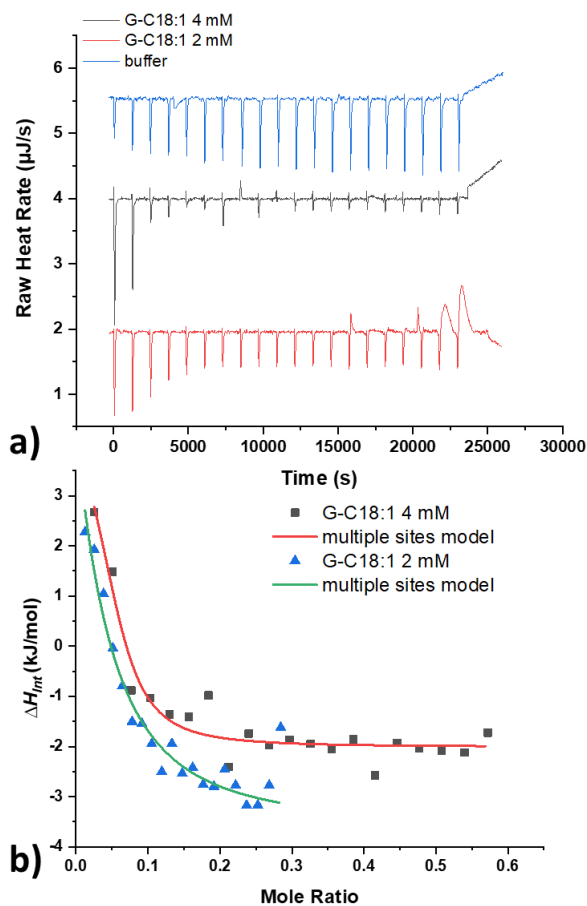


Figure 7 - a) ITC heat rate profiles of buffer (blue) and G-C18:1 ($C = 4$ mM, black; $C = 2$ mM, red) solutions injected into a PLL solution ($C = 2$ mM). **b)** Evolution of the ΔH_{Int} ($= \Delta H_{G-C18:1/PLL} - \Delta H_{Buffer}$) with PLL/G-C18:1 molar ratio derived from (a). The fit is performed with a “multiple site” model provided by the Nanoanalyze software.

In this work, the independent model is not able to fit the data and it is then discarded. The evolution of the enthalpy change of interaction, ΔH_{Int} , with mole ratio (Figure 7b) can be satisfactorily fitted with both the “multiple site” and “sequential (two sites)” models. However, one should be aware of the fact Langmuir-type binding isotherms do make some assumptions which are not completely satisfied for the experiments and results should be interpreted with caution and with an eye on the underlying physics. Here, the highest consistency between the fitting results and the physics of adsorption of G-C18:1 onto PLL is obtained with the “multiple site” model, interpreted hereafter.

The thermodynamic parameters extracted from the fit of the enthalpy profile are given in Table 3. The first interaction has a positive enthalpy change ($\Delta H_1 = 28.9 \pm 0.9$ kJ/mol) and an entropy variation of $T\Delta S_1 = 76.7 \pm 22.8$ kJ/mol. The second interaction shows a negative

entropy change ($\Delta H_2 = -2.8 \pm 0.8$ kJ/mol) and a smaller entropy variation ($T\Delta S_2 = 33.6 \pm 1.1$ kJ/mol). Please note that the denominations first and second do not specify sequential interactions, i.e. they can occur in any random order, as both sites are independent. These data illustrate that the first interaction is endothermic, non-specific and essentially entropy-dependent, most likely driven by the hydrophobic effect. On the contrary, the second is exothermic, specific and most likely driven by electrostatic and/or of H-bonding interactions,⁹⁸ as also found for β -lactoglobulin/sodium alginate in the pH range where they are oppositely charged.¹⁰² Both interactions are of equivalent importance for the association of G-C18:1 and PLL, considering that both Gibbs free energies (ΔG) are negative and of the same order of magnitude.

From a mechanistic point of view, we interpret these data with a standard surfactant-polyelectrolyte approach:⁹⁸ G-C18:1 strongly binds to PPL through specific interactions ($\Delta H_2 < 0$) with an entropic ($T\Delta S_2 > 0$) component, most likely coming from the release of water and counterions initially associated to the charged binding sites. The stoichiometry of the interaction in Table 3 corresponds to the monomer stoichiometry, also evaluated by NMR in Table 2 ($n_2 \equiv \frac{[COOH]_F}{[NH_2]_F}$). ITC provides $n_2 = 3.8 \pm 0.7$ with an affinity of $K_{a2} = 2.62 \pm 1.48 \cdot 10^6$ M⁻¹, where n_2 is in very good agreement, within the error, with $\langle \frac{[COOH]_F}{[NH_2]_F} \rangle = 6.8 \pm 2.2$, the average monomer ratio found by NMR. ITC and NMR experiments are performed under different experimental and sample preparation conditions; the agreement between n_2 and $\frac{[COOH]_F}{[NH_2]_F}$ strongly support the reliability of the hypothesis formulated in Figure 6. The order of magnitude of the interactions and affinity constants found here are in also good agreement with the values published in the literature for similar systems, where $|\Delta H|$ varies between 1 and 20 kJ/mol, $|T\Delta S|$ between 1 and 50 kJ/mol with affinity constants in the order of 10^7 M⁻¹.^{97,103–105}

The second energetic contribution found in the [G-C18:1+PLL] system is non-specific ($\Delta H_2 > 0$) and it corresponds to the clustering, or grouping, of the non-polar tails of G-C18:1 molecules, driven by the release of water ($T\Delta S_2 > 0$). Similar coexisting specific and non-specific interactions were reported in hyaluronan/cationic vesicles system¹⁰⁶ or gum acacia/bovine serum albumin system¹⁰⁷ and are well-known in polyelectrolyte-micelle coacervation (“polymer-driven micellization”).⁹⁸

Table 3 - Thermodynamic parameters extracted from fitted data in Figure 7b using a “multiple site” model at $T = 298$ K. Data are averaged for the two experiments, of which the corresponding parameters of the fits are given in the Supporting Information (Table S 2 and Table S 3). k_a is the association constant, n is the

G-C18:1 to PLL monomer stoichiometry ($\equiv \frac{[COOH]_F}{[NH_2]_F}$) and ΔH , ΔG and ΔS are respectively the enthalpy, Gibbs' free energy and entropy change.

Interaction type	Parameter	Value
Non-specific Endothermic (entropic, hydrophobic effect)	K_{a1}	$2.4 \pm 0.8 \cdot 10^8 \text{ M}^{-1}$
	n_1	0.03 ± 0.02
	ΔG_1	$-47.7 \pm 1.2 \text{ kJ/mol}$
	ΔH_1	$28.9 \pm 0.9 \text{ kJ/mol}$
	ΔS_1	$0.3 \pm 0.1 \text{ kJ/mol} \cdot \text{K}$
Specific Exothermic (electrostatic, H-bonding)	K_{a2}	$2.6 \pm 1.5 \cdot 10^6 \text{ M}^{-1}$
	n_2	3.8 ± 0.7
	ΔG_2	$-36.4 \pm 1.9 \text{ kJ/mol}$
	ΔH_2	$-2.8 \pm 0.8 \text{ kJ/mol}$
	ΔS_2	$0.10 \pm 0.04 \text{ kJ/mol} \cdot \text{K}$

Discussion

Figure 8 summarizes the major findings of this work. SL-C18:0 is a lipid which undergoes a direct micelle-to-fiber transition in water in the vicinity of pH 7. We had proposed a nucleation and growth mechanism of the fibers with no apparent structural continuity with the micelles, which act as reservoir of matter.^{49,59} In the presence of a polyelectrolyte, such mechanism persists. Above pH 7.5, the negatively-charged micelles are complexed by the polyelectrolyte into a complex coacervate (*Co* phase), of which we find two major structures by cryo-TEM, a dense cluster of micelles (panel 1 in Figure 3) coexisting with a PLL-rich (*sc* in Figure 3) and textured, “pearl-necklace”-like, glycolipid-rich medium (panels 2,3 in Figure 3). Below pH 7.5, the coacervate phase disassembles in favour of a twisted ribbon phase, only composed of SL-C18:0 only, as confirmed by ¹H solution NMR experiments (Figure S 11c,d). Interestingly, ribbons were shown to form by the interaction of bile salts with block copolymers,⁴⁶ and for this reason we speculate that SL-C18:0 fibers are either neutral objects of their surface charge is too low for complexation to occur. We stress however the fact that at the moment we do not have a direct measurement of the fibers' surface charge. As in the PEC-free system, the coacervate-to-fiber transition occurs in less than a pH unit and without any intermediate. This general mechanism is shown in Figure 8a. The best hypothesis, to be eventually verified with other complementary techniques, is that upon charge compensation during lowering pH, SL-C18:0 molecules are progressively acidified and slowly diffuse from the micellar environment to the solution. The solubility of acidic SL-C18:0 in water is low and

for this reason, after reaching a critical concentration, nucleation of the twisted ribbons occurs, followed by growth and concomitant disruption of the coacervate. Last but not least, the nature of the PEC has no influence on the coacervate-to-fiber transition, indicating that PEC rigidity and charge density play no significant role.

In the absence of a polyelectrolyte, G-C18:1 undergoes a micelle-to-vesicle-to-lamellar phase transition, characterized by a structural and morphological continuity.⁴⁹ In the presence of PLL (generalization to other PEC is presented elsewhere),⁶⁴ G-C18:1 forms a *Co* phase in the micelle region of its phase diagram at $\text{pH} > 7$. If combination of cryo-TEM and SAXS suggests a textured worm-like structure of the coacervate (Figure 3d) rather than a “pearl-necklace”, complexation by the polyelectrolyte does not induce shape transition in the G-C18:1 micelles. This is in line with the body of data published on surfactant-polyelectrolyte coacervates²¹ and probably explained by the low binding affinity of ammonium groups.¹⁰⁸ Below approximately $\text{pH} 7.5$, we find a transition between the complex coacervate and multilamellar walls vesicles. This is driven by an isostructural and isodimensional (Figure 6c,d) micelle-to-membrane transition (Figure 6a,b): the diameter of the micelles, embedded in the coacervate phase, is equivalent to the thickness of the membrane. The thickness corresponds to the length of a single G-C18:1 molecule (Figure 6d), as previously found for this systems⁴⁹ and expected for bolaamphiphiles.⁷¹ *MLWV* are stable in the pH interval between 7 and 5. A decrease in pH corresponds to an increasing content of the acidic form of G-C18:1 in the membrane and a consequent lowering of the membrane charge density. For this reason, the interlamellar distance increases by decreasing pH , due to the increasing thickness of PLL, hence causing an increase in repulsive pressure, upon lowering the charge density of the membrane (Figure 6e).⁷⁴ Quantitative ^1H NMR experiments confirm that *MLWV* are composed of both G-C18:1 and PLL with an average monomer stoichiometry of 6.8 ± 2.2 . Considerations about the pK_a (here assumed to be about 7) and pH at which *MLWV* are prepared (5) suggest a situation of charge compensation between carboxylic acids and ammonium groups. Such specific interactions ($\Delta H_2 = -2.8 \pm 0.8$ kJ/mol) with a comparable stoichiometry (3.8 ± 0.7) and high affinity ($K_{a2} = 2.6 \pm 1.5 \cdot 10^6$ M⁻¹) are also confirmed by independent ITC experiments. When the amount of negative charges has lowered at a point below which attractive interaction with PLL can no longer hold the membranes together (between $\text{pH} 5$ and $\text{pH} 4$), *MLWV* experience a loss in the long-range lamellar order. This is followed by the complete disruption of the *MLWV*, causing the expulsion of PLL and eventually followed, below $\text{pH} 3$, by precipitation of a polyelectrolyte-free lamellar phase only composed of G-C18:1 (Figure 6e and Figure 8b). If pH is increased again, *MLWV* form again in their pH stability range. However, further increase

in pH does not induce a reversed *MLWV*-to-*Co* transition, but rather the formation of free micelles and PLL.

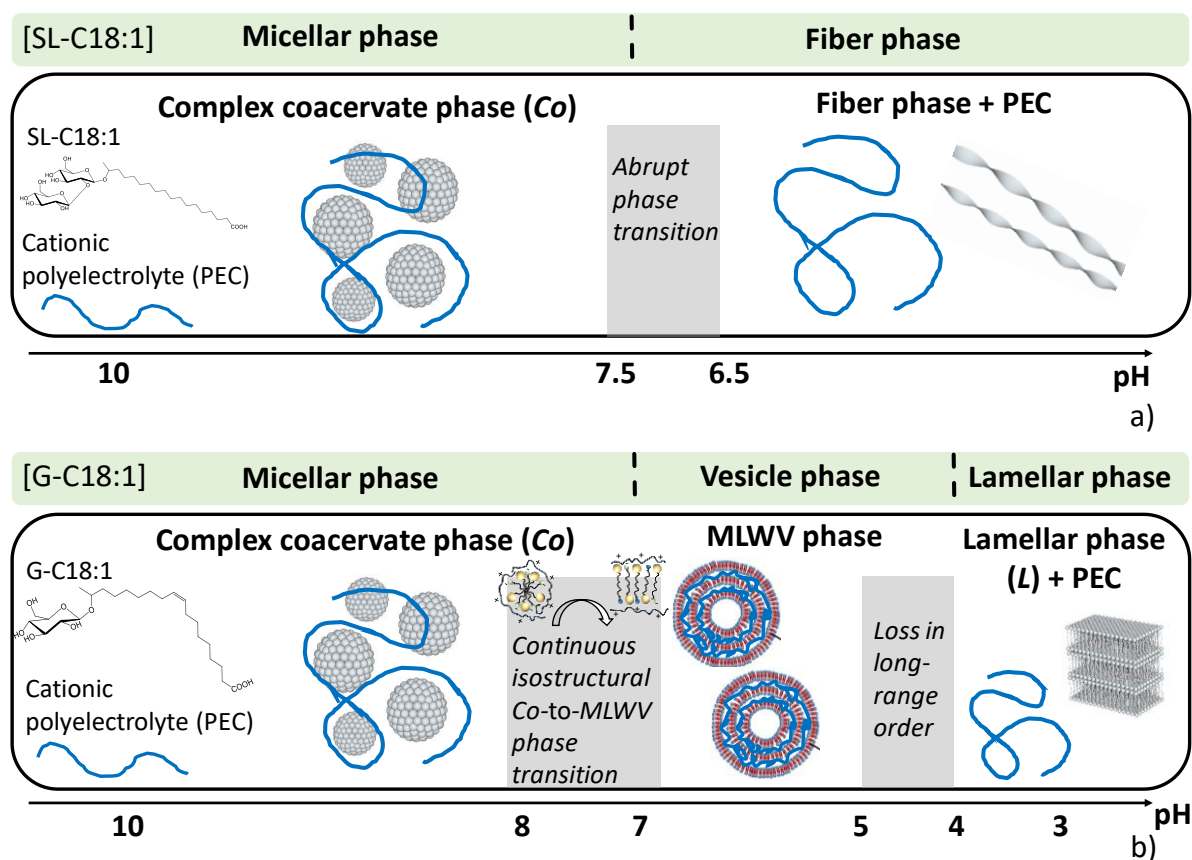


Figure 8 – Summary of the pH-driven phase transitions of (a) SL-C18:0 and (b) G-C18:1 lipids alone and in the presence of PLL polyelectrolyte in water at room temperature and $C < 1$ wt%.

Our data show that the *Co*-to-*MLWV* transition is driven by the dynamic variation in the effective packing parameter of G-C18:1 and which depends on the transition from its ionic to neutral form. If this result is coherent with previous studies on the equilibrium phase diagrams of PESC, where the packing parameter of the PESC was modified either by using a cosurfactant^{6,24} or by varying the nature of the polar headgroup,³⁵ we do not find a major influence of the type of polyelectrolyte, as proposed elsewhere.⁷ This is unexpected, especially considering the strong impact of polyelectrolytes on the membrane bending energy already discussed above. It has been recently shown that the pH-driven micelle-to-vesicle transition in free ethoxy fatty acids solutions³⁴ can be inhibited in the presence of a polyelectrolyte.³⁵ In fact, to the best of our knowledge, evidence of isostructural and isodimensional micelle-to-vesicle transition in PESC at concentrations as low as 0.2 wt% have hardly been described. Lamellar or multilamellar PESC phases are far from being uncommon but they are generally obtained

for calibrated formulations³⁵ and often at high lipid concentrations (generally above 10 wt%).²⁴ Furthermore, similar phase transitions were never reported in specific polyelectrolyte-surfactant complex coacervate systems.

It is worth mentioning a short comment on the *MLWV* structure, which we systematically find, instead of flat lamellar phase or agglutinated single-wall vesicles. We have discussed the former situation as the overwhelming effect of the intrinsic bending energy of the G-C18:1 interdigitated layered membrane overwhelming the competing structuring effect of the polyelectrolyte. Although we cannot quantify it, it seems clear that any of the polyelectrolytes employed in this study are neither rigid enough nor bind strongly enough to generate a flat membrane.

Whether the non-equilibrium continuous pH variation to cross the micelle-vesicle boundary of G-C18:1 has any impact on the *Co*-to-*MLWV* transition is an open question to which we can answer only partially. Vesicles are generally considered as metastable structures, although in some cases, when the structure does not evolve for an “infinitely” long time, they are assumed to be at equilibrium. G-C18:1 spontaneously self-assembles into vesicles upon pH variation from alkaline to acidic pH under conditions of both pseudo-⁵⁴ and non-equilibrium (Figure 5a).⁴⁹ Furthermore, unpublished in-lab tests show that G-C18:1 in fact spontaneously forms vesicles by a simple dispersion in water at pH below 7 and by application of moderate amounts of energy (e.g., bath sonication). G-C18:1 vesicles tend to be colloiddally stable over long periods of time (months). On the basis of these observation, one can qualitatively say that the vesicle phase is the thermodynamic phase of G-C18:1 under acidic pH conditions. Given the above, *MLWV* structures should be systematically obtained if pH is varied extremely slow or if a G-C18:1 pre-formed vesicles and PEC solutions are mixed at acidic pH. In the first approach, it would be hard and ridiculously long to determine which rate of pH variation would be considered to be compatible with equilibrium conditions. For instance, Chiappisi *et al.* have employed equilibration times for a given pH value between 2 and 15 days.^{35,68} For this reason, we have employed the second approach, reported elsewhere,⁶⁴ and which does not show the formation of a single *MLWV* phase but rather a multiphasic system composed of agglutinated vesicles, cabbage-like structure and *MLWV*.

Agglutination of single-wall vesicles (SWV)^{25,109,110} against the formation of *MLWV* is an open, and important, question in the literature both from a fundamental¹¹⁰ and applicative points of view, as agglutination is important in the field of life science,¹¹⁰ while *MLWV* have a specific interest in gene transfection applications.¹¹¹ If several authors have explained the origin of *MLWV* structures as a simple matter of lipid-to-polyelectrolyte ratio,^{3,111,112} other authors

show contradictory data, where a mixture of both can be found.¹¹³ In the present system, we rather believe that the systematic production of *MLWV*, instead of agglutinated *SWV*, depends on the combination between the pre-existing complex coacervate phase, inside which the isostructural and isodimensional micelle-to-vesicle phase transition occurs, and the non-equilibrium pH variation, which traps the system in the *MLWV* phase. Separation between these mechanisms is shown elsewhere.⁶⁴

Finally, the *Co*-to-*MLWV* transition is driven by a pH jump process, meaning that salt is continuously generated. Ionic strength is an important parameter with a strong impact on the stability of PESC, but the charge density on both the polymer and the colloid, equally pH-dependent, are also very important for the PESC stability.²¹ Under the experimental conditions of this work, the amount of generated salt is in the order of 50 mM. Such concentration is modest compared to other studied reaching ionic strength as high as 0.4 M,⁶² but it could play a role in the overall electroneutrality and charge stoichiometry of both coacervates and *MLWV*. However, the pH jump process, necessary to drive the *Co*-to-*MLWV* transition, does not prevent the formation of both the *Co* and *MLWV* phases. Even if preliminary data (not displayed here) seem to show that *MLWV* are stable up to 0.5 M NaCl, we suspect salt to be responsible for the lack of reversibility of the *Co*-to-*MLWV*-to-*Co* transition (Figure S 10), meaning that this parameter certainly deserves to be studied in detail in relationship to the stability of PESC containing G-C18:1.

Conclusion

Non-equilibrium phase transitions in polyelectrolyte-surfactant complex (PESC) coacervates (*Co*) are addressed in this work by mean of stimuli-responsive negatively-charged amphiphiles and cationic polyelectrolytes. We employ two microbial glycolipid biosurfactants known to undergo micelle-to-fiber (deacetylated acidic C18:0 sophorolipids, SL-C18:0) and micelle-to-vesicle (deacetylated acidic C18:1 glucolipids, G-C18:1) phase transition when pH is lowered from alkaline to acidic. In the alkaline pH domain, both amphiphiles mainly form a phase characterized by negatively-charged micelles. Upon mixing with a positively-charged polyelectrolyte, pH-resolved *in situ* SAXS, DLS and ζ -potential combined with cryo-TEM show the formation of globally neutral PESC polyelectrolyte-surfactant coacervates. Upon acidification of the solution, the SL-C18:0 amphiphile undergoes a micelle-to-fiber transition, independently from the presence of the polyelectrolyte, which, according to ¹H NMR arguments, is most likely released in solution and it coexists with the fibers, but without specific interactions, differently than other similar systems.⁴⁶ The micelle-to-fiber transition is hence

responsible for the disruption of the complex coacervate, which becomes unstable below pH ~ 7 , the transition pH of the SL-C18:0 surfactant alone.

At the micelle-vesicle boundary, we find a continuous isostructural and isodimensional transition between complex coacervate (*Co*) and multilamellar wall vesicles (*MLWV*). By reducing the negative charge density during acidification, the micellar aggregates embedded in the *Co* phase are characterized by a decrease in the local curvature, which drives the transition from spheres to membranes, composed of interdigitated G-C18:1 molecules. The residual negative charge density guarantees electrostatic interaction with the polyelectrolyte, which keeps the membranes together. This is supported by both NMR and ITC experiments, providing a comparable charge stoichiometry and the latter showing specific interactions ($\Delta H < 0$). The bending energy associated to the polyelectrolyte-membrane complex is low enough for the lipid membrane to bend and drive the formation of vesicular colloids, characterized by multilamellar walls. The membrane thickness is equivalent to the micellar radius and compatible with the length of G-C18:1, testifying the isostructural and isodimensional transition. At lower pH, the membrane charge density becomes low and interactions with the polyelectrolyte less strong. This phenomenon promotes intra-chain electrostatic repulsion interactions and eventual swelling of the lamellar region. Finally, when the membrane becomes neutral, polymeric repulsion becomes strong enough to disassemble the lamellae. The polyelectrolyte will most likely be entirely solvated and at sufficiently low pH (< 3) the G-C18:1 precipitated in the form of a poorly-ordered, polyelectrolyte-free, lamellar phase, as found in the control lipid solution at the same pH. Upon increasing pH, *MLWV* form again but we do not find reversibility in the *MLWV*-to-*Co* transition.

This work shows that surfactant phase transitions driven by a non-equilibrium pH variation drive the complex coacervate out of its stability region. This occurs either through the loss of the polyelectrolyte-surfactant aggregation or through the formation of a new complex phase. In both cases, the nature of the polyelectrolyte (e.g., rigidity or charge density) does not have any significant influence on the fate of the transition, as found for most PESC. For the *MLWV* phase, the bending energy of the lipid membrane is low enough to counterbalance the strong adsorption and stiffness of the polyelectrolyte, which could otherwise drive the formation of a flat lamellar phase. At the same time, combination between the isostructural and isodimensional transition occurring in the confined micellar complex coacervate with non-equilibrium pH variation drive the formation of a *MLWV* phase, interesting for biomedical applications, rather than of a system composed of agglutinated single-wall vesicles, as found in many other systems. Finally, we stress the fact that this work demonstrates the possibility to

prepare a new generation of stimuli-responsive and fully sustainable PESC's due to the use of biosurfactants.

Acknowledgements

Diamond synchrotron radiation facility (U. K.) is acknowledged for accessing to the B21 beamline and financial support (proposal N° 23247). Ghazi Ben Messaoud (DWI-Leibniz Institute for Interactive Materials, Aachen, Germany) is kindly acknowledged for helpful discussions. We thank Dr. S. Roelants, Prof. W. Soetaert and Prof. C. V. Stevens at Gent University for providing us the glycolipids. We thank P. Dhasaiyan (Institute for Basic Science Center for Self Assembly and Complexity, Gyeongsangbuk-do, South Korea) for helpful suggestions. This work benefited from the use of the SasView application, originally developed under NSF award DMR-0520547. SasView contains code developed with funding from the European Union's Horizon 2020 research and innovation program under the SINE2020 project, grant agreement No. 654000. WT and GK acknowledge financial support from KU Leuven (grants C14/18/061 and IDN/19/014) and Research Foundation - Flanders (grant G.0C60.13N). Soleil Synchrotron facility for accessing the Swing beamline and financial support (proposal N° 20190961). Sorbonne Université (contract N°3083/2018) is acknowledged for financial support of CS. The authors acknowledge the French ANR for financial support, project N° SELFAMPHI - 19-CE43-0012-01.

Supporting Information: Figure S1 to Figure S11, Table S1 to Table S3, explicative text.

References

- (1) Kronberg, B.; Holmberg, K.; Lindman, B. *Surface Chemistry of Surfactants and Polymers*; John Wiley & Sons, Inc., 2014.
- (2) *Dna Interactions With Polymers and Surfactants*; Dias, R., Lindman, B., Eds.; John Wiley & Sons, Inc.: Hoboken, New Jersey, 2008.
- (3) Gradzielski, M.; Hoffmann, I. Polyelectrolyte-Surfactant Complexes (PESC's) Composed of Oppositely Charged Components. *Curr. Opin. Colloid Interface Sci.* **2018**, *35*, 124–141.
- (4) Ferreira, G. A.; Loh, W. Liquid Crystalline Nanoparticles Formed by Oppositely Charged Surfactant-Polyelectrolyte Complexes. *Curr. Opin. Colloid Interface Sci.* **2017**, *32*, 11–22.
- (5) Lindman, B.; Antunes, F.; Aidarova, S.; Miguel, M.; Nylander, T. Polyelectrolyte-

- Surfactant Association—from Fundamentals to Applications. *Colloid J.* **2014**, *76*, 585–594.
- (6) Piculell, L. Understanding and Exploiting the Phase Behavior of Mixtures of Oppositely Charged Polymers and Surfactants in Water. *Langmuir* **2013**, *29*, 10313–10329.
- (7) Chiappisi, L.; Hoffmann, I.; Gradzielski, M. Complexes of Oppositely Charged Polyelectrolytes and Surfactants - Recent Developments in the Field of Biologically Derived Polyelectrolytes. *Soft Matter* **2013**, *9*, 3896–3909.
- (8) Schmitt, C.; Turgeon, S. L. Protein/Polysaccharide Complexes and Coacervates in Food Systems. *Adv. Colloid Interface Sci.* **2011**, *167*, 63–70.
- (9) Winslow, B. D.; Shao, H.; Stewart, R. J.; Tresco, P. A. Biocompatibility of Adhesive Complex Coacervates Modeled after the Sandcastle Glue of *Phragmatopoma Californica* for Craniofacial Reconstruction. *Biomaterials* **2010**, *31*, 9373–9381.
- (10) Johnson, N. R.; Wang, Y. Coacervate Delivery Systems for Proteins and Small Molecule Drugs. *Expert Opin. Drug Deliv.* **2014**, *11*, 1829–1832.
- (11) Hwang, D. S.; Zeng, H.; Srivastava, A.; Krogstad, D. V.; Tirrell, M.; Israelachvili, J. N.; Waite, J. H. Viscosity and Interfacial Properties in a Mussel-Inspired Adhesive Coacervate. *Soft Matter* **2010**, *6*, 3232–3236.
- (12) Baccile, N.; Reboul, J.; Blanc, B.; Coq, B.; Lacroix-Desmazes, P.; In, M.; Gérardin, C. Ecodesign of Ordered Mesoporous Materials Obtained with Switchable Micellar Assemblies. *Angew. Chemie - Int. Ed.* **2008**, *47*, 8433–8437.
- (13) Chiappisi, L.; Simon, M.; Gradzielski, M. Toward Bioderived Intelligent Nanocarriers for Controlled Pollutant Recovery and PH-Sensitive Binding. *ACS Appl. Mater. Interfaces* **2015**, *7*, 6139–6145.
- (14) Hiwatari, Y.; Yoshida, K.; Akutsu, T.; Yabu, M.; Iwai, S. Polyelectrolyte-Micelle Coacervation: Effect of Coacervate on the Properties of Shampoo. *J. Soc. Cosmet. Chem. Japan* **2004**, *26*, 315–316.
- (15) Burgess, D. J.; Ponsart, S. B-Glucuronidase Activity Following Complex Coacervation and Spray Drying Microencapsulation. *J. Microencapsul.* **1998**, *15*, 569–579.
- (16) Wang, Y. F.; Gao, J. Y.; Dubin, P. L. Protein Separation via Polyelectrolyte Coacervation: Selectivity and Efficiency. *Biotechnol. Prog.* **1996**, *12*, 356–362.
- (17) Jones, O. G.; Lesmes, U.; Dubin, P.; McClements, D. J. Effect of Polysaccharide Charge on Formation and Properties of Biopolymer Nanoparticles Created by Heat Treatment of β -Lactoglobulin-Pectin Complexes. *Food Hydrocoll.* **2010**, *24*, 374–383.

- (18) Israelachvili, J. N.; Mitchell, D. J.; Ninham, B. W. Theory of Self-Assembly of Hydrocarbon Amphiphiles into Micelles and Bilayers. *J. Chem. Soc. Faraday Trans. 2* **1976**, *72*, 1525.
- (19) Bilalov, A.; Olsson, U.; Lindman, B. Complexation between DNA and Surfactants and Lipids: Phase Behavior and Molecular Organization. *Soft Matter* **2012**, *8*, 11022–11033.
- (20) Kogej, K. Association and Structure Formation in Oppositely Charged Polyelectrolyte-Surfactant Mixtures. *Adv. Colloid Interface Sci.* **2010**, *158*, 68–83.
- (21) Kizilay, E.; Kayitmazer, A. B.; Dubin, P. L. Complexation and Coacervation of Polyelectrolytes with Oppositely Charged Colloids. *Adv. Colloid Interface Sci.* **2011**, *167*, 24–37.
- (22) Sing, C. E.; Perry, S. L. Recent Progress in the Science of Complex Coacervation. *Soft Matter* **2020**, *16*, 2885–2914.
- (23) Kizilay, E.; Dinsmore, A. D.; Hoagland, D. A.; Sun, L.; Dubin, P. L. Evolution of Hierarchical Structures in Polyelectrolyte-Micelle Coacervates. *Soft Matter* **2013**, *9*, 7320–7332.
- (24) Piculell, L.; Norrman, J.; Svensson, A. V.; Lynch, I.; Bernardes, J. S.; Loh, W. Ionic Surfactants with Polymeric Counterions. *Adv. Colloid Interface Sci.* **2009**, *147–148*, 228–236.
- (25) Antunes, F. E.; Marques, E. F.; Miguel, M. G.; Lindman, B. Polymer-Vesicle Association. *Adv. Colloid Interface Sci.* **2009**, *147–148*, 18–35.
- (26) Stanic, V.; Mancuso, M.; Wong, W.; Dimasi, E.; Strey, H. H. Phase Diagrams of Electrostatically Self-Assembled Amphiplexes. *Macromolecules* **2011**, *44*, 7423–7429.
- (27) Mekhloufi, G.; Sanchez, C.; Renard, D.; Guillemin, S.; Hardy, J. PH-Induced Structural Transitions during Complexation and Coacervation of β -Lactoglobulin and Acacia Gum. *Langmuir* **2005**, *21*, 386–394.
- (28) Rawat, K.; Aswal, V. K.; Bohidar, H. B. DNA-Gelatin Complex Coacervation, UCST and First-Order Phase Transition of Coacervate to Anisotropic Ion Gel in 1-Methyl-3-Octylimidazolium Chloride Ionic Liquid Solutions. *J. Phys. Chem. B* **2012**, *116*, 14805–14816.
- (29) Vieregge, J. R.; Lueckheide, M.; Marciel, A. B.; Leon, L.; Bologna, A. J.; Rivera, J. R.; Tirrell, M. V. Oligonucleotide-Peptide Complexes: Phase Control by Hybridization. *J. Am. Chem. Soc.* **2018**, *140*, 1632–1638.
- (30) Love, C.; Steinkühler, J.; Gonzales, D. T.; Yandrapalli, N.; Robinson, T.; Dimova, R.;

- Tang, T. Y. D. Reversible PH-Responsive Coacervate Formation in Lipid Vesicles Activates Dormant Enzymatic Reactions. *Angew. Chemie - Int. Ed.* **2020**, *59*, 5950–5957.
- (31) Last, M. G. F.; Deshpande, S.; Dekker, C. PH-Controlled Coacervate-Membrane Interactions within Liposomes. *ACS Nano* **2020**, 10.1021/acsnano.9b10167.
- (32) Lasic, D. D. *Liposomes: From Physics to Applications*; Elsevier, Ed.; 1993.
- (33) Leng, J.; Egelhaaf, S. U.; Cates, M. E. Kinetics of the Micelle-to-Vesicle Transition: Aqueous Lecithin-Bile Salt Mixtures. *Biophys. J. Vol.* **2003**, *85*, 1624–1646.
- (34) Hayward, D. W.; Chiappisi, L.; Teo, J. H.; Prévost, S.; Schweins, R.; Gradzielski, M. Neutralisation Rate Controls the Self-Assembly of PH-Sensitive Surfactants. *Soft Matter* **2019**, *15*, 8611–8620.
- (35) Chiappisi, L.; Prévost, S.; Grillo, I.; Gradzielski, M. From Crab Shells to Smart Systems: Chitosan-Alkylethoxy Carboxylate Complexes. *Langmuir* **2014**, *30*, 10615–10616.
- (36) Brooks, J. T.; Marques, C. M.; Cates, M. E. The Effect of Adsorbed Polymer on the Elastic Moduli of Surfactant Bilayers. *J. Phys. II* **1991**, *1*, 673–690.
- (37) Harries, D.; Ben-Shaul, A.; Szleifer, I. Enveloping of Charged Proteins by Lipid Bilayers. *J. Phys. Chem. B* **2004**, *108*, 1491–1496.
- (38) May, S.; Ben-Shaul, A. DNA-Lipid Complexes: Stability of Honeycomb-like and Spaghetti-like Structures. *Biophys. J.* **1997**, *73*, 2427–2440.
- (39) May, S. Stability of Macroion-Decorated Lipid Membranes. *J. Phys. Condens. Matter* **2005**, *17*.
- (40) Sjöström, L.; Åkesson, T.; Jönsson, B. Interaction and Conformation of Polyelectrolyte Chains Adsorbed on Neutral Surfaces. *J. Chem. Phys.* **1993**, *99*, 4739–4747.
- (41) Fleer, G. J.; Stuart, M. A. C.; Scheutjens, J. M. H. M.; Cosgrove, T.; Vincent, B. *Polymers at Interfaces*, 1998th ed.; Springer-Science, 1998.
- (42) Wang, J.; Guo, K.; Qiu, F.; Zhang, H.; Yang, Y. Predicting Shapes of Polymer-Chain-Anchored Fluid Vesicles. *Phys. Rev. E - Stat. Nonlinear, Soft Matter Phys.* **2005**, *71*, 1–5.
- (43) Li, D.; Wagner, N. J. Universal Binding Behavior for Ionic Alkyl Surfactants with Oppositely Charged Polyelectrolytes. *J. Am. Chem. Soc.* **2013**, *135*, 17547–17555.
- (44) Okesola, B. O.; Smith, D. K. Applying Low-Molecular Weight Supramolecular Gelators in an Environmental Setting-Self-Assembled Gels as Smart Materials for Pollutant Removal. *Chem. Soc. Rev.* **2016**, *45*, 4226–4251.

- (45) Liu, X. Y.; Sawant, P. D. Formation Kinetics of Fractal Nanofiber Networks in Organogels. *Appl. Phys. Lett.* **2001**, *79*, 3518–3520.
- (46) Di Gregorio, M. C.; Gubitosi, M.; Travaglini, L.; Pavel, N. V.; Jover, A.; Meijide, F.; Vázquez Tato, J.; Sennato, S.; Schillén, K.; Tranchini, F.; et al. Supramolecular Assembly of a Thermoresponsive Steroidal Surfactant with an Oppositely Charged Thermoresponsive Block Copolymer. *Phys. Chem. Chem. Phys.* **2017**, *19*, 1504–1515.
- (47) Dhasaiyan, P.; Prasad, B. L. V. Self-Assembly of Bolaamphiphilic Molecules. *Chem. Rec.* **2017**, *17*, 597–610.
- (48) Kitamoto, D.; Morita, T.; Fukuoka, T.; Konishi, M.; Imura, T. Self-Assembling Properties of Glycolipid Biosurfactants and Their Potential Applications. *Curr. Op. Coll. Interf. Sci.* **2009**, *14*, 315–328.
- (49) Baccile, N.; Cuvier, A.-S.; Prévost, S.; Stevens, C. V.; Delbeke, E.; Berton, J.; Soetaert, W.; Van Bogaert, I. N. A.; Roelants, S. Self-Assembly Mechanism of PH-Responsive Glycolipids: Micelles, Fibers, Vesicles, and Bilayers. *Langmuir* **2016**, *32*, 10881–10894.
- (50) Palareti, G.; Legnani, C.; Cosmi, B.; Antonucci, E.; Erba, N.; Poli, D.; Testa, S.; Tosetto, A. Comparison between Different D-Dimer Cutoff Values to Assess the Individual Risk of Recurrent Venous Thromboembolism: Analysis of Results Obtained in the DULCIS Study. *Int. J. Lab. Hematol.* **2016**, *38*, 42–49.
- (51) Baccile, N.; Pedersen, J. S.; Pehau-Arnaudet, G.; Van Bogaert, I. N. a. Surface Charge of Acidic Sophorolipid Micelles: Effect of Base and Time. *Soft Matter* **2013**, *9*, 4911–4922.
- (52) Baccile, N.; Babonneau, F.; Jestin, J.; Pehau-Arnaudet, G.; Van Bogaert, I. Unusual, PH-Induced, Self-Assembly of Sophorolipid Biosurfactants. *ACS Nano* **2012**, *6*, 4763–4776.
- (53) Ben Messaoud, G.; Promeneur, L.; Brennich, M.; Roelants, S. L. K. W.; Le Griel, P.; Baccile, N. Complex Coacervation of Natural Sophorolipid Bolaamphiphile Micelles with Cationic Polyelectrolytes. *Green Chem.* **2018**, *20*, 3371–3385.
- (54) Baccile, N.; Selmane, M.; Le Griel, P.; Prévost, S.; Perez, J.; Stevens, C. V.; Delbeke, E.; Zibek, S.; Guenther, M.; Soetaert, W.; et al. PH-Driven Self-Assembly of Acidic Microbial Glycolipids. *Langmuir* **2016**.
- (55) Cuvier, A. S.; Berton, J.; Stevens, C. V.; Fadda, G. C.; Babonneau, F.; Van Bogaert, I. N. A.; Soetaert, W.; Pehau-Arnaudet, G.; Baccile, N. PH-Triggered Formation of Nanoribbons from Yeast-Derived Glycolipid Biosurfactants. *Soft Matter* **2014**, *10*,

3950–3959.

- (56) Liu, W.; Sun, S.; Cao, Z.; Zhang, X.; Yao, K.; Lu, W. W.; Luk, K. D. K. An Investigation on the Physicochemical Properties of Chitosan/DNA Polyelectrolyte Complexes. *Biomaterials* **2005**, *26*, 2705–2711.
- (57) Lewis, S. R.; Datta, S.; Gui, M.; Coker, E. L.; Huggins, F. E.; Daunert, S.; Bachas, L.; Bhattacharyya, D. Reactive Nanostructured Membranes for Water Purification. *Proc. Natl. Acad. Sci. U. S. A.* **2011**, *108*, 8577–8582.
- (58) Mady, M. M.; Mohammed, W. A.; El-Guendy, N. M.; Elsayed, A. A. Effect of Polymer Molecular Weight on the Dna/Pei Polyplexes Properties. *J. Biophys* **2011**, *21*, 151–165.
- (59) Ben Messaoud, G.; Le Griel, P.; Hermida-Merino, D.; Roelants, S. L. K. W.; Soetaert, W.; Stevens, C. V.; Baccile, N. PH-Controlled Self-Assembled Fibrillar Network (SAFiN) Hydrogels: Evidence of a Kinetic Control of the Mechanical Properties. *Chem. Mater.* **2019**, *31*, 4817–4830.
- (60) Schindelin, J.; Arganda-Carreras, I.; Frise, E.; Kaynig, V.; Longair, M.; Pietzsch, T.; Preibisch, S.; Rueden, C.; Saalfeld, S.; Schmid, B.; et al. Fiji: An Open-Source Platform for Biological-Image Analysis. *Nat. Methods* **2012**, *9*, 676–682.
- (61) Koga, S.; Williams, D. S.; Perriman, A. W.; Mann, S. Peptide-Nucleotide Microdroplets as a Step towards a Membrane-Free Protocell Model. *Nat. Chem.* **2011**, *3*, 720–724.
- (62) Swanson-Vethamuthu, M.; Dubin, P. L.; Almgren, M.; Yingjie, L. Cryo-TEM of Polyelectrolyte – Micelle Complexes. *J. Colloid Interface Sci.* **1997**, *186*, 414–419.
- (63) Rinaudo, M. Chitin and Chitosan: Properties and Applications. *Prog. Polym. Sci.* **2006**, *31*, 603–632.
- (64) Seyrig, C.; Griel, P. Le; Cowieson, N.; Perez, J.; Baccile, N. Synthesis of Multilamellar Walls Vesicles Polyelectrolyte-Surfactant Complexes from PH-Stimulated Phase Transition Using Microbial Biosurfactants. *J. Colloid Interface Sci.* **2020**, 10.1016/j.jcis.2020.07.021.
- (65) Xu, A. Y.; Melton, L. D.; Ryan, T. M.; Mata, J. P.; Rekas, A.; Williams, M. A. K.; McGillivray, D. J. Effects of Polysaccharide Charge Pattern on the Microstructures of β -Lactoglobulin-Pectin Complex Coacervates, Studied by SAXS and SANS. *Food Hydrocoll.* **2018**, *77*, 952–963.
- (66) Kronberg, B.; Holmberg, K.; Lindman, B. Surfactant–Polymer Systems. In *Surface Chemistry of Surfactants and Polymers*; Kronberg, B., Holmberg, K., Lindman, B.,

- Eds.; John Wiley & Sons, Ltd., 2014; pp 271–294.
- (67) Dias, R. S.; Dawson, K.; Miguel, M. G. Interaction of DNA with Surfactants in Solution. In *DNA Interactions with Polymers and Surfactants*; Dias, R., Lindman, B., Eds.; Hoboken, New Jersey, 2008; pp 89–117.
- (68) Chiappisi, L.; David Leach, S.; Gradzielski, M. Precipitating Polyelectrolyte-Surfactant Systems by Admixing a Nonionic Surfactant—a Case of Cononsurfactancy. *Soft Matter* **2017**, *13*, 4988–4996.
- (69) Israelachvili, J. N.; Mitchell, D. J. A Model for the Packing of Lipids in Bilayer Membranes. *Biochim. Biophys. Acta* **1975**, *389*, 13–19.
- (70) Tanford, C. *The Hydrophobic Effect: Formation of Micelles and Biological Membranes*; Wiley-Interscience, 1973.
- (71) Nagarajan, R. Self-Assembly of Bola Amphiphiles. *Chem. Eng. Commun.* **1987**, *55*, 251–273.
- (72) Manet, S.; Cuvier, A. S.; Valotteau, C.; Fadda, G. C.; Perez, J.; Karakas, E.; Abel, S.; Baccile, N. Structure of Bolaamphiphile Sophorolipid Micelles Characterized with SAXS, SANS, and MD Simulations. *J. Phys. Chem. B* **2015**, *119*, 13113–13133.
- (73) Borukhov, I.; Andelman, D.; Orland, H. Polyelectrolyte Solutions between Charged Surfaces. *Europhys. Lett.* **1995**, *32*, 499–504.
- (74) Dobrynin, A. V.; Rubinstein, M. Theory of Polyelectrolytes in Solutions and at Surfaces. *Prog. Polym. Sci.* **2005**, *30*, 1049–1118.
- (75) Dan, N.; Pincus, P.; Safran, S. A. Membrane-Induced Interactions between Inclusions. *Langmuir* **1993**, *9*, 2768–2771.
- (76) Winterhalter, M.; Helfrich, W. Effect of Surface Charge on the Curvature Elasticity of Membranes. *J. Phys. Chem* **1988**, *92*, 6865–6867.
- (77) Zinchenko, A. A.; Pyshkina, O. A.; Lezov, A. V.; Sergeyev, V. G.; Yoshikawa, K. Single DNA Molecules: Compaction and Decompaction. In *DNA Interactions with Polymers and Surfactants*; Dias, R., Lindman, B., Eds.; John Wiley & Sons, Inc.: Hoboken, New Jersey, 2008; pp 59–88.
- (78) He, T. Estimating Cross-sectional Area of a Polymer Chain by Additive Method. *J. Appl. Polym. Sci.* **1986**, *31*, 1521–1524.
- (79) Heath, G. R.; Li, M.; Polignano, I. L.; Richens, J. L.; Catucci, G.; O’Shea, P.; Sadeghi, S. J.; Gilardi, G.; Butt, J. N.; Jeuken, L. J. C. Layer-by-Layer Assembly of Supported Lipid Bilayer Poly-l-Lysine Multilayers. *Biomacromolecules* **2016**, *17*, 324–335.
- (80) Netrabukkana, R.; Lourvanij, K.; Rorrer, G. L. Diffusion of Glucose and Glucitol in

- Microporous and Mesoporous Silicate/Aluminosilicate Catalysts. *Ind. Eng. Chem. Res.* **1996**, *35*, 458–464.
- (81) Parsegian, V. A.; Zemb, T. Hydration Forces: Observations, Explanations, Expectations, Questions. *Curr. Opin. Colloid Interface Sci.* **2011**, *16*, 618–624.
- (82) Leikin, S.; Parsegian, V. A.; Rau, D. C.; Rand, R. P. Hydration Forces. *Annu. Rev. Phys. Chem.* **1993**, *44*, 369–395.
- (83) Dubois, M.; Zemb, T.; Fuller, N.; Rand, R. P.; Parsegian, V. A. Equation of State of a Charged Bilayer System: Measure of the Entropy of the Lamellar-Lamellar Transition in DDABr. *J. Chem. Phys.* **1998**, *108*, 7855–7869.
- (84) Ricoul, F.; Dubois, M.; Belloni, L.; Zemb, T.; André-Barrès, C.; Rico-Lattes, I. Phase Equilibria and Equation of State of a Mixed Cationic Surfactant-Glycolipid Lamellar System. *Langmuir* **1998**, *14*, 2645–2655.
- (85) Leneveu, D. M.; Rand, R. P.; Parsegian, V. A. Measurement of Forces between Lecithin Bilayers. *Nature* **1976**, *259*, 601–603.
- (86) Claesson, P. M. Interactions Between Surfaces Coated with Carbohydrates, Glycolipids, and Glycoproteins. In *Biopolymers at Interfaces, Second Edition*; Malmsten, M., Ed.; CRC Press, 2003; p 165.
- (87) Chatellier, X.; Joanny, J.-F. Adsorption of Polyelectrolyte Solutions on Surfaces: A Debye-Hueckel Theory. *J. Phys. II Fr.* **1996**, *6*, 1669–1686.
- (88) Yethiraj, A. Forces between Surfaces Immersed in Polyelectrolyte Solutions. *J. Chem. Phys.* **1999**, *111*, 1797–1800.
- (89) Dobrynin, A. V.; Deshkovski, A.; Rubinstein, M. Adsorption of Polyelectrolytes on Oppositely Charged Surfaces. *Macromolecules* **2001**, *34*, 3421–3436.
- (90) Rand, R. P.; Parsegian, V. A. Hydration Forces between Phospholipid Bilayers. *BBA - Rev. Biomembr.* **1989**, *988*, 351–376.
- (91) Kanicky, J. R.; Shah, D. O. Effect of Degree, Type, and Position of Unsaturation on the PKa of Long-Chain Fatty Acids. *J. Colloid Interface Sci.* **2002**, *256*, 201–207.
- (92) Lieckfeldt, R.; Villalaín, J.; Gómez-Fernández, J.-C.; Lee, G. Apparent Pka of the Fatty Acids Within Ordered Mixtures of Model Human Stratum Corneum Lipids. *Pharm. Res.* **1995**, *12*, 1614–1617.
- (93) Satake, I.; Yang, J. T. Interaction of Sodium Decyl Sulfate with Poly(L-ornithine) and Poly(L-lysine) in Aqueous Solution. *Biopolymers* **1976**, *15*, 2263–2275.
- (94) Nishio, T.; Shimizu, T.; Kwak, J. C. T.; Minakata, A. The Cooperative Binding of Large Ligands to a One-Dimensional Lattice: The Steric Hindrance Effect. *Biophys.*

Chem. **2003**, *104*, 501–508.

- (95) Nishio, T.; Shimizu, T. Model Analysis of Surfactant-Polymer Interaction as Cooperative Ligand Binding to Linear Lattice. *Biophys. Chem.* **2005**, *117*, 19–25.
- (96) Instruments, T. Microcalorimetry Introduction to Characterizing Biopolymer Binding and Kinetics Reactions by ITC. **2009**, 1–42.
- (97) Aberkane, L.; Jasniewski, J.; Gaiani, C.; Scher, J.; Sanchez, C. Thermodynamic Characterization of Acacia Gum- β -Lactoglobulin Complex Coacervation. *Langmuir* **2010**, *26*, 12523–12533.
- (98) Kayitmazer, A. B. Thermodynamics of Complex Coacervation. *Adv. Colloid Interface Sci.* **2017**, *239*, 169–177.
- (99) Freire, E.; Mayorga, O. L.; Straume, M. Isothermal Titration. *Anal. Chem.* **1990**, *62*, 950A-959A.
- (100) van Holde, K. E. No Title. In *Physical Biochemistry, 2nd éd.*; Prentice-Hall: Englewood Cliffs, NJ,; 1985; p chapter 3.
- (101) Cantor, C. R.; Schimmel, P. R. No Title. In *Cantor, C. R.; Schimmel, P. R. Biophysical Chemistry, Part III: The Behavior of Biological Macromolecules*; W. H. Freeman: New York; 1980; p chapter 15.
- (102) Harnsilawat, T.; Pongsawatmanit, R.; McClements, D. J. Characterization of β -Lactoglobulin-Sodium Alginate Interactions in Aqueous Solutions: A Calorimetry, Light Scattering, Electrophoretic Mobility and Solubility Study. *Food Hydrocoll.* **2006**, *20*, 577–585.
- (103) Du, X.; Dubin, P. L.; Hoagland, D. A.; Sun, L. Protein-Selective Coacervation with Hyaluronic Acid. *Biomacromolecules* **2014**, *15*, 726–734.
- (104) Priftis, D.; Laugel, N.; Tirrell, M. Thermodynamic Characterization of Polypeptide Complex Coacervation. *Langmuir* **2012**, *28*, 15947–15957.
- (105) Yu, S.; Xu, X.; Yigit, C.; Van Der Giet, M.; Zidek, W.; Jankowski, J.; Dzubiella, J.; Ballauff, M. Interaction of Human Serum Albumin with Short Polyelectrolytes: A Study by Calorimetry and Computer Simulations. *Soft Matter* **2015**, *11*, 4630–4639.
- (106) Krouská, J.; Pekař, M.; Klučáková, M.; Šarac, B.; Bešter-Rogač, M. Study of Interactions between Hyaluronan and Cationic Surfactants by Means of Calorimetry, Turbidimetry, Potentiometry and Conductometry. *Carbohydr. Polym.* **2017**, *157*, 1837–1843.
- (107) Vinayahan, T.; Williams, P. A.; Phillips, G. O. Electrostatic Interaction and Complex Formation between Gum Arabic and Bovine Serum Albumin. *Biomacromolecules*

- 2010**, *11*, 3367–3374.
- (108) Dubin, P. L.; Gruber, J. H.; Xia, J.; Zhang, H. The Effect of Cations on the Interaction between Dodecylsulfate Micelles and Poly(Ethyleneoxide). *J. Colloid Interface Sci.* **1992**, *148*, 35–41.
- (109) Marques, E. F.; Regev, O.; Khan, A.; Miguel, M. D. G.; Lindman, B. Interactions between Catanionic Vesicles and Oppositely Charged Polyelectrolytes - Phase Behavior and Phase Structure. *Macromolecules* **1999**, *32*, 6626–6637.
- (110) De Souza, T. P.; Bossa, G. V.; Stano, P.; Steiniger, F.; May, S.; Luisi, P. L.; Fahr, A. Vesicle Aggregates as a Model for Primitive Cellular Assemblies. *Phys. Chem. Chem. Phys.* **2017**, *19*, 20082–20092.
- (111) Weisman, S.; Hirsch-Lerner, D.; Barenholz, Y.; Talmon, Y. Nanostructure of Cationic Lipid-Oligonucleotide Complexes. *Biophys. J.* **2004**, *87*, 609–614.
- (112) Ram-On, M.; Cohen, Y.; Talmon, Y. Effect of Polyelectrolyte Stiffness and Solution PH on the Nanostructure of Complexes Formed by Cationic Amphiphiles and Negatively Charged Polyelectrolytes. *J. Phys. Chem. B* **2016**, *120*, 5907–5915.
- (113) Gasperini, A. A. M.; Puentes-Martinez, X. E.; Balbino, T. A.; De Paula Rigoletto, T.; De Sá Cavalcanti Corrêa, G.; Cassago, A.; Portugal, R. V.; De La Torre, L. G.; Cavalcanti, L. P. Association between Cationic Liposomes and Low Molecular Weight Hyaluronic Acid. *Langmuir* **2015**, *31*, 3308–3317.

Supporting Information

Stimuli-induced non-equilibrium phase transitions in polyelectrolyte-surfactant complex coacervates

Chloé Seyrig,^a Gertrude Kignelman,^b Wim Thielemans,^b Patrick Le Griel,^a Nathan Cowieson,^c Javier Perez,^d Niki Baccile^{a,*}

^a Sorbonne Université, Centre National de la Recherche Scientifique, Laboratoire de Chimie de la Matière Condensée de Paris, LCMCP, F-75005 Paris, France

^b Sustainable Materials Lab, Department of Chemical Engineering, KU Leuven, campus Kulak Kortrijk, Etienne Sabbelaan 53, 8500 Kortrijk, Belgium

^c Diamond Light Source Ltd, Harwell Science and Innovation Campus, Didcot, OX11 0QX, U.K.

^d SWING, Synchrotron Soleil, BP 48, 91192 Gif-sur-Yvette, France

* Corresponding author: niki.baccile@sorbonne-universite.fr

Content:

Pages S1 to S16

Figure S1 to Figure S11

Table S1 to Table S3

3 references

Explicative text

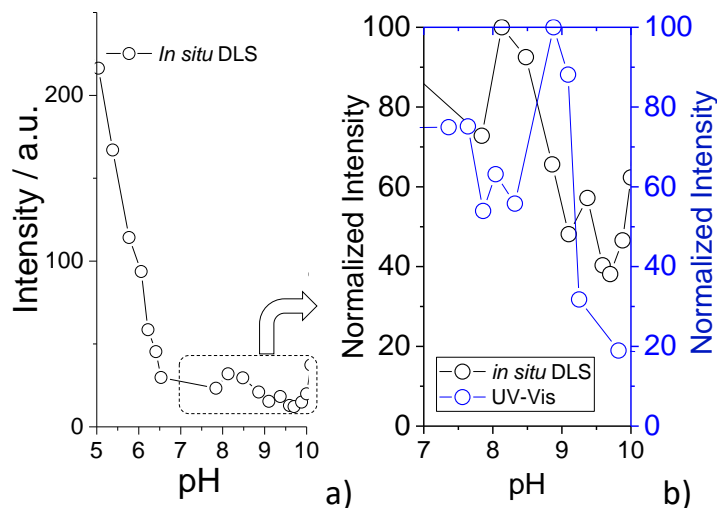


Figure S 1 – a) pH-resolved *in situ* turbidimetric experiment (DLS apparatus) performed on a [SL-C18:0 + PLL] solution at $C_{\text{SL-C18:0}} = 2.5 \text{ mg}\cdot\text{mL}^{-1}$ $C_{\text{PLL}} = 2.5 \text{ mg}\cdot\text{mL}^{-1}$. b)-panel shows the normalized intensity recorded in turbidimetry experiments using the pH-resolved *in situ* DLS and UV-Vis apparatus.

To avoid sedimentation issues in the SL-C18:0 fibrillar system, we have repeated the turbidimetric titration of the [SL-C18:0 + PLL] mixture using a continuous flow-through device installed on a light scattering instrument and which guarantees a better homogenization of the sample solution. Data in Figure S 1 show a scattering behavior, in which one can identify some scattering above pH 10, due to the formation of platelets in the SL-C18:0 system alone,¹ and a strong scattering below pH 7, as reported elsewhere for the SL-C18:0 system alone.² Interestingly, the region between pH 7 and 10 is characterized by a mild scattering but comparable, after normalization, to the scattering observed in UV-Vis experiments (Figure S 1b). Whichever the method of analysis employed, we systematically find a region of pH, generally between 7 and 10, in which the lipid-PEC mixed solution becomes turbid, differently than the controls.

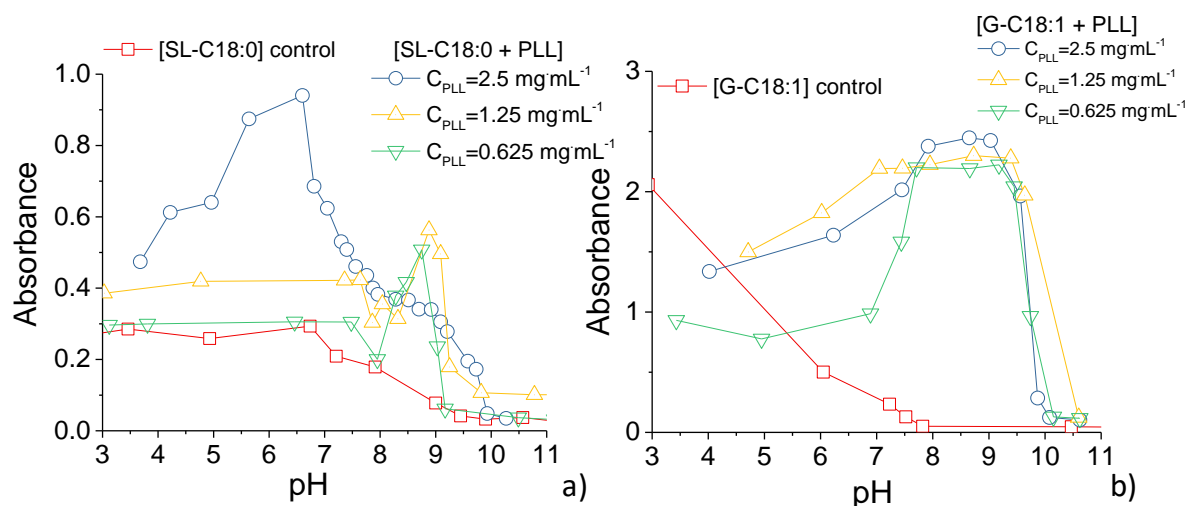


Figure S 2 - Room temperature turbidimetric analysis of a) SL-C18:0 and b) G-C18:1 glycolipid solutions with different concentrations of PLL as a function of pH. The typical sample preparation is described in the materials and method section. The final lipid and PLL concentrations are $C_{G-C18:1} = C_{SL-C18:0} = 2.5 \text{ mg mL}^{-1}$, $C_{PLL} = 2.5, 1.25$ or 0.625 mg mL^{-1} . pH is decreased from 11 to 3.

The red square curve Figure S 2 refers to the control lipid solutions, displaying a similar behavior: the micellar region at alkaline pH shows poor scattering, while the intensity increases at acidic pH, when SL-C18:0 and G-C18:1 respectively self-assemble into fibers and vesicles. When mixed with different concentrations of PLL, all scattering profiles show a common bell-like shape, with an enhanced signal between pH 7 and 10. Indeed, blue, yellow and green curves, respectively standing for concentration of PLL of 2.5 mg mL^{-1} , 1.25 mg mL^{-1} and 0.625 mg mL^{-1} , show an intensity peak at around pH 8.5 - 9. This behavior clearly identifies a preferred pH range of interaction between lipids and PLL, precisely from pH 7 to pH 9.

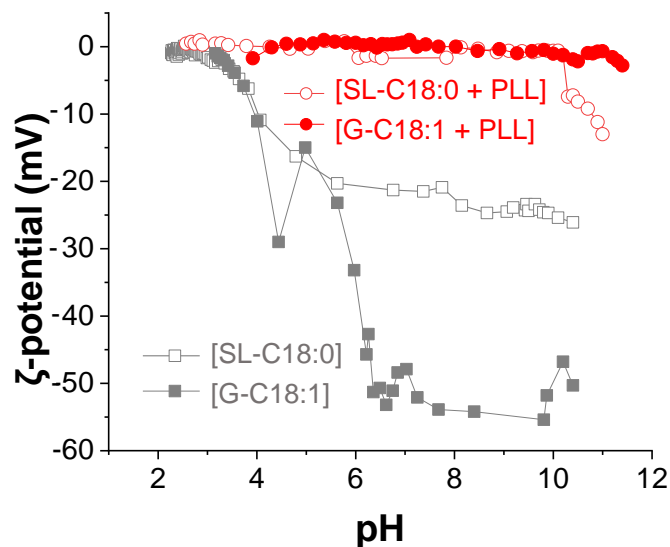


Figure S 3 – ζ -potential measurements of: [SL-C18:0] and [G-C18:1] controls (grey curves); [SL-C18:0 + PLL] and [G-C18:1 + PLL] solutions (red curves) $C_{G-C18:1} = C_{SL-C18:0} = 2.5 \text{ mg mL}^{-1}$, $C_{PLL} = 2.5 \text{ mg mL}^{-1}$

ζ -potential experiments shown in Figure S 3 show that control lipid solutions have the same behavior: they are strongly negative (SL-C18:0 and G-C18:1 respectively show a plateau at -20 mV and -55 mV) under alkaline conditions, but their ζ -potentials slightly increase around pH 6 to finally be close to zero, putting in evidence the neutralization of the carboxylate group. When lipids are mixed with PLL, the resulting curve oscillates around neutral ζ -potential, and charges are perfectly compensated in the pH region of interest, from pH 7 to 9, an argument in favor of coacervation, a process likely occurring in electroneutralization conditions³

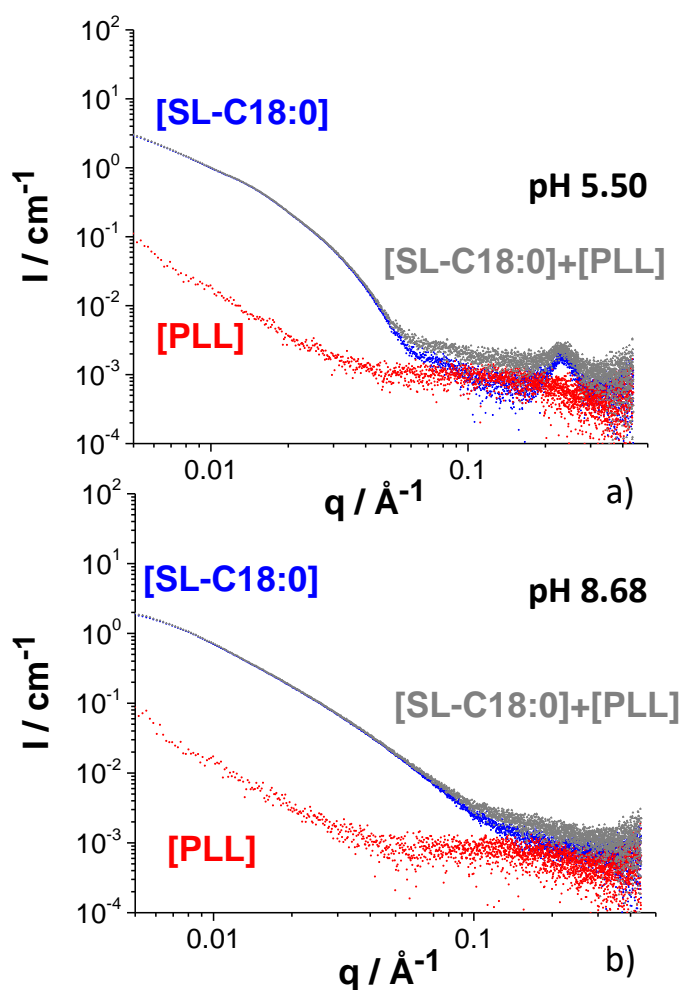


Figure S 4 - SAXS profiles of [SL-C18:0] and [PLL] controls at acidic and basic pH. $C_{\text{SL-C18:0}} = 2.5 \text{ mg mL}^{-1}$, $C_{\text{PLL}} = 2.5 \text{ mg mL}^{-1}$. [SL-C18:0] + [PLL] refers to the arithmetic sum of individual [SL-C18:0] and [PLL] signals.

Figure S 4 shows the control signals of single components: the red curve for [PLL] alone and the blue one for [SL-C18:0] alone. The grey curve corresponds to the simple arithmetic sum of both signals.

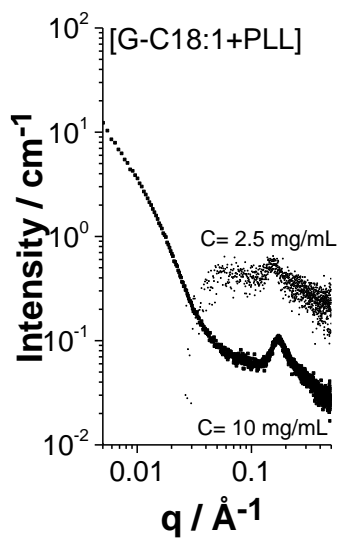


Figure S 5 - SAXS profiles of [G-C18:1 + PLL] solutions at two concentrations ($C_{G-C18:1} = C_{PLL}$) and pH 8.

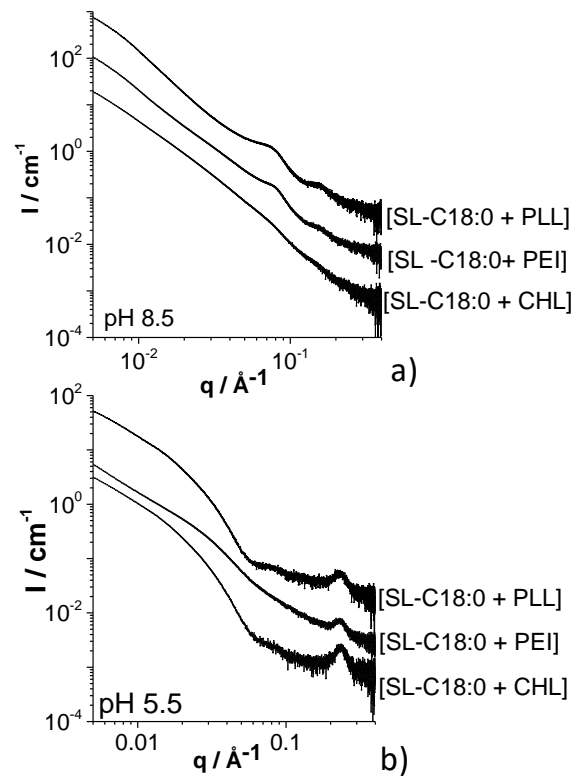


Figure S 6 - SAXS profiles of SL-C18:0 mixed with different polyelectrolytes at acidic and basic pH. $C_{\text{SL-C18:0}} = C_{\text{PLL}} = C_{\text{PEI}} = C_{\text{CHL}} = 2.5 \text{ mg}\cdot\text{mL}^{-1}$

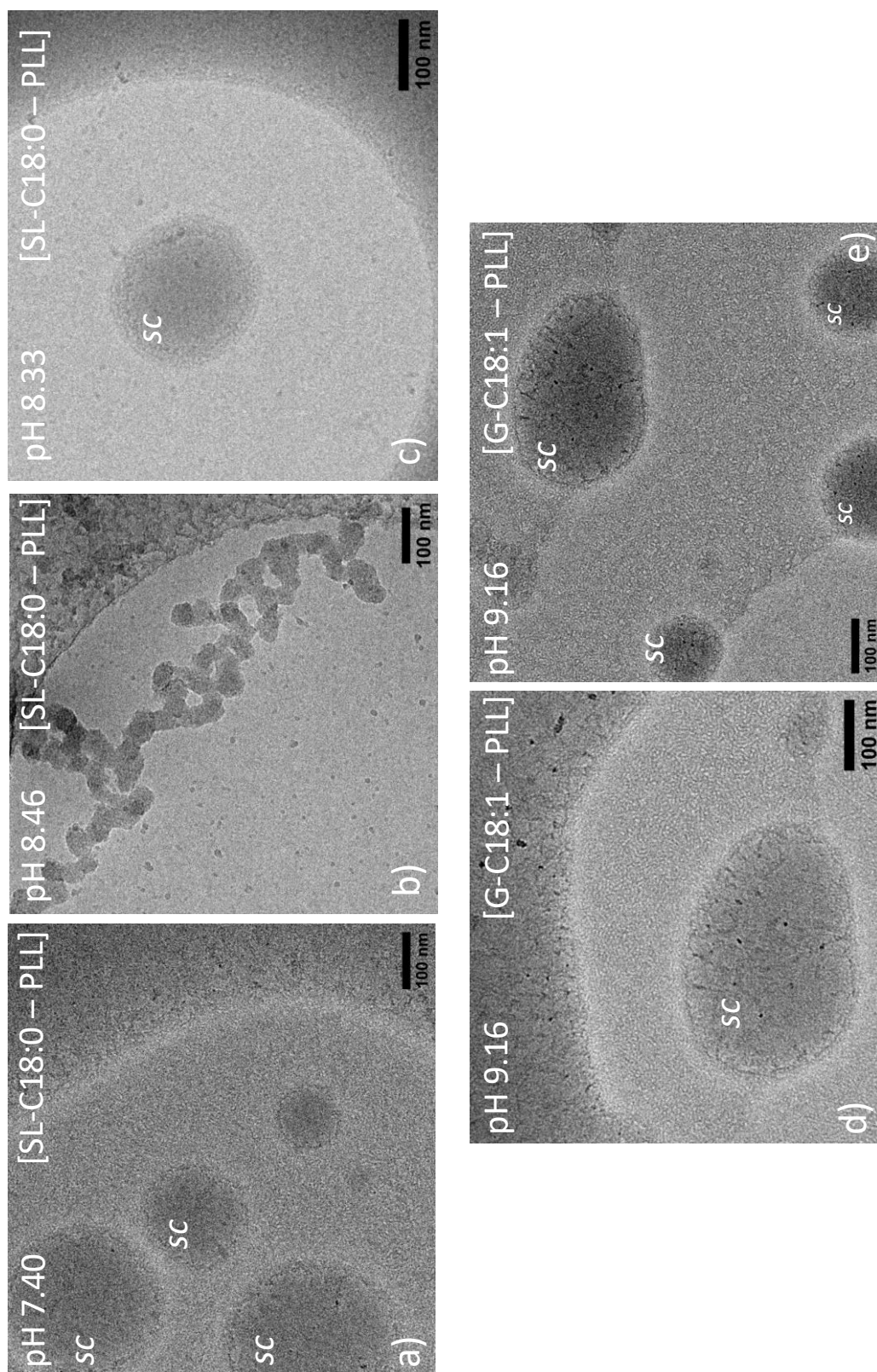


Figure S 7 - Cryo-TEM images of [SL-C18:0 + PLL] and [G-C18:1 + PLL] complex coacervates recorded at various pH values. $C_{\text{SL-C18:0}} = C_{\text{G-C18:1}} = 2.5 \text{ mg mL}^{-1}$; $C_{\text{PLL}} = 1.25 \text{ mg mL}^{-1}$. *sc* stands for spherical colloid.

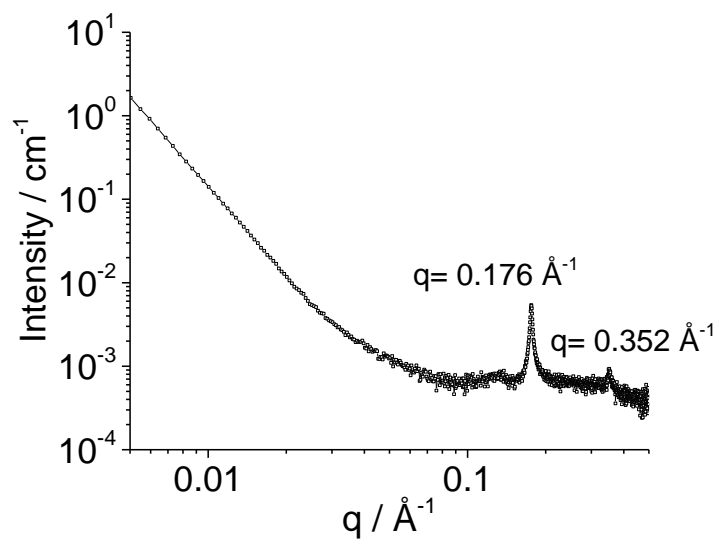


Figure S 8 - SAXS plots of the G-C18:1 control solution at $C = 2.5 \text{ mg mL}^{-1}$ and pH 3. Experiment extracted from 2D contour plot in Figure 5a in the main text.

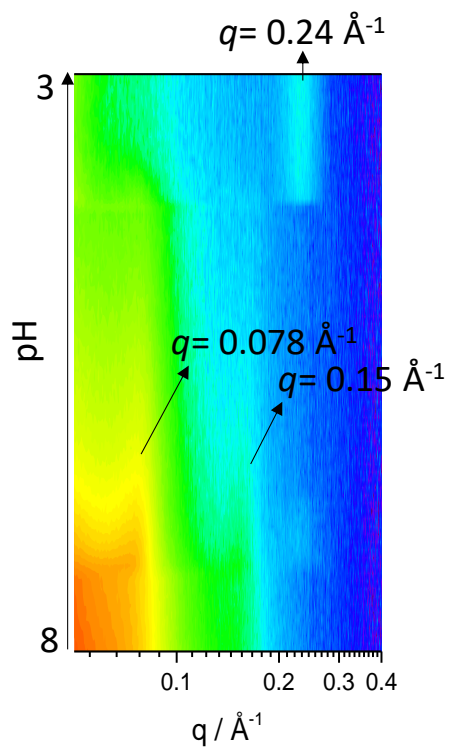


Figure S 9 - pH-resolved *in situ* SAXS 2D contour plot of the [SL-C18:0 + PLL] solution at $C_{\text{SL-C18:0}} = C_{\text{PLL}} = 2.5 \text{ mg/mL}^{-1}$. Highlight of the coacervate-to-fiber transition between pH 8 and 3.

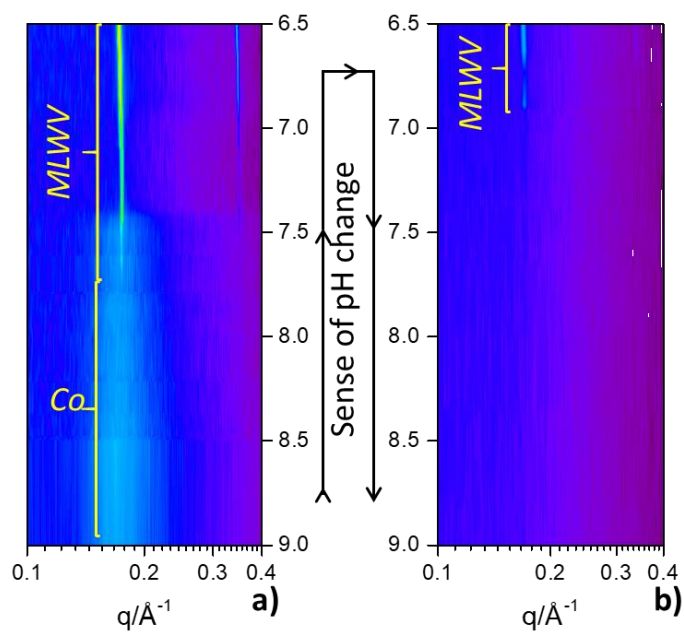
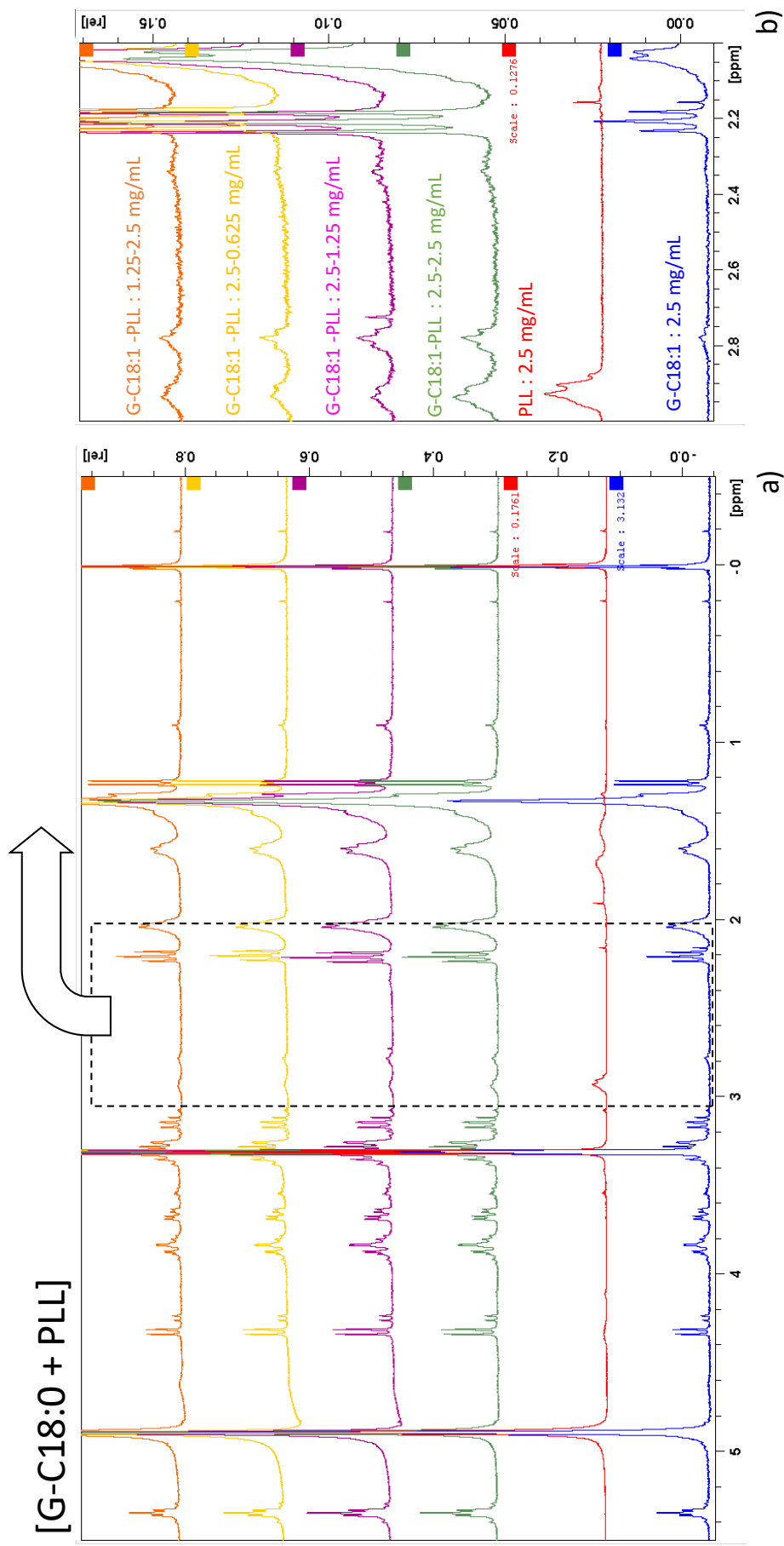


Figure S 10 - pH-resolved *in situ* SAXS 2D contour plots of the [G-C18:1 + PLL] solutions at $C_{G-C18:1} = C_{PLL} = 2.5 \text{ mg mL}^{-1}$: highlight of the *Co*-to-*MLWV* transition between pH 9 and 6.5. In a), pH is reduced from 10 to 3. Contour plot in b) is recorded on the same sample as in a), to which pH is increased from 3 to 10.



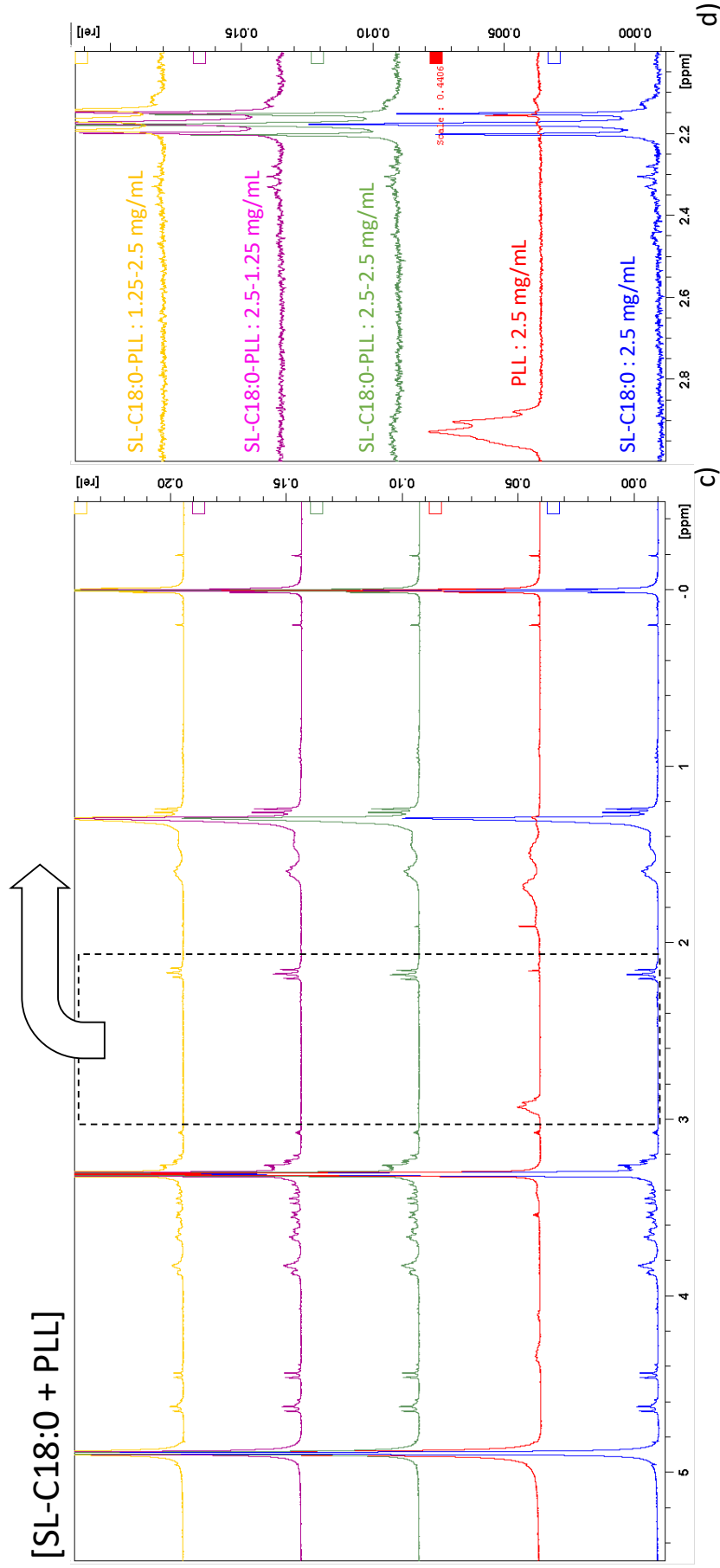


Figure S 11 – ^1H NMR spectra of a,b) G-C18:1, PLL, [G-C18:0 + PLL] and c,d) SL-C18:0, PLL, [SL-C18:0 + PLL] samples in MeOD-d4 ($V = 500 \mu\text{L}$) and corresponding zoom (b, d) of the $3.0 < \delta / \text{ppm} < 2.0$ region. Concentrations given next to each [SL-C18:0 + PLL] spectrum refer to the initial concentration of each component in water at pH 5. Under these conditions, [SL-C18:0 + PLL] form fibers while [G-C18:1 + PLL] forms *MLWV*. Both fibers and *MLWV* are centrifuged out of the parent solution, dried at 40°C during two days and dispersed in $500 \mu\text{L}$ MeOD-d4 for NMR analysis.

Table S 1 – Quantitative analysis of the integrals corresponding to the ¹H NMR spectra of the [G-C18:1 +PLL] samples in MeOD-d4, shown in Figure S 11. PLL is represented by the (RCH₂NH₂)_x (x ~ 20) peak at δ= 2.92 ppm. The M_w (PLL)≈ 1-5 KDa, we then consider an average M_w (PLL)= 2.5 kDa, whereas the M_w of each monomer is 128 g/mol, yielding an average of 20 monomers per PLL chain. The valence of the (RCH₂NH₂)_x (x ~ 20) peak is then taken as 40. G-C18:1 is represented by the RCH₂C=O peak at δ= 2.2 ppm. The M_w (G-C18:1)= 460 g/mol and each G-C18:1 bears a single COOH group. The valence of the RCH₂C=O peak is then taken as 2. The peak at δ=0 ppm corresponds to the reference (TMSP-d4, 1 mg.mL⁻¹≡ 5.8 mM), having a valence of 9.

Explanation of columns: C_{ln} represents the nominal concentration of G-C18:1 and PLL in 1 mL water at pH 5; the Integrals column provides the values of the integrals of G-C18:1, PLL and TMSP-d4 normalized to the valence of each peak and collected on centrifuged MLWV dispersed in 500 μL MeOD-d4; C_F represents the concentration of G-C18:1 and PLL in MLWV calculated from their respective integrals with respect to TMSP-d4 (I_{average} @ 0 ppm/9= 9708296 ± 120685) for an equivalent 1 mL of solution. C_F/C_l represents the amount (%) of G-C18:1 and PLL consumed in the formation of MLWV. The Molar ratio column gives the G-C18:1-to-PLL molar ratio in the initial solution and in the MLWV. $\frac{[COOH]_F}{[NH_2]_F}$ represents the G-C18:1-to-PLL monomer molar ratio in MLWV. All errors are calculated from the propagation of errors in respect of the integral of the reference.

C _{ln}		Integrals			C _F		C _F /C _{ln}		Molar ratio		Function al group ratio in MLWV
[G - C18: 1] _{ln} mM (mg.mL ⁻¹)	[PLL] _{ln} mM (mg.mL ⁻¹)	G-C18:1 I _{2.2 ppm} /2	PLL I _{2.8 ppm} /40	TMSP-d4 I _{0 ppm} /9	[G - C18: 1] _F mM	[PLL] _F x 10 ⁻² mM	$\frac{[G-C18:1]_F}{[G-C18:1]_{ln}}$ %	$\frac{[PLL]_F}{[PLL]_{ln}}$ %	$\frac{[G - C18:1]_{ln}}{[PLL]_{ln}}$ (in solution)	$\frac{[G - C18:1]_F}{[PLL]_F}$ (in MLWV)	$\frac{[COOH]_F}{[NH_2]_F}$
5.4 (2.5)	1 (2.5)	11320838	122969	9725633	3.4 ± 0.6	3.7 ± 0.6	63 ± 11	3.7 ± 0.6	5.4	92 ± 22	4.6 ± 1.1
5.4 (2.5)	0.5 (1.25)	12427299	64857	9728182	3.7 ± 0.6	1.9 ± 0.3	69 ± 12	3.9 ± 0.7	10.8	192 ± 46	9.6 ± 2.3
5.4 (2.5)	0.25 (0.625)	8480098	58866	9835125	2.5 ± 0.4	1.8 ± 0.3	47 ± 8	7.0 ± 1.2	21.6	144 ± 35	7.2 ± 1.7
2.75 (1.25)	1 (2.5)	8687840	76772	9544245	2.6 ± 0.4	2.3 ± 0.4	94 ± 16	2.3 ± 0.4	2.75	113 ± 27	5.7 ± 1.4

Table S 2 - ITC experiments: parameters extracted from the “multiple sites” model fit of G-C18:1 4 mM into PLL 2 mM data after subtracting the buffer contribution.

Interaction type	Parameter	Value
Non-specific Endothermic (entropic, hydrophobic effect)	K_{a1}	$3.2 \cdot 10^8 \text{ M}^{-1}$
	n_1	0.05
	ΔG_1	-48.6 kJ/mol
	ΔH_1	5.3 kJ/mol
	ΔS_1	0.18 kJ/mol·K
Specific Exothermic (electrostatic, H-bonding)	K_{a2}	$1.1 \cdot 10^6 \text{ M}^{-1}$
	n_2	4.3
	ΔG_2	-34.6
	ΔH_2	-2.0 kJ/mol
	ΔS_2	0.11 kJ/mol·K

Table S 3 - ITC experiments: parameters extracted from the “multiple sites” model fit of G-C18:1 2 mM into PLL 2 mM data after subtracting the buffer contribution.

Interaction type	Parameter	Value
Non-specific Endothermic (entropic, hydrophobic effect)	K_{a1}	$1.7 \cdot 10^8 \text{ M}^{-1}$
	n_1	0.01
	ΔG_1	-46.8 kJ/mol
	ΔH_1	52.6 kJ/mol
	ΔS_1	0.33 kJ/mol·K
Specific Exothermic (electrostatic, H-bonding)	K_{a2}	$4.1 \cdot 10^6 \text{ M}^{-1}$
	n_2	3.3
	ΔG_2	-38.3
	ΔH_2	-3.6 kJ/mol
	ΔS_2	0.12 kJ/mol·K

References

- (1) Cuvier, A. S.; Babonneau, F.; Berton, J.; Stevens, C. V.; Fadda, G. C.; Péhau-Arnaudet, G.; Le Griel, P.; Prévost, S.; Perez, J.; Baccile, N. Nanoscale Platelet Formation by Monounsaturated and Saturated Sphorolipids under Basic PH Conditions. *Chem. - A Eur. J.* **2015**, *21*, 19265–19277.
- (2) Cuvier, A. S.; Berton, J.; Stevens, C. V.; Fadda, G. C.; Babonneau, F.; Van Bogaert, I. N. A.; Soetaert, W.; Pehau-Arnaudet, G.; Baccile, N. PH-Triggered Formation of Nanoribbons from Yeast-Derived Glycolipid Biosurfactants. *Soft Matter* **2014**, *10*, 3950–3959.
- (3) Wang, Y.; Kimura, K.; Huang, Q.; Dubin, P. L. Effects of Salt on Poly Electrolyte-Micelle Coacervation. *Macromolecules* **1999**, *32*, 7128–7134.



HAL
open science

Synthesis of multilamellar walls vesicles polyelectrolyte-surfactant complexes from pH-stimulated phase transition using microbial biosurfactants

Chloé Seyrig, Patrick Le Griel, Nathan Cowieson, Javier Perez, Niki Baccile

► **To cite this version:**

Chloé Seyrig, Patrick Le Griel, Nathan Cowieson, Javier Perez, Niki Baccile. Synthesis of multilamellar walls vesicles polyelectrolyte-surfactant complexes from pH-stimulated phase transition using microbial biosurfactants. *Journal of Colloid and Interface Science*, Elsevier, 2020, 580, pp.493-502. 10.1016/j.jcis.2020.07.021 . hal-02905980

HAL Id: hal-02905980

<https://hal.archives-ouvertes.fr/hal-02905980>

Submitted on 23 Jul 2020

HAL is a multi-disciplinary open access archive for the deposit and dissemination of scientific research documents, whether they are published or not. The documents may come from teaching and research institutions in France or abroad, or from public or private research centers.

L'archive ouverte pluridisciplinaire **HAL**, est destinée au dépôt et à la diffusion de documents scientifiques de niveau recherche, publiés ou non, émanant des établissements d'enseignement et de recherche français ou étrangers, des laboratoires publics ou privés.

Synthesis of multilamellar walls vesicles polyelectrolyte-surfactant complexes from pH-stimulated phase transition using microbial biosurfactants

Chloé Seyrig^a, Patrick Le Griel^a, Nathan Cowieson,^b Javier Perez,^c Niki Baccile^a

^a Sorbonne Université, Centre National de la Recherche Scientifique, Laboratoire de Chimie de la Matière Condensée de Paris, LCMCP, F-75005 Paris, France

^b Diamond Light Source Ltd, Diamond House, Harwell Science & Innovation Campus, Didcot, Oxfordshire, OX11 0DE

^c Synchrotron SOLEIL, L'Orme des Merisiers Saint-Aubin, BP 48 91192 Gif-sur-Yvette Cedex

Abstract

Multilamellar wall vesicles (MLWV) are an interesting class of polyelectrolyte-surfactant complexes (PESCs) for wide applications ranging from house-care to biomedical products. If MLWV are generally obtained by a polyelectrolyte-driven vesicle agglutination under pseudo-equilibrium conditions, the resulting phase is often a mixture of more than one structure. In this work, we show that MLWV can be massively and reproductively prepared from a recently developed method involving a pH-stimulated phase transition from a complex coacervate phase (*Co*). We employ a biobased pH-sensitive microbial glucolipid biosurfactant in the presence of a natural, or synthetic, polyamine (chitosan, poly-L-Lysine, polyethylene imine, polyallylamine). *In situ* small angle X-ray scattering (SAXS) and cryogenic transmission electron microscopy (cryo-TEM) show a systematic isostructural and isodimensional transition from the *Co* to the *MLWV* phase, while optical microscopy under polarized light experiments and cryo-TEM reveal a massive, virtually quantitative, presence of MLWV. Finally, the multilamellar wall structure is not perturbed by filtration and sonication, two typical methods employed to control size distribution in vesicles. In summary, this work highlights a new, robust, non-equilibrium phase-change method to develop biobased multilamellar wall vesicles, promising soft colloids with applications in the field of personal care, cosmetics and pharmaceuticals among many others.

Keywords. Polyelectrolyte-Surfactant Complex, complex coacervates, biosurfactants, polyelectrolytes, multilamellar walls vesicles

Introduction

Polyelectrolytes and surfactants may assemble into complex structures known as polyelectrolyte-surfactant complexes (PESCs). When these compounds are oppositely charged, their self-assembly process is mainly driven by electrostatic interactions and it results in the formation of aggregates, which have a broad range of applications in biological materials,¹⁻⁵ drug delivery,⁶⁻⁸ surface modifications,⁹ colloid stabilization¹⁰ and flocculation¹¹ and consumer health-care products. The rich mesoscopical and structural organisation of surfactants combined with the electrostatic interactions with polyelectrolytes give rise to a wide range of structures and phases.¹²⁻¹⁸ Many works reported cubic or hexagonal mesophases^{15,16} but also a number of micellar-based structures: pearl-necklace morphologies,^{2,19,20} interpenetrated polyelectrolyte-wormlike/cylindrical micelles network,^{19,21-23} spheroidal clusters composed of densely packed micelles held by the polyelectrolyte, the latter known as complex coacervates (*Co*) when they form a liquid-liquid phase separation.^{19,24,25}

Very interesting PESCs structures are formed when the surfactant forms low curvature vesicular morphologies. It is in fact generally admitted that modifying vesicles by the addition of polyelectrolytes is an interesting, cheap and simple approach to obtain nanocapsules,²³ which are good candidates to be used as versatile delivery systems,^{19,23} like gene delivery,^{1,22,26,27} or as MRI contrast agents.²⁸ One of the first PESCs vesicular systems has been reported more than 20 years ago in DNA-CTAB (cetyltrimethylammonium bromide) systems, which were the precursors of a number of carriers for gene transfection and often referred to as lipoplexes, when cationic lipids replace surfactants in DNA complexation.^{29,30} If the term lipoplex supposes the use of nucleic acids as complexing agents, similar structures, often addressed to as onion-like structures³¹ or multilamellar vesicles,¹³ were observed using both lipids and surfactants complexed by a wide range of polyelectrolytes. However, multilamellar, or onion-like, vesicles are rather characterized by single-wall membranes concentrically distributed from the outer to the inner core of the vesicle. Lipoplexes, on the contrary, are vesicular objects with a large lumen and a dense multilamellar wall. For this reason, in this work we employ the name multilamellar wall vesicles (MLWV).

The mechanism of formation of MLWV was addressed by several authors, but a common agreement is not achieved, yet. Several works propose that the lipid:polyelectrolyte ratio controls the fusion of single-wall vesicles into MLWV,^{19,29,32-35} while others rather observe vesicular agglutination under similar conditions.³⁶⁻³⁸ In fact, a general consensus has not been found and a multiphasic system including agglutinated vesicles and MLWV are actually observed.³⁹ The question whether or not MLWV, and PESCs in general, are

equilibrium structures and how they are formed is still open, especially when they are prepared under non-equilibrium conditions.¹⁹ To the best of our knowledge, the only works exploring a stimuli-induced approach in the synthesis of MLWV in particular, and PESC in general, were proposed by Chiappisi *et al.*^{21,40} However, the pH variation in these works was still performed under pseudo-equilibrium conditions with equilibration times ranging from 2 to 15 days for each pH value.

In a recent work, we have explored a *Co*-to-*MLWV* phase transition under non-equilibrium conditions using a continuous variation in pH,⁴¹ as illustrated by Figure 1. We could show that in the presence of G-C18:1, an acidic microbial glycolipid biosurfactant,^{42,43} and poly-L-lysine (PLL), a cationic polyelectrolyte (PEC), the pH-stimulated micelle-to-vesicle phase transition of the lipid drives a continuous, isostructural and isodimensional, transition between complex coacervates and MLWV. PLL strongly binds to the lipid monolayers thus favouring ($\Delta G = -36.4 \pm 1.9$ kJ/mol) the formation of the multilamellar wall through both specific ($\Delta H = -2.8 \pm 0.8$ kJ/mol, electrostatic and possibly hydrogen bonding) and non-specific ($\Delta H = 28.9 \pm 0.9$ kJ/mol, entropic, hydrophobic effect) interactions, as quantified by isothermal titration calorimetry experiments.⁴¹

In the present work, we generalize the method of preparing MLWV through a phase transition approach performed under non-equilibrium conditions and we show its performance in comparison to the more accepted method of vesicular agglutination. We show that the former can be applied to a broader set of polyelectrolytes and we explore in more detail the structure and size control of MLWV.

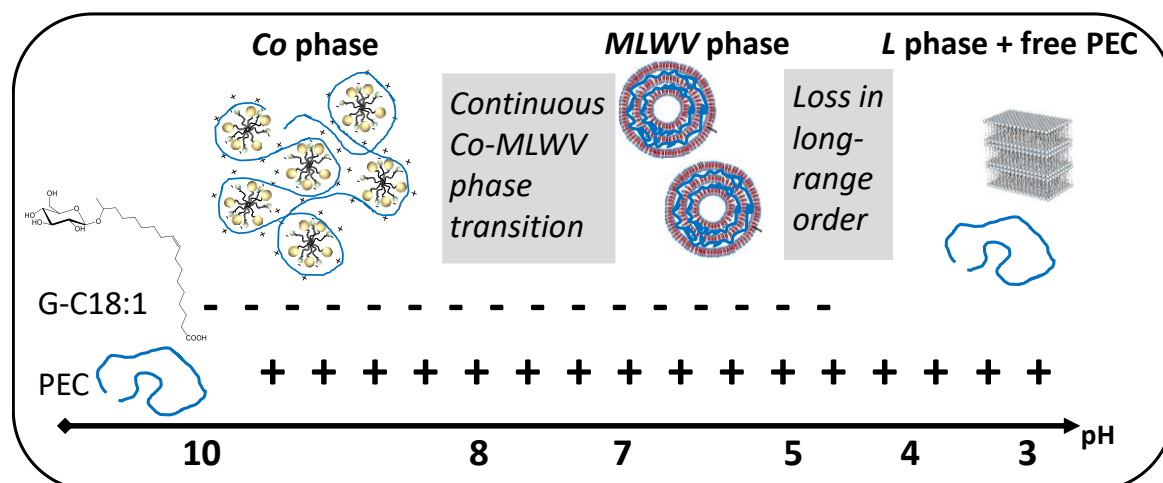


Figure 1 – Phase transition and structures obtained by mixing G-C18:1 and PEC (chitosan, poly-L-lysine, polyallylamine or polyethylenimine) upon a rapid variation of pH. G-C18:1 is negatively charged between about pH 4 and alkaline pH, while PECs are positively charged below pH ~10 (depending on the exact pKa, given in the materials and method section). Complex coacervates (*Co*) composed of G-C18:1 and PEC form

at pH ~10. They progressively rearrange into MLWV and dissociate below pH ~4, where G-C18:1 forms a lamellar (*L*) phase coexisting with free polymer chains.⁴¹

Experimental section

Chemicals

In this work we use microbial glycolipids G-C18:1, made of a single β -D-glucose hydrophilic headgroup and a C18 fatty acid tail (monounsaturated in position 9,10). From alkaline to acidic pH, the former undergoes a micelle-to-vesicle phase transition.⁴² Syntheses of glucolipid G-C18:1 are described in Ref ⁴⁴ and ⁴³, where the typical ¹H NMR spectra and HPLC chromatograms are given. The compound used in this work have a molecular purity of more than 95%.

The polyelectrolytes used in this work are chitosan, obtained from the deacetylation of chitin from crusteans' shells, poly-L-lysine, widely used in biomedical field, polyallylamine and polyethylenimine. Chitosan oligosaccharide lactate (CHL) ($M_w \approx 5$ KDa, $pK_a \sim 6.5$)⁴⁵ with a deacetylation degree >90%, poly-L-lysine (PLL) hydrobromide ($M_w \approx 1-5$ KDa, $pK_a \sim 10-10.5$)⁴⁶ and polyallyllamine hydrochloride (PAH) ($M_w \approx 1-5$ KDa, $pK_a \sim 9.5$),⁴⁶ polyethylenimine (PEI) hydrochloride (linear, $M_w \approx 4$ KDa, $pK_a \sim 8$)⁴⁷ are purchased from Sigma-Aldrich. We also employ a polyampholite, gelatin (Aldrich, type A, from porcine skin, $M_w \approx 50-100$ KDa, isoelectric point 7-9), as a control. All other chemicals are of reagent grade and are used without further purification.

Preparation of stock solutions

G-C18:1 ($C = 5$ mg·mL⁻¹, $C = 20$ mg·mL⁻¹), CHL ($C = 2$ mg·mL⁻¹), PLL ($C = 5$ mg·mL⁻¹, $C = 20$ mg·mL⁻¹), PEI ($C = 5$ mg·mL⁻¹), PAH ($C = 2$ mg·mL⁻¹) and gelatin ($C = 5$ mg·mL⁻¹) stock solutions ($V = 10$ mL) are prepared by dispersing the appropriate amount of each compound in the corresponding amount of Milli-Q-grade water. The solutions are stirred at room temperature ($T = 23 \pm 2$ °C) and the final pH is increased to 11 by adding a few μ L of NaOH ($C = 0.5$ M or $C = 1$ M).

Preparation of samples

Samples are prepared by mixing appropriate volume ratios of G-C18:1 stock solutions at pH 11 and cationic polyelectrolyte (PEC) stock solutions, as defined in Table 1. The final total volume is generally set to $V = 1$ mL or $V = 2$ mL, the solution pH is about 11 and the final concentrations are given in Table 1. The pH of the mixed lipid-PEC solution is eventually

decreased by the addition of 1-10 μL of a HCl solution at $C= 0.5 \text{ M}$ or $C= 1 \text{ M}$. The rate at which pH is changed is generally not controlled although it is in the order of several $\mu\text{L}\cdot\text{min}^{-1}$. Differently than in other systems,^{48,49} we did not observe unexpected effects on the PESC structure to justify a tight control over the pH change rate.

Table 1 - Relative volumes of G-C18:1 and PEC solutions to mix to obtain given concentrations

Volume			Concentration	
G-C18:1 stock solution / mL	PEC stock solution / mL	Water / mL	$C_{\text{G-C18:1}} / \text{mg}\cdot\text{mL}^{-1}$	$C_{\text{PEC}} / \text{mg}\cdot\text{mL}^{-1}$
0.5	0.5	0	2.5 or 10	2.5 or 10
	0.25	0.25	2.5	1.25
	0.125	0.375	2.5	0.625

Dynamic light scattering measurements (DLS)

DLS experiments are performed using a Malvern Zetasizer Nano ZS90 (Malvern Instruments Ltd, Worcestershire, UK) equipped with a 4 mW He-Ne laser at a wavelength of 633 nm. Measurements were made at 25 °C with a fixed angle of 90° and three acquisitions per sample.

pH-resolved *in situ* Small angle X-ray scattering (SAXS)

In situ SAXS experiments during pH variation are performed at room temperature on two different beamlines. The B21 beamline at Diamond Light Source Synchrotron (Harwell, England) is employed using an energy of $E= 13.1 \text{ keV}$ and a fixed sample-to-detector (Eiger 4M) distance of 2.69 m. The Swing beamline at Soleil Synchrotron (Saint-Aubin, France) is employed using an energy of $E= 12 \text{ keV}$ and a fixed sample-to-detector (Eiger X 4M) distance of 1.995 m. For all experiments: the q -range is calibrated to be contained between $\sim 5 \cdot 10^{-3} < q/\text{\AA}^{-1} < \sim 4.5 \cdot 10^{-1}$; raw data collected on the 2D detector are integrated azimuthally using the in-house software provided at the beamline and so to obtain the typical scattered intensity $I(q)$ profile, with q being the wavevector ($q = 4\pi \sin \theta / \lambda$, where 2θ is the scattering angle and λ is

the wavelength). Defective pixels and beam stop shadow are systematically masked before azimuthal integration. Absolute intensity units are determined by measuring the scattering signal of water ($I_{q=0} = 0.0163 \text{ cm}^{-1}$).

The same sample experimental setup is employed on both beamlines: the sample solution ($V = 1 \text{ mL}$) with the lipid and PEC at their final concentration and $\text{pH} \sim 11$ is contained in an external beaker under stirring. The solution is continuously flushed through a 1 mm glass capillary using an external peristaltic pump. The pH of the solution in the beaker is changed using an interfaced push syringe, injecting microliter amounts of a 0.5 M HCl solution. pH is measured using a micro electrode (Mettler-Toledo) and the value of pH is monitored live and manually recorded from the control room via a network camera pointing at the pH-meter located next to the beaker in the experimental hutch. Considering the fast pH change kinetics, the error on the pH value is ± 0.2 .

Polarized Light Microscopy (PLM)

PLM experiments are performed with a transmission Zeiss AxioImager A2 POL optical microscope. A drop of the given sample solution is deposited on a slide covered with a cover slip. The microscope is equipped with a polarized light source, crossed polarizers and an AxioCam CCD camera.

Cryogenic transmission electron microscopy (cryo-TEM)

Cryo-TEM experiments are carried out on an FEI Tecnai 120 twin microscope operated at 120 kV and equipped with a Gatan Orius CCD numeric camera. The sample holder is a Gatan Cryoholder (Gatan 626DH, Gatan). Digital Micrograph software is used for image acquisition. Cryofixation is done using a homemade cryofixation device. The solutions are deposited on a glow-discharged holey carbon coated TEM copper grid (Quantifoil R2/2, Germany). Excess solution is removed and the grid is immediately plunged into liquid ethane at -180°C before transferring them into liquid nitrogen. All grids are kept at liquid nitrogen temperature throughout all experimentation. Images were analyzed using Fiji software, available free of charge at the developer's website.⁵⁰

Results

In recent publications,^{41,51} we have explored the complex coacervation between microbial glycolipids and PEC. For this reason, this aspect is only briefly shown here. Cryo-

TEM images presented in Figure 2 show the structure of PEC-complexed G-C18:1 complex coacervates above pH 7. Above this value, we expect the G-C18:1 to be negatively charged and PEC positively charged, whereas the apparent pK_a of G-C18:1 is expected to be between 6 and 7, similarly to oleic acid,⁵² and the pK_a of PECs being provided in the materials and methods section. Irrespective of the selected PEC, all systems show spheroidal colloids of variable size in the 100 nm range. One can identify two types of structures, both typical of complex coacervates:^{24,25,51,53} dense aggregated structures, shown in Figure 2a,c and very similar to what was found by us^{41,51} and others,²⁴ are attributed to dehydrated, densely-packed, micelles tightly interacting with the polyelectrolyte; a biphasic medium composed of spheroidal, poorly-contrasted, polymer-rich, colloids embedded in a textured, surfactant-rich, medium. The latter were also reported by us^{41,51} and others.^{53,54} In all cases, *Co* phase is a PESC forming in the micellar region of the surfactant's phase diagram and having the specificity of a liquid-liquid phase separation,^{19,25} compared to other supramicellar PESC's undergoing a solid-liquid phase separation.¹⁹

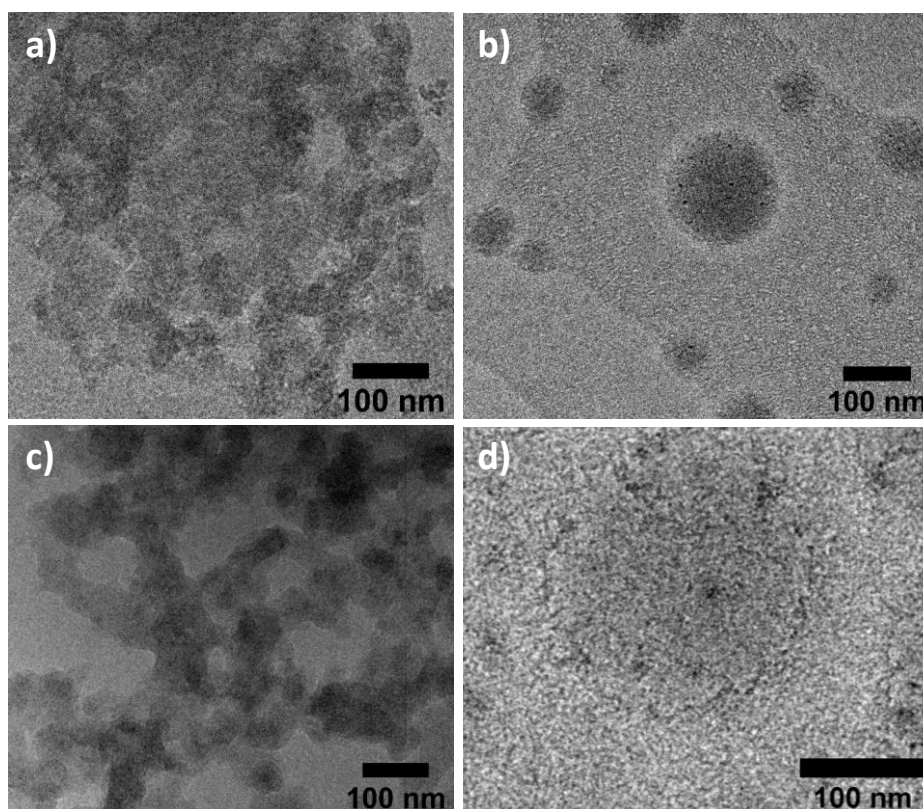


Figure 2 – Cryo-TEM images of PESC solutions in the complex coacervate phase composed of G-C18:1 lipid complexed with a) CHL (pH 7.16), b) PLL (pH 9.16), c) PAH (pH 8.96) and d) PEI (pH 9.02). $C_{G-C18:1} = C_{PEI} = 2.5 \text{ mg mL}^{-1}$, $C_{CHL} = 1 \text{ mg mL}^{-1}$, $C_{PAH} = 0.25 \text{ mg mL}^{-1}$, $C_{PLL} = 1.25 \text{ mg mL}^{-1}$

The difference between dense and poorly-contrasted structures is PEC-independent and it is more related to the stage of coacervation. At an early stage, colloids with a relatively low electron density form and coexist with a rich micellar phase. Free micelles progressively interact with residual polymer chains. At a later, entropy-driven (dehydration and counterion release),⁵⁵ stage of coacervation, droplets with a higher electron density massively form. Unfortunately, neither the texture of the particles nor their internal structure can be easily controlled as they strongly depend on the type of PEC, its stiffness, charge density, stage of coacervation and even kinetics. For these reasons, isolating a specific structure in a *Co* phase can be challenging and we have ourselves found coexisting dense and poorly-contrasted structures,⁴¹ thus preventing any reasonable structure-composition generalization concerning the images presented in Figure 2.

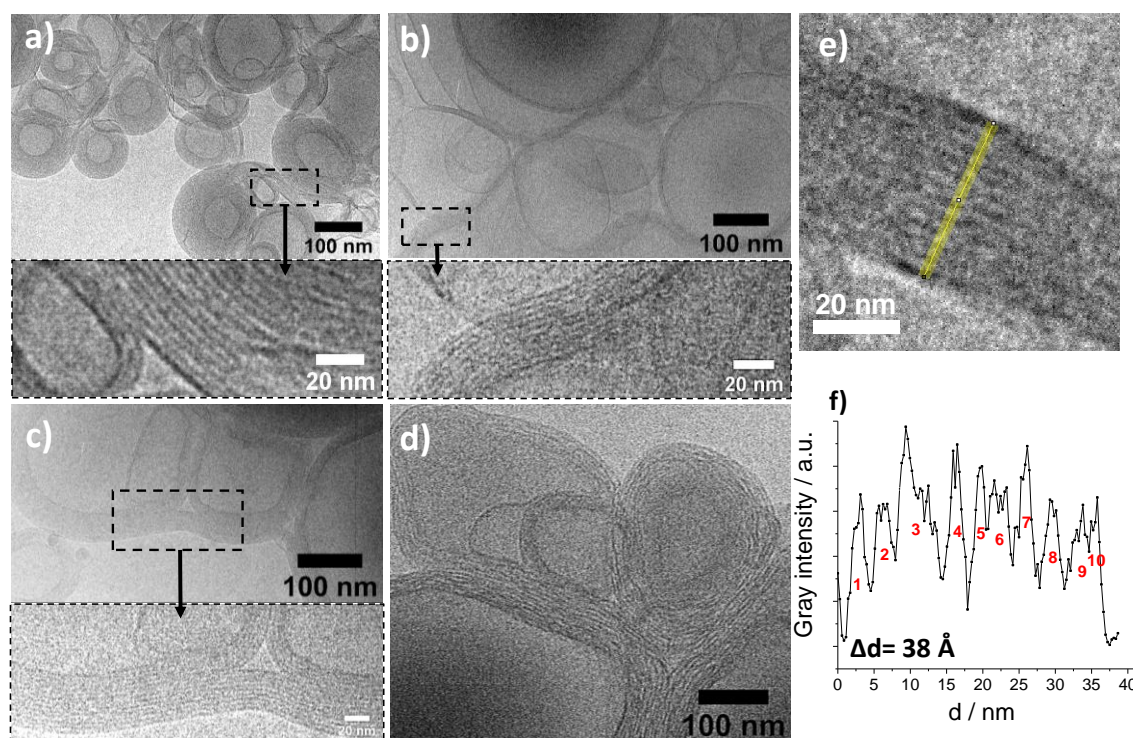


Figure 3 – Cryo-TEM images of a *MLWV* phase composed of acidic G-C18:1 lipid complexed with a) CHL (pH 4.87), b) PLL (pH 4.70), c) PAH (pH 4.25) and d) PEI (pH 5.33). $C_{G-C18:1} = C_{PEI} = C_{PLL} = 2.5 \text{ mg mL}^{-1}$, $C_{CHL} = 1 \text{ mg mL}^{-1}$, $C_{PAH} = 0.25 \text{ mg mL}^{-1}$. e) Zoomed cryo-TEM image of [G-C18:1 + PLL] mixture and its corresponding profile (f) allowing the determination of the interlamellar distance. Cryo-TEM data have been analyzed using Fiji software.⁵⁰

At pH below 7, vesicular structures with multilamellar walls (*MLWV* phase) are observed by cryo-TEM for all PEC samples (Figure 3 and Figure S 1). These structures are closely-related to a lipoplex-type phase rather than to an onion-like phase: the latter is composed of concentric single-wall vesicles, while the former keeps a free lumen and a thick multilamellar

wall.²⁹ Figure 3 also shows a strong packing of the multilamellar walls as well as a strong interconnection between adjacent vesicular objects, in agreement with lipoplexes and other MLWV reported in the literature.²³ The walls are constituted of alternating sandwiched layers composed of tightly packed polyelectrolyte chains and interdigitated monolayers of G-C18:1.⁴¹ d -spacing can be directly estimated from cryo-TEM images (Figure 3e,f) and we find a set of values of $d= 33.7 \pm 4.95 \text{ \AA}$ for the PLL system and $d= 31.6 \pm 3.00 \text{ \AA}$, $25.3 \pm 4.60 \text{ \AA}$ and $41.1 \pm 0.30 \text{ \AA}$ respectively for CHL, PAH and PEI systems. Within the error, these values are compatible with interdigitated G-C18:1 layers,⁴¹⁻⁴³ of which the thickness can be estimated to be about 25 \AA by applying the Tanford relationship,⁵⁶ but also close to what is classically recorded for lipoplexes.^{22,23,33} One may note that the multilamellar walls of the PECSs involving PEI (Figure 3d) appear more disordered than for other PESCs. At the moment, we do not have a clear explanation for that and we actually believe it to be an artifact due to freezing, because the full width at half maximum of the corresponding lamellar peak in SAXS experiments is $\Delta q \sim 2.10^{-3} \text{ \AA}^{-1}$, the same value found for the PLL system.

Cryo-TEM images recorded on the *Co* (Figure 2) and *MLWV* (Figure 3) phases show that the *Co*-to-*MLWV* transition is a general property of G-C18:1 PESCs: it strictly depends on the lipid phase behavior, while the polyelectrolyte only guarantees the cohesion between the lipid membranes. We highlighted elsewhere⁴¹ by pH-resolved *in situ* SAXS experiments an explicit isostructural and isodimensional continuity in the *Co*-to-*MLWV* phase transition: the broad correlation peak at $q= 0.171 \text{ \AA}^{-1}$ (d -spacing of 36.7 \AA) of the coacervate phase coexists with the sharp diffraction peak of the *MLWV* phase at $q_1= 0.178 \text{ \AA}^{-1}$ (d -spacing of 35.3 \AA) in a narrow range around pH 7.⁴¹ Restructuring is driven by the progressive hydrogenation of the carboxylate group and the resulting conformational change of the lipid, which favors the formation of low curvature colloids, while inter-lipid repulsive electrostatic interactions disappear in the meanwhile.

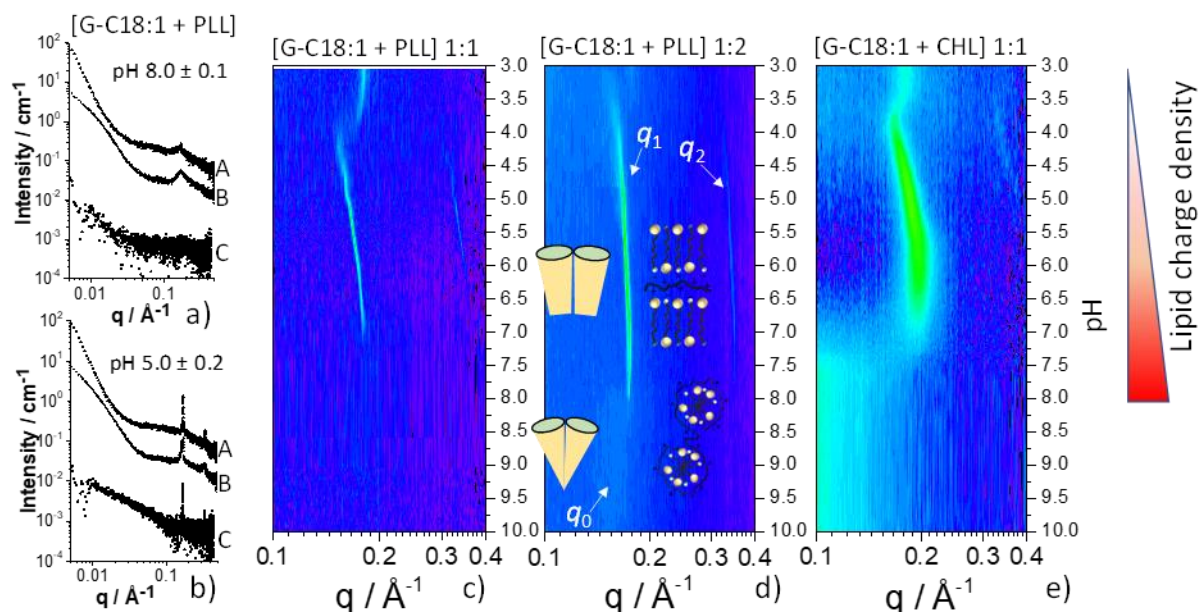


Figure 4 - SAXS profiles of [G-C18:1 + PLL] PESC at a) basic and b) acidic pH with G-C18:1:PLL concentration ratios in $\text{mg}\cdot\text{mL}^{-1}$: A= 2.5:5, B= 10:10, C= 2.5:2.5. c-e) 2D SAXS contour plots of G-C18:1:PLL concentration ratios in $\text{mg}\cdot\text{mL}^{-1}$: c) 2.5:2.5, d) 2.5:5 and e) 2.5:2.5. pH is varied from basic to acidic.

SAXS profiles presented Figure 4 show two different behaviors of the mixture [G-C18:1 + PLL]: at basic pH (Figure 4a), a broad correlation peak is observed at about $q = 0.17 \text{ \AA}^{-1}$ for all lipid:PLL ratios, where the peak can be more pronounced either with concentration (B profile) or lipid:PLL ratio (A profile). SAXS profiles B and C were previously assigned to complex coacervates, and more details on the structure of the *Co* phase can be found in Ref. ⁴¹. In similar systems, the slope at low q was shown to be indicative of the shape of the PESC;⁴⁰ here, the slope is below -3. If such values are typical of fractal interfaces,^{57,58} we cannot unfortunately draw any conclusion on the structure of the complex coacervates, most likely because the *Co* phase in these systems is heterogeneous.⁴¹

Below pH 7 (Figure 4b), a sharp diffraction peak and its first harmonics are visible respectively around $q_1 = 0.17 \text{ \AA}^{-1}$ and $q_2 = 0.34 \text{ \AA}^{-1}$, characteristic of the (100) and (200) reflections of a lamellar order in the walls, described previously and shown in Figure 3. The d -spacing of 37 \AA is in agreement with the ones deduced from cryo-TEM (Figure 3e,f). Similar results are obtained at different lipid:PLL ratios (Figure 4c,d) but also for other PEC. Figure S 2 presents the SAXS signals of [G-C18:1 + CHL] solutions at basic and acidic pH, compared to the control solutions of [G-C18:1] and [CHL] alone as well as their arithmetic sum. If at acidic pH the signature of the lamellar wall of the mixture compared to the controls is out of

doubt, the signal at basic pH is less straightforward to interpret, due to the scattering of CHL alone, known to precipitate above pH 7.⁵⁹ This result is similar to what was found for acidic deacetylated sophorolipids,^{41,51} however, considering the fact that cryo-TEM experiments suggest the presence of complex coacervates, we cannot exclude their formation, although their content may constitute a small minority, if compared to the PLL-based PESCs in the same pH range. Another argument for the formation of *Co* in the presence of CHL will be given later.

Figure 4c-e show the pH-resolved *in situ* contour plots of [G-C18:1 + PLL] PESCs at various lipid:PLL ratio and with CHL. They are recorded between pH 10 and 3 and focus on the high-*q* region of the SAXS pattern, sensitive to the structural *Co*-to-*MLWV* phase transition. All pH-resolved *in situ* contour plots in Figure 4 show three common features: 1) the *Co*-to-*MLWV* transition between pH 8 and 7, where q_1 and q_2 refer to the first and second order peaks of the lamellar wall; 2) a low-*q* shift of q_1 and q_2 when pH decreases to about 4.5, indicating a swelling of the lamellar period, and 3) a loss of the signal between about pH 4.5 and pH 3.5, below which a constant peak at higher *q*-values (generally around $q = 0.2 \text{ \AA}^{-1}$) appears. These phenomena were quantitatively described in more detail in Ref. ⁴¹ and will only be summarized hereafter.

When fully deprotonated at basic pH, G-C18:1 is in a high curvature, micellar, environment (*Co* phase). This state, represented by the drawing superimposed on Figure 4d, is proven by both cryo-TEM and the broad correlation peak at about $q_0 = 0.17 \text{ \AA}^{-1}$. After crossing the transition pH range between 8 and 7, the number of negative charges decreases and G-C18:1 is entrapped in a low-curvature, interdigitated layer, environment. The continuity between q_0 and q_1 strongly suggests an isostructural and isodimensional transition between the micelle and membrane configurations, without any loss of the interaction with the polyelectrolyte. This is also sketched on Figure 4d. When the pH is decreased further, the COOH content increases and thus the membrane charge density decreases. The interlamellar distance consequently increases due to the repulsive pressure exerted by the charged polyelectrolyte, which undergoes hydration and increase internal electrostatic repulsion.^{2,60,61} When hydrogenation of carboxylate groups reach a certain extent, attractive interaction with PLL can no longer hold the membranes together and *MLWV* then lose their long-range lamellar order, which results in their complete disruption and the concomitant expulsion of PLL. Below pH 3, this mechanism leads to the precipitation of a polyelectrolyte-free lamellar, *L*, phase, which is also observed for PEC-free G-C18:1 solutions.⁴¹

A closer look at the experiments in Figure 4 indicates two additional features. The pH stability domain of the *MLWV* phase seems to vary with the lipid:PLL ratio. Comparison of

Figure 4c and Figure 4d, respectively recorded at lipid:PLL= 1:1 and 1:2 reveal that the q_1 peak of the *MLWV* phase is observed between pH 8 and 7. At the 1:2 ratio the *MLWV* phase starts at about pH 8 while at the 1:1 ratio the *MLWV* phase is only visible at pH below 7. At higher concentrations ($C= 10 \text{ mg}\cdot\text{mL}^{-1}$), but still for a 1:1 ratio, the stability frontier seems to be shifted at pH of about 7.5.⁴¹ Although we do not have enough data to draw a general trend, it is well-known that the lipid:polyelectrolyte ratio reflects the negative:positive charge ratio and for this reason it has a direct impact on the electroneutrality, thus affecting a number of structural features of PESC: the wall thickness of the multilamellar structure,^{21,62} the PESC morphology and colloidal stability.¹⁹ For instance, order is noticeably improved when the charge ratio approaches 1:1,⁶³ and micelle-polyelectrolyte complex coacervation can be favored or not.⁶⁴ This ratio is particularly crucial to control the properties of the lipoplexes and thus their applications: lipid/DNA ratio was reported to influence both the formation of lipoplexes and the release of DNA⁶⁵ and gene transfer activity.⁶⁶ Many authors have shown that the lipid:polyelectrolyte ratio actually controls the formation of *MLWV* structures^{19,29,32–35} over agglutinated single-wall vesicles,^{36–38} but in fact it is more likely that a general consensus has not been found, yet, and reality often consists in a mixtures of *MLWV* and agglutinated vesicles,³⁹ although many authors do not specify it. One of the reasons that could explain such discrepancy is the parallel influence of several other parameters like the charge density on both the lipid membrane and in the polyelectrolytes, the rigidity of the latter, the bending energy of the lipid membrane, the ionic strength and so on.^{14,19} In the present case, it is important to note that: 1) G-C18:1 forms a stable *MLWV* phase with all PEC tested in this work and of different origin (biobased vs. synthetic) and rigidity. 2) *MLWV* are stable in the neutral pH range, which can be a good opportunity for applications in the biomedical field, for instance.

An interesting remark concerns the long-range order inside the vesicular multilamellar walls. The width of the lamellar peak around $q \sim 0.2 \text{ \AA}^{-1}$ is more than ten times larger for the CHL (Figure 4e, $\Delta q \sim 3 \cdot 10^{-2} \text{ \AA}^{-1}$) than the PLL (Figure 4c,d, $\Delta q \sim 2 \cdot 10^{-3} \text{ \AA}^{-1}$) system, either suggesting an average smaller size of the lamellar domains or a poorer lamellar order in the case of the *MLWV* obtained from CHL. The reason behind such difference could be the bulkiness and stiffness of CHL with respect to PLL,³² but one should recall from Figure 2 and related discussion that [G-C18:1 + CHL] solutions do not form an extensive *Co* phase. We have already made the hypothesis that the *Co* phase is necessary to form the *MLWV* phase,⁴¹ and we will reinforce this assumption in the next part of this work.

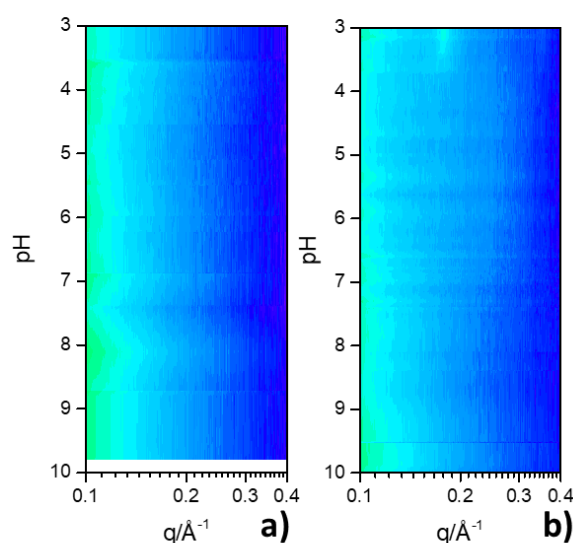


Figure 5 – pH-resolved *in situ* 2D SAXS contour plots of a) gelatin ($C = 2.5 \text{ mg.mL}^{-1}$) and b) [G-C18:1 + gelatin] mixture ($C_{\text{G-C18:1}} = C_{\text{Gelatin}} = 2.5 \text{ mg.mL}^{-1}$).

The data collected so far show that G-C18:1 interacts with all polyelectrolytes tested in this work and that its micelle-to-vesicle phase transition drives the *Co*-to-*MLWV* transition. As one could reasonably expect, and actually confirmed by ITC,⁴¹ strong specific electrostatic interactions, electrostatic in nature, between the positively charged PEC and negatively charged G-C18:1 drive the PESC formation across the entire pH range. To test the solidity of the PESC synthesis using G-C18:1 and PECs, we employ gelatin, a polyampholyte, as a possible alternative to polyelectrolytes and which could be interesting to prepare biobased PESC. We use a commercial (Aldrich) source of gelatin type A, a natural protein of isoelectric point between 7.0-9.0, below which the charge becomes positive. Figure 5 shows pH-resolved *in situ* contour plots of gelatin and [G-C18:1 + gelatin] samples. The control gelatin sample in Figure 5a shows no specific contribution across the entire pH range between $0.1 < q / \text{\AA}^{-1} < 0.4$. Interestingly, the [G-C18:1 + gelatin] sample presented in Figure 5b does not show any signal either in the same pH and q range, except for the systematic signal of the lamellar, *L*, phase of G-C18:1 below pH 4.^{41,42}

Despite an expected positive charge density of gelatin, the *in situ* SAXS experiment shows no sign of the *Co* phase above pH 7, indicating that the charge density is probably too low to interact with negatively charged G-C18:1 micelles. Although somewhat unexpected because interactions with negatively charged sodium dodecyl sulfate micelles across a wide compositional and pH range were reported in other studies,⁶⁷ this result is not a surprise. What

it is more interesting from a mechanistic point of view is the lack of the *MLWV* phase below pH 7. Given its isoelectric point, type A gelatin is positively charged below pH 7 and it is then expected to interact with G-C18:1 negative membranes.

In this work we have used a broad set of polyelectrolytes, of which the different chemical nature let us explore various aspects of their interactions with G-C18:1. If the nature of the polyelectrolyte (stiffness, charge density, ...) is known to strongly affect the morphology and structure of PESCs,^{14,32} in this work we show that: 1) when the *Co* and *MLWV* phases are formed, the structure of the corresponding colloidal structures is very similar, whichever the polyelectrolyte used, even if local phenomena like swelling or long-range order may vary from one polyelectrolyte to another. 2) The *Co* and *MLWV* phases are only obtained with polyelectrolytes with a net positive charge, that is polycations. 3) The *MLWV* phase is always preceded by the *Co* phase, which seems to be a necessary condition to drive the isostructural and isodimensional *Co*-to-*MLWV* transition. This phenomenon does not occur when gelatin is employed and where the *MLWV* phase is not observed. On the contrary, the *MLWV* phase is obtained for the CHL system, despite the fact that we do not have a proof by SAXS of the *Co* phase. In this regard, we must outline that the SAXS signal for the [G-C18:1 + CHL] system at basic pH is dominated by the precipitated CHL phase, which we think to be in major amount but not the only phase. Cryo-TEM shows the presence of an unknown fraction of complex coacervates, which we believe to be source of the *MLWV* phase at pH below 7. We also believe that the higher disorder of the *MLWV* phase in the [G-C18:1 + CHL] system (broader first order diffraction peak compared to the PLL-derived *MLWV* in Figure 4e) could be attributed to the smaller fraction of the initial *Co* phase. In other words, the presence of a less ordered *MLWV* phase in the CHL system could then be the indirect proof that probably a small fraction of the *Co* phase forms in the CHL system.

Quantitativity and size control

If the synthesis of PESCs involving vesicles and polyelectrolytes, and eventually forming *MLWV*, has long been addressed in the literature,^{37,68,69} very few studies, if none, address the issue of quantitativity in relationship to the mechanism of formation. In particular, the synthesis of *MLWV* from a continuous isostructural phase transition from a coacervate phase has not been addressed before, because *MLWV* are generally obtained by mixing vesicles and polyelectrolytes in solution.^{19,29,32–35,37} If some authors state that the formation of *MLWV* is driven by the lipid:polyelectrolyte ratio, other authors show that a mix of agglutinated vesicles and *MLWV* are actually obtained.^{38,39} Other procedures could probably be followed to

increase this control when working with pre-formed vesicles, such as the insertion of the polymer into the hydrophobic vesicle bilayer, which was reported in the case of polycations bearing pendant hydrophobic groups.^{37,70} However, it was found that such interaction could be accompanied by lateral lipid segregation, highly accelerated transmembrane migration of lipid molecules (polycation-induced flip-flop), incorporation of adsorbed polycations into vesicular membrane as well as aggregation and disruption of vesicles.⁷⁰

To evaluate the amount of MLWV with respect to agglutinated vesicles, we compare the sample obtained by continuous *Co-to-MLWV* phase transition with a sample obtained by the more classical approach consisting in mixing G-C18:1 single-wall vesicles and polyelectrolyte, the main one employed in the literature of MLWV. If SAXS can prove the presence of a multilamellar structure, it cannot be easily employed to quantify and discriminate between the two structures. For this reason, instead of SAXS, we evaluate the content of MLWV between the two methods of preparation by combining cryo-TEM with optical microscopy using crossed polarizers. If cryo-TEM can differentiate between agglutination and MLWV, its high magnification is poorly compatible with good statistics, unless a large number of images are recorded. On the contrary, optical microscopy using cross polarizers is the ideal technique to differentiate, on the hundreds of micron scale, between MLWV and agglutinated vesicles: multilamellar structures (but not single-wall vesicles) show a characteristic maltese cross pattern⁷¹ under crossed polarizers, found both in concentric lamellar emulsions⁷² and in spherical lamellar structures.⁷³

Cryo-TEM of samples obtained from a *Co-to-MLWV* phase transition was shown in Figure 4 and, as already commented above, they show a massive presence of vesicular structures having multilamellar walls, as also confirmed by the corresponding SAXS data presented in Figure 4. Figure 6 shows two representative microscopy images of a typical sample prepared with the same approach; images are collected under white (a,d) and polarized light with polarizers at 0°-90° (b,e) and 45°-135° (c,f). The system is characterized by a large number of vesicles highly heterogeneous in size but all below ~10 μm. Under polarized light and crossed polarizers, the entire material displays a typical maltese cross colocalized with each vesicle. Despite the aggregation of the vesicles, also observed with cryo-TEM, maltese crosses are well-defined and nicely separated and each identifying single multilamellar wall vesicles. The entire material displays such a characteristic birefringency, strongly suggesting a quantitative presence of MLWV.

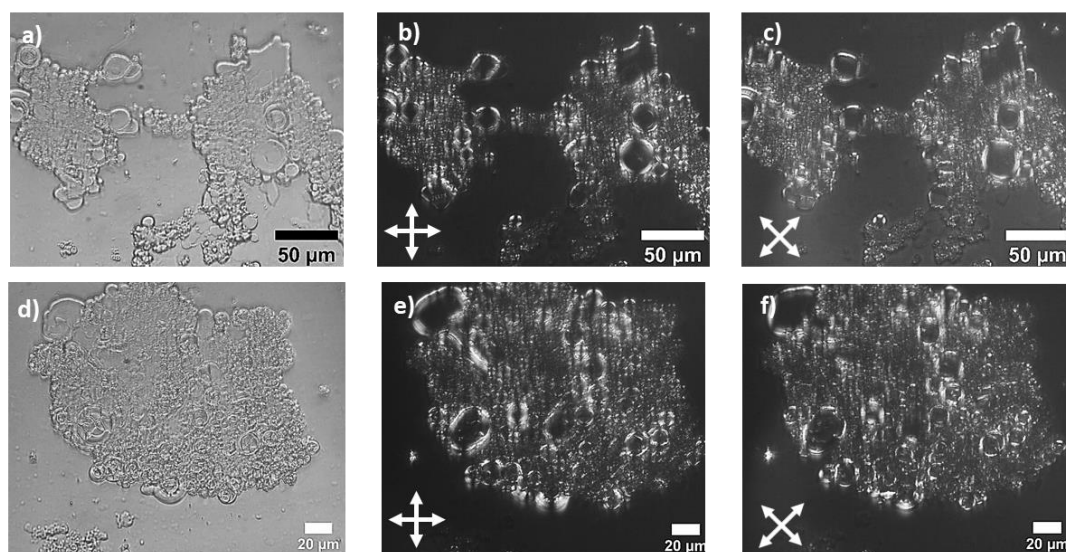


Figure 6 – Optical microscopy images recorded on a [G-C18:1 + PLL] solution ($C_{G-C18:1} = C_{PLL} = 2.5 \text{ mg}\cdot\text{mL}^{-1}$) at pH 3.9 obtained from a *Co-to-MLWV* phase transition. a,d) white light and polarized light with cross polarizers set at b,e) 0-90° and c,f) 45-135°.

The experiment consisting in mixing acidic solutions (pH 3.8) of pre-formed G-C18:1 single-wall vesicles and PLL is shown in Figure 7. A preliminary investigation by optical microscopy results in a different behavior and distribution of signal with respect to the sample obtained through the *Co-to-MLWV* phase transition. Figure 7a shows representative images of a sample being constituted of aggregated objects, each of size below 1 μm , expected for G-C18:1 vesicles.⁴³ The corresponding images recorded using crossed polarizers (Figure 7b,d) show a broad, undefined, birefringency associated to the aggregates with little, if no, content of maltese crosses. The featureless, generalized, birefringency signal suggests that MLWV are either not formed or they form in small amounts, in good agreement with the data presented by others.^{38,39} This assumption is confirmed by cryo-TEM images recorded on the same system and showing a mixture of structures including agglutinated vesicles but also “cabbage-like” and multilamellar structures (Figure 7e-f).

The massive presence of MLWV structures obtained through the phase transition process compared to the mixture of structure obtained from a direct mixing of pre-formed vesicles-polyelectrolyte solutions confirms the crucial role of the complex coacervates in the formation of MLWV: coacervation seems to be a requirement to the extensive formation of vesicular structures with multilamellar walls.⁴¹ This is also in agreement with the data obtained from the [G-C18:1 + gelatin] system presented in Figure 5 and prepared using the pH variation approach. Also in that case, the absence of a complex coacervate phase had as a consequence

the absence of the *MLWV* phase. An additional piece of evidence comes from the *CHL* system, in which the limited amount of the *Co* phase generates a more disordered *MLWV* phase. Combination of the data obtained with gelatin and employing the *in situ* pH variation with the data obtained by mixing vesicle and polyelectrolyte solutions at a given pH demonstrates the importance of the precursor *Co* phase during the phase change method in order to obtain a massive presence of *MLWV* structures.

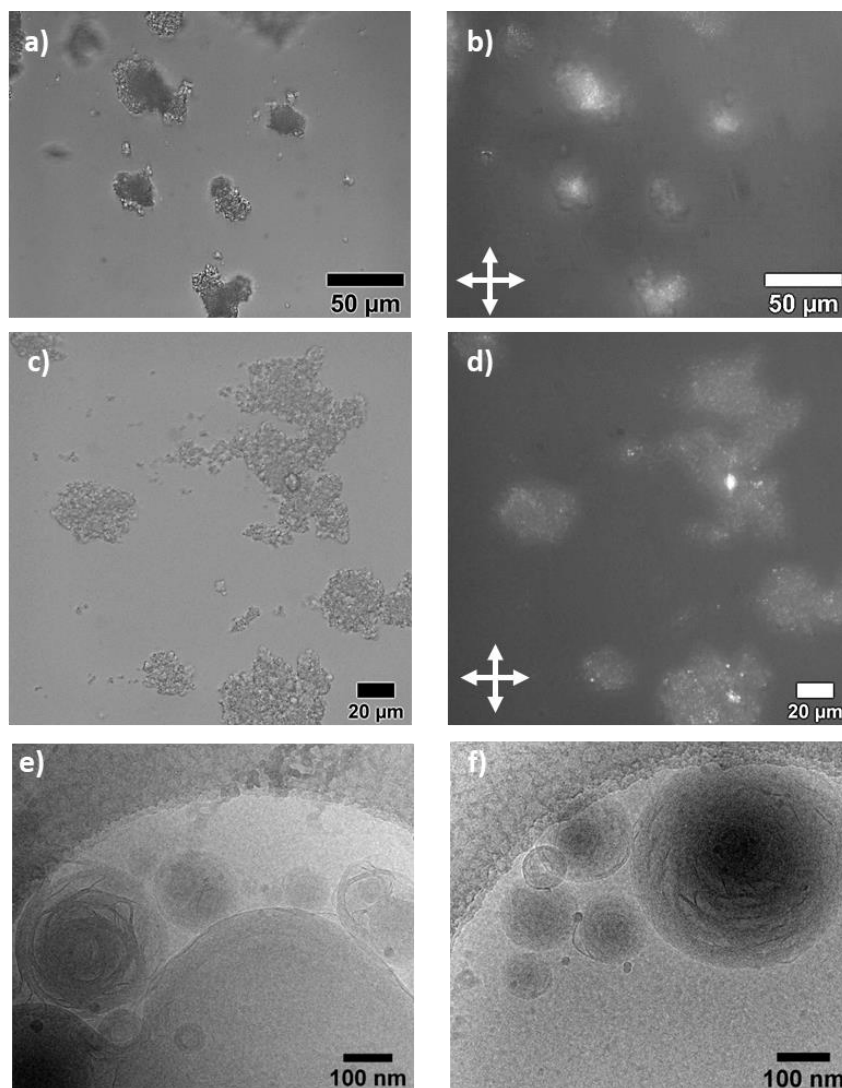


Figure 7 – a-d) Optical microscopy images recorded on a mixture of [G-C18:1] single-wall vesicles and [PLL] solutions ($C_{G-C18:1} = C_{PLL} = 2.5 \text{ mg.mL}^{-1}$) both prepared at pH= 3.8. a,c) white light and b,d) polarized light with cross polarizers set at 0-90°. Images in e,f) are recorded on the same sample by mean of cryo-TEM.

If the *Co*-to-*MLWV* phase transition is able to quantitatively produce *MLWV*, its main drawback is the poor control over their size distribution, as shown both by TEM and optical microscopy. To improve this point, we employed filtration (Figure 8a-c) and sonication (Figure 8d-f), these methods being known to efficiently control vesicles size distribution,⁷⁴ but unclear

whether or not they have any deleterious impact on the MLWV structure. According to the cryo-TEM data in Figure 8a-c, filtration (pore size, $\phi = 450$ nm) promotes the stabilization of colloidally-stable spherical MLWV, of which the diameter seems to be contained between 50 nm and about 300 nm, in agreement with the filter pore size. Concerning the effect of sonication, Figure 8d-f also shows a large number of spherical, un-aggregated, MLWV colloids, although the diameter appears to be bigger of several hundred nanometers if compared to the filtered sample. The cryo-TEM results are confirmed by intensity-filtered DLS experiments, presented in Figure 8g. The as-prepared sample (black curve) shows a MLWV distribution centered at 716 nm, while the filtered sample shows a distribution centered at 460 nm. To better evaluate the impact of sonication, we tested the influence of sonication time and according to DLS data (Figure 8g) we find that at $t = 30'$ the size distribution is centered at higher diameter values and it is even broader than the as-prepared sample. Applying the same sonication conditions, but over a longer period of time ($t = 1'$ or $t = 1'30''$), it is possible to reduce the MLWV diameter even if the size distribution is broader than the filtration approach, in agreement with the cryo-TEM data.

These experiments show that control of the size distribution of MLWV is possible using standard methods employed in liposome science without perturbing the multilamellar wall structure.

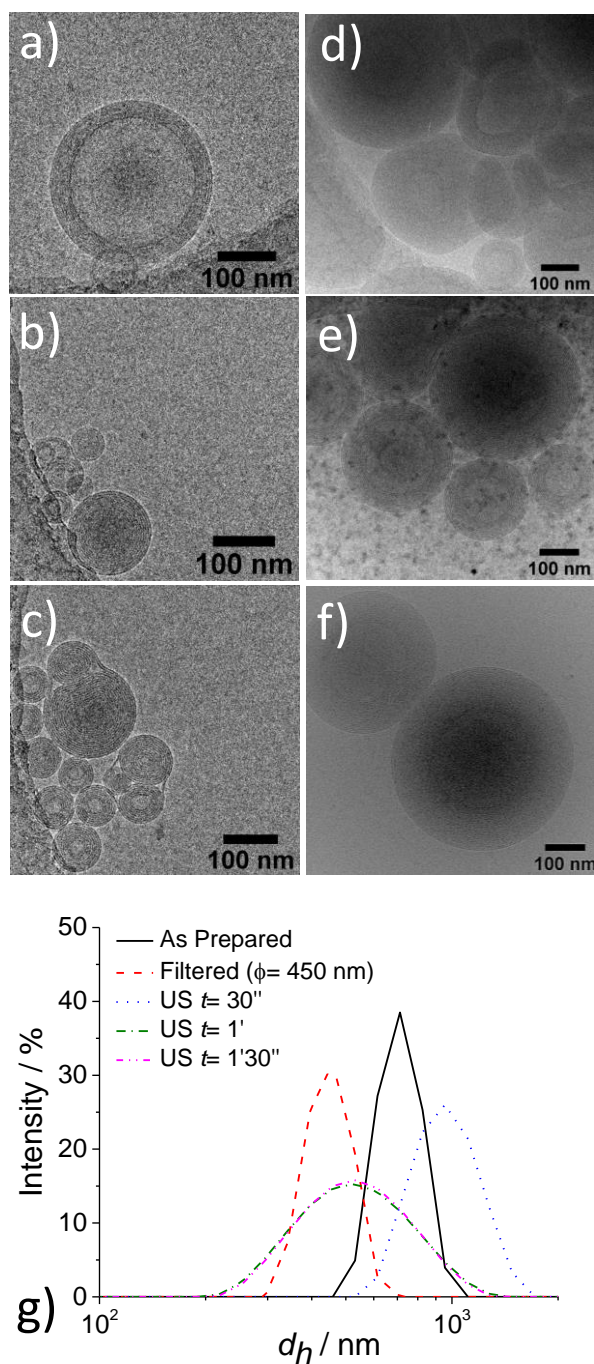


Figure 8 - Cryo-TEM images of a [G-C18:1 + PLL] solution ($\text{pH}=5$, $C_{\text{G-C18:1}}=C_{\text{PLL}}=2.5 \text{ mg.mL}^{-1}$) prepared using the *Co-to-MLWV* approach and a-c) filtered through a $\phi=450$ nm pores membrane or d-f) sonicated (ultrasound, US, technical data: $t=1'$, $P=40$ W, $\text{Ampl.}=40\%$, $\text{freq.}=100\%$). g) profiles of the as prepared (black curve), filtered ($\phi=450$ nm pores membranes, red curve) and sonicated (US, technical data: $P=40$ W, $\text{Ampl.}=40\%$, $\text{freq.}=100\%$, time is given on graph) MLWV samples

Conclusion

This work addresses the synthesis of multilamellar wall vesicles (MLWV) using a recently developed method involving a pH-stimulated transition from a complex coacervate phase (*Co*) instead of a polyelectrolyte-driven vesicle agglutination, classically-employed in the preparation of MLWV polyelectrolyte surfactant complexes (PESCs). We use a combination of a stimuli-responsive microbial glycolipid biosurfactant and a polyelectrolyte, mainly polyamines (either synthetic or natural). The deacetylated acidic C18:1 glucolipid, G-C18:1, undergoes a micelle-to-vesicle phase transition from alkaline to acidic pH. In the alkaline pH domain, its phase behavior is mainly characterized by negatively-charged micelles. In the presence of a positively charged polyelectrolyte, G-C18:1 forms a *Co* phase. Upon lowering pH below the micelle-vesicle boundary, *in situ* SAXS experiments show a continuous isostructural and isodimensional transition between the *Co* and *MLWV* phase. The acidification process reducing the negative charge density, the micellar aggregates embedded in the *Co* phase undergo a decrease in the local curvature, which drives the transition from spheres to membranes, made of interdigitated G-C18:1 molecules. The membrane has a residual negative charge density, responsible for the strong electrostatic interaction with the polyelectrolyte, crucial to maintain the membranes together. At lower pH, the membrane charge density becomes low and interactions with the polyelectrolyte decrease. This phenomenon promotes intra-chain electrostatic repulsion interactions and eventually encourage the lamellar region to swell. Finally, when the membrane reaches neutrality, polymeric repulsion becomes strong enough to disassemble the lamellae. The polyelectrolyte will most likely be entirely solvated and at sufficiently low pH (< 3) the G-C18:1 precipitates in the form of a lamellar phase, possibly free of the polyelectrolyte, a behavior characteristic of the control lipid solution at the same pH.

We employ four polyelectrolytes, synthetic and natural and with different characteristics of rigidity and charge density (chitosan, poly-L-Lysine, polyethylene imine, polyallylamine); however, the nature of the polyelectrolyte does not seem to be a relevant parameter concerning the fate of the transition, as otherwise found for most PESCs. This may be explained by the strong proximity between the lipid and the polyelectrolyte throughout the isostructural *Co*-to-*MLWV* transition. If the method described in this work does not allow a tight control over the size distribution of MLWV, we also find that the multilamellar wall structure is stable against filtration and sonication, two common methods employed to control the size of vesicles. Last but not least, we show that if we employ the classical approach consisting in mixing pre-formed vesicles with a cationic polyelectrolyte solution at a given pH, we find a much broader structural

diversity, including agglutinated single-wall vesicles, multilamellar but also cabbage-like structures, in agreement with previous literature studies.

All in all, this work establishes the ground for the preparation of a new generation of fully biobased, stimuli-responsive, PESC, of which the potential fields of applications could span from cosmetics to home-care products.

Acknowledgements

Diamond synchrotron radiation facility (U. K.) is acknowledged for accessing to the B21 beamline and financial support (proposal N° 23247), as well as Soleil Synchrotron facility for accessing the Swing beamline and financial support (proposal N° 20190961). Ghazi Ben Messaoud (DWI-Leibniz Institute for Interactive Materials, Aachen, Germany) is kindly acknowledged for helpful discussions. We thank Dr. S. Roelants, Prof. W. Soetaert and Prof. C. V. Stevens at Gent University for providing us the glycolipid. Sorbonne Université (contract N°3083/2018) is acknowledged for financial support of CS. Authors kindly acknowledge the French ANR, Project N° SELFAMPHI - 19-CE43-0012-01.

Authors' contributions

CS performed the experiments, analyzed the data and wrote the manuscript. PG performed the cryo-TEM experiments. NC and JP assisted the SAXS experiments. NB conceived and supervised the work and wrote the manuscript.

Supporting Information: Figure S1

References

- (1) Morán, M. C.; Miguel, M. G.; Lindman, B. Surfactant–DNA Gel Particles: Formation and Release Characteristics. *Biomacromolecules* **2007**, *8*, 3886–3892.
- (2) Dobrynin, A. V.; Rubinstein, M. Theory of Polyelectrolytes in Solutions and at Surfaces. *Prog. Polym. Sci.* **2005**, *30*, 1049–1118.
- (3) Wong, G. C. L. Electrostatics of Rigid Polyelectrolytes. *Curr. Opin. Colloid Interface Sci.* **2006**, *11*, 310–315.
- (4) Boroudjerdi, H.; Kim, Y. W.; Naji, A.; Netz, R. R.; Schlagberger, X.; Serr, A. Statics

- and Dynamics of Strongly Charged Soft Matter. *Phys. Rep.* **2005**, *416*, 129–199.
- (5) White, S. R.; Moore, J. S.; Sottos, N. R.; Krull, B. P.; Santa Cruz, W. A.; Gergely, R. C. R. Restoration of Large Damage Volumes in Polymers. *Science (80-.)*. **2014**, *344*, 620–623.
 - (6) Prausnitz, M. R.; Langer, R. Transdermal Drug Delivery. *Nat. Biotechnol.* **2008**, *26*, 1261–1268.
 - (7) Drummond, C. J.; Fong, C. Surfactant Self-Assembly Objects as Novel Drug Delivery Vehicles. *Curr. Opin. Colloid Interface Sci.* **1999**, *4*, 449–456.
 - (8) Singh, M.; Briones, M.; Ott, G.; Hagan, D. O. Cationic Microparticles: A Potent Delivery System for DNA Vaccines. *PNAS* **2000**, *97*, 811–816.
 - (9) Takahashi, A.; Kawaguchi, M. The Structure of Macromolecules Adsorbed on Interfaces. *Adv. Polym. Sci.* **1982**, *46*, 1–65.
 - (10) Müller, M. *Polyelectrolyte Complexes in the Dispersed and Solid State II Application Aspects*; 2013.
 - (11) Petzold, G.; Schwarz, S. Polyelectrolyte Complexes in Flocculation Applications. *Adv. Polym. Sci.* **2014**, *256*, 25–65.
 - (12) Kötz, J.; Kosmella, S.; Beitz, T. Self-Assembled Polyelectrolyte Systems. *Prog. Polym. Sci.* **2001**, *26*, 1199–1232.
 - (13) Langevin, D. Complexation of Oppositely Charged Polyelectrolytes and Surfactants in Aqueous Solutions. A Review. *Adv. Colloid Interface Sci.* **2009**, *147–148*, 170–177.
 - (14) Chiappisi, L.; Hoffmann, I.; Gradzielski, M. Complexes of Oppositely Charged Polyelectrolytes and Surfactants - Recent Developments in the Field of Biologically Derived Polyelectrolytes. *Soft Matter* **2013**, *9*, 3896–3909.
 - (15) Piculell, L.; Norrman, J.; Svensson, A. V.; Lynch, I.; Bernardes, J. S.; Loh, W. Ionic Surfactants with Polymeric Counterions. *Adv. Colloid Interface Sci.* **2009**, *147–148*, 228–236.
 - (16) Piculell, L. Understanding and Exploiting the Phase Behavior of Mixtures of Oppositely Charged Polymers and Surfactants in Water. *Langmuir* **2013**, *29*, 10313–10329.
 - (17) Lindman, B.; Antunes, F.; Aidarova, S.; Miguel, M.; Nylander, T. Polyelectrolyte-Surfactant Association—from Fundamentals to Applications. *Colloid J.* **2014**, *76*, 585–594.
 - (18) Schillén, K.; Galantini, L.; Du, G.; Del Giudice, A.; Alfredsson, V.; Carnerup, A. M.; Pavel, N. V.; Masci, G.; Nyström, B. Block Copolymers as Bile Salt Sequestrants:

- Intriguing Structures Formed in a Mixture of an Oppositely Charged Amphiphilic Block Copolymer and Bile Salt. *Phys. Chem. Chem. Phys.* **2019**, *21*, 12518–12529.
- (19) Gradzielski, M.; Hoffmann, I. Polyelectrolyte-Surfactant Complexes (PESCs) Composed of Oppositely Charged Components. *Curr. Opin. Colloid Interface Sci.* **2018**, *35*, 124–141.
- (20) Kronberg, B.; Holmberg, K.; Lindman, B. Surfactant–Polymer Systems. In *Surface Chemistry of Surfactants and Polymers*; Kronberg, B., Holmberg, K., Lindman, B., Eds.; John Wiley & Sons, Ltd., 2014; pp 271–294.
- (21) Chiappisi, L.; Prévost, S.; Grillo, I.; Gradzielski, M. From Crab Shells to Smart Systems: Chitosan-Alkylethoxy Carboxylate Complexes. *Langmuir* **2014**, *30*, 10615–10616.
- (22) Bilalov, A.; Olsson, U.; Lindman, B. Complexation between DNA and Surfactants and Lipids: Phase Behavior and Molecular Organization. *Soft Matter* **2012**, *8*, 11022–11033.
- (23) Ferreira, G. A.; Loh, W. Liquid Crystalline Nanoparticles Formed by Oppositely Charged Surfactant-Polyelectrolyte Complexes. *Curr. Opin. Colloid Interface Sci.* **2017**, *32*, 11–22.
- (24) Kizilay, E.; Dinsmore, A. D.; Hoagland, D. A.; Sun, L.; Dubin, P. L. Evolution of Hierarchical Structures in Polyelectrolyte-Micelle Coacervates. *Soft Matter* **2013**, *9*, 7320–7332.
- (25) Kizilay, E.; Kayitmazer, A. B.; Dubin, P. L. Complexation and Coacervation of Polyelectrolytes with Oppositely Charged Colloids. *Adv. Colloid Interface Sci.* **2011**, *167*, 24–37.
- (26) Duarte, S.; Faneca, H.; Pedroso De Lima, M. C. Non-Covalent Association of Folate to Lipoplexes: A Promising Strategy to Improve Gene Delivery in the Presence of Serum. *J. Control. Release* **2011**, *149*, 264–272.
- (27) Dias, R. S.; Dawson, K.; Miguel, M. G. Interaction of DNA with Surfactants in Solution. In *DNA Interactions with Polymers and Surfactants*; Dias, R., Lindman, B., Eds.; Hoboken, New Jersey, 2008; pp 89–117.
- (28) Chen, Y.; Zhu, Q.; Tian, Y.; Tang, W.; Pana, F.; Rulin Xiong, Y.; Yuan, Y.; Hu, A.; 5. Supramolecular Aggregates from Polyacrylates and Gd(III)-Containing Cationic Surfactant as High-Relaxivity MRI Contrast Agents. *Polym. Chem.* **2015**, *6*, 1521–1526.
- (29) Zinchenko, A. A.; Pyshkina, O. A.; Lezov, A. V.; Sergeyev, V. G.; Yoshikawa, K.

- Single DNA Molecules: Compaction and Decompaction. In *DNA Interactions with Polymers and Surfactants*; Dias, R., Lindman, B., Eds.; John Wiley & Sons, Inc.: Hoboken, New Jersey, 2008; pp 59–88.
- (30) Rafael, D.; Andrade, F.; Arranja, A.; Luís, S.; Videira, M. Lipoplexes and Polyplexes: Gene Therapy. *Encycl. Biomed. Polym. Polym. Biomater.* **2015**, No. August 2016, 4335–4347.
- (31) Golan, S.; Talmon, Y. Nanostructure of Complexes between Cationic Lipids and an Oppositely Charged Polyelectrolyte. *Langmuir* **2012**, *28*, 1668–1672.
- (32) Ram-On, M.; Cohen, Y.; Talmon, Y. Effect of Polyelectrolyte Stiffness and Solution PH on the Nanostructure of Complexes Formed by Cationic Amphiphiles and Negatively Charged Polyelectrolytes. *J. Phys. Chem. B* **2016**, *120*, 5907–5915.
- (33) Weisman, S.; Hirsch-Lerner, D.; Barenholz, Y.; Talmon, Y. Nanostructure of Cationic Lipid-Oligonucleotide Complexes. *Biophys. J.* **2004**, *87*, 609–614.
- (34) Huebner, S.; Battersby, B. J.; Grimm, R.; Cevc, G. Lipid-DNA Complex Formation: Reorganization and Rupture of Lipid Vesicles in the Presence of DNA as Observed by Cryoelectron Microscopy. *Biophys. J.* **1999**, *76*, 3158–3166.
- (35) Chiappisi, L.; Gradzielski, M. Co-Assembly in Chitosan-Surfactant Mixtures: Thermodynamics, Structures, Interfacial Properties and Applications. *Adv. Colloid Interface Sci.* **2015**, *220*, 92–107.
- (36) Marques, E. F.; Regev, O.; Khan, A.; Miguel, M. D. G.; Lindman, B. Interactions between Catanionic Vesicles and Oppositely Charged Polyelectrolytes - Phase Behavior and Phase Structure. *Macromolecules* **1999**, *32*, 6626–6637.
- (37) Antunes, F. E.; Marques, E. F.; Miguel, M. G.; Lindman, B. Polymer-Vesicle Association. *Adv. Colloid Interface Sci.* **2009**, *147–148*, 18–35.
- (38) De Souza, T. P.; Bossa, G. V.; Stano, P.; Steiniger, F.; May, S.; Luisi, P. L.; Fahr, A. Vesicle Aggregates as a Model for Primitive Cellular Assemblies. *Phys. Chem. Chem. Phys.* **2017**, *19*, 20082–20092.
- (39) Gasperini, A. A. M.; Puentes-Martinez, X. E.; Balbino, T. A.; De Paula Rigoletto, T.; De Sá Cavalcanti Corrêa, G.; Cassago, A.; Portugal, R. V.; De La Torre, L. G.; Cavalcanti, L. P. Association between Cationic Liposomes and Low Molecular Weight Hyaluronic Acid. *Langmuir* **2015**, *31*, 3308–3317.
- (40) Chiappisi, L.; David Leach, S.; Gradzielski, M. Precipitating Polyelectrolyte-Surfactant Systems by Admixing a Nonionic Surfactant-a Case of Conosurfactancy. *Soft Matter* **2017**, *13*, 4988–4996.

- (41) Seyrig, C.; Griel, P. Le; Cowieson, N.; Perez, J.; Baccile, N. Stimuli-Induced Non-Equilibrium Phase Transitions in Polyelectrolyte-Surfactant Complex Coacervates. *Langmuir* **2020**, 10.1021/acs.langmuir.0c01177.
- (42) Baccile, N.; Cuvier, A.-S.; Prévost, S.; Stevens, C. V.; Delbeke, E.; Berton, J.; Soetaert, W.; Van Bogaert, I. N. A.; Roelants, S. Self-Assembly Mechanism of PH-Responsive Glycolipids: Micelles, Fibers, Vesicles, and Bilayers. *Langmuir* **2016**, *32*, 10881–10894.
- (43) Baccile, N.; Selmane, M.; Le Griel, P.; Prévost, S.; Perez, J.; Stevens, C. V.; Delbeke, E.; Zibek, S.; Guenther, M.; Soetaert, W.; et al. PH-Driven Self-Assembly of Acidic Microbial Glycolipids. *Langmuir* **2016**.
- (44) Cuvier, A. S.; Berton, J.; Stevens, C. V.; Fadda, G. C.; Babonneau, F.; Van Bogaert, I. N. A.; Soetaert, W.; Pehau-Arnaudet, G.; Baccile, N. PH-Triggered Formation of Nanoribbons from Yeast-Derived Glycolipid Biosurfactants. *Soft Matter* **2014**, *10*, 3950–3959.
- (45) Liu, W.; Sun, S.; Cao, Z.; Zhang, X.; Yao, K.; Lu, W. W.; Luk, K. D. K. An Investigation on the Physicochemical Properties of Chitosan/DNA Polyelectrolyte Complexes. *Biomaterials* **2005**, *26*, 2705–2711.
- (46) Lewis, S. R.; Datta, S.; Gui, M.; Coker, E. L.; Huggins, F. E.; Daunert, S.; Bachas, L.; Bhattacharyya, D. Reactive Nanostructured Membranes for Water Purification. *Proc. Natl. Acad. Sci. U. S. A.* **2011**, *108*, 8577–8582.
- (47) Mady, M. M.; Mohammed, W. A.; El-Guendy, N. M.; Elsayed, A. A. Effect of Polymer Molecular Weight on the Dna/Pei Polyplexes Properties. *J. Biophys* **2011**, *21*, 151–165.
- (48) Ben Messaoud, G.; Le Griel, P.; Hermida-Merino, D.; Roelants, S. L. K. W.; Soetaert, W.; Stevens, C. V.; Baccile, N. PH-Controlled Self-Assembled Fibrillar Network (SAFiN) Hydrogels: Evidence of a Kinetic Control of the Mechanical Properties. *Chem. Mater.* **2019**, *31*, 4817–4830.
- (49) Hayward, D. W.; Chiappisi, L.; Teo, J. H.; Prévost, S.; Schweins, R.; Gradzielski, M. Neutralisation Rate Controls the Self-Assembly of PH-Sensitive Surfactants. *Soft Matter* **2019**, *15*, 8611–8620.
- (50) Schindelin, J.; Arganda-Carreras, I.; Frise, E.; Kaynig, V.; Longair, M.; Pietzsch, T.; Preibisch, S.; Rueden, C.; Saalfeld, S.; Schmid, B.; et al. Fiji: An Open-Source Platform for Biological-Image Analysis. *Nat. Methods* **2012**, *9*, 676–682.
- (51) Ben Messaoud, G.; Promeneur, L.; Brennich, M.; Roelants, S. L. K. W.; Le Griel, P.;

- Baccile, N. Complex Coacervation of Natural Sophorolipid Bolaamphiphile Micelles with Cationic Polyelectrolytes. *Green Chem.* **2018**, *20*, 3371–3385.
- (52) Lieckfeldt, R.; Villalaín, J.; Gómez-Fernández, J.-C.; Lee, G. Apparent Pka of the Fatty Acids Within Ordered Mixtures of Model Human Stratum Corneum Lipids. *Pharm. Res.* **1995**, *12*, 1614–1617.
- (53) Swanson-Vethamuthu, M.; Dubin, P. L.; Almgren, M.; Yingjie, L. Cryo-TEM of Polyelectrolyte – Micelle Complexes. *J. Colloid Interface Sci.* **1997**, *186*, 414–419.
- (54) Koga, S.; Williams, D. S.; Perriman, A. W.; Mann, S. Peptide-Nucleotide Microdroplets as a Step towards a Membrane-Free Protocell Model. *Nat. Chem.* **2011**, *3*, 720–724.
- (55) Kayitmazer, A. B.; Strand, S. P.; Tribet, C.; Jaeger, W.; Dubin, P. L. Effect of Polyelectrolyte Structure on Protein - Polyelectrolyte Coacervates: Coacervates of Bovine Serum Albumin with Poly(Diallyldimethylammonium Chloride) versus Chitosan. *Biomacromolecules* **2007**, *8*, 3568–3577.
- (56) Tanford, C. *The Hydrophobic Effect: Formation of Micelles and Biological Membranes*; Wiley-Interscience, 1973.
- (57) Cuvier, A. S.; Babonneau, F.; Berton, J.; Stevens, C. V.; Fadda, G. C.; Péhau-Arnaudet, G.; Le Griel, P.; Prévost, S.; Perez, J.; Baccile, N. Nanoscale Platelet Formation by Monounsaturated and Saturated Sophorolipids under Basic PH Conditions. *Chem. - A Eur. J.* **2015**, *21*, 19265–19277.
- (58) Teixeira, J. Small-Angle Scattering by Fractal Systems. *J. Appl. Crystallogr.* **1988**, *21*, 781–785.
- (59) Rinaudo, M. Chitin and Chitosan: Properties and Applications. *Prog. Polym. Sci.* **2006**, *31*, 603–632.
- (60) Sjöström, L.; Åkesson, T.; Jönsson, B. Interaction and Conformation of Polyelectrolyte Chains Adsorbed on Neutral Surfaces. *J. Chem. Phys.* **1993**, *99*, 4739–4747.
- (61) Fleer, G. J.; Stuart, M. A. C.; Scheutjens, J. M. H. M.; Cosgrove, T.; Vincent, B. *Polymers at Interfaces*, 1998th ed.; Springer-Science, 1998.
- (62) Gerelli, Y.; Di Bari, M. T.; Deriu, A.; Clemens, D.; Almásy, L. Lipid Multilayered Particles: The Role of Chitosan on Structure and Morphology. *Soft Matter* **2010**, *6*, 2533–2538.
- (63) Kogej, K.; Evmenenko, G.; Theunissen, E.; Berghmans, H.; Reynaers, H. Investigation of Structures in Polyelectrolyte/Surfactant Complexes by X-Ray Scattering. *Langmuir* **2001**, *17*, 3175–3184.

- (64) Wang, Y.; Kimura, K.; Dubin, P. L.; Jaeger, W. Polyelectrolyte-Micelle Coacervation: Effects of Micelle Surface Charge Density, Polymer Molecular Weight, and Polymer/Surfactant Ratio. *Macromolecules* **2000**, *33*, 3324–3331.
- (65) Tarahovsky, Y. S.; Koynova, R.; MacDonald, R. C. DNA Release from Lipoplexes by Anionic Lipids: Correlation with Lipid Mesomorphism, Interfacial Curvature, and Membrane Fusion. *Biophys. J.* **2004**, *87*, 1054–1064.
- (66) Zhou, S.; Chu, B. Assembled Materials: Polyelectrolyte-Surfactant Complexes. *Adv. Mater.* **2000**, *12*, 545–556.
- (67) Greener, J.; Contestable, B. A.; Bale, M. D. Interaction of Anionic Surfactants with Gelatin: Viscosity Effects. *Macromolecules* **1987**, *20*, 2490–2498.
- (68) Bordi, F.; Cametti, C.; Diociaiuti, M.; Gaudino, D.; Gili, T.; Sennato, S. Complexation of Anionic Polyelectrolytes with Cationic Liposomes: Evidence of Reentrant Condensation and Lipoplex Formation. *Langmuir* **2004**, *20*, 5214–5222.
- (69) Rozenfeld, J. H. K.; Duarte, E. L.; Barbosa, L. R. S.; Lamy, M. T. The Effect of an Oligonucleotide on the Structure of Cationic DODAB Vesicles. *Phys. Chem. Chem. Phys.* **2015**, *17*, 7498–7506.
- (70) Yaroslavov, A.; Kabanov, V. What Happens to Negatively Charged Vesicles upon Interacting with Polycation Species? *Am. Chem. Soc. Polym. Prepr. Div. Polym. Chem.* **2000**, *41*, 1613.
- (71) Regev, O. Various Bilayer Organizations in a Single-Tail Nonionic Surfactant: Unilamellar Vesicles, Multilamellar Vesicles, and Flat-Stacked Lamellae. *Langmuir* **1999**, *15*, 4357–4364.
- (72) Park, B. D.; Youm, J. K.; Jeong, S. K.; Choi, E. H.; Ahn, S. K.; Lee, S. H. The Characterization of Molecular Organization of Multilamellar Emulsions Containing Pseudoceramide and Type III Synthetic Ceramide. *J. Invest. Dermatol.* **2003**, *121*, 794–801.
- (73) Harris, J. K.; Rose, G. D.; Bruening, M. L. Spontaneous Generation of Multilamellar Vesicles from Ethylene Oxide/Butylene Oxide Diblock Copolymers. *Langmuir* **2002**, *18*, 5337–5342.
- (74) Pereira-Lachataignerais, J.; Pons, R.; Panizza, P.; Courbin, L.; Rouch, J.; López, O. Study and Formation of Vesicle Systems with Low Polydispersity Index by Ultrasound Method. *Chem. Phys. Lipids* **2006**, *140*, 88–97.

Supplementary information

Synthesis of multilamellar walls vesicles polyelectrolyte-surfactant complexes from pH-stimulated phase transition using microbial biosurfactants

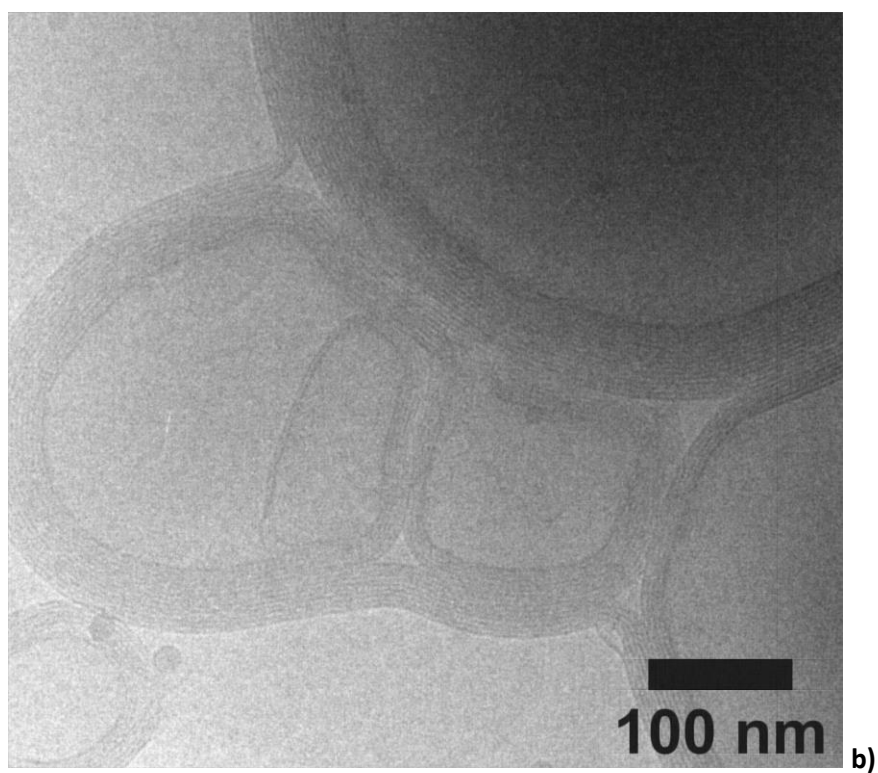
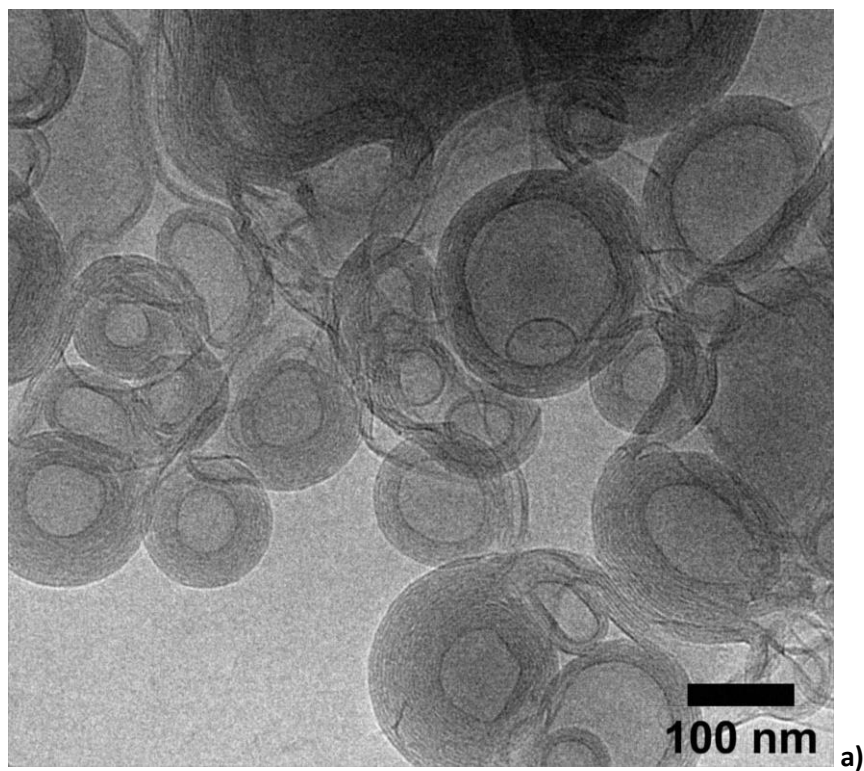
Chloé Seyrig^a, Patrick Le Griel^a, Nathan Cowieson,^b Javier Perez,^c Niki Baccile^a

^a Sorbonne Université, Centre National de la Recherche Scientifique, Laboratoire de Chimie de la Matière Condensée de Paris , LCMCP, F-75005 Paris, France

^b Diamond Light Source Ltd, Diamond House, Harwell Science & Innovation Campus, Didcot, Oxfordshire, OX11 0DE

^c Synchrotron SOLEIL, L'Orme des Merisiers Saint-Aubin, BP 48 91192 Gif-sur-Yvette Cedex

Content : Figure S1, Figure S2



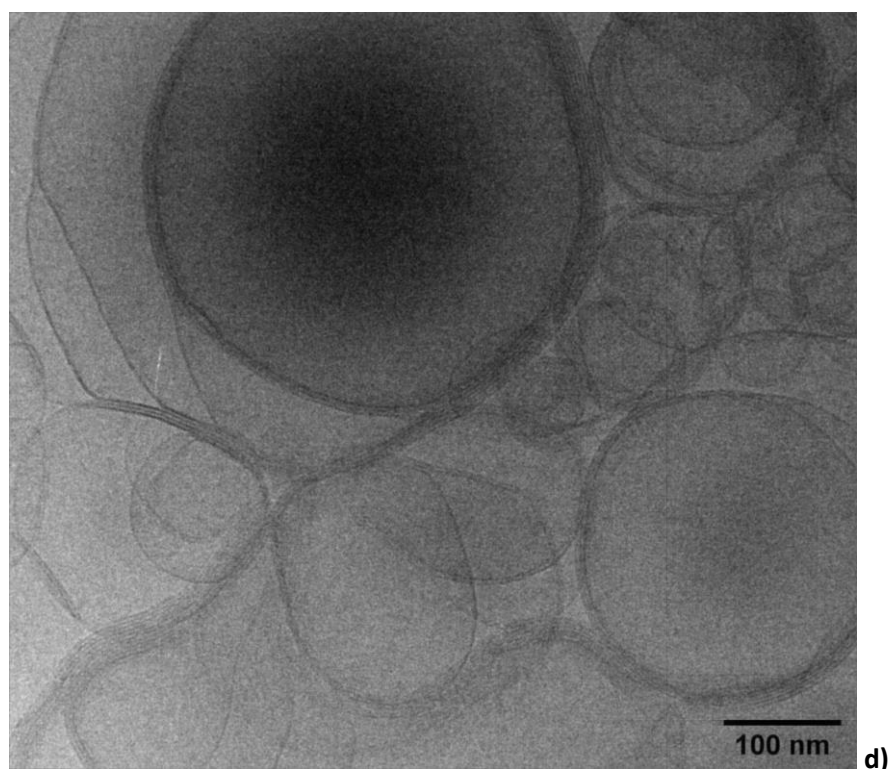
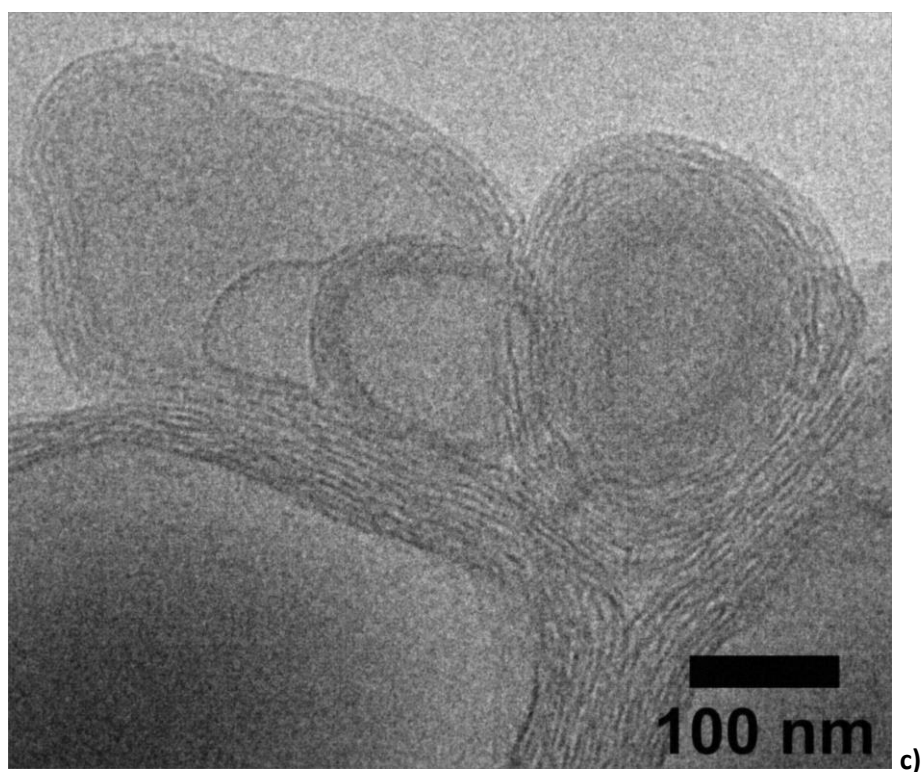


Figure S 1 - Additional cryo-TEM images and zooms on layers of *MLWV* made of G-C18:1 (2.5 mg.mL⁻¹) + a) CHL (1 mg.mL⁻¹, pH 4.87) , b) PAH (0.25 mg.mL⁻¹, pH 4.25), c) PEI (2.5 mg.mL⁻¹, pH 5.33) and d) PLL (2.5 mg.mL⁻¹, pH 4.70)

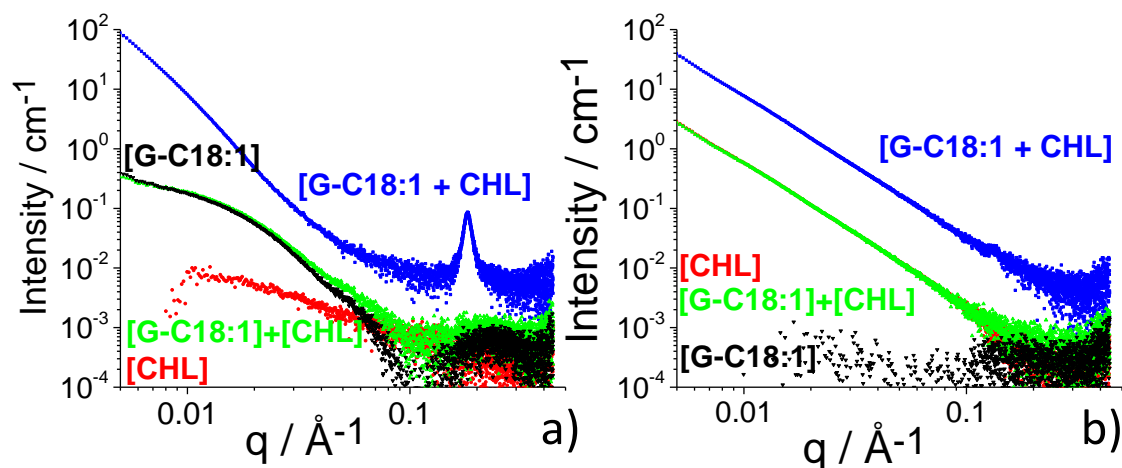


Figure S 2 - SAXS profiles of [G-C18:1] (black) and [CHL] (red) control and [G-C18:1 + CHL] (blue) solutions ($C_{G-C18:1} = 2.5 \text{ mg}\cdot\text{mL}^{-1}$, $C_{CHL} = 1 \text{ mg}\cdot\text{mL}^{-1}$) at a) pH= 4.73 and b) pH= 8.81. The green [G-C18:1] + [CHL] profiles correspond to the arithmetic sum of [G-C18:1] + [CHL] individual SAXS profiles.

Glycolipid Biosurfactants as Multilamellar Vesicular Drug Carriers

Silvia Alonso-de-Castro,^a Chloé Seyrig,^a Korin Ozkaya^a, Julien Dumond,^b Luisa Riancho,^c Javier Perez,^d Christophe Hélyary^{a,*}, Niki Baccile^{a,*}

^a Sorbonne Université, Centre National de la Recherche Scientifique, Laboratoire de Chimie de la Matière Condensée de Paris, LCMCP, F-75005 Paris, France

^b Centre interdisciplinaire de recherche biologique, Collège de France, 75005 Paris, France

^c Centre de Recherche INSTITUT DE LA VISION, UMR_S968 Inserm / UPMC / CHNO des Quinze-Vingts, 75012, Paris, France

^d Synchrotron Soleil, L'Orme des Merisiers, Saint-Aubin, BP48, 91192 Gif-sur-Yvette Cedex, France

Abstract

In this study, multilamellar wall vesicles (MLWV) consisting of microbial glucolipids (GC) and Polylysine (PLL) have been assessed as novel drug delivery system. First, the stability of GCPLL MLWV is established in culture medium at physiological pH. Second, the GCPLL cytotoxicity has been evaluated in mouse fibroblasts L929, normal human dermal fibroblasts NHDF, macrophages derived THP-1 and human cervical carcinoma HeLa. The nanocarriers do not present any cytotoxicity on cells when the dose is lower than 250 µg/mL regardless of the cell type. Curcumin, a highly lipophilic molecule, has been used as drug model to evaluate the **GCPLL** MLWVs as potential nanocarrier to specifically deliver drugs into cancer cells. The curcumin loaded MLWVs uptake measured by flow cytometry is much higher in HeLa cells (50%) compared to NHDF (35%) and THP-1 derived macrophages (20%). The large GCPLL uptake by HeLa cells is correlated to a large amount of curcumin released, responsible for cell cytotoxicity. No significant cytotoxic effect is observed in NHDF and macrophages. A dedicated mechanistic study shows that the cytotoxic effect is based on MLWV fusion with the cell membrane and the curcumin release within the cellular cytoplasm. Taken together, these results demonstrate the use of GCPLL MLWVs as novel drug delivery system to efficiently target cancer cells.

Introduction

Biological amphiphiles, sometimes referred to as biosurfactants, are molecules produced by microorganisms and developed for their high ecosustainable profile.¹ Among the different families of biosurfactants available (glycolipids, lipoproteins or lipopeptides, polymeric), glycolipids are certainly the most relevant one for their high-throughput production process and broadness of applications. In particular, their use in the biomedical field² has long been reported, but is mainly focused on the development of antibiotics.² In the pharmacological field, there have been spurious reports^{3,4} on the anticancer properties of specific microbial glycolipids (e.g., sophorolipids),⁵ but these results are still under debate.⁶ Biosurfactants-based carriers have been proposed in the past years,⁷ but in the best case scenario, the main lipidic vehicle is generally constituted by a classical phospholipid liposome.^{8,9} Hence, a better understanding of the effects of biosurfactants on pre-formed bilayer membranes,¹⁰⁻¹² thus

making the liposomal vector is necessary to obtain more complex particles. In the several cases, the lipid particle formation leads to an uncontrolled structure.¹³

The analysis of the self-assembly properties of microbial glycolipids^{14,15} has opened the opportunity to conceive phospholipid-free stimuli-responsive complex colloidal structures, only composed of bioamphiphiles. Multilamellar wall vesicles (MLWV), belonging to the family of polyelectrolyte-surfactant complexes (PESC), are interesting colloids, originally employed in gene transfection,¹⁶ for which the stability is generally considered better than single-wall vesicles. In recent reports, we have controlled the attractive electrostatic interactions between microbial C18:1-*cis* single-glucose lipid (G-C18:1, **GC**) and poly-L-lysine (**PLL**) at the micelle-to-vesicle phase transition of **GC** and shown the formation of phospholipid-free, stable, MLWV.^{17,18} The multilamellar wall structure is composed of alternating layers of GC and PLL and is prepared from a pH-stimulated phase transition in water around pH 7.¹⁷ Indeed, microbial glycolipids in general, and **GC** in particular, have a curious asymmetric bolaform structure with a free-standing COOH group, making the molecule pH-sensitive with a more complex phase behavior than classical lipids or surfactants.

Drug delivery systems are engineered technologies which allow the targeting and/or the controlled release of active principles. They overcome several drawbacks related to the systemic administration of free pharmacological molecules such as side effects, drug solubility, stability in biological environment, rapid clearance or non-specific delivery, etc.¹⁹ Thus, the therapeutic index of a pharmacological drug can be improved thanks to drug delivery technologies. These systems are often in the form of a drug carrier, which specifically distributes and protects the active principle from degradation and removal by the reticuloendothelial system (RES).¹⁹

Several examples of such delivery systems have been extensively reported in the literature, which include liposomes,²⁰ polymers²¹ and polymeric micelles,²² peptide based biomaterials,²³ inorganic nanoparticles,²⁴ and gels among others.²⁵ Liposomes are the most common form, investigated as nanocarriers for drug encapsulation. They have a characteristic bilayer assembly mimicking the cellular membrane, are easy-to-prepare and bio-compatible.²⁰ Despite their benefits, liposomes also face several drawbacks, such as the reticuloendothelial clearance and/or immune response.²⁶ A similar behavior has been reported for PEGylated constructs with an augmented immune response after several doses.²⁶ Therefore, there is an emergent and continuous need to discover alternatives for drug delivery strategies to overcome such issues.

In this perspective, it is of particular interest to evaluate engineered MLWV composed of glycolipid biosurfactant and biocompatible polyelectrolyte as a carrier of hydrophobic, as well as hydrophilic, drugs. Both small hydrophilic and hydrophobic drugs have been widely demonstrated that are effective against several diseases, but their therapeutic effect can be limited by the rapid clearance from the systemic circulation or a local site of administration, lipophilicity and therefore lower bioavailability.^{27,28} In this study, the drug-loading and targeting potential of MLWV composed of GC and PLL (**GCPLL MLWV**) is evaluated towards mouse fibroblasts L929, normal human dermal fibroblasts NHDF, macrophages derived THP-1 and human cervical carcinoma HeLa. For this purpose, the encapsulation and mechanism of released curcumin, the active component of *Curcuma longa* plant, which combines lipophilicity, fluorescence but also anticancer properties, are analyzed.^{29,30} In addition **GCPLL MLWV** carriers are also evaluated to deliver other commercial drugs with different degree of lipophilicity.

Experimental

Materials

Microbial glycolipids G-C18:1 are made of a single β -D-glucose hydrophilic headgroup and a C18 fatty acid tail (monounsaturations in positions 9,10). The synthesis of glycolipid G-C18:1 is described in Ref. ³¹, where the typical ¹H NMR spectra and HPLC chromatograms are given. The compound used in this work has a molecular purity of more than 95%. Poly-L-lysine (PLL) hydrobromide ($M_w \approx 1-5$ kDa, $pK_a \sim 10-10.5$)³² is purchased from Sigma-Aldrich. All other chemicals are of reagent grade and are used without further purification. Curcumin (Cur) is purchased from Sigma-Aldrich without further purification. 18:1 Liss Rhod PE: 1,2-dioleoyl-sn-glycero-3-phosphoethanolamine-N-(lissamine rhodamine B sulfonyl) (ammonium salt) (Liss-Rhod) ($M_w = 1301.7$ g/mol, $\lambda_{abs} = 560$ nm, $\lambda_{em} = 583$ nm) is purchased from Avanti Lipids. Lipopolysaccharides (LPS), Phorbol 12-myristate 13-acetate (PMA), paraformaldehyde (PFA), Docetaxel, Paclitaxel and Doxorubicin are purchased from Sigma Aldrich-Merck. DAPI (4',6-Diamidino-2-Phenylindole, Dihydrochloride) is purchased from Life Technologies-ThermoFisher Scientific.

Cell culture

L929 (mouse fibroblast) cells (Merck), HeLa (human cervical carcinoma) cells and NHDF (Normal human dermal fibroblast) (Merck) cells are cultured in Dulbecco's Modified Eagle Medium (DMEM) supplemented with 10% fetal bovine serum (FBS) and 1% penicillin/streptomycin and 1% Amphotericin B. THP-1 (human monocyte) (Promocell) cells are cultured in RPMI 1640 medium supplemented with 10% fetal bovine serum (FBS) and 1% penicillin/streptomycin and 1% Amphotericin B. Cells are cultivated at 37°C and 5% CO₂ under 100% humidity.

Preparation G-C18:1-PLL (**GCPLL**) multilamellar wall vesicles (MLWVs)

GCPLL MLWVs are prepared according to previous work.^{17,18} Stock solutions are prepared by dissolving 5 mg of **GC** or PLL in 1 mL of DMEM cell culture medium supplemented with 10% FBS. Both solutions are raised to pH 10 with NaOH 1 M, a step necessary to solubilize **GC** (micellar phase), and mixed in a 1:1 volume ratio, followed by vortexing. The final concentration of **GC** and PLL is 2.5 mg/mL. pH is then lowered to 7 with HCl 1 M to trigger MLWV formation. The solution is slightly cloudy at pH 7, confirming the presence of MLWV colloids.^{17,18}

Encapsulation of curcumin (**Cur**) in GCPLL (**GCPLL-Cur**)

After the formation of **GCPLL** MLWVs in cell culture medium at pH 7 (once the solution becomes cloudy), an aliquot (10 μ L) of **Cur** from 13.5 mM stock solution prepared in absolute ethanol is added to 1 mL of **GCPLL** solution to reach the final concentration 135 μ M. After vortexing, the suspension is centrifuged at 3000 rpm for 5 min to collect a pellet of **GCPLL-Cur** MLWVs and remove the excess, non-encapsulated, **Cur** in the supernatant. The pellet is resuspended in fresh cell culture medium by vortexing.

Encapsulation of Doxorubicin, Paclitaxel and Docetaxel

As described for Curcumin in the previous paragraph, an aliquot (10 μ L) of drug (Doxorubicin: 1 mg/ml in DMSO; Paclitaxel: 0.1 mg/ml in ethanol; Docetaxel 0.1 mg/ml in

ethanol) were added to **GCPLL** MLWVs following the same protocol of centrifugation and resuspension in fresh cell culture medium by vortexing.

Characterization of the drug loading

The loading capacity (LC %) expressed as a percentage is the ratio: quantity of encapsulated drugs (**Cur**) over the total amount of the delivery vehicles, in this case the weight of **GCPLL** MLWVs.

The encapsulation efficiency (EE %) is calculated by dividing the amount of encapsulated drug by the total amount of drug used during the encapsulation process, expressed as a percentage.

Labelling of GCPLL and GCPLL-Cur with rhodamine (GCPLL-Rhod and GCPLL-Rhod-Cur)

Both **GCPLL** and **GCPLL-Cur** MLWVs are prepared as described above. To their corresponding solution, an aliquot of 10 μ L of 18:1 Liss-Rhod PE in ethanol (4 mg/mL, 3.08 mM) is added to the mixture solution so that the molar **GC**:rhodamine ratio is 200:1. After vortexing, the solution is centrifuged at 3000 rpm for 5 min and the pink pellet is resuspended in fresh cell culture media. 18:1 Liss-Rhod PE is a standard dye labelling lipid bilayers as its lipid backbone intercalates in the lipid bilayer without any perturbation, when the lipid:dye molar ratio ≥ 100 .^{33,34}

Small Angle X-Ray Scattering (SAXS)

pH-resolved *in situ* SAXS experiments are performed at room temperature on the Swing beamline at Soleil Synchrotron (Saint-Aubin, France) during the proposal N° 20190961. The beam energy is $E = 12$ keV and the sample-to-detector (Eiger X 4M) distance is 1.995 m. Silver behenate ($d(100) = 58.38$ Å) is used as standard to calibrate the q -scale. Raw data collected on the 2D detector are integrated azimuthally using the in-house Foxtrot software, provided at the beamline and so to obtain the typical scattered intensity $I(q)$ profile, with q being the wavevector ($q = (4\pi \sin \theta) / \lambda$, where 2θ is the scattering angle and λ is the wavelength). Defective pixels and beam stop shadow are systematically masked before azimuthal integration. Absolute intensity units are determined by measuring the scattering signal of water ($I_{\text{H}_2\text{O}} = 0.0163 \text{ cm}^{-1}$). SAXS profiles are processed with SasView software, version 3.1.2, available at the developer's website (sasview.org).

The experimental setup is reproduced from the Ref.¹⁷ as follows. The sample solution ($V = 1$ mL, $C_{\text{GC}} = C_{\text{PLL}} = 2.5$ mg/mL) in DMEM and pH ~ 11 is contained in an external beaker under stirring at room temperature ($T = 23 \pm 2^\circ\text{C}$). The solution is continuously flushed through a 1 mm glass capillary using an external peristaltic pump. The pH of the solution in the beaker is changed using an interfaced push syringe, injecting microliter amounts of a 0.5 M HCl solution. pH is measured using a micro electrode (Mettler-Toledo) and the value of pH is monitored live and manually recorded from the control room via a network camera pointing at the pH-meter located next to the beaker in the experimental hutch. Considering the fast pH change kinetics, the error on the pH value is ± 0.5 .

Polarized Light Microscopy (PLM)

PLM images are obtained with a transmission Zeiss AxioImager A2 POL optical microscope. A drop of the given sample solution was deposited on a glass slide covered with a

cover slip. The microscope is equipped with a polarized light source, crossed polarizers and an AxioCam CCD camera.

¹H solution nuclear magnetic resonance (NMR)

¹H solution NMR experiments of the various samples are recorded on an AVANCE III Bruker 300 NMR spectrometer using standard pulse programs and a 5 mm ¹H-X BBFO probe. The number of transients is 32 with 7.3 s recycling delay, an acquisition time of 2.73 s, and a receiver gain of 322. Chemical shifts are reported in parts-per-million (δ , ppm) and referenced to the 3-(Trimethylsilyl)propionic-2,2,3,3-d₄ acid sodium salt (TMSP-d₄) (Sigma-Aldrich) peak at 0 ppm at 1 mg/mL (5.8 mM). All samples are prepared by the protocol described above. We have employed a 5 mm NMR tube containing 500 μ L of solution. This solution is obtained by solubilizing the pellet of MLWVs GCPLL in MeOD. This pellet is obtained by centrifugation during 5 min at 3000 rpm. The signals that have been used for calculations are: δ (PLL) = 2.8 ppm (t) and δ (GC) = 2.25 ppm (t). All experiments were performed under the same conditions. (Figures S2-S5).

Dynamic light scattering (DLS) and Zeta potential measurements

Dynamic light scattering measurements (DLS) DLS experiments are performed using a Malvern Zetasizer Nano ZS90 (Malvern Instruments Ltd, Worcestershire, UK) equipped with a 4 mW He–Ne laser at a wavelength of 633 nm. Measurements were made at 25 °C with a fixed angle of 90° and three acquisitions per sample.

Cell viability assay

The impact of GCPLL on cell viability is first assessed using the cell line L929 of mouse fibroblasts to determine the optimal dose enabling optimal cell viability. For this purpose, 5x10⁴ cells/mL are seeded in wells of a 24 well plate and cultivated for 24 hours. Then, different GCPLL MLWV concentrations up to 0.25 mg/ml are added to the fibroblasts L929. Cells are cultivated with GCPLL for another 24-hour period. Besides, fibroblasts are also cultivated in presence of free G-C18:1, PLL and DMEM impacted by pH changes. L929 fibroblasts cultivated in complete medium are used as control samples.

Cell viability is determined by measuring the metabolic activity using Alamar Blue assay. Basically, GCPLL particles are taken out from the wells and L929 cells are rinsed twice with fresh medium. Then, 300 μ L of a resazurin solution at 0.01 % (w/v) in colourless fresh DMEM medium is added to cells and incubated for 4 hours. The supernatant in each well is then collected, diluted with 700 μ L of fresh medium, and the absorbance measured at λ = 570 nm and λ = 600 nm. The percentage of resazurin reduction is calculated following the formula provided by the supplier. Cell metabolic activity of the samples is compared to control samples. The arbitrary value 100 % is given to controls.

After determination of the optimal dose, the antiproliferative activity of GCPLL, GCPLL-Cur and Cur is assessed for 3 different human cell lines: HeLa, Normal Human Dermal Fibroblasts (NHDF) and macrophage derived THP-1 cells.

HeLa and NHDF are seeded 24 hours prior to the experiment in 24-well plates with a density of 5x10⁴ cells/ml and grown under standard conditions (DMEM medium supplemented with 10% fetal bovine serum, 1% penicillin/streptomycin and 1% Anphotericin B at 37°C, 5% CO₂ and 90% humidity). Non adherent THP-1 cells are seeded at a density of 4x10⁵ cells/mL in wells

and incubated for 24 hours with PMA 10 µg/mL in deprived RPMI 1640 medium to differentiate them into adherent macrophage like cells. Then, the cell culture media was replaced by fresh complete RPMI 1640. After 24 hours in culture, the different concentrations of particles are administered to the cells and cells cultured for another 24h. The Alamar Blue colorimetric assay is used for cell viability evaluation for all types of cells as previously described.

Optical fluorescence microscopy

5 x10⁴ cells/well are seeded into a 6 well-plate and grown under standard conditions as previously described. After 24 h, solutions of GCPLL and GCPLL-Cur, analogously GCPLL-Rhod and GCPLL-Rhod-Cur are added at the final concentration of 100 µg/mL and incubated for another 24 h period. Then, samples are rinsed 3 times with PBS, fixed for 1 hour by adding 1 mL of 4% PFA in PBS. After 3 rinses with PBS, cells are incubated for 15 min in a solution of PBS-Tween at 0.2% to permeabilize them. Then, 300 µL/well of DAPI (1/50000) are added and cells incubated for 10 min. Last cells are rinsed 3 times with PBS and kept at 4°C protected from the light until analysis. Cells are observed using a ZEISS fluorescence microscope, equipped with camera AxioCam MRm.

Flow Cytometry Analysis

1x10⁵ cells/well are seeded into a 6 well-plate, cultivated for 24 h, then treated with MLWV particles using a concentration of 100 µg/mL and incubated for another 24 h. Samples for FACS analysis are obtained by detaching cells with 300 µL/well of trypsin for approximately 5 min, and collected within 1 mL of cell culture medium in microfuge tubes. Detached cells are collected in tubes and are centrifuged at 300 g for 5 min. After supernatant removal, the pellet is resuspended in 1 mL of PBS containing 0.5% paraformaldehyde (PFA). Flow Cytometry is performed on a CELESTA SORP flow cytometer (BD Biosciences, Franklin Lakes, NJ, USA). Acquisition gate is set to record 10⁵ events total for each sample.

Confocal laser scanning microscopy

Samples are prepared using the same protocol than that for regular fluorescence microscopy, except cells are cultured in a Thermo Scientific™ Nunc™ Lab-Tek™ II Chamber Slide™ with 2 wells for an optimal visualization.

Analyses are performed in a spinning-disk head X1 (Yokogawa) mounted on a Nikon Eclipse Ti inverted microscope. Cells are observed with a 60x/1.4 Plan Apo objective and a Hamamatsu Orca Flash SCMOS camera.

Results and discussion

GCPLL MLWVs are stable in cell culture medium

Multilamellar wall vesicles only composed of glycolipid biosurfactant **GC** and polyelectrolyte **PLL** have been previously reported to form in mQ-grade water below pH ~ 7.5.^{17,18} Study of their formation in cell culture medium is then a necessary step to develop carriers for biological applications. A typical cell culture medium contains a wide variety of compounds such as salts, glucose and amino acids, but also proteins coming from the supplemented Fetal Bovine Serum (FBS). Such a physicochemical complexity may alter the

charge, composition and/or the pH-range of stability of **GCPLL** MLWV. This latter is prepared by pH modulation as described elsewhere,^{17,18} except for the replacement of water by FBS supplemented DMEM cell culture medium.

SAXS experiments using synchrotron radiation performed during the pH-controlled synthesis process provide the necessary real-time structural information proving the existence of multilamellar structure of the nanocarriers.¹⁷ pH-resolved *in situ* synchrotron SAXS is then performed on the GCPLL system from alkaline to acidic pH in DMEM and the corresponding contour plot between $q=0.1$ and 0.4 \AA^{-1} is shown in Figure 1a.

Below pH 8 and approximately until pH ~ 5 , two sharp diffraction peaks correspond to the first ($q_{(001)}$) and second ($q_{(002)}$) order reflections ($q_{(001)}=0.171 \text{ \AA}^{-1}$, $q_{(002)}=0.341 \text{ \AA}^{-1}$) of the multilamellar wall vesicles MLWV phase (Figure 1a), evolving during pH decrease. This is in full agreement with our previous observations in water.^{17,18} Below pH ~ 5 , a structural gap at $q_{(001)}$ reveals the previously-reported transition between MLWV and a PLL-free lamellar phase composed of GC only, characterized by a peak at $q=0.169 \text{ \AA}^{-1}$.¹⁷ Previously, it was shown that **GCPLL** MLWVs synthesized in H₂O are stable at a pH ranging from 4 to ~ 7.5 (2.5 mg/mL), the exact extreme pH values however depending on experimental conditions, like the GC-to-PLL ratio and possibly the salt content.^{17,18} The present experiment shows that the use of DMEM cell culture medium does not influence at all the formation of **GCPLL** MLWV and it even seems that the domain of pH stability may even be increased to higher pH values (~ 8) than in pure water (~ 7.5) (Figure 1a). Variations in the limits of the pH transition are not unexpected and they can be qualitatively explained as follows. **GCPLL** MLWV are stabilized by attractive electrostatic forces between negatively-charged **GC** and positively-charged **PLL**. If both NMR and ITC experiments have shown that most negative charges are compensated by positive charges,¹⁷ the exact amount of both negative and positive charges varies with pH and ionic strength for both **GC** and **PLL**. In pure water and absence of added salt, the optimal balance of charges for the MLWV phase starts at pH ~ 7.5 ; in DMEM, rich in salt, one expects that the optimal charge balance occurs at higher pH, when part of the higher content of negative charges are counterbalanced by the free cations in solution.

Being multilamellar systems, MLWVs are birefringent under polarized light.¹⁸ Polarized light microscopy (PLM, Figure 1b and Figure S1) images are obtained under white (b1) and polarized light (b2 and b3) with polarizers at 0° - 90° and 45° - 135° respectively. PLM reveals the presence of vesicular structures displaying optical birefringence in the shape of typical maltese cross, colocalized with the vesicle, in agreement with previous work.¹⁸ PLM thereby confirms both the vesicular shape and multilamellar wall structure of GCPLL colloids in solution.

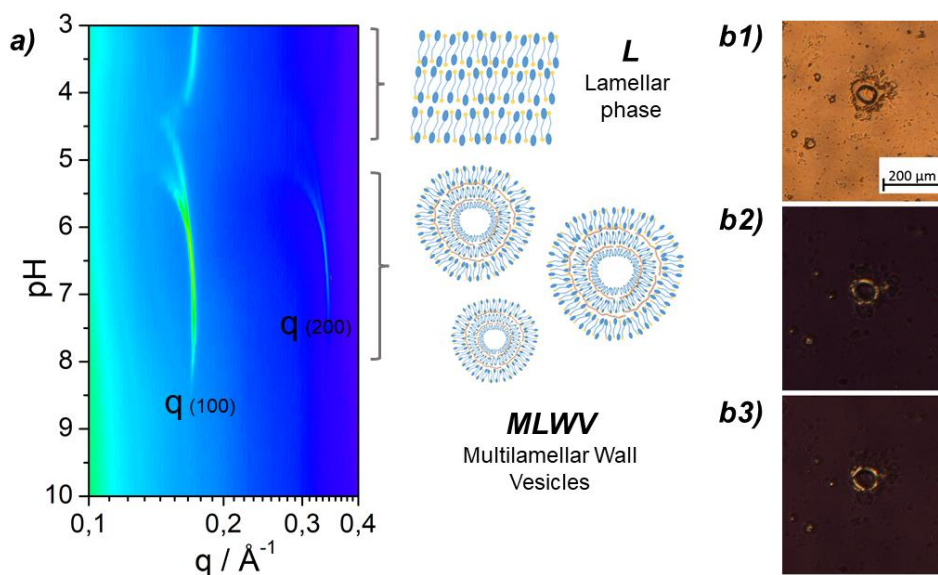


Figure 1. a) Graphical representation of SAXS at different pH values of 2.5 mg/ml of G-C18:1PLL (1:1) in DMEM cell culture medium, where L: Lamellar phase and MLWV: Multilamellar wall vesicles. **b1)** PLM images of GCPLL 2.5 mg/mL in DMEM cell culture medium containing birefringent patterns on the surface evidenced by rotation of the polarizers from 45°–135° (**b2**) to 0–90° (**b3**)

Quantitative ^1H solution NMR, using methanol- d_4 as common solvent, is employed to determine the content of **GC** and **PLL** within MLWVs compared to a reference standard TMSP- d_4 . ^1H NMR spectra show that **GCPLL** MLWVs in H_2O (pH= 5.5) have a molar ratio of molecules consisting of 6.5 % of the initial content of PLL and 70% of the initial content of GC. Otherwise, when **GCPLL** MLWVs are prepared in DMEM cell culture medium (pH = 7.4), one observes a proportional decrease of both PLL and GC molar ratios, 4 and 45 % respectively (Table 1 and Figures S2-S5). A reduced content of both **GC** and **PLL** in DMEM with respect to water samples agrees well with the higher pH at which MLWV formation occurs. As previously measured by SAXS (Figure 1a), MLWVs in DMEM are formed in the pH range 4.5-8, whereas pH 8 constitutes the upper pH limit above which MLWV start to disassemble. It is reasonable to suppose that for pH values close to the limit of pH 8, part of the MLWV have started to disassemble and the composition decreases. This issue could be easily solved by adapting the initial content of **GC** and **PLL**, but this was out of the scope of this work. All in all, this structural analysis shows that the **GCPLL** MLWV prepared as such can be used for biological applications at physiological pH in culture medium. In addition, the final molar ratio GC_f/PLL_f in H_2O and DMEM after preparation of MLWV remains practically constant (57 and 60 respectively). The ratio between COOH and NH_2 functional groups, partially reflecting the charge ratio, is given in Table 1 as $[\text{COOH}]/[\text{NH}_2]$ and one respectively finds 2.8 and 3 for H_2O and DMEM, concluding that the composition of MLWVs is comparable independently of the nature of the aqueous medium.

Table 1. Quantitative evaluation of G-C18:1 and PLL in MLWV by ¹H Solution NMR. Explanation of the calculation is described in Table S1.

	C _{initial} (mM)		C _{final} (mM)		C _f /C _{in} (%)		Molar ratio		Functional group
	[GC] _{in}	[PLL] _{in}	[GC] _f	[PLL] _f	GC _{f/in}	PLL _{f/in}	GC _{in} / PLL _{in}	GC _f / PLL _f	[COOH]/ [NH ₂]
H ₂ O	5.4	1	3.7	0.065	70	6.5	5.4	57	2.8
DMEM	5.4	1	2.4	0.04	45	4	5.4	60	3

GCPLL MLWVs less cytotoxic than GC alone

The cytotoxicity of **GCPLL** MLWVs is not known. This parameter is evaluated in mouse fibroblasts L929 cell line by dilution of the initial 2.5 mg/mL mixture to obtain different concentrations (range from 0 to 1 mg/ml). All the concentrations are referred to as the initial quantity employed in the preparation. As controls, the viability of cells is evaluated after incubation with **GC** and **PLL** independently, as well as the medium at the same pH. The latter corresponds to a **GC**- and **PLL**-free DMEM medium which has undergone the same pH changes required to prepare **GCPLL** MLWVs. These results are shown in Figures S6, S7.

PLL and pH medium controls show no significant cytotoxic effect under the studied conditions. On the contrary, **GC** (Figure S7) has a significant impact on the L929 viability, as only 80 % of the control metabolic activity is measured when C_{GC}= 250 µg/mL is used and dramatically decreases to less than 10% from 500 µg/mL on. Regarding **GCPLL** MLWVs, a cytotoxic effect is observed from 250 µg/mL as the metabolic activity drops to 60%. From 500 µg/mL, only 20% of cells are alive (Figure S6). However, no significant cytotoxicity is observed with C_{GCPLL}= 100 µg/mL.

According to the ¹H solution NMR analysis (Figure S2-5 and Table S1), about 95 % of free PLL and 50% of free GC are detected in a **GCPLL** colloidal solution fabricated with DMEM cell culture medium. For this reason, we suspect that most of the cytotoxic effect of the GCPLL solution is associated to free GC molecules. We then develop an alternative strategy to evaluate the cell viability without the presence of extra **GC** free molecules in solution. **GCPLL** MLWVs are prepared in DMEM as described previously,¹⁸ but they are centrifuged at 3000 rpm for 5 min, then the supernatant is discarded (thus eliminating the free forms of **GC** and **PLL**) and replaced by the same volume of fresh DMEM, prior to their analysis and further use. The **GCPLL** pellet is resuspended by vortexing and sonicating for few seconds, recovering its initial colloidal stability.¹⁸ The latter is most likely explained by surface charge arguments, an important physicochemical parameter that influences the colloidal stability of the suspensions. The zeta-potential of **GCPLL** MLWVs in cell culture medium is found to be of -11.9 ± 0.4 mV, meaning that **GCPLL** MLWVs have a slight negative surface charge, which may prevent aggregation.^{35,36}

The cell viability measured after incubation with **GCPLL** MLWVs after centrifugation is presented in Figure S6, now showing no significant cytotoxicity of **GCPLL** MLWVs up to 250 µg/mL in L929 mouse fibroblast cell line, while the as-prepared MLWVs containing free **GC** exhibits a viability of about 50%. This result confirms that the cytotoxic effect previously found for GCPLL MLWVs is essentially attributable to the free **GC** in solution. Finally, Figure S7 shows no cytotoxicity associated to the controls, that is **PLL** and DMEM, the latter undergone with pH changes as described above. The cytotoxicity of **GCPLL** MLWVs is eventually assessed on several

cell lines (blue bars on Figure 2): macrophages derived THP-1, Normal Human Dermal fibroblasts and HeLa cells. The concentration range settles within the range contained between 20 and 1000 $\mu\text{g}/\text{mL}$, comparable to other drug delivery systems, such as loaded and blank liposomes.^{37–39}

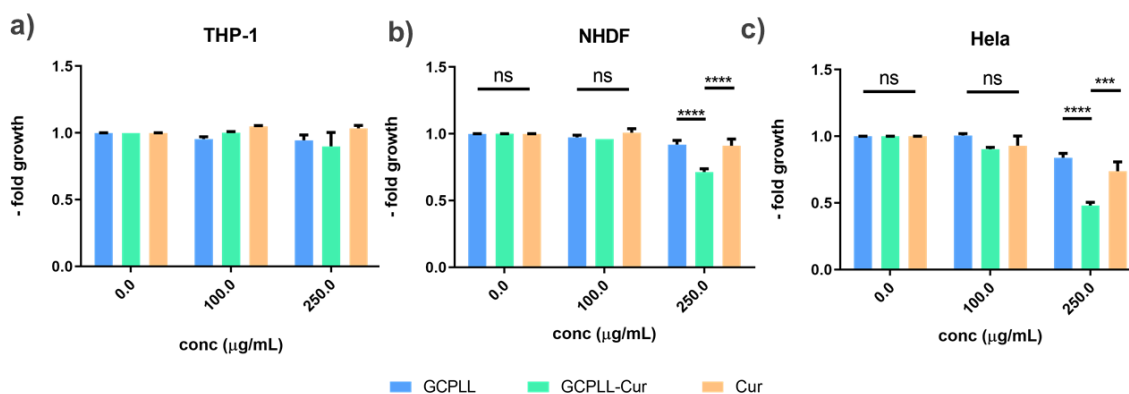


Figure 2. a-c) Cell viability of GCPLL (blue), GCPLL-Cur (green) and Cur (orange) in a) THP-1 cells; b) NHDF cells; and c) HeLa cells. All concentrations herein are referred to the concentrations employed initially in the preparation of GCPLL. In particular: 100 $\mu\text{g}/\text{ml}$ corresponds to 45 $\mu\text{g}/\text{ml}$ GC: 4 $\mu\text{g}/\text{ml}$ PLL and 1.2 $\mu\text{g}/\text{ml}$ Cur (3.25 μM Cur); and 250 $\mu\text{g}/\text{ml}$ corresponds to 112.5 $\mu\text{g}/\text{ml}$ GC: 10 $\mu\text{g}/\text{ml}$ PLL and 3 $\mu\text{g}/\text{ml}$ Cur (8.1 μM Cur), considering the values obtained from ^1H NMR evaluation (Table1).

Curcumin is efficiently encapsulated within MLWVs

The multilamellar lipid structure, the stability of **GCPLL** MLWVs in physiological culture medium and their absence of cytotoxicity make them ideal candidates as phospholipid-free drug delivery system based on biological amphiphiles alone. MLWVs may combine the advantages of drug loading capacity, biodegradability, and biocompatibility based on biosurfactants obtained from microbial source.

Curcumin, the active component of *Curcuma longa* plant, is a molecule widely used as drug due to its antioxidant, anti-inflammatory and anticancer properties.^{29,40} Curcumin is highly lipophilic, with a water-octanol partition coefficient, logP, in the order of 2.6 and a membrane partition constant above 10^4 M^{-1} .³⁰ Similarly to other hydrophobic drugs,⁴¹ curcumin has limited applicability due to its poor oral bioavailability, low chemical stability⁴² as well as its weak cellular uptake.²⁹ As a consequence, the accumulation of curcumin is low within the cytoplasm.^{43,44} The cell uptake process of curcumin has been reported to penetrate the cell membrane and interact with the lipids of the membrane through H-bonding and hydrophobic interactions. Different strategies could be followed to overcome these limitations, such as the synthesis of curcumin derivatives,²⁹ or the development of drug delivery systems to enhance the stability and increase its cellular uptake.⁴⁵

Therefore, curcumin was chosen as model natural drug to load the **GCPLL** system with the aim of probing the encapsulation capacity of MLWVs and to show their potential to enhance the therapeutic index of the encapsulated drug curcumin.

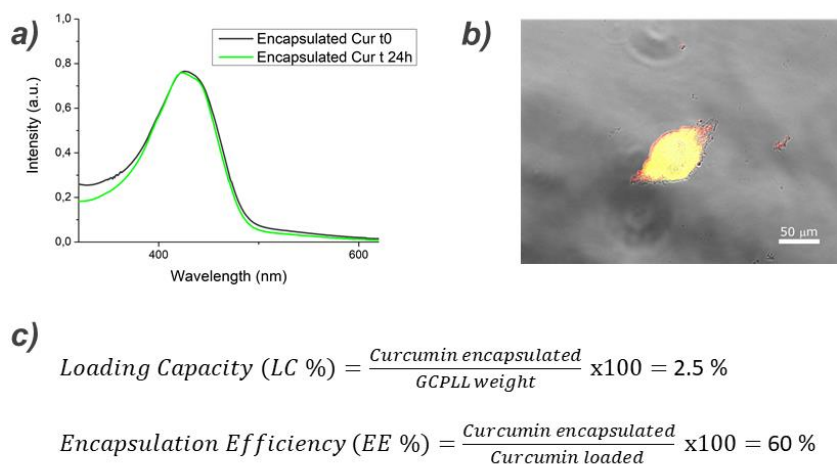


Figure 3. a) UV-Vis spectra of Curcumin encapsulated in GCPLL at t= 0 and t= 24h in DMEM cell culture medium. GCPLL-Cur is centrifuged out and resuspended in ethanol for analysis. b) Fluorescence microscopy image of GCPLL-Rhod-Cur at 2.5 mg/mL in DMEM cell culture medium. Liss-Rhod (red) and Curcumin (green) are loaded within particles. c) Calculation of Loading capacity (LC%) and Encapsulation Efficiency (EE%), where the amount of Cur encapsulated is 30 μg, the loaded quantity 50 μg and the weight of GCPLL 1225 μg considering the values obtained from ¹H NMR evaluation (Table1).

The process of curcumin (**Cur**) encapsulation is based on a straightforward and fast mixture and vortexing protocol described in the experimental section. Addition of **Cur** does not modify the zeta potential of **GCPLL-Cur** MLWVs, which is -13.2 ± 0.3 mV, thus justifying the colloidal stability after resuspension.

UV-vis absorbance measurements are performed to quantify the **Cur** encapsulated in **GCPLL** MLWVs just after fabrication and after 24 hours of incubation in culture medium. (Figure 3a). These experiments involve dissolution of the **GCPLL-Cur** MLWVs pellet in ethanol, a common solvent for all components. The absorption spectra are superimposable, thereby showing that **Cur** is stable within the MLWVs aqueous solution over 24 h. In addition, this result shows that **Cur** is encapsulated in **GCPLL** in its native form. This can be considered as a crucial advantage compared to free **Cur** in solution. Indeed, it has been reported that **Cur** decomposes approximately by 50% in cell culture medium supplemented with 10% serum after 8 hours of incubation.⁴⁶ The encapsulated concentration corresponds to 80 μM **Cur**, and this concentration is calculated using the calibration curve reported in Figure S8.

To exclude coprecipitation and to confirm that **Cur** is actually colocalized in the **GCPLL** MLWVs, we perform fluorescence microscopy on a drop of **GCPLL-Cur** MLWVs solution. **GCPLL** MLWVs are simultaneously labelled with rhodamine using a rhodamine-modified C18:1 lipid (Liss-Rhod PE), known to intercalate in the glucolipid membrane without interfering with the structure for lipid-to-dye molar ratio above 200.⁴⁷ The colocalized fluorescence, red for Liss-Rhod PE and green for **Cur** as well as the DIC white light for GCPLL confirm the encapsulation of Cur within MLWVs, rather than coprecipitation (Figure 3b). Colocalization of Cur (green) and Liss-Rhod PE (red) is also demonstrated within the cellular compartment, as shown and discussed later.

A key parameter to characterize drug delivery systems is the encapsulation efficiency (EE %), defined in the formula given in Figure 3c. EE % is sensitive to different properties related

to each system such as morphology, hydrophobicity, charge of the surface, permeability, the structure of the encapsulated molecule as well as the encapsulation process.^{48,49} Taking into account the molar concentration of **Cur** obtained by UV-Vis (80 μM) and the total loaded Cur (135 μM), one can then calculate the drug loading of this system and finds $\text{EE}\% = 60\%$. This value is higher than other $\text{EE}\%$ estimated for other vesicular systems, which show a high variability, ranging from 1 to 68% for vesicles and 6 to 31% for multilamellar vesicles (MLV).⁵⁰ The broad spectrum of reported $\text{EE}\%$ values between unilamellar vesicles (ULVs) and MLVs is commonly explained by the presence of a lumen in ULVs, allowing a higher loading volume of drug compared to the actual lipid content.⁵⁰ Despite the structure differences, we have reached comparable $\text{EE}\%$ in MLVs compared to ULVs.

The loading capacity (LC %, Figure 3c) is defined as the ratio between the amount of **Cur** encapsulated (30 μg) and the weight of GCPLL system calculated by ^1H NMR (1225 μg). The loading capacity that we obtain for **GCPLL-Cur** is about 2.5% (Figure 3c). In the present case, the two-step preparation protocol of **GCPLL-Cur** may explain the low LC % value: considering that MLWVs are already formed when **Cur** is added, encapsulation may occur only in the outer layers of the MLWVs. The strong discrepancy between LC % and $\text{EE}\%$ may confirm this hypothesis: the drug is mainly encapsulated in the outer lipid layer of the MLWVs, which would involve a good encapsulation process but a low drug-to-lipid content. Different protocols could probably improve both the EE and LC% of Cur, but this is out of the scope of the present work.

Curcumin is selectively delivered to HeLa cells via a membrane-fusion mechanism

The antiproliferative activity of curcumin loaded MLWVs is explored in three different human cell lines (Figure 2a-c): Normal Dermal Human Fibroblasts (NHDF), cervical carcinoma HeLa cells and THP-1 monocyte-derived macrophages.

HeLa cells are chosen as model to evaluate the GCPLLs as drug carriers to target cancer cells, i.e with high proliferative activities. On the opposite, NHDF are used as model of normal cells with moderate proliferative activities to assess the effect of MLWVs with regards to the multiplication potential. Last, THP1 derived macrophages are used in this study to evaluate the targeting of GCPLL toward cancer cells. Macrophages are members of the reticulo endothelial system (RES) and possess high phagocytic activities to clear particles from the human body.

First of all, free **Cur** control (yellow bar) has no toxic effect on THP-1 derived macrophages and NHDF and it only slightly reduces cell viability of HeLa cells for the 250 $\mu\text{g}/\text{mL}$ concentration. Similarly, the **GCPLL** (blue bar) control has no cytotoxic effect neither on THP-1 derived macrophages nor on NHDF, with a slight reduction in cell viability ($>80\%$) on the HeLa cells for the 250 $\mu\text{g}/\text{mL}$ concentration. Finally, the Curcumin-loaded MLWV system, **GCPLL-Cur** (green bar), has no effect on the THP-1, for 100 and 250 $\mu\text{g}/\text{mL}$, and NHDF up 100 $\mu\text{g}/\text{mL}$, while a slight cytotoxicity is measured at 250 $\mu\text{g}/\text{mL}$ (cell viability at about 75%, Figure 2b). Regarding the HeLa cancer cell line, a dramatic effect (50% cell viability) is observed for **GCPLL-Cur** at concentration of 250 $\mu\text{g}/\text{mL}$, when compared to **Cur** (75% cell viability) and **GCPLL** controls (Figure 2c). It is worth noticing that the cytotoxic effect of GCPLL-Cur is greater than that of free curcumin despite a lower cargo. Indeed, the amount of curcumin introduced in the culture well is 60% of the free curcumin dose because of the encapsulation efficiency is 60%.

As the cytotoxic effect of curcumin encapsulated within GCPLL MLWVs is greater in HeLa cells compared to NHDF and macrophages, it seems to be positively correlated with the proliferative

rate of cells. Indeed, cancer cells such HeLa possess a very short doubling time, NHDF have moderate proliferative activities and macrophages derived THP-1 do not proliferate. Liposomal curcumin systems applied in pharmacology,³⁹ in particular the studies of Huang *et al.*⁵¹ employed carboxymethyl dextran (CMD) modifying liposomal curcumin in HeLa cells, reporting an IC_{50} of 6.6 μ M, and in another study by Saengkrit *et al.*⁵² involving curcumin loaded cationic liposomes showed IC_{50} in HeLa and SiHa cells of 21 μ M and 16 μ M, respectively. In comparison with our results, we employed 8.1 μ M loaded curcumin in MLWVs to reach 50 % cytotoxicity in HeLa cells (Figure 2c), which is comparable to CMD IC_{50} in HeLa cells.

These results put in evidence the remarkable activity of **GCPLL-Cur** MLWVs towards cancer cell line HeLa, with little cytotoxic effect in both normal cells, i.e fibroblasts and no dividing cells such as macrophages, thus avoiding the potential damage in normal tissue and the clearance by the reticuloendothelial system (RES), which is dedicated for the foreign particles elimination. Cytotoxicity of curcumin encapsulated within GCPLL MLWVs seems to be correlated, on one side, with the proliferative rate of cells, and on the other side, with the encapsulation efficiency. They are highly toxic for cancer cells which possess a high doubling time but not on no dividing cells such as macrophages.

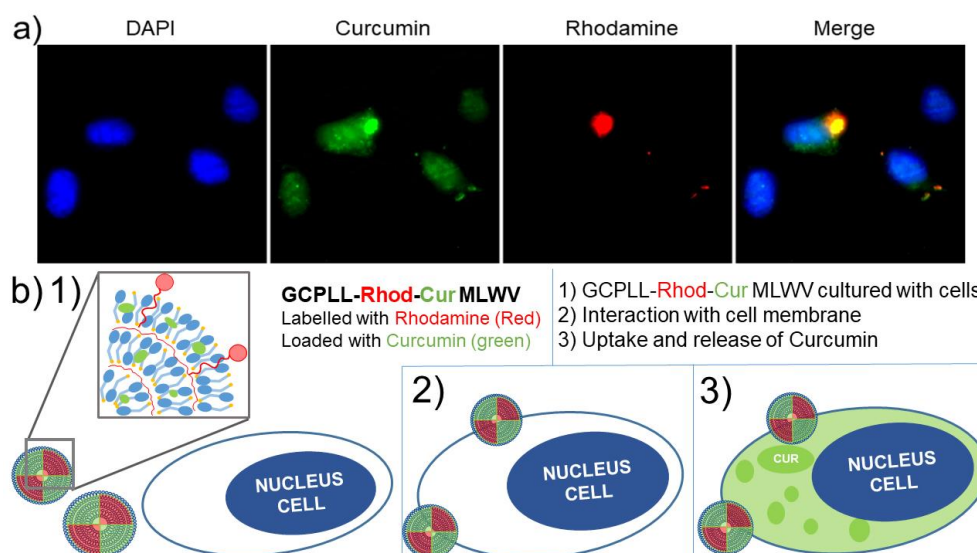


Figure 4. a) Fluorescence microscopy images on HeLa cells treated with GCPLL-Cur 100 μ g/ml and nucleus stained in blue with DAPI, green fluorescence from Curcumin, red from rhodamine and the merged image of the three channels. b) Schematic representation of the uptake mechanism of GCPLL-Rhod-Cur.

To better understand the mechanism of action of the **GCPLL-Cur** MLWVs on HeLa cells, we couple fluorescence (Figure 4) and confocal microscopy (Figure 5, Figures S9-15) with flow cytometry (Figure 5, Figures S16-18). Figure 4a shows three fluorescence microscopy images, each corresponding to different channels: the nucleus (stained with DAPI, blue), **Cur** (green) and **GCPLL** (stained with rhodamine, red). All channels are eventually combined in a fourth image (merge).

Colocalization of curcumin and rhodamine (yellow) in the merge image and presence of green curcumin around the blue nucleus demonstrate the mechanism of cell uptake occurring in HeLa cells. **GCPLL** MLWVs labelled with rhodamine (Liss-Rhod) and loaded with **Cur** penetrate

into the cell membrane and **Cur** is eventually released within the cytoplasm. At the same time, no red fluorescence signal alone is detected inside the cell, meaning that **GCPLL** MLWVs fuse with the cell membrane and deliver **Cur** within the the cytoplasm. A schematic representation of the uptake mechanism is illustrated in Figure 4b.

Figures S9-15 in the supporting information show the fluorescence microscopy images of HeLa, NHDF and THP-1 cells with the corresponding images for control, Cur alone (with and without Liss-Rhod), **GCPLL** (and **GCPLL-Rhod**) and **GCPLL-Cur** (and **GCPLL-Cur-Rhod**). It is worth noticing that fluorescent grains are observed within HeLa cells when they are incubated with **GCPLL-Cur** (Figure S11 and S12, green) and **GCPLL-Cur-Rhod** (Figure S13, red and overlapped green and red respectively). On the opposite, a blurry and weak green fluorescence is detected when free curcumin is used (Figure S11). This shows an accumulation of curcumin within HeLa cells when GCPLL particles are used, thereby evidencing their efficacy to deliver drugs inside the cancer cells. This effect is specific as no granny fluorescence is detected in NHDF or macrophages derived THP-1 (Figure S9, S10, S14, S15).

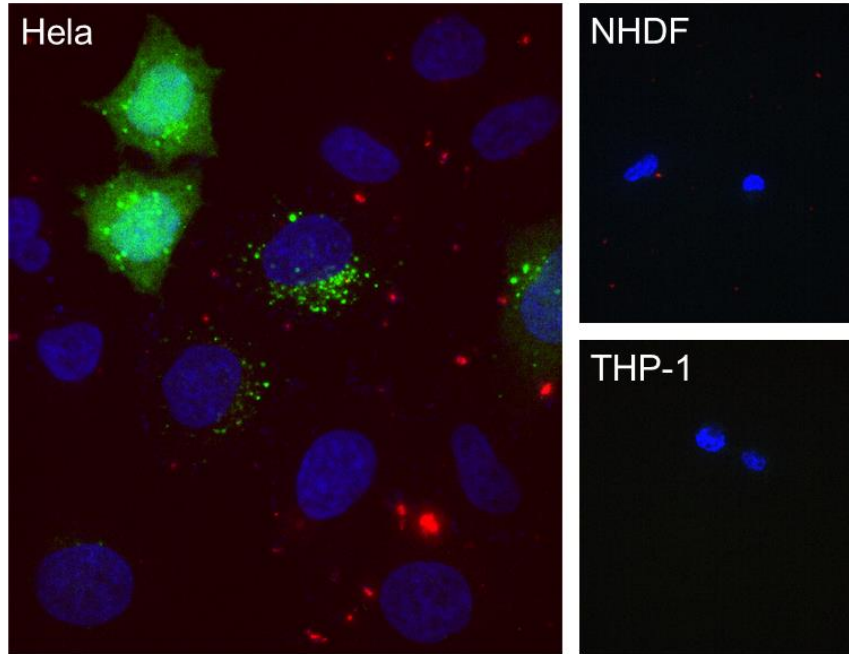
Confocal microscopy imaging in Figure 5a shows images of HeLa, NHDF and THP-1 cells incubated with GCPLL-Cur-Rhod and nucleus stained with DAPI. In addition to HeLa cells, both planes yz and zx were included (Figure S19), which confirms the proposed mechanism: **GCPLL** labelled with rhodamine (red) is localized in the outer part of the cell while **Cur** (green) is released in the cytoplasm of the HeLa cells (Figure 5a) and it surrounds the nucleus (blue).

Flow cytometry measurements of the three different cell lines tested (THP-1, NHDF, and HeLa) are presented in Figure 5b and in the Supporting Information (Figure S16-18) and they evidence different uptake quantities of the MLWVs by measuring the intensity of rhodamine in cells. The results demonstrate that HeLa cells have the highest percentage of rhodamine labelling (41% for **GCPLL-Rhod** and 50% for **GCPLL-Rhod-Cur**), which explains the higher uptake, and therefore higher cytotoxicity, compared to both THP-1 and NHDF, which respectively show a rhodamine signal of 20% and 34% for **GCPLL-Rhod-Cur**.

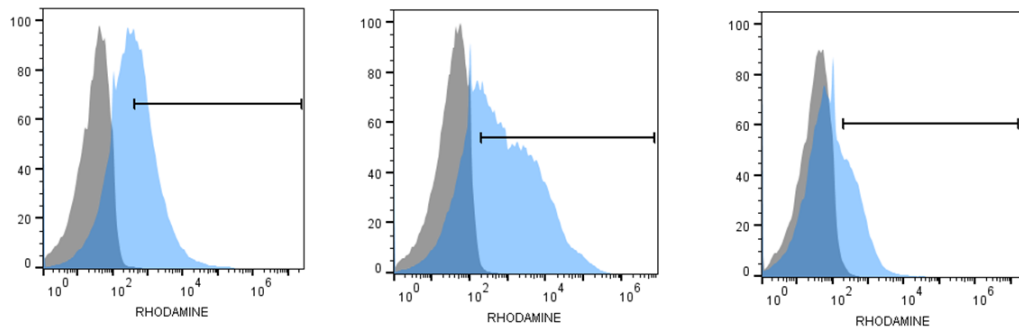
The lipid-based particles can be uptaken by the cells following different cellular mechanisms. Nanoparticles ranging from 50-100 nm can be engulfed by endocytosis, those less than 400 nm by micropinocytosis and micrometric particles can enter the cells by phagocytosis.⁵³ The latter phenomenon is dedicated to immune cells of the reticuloendothelial system such as macrophages and neutrophils. The curcumin loaded MLWVs are poorly engulfed by macrophages, thereby showing phagocytosis is not involved in the intracellular delivery of curcumin. The MLWVs population is quite polydisperse ranging from 10 nm up to 10 μ m. A fraction of particles could be uptaken by macropinocytosis. However, no rhodamine fluorescence, evidencing the presence of micropinocytosis vesicles, is observed within the cellular cytoplasm of NHDF and HeLa cells. Hence, the major mechanism of curcumin delivery seems to be based on MLWVs fuse with the cell membrane. This fusion is much easier in dividing cells as their lipid membrane is more fluid and favors MLWVs interaction. Particle interaction with dividing cells does not seem to depend on the cell doubling time as HeLa and NHDF exhibit the same quantity of cells labeled with rhodamine, as quantified by FACS (Figure 5b). However, the quantity of curcumin delivered within HeLa cells is much larger than that in normal fibroblasts (Figure 5a). Hence the process of fusion is favored by the proliferative activities of cells, which is an asset to target and kill cancer cells. Curcumin toxicity has been improved by its encapsulation in GCPLL MLWVs compared to the free form despite a smaller quantity as the loading efficiency does not exceed 60%.

In addition to FACS and fluorescence microscopy, cell viability results correlate to the higher fluorescence detected of the uptaken Curcumin in HeLa cells than in NHDF (Figure 5a), demonstrating a higher toxicity in HeLa cells than in NHDF cells (Figure 2).

a) GCPLL-Cur-Rhod



b) HeLa NHDF THP-1



Flow cytometry	HeLa	NHDF	THP-1
GCPLL-Rhod	26.4 ± 0.6 %	46.8 ± 2.0 %	15.3 ± 10 %
GCPLL-Rhod-Cur	41.8 ± 9.2 %	33.3 ± 3.0 %	15.8 ± 8.7 %

Figure 5. a) Confocal microscopy images of HeLa, NHDF and THP-1 cells treated with GCPLL-Rhod-Cur 100 µg/mL. Color code: green= Curcumin, red= rhodamine –stained GCPLL MLWV, blue= cell nucleus. b) Flow cytometry FACS data of HeLa, NHDF and THP-1 cells of incubated with 100 µg/mL GCPLL and GCPLL-Cur labelled with Liss-Rhod. Table with mean ± SD values of triplicate of triplicates of GCPLL and GCPLL-Cur both labelled with Liss-Rhod for the three cell lines tested.

In order to extend the encapsulation feasibility of this MLWV system with a wider variety of drugs which display different hydrophobicities, we screened the GCPLL encapsulation and cell cytotoxicity of Doxorubicin ($\log P = 1.41$),⁵⁴ Paclitaxel ($\log P = 3$)⁵⁵ and Docetaxel ($\log P = 2.4$)⁵⁶ in Hela and NHDF cells (Table 2).

Results demonstrated the possibility to exploit the MLWVs with other encapsulated small molecules which provoked a higher cytotoxic effect preferentially over Hela cells than in NHDF for all drug types tested. In the case on Doxorubicin (Dox), there is a great decrease in viability reaching $26.8 \pm 1.6\%$ at $250 \mu\text{g/mL}$ GCPLL-Dox, compared to empty GCPLL $89 \pm 3\%$ in Hela cells, while in NHDF cells there is a slighter decrease in viability being $69.2 \pm 0.9\%$ at $250 \mu\text{g/mL}$ GCPLL-Dox. For Paclitaxel and Docetaxel, both GCPLL loaded systems at $250 \mu\text{g/mL}$ showed a cell viability higher than 65% in NHDF cells. On the contrary, in Hela cells the effect is again increased compared with analogous NHDF experiments. GCPLL-Pac at $250 \mu\text{g/mL}$ is $59.3 \pm 0.5\%$ and GCPLL-Doc at $250 \mu\text{g/mL}$ is $44.3 \pm 1.3\%$. In this last two systems, it is observed a milder effect in the cytotoxicity compared with Doxorubicin experiments.

Cell viability \pm SEM (%)	Hela cells		NHDF cells	
	100 $\mu\text{g/mL}$	250 $\mu\text{g/mL}$	100 $\mu\text{g/mL}$	250 $\mu\text{g/mL}$
GCPLL	93.3 ± 6.9	89.5 ± 3.0	95.9 ± 2.9	98.7 ± 1.3
GCPLL-DOX	66.9 ± 1.8	26.8 ± 1.7	81.3 ± 1.4	69.3 ± 0.9
DOX	38.0 ± 1.2	15.5 ± 0.2	49.1 ± 2.2	53.2 ± 1.2

Cell viability \pm SEM (%)	Hela cells		NHDF cells	
	100 $\mu\text{g/mL}$	250 $\mu\text{g/mL}$	100 $\mu\text{g/mL}$	250 $\mu\text{g/mL}$
GCPLL	98.7 ± 1.8	80.9 ± 2.3	78.3 ± 9.8	65.3 ± 6.6
GCPLL-PAC	98.7 ± 1.2	59.3 ± 0.6	91.6 ± 5.6	77.7 ± 6.2
PAC	39.6 ± 4.0	40.5 ± 4.63	61.3 ± 10.5	51.8 ± 0.8

Cell viability \pm SEM (%)	Hela cells		NHDF cells	
	100 $\mu\text{g/mL}$	250 $\mu\text{g/mL}$	100 $\mu\text{g/mL}$	250 $\mu\text{g/mL}$
GCPLL	99.6 ± 0.3	87.9 ± 6.1	87.5 ± 7.7	57.4 ± 3.0
GCPLL-DOC	79.5 ± 8.1	44.3 ± 1.3	85.5 ± 4.2	67.0 ± 2.0
DOC	37.4 ± 1.2	33.5 ± 2.3	48.0 ± 1.3	49.5 ± 0.1

Table 2. Cell viability data of three different drug experiment tested in Hela and NHDF cells treated with 100 $\mu\text{g/mL}$ and 250 $\mu\text{g/mL}$ of: GCPLL, GCPLL-drug and drug. Being the drugs tested: Doxorubicin (DOX), Paclitaxel (PAC) and Docetaxel (DOC). Table with mean \pm SEM values of triplicate of triplicates.

Conclusions

In this study, stable GCPLL particles have been synthesized in cell culture medium. GCPLL particles exhibit a multilamellar anisotropic structure (MLWVs) at physiological pH observed by in-situ SAXS measurements and polarized light microscopy.

With the aim of evaluating GCPLL as novel drug delivery system, curcumin, used as lipophilic drug model have been efficiently encapsulated within GCPLL. Curcumin loaded GCPLL shows a greater

therapeutic effect towards cancer Hela cells compared to free curcumin. In addition, this cytotoxic impact is exclusive to cancer cells, as no significant effect is observed on normal human dermal fibroblasts NHDF and THP-1 derived macrophages. This suggests that GCPLL-Cur MLWVs would avoid side effects. In addition, this system would increase the circulation time of therapeutic drugs in the bloodstream since GCPLL are not engulfed by macrophages, cells in charge of the clearance of foreign particles *in vivo*. Taken together, these results demonstrate the novel use of biosurfactant based MLWVs assemblies, in particular the GCPLL MLWVs, what opens an alternative composition of drug delivery systems.

5. References

1. Desai, J. D. & Banat, I. M. Microbial production of surfactants and their commercial potential. *Microbiol. Mol. Biol. Rev.* **61**, 47–64 (1997).
2. Rodrigues, L. R. & Teixeira, J. A. Biomedical and therapeutic applications of biosurfactants. *Adv. Exp. Med. Biol.* **672**, 75–87 (2010).
3. Haque, F., Khan, M. S. A. & AlQurashi, N. ROS-Mediated Necrosis by Glycolipid Biosurfactants on Lung, Breast, and Skin Melanoma Cells. *Front. Oncol.* **0**, 253 (2021).
4. Thakur, P. *et al.* Rhamnolipid the Glycolipid Biosurfactant: Emerging trends and promising strategies in the field of biotechnology and biomedicine. *Microb. Cell Factories 2021 201* **20**, 1–15 (2021).
5. Fu, S. L. *et al.* Sophorolipids and Their Derivatives Are Lethal Against Human Pancreatic Cancer Cells. *J. Surg. Res.* **148**, 77–82 (2008).
6. Callaghan, B. *et al.* Lactonic sophorolipids increase tumor burden in Apcmin[±] mice. *PLoS One* **11**, 1–16 (2016).
7. Rodrigues, L. R. Microbial surfactants: Fundamentals and applicability in the formulation of nano-sized drug delivery vectors. *J. Colloid Interface Sci.* **449**, 304–316 (2015).
8. Nakanishi, M., Inoh, Y., Kitamoto, D. & Furuno, T. Nano vectors with a biosurfactant for gene transfection and drug delivery. *J. Drug Deliv. Sci. Technol.* **19**, 165–169 (2009).
9. Sanches, B. C. P. *et al.* Rhamnolipid-based liposomes as promising nano-carriers for enhancing the antibacterial activity of peptides derived from bacterial toxin-antitoxin systems. *Int. J. Nanomedicine* **16**, 925–939 (2021).
10. Ortiz, A. *et al.* Interactions of a bacterial biosurfactant trehalose lipid with phosphatidylserine membranes. *Chem. Phys. Lipids* **158**, 46–53 (2009).
11. Ortiz, A. *et al.* Effects of a bacterial trehalose lipid on phosphatidylglycerol membranes. *Biochim. Biophys. Acta - Biomembr.* **1808**, 2067–2072 (2011).
12. Otzen, D. E. Biosurfactants and surfactants interacting with membranes and proteins: Same but different? *Biochim. Biophys. Acta - Biomembr.* **1859**, 639–649 (2017).
13. Müller, F. *et al.* Rhamnolipids form drug-loaded nanoparticles for dermal drug delivery. *Eur. J. Pharm. Biopharm.* **116**, 31–37 (2017).
14. Baccile, N. *et al.* Self-Assembly Mechanism of pH-Responsive Glycolipids: Micelles, Fibers, Vesicles, and Bilayers. *Langmuir* **32**, 10881–10894 (2016).
15. Baccile, N. *et al.* Self-assembly, interfacial properties, interactions with macromolecules and molecular modelling and simulation of microbial bio-based amphiphiles (biosurfactants). A tutorial review. *Green Chem.* **23**, 3842–3944 (2021).
16. Safinya, C. R. Structures of lipid-DNA complexes: Supramolecular assembly and gene

- delivery. *Curr. Opin. Struct. Biol.* **11**, 440–448 (2001).
17. Seyrig, C. *et al.* Stimuli-induced non-equilibrium phase transitions in polyelectrolyte-surfactant complex coacervates. *Langmuir* **36**, 8839–8857 (2020).
 18. Seyrig, C., Griel, P. Le, Cowieson, N., Perez, J. & Baccile, N. Synthesis of multilamellar walls vesicles polyelectrolyte-surfactant complexes from pH-stimulated phase transition using microbial biosurfactants. *J. Colloid Interface Sci.* **580**, 493–502 (2020).
 19. Majumder, J. & Minko, T. Multifunctional and stimuli-responsive nanocarriers for targeted therapeutic delivery. *Expert Opin. Drug Deliv.* **18**, 205–227 (2021).
 20. Filipczak, N., Pan, J., Yalamarty, S. S. K. & Torchilin, V. P. Recent advancements in liposome technology. *Adv. Drug Deliv. Rev.* **156**, 4–22 (2020).
 21. Kopeček, J. & Yang, J. Polymer nanomedicines. *Advanced Drug Delivery Reviews* vol. 156 40–64 (2020).
 22. Hwang, D., Ramsey, J. D. & Kabanov, A. V. Polymeric micelles for the delivery of poorly soluble drugs: From nanoformulation to clinical approval. *Adv. Drug Deliv. Rev.* **156**, 80–118 (2020).
 23. Varanko, A., Saha, S. & Chilkoti, A. Recent trends in protein and peptide-based biomaterials for advanced drug delivery. *Advanced Drug Delivery Reviews* vol. 156 133–187 (2020).
 24. Luther, D. C. *et al.* Delivery of drugs, proteins, and nucleic acids using inorganic nanoparticles. *Advanced Drug Delivery Reviews* vol. 156 188–213 (2020).
 25. Jain, K. K. An Overview of Drug Delivery Systems. in *Drug Delivery Systems. Methods in Molecular Biology* vol. 2059 1–54 (Humana Press Inc., 2020).
 26. Sercombe, L. *et al.* Advances and challenges of liposome assisted drug delivery. *Frontiers in Pharmacology* vol. 6 286 (2015).
 27. Senapati, S., Mahanta, A. K., Kumar, S. & Maiti, P. Controlled drug delivery vehicles for cancer treatment and their performance. *Signal Transduct. Target. Ther.* **2018 31** **3**, 1–19 (2018).
 28. Li, Q., Li, X. & Zhao, C. Strategies to Obtain Encapsulation and Controlled Release of Small Hydrophilic Molecules. *Front. Bioeng. Biotechnol.* **0**, 437 (2020).
 29. Tomeh, M. A., Hadianamrei, R. & Zhao, X. A review of curcumin and its derivatives as anticancer agents. *International Journal of Molecular Sciences* vol. 20 (2019).
 30. Heger, M., Golen, R. F. Van, Broekgaarden, M. & Michel, M. C. The Molecular Basis for the Pharmacokinetics and Pharmacodynamics of Curcumin and Its Metabolites in Relation to Cancer. *Pharmacol. Rev.* **66**, 222–307 (2014).
 31. Baccile, N. *et al.* PH-Driven Self-Assembly of Acidic Microbial Glycolipids. *Langmuir* **32**, 6343–6359 (2016).
 32. Lewis, S. R. *et al.* Reactive nanostructured membranes for water purification. *Proc. Natl. Acad. Sci.* **108**, 8577–8582 (2011).
 33. Novaira, A. I., Avila, V., Montich, G. G. & Previtali, C. M. Fluorescence quenching of anthracene by indole derivatives in phospholipid bilayers. *J Photochem Photobiol B* **60**, 25–31 (2001).
 34. Leonard-Latour, M., Morelis, R. M. & Coulet, P. R. Influence of Pyrene-Based Fluorescent Probes on the Characteristics of DMPA/DMPC Langmuir-Blodgett Films. *Langmuir* **12**, 4797–4802 (1996).
 35. Patil, S., Sandberg, A., Heckert, E., Self, W. & Seal, S. Protein adsorption and cellular

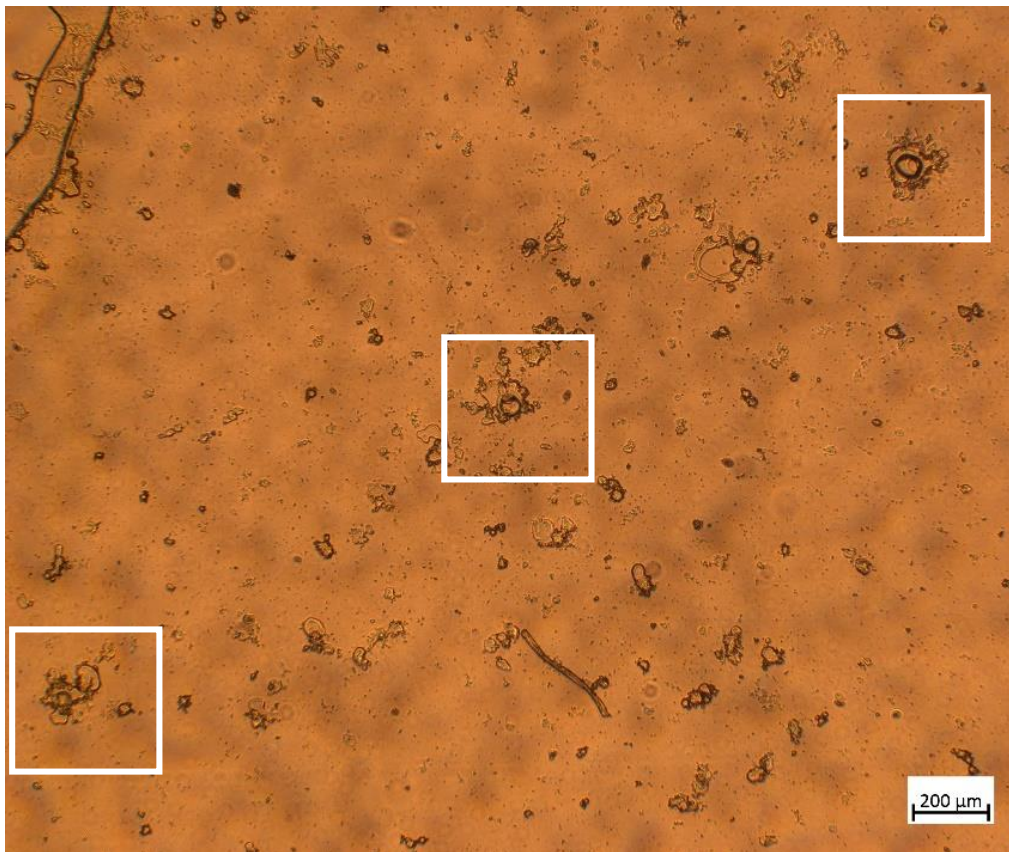
- uptake of cerium oxide nanoparticles as a function of zeta potential. *Biomaterials* **28**, 4600–4607 (2007).
36. Puttipipatkachorn, S., Nunthanid, J., Yamamoto, K. & Peck, G. E. Drug physical state and drug-polymer interaction on drug release from chitosan matrix films. *J. Control. Release* **75**, 143–153 (2001).
 37. Nandi, U., Onyesom, I. & Douroumis, D. An in vitro evaluation of antitumor activity of sirolimus-encapsulated liposomes in breast cancer cells. *J. Pharm. Pharmacol.* **73**, 300–309 (2021).
 38. Wang, W. *et al.* Flexible liposomal gel dual-loaded with all-trans retinoic acid and betamethasone for enhanced therapeutic efficiency of psoriasis. *J. Nanobiotechnology* **18**, (2020).
 39. Feng, T., Wei, Y., Lee, R. J. & Zhao, L. Liposomal curcumin and its application in cancer. *Int. J. Nanomedicine* **12**, 6027–6044 (2017).
 40. Goel, A., Kunnumakkara, A. B. & Aggarwal, B. B. Curcumin as ‘Curecumin’: From kitchen to clinic. *Biochem. Pharmacol.* **75**, 787–809 (2008).
 41. Kalepu, S. & Nekkanti, V. Insoluble drug delivery strategies: Review of recent advances and business prospects. *Acta Pharmaceutica Sinica B* vol. 5 442–453 (2015).
 42. Quitschke, W. W. Differential solubility of curcuminoids in serum and albumin solutions: Implications for analytical and therapeutic applications. *BMC Biotechnol.* **8**, 84 (2008).
 43. Barry, J. *et al.* Determining the effects of lipophilic drugs on membrane structure by solid-state NMR spectroscopy: The case of the antioxidant curcumin. *J. Am. Chem. Soc.* **131**, 4490–4498 (2009).
 44. Tsukamoto, M., Kuroda, K., Ramamoorthy, A. & Yasuhara, K. Modulation of raft domains in a lipid bilayer by boundary-active curcumin. *Chem. Commun.* **50**, 3427–3430 (2014).
 45. Karthikeyan, A., Senthil, N. & Min, T. Nanocurcumin: A Promising Candidate for Therapeutic Applications. *Front. Pharmacol.* **0**, 487 (2020).
 46. Wang, Y. J. *et al.* Stability of curcumin in buffer solutions and characterization of its degradation products. *J. Pharm. Biomed. Anal.* **15**, 1867–1876 (1997).
 47. Ben Messaoud, G. *et al.* Single-Molecule Lamellar Hydrogels from Bolaform Microbial Glucolipids. *Soft Matter* **16**, 2528–2539 (2020).
 48. Nicholas, A. R., Scott, M. J., Kennedy, N. I. & Jones, M. N. Effect of grafted polyethylene glycol (PEG) on the size, encapsulation efficiency and permeability of vesicles. *Biochim. Biophys. Acta - Biomembr.* **1463**, 167–178 (2000).
 49. Kulkarni, S. B., Betageri, G. V. & Singh, M. Factors affecting microencapsulation of drugs in liposomes. *J. Microencapsul.* **12**, 229–246 (1995).
 50. Sun, B. & Chiu, D. T. Determination of the encapsulation efficiency of individual vesicles using single-vesicle photolysis and confocal single-molecule detection. *Anal. Chem.* **77**, 2770–2776 (2005).
 51. Huang, Q. *et al.* Coating of carboxymethyl dextran on liposomal curcumin to improve the anticancer activity. *RSC Adv.* **4**, 59211–59217 (2014).
 52. Saengkrit, N., Saesoo, S., Srinuanchai, W., Phunpee, S. & Ruktanonchai, U. R. Influence of curcumin-loaded cationic liposome on anticancer activity for cervical cancer therapy. *Colloids Surfaces B Biointerfaces* **114**, 349–356 (2014).

53. Manzanares, D. & Ceña, V. Endocytosis: The Nanoparticle and Submicron Nanocompounds Gateway into the Cell. *Pharm.* 2020, Vol. 12, Page 371 12, 371 (2020).
54. Doxorubicin hydrochloride | DrugBank Online.
55. Paclitaxel: Uses, Interactions, Mechanism of Action | DrugBank Online.
56. Docetaxel: Uses, Interactions, Mechanism of Action | DrugBank Online.

Glycolipid Biosurfactants as Multilamellar Vesicular Drug Carriers

Supporting Information

PLM



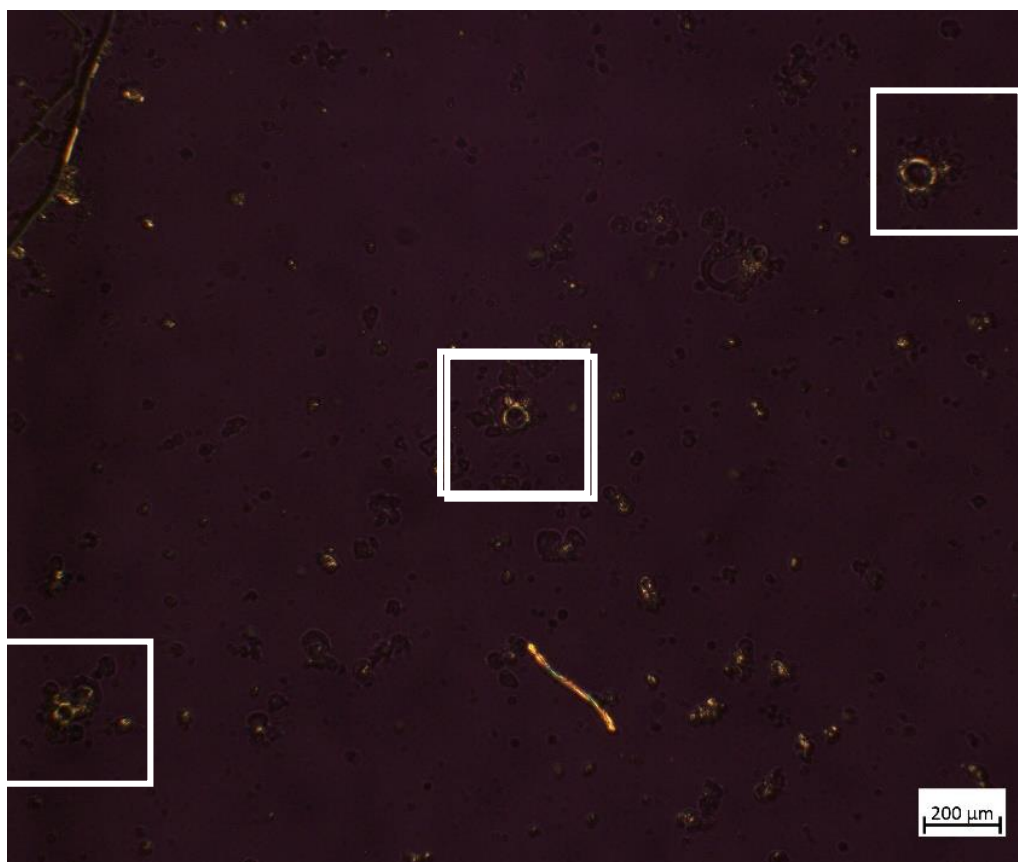
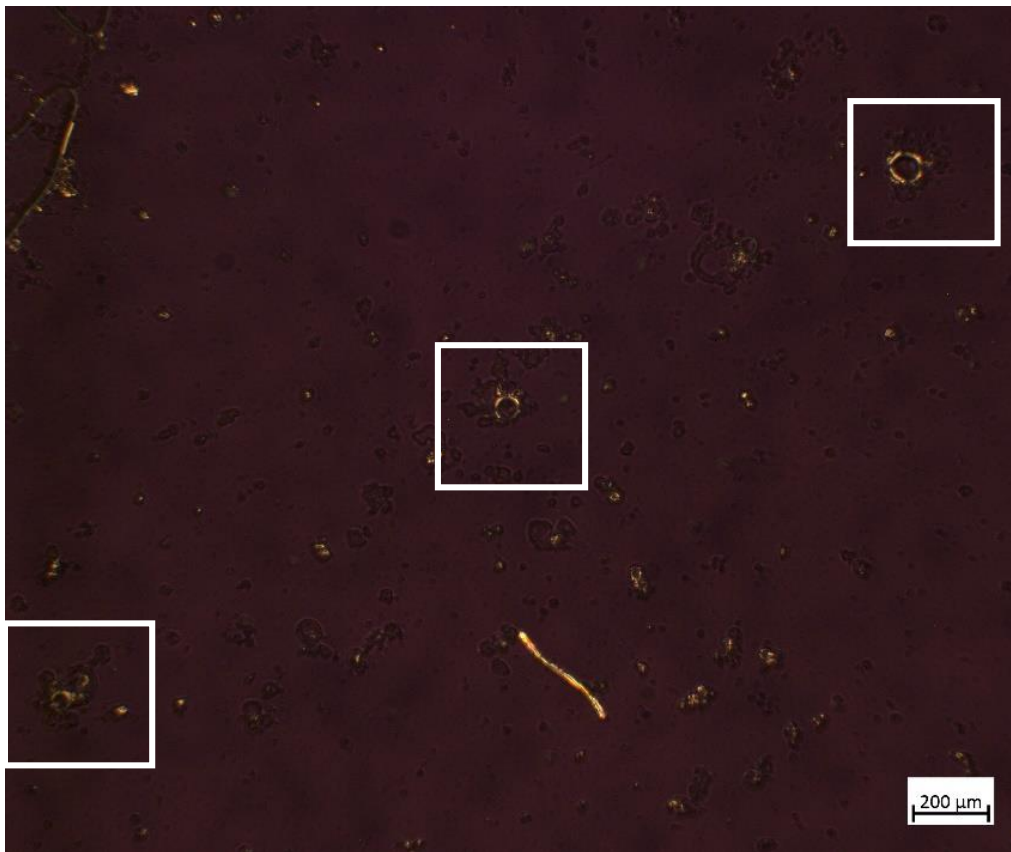


Figure S1. PLM images of GCPLL 2.5 mg/mL in DMEM cell culture media containing birefringent patterns on the surface evidenced by rotating the polarizers from 45°–135° (b) to 0–90°(c).

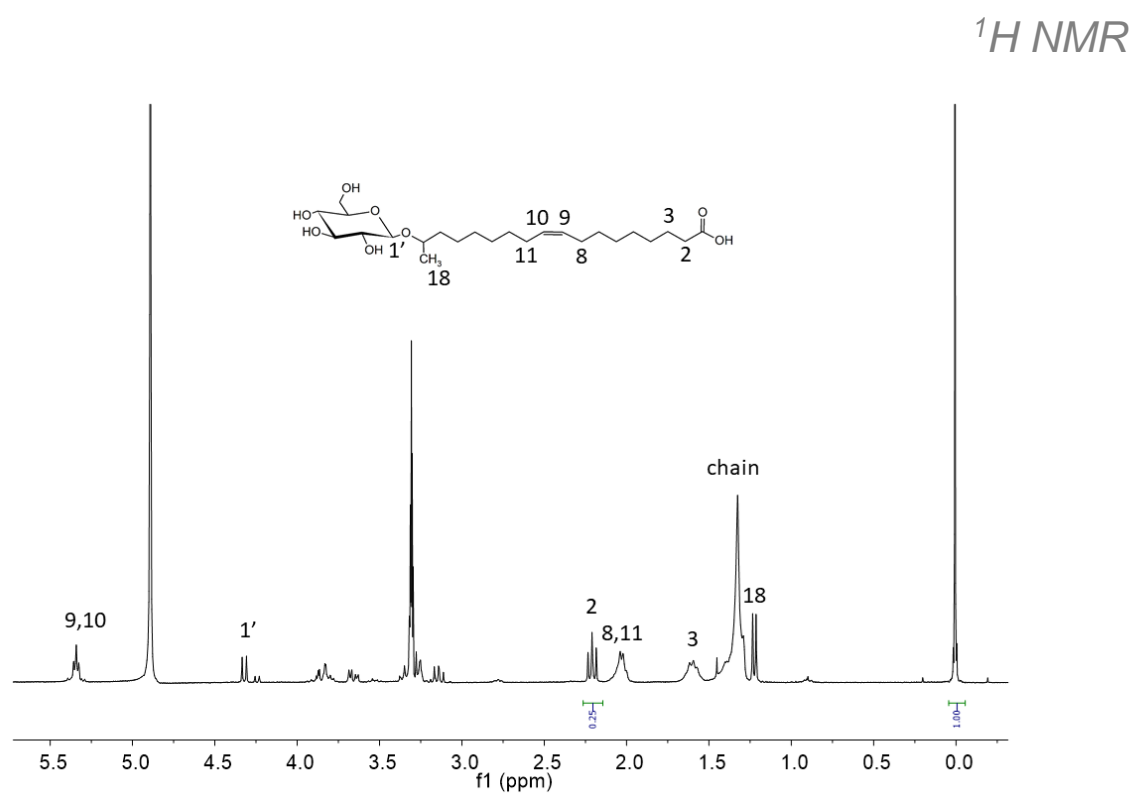


Figure S2. ¹H NMR of control GC in methanol-d₄.

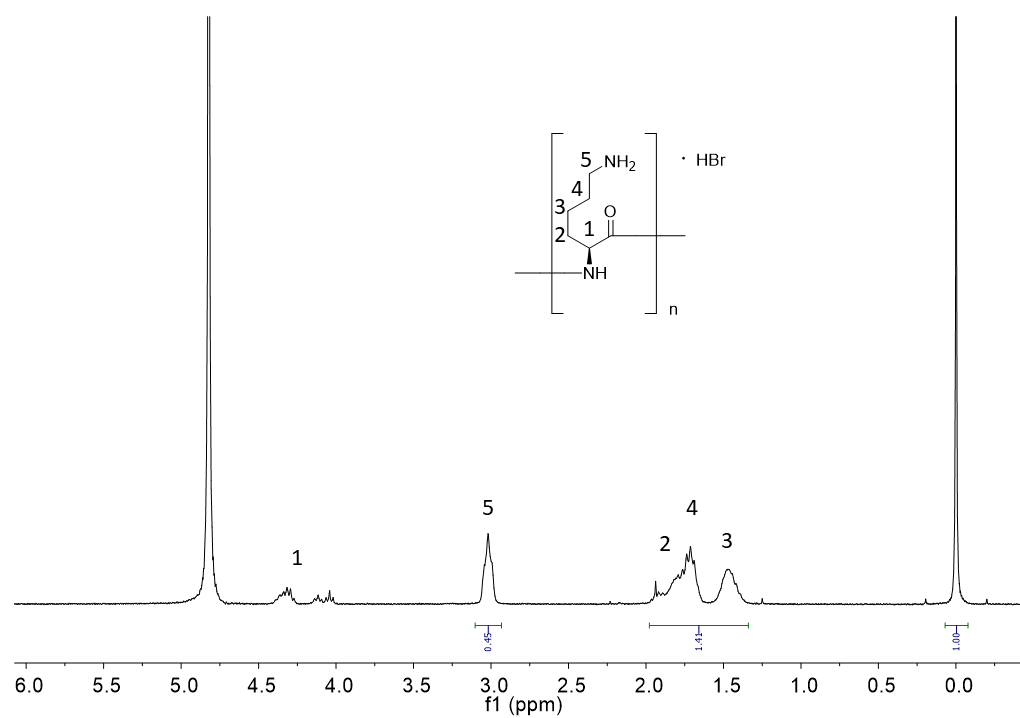


Figure S3. ¹H NMR of control PLL in D₂O.

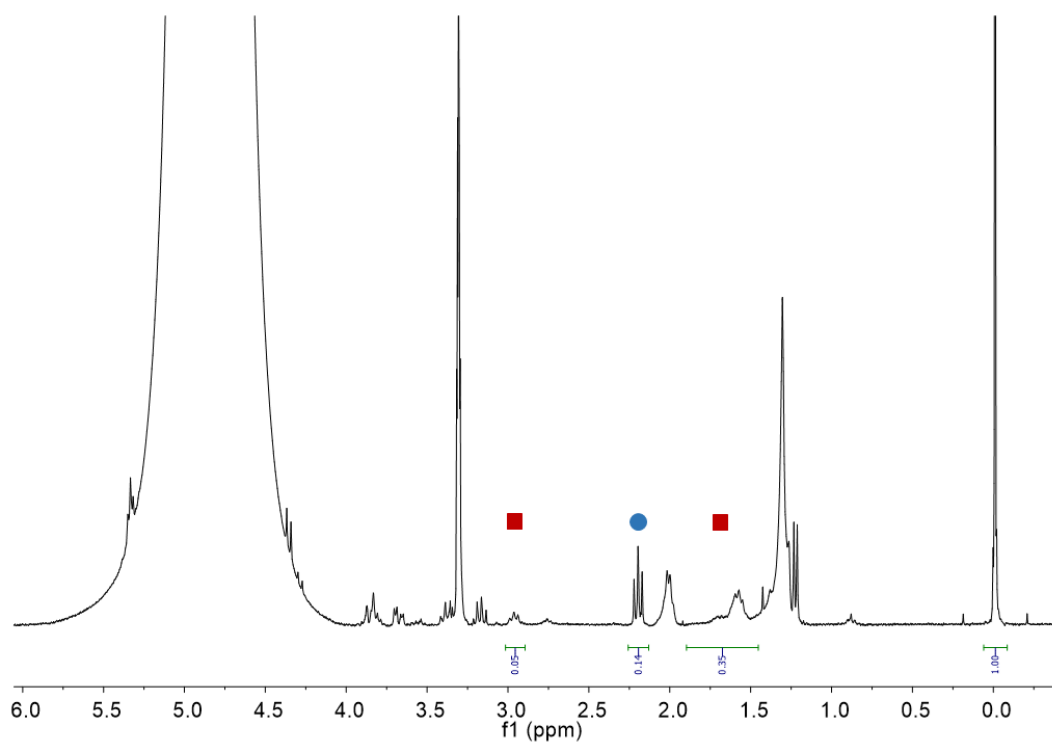


Figure S4. ¹H NMR from sample GCPLL in H₂O, centrifuged pellet and dissolved in methanol-d₄, where peaks assigned with ■ and ● correspond to PLL and GC, respectively.

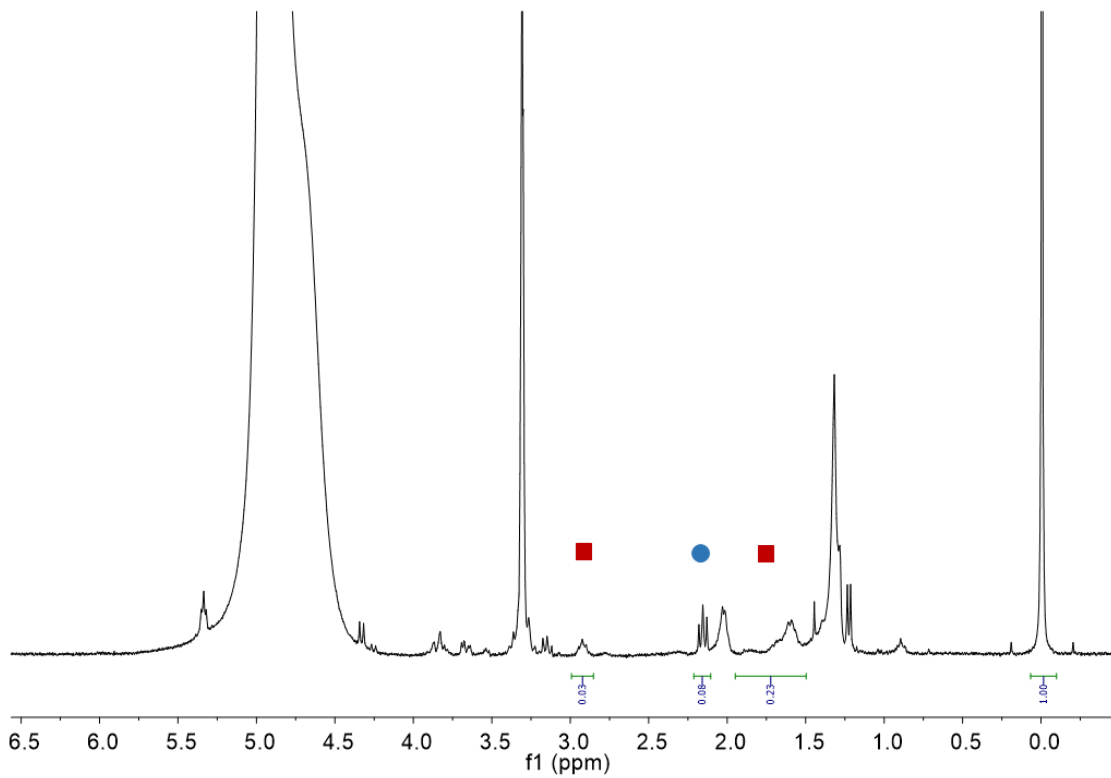


Figure S5 ^1H NMR from sample GCPLL in DMEM, centrifuged and dissolved in methanol- d_4 , where peaks assigned with \blacksquare and \bullet correspond to PLL and GC, respectively.

Table S1. Quantitative analysis of the integrals corresponding to the ^1H NMR spectra of the GCPLL prepared in H_2O (pH 5) and DMEM cell culture media (pH 7.5) and the resulting pellet dissolved in MeOD-d_4 , shown in Figures S2-5. PLL is represented by the $(\text{RCH}_2\text{NH}_2)_x$ (where $x \sim 20$) peak at $\delta = 2.8$ ppm. The M_w (PLL) $\approx 1\text{-}5\text{ kDa}$, then we consider an average M_w (PLL) $= 2.5\text{ kDa}$, whereas the M_w of each monomer is 128 g/mol , yielding an average of 20 monomers per PLL chain. The valence of the $(\text{RCH}_2\text{NH}_2)_x$ ($x \sim 20$) peak is then taken as 40. G-C18:1 is represented by the $\text{RCH}_2\text{C}=\text{O}$ peak at $\delta = 2.2$ ppm. The M_w (G-C18:1) $= 460\text{ g/mol}$ and each G-C18:1 bears a single COOH group. The valence of the $\text{RCH}_2\text{C}=\text{O}$ peak is then taken as 2. The peak at $\delta = 0$ ppm corresponds to the reference ($\text{TMSP-d}_4, 1\text{ mg}\cdot\text{mL}^{-1} \equiv 5.8\text{ mM}$), having a valence of 9.

	Integrals			C_{initial} (mM)		C_{final} (mM)		$C_{\text{F}}/C_{\text{In}}$ (%)		Molar ratio		Functional group
	GC (2H)	PLL (40H)	TMSP-d4 (9H)	$[\text{GC}]_{\text{in}}$	$[\text{PLL}]_{\text{in}}$	$[\text{GC}]_{\text{f}}$	$[\text{PLL}]_{\text{f}}$	$\text{GC}_{\text{f/in}}$	$\text{PLL}_{\text{f/in}}$	$\text{GC}_{\text{in}}/\text{PLL}_{\text{in}}$	$\text{GC}_{\text{f}}/\text{PLL}_{\text{f}}$	$[\text{COOH}]/[\text{NH}_2]$
H_2O	0.14	0.05	1	5.4	1	3.7	0.065	70	6.5	5.4	57	2.8
DMEM	0.09	0.03	1	5.4	1	2.4	0.04	45	4	5.4	60	3

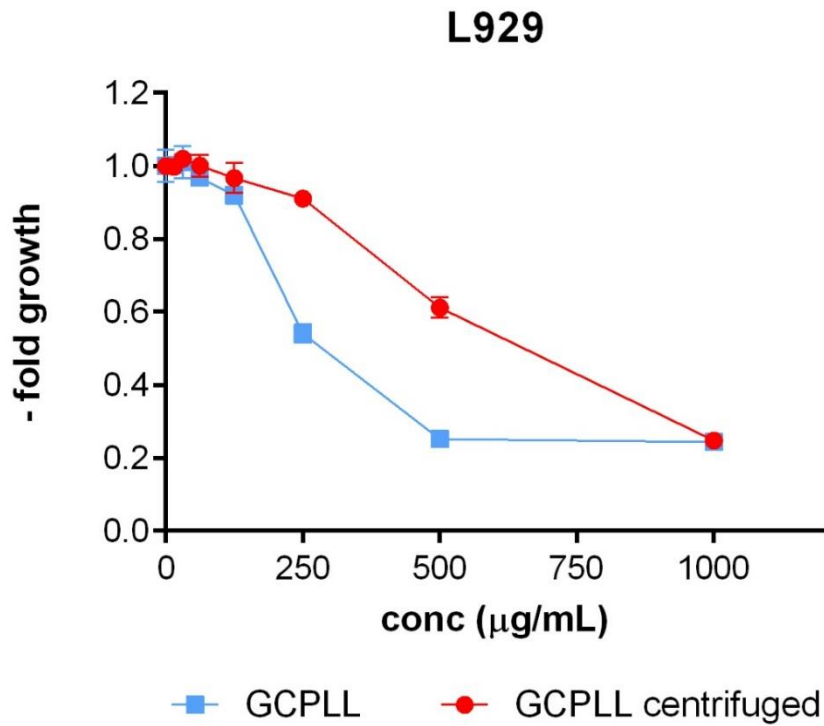


Figure S6. Cell viability comparison of both GCPLL and GCPLL centrifugated at 3000 rpm during 5 min and resuspended with new cell culture media on L929 fibroblasts mouse cell line.

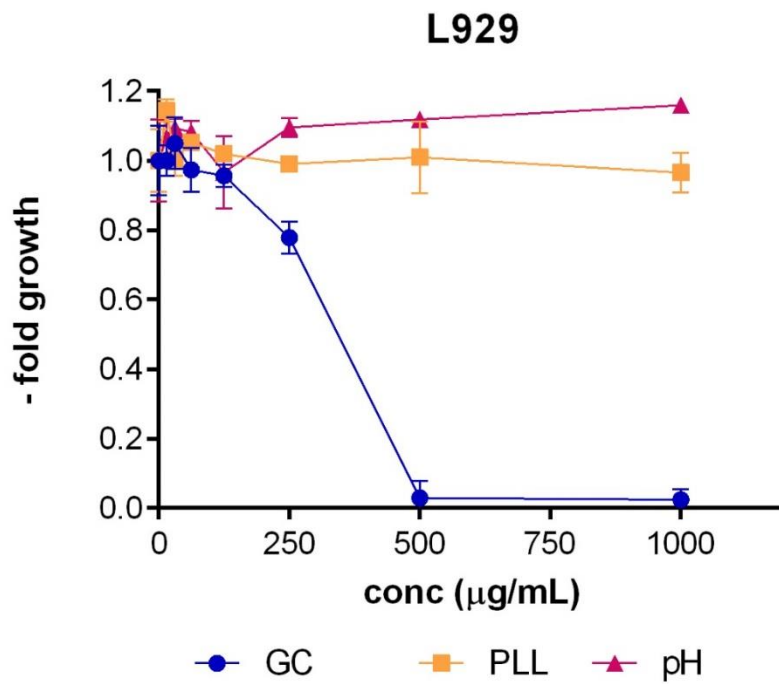


Figure S7. Cell viability of DMEM cell culture medium altered with changes in pH, glucolipid GC18:1 (GC) and poly-L-lysine (PLL) on L929 fibroblasts mouse cell line.

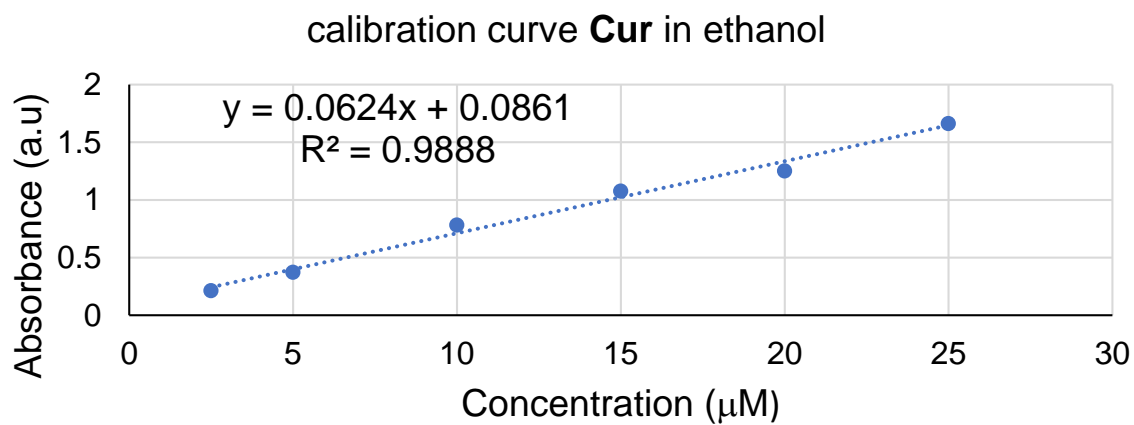
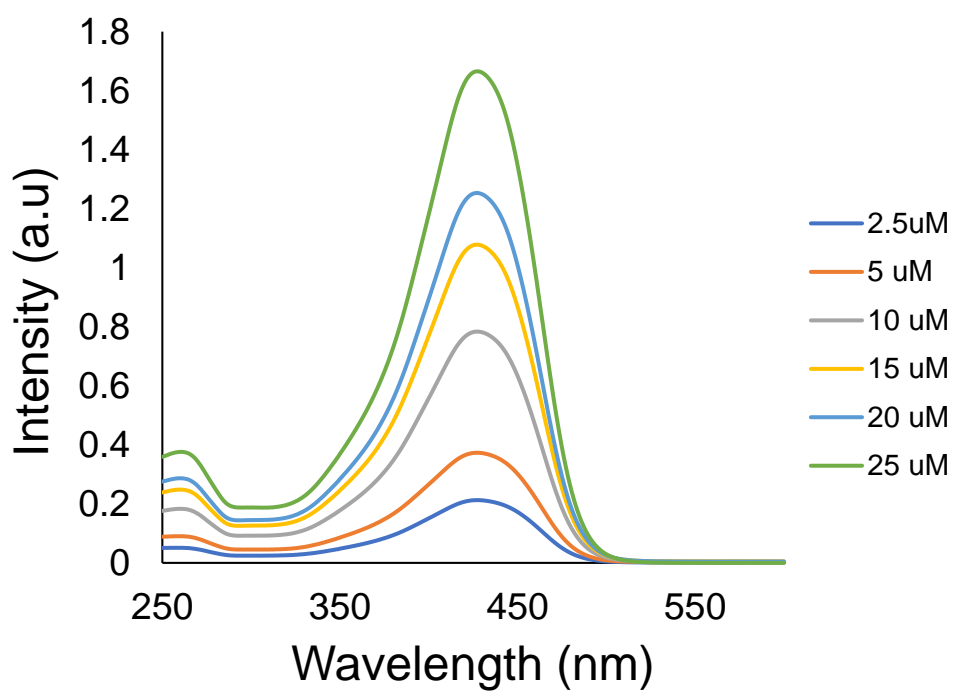


Figure S8. UV-Vis spectra of the calibration curve of Curcumin in ethanol.

Fluorescence Microscopy

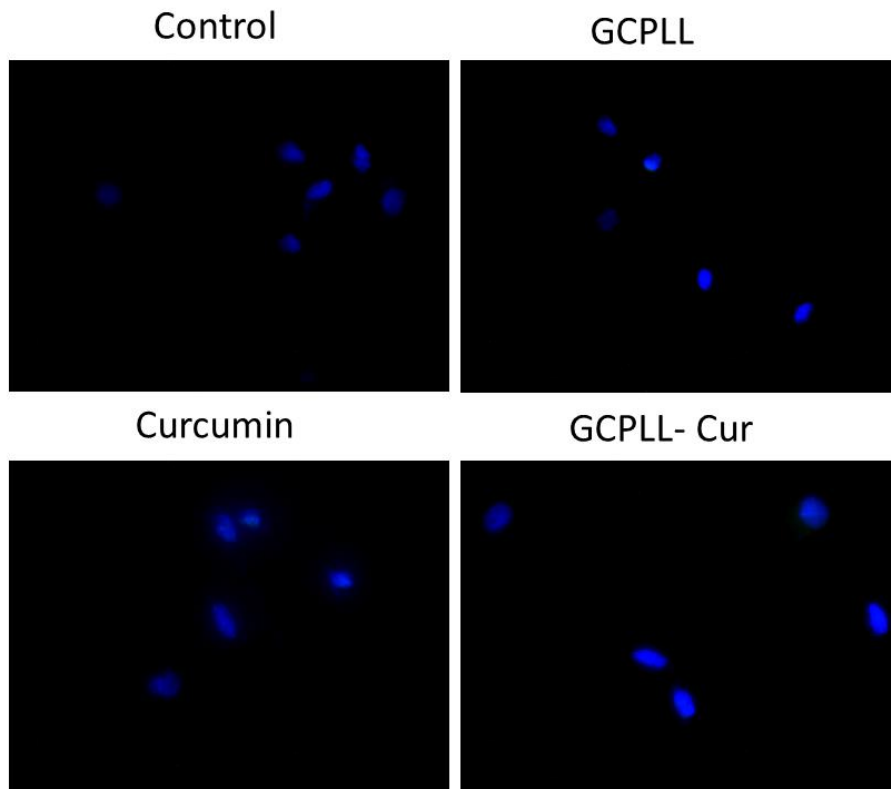


Figure S9. Fluorescence microscopy of **NHDF** cells stained with DAPI dye for nucleus.

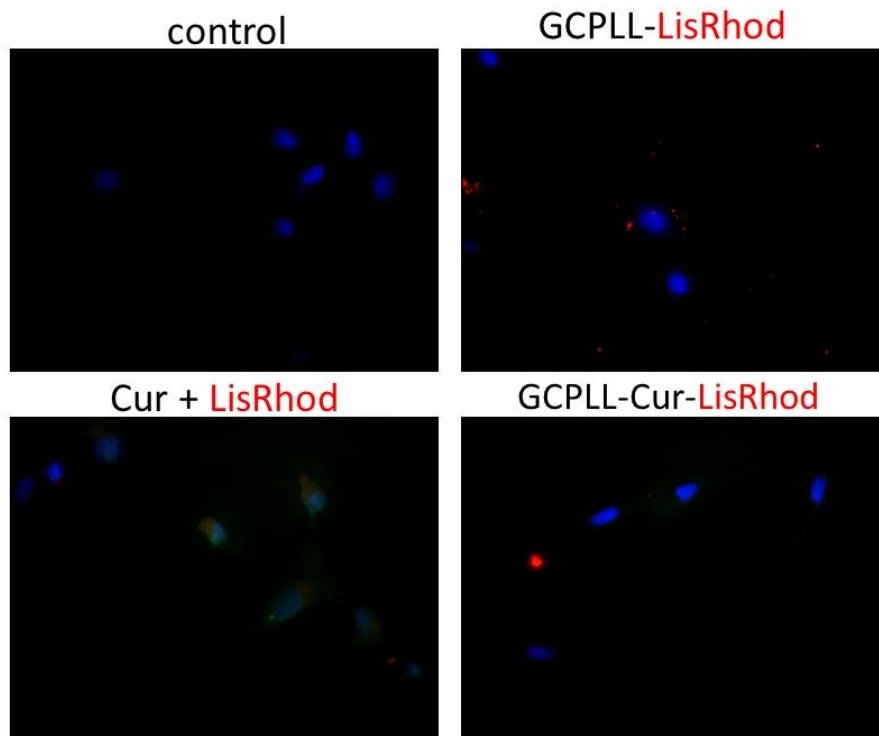


Figure S10. Fluorescence microscopy of **NHDF** cells stained with DAPI dye for nucleus and GCPLL labelled with Rhodamine-lipid (Liss-Rhod).

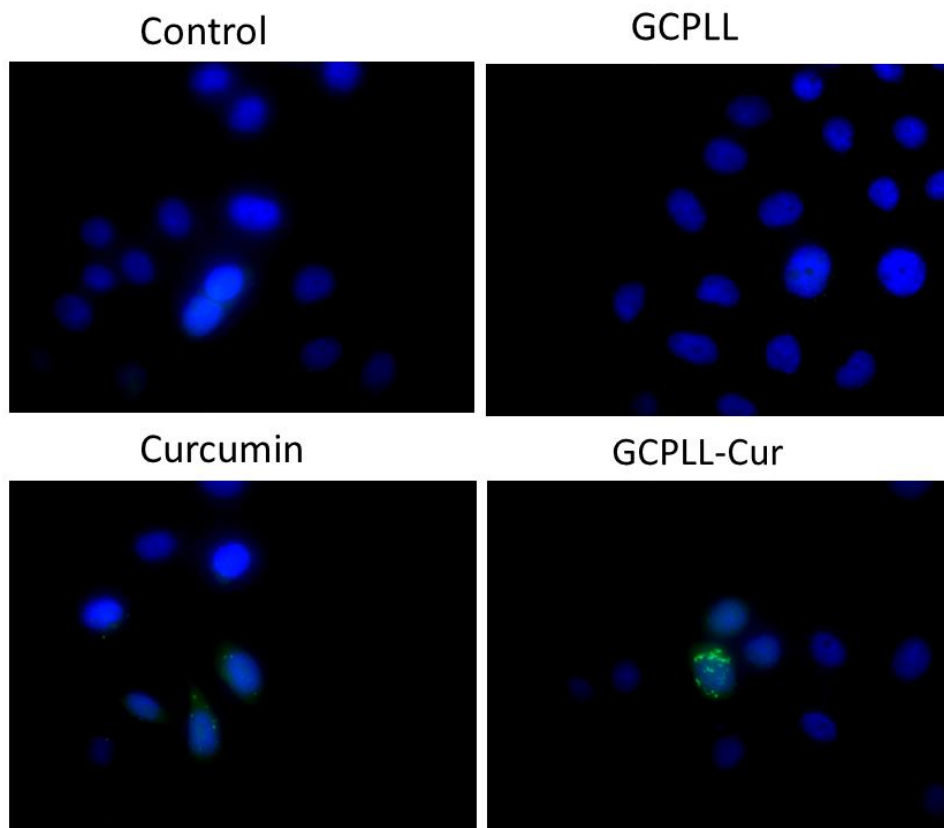


Figure S11. Fluorescence microscopy of **HeLa** cells stained with DAPI dye for nucleus.

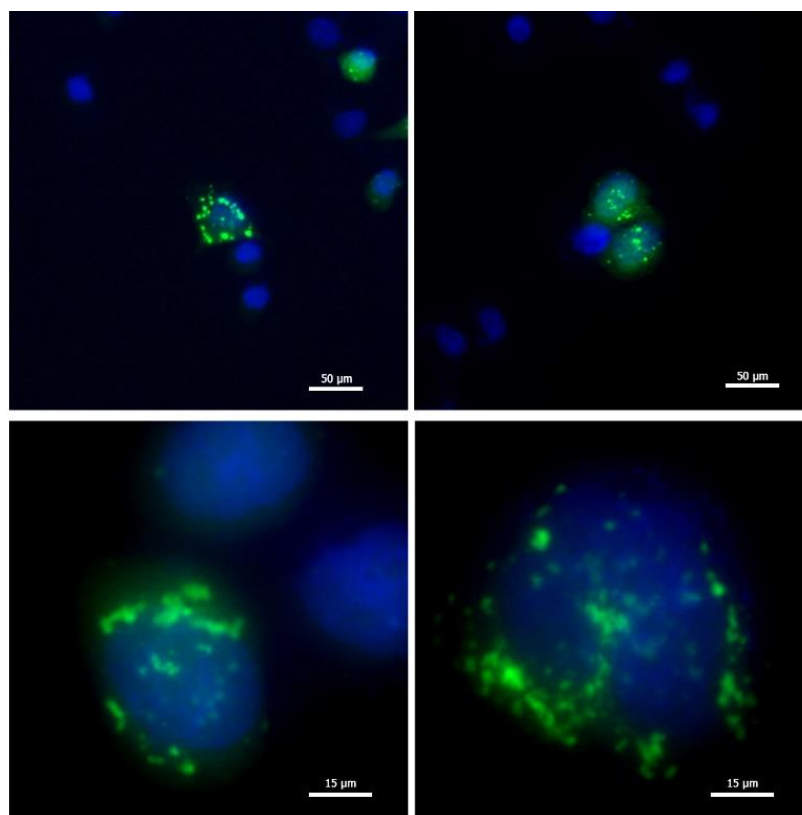


Figure S12. Fluorescence microscopy zoom images of **HeLa** cells stained with DAPI dye for nucleus after administration with GCPLL-Cur.

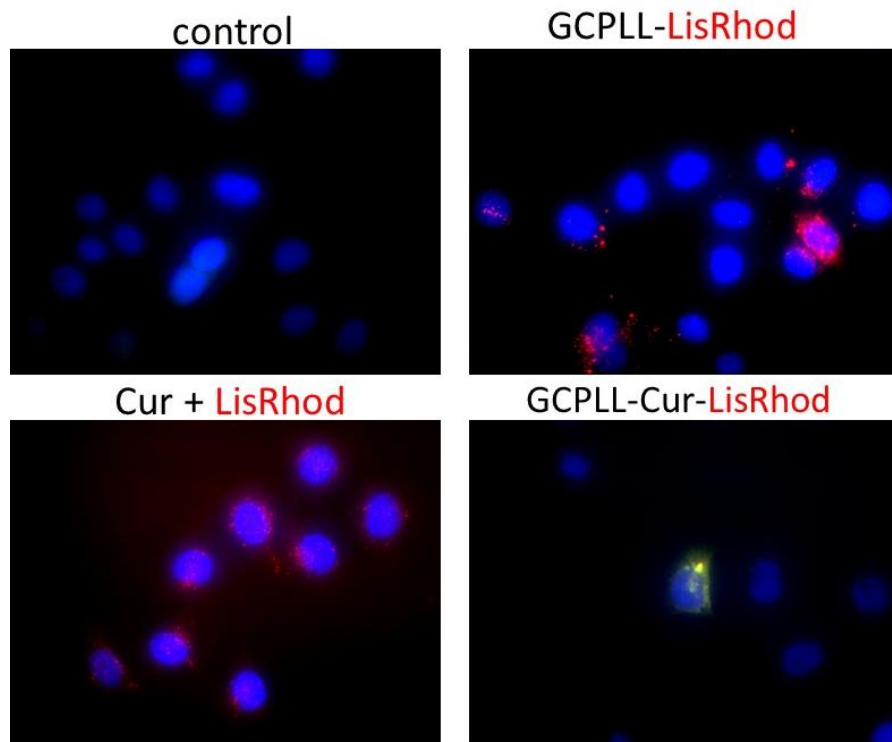


Figure S13. Fluorescence microscopy of **HeLa** cells stained with DAPI dye for nucleus and GCPLL labelled with Rhodamine-lipid (Liss-Rhod).

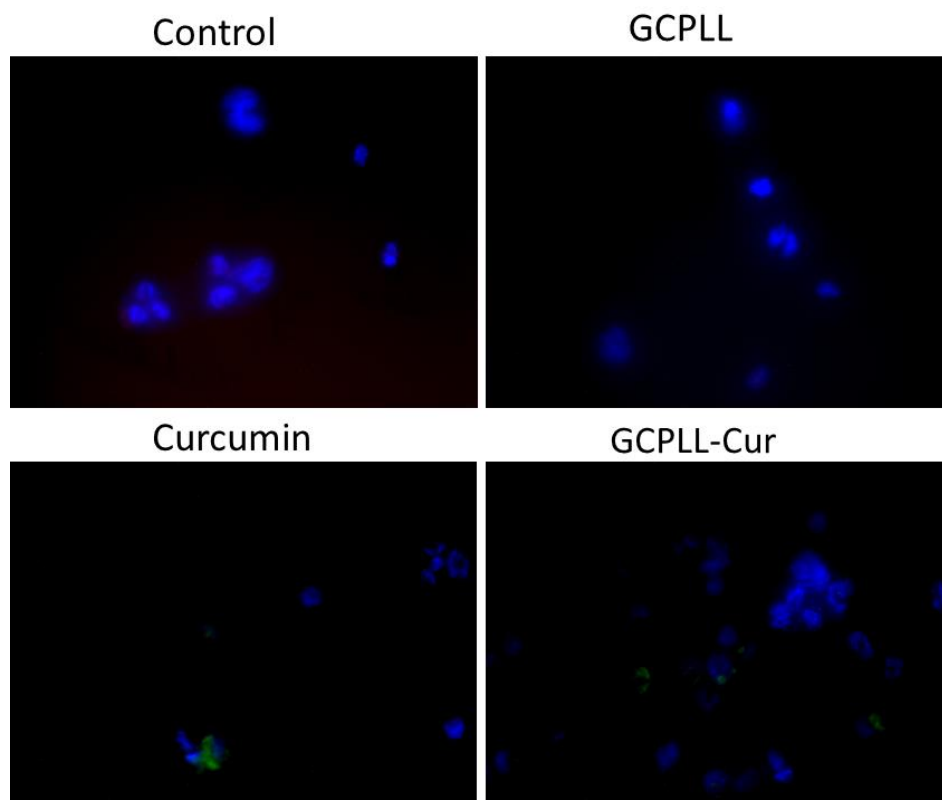


Figure S14. Fluorescence microscopy of **THP-1** cells stained with DAPI dye for nucleus.

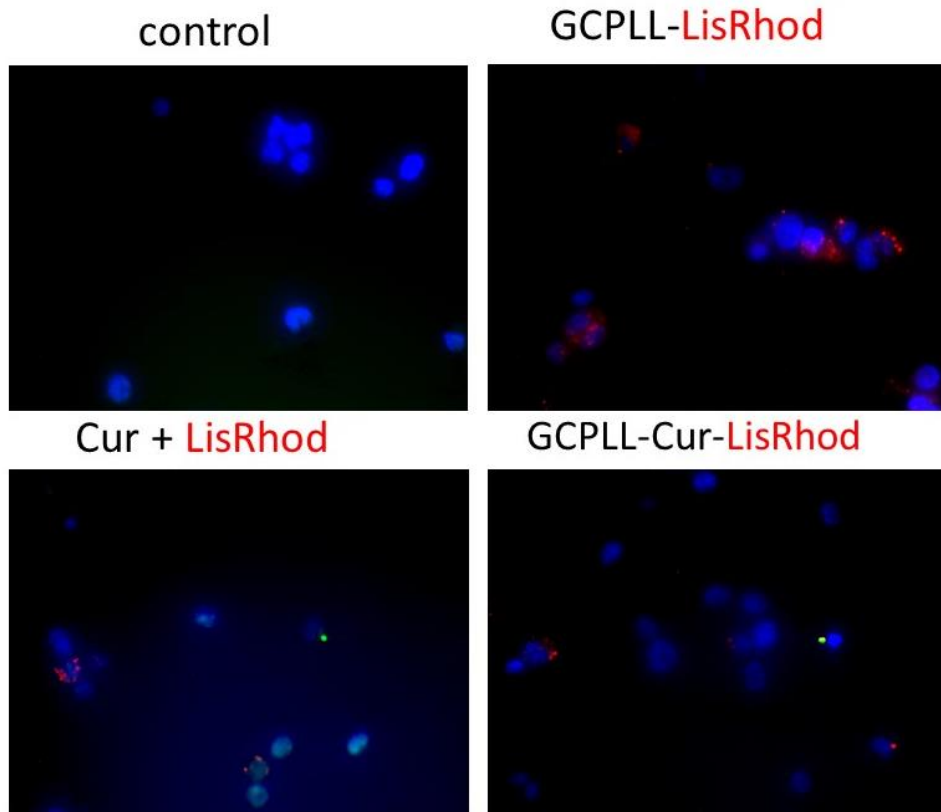
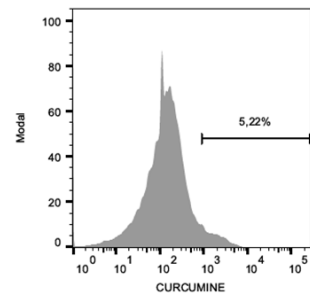
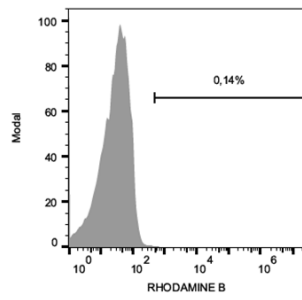
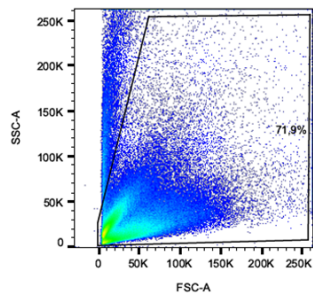


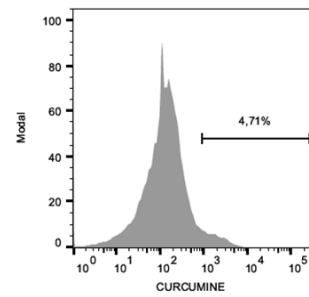
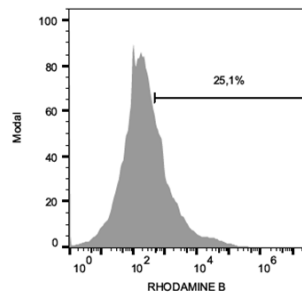
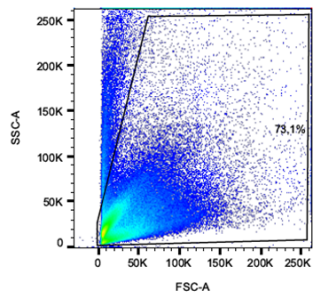
Figure S15. Fluorescence microscopy of **THP-1** cells stained with DAPI dye for nucleus and GCPLL labelled with Rhodamine-lipid (Liss-Rhod).

Flow Cytometry FACS

HeLa
blank



HeLa
GCPLL-Rhod



HeLa
GCPLL-Rhod-Cur

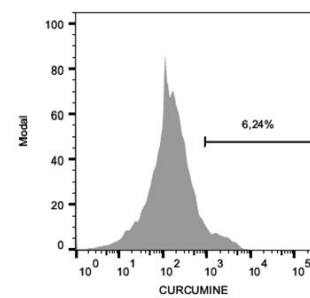
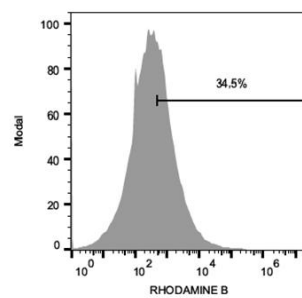
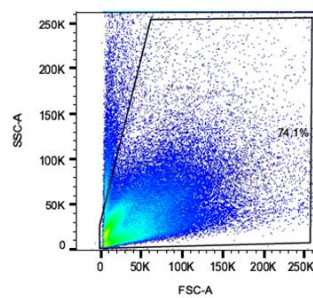
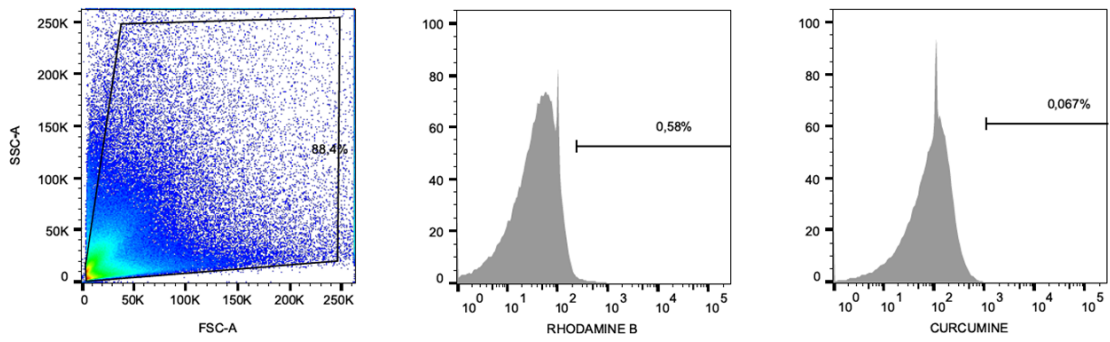
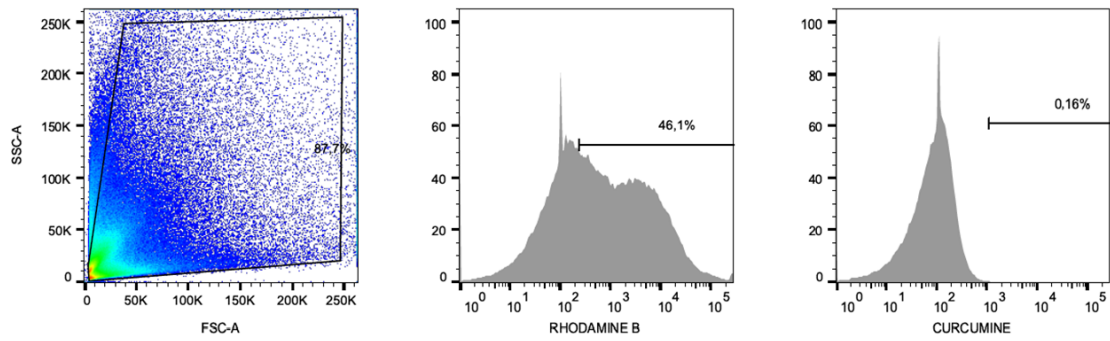


Figure S16. Flow cytometry raw data examples of the triplicate experiments with 3 replicates each one in Hela cells, for: blank; GCPLL-Rhod and GCPLL-Rhod-Cur.

NHDF
blank



NHDF
GCPLL-Rhod



NHDF
GCPLL-Rhod-Cur

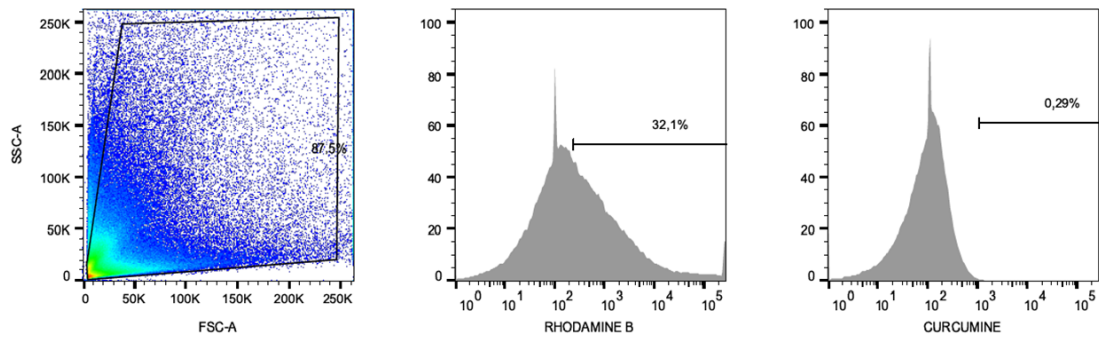
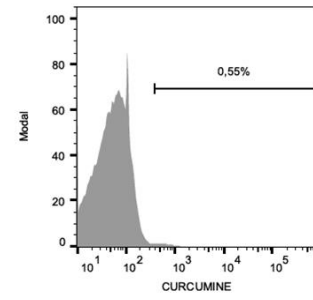
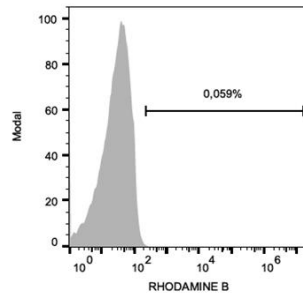
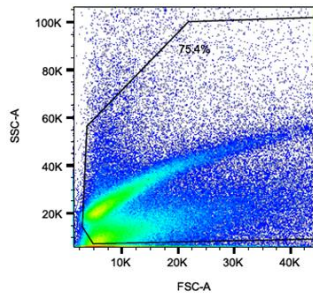
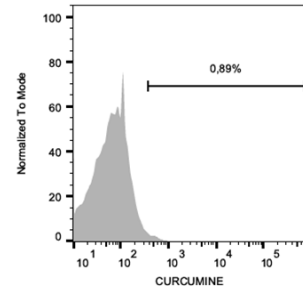
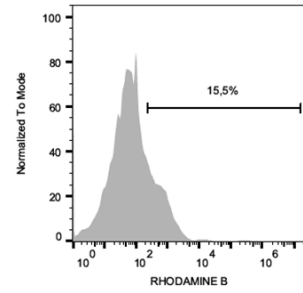
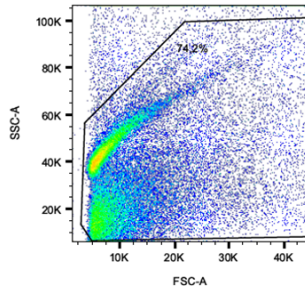


Figure S17. Flow cytometry raw data examples of the triplicate experiments with 3 replicates each one in NHDF cells, for: blank; GCPLL-Rhod and GCPLL-Rhod-Cur.

THP-1
blank



THP-1
GCPLL-Rhod



THP-1
GCPLL-Rhod-Cur

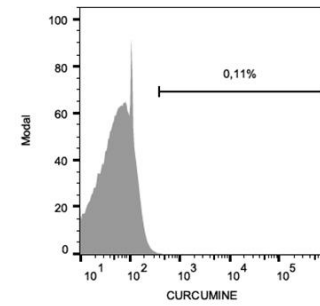
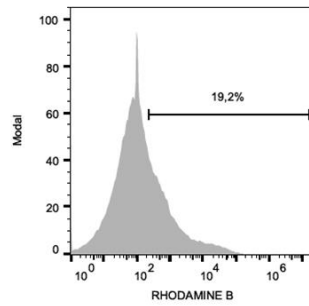
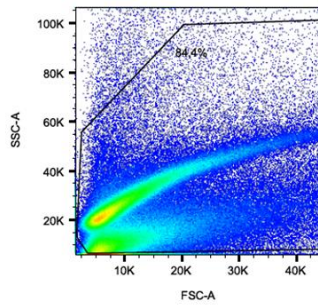


Figure S18. Flow cytometry raw data examples of the triplicate experiments with 3 replicates each one in THP-1 cells, for: blank; GCPLL-Rhod and GCPLL-Rhod-Cur.

Confocal Microscopy

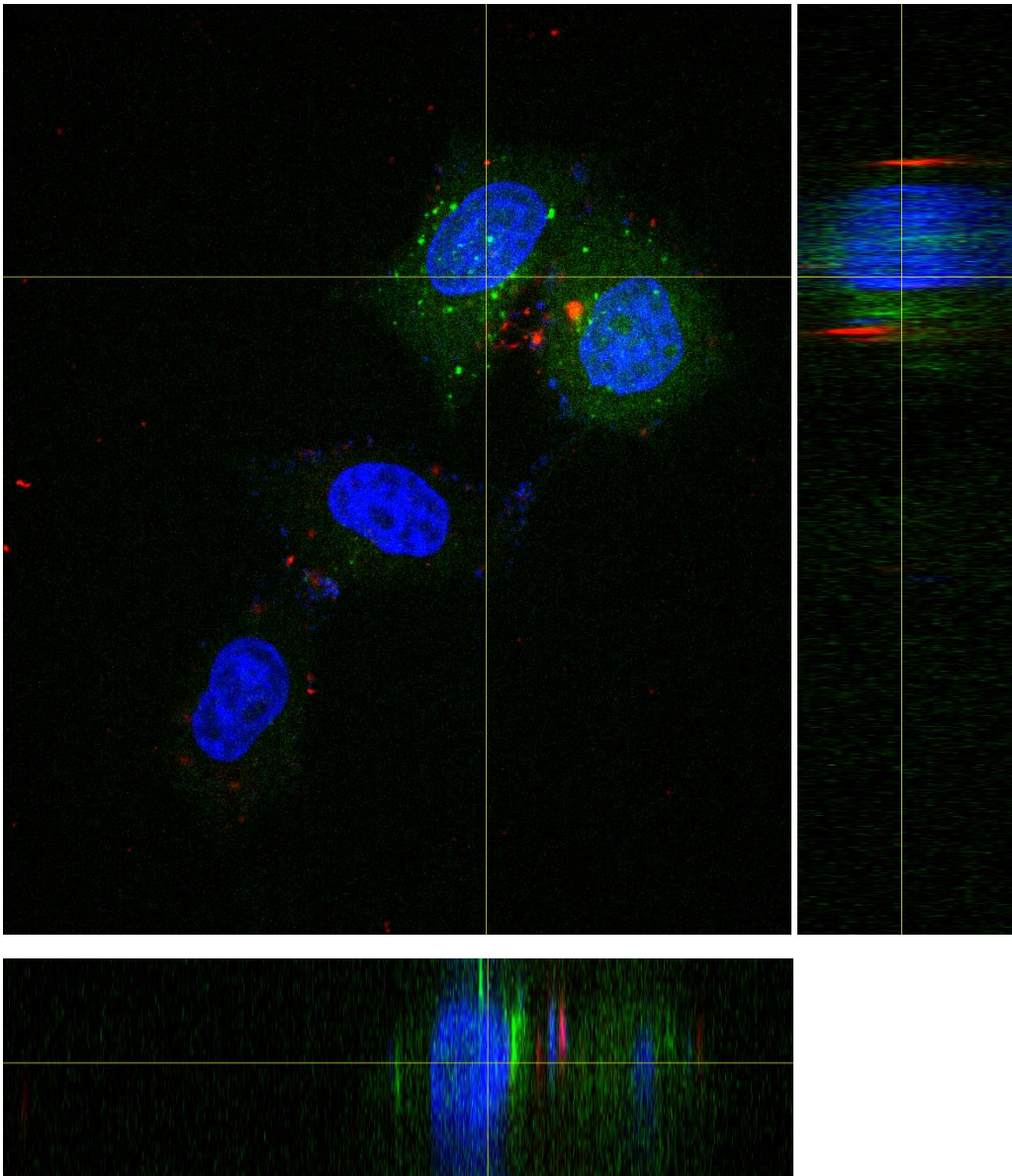


Figure S19. Orthogonal views of confocal microscopy images

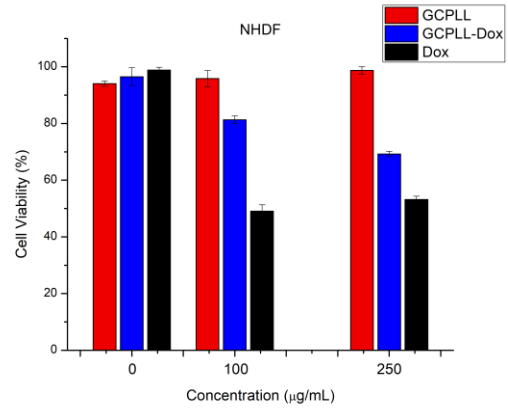
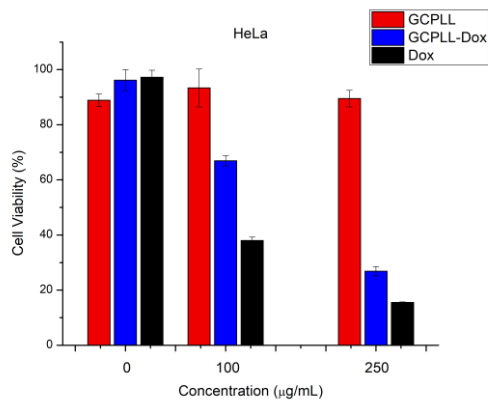


Figure S20. Cell viability of HeLa and NHDF cells after 48h treated with different concentrations of GCPLL, GCPLL-Dox and free Doxorubicin.

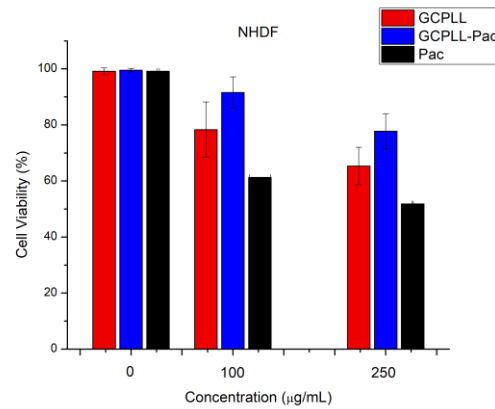
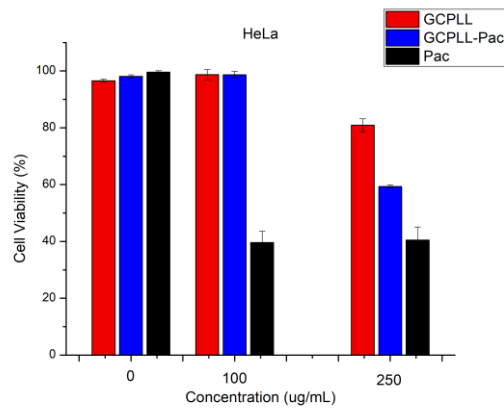


Figure S21. Cell viability of HeLa and NHDF cells after 48h treated with different concentrations of GCPLL, GCPLL-Pac and free Paclitaxel.

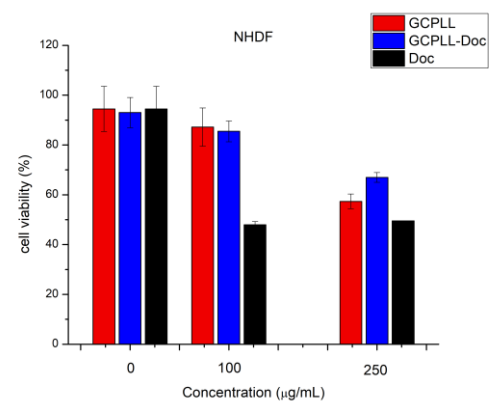
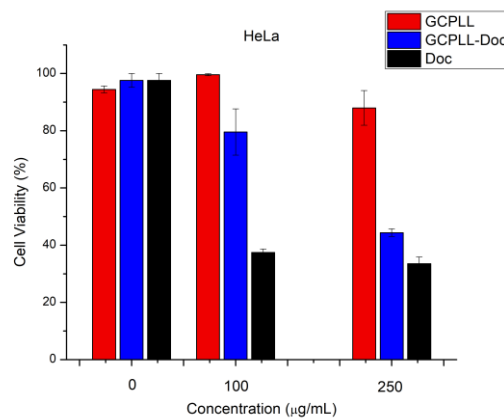


Figure S22. Cell viability of HeLa and NHDF cells after 48h treated with different concentrations of GCPLL, GCPLL-Doc and free Docetaxel.

Mechanical reinforcement of biosurfactant/biopolymer hydrogels through Interpenetrating Networks

Chloé Seyrig^a, Alexandre Poirier^a, Javier Perez,^b Niki Baccile^a

^aSorbonne Université, Centre National de la Recherche Scientifique, Laboratoire de Chimie de la Matière Condensée de Paris , LCMCP, F-75005 Paris, France

^bSynchrotron SOLEIL, L'Orme des Merisiers Saint-Aubin, BP 48 91192 Gif-sur-Yvette Cedex

Abstract

Controlling the viscoelastic properties of hydrogels is a main challenge for many applications. Low Molecular Weight Gelators (LMWG) (bile salt, glycolipids) and biopolymers are good candidates to develop fully biobased hydrogels benefiting from both components' advantages. We selected microbial surfactants and biopolymers (gelatine, chitosan HMW and alginate) able to form hydrogels by themselves. pH drives the behavior of the biosurfactant which can be solubilized within different aspects: it can thus be used as micelles, vesicles or even fibers in presence of calcium. The choice of these phases should be considered in terms of elasticity modulator of the biosurfactant/biopolymer hydrogel.

Introduction

Classical hydrogels are of great interest for biomedical applications, despite they may suffer from drawbacks such as weak and static mechanical properties or difficulties to perfectly replicate all the aspects of the cellular microenvironment. These points can be challenged through the incorporation of a second network, resulting in the formation of interpenetrating polymer network (IPN) hydrogels. Advantages of incorporating secondary networks into traditional biopolymer-based hydrogels include mechanical reinforcement, ability to respond to external stimuli or tuning cell-material interactions.

Biopolymer-based hydrogels can result either from the leverage of their native intermolecular interactions or from chemical cross-linking. They have the advantage to benefit from the inherent properties of biopolymers, especially their bioactivity, degradability and biocompatibility. Despite their promising profile, biopolymers generally have weaker mechanical properties, wider distributions in molecular weights, undefined chemical compositions and eventual immune response due to its sourcing than classical petro-derived polymers.

Several reasons may explain the lack of mechanical strength in hydrated single network (SN) biopolymer hydrogels. The main ones are heterogeneous distributions of crosslinking sites, varying molecular weights between crosslinks and the lack of stress dissipation mechanisms to prevent crack propagation.^{1,2} Increasing the polymer concentration and/or the crosslinking density can efficiently improve the mechanical properties of SN biopolymer hydrogels, but present however major drawbacks : these approaches can inhibit nutrient transport or adversely affect cell mechano-transduction and finally disturb the cellular behavior. Mechanical reinforcement through interpenetrating network has progressively been favored to address these issues, since the first report by the Gong laboratory on the fabrication of double network hydrogels (DN), a special class of IPN formed by sequential polymerization of each network.^{1,3,4} Many multicomponent systems have been developed ever since and related studies highlighted some main trends/conclusions, especially concerning the importance of the components choice. Indeed, storage modulus of the final system depends on the combination of selected gelators.⁵

A hybrid gel can be composed of two polymers but also of a polymer and other self-assembled phases expected to provide their functionality, such as micelles, fibers or vesicles. These latter are useful for encapsulation and release purposes, as illustrated by the work of Dowling *et al.* who efficiently encapsulated calcein in NaOA vesicles loaded gelatin hydrogel and control its release.⁶

In this work, we study the effect of various self-assembled phases obtained by a biobased amphiphile of microbial origin, on the elastic properties of three biobased macromolecules. G-C18:1 is a part of microbial surfactants family, resulting from the fermentation of the yeast *S. Bombicola*. Its structure is composed of a single β -D-glucose hydrophilic headgroup and a C18 fatty acid tail (monounsaturated in position 9,10). It evolves from micelles to vesicles upon lowering the pH.⁷⁻⁹ The interaction between G-C18:1 and biopolymers was recently reported under dilute conditions, forming either complex coacervates or unusual multilamellar walls vesicles.^{10,11} The biopolymers selected for this work are gelatin, chitosan and alginate. Gelatin is obtained by the denaturation of collagen protein and has many potential applications due to its ability to stabilize colloids and its gelation below 30°C.¹² Interactions with anionic surfactants are reported for many proteins, including gelatin. Below its isoelectric point, gelatin bears a positive net charge and is expected to interact with a negatively charged polymer, resulting in the precipitation of polymer-surfactant complexes.¹³⁻¹⁵ Alginate is a polysaccharide composed of β -D-mannuronic acid (M-blocks) and α -L-guluronic acid (G-blocks), as well as regions of interspersed M and G units.¹⁶ Alginates form hydrogels in aqueous solution under mild conditions through interaction with divalent cations, mainly Ca^{2+} , whose cooperative binding between the G-blocks of adjacent alginate chains create reversible ionic interchain bridges.¹⁷ Finally, chitosan is obtained by the deacetylation of chitin, the second most widespread natural polysaccharide. Its structure involves both N-acetylglucosamine and glucosamine, linked together into linear chains through β -(1-4) connections.¹⁸ Biocompatibility, biodegradability, anti-microbial activity, or promotion of wound healing are some examples of chitosan's advantages. Its structure is not so different from the one of the glycosaminoglycans, main constituents of the natural extracellular matrix, opening thus serious trails in tissue engineering applications.¹⁹

By a combination of rheology and small angle X-ray scattering (SAXS), this work shows the improvement of the mechanical properties of the biopolymer hydrogels upon mixing with a fibrillar phase of G-C18:1.

Experimental

Chemicals

In this work we employ microbial glycolipids G-C18:1, composed of a single β -D-glucose hydrophilic headgroup and a C18:1 fatty acid tail (monounsaturated in position 9,10). The compound is purchased from Bio Base Europe Pilot Plant, Gent, Belgium, lot N° APS F06/F07,

Inv96/98/99 and used as such. Its synthesis of G-C18:1 is described in Refs.^{8,9}, where the typical ¹H NMR spectra and HPLC chromatograms are also given. The molecular purity of G-C18:1 exceeds 95%.

The three polymers used in this work, gelatin (type A, from porcine skin, $M_w \approx 50\text{--}100$ kDa, isoelectric point 7–9), alginate (from brown algae, medium viscosity, $M_w \approx 20\text{--}240$ kDa, $pK_a \approx 4$) and chitosan (high molecular weight, HMW, from shrimp shell, practical grade, $M_w \approx 190\text{--}375$ kDa, $pK_a \approx 6.5$), are purchased from Sigma Aldrich.

Preparation of the hydrogels

Stock solutions. The G-C18:1 stock solution at concentration, $C_{G-C18:1} = 40$ mg/mL, is prepared by dissolving the G-C18:1 powder in the appropriate volume of milli-Q grade water at pH= 10, adjusted with a few μL of NaOH 5 or 1 M solution. The stock solutions for each biopolymer are prepared as follows. *Gelatin:* 80 mg of gelatin powder is dispersed in 2 mL of milli-Q water, for a concentration of $C_{\text{gelatin}} = 40$ mg/mL. The gelatin stock solution is vortexed and set in the oven at 50°C. Once the solution is homogeneous, pH is increased up to pH 10 with a few μL of a 0.5 M - 1 M NaOH solution. *Chitosan:* 100 mg of chitosan dispersed in 10 mL of 0.1 M acetic acid aqueous solution for a concentration $C = 10$ mg/mL. For an optimal solubilisation, the chitosan stock solution is stirred for one day before use. *Alginate:* 100 mg of alginate powder is dispersed in 10 mL of Milli-q water for a concentration $C = 10$ mg/mL and stirred until complete solubilization. The magnetic stirrer usually sticks upon water addition; in this case, a manual help may be required to improve stirring. For a typical volume of 10 mL, pH is then increased to 10 with a 1-10 μL of a 5 M or 1 M NaOH solution under stirring. Stirring and vortexing are eventually necessary to obtain a homogeneous alginate solution. Additional protocol details are given below for each biopolymer.

Fibrillar G-C18:1 gels, {F}G-C18:1. For a 1 mL sample, one increases the pH of 1 mL of the G-C18:1 stock solution up to ≈ 8 using 2-5 μL of a 5 M or 1 M NaOH solution. CaCl_2 solution (1 M, $V_{\text{CaCl}_2} = 33.5$ μL , $[\text{CaCl}_2] = 33.5$ mM) is manually added for a total $[\text{CaCl}_2] : [\text{G-C18:1}] = 1 : 1.3$ molar ratio. The final solution is stirred and a gel is obtained after resting a few hours at room temperature.

{F}G-C18:1/gelatin gels. A volume of 500 μL of the gelatin stock solution is mixed with 500 μL of either water (reference) or G-C18:1 stock solution (sample). For a typical volume of 1 mL, CaCl_2 solution (1 M, $V_{\text{CaCl}_2} = 33.5$ μL , $[\text{CaCl}_2] = 33.5$ mM) is manually added for a total

$[\text{CaCl}_2] : [\text{G-C18:1}] = 1 : 1.3$ molar ratio. The final solution is stirred and a gel is obtained after resting a few hours at room temperature.

{F}G-C18:1/chitosan gels. The pH of a 1 mL of the acidic chitosan stock acidic solution is increased above about 8. Typically, for 1 mL, one adds 5-10 μL of a 5 M or 1 M NaOH solution. The solution, initially viscous, is vigorously stirred and vortexed to obtain a heterogeneous gel. Due to the heterogeneity of the chitosan gel at basic pH, 500 mg of the chitosan gel are weighted and mixed with 500 μL of a glycolipid solution under vigorous stirring and vortexing. To this mixture, 33.5 mM ($V_{\text{CaCl}_2} = 67 \mu\text{L}$) of a CaCl_2 solution ($[\text{CaCl}_2] = 1 \text{ M}$) are added, followed by further mixing. The final concentration of CaCl_2 in the sample is 33.5 mM, for a total $[\text{CaCl}_2] : [\text{G-C18:1}] = 1 : 1.3$ molar ratio. A homogeneous gel is obtained after resting a few hours at room temperature.

{F}G-C18:1/alginate gels. 500 μL of the alginate viscous stock solution are added either to 500 μL water (reference) or to 500 μL of the G-C18:1 stock solution under stirring. A volume of $V_{\text{CaCl}_2} = 50 \mu\text{L}$ of a CaCl_2 solution ($[\text{CaCl}_2] = 1 \text{ M}$) is added, for a final CaCl_2 concentration of 50 mM and $[\text{CaCl}_2] : [\text{G-C18:1}] = 1 : 0.86$ molar ratio and $[\text{CaCl}_2] : [\text{alginate}] \approx 1 : 0.0015$ molar ratio. The final solution is magnetically stirred for several hours to obtain a homogeneous gel.

Table 1 summarizes the reference, sample and stock solution concentrations in wt% employed throughout this study.

Table 1 – Concentration of stock solutions, volumes from stock solutions and final concentration in the samples

	G-C18:1	gelatin	alginate	chitosan
Stock solution concentration (wt%)	4	4	2	2
V (mL)	0.5 (1 for the second procedure with chitosan)	0.5	0.5	0.5/1 (first/second procedure)
Reference and sample concentration (wt%)	2	2	1	1

Rheology

Viscoelastic measurements are carried out using an Anton Paar MCR 302 rheometer equipped with parallel titanium or stainless-steel sandblasted plates (diameter = 25 mm, gap = 1 mm). Unless otherwise stated, all experiments are conducted at 25 °C, whereas the temperature is controlled by the stainless-steel lower Peltier plate. During the experiments, the measuring geometry is covered with a humidity chamber to minimize water evaporation. To investigate the pH-dependence of the mechanical properties, samples containing {F}G-C18:1 and the biopolymer are mixed with the appropriate amount of glucono- δ -lactone, GDL, and immediately vortexed during 20 s. Half of the sample is immediately loaded on the bottom plate, while the pH is monitored automatically on the other half. Dynamic oscillatory and time sweep experiments are performed by applying a constant oscillation frequency ($f = 1$ Hz) and a shear strain (γ) within the linear viscoelastic regime (LVER).

Small angle X-ray scattering (SAXS)

SAXS experiments are performed at 25 °C at the Swing beamline at the Soleil synchrotron facility (Saint-Aubin, France). Samples have been analyzed during the run N° 20201747 using a beam at 12.00 keV and a sample-to-detector distance of 2.00 m. Samples are prepared *ex situ*, pushed through a 1 mm quartz tube with a 1 mL syringe and analyzed directly by setting them in front of the X-ray beam. The signal of the same quartz tube containing water is subtracted as background. The quartz tubes are rinsed with water and ethanol after each use. The signal of the Pilatus 1M 2D detector (172 x 172 mm pixel size), used to record the data, is integrated azimuthally with PyFAI to obtain the $I(q)$ vs. q spectrum ($q = 4\pi \sin \theta/\lambda$, where 2θ is the scattering angle) after masking systematically wrong pixels and the beam stop shadow. Silver behenate ($d_{(001)} = 58.38$ Å) is used as SAXS standards to calibrate the q -scale. Data are not scaled to absolute intensity.

Rheo-SAXS

Experiments coupling rheology and SAXS are performed at the SWING beamline of the Soleil synchrotron facility (Saint-Aubin, France) during the run N° 20200532, using a beam energy of 12.00 keV and a sample-to-detector distance of 1.65 m. Tetradecanol ($d_{(001)} = 39.77$ Å) is used as the q -calibration standard. The signal of the Pilatus 1 M 2D detector (172 x 172 mm pixel size) is integrated azimuthally with Foxtrot software to obtain the $I(q)$ spectrum ($q = 4\pi \sin \theta/\lambda$, where 2θ is the scattering angle) after masking systematically defective pixels and the beam stop shadow. A MCR 501 rheometer (Anton Paar, Graz, Austria) equipped with a

Couette polycarbonate cell (gap= 0.5 mm, volume, \approx 2 mL) is coupled to the beamline and controlled through an external computer in the experimental hutch using the Rheoplus/32 software, version 3.62. The experiments are performed in a radial configuration, where the X-ray beam is aligned along the center of the Couette cell. Data are not scaled to absolute intensity.

RESULTS

The phase behaviour of G-C18:1 against pH, summarized in Figure 1a,⁷ shows micelles above and unilamellar vesicles below pH~6.5-7,⁸ none of them having any gelling property. An additional phase has recently been put in evidence when adding metal ions, and in particular a Ca²⁺ salt, to the micellar phase (pH above ≈7.8): self-assembled fibers spontaneously and immediately form, as supported by cryo-TEM and their characteristic SAXS profile. Fibrillation occurs homogeneously, followed by prompt gelling.²⁰ The typical G' of G-C18:1 hydrogels settles around 100 Pa at about 2 wt% for an equimolar amount of positive-to-negative charge, [Ca²⁺]/[G-C18:1] > 0.6 (Figure S 1a).²⁰

The viscoelastic behaviour of all biopolymers studied in this work is given in Figure S 1 for selected controls at two pH values in the form of storage and loss moduli measured few minutes after loading the rheometer. As expected, all reference samples are gels, of which the magnitude of the elastic modulus depends on the nature of the biopolymer, but not the pH.

Hybrid {F}G-C18:1/gelatin hydrogels

Network interpenetration between polymer gels and self-assembled fibrillar network (SAFiN) hydrogels could generate a synergetic interaction improving the elastic performance of the gels. This is studied for gelatin {F}G-C18:1 SAFiN hybrid hydrogels in Figure 1 and Figure 2. According to Figure 1b, the aqueous vesicular and micellar solutions mixed with a 2 wt% gelatin have comparable G' (~ 30 Pa) and do not have significant differences in the final properties of the gel, although they seem to have a moderate detrimental impact on the G', if compared to gelatin alone (~ 55 Pa, Figure S 1). On the other hand, the addition of a Ca²⁺ solution to the gelatin-micelle gel strongly improves, by almost one order of magnitude, the corresponding G'. The mechanical properties of the hybrid gelatin-SAFiN gel are also superior to the ones of each component alone, {F}G-C18:1 and gelatin, compared on Figure 2a, showing how the combination of both fibrillar and polymeric components generates a stronger gel.

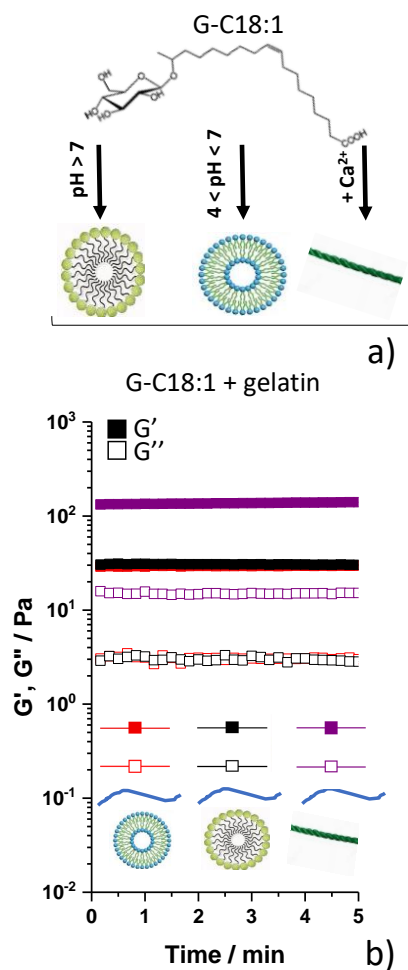


Figure 1 - Mechanical properties of hybrid gels made of gelatin (2 wt%) mixed with the three different solutions, each containing a different phase of G-C18:1 (2 wt%).

SAXS is employed to draw a clearer picture of hybrid hydrogel's structure, in comparison to the single components. Figure 2b presents the typical SAXS profile of {F}G-C18:1 fibrillar hydrogels (purple), showing the characteristic low- q slope with a -2 dependency and a crystalline structure within the fiber network,²⁰ and gelatin (green), classical for polymers in a good solvent.²¹ The experimental SAXS signal of the hybrid gel (red) is in very good agreement with the arithmetic sum of each individual's SAXS profile (Figure 2c), which is rather a proof of interpenetration of SAFiN and polymer networks, but not a mutual interaction. This is in agreement with our previous work, showing no interactions between G-C18:1 and gelatin solutions in a broad pH range.¹¹ Figure 2e presents the rheo-SAXS experiment probing elastic behaviour of the hybrid gel under strain sweep: about 80 % of the G' is recovered within 30 s, and that at least over the three cycles of the experiment. According to the corresponding

scattering analysis (Figure 2d), which shows that SAXS profiles *a* (initial gel) through *c* (after two and three cycles) are superimposed, the structure of the hybrid gel is not affected.

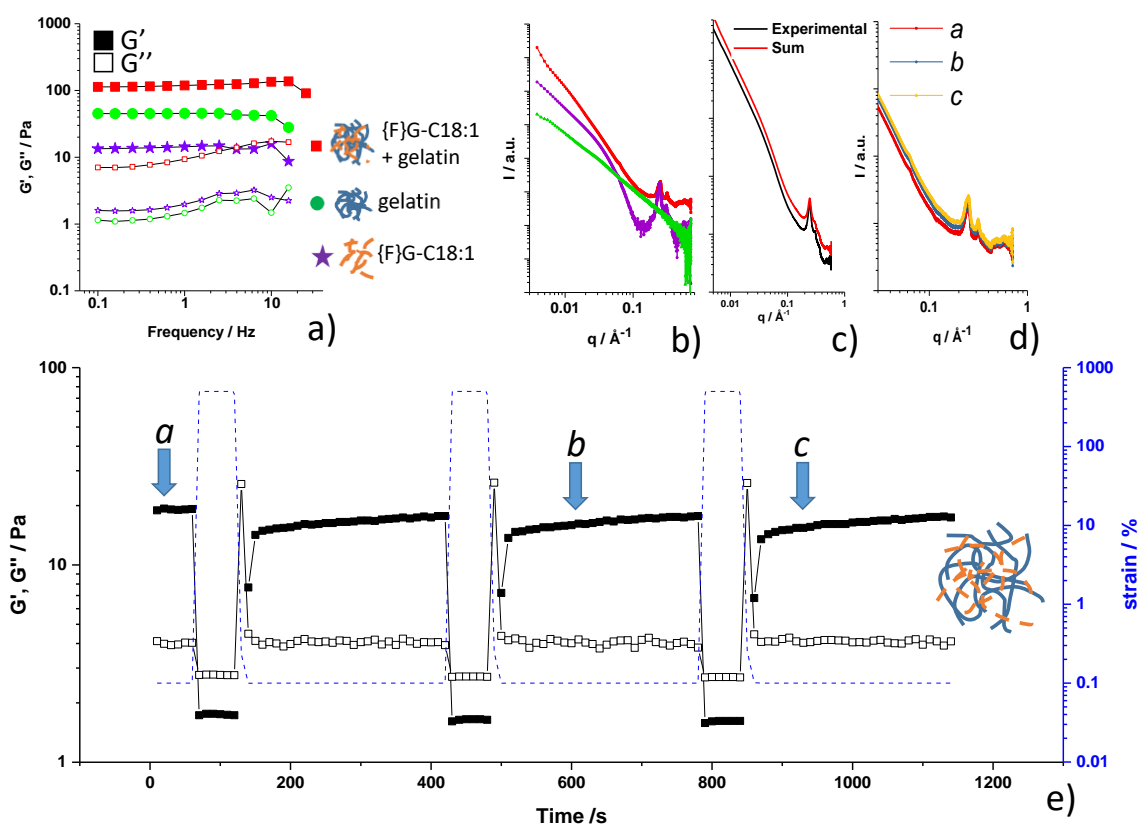


Figure 2– (a) Mechanical properties and (b) SAXS of {F}G-C18:1, gelatin and {F}G-C18:1/gelatin hybrid gels. (c) SAXS profiles of {F}G-C18:1/gelatin and the arithmetical sum of G-C18:1 and gelatin. Rheo-SAXS of hybrid {F}G-C18:1: (e) mechanical properties and (d) resulting SAXS of {F}G-C18:1/gelatin hybrid gels in function of shear strain

Hybrid {F}G-C18:1/alginate gels

Alginate is a biopolymer, of which the hydrogelation process is triggered by addition of Ca^{2+} ions.²² Upon mixing a Ca^{2+} -free alginate solution with a G-C18:1 solution, either in a micellar or vesicle phase, no gelation occurs, while adding a source of Ca^{2+} to the alginate-micelles solution at basic pH, gelation is immediate (Figure 3a), with G' above 100 Pa.

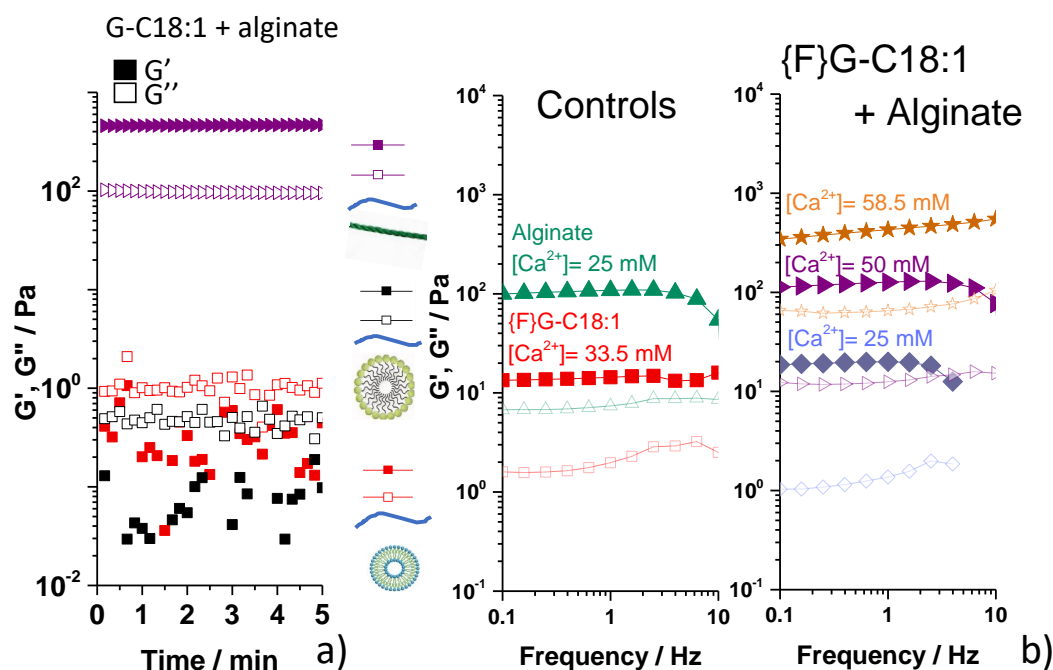


Figure 3 – (a) Mechanical properties of hybrid systems composed of alginate (1 wt%) and G-C18:1 in its micellar, vesicle or fiber phase ([Ca²⁺] = 58 mM). (b) Mechanical properties of {F}G-C18:1/alginate hybrid gel as a function of calcium concentration. GC and A stand for {F}G-C18:1 and alginate, respectively.

It is not surprising that alginate/micelle and alginate/vesicle hybrid samples are liquid solutions, alginate being known to form gels only in the presence of calcium.^{22–25} Simultaneous responsivity to Ca²⁺ ions for both alginate and G-C18:1 make this sample particularly interesting. The G-C18:1/alginate system involves two partners, both containing carboxylic acid groups, and of which gelation is triggered by calcium, thus creating a competition. Figure 3 **Erreur ! Source du renvoi introuvable.** b presents the mechanical properties of each component's solution in the presence of a calcium source: {F}G-C18:1 (2 wt%, 33.5 mM CaCl₂) and alginate (1 wt%, 25 mM CaCl₂). Upon addition of 25 mM CaCl₂ to the mixed alginate and G-C18:1 sample, the hybrid {F}G-C18:1/alginate hydrogel reaches the mechanical properties of {F}G-C18:1 alone. When providing an additional source of calcium (50 mM), the hybrid gel reaches the mechanical properties of the pure alginate gel. This simple experiment, which could be further verified by more advanced microcalorimetry tests, suggests that {F}G-C18:1 sequesters calcium ions and eventually forms gels faster than alginate, which reacts with calcium only afterwards. Interestingly, the mechanical properties of the hybrid system can even be improved by adding an excess of calcium, here increased up to 58.5 mM, and corresponding to the sum of the quantities required to gel each component. The possibility to obtain a stronger hybrid gel than each component taken separately by adding the amount of

calcium required to gel them demonstrates a cooperative effect between alginate and {F}G-C18:1, as also reported above for gelatin. Further experiments however show that a threshold calcium concentration should not be exceeded to obtain a homogeneous gel (data not shown).

This mechanism is supported by microcalorimetry data: a colleague (A. Poirier) reported the binding enthalpy between G-C18 :1 and Ca^{2+} to be lower than 4 kJ/mol, the enthalpy of binding between alginate and Ca^{2+} reported in the literature.²² This result is indeed in favor of a preferential binding of calcium to G-C18 :1, in agreement with our observations, but is however to be used with caution (we identified a strong signal due to calcium in the buffer solution we used for instance) and further experiments are on going.

Figure 4a-c presents the structural characterization of alginate glucolipid hydrogels studied by SAXS. As similarly commented for gelatin, the SAXS profiles of {F}G-C18:1 and alginate alone (Figure 4a) are respectively typical of fibers²⁰ and polymer in a good solvent.²¹ The signature of the fibrillar phase (purple stars) is on the contrary very similar to the SAXS of the hybrid gel (red squares), the latter being close enough to the arithmetic sum of the alginate and {F}G-C18:1 SAXS profiles (Figure 4b), and reasonably suggesting interpenetration between the SAFiN and polymer chains. Figure 4c, d presents the resulting rheo-SAXS experiment, probing the mechanical properties of the hybrid gel over several cycles of shear strain: 85% of G' is recovered within 15 s at least over three consecutive cycles. According to Figure 4d, the structure of the gel is not affected, highlighted by the superimposable SAXS profiles corresponding to regions *a* through *c* of Figure 4c.

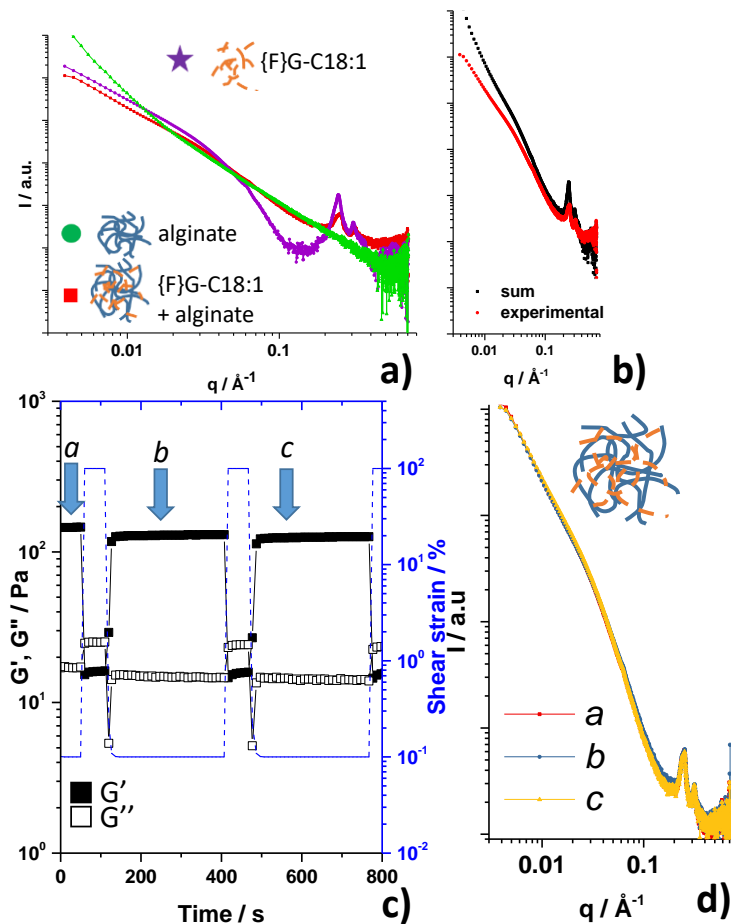


Figure 4 - (a) SAXS profiles of {F}G-C18:1, gelatin, and hybrid gels (b) Arithmetical sum of {F}G-C18:1 and alginate profiles compared to hybrid {F}G-C18:1/alginate profile. (c, d) Rheo SAXS experiment probing the (c) elastic properties and (d) corresponding structures of {F}G-C18:1/alginate hybrid gels in function of shear strain.

Hybrid {F}G-C18:1/chitosan gels

Chitosan is a biopolymer, which is able to form a hydrogel above its pK_a . Each G-C18:1 phase, micellar, vesicular and fibrillar is combined with a chitosan gel, prepared by manual increase of the pH. Figure 5 shows that $G'' > G'$ when chitosan is mixed with vesicles, meaning that these latter do not provide any elastic properties to the system. In the case of a micellar solution, the viscous chitosan sample does easily mix with the fluid micellar solution and the hybrid sample is too heterogeneous to measure reliable elastic properties. However, when calcium is added to the latter micellar/chitosan solution, the sample immediately forms a gel, more homogenous by the eye. The hybrid gel exhibits enhanced mechanical properties.

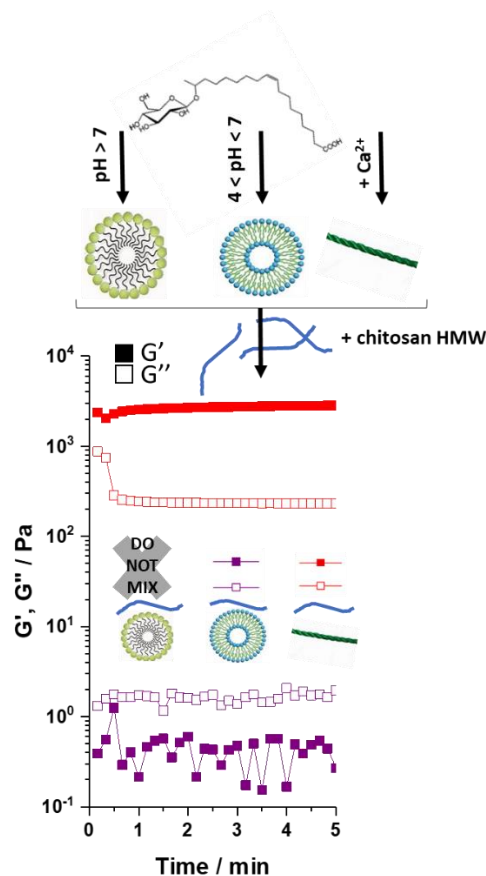


Figure 5 - Mechanical properties of hybrid gels made of chitosan mixed with the different phases of the biosurfactant {F}G-C18:1

Figure 6a presents the mechanical properties of the hybrid gel compared to the ones of each component alone: the combination of both components allows to obtain a gel with enhanced mechanical properties compared to the controls. Their corresponding SAXS profiles, given in Figure 6b, show the characteristic scattering pattern of {F}G-C18:1, indicating its presence and confirming its important role in the formation of the hybrid scaffold, while Figure 7 shows the good matching between the {F}G-C18:1 and {F}G-C18:1 + chitosan SAXS patterns, indicating the orthogonality between the two networks. Figure 6c presents the rheo-SAXS experiment associated to the step strain experiment performed on the hybrid gel: about 85% of the initial elastic properties are recovered within 30 s after releasing 100% strain over three cycles of the experiment. The superimposed SAXS data in Figure 6d, collected after each step-strain cycle, show that, similarly to alginate and gelatin-based hybrid gels, the structure is not affected (a, b and c profiles correspond to a, b and c arrows on Figure 6c).

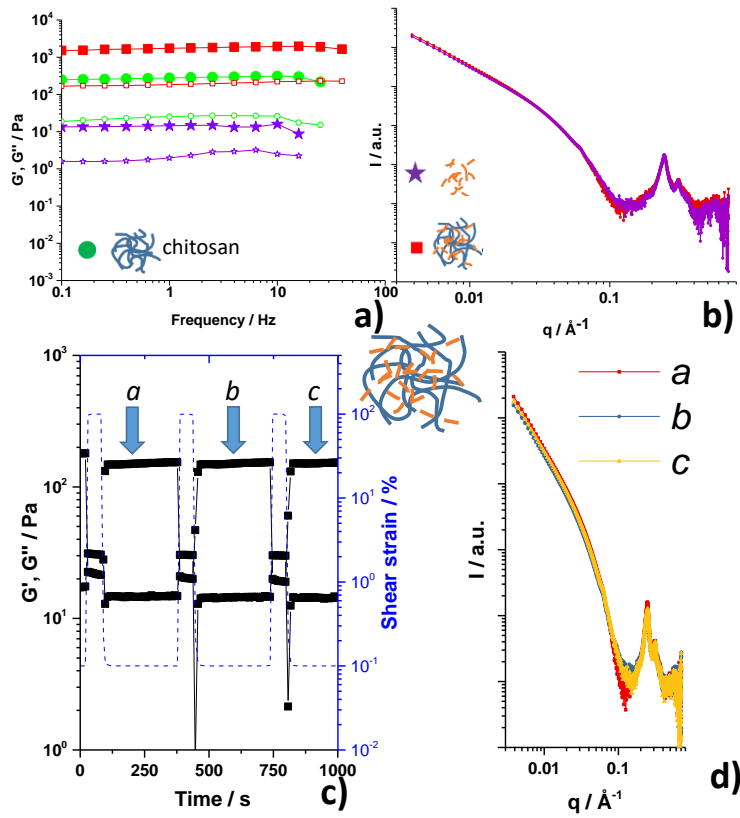


Figure 6 - (a) Mechanical properties and (b) SAXS profile of {F}G-C18:1/chitosan hybrid gels as a function of frequency. Rheo-SAXS experiment: (c) step-strain evolution of G' and (d) corresponding SAXS profiles in hybrid {F}G-C18:1/chitosan gels.

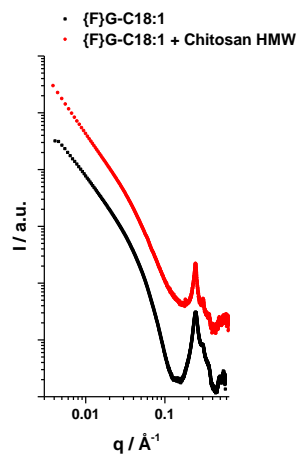


Figure 7 - SAXS profiles of {F}G-C18:1 and mixed {F}G-C18:1 + chitosan HMW hydrogels

Discussion

Conclusion

Acknowledgements

Soleil Synchrotron facility is acknowledged for accessing the Swing beamline and financial support (proposal N° 20200532). Ghazi Ben Messaoud (DWI-Leibniz Institute for Interactive Materials, Aachen, Germany) is kindly acknowledged for helpful discussions. We thank Dr. S. Roelants, Prof. W. Soetaert and Prof. C. V. Stevens at Gent University for providing us the glycolipid. Sorbonne Université (contract N° 3083/2018) is acknowledged for financial support of CS. Authors kindly acknowledge the French ANR, Project N° SELFAMPHI - 19-CE43-0012-01.

References

- (1) Gong, J. P. Why Are Double Network Hydrogels so Tough? *Soft Matter* **2010**, *6*, 2583–2590.
- (2) Costa, A. M. S.; Mano, J. F. Extremely Strong and Tough Hydrogels as Prospective Candidates for Tissue Repair -a Review. *Eur. Polym. J.* **2015**, *72*, 344–364.
- (3) Higa, K. Fundamental Biomaterial Properties of Tough Glycosaminoglycan-Containing Double Network Hydrogels Newly Developed Using the Molecular Stent Method. *Acta Biomater.* **2016**, *43*, 38–49.
- (4) Mredha, M. T. I. Anisotropic Tough Double Network Hydrogel from Fish Collagen and Its Spontaneous in Vivo Bonding to Bone. *Biomaterials* **2017**, *132*, 85–95.
- (5) Colquhoun, C.; Draper, E. R.; Eden, E. G. B.; Cattoz, B. N.; Morris, K. L.; Chen, L.; McDonald, T. O.; Terry, A. E.; Griffiths, P. C.; Serpell, L. C.; et al. The Effect of Self-Sorting and Co-Assembly on the Mechanical Properties of Low Molecular Weight Hydrogels. *Nanoscale* **2014**, *6*, 13719–13725.
- (6) Dowling, M. B.; Lee, J. H.; Raghavan, S. R. PH-Responsive Jello: Gelatin Gels Containing Fatty Acid Vesicles. *Langmuir* **2009**, *25*, 8519–8525.
- (7) Baccile, N.; Cuvier, A.-S.; Prévost, S.; Stevens, C. V.; Delbeke, E.; Berton, J.; Soetaert, W.; Van Bogaert, I. N. A.; Roelants, S. Self-Assembly Mechanism of PH-Responsive Glycolipids: Micelles, Fibers, Vesicles, and Bilayers. *Langmuir* **2016**, *32*, 10881–10894.
- (8) Baccile, N.; Selmane, M.; Le Griel, P.; Prévost, S.; Perez, J.; Stevens, C. V.; Delbeke, E.; Zibek, S.; Guenther, M.; Soetaert, W.; et al. PH-Driven Self-Assembly of Acidic Microbial Glycolipids. *Langmuir* **2016**.
- (9) Cuvier, A. S.; Berton, J.; Stevens, C. V.; Fadda, G. C.; Babonneau, F.; Van Bogaert, I. N. A.; Soetaert, W.; Pehau-Arnaudet, G.; Baccile, N. PH-Triggered Formation of Nanoribbons from Yeast-Derived Glycolipid Biosurfactants. *Soft Matter* **2014**, *10*,

3950–3959.

- (10) Seyrig, C.; Le Griel, P.; Cowieson, N.; Perez, J.; Baccile, N. Synthesis of Multilamellar Walls Vesicles Polyelectrolyte-Surfactant Complexes from PH-Stimulated Phase Transition Using Microbial Biosurfactants. *J. Colloid Interface Sci.* **2020**, *580*, 493–502.
- (11) Seyrig, C.; Kignelman, G.; Thielemans, W.; Le Griel, P.; Cowieson, N.; Perez, J.; Baccile, N. Stimuli-Induced Nonequilibrium Phase Transitions in Polyelectrolyte-Surfactant Complex Coacervates. *Langmuir* **2020**, *36*, 8839–8857.
- (12) Djabourov, M. Architecture of Gelatin Gels. *Contemp. Phys.* **1988**, *29*, 273.
- (13) Pankhurst, K. G. A.; Smith, R. C. M. The Adsorption of Paraffin-Chain Salts to Proteins. Part I. Some Factors Influencing the Formation and Separation of Complexes between Gelatin and Dodecyl Sodium Sulfate. *Trans. Faraday Soc.* **1944**, *40*, 465.
- (14) Tamaki, K.; Tamamushi, B. The Interaction of Gelatin Molecule with Surface Active Ions. *Bull. Chem. Soc. Jpn.* **1955**, *28*, 555.
- (15) Know, W. J.; Wright, J. F. The Interaction of Sodium Dodecyl Sulfate with Gelatin. *J. Colloid Sci.* **1965**, *20*, 177.
- (16) Martinsen, A.; Skjaak-Braek, G.; Smidsroed, O. Alginate as Immobilization Material: I. Correlation between Chemical and Physical Properties of Alginate Gel Beads. *Biotechnol. Bioeng.* **1989**, *33*, 79–89.
- (17) Rowley, J. A.; Madlambayan, G.; Mooney, D. J. Alginate Hydrogels as Synthetic Extracellular Matrix Materials. *Biomaterials* **1999**, *20*, 45–53.
- (18) Zargar, V.; Asghari, M.; Dashti, A. A Review on Chitin and Chitosan Polymers : Structures, Chemistry, Solubility, Derivatives, and Applications. *Chem. Bio. Eng. Rev.* **2015**, *2*, 204–226.
- (19) Ullah, S.; Zainol, I.; Idrus, R. H. Incorporation of Zinc Oxide Nanoparticles into Chitosan-Collagen 3D Porous Scaffolds : Effect on Morphology, Mechanical Properties and Cytocompatibility of 3D Porous Scaffolds. *Int. J. Biol. Macromol.* **2017**, *104*, 1020–1029.
- (20) Poirier, A. et al. No Title. *Prep.*
- (21) Pedersen, J. S.; Schurtenbercer, P. Scattering Functions of Semidilute Solutions of Polymers in a Good Solvent. *J. Polym. Sci. Part B Polym. Phys.* **2004**, *42*, 3081–3094.
- (22) Fang, Y.; Al-Assaf, S.; Phillips, G. O.; Nishinari, K.; Funami, T.; Williams, P. A.; Li, A. Multiple Steps and Critical Behaviors of the Binding of Calcium to Alginate. *J. Phys. Chem. B* **2007**, *111*, 2456–2462.
- (23) Grant, G. T.; Morris, E. R.; Rees, D. A.; Smith, P. J. C.; Thom, D. Biological Interactions

- between Polysaccharides and Divalent Cations: The Egg-box Model. *FEBS Lett.* **1973**, 32, 195.
- (24) Morris, E. R.; Rees, D. A.; Thom, D.; Boyd, J. Chiroptical and Stoichiometric Evidence of a Specific, Primary Dimerisation Process in Alginate Gelation. *Carbohydr. Res.* **1978**, 66, 145.
- (25) Thom, D.; Grant, G. T.; Morris, E. R.; Rees, D. A. Characterisation of Cation Binding and Gelation of Polyuronates by Circular Dichroism. *Carbohydr. Res.* **1982**, 100, 29.

Supplementary information

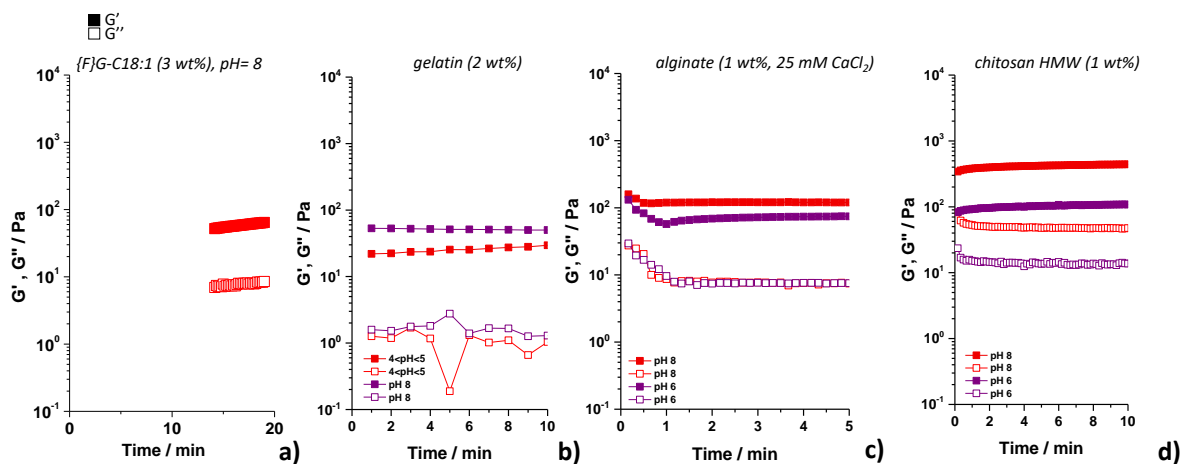


Figure S 1 – Time dependence of storage and loss modulus of a) gelatin, b) alginate and c) chitosan HMW at acidic and basic pH

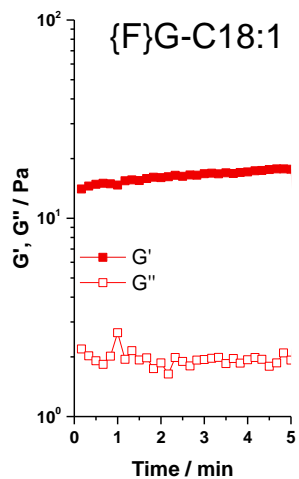


Figure S 2 – Time dependence of storage and loss modulus of {F}G-C18 :1 (2 wt%), with $[Ca^{2+}] = 33.5$ mM gel (pH 8)

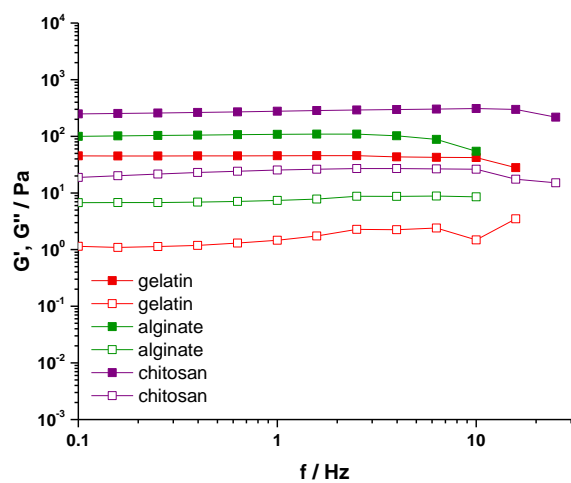


Figure S 3 – Frequency dependence of storage and loss modulus of gelatin, alginate and chitosan (2 wt%) gels at pH 8.

pH and temperature responsivity of biosurfactant/biopolymer interpenetrated network hydrogels

Chloé Seyrig^a, Alexandre Poirier^a, Thomas Bizien,^b Niki Baccile^a

^aSorbonne Université, Centre National de la Recherche Scientifique, Laboratoire de Chimie de la Matière Condensée de Paris, LCMCP, F-75005 Paris, France

^bSynchrotron SOLEIL, L'Orme des Merisiers Saint-Aubin, BP 48 91192 Gif-sur-Yvette Cedex

Abstract

Hydrogels can serve a wide range of applications which makes them a hot topic in soft matter community. Control over the viscoelastic properties of the gel has been shown to directly impact cell proliferation in tissue engineering applications, for instance. This work is motivated by the development of a dual system composed of low molecular weight gelators (LMWG) and biopolymers. This new form of hydrogels is expected to benefit from the stimuli-responsive properties of LMWG and the higher stiffness of the polymers. The hydrogel conception includes a safe-by-design approach. Indeed, only biodegradable and biocompatible molecules are selected: a microbial surfactant (G-C18:1, able to gelify in presence of calcium) and biopolymers (gelatin, chitosan and alginate). *In situ* acidification of the gel using glucono- δ -lactone (GDL) evidences a loss of mechanical properties following a decrease of the pH while heating the gel does not destroy it, contrary to some of the individual components gels. pH and temperature appear thus as two efficient tools to tune the properties of the gel for a desired application.

Introduction

Classical hydrogels commonly suffer from limited mechanical strength and undergo permanent breakage. The lack of desired dynamic and structural complexity within the hydrogels are other drawbacks limiting their functions. Advanced engineering of parameters such as mechanics and spatially/temporally controlled release of (bio)active moieties, as well as manipulation of multiscale shape, structure, and architecture, could significantly widen the applications of hydrogels.

One strategy increasingly employed to address such challenges is the incorporation of a second polymeric network, resulting in IPN hydrogels displaying both networks' properties.¹ Smart IPN hydrogels can be categorized based on the stimuli driving hydrogel properties : temperature-responsive, glucose-responsive, pH-responsive, magnetically-responsive, enzyme-responsive, light-responsive, mechanically-responsive or multistimuli-responsive IPN hydrogels. In IPN literature, some examples of stimuli-responsive systems are reported. Among response to a wide range of stimuli, pH-responsiveness has attracted increasing interest due to practical purposes: indeed, it can be readily adapted to various tissues (e.g., tumor microenvironment, gastric fluid, colon), where the IPN hydrogel is designed to release locally a bioactive component based on the acido-basic conditions of the tissue targeted. For example, to deal with chronic wound dressings, chemically crosslinked PEG diacrylate (PEGDA) and acrylic acid networks within alginate hydrogels with pH modulation guarantee to the hydrogel an essential high swelling capacity to absorb the secreted exudates.² Temperature is another stimuli widely studied. Reversible bound of growth factors such as vascular endothelial growth factor (VEGF) and bone morphogenetic protein 2 (BMP-2) to the hydrogel was for example achieved upon incorporation of heparin into thermoresponsive star poly(ethylene glycol) (PEG)-heparin/(PNIPAAm) IPN hydrogels with benefit from PNIPAAm temperature-dependant behavior.³ The development of multifunctional hydrogels able to respond to multiple stimuli remains challenging. To achieve this, IPN hydrogels can be designed based on multiple « smart » networks, each of them being sensitive to a different stimulus. Some temperature/pH dual responsive systems already exist and exhibit an efficient additional control over the delivery of therapeutic drugs and proteins.^{4,5}

It is possible to go further by mixing a polymer hydrogel with self-assembled systems, especially fibrillar phases.⁶ Many advantages are reported, but stimuli-responsivity remains however poorly explored in literature.

This work aims at synthesizing and characterizing an IPN-like hydrogel, whereas one polymeric component is constituted by a biopolymer (gelatin, chitosan HMW, alginate...) but where the second polymer is substituted by a self-assembled biosurfactant. The role of the biopolymer is then essentially to generate a mechanically strong scaffold, the properties of which may be stimuli-dependent (pH, ion, T). The impact of the known phases of the biosurfactants on the biopolymer hydrogels will then be evaluated. The interesting aspect of this approach is that the phase behavior of the surfactant can also be externally triggered, in principle modifying the properties of the hybrid network. One should also note that the stimuli may not be the same for the biosurfactant and the biopolymer, thus making the hybrid system potentially responsive to a multitude of stimuli at once.

To study the dynamics of hybrid polymer amphiphile networks, we employ a system which undergoes phase transitions upon application of external stimuli, like pH or temperature. G-C18:1 is a microbial surfactant obtained by fermentation of the yeast *S. Bombicola*. It is made of a single β -D-glucose hydrophilic headgroup and a C18:1 fatty acid tail. From alkaline to acidic pH, the former undergoes a micelle-to-vesicle phase transition.⁷⁻⁹ Its interactions with biopolymers in dilute conditions were recently investigated and an astonishing coacervate-to-multilamellar walls vesicles was evidenced.^{10,11}

We explore the effect of fiber-to-micelles and fiber-to-vesicle phase transitions on the elastic properties of biopolymers, gelatin, chitosan and alginate. Gelatin is derived from the denaturation of collagen and it undergoes a gel-to-sol transition above 30°C.¹² Alginates are naturally derived polysaccharide block copolymers composed of β -D-mannuronic acid monomers (M-blocks), α -L-guluronic acid (G-blocks) and regions of interspersed M and G units, forming hydrogels upon addition of a calcium source.^{13,14} Chitosan results from the deacetylation of chitin, the second most widespread natural polysaccharide. Both the biobased amphiphile and biopolymers are biocompatible and have either established or potential interest in biomedical applications, like tissue engineering or wound healing.

In a parent article, we report the improved mechanical properties of gelatin, alginate or chitosan hydrogels in the presence of self-assembled fibers composed of G-C18:1. The present work reveals another aspect of these hybrid interpenetrated hydrogels: the impact of the fiber-to-micelle (vesicle) transition of G-C18:1 within the hybrid network. This work thus joins an increasing literature reporting LMWG remaining pH-responsive within a polymeric network which guarantees integrity of the gel.^{15,16} This latter may have an influence on LMWG assembly kinetics and morphology.¹⁷

Experimental section

Chemicals

Microbial glycolipids, G-C18:1, are composed of a single β -D-glucose hydrophilic headgroup and a C18:1 fatty acid tail (monounsaturations in positions 9,10). From alkaline to acidic pH, G-C18:1 undergoes a micelle-to-vesicle phase transition.⁷ The synthesis of G-C18:1 is described in Refs.^{8,9}, where the typical ¹H NMR spectra and HPLC chromatograms are given. The compound is provided by Bio Base Europe Pilot Plant, Gent, Belgium, lot N° APS F06/F07, Inv96/98/99 and used as such. The molecular purity of G-C18:1 exceeds 95%.

The three polymers used in this work, gelatin (type A, from porcine skin, $M_w \approx 50$ – 100 kDa, isoelectric point 7–9), alginate (from brown algae, medium viscosity, $M_w \approx 20$ – 240 kDa, $pK_a \approx 4$) and chitosan (high molecular weight, HMW, from shrimp shell, practical grade, $M_w \approx 190$ – 375 kDa, $pK_a \approx 6.5$), are purchased from Sigma Aldrich.

Preparation of the hydrogels

Stock solutions. The G-C18:1 stock solution at concentration, $C_{G-C18:1} = 40$ mg/mL, is prepared by dissolving the G-C18:1 powder in the appropriate volume of milli-Q grade water at pH = 10, adjusted with 5–10 μ L of NaOH 5 or 1 M solution. The stock solutions for each biopolymer are prepared as follows. *Gelatin:* 80 mg of gelatin powder is dispersed in 2 mL of milli-Q water, for a concentration of $C_{gelatin} = 40$ mg/mL. The gelatin stock solution is vortexed and set in the oven at 50°C. Once the solution is homogeneous, pH is increased up to pH 10 with a few μ L of a 0.5 M - 1 M NaOH solution. *Chitosan:* 200 mg of chitosan dispersed in 10 mL of 0.1 M acetic acid aqueous solution for a concentration $C = 20$ mg/mL. For an optimal solubilisation, the chitosan stock solution is stirred for one day before use. The pH of the acidic chitosan stock solution is increased above about 8. Typically, for 1 mL, one adds 5–10 μ L of a 5 M or 1 M NaOH solution. The solution, initially viscous at acidic pH, is vigorously stirred and vortexed upon pH increase to obtain a heterogeneous gel. *Alginate:* 200 mg of alginate powder is dispersed in 10 mL of Milli-q water for a concentration $C = 20$ mg/mL and stirred until complete solubilization. The magnetic stirrer usually sticks upon water addition; in this case, a manual help may be required to improve stirring. For a typical volume of 10 mL, pH is then increased to 10 with a 1–5 μ L of a 5 M or 1 M NaOH solution under stirring. Stirring and vortexing are eventually necessary to obtain a homogeneous alginate solution. Additional protocol details are given below for each biopolymer.

Fiber G-C18:1 hydrogels, {F}G-C18:1. For a 1mL sample, one increases the pH of 1 mL of the G-C18:1 stock solution up to ≈ 8 using 2-5 μL of a 5 M or 1 M NaOH solution. CaCl_2 solution (1 M, $V_{\text{CaCl}_2} = 33.5 \mu\text{L}$, $[\text{CaCl}_2] = 33.5 \text{ mM}$) is manually added for a total $[\text{CaCl}_2] : [\text{G-C18:1}] = 1 : 1.3$ molar ratio. The final solution is stirred and a gel is obtained after resting a few hours at room temperature.

{F}G-C18:1/gelatin gels. A volume of 500 μL of the gelatin stock solution is mixed with 500 μL of either water (reference) or G-C18:1 stock solution (sample). For a typical volume of 1 mL, CaCl_2 solution (1 M, $V_{\text{CaCl}_2} = 33.5 \mu\text{L}$, $[\text{CaCl}_2] = 33.5 \text{ mM}$) is manually added for a total $[\text{CaCl}_2] : [\text{G-C18:1}] = 1 : 1.3$ molar ratio. The final solution is stirred and a gel is obtained after resting a few hours at room temperature.

{F}G-C18:1/chitosan gels. Due to the heterogeneity of the chitosan gel at basic pH, 500 mg of the chitosan gel are weighted and mixed with 500 μL of a glycolipid solution under vigorous stirring and vortexing. To this mixture, 33.5 mM ($V_{\text{CaCl}_2} = 67 \mu\text{L}$) of a CaCl_2 solution ($[\text{CaCl}_2] = 1 \text{ M}$) are added, followed by further mixing. The final concentration of CaCl_2 in the sample is 33.5 mM, for a total $[\text{CaCl}_2] : [\text{G-C18:1}] = 1 : 1.3$ molar ratio. A homogeneous gel is obtained after resting a few hours at room temperature.

{F}G-C18:1/alginate gels. 500 μL of the alginate viscous stock solution are added either to 500 μL water (reference) or to 500 μL of the G-C18:1 stock solution under stirring. A volume of $V_{\text{CaCl}_2} = 50 \mu\text{L}$ of a CaCl_2 solution ($[\text{CaCl}_2] = 1 \text{ M}$) is added, for a final CaCl_2 concentration of 50 mM and $[\text{CaCl}_2] : [\text{G-C18:1}] = 1 : 0.86$ molar ratio and $[\text{CaCl}_2] : [\text{alginate}] \approx 1 : 0.0015$ molar ratio. The final solution is magnetically stirred for several hours to obtain a homogeneous gel.

Table 1 summarizes the reference, sample and stock solution concentrations in wt% employed throughout this study.

Table 1 – Concentration of stock solutions, volumes from stock solutions and final concentration in the samples

	G-C18:1	gelatin	alginate	chitosan
Stock solution concentration (wt%)	4	4	2	2
V (mL)		0.5	0.5	0.5

	0.5			
Reference and sample concentration (wt%)	2	2	1	1

Rheology

Viscoelastic measurements are carried out using an Anton Paar MCR 302 rheometer equipped with parallel titanium or stainless steel sandblasted plates (diameter = 25 mm, gap = 1 mm). Unless otherwise stated, all experiments are conducted at 25 °C, whereas the temperature is controlled by the stainless steel lower Peltier plate. During the experiments, the measuring geometry is covered with a humidity chamber to minimize water evaporation. To investigate the pH-dependence of the mechanical properties, samples containing {F}G-C18:1 and the biopolymer are mixed with the appropriate amount of glucono- δ -lactone, GDL, and immediately vortexed during 20 s. Volumes have been doubled and concentrations have been adapted (divided by two) for an easier dispersion of GDL powder. Half of the sample is immediately loaded on the bottom plate, while the pH is monitored automatically on the other half. Dynamic oscillatory and time sweep experiments are performed by applying a constant oscillation frequency ($f = 1$ Hz) and a shear strain (γ) within the linear viscoelastic regime (LVER).

pH monitoring

In situ pH monitoring after addition of GDL is performed using a Mettler Toledo microelectrode connected to a Hanna scientific pH-meter, model HI 5221. The pH meter is connected to a computer, equipped with the fabricant's software [HI 92000, version 5.0.28]. The frequency of pH recording is 10 s^{-1} .

Rheo-SAXS

Experiments coupling rheology and SAXS are performed at the SWING beamline of the Soleil synchrotron facility (Saint-Aubin, France) during the run N° 20200532, using a beam energy of 12.00 keV and a sample-to-detector distance of 1.65 m. Tetradecanol ($d(001) = 39.77 \text{ \AA}$) is used as the q-calibration standard. The signal of the Pilatus 1 M 2D detector (172 x 172 mm pixel size) is integrated azimuthally with Foxtrot software to obtain the $I(q)$ spectrum ($q = 4\pi \sin \theta/\lambda$, where 2θ is the scattering angle) after masking systematically defective pixels and the beam stop shadow. A MCR 501 rheometer (Anton Paar, Graz, Austria) equipped with a

Couette polycarbonate cell (gap= 0.5 mm, volume, \approx 2 mL) is coupled to the beamline and controlled through an external computer in the experimental hutch using the Rheoplus/32 software, version 3.62. The experiments are performed in a radial configuration, where the X-ray beam is aligned along the center of the Couette cell. The rheology and SAXS acquisitions are triggered manually with an estimated delay of less than 5 s. Due to standard compulsory security procedures required at the beamline, the first rheo-SAXS experimental point is systematically acquired with a delay of about 2–3 minutes with respect to the rheometer. Data are not scaled to absolute intensity.

RESULTS

pH-stimulated hybrid hydrogels

G-C18:1 was shown to undergo a micelle-to-vesicle phase transition stimulated by pH: above and below $\text{pH} \approx 6.5$, G-C18:1 self-assembles respectively into micelles and vesicles. By adding an aqueous calcium solution in the micellar phase at pH above ≈ 7.8 for an equimolar amount of positive-to-negative charge, $[\text{Ca}^{2+}]/[\text{G-C18:1}] > 0.6$, G-C18:1 immediately forms a homogeneous fibrillar hydrogel at $C_{\text{G-C18:1}}$ above 0.5 wt%, referred in this work to {F}G-C18:1. At acidic pH below 7, calcium induces precipitation of a powder with lamellar order.¹⁸

In this work, we make the hypothesis that the elastic properties of hybrid hydrogels composed of a biopolymer and G-C18:1 can be controlled by switching from one G-C18:1 phase to another. We test this hypothesis by monitoring *in-situ* the structural and mechanical properties of biopolymer/{F}G-C18:1 hydrogels upon pH lowering, the latter performed in bulk by mean of glucono- δ -lactone (GDL) hydrolysis.

The mechanical properties of each biopolymer alone are measured at pH 8 and 6, as controls. According to Figure S 1, the absolute magnitude of storage (G') and loss (G'') moduli depend on the biopolymer : 20-50, 50-100 and ≈ 2000 Pa for gelatin, alginate and chitosan respectively, but, as a general trend, pH does not sensibly affect G' and G'' , except for chitosan, known to be more soluble at acidic pH. In the 8-10 pH range, all control ($G' \approx 10, 50, 100, 1000$ Pa for {F}G-C18:1, gelatin, alginate and chitosan, respectively) and hybrid {F}G-C18:1/biopolymer (≈ 100 Pa) gels are mechanically strong.

Rheological measurements of all hybrid {F}G-C18:1/biopolymer hydrogels at pH 10 before pH variation are acquired on the SAXS-coupled rheometer before triggering the pH variation. The *ex situ* panel in Figure 1a, Figure 2a and Figure 3a shows that hybrid gels made of {F}G-C18:1 and respectively gelatin, alginate and calcium have a storage modulus around 100 Pa at pH 10. After adding GDL to the hybrid hydrogels pH 10, the sample is split in two

halves for two parallel *in situ* measurements: the mechanical and structural properties are collected by rheo-SAXS on one half while pH is measured using an automated pH meter on the other half. The results are combined in Figure 1, Figure 2 and Figure 3 respectively for gelatin, alginate and chitosan. Due to the unavoidable security constraints of the SAXS beamline, a lag time of about 2 min systematically precedes rheo-SAXS acquisitions.

The elastic properties of the hybrid {F}G-C18:1/gelatin hydrogel dramatically decrease to ~5 Pa during acidification at pH 7, below which the gel becomes a liquid, characterized by a loss modulus higher than the storage modulus (Figure 1a). Evolution of the mechanical properties of control gelatin gels are not as significant and are given in Figure S 1a. Figure 1b shows the concomitant SAXS signature, identifying the structural features of the gels. SAXS highlights a decrease in intensity of the peaks at $q=0.25 \text{ \AA}^{-1}$ and $q=0.31 \text{ \AA}^{-1}$, both characteristics of the crystalline structure of {F}G-C18:1 fibers¹⁸ visible at pH 10 and progressively disappearing at more acidic pH, suggesting a structural perturbation of the system around pH ≈ 7 . The SAXS profile at pH 6.47 (Figure 1b) is typical of elongated micelles in solution, as expected for this compound in the pH transition region between 7 and 6,⁷ thus suggesting that the change in physical properties of the gel recorded by SAXS are explained by a fiber-to-micelle phase transition of {F}G-C18:1.⁸

A closer comparison between rheology and SAXS clearly associates the loss of the mechanical properties to a loss in structure of {F}G-C18:1 fibers. The pH-dependent 2D SAXS contour plot centered around the fibers' structural diffraction peaks at $q=0.25 \text{ \AA}^{-1}$ and $q=0.31 \text{ \AA}^{-1}$ is superposed to the $G'(\text{pH})$ profile in Figure 1a, both synchronized within the same rheo-SAXS experiment. The loss in structural properties, pointed at by the b-tagged arrow, occurs in the same pH range during which the structural peak disappears.

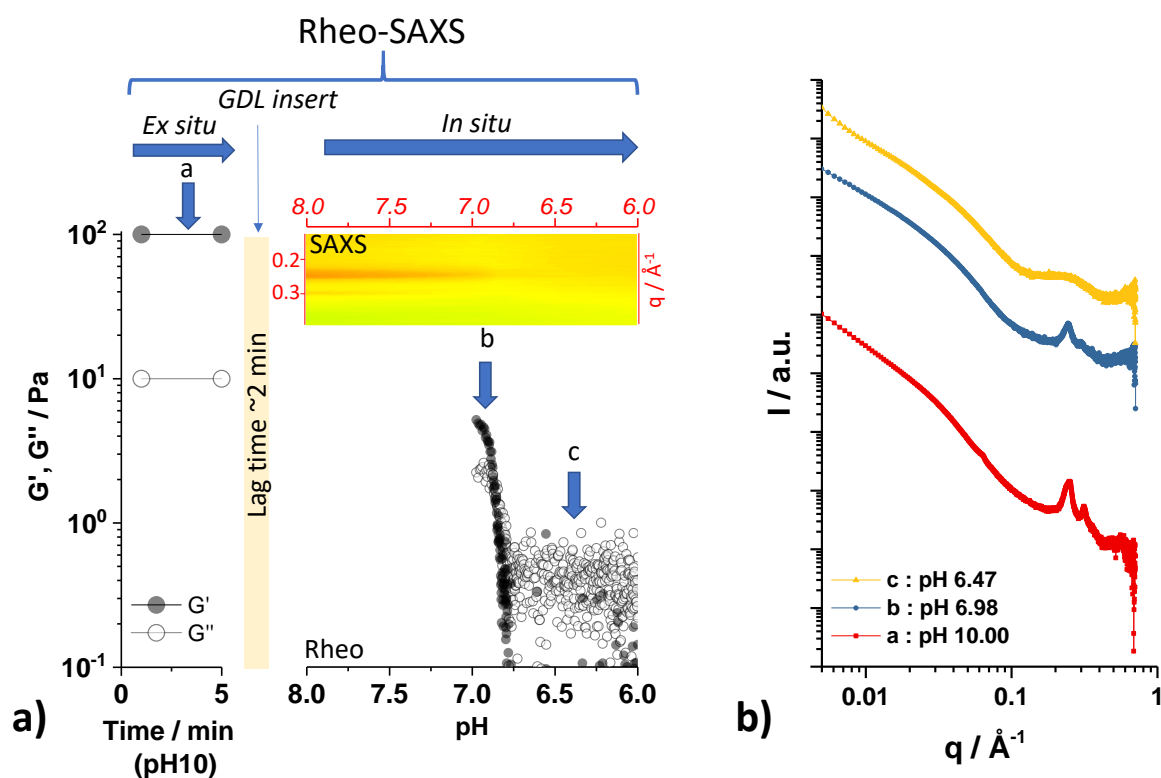


Figure 1 – GDL-induced acidification of {F}G-C18:1/gelatin hydrogel. Rheo-SAXS experiment: a) mechanical properties and b) corresponding SAXS profiles. The 2D contour plot profile superposed to the $G'(\text{pH})$ evolution in a) corresponds to the full SAXS experiment. $C_{\text{GDL}} = 1 \text{ wt}\%$, $C_{\text{G-C18:1}} = 1 \text{ wt}\%$, $C_{\text{gelatin}} = 1 \text{ wt}\%$, $[\text{Ca}^{2+}] = 33.5 \text{ mM}$.

After addition of GDL to the hybrid {F}G-C18:1/alginate hydrogels, the mechanical properties decrease with pH, but not more than one order of magnitude. Differently than to the case of gelatin described above, the {F}G-C18:1/alginate systems remains a gel on the whole pH range (the storage modulus is above the loss modulus). This result is similar to the alginate control hydrogels, which have comparable mechanical properties at pH 6 and 8 (Figure S 1b). From a structural point of view, Figure 2b shows that the peaks ($q = 0.25$ and 0.31 \AA^{-1}) at pH 10, typical of the fiber phase of {F}G-C18:1, progressively disappear in favor of a lamellar phase at acidic pH,¹⁰ meaning that the G-C18:1 self-assembled structure undergoes a significant change. This is well-illustrated by the pH-dependent 2D contour plot associated to the full rheo-SAXS experiment (2D SAXS panel superposed to its synchronized $G'(\text{pH})$ profile), which nicely shows that the fiber ($\text{pH} > \sim 7$) to lamellar ($\text{pH} < \sim 6.5$) phase transition occurs at the same time as partial loss in elastic properties of the hybrid {F}G-C18:1/alginate hydrogels. However, all in all, the loss in the structural and elastic properties of {F}G-C18:1 does not have as much

effect on the elastic modulus of the hybrid {F}G-C18:1/alginate hydrogels as observed for gelatin.

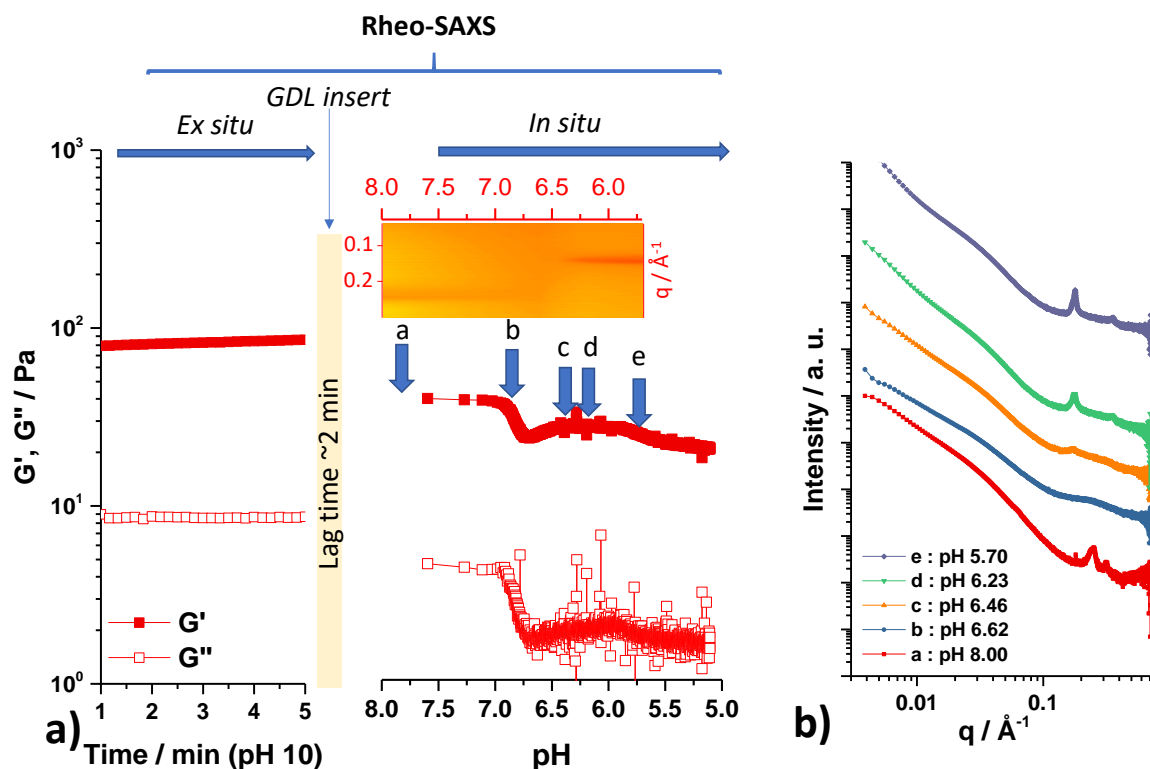


Figure 2 - GDL-induced acidification of {F}G-C18:1/alginate/calcium gel. Rheo-SAXS experiment: a) mechanical properties and b) corresponding SAXS profiles. The 2D contour plot profile superposed to the G' (pH) evolution in a) corresponds to the full SAXS experiment. $C_{\text{GDL}} = 2 \text{ wt\%}$, $C_{\text{G-C18:1}} = 1 \text{ wt\%}$, $C_{\text{alginate}} = 0.5 \text{ wt\%}$, $[\text{Ca}^{2+}] = 25 \text{ mM}$.

Hybrid {F}G-C18:1/chitosan hydrogels undergo a GDL-induced variation of pH and the mechanical properties of the gel are monitored by rheo-SAXS, as well (Figure 3a). When pH is in the order of 8, the G' has already lost one order of magnitude, while at pH below 6, the gel has lost its properties and forms a viscous solution. This behavior is intermediate between the hybrid gels involving gelatin and alginate, which become viscous or remain a gel, respectively. According to the control experiment in Figure S 1c and to its known solubility at pH below its pKa (6.5), chitosan is expected to lose its elastic properties below pH 6. However, the strong loss in G' between pH 10 and pH 7, above its pKa, also indicates that the pH-induced phase transition of {F}G-C18:1 at pH 8. On the basis of the experiments performed on the

gelatin and alginate hybrid gels, it is not unreasonable to expect a fiber-to-vesicle phase transition of {F}G-C18:1 below pH 8.

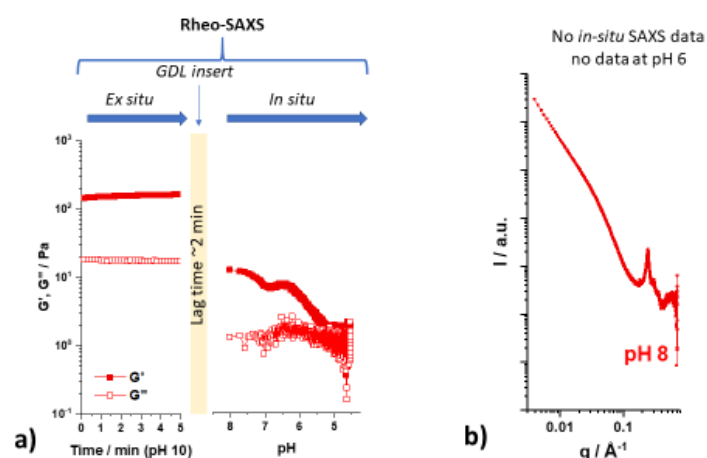


Figure 3 - GDL-induced (100 mg.mL^{-1}) acidification of G-C18:1 (2 wt%)/chitosan HMW (1wt%)/calcium (33.5 mM) gel : mechanical properties (a) and resulting structure (b)

Temperature-stimulated hybrid hydrogels

Apart from pH, temperature has been tested as another stimulus to control the viscoelastic properties of the hybrid hydrogels. It is indeed another simple stimulus and it is already reported to significantly impact the mechanical properties of polymeric hydrogels, like pNiPAAm-based ones.^{19–21} Both gelatin [Ref] and {F}G-C18:1 [Ref Alexandre] hydrogels undergo a temperature-driven gel-to-sol transition, while alginate and chitosan are less sensitive to temperature, as shown by the control rheology experiments in Figure S 2. It is then of particular interest to study the double temperature-sensitivity of {F}G-C18:1/gelatin hydrogels but also the gel-to-sol transition of {F}G-C18:1 in alginate and chitosan hybrids.

The evolution of the storage and loss moduli of {F}G-C18:1, biopolymer and {F}G-C18:1/biopolymer gels was investigated between 20°C and 50°C via a heating then cooling protocol. Figure 4a shows that, as expected, gelatin gel loses its mechanical properties above 28°C and does not reform a gel upon cooling, at least on the experiment time range. On the contrary, Figure S 2 illustrates that alginate and chitosan are not sensitive to temperature up to 50°C . Concerning {F}G-C18:1 gels, Figure 4b confirms previous results [Ref Alex], as it shows that the biosurfactant undergoes a reversible sol-gel transition, corresponding to a fiber-micelle phase change, above 45°C .

The hybrid {F}G-C18:1/gelatin gels are also sensitive to temperature in correspondence of the sol-gel transition of each individual component. Rheo-SAXS of the hybrid {F}G-C18:1/gelatin gel (Figure 4) is performed to associate the elastic and structural properties.

Figure 4c shows that the mechanical properties of the hybrid gel initially decrease above 25°C, following the gel-to-sol transition of gelatin (Figure 4a). A second gel-to-sol transition occurs around 45°C, this time corresponding to the gel-to-sol transition of {F}G-C18:1, as compared to the control of Figure 4b. Upon cooling, the elastic properties of {F}G-C18:1 increase again, as explained by the reversible sol-gel transition of {F}G-C18:1 rather than gelatin (Figure 4a,b). [Ref Alexandre] The contributions of both components are thus nicely established, while the advantage of introducing a fast-responsive self-assembled fibrillary network within a polymer gel now become self-evident: the rapid sol-gel transition of {F}G-C18:1 overwhelms the slow recovery of gelatin alone.

Figure 4d provides the SAXS profiles associated to the gels at 25°C (a), 50°C (b) and 25°C after cooling (c). The SAXS profiles acquired at different temperatures are perfectly superimposed, showing that the structure of the gel is not sensitive to temperature at least up to about 50°C, which can be quite surprising considering the low T_m of the oleic acid moiety of G-C18:1. However, dynamic scanning calorimetry experiments show that the T_m of {F}G-C18:1 is rather in the range of 70°C.¹⁸ Considering our previous work,⁸ {F}G-C18:1 hydrogels undergo a fiber-to-micelle phase transition just above 50°C, although the elastic properties start to decrease in the order of 50°C, probably due to a disentanglement mechanism.

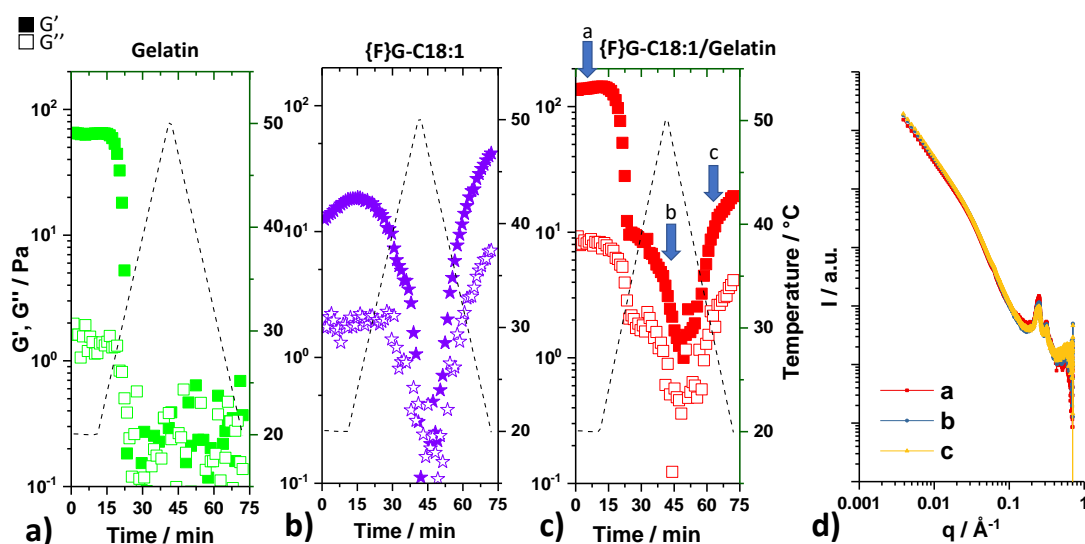


Figure 4 – Combined rheo-SAXS experiment. Rheological measurements of storage (G') and loss (G'') moduli of a) gelatin gel, b) {F}G-C18:1 gel and c) hybrid {F}G-C18:1/gelatin gel as a function of temperature. $C_{G-C18:1}$ = 2 wt%, $C_{gelatin}$ = 2 wt%, $[CaCl_2]$ = 33.5 mM, pH = 7.8. d) SAXS profiles of hybrid {F}G-C18:1/gelatin hydrogels corresponding to arrows in c).

Hybrid gels composed of chitosan and alginate were also tested against temperature, knowing that the controls are not temperature-sensitive (Figure S 2). According to the data shown in

Figure 5a, the hybrid {F}G-C18:1/alginate gel is only slightly sensitive to temperature, and mainly around 50°C, in correspondence of the gel-to-sol transition of {F}G-C18:1. In this case, the alginate network compensates the weakness of {F}G-C18:1 towards temperature. From a structural point of view, the SAXS profiles acquired at different temperatures (Figure 5b) are identical, thus showing that the gel structure is unaffected by temperature.

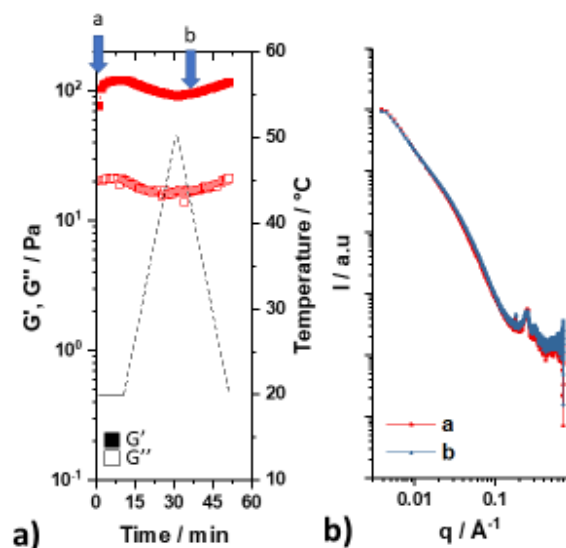


Figure 5 – Combined rheo-SAXS experiment. a) Rheological measurements and b) SAXS profiles of hybrid {F}G-C18:1/alginate gel as a function of temperature. $C_{G-C18:1} = 2$ wt%, $C_{alginate} = 1$ wt%, $[CaCl_2] = 50$ mM, $pH = 7.8$.

Concerning the properties of hybrid {F}G-C18:1/chitosan gels against temperature, results are quite similar to the ones of alginate : Figure 6a shows that the hybrid {F}G-C18:1/chitosan gel does not have any obvious temperature-responsive property, as also found for the chitosan gel control (Figure S 2b). In this case, chitosan strengthens the hybrid gel. The SAXS profiles given in Figure 6b demonstrate that, as for the other biopolymers tested, temperature is not a parameter governing the gel structure, at least not up to 50°C.

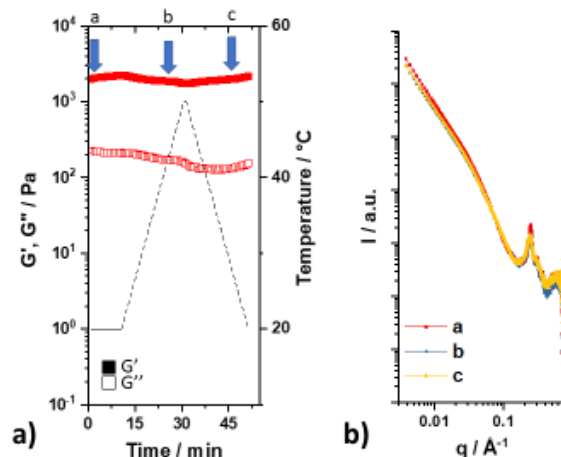


Figure 6 - Combined rheo-SAXS experiment. a) Rheological measurements and b) SAXS profiles of hybrid {F}G-C18:1/chitosan gel as a function of temperature. $C_{G-C18:1}$ = 2 wt%, $C_{chitosan}$ = 1 wt%, $[CaCl_2]$ = 33.5 mM, pH= 7.8.

Discussion

Conclusion

Acknowledgements

Soleil Synchrotron facility is acknowledged for accessing the Swing beamline and financial support (proposal N° 20200532). Ghazi Ben Messaoud (DWI-Leibniz Institute for Interactive Materials, Aachen, Germany) is kindly acknowledged for helpful discussions. We thank Dr. S. Roelants, Prof. W. Soetaert and Prof. C. V. Stevens at Gent University for providing us the glycolipid. Sorbonne Université (contract N° 3083/2018) is acknowledged for financial support of CS. Authors kindly acknowledge the French ANR, Project N° SELFAMPHI - 19-CE43-0012-01.

References

- (1) Dhand, A. P.; Galarraga, J. H.; Burdick, J. A. Enhancing Biopolymer Hydrogel Functionality through Interpenetrating Networks. *Trends Biotechnol.* **2021**, *39*, 519–538.
- (2) Koehler, J. PH-Modulating Poly(Ethylene Glycol)/Alginate Hydrogel Dressings for the Treatment of Chronic Wounds. *Macromol. Biosci.* **2017**, *17*, 1–11.
- (3) Sievers, J. Temperature-Induced Mechanomodulation of Interpenetrating Networks of Star Poly(Ethylene Glycol)-Heparin and Poly(N-Isopropylacrylamide). *ACS Appl.*

- Mater. Interfaces* **2019**, *11*, 41862–41874.
- (4) Kim, A. R.; Lee, S. L.; Park, S. N. Properties and in Vitro Drug Release of PH- and Temperature-Sensitive Double Cross-Linked Interpenetrating Polymer Network Hydrogels Based on Hyaluronic Acid/Poly (N-Isopropylacrylamide) for Transdermal Delivery of Luteolin. *Int. J. Biol. Macromol.* **2018**, *118*, 731–740.
 - (5) Zhao, J.; Zhao, X.; Guo, B.; Ma, P. X. Multifunctional Interpenetrating Polymer Network Hydrogels Based on Methacrylated Alginate for the Delivery of Small Molecule Drugs and Sustained Release of Protein. *Biomacromolecules* **2014**, *15*, 3246–3252.
 - (6) Cornwell, D. J.; Smith, D. K. Expanding the Scope of Gels - Combining Polymers with Low-Molecular-Weight Gelators to Yield Modified Self-Assembling Smart Materials with High-Tech Applications. *Materials Horizons*. 2015.
 - (7) Baccile, N.; Cuvier, A.-S.; Prévost, S.; Stevens, C. V.; Delbeke, E.; Berton, J.; Soetaert, W.; Van Bogaert, I. N. A.; Roelants, S. Self-Assembly Mechanism of PH-Responsive Glycolipids: Micelles, Fibers, Vesicles, and Bilayers. *Langmuir* **2016**, *32*, 10881–10894.
 - (8) Baccile, N.; Selmane, M.; Le Griel, P.; Prévost, S.; Perez, J.; Stevens, C. V.; Delbeke, E.; Zibek, S.; Guenther, M.; Soetaert, W.; et al. PH-Driven Self-Assembly of Acidic Microbial Glycolipids. *Langmuir* **2016**.
 - (9) Cuvier, A. S.; Berton, J.; Stevens, C. V.; Fadda, G. C.; Babonneau, F.; Van Bogaert, I. N. A.; Soetaert, W.; Pehau-Arnaudet, G.; Baccile, N. PH-Triggered Formation of Nanoribbons from Yeast-Derived Glycolipid Biosurfactants. *Soft Matter* **2014**, *10*, 3950–3959.
 - (10) Seyrig, C.; Le Griel, P.; Cowieson, N.; Perez, J.; Baccile, N. Synthesis of Multilamellar Walls Vesicles Polyelectrolyte-Surfactant Complexes from PH-Stimulated Phase Transition Using Microbial Biosurfactants. *J. Colloid Interface Sci.* **2020**, *580*, 493–502.
 - (11) Seyrig, C.; Kignelman, G.; Thielemans, W.; Le Griel, P.; Cowieson, N.; Perez, J.; Baccile, N. Stimuli-Induced Nonequilibrium Phase Transitions in Polyelectrolyte-Surfactant Complex Coacervates. *Langmuir* **2020**, *36*, 8839–8857.
 - (12) Djabourov, M. Architecture of Gelatin Gels. *Contemp. Phys.* **1988**, *29*, 273.
 - (13) Martinsen, A.; Skjåk-Braek, G.; Smidsroed, O. Alginate as Immobilization Material: I. Correlation between Chemical and Physical Properties of Alginate Gel Beads. *Biotechnol. Bioeng.* **1989**, *33*, 79–89.

- (14) Rowley, J. A.; Madlambayan, G.; Mooney, D. J. Alginate Hydrogels as Synthetic Extracellular Matrix Materials. *Biomaterials* **1999**, *20*, 45–53.
- (15) Cornwell, D. J.; Okesola, B. O.; Smith, D. K. Hybrid Polymer and Low Molecular Weight Gels-Dynamic Two-Component Soft Materials with Both Responsive and Robust Nanoscale Networks. *Soft Matter* **2013**, *9*, 8730–8736.
- (16) Vieira, V. M. P.; Hay, L. L.; Smith, D. K. Multi-Component Hybrid Hydrogels-Understanding the Extent of Orthogonal Assembly and Its Impact on Controlled Release. *Chem. Sci.* **2017**, *8*, 6981–6990.
- (17) Cornwell, D. J.; Okesola, B. O.; Smith, D. K. Multidomain Hybrid Hydrogels: Spatially Resolved Photopatterned Synthetic Nanomaterials Combining Polymer and Low-Molecular-Weight Gelators. *Angew. Chemie - Int. Ed.* **2014**, *53*, 12461–12465.
- (18) Poirier, A. et al. No Title. *Prep.*
- (19) Yin, X.; Hoffman, A. S.; Stayton, P. S. Poly(N-Isopropylacrylamide-Co-Propylacrylic Acid) Copolymers That Respond Sharply to Temperature and PH. *Biomacromolecules* **2006**, *7*, 1381–1385.
- (20) Nakayama, M.; Okano, T.; Miyazaki, T.; Kohori, F.; Sakai, K.; Yokoyama, M. Molecular Design of Biodegradable Polymeric Micelles for Temperature-Responsive Drug Release. *J. Control. Release* **2006**, *115*, 46–56.
- (21) Coughlan, D. C.; Quilty, F. P.; Corrigan, O. I. Effect of Drug Physicochemical Properties on Swelling/Deswelling Kinetics and Pulsatile Drug Release from Thermoresponsive Poly(N-Isopropylacrylamide) Hydrogels. *J. Control. Release* **2004**, *98*, 97–114.

Supplementary Information

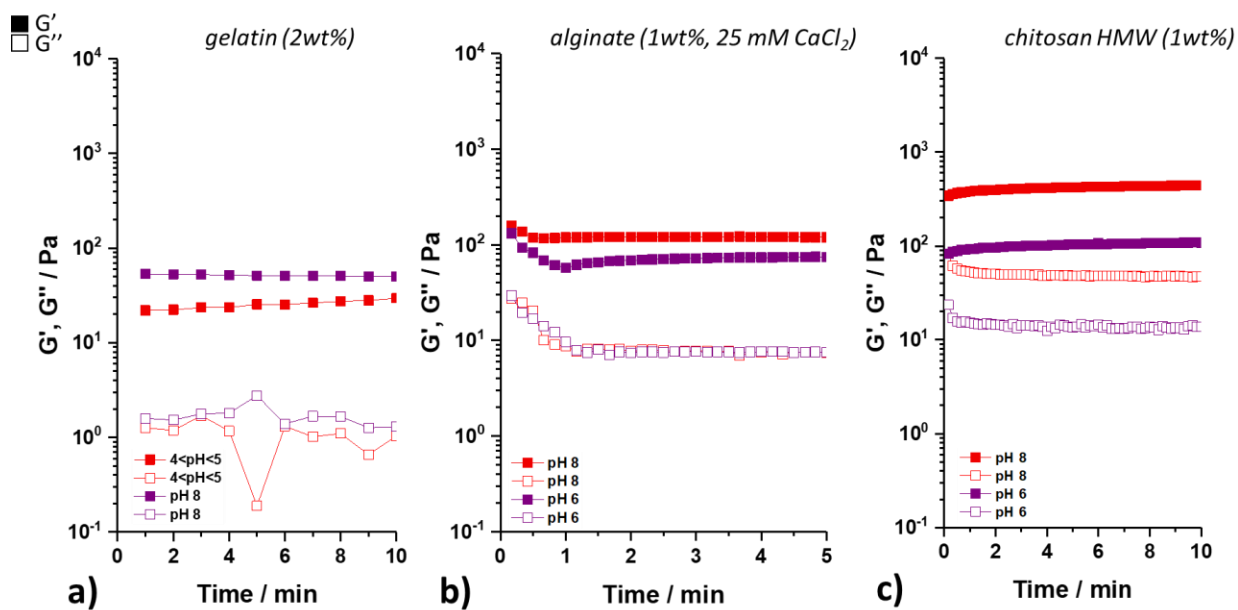


Figure S 1 - Rheological measurements of storage and loss moduli of gelatin (a), alginate (b) and chitosan HMW (c) gels at basic and acidic pH.

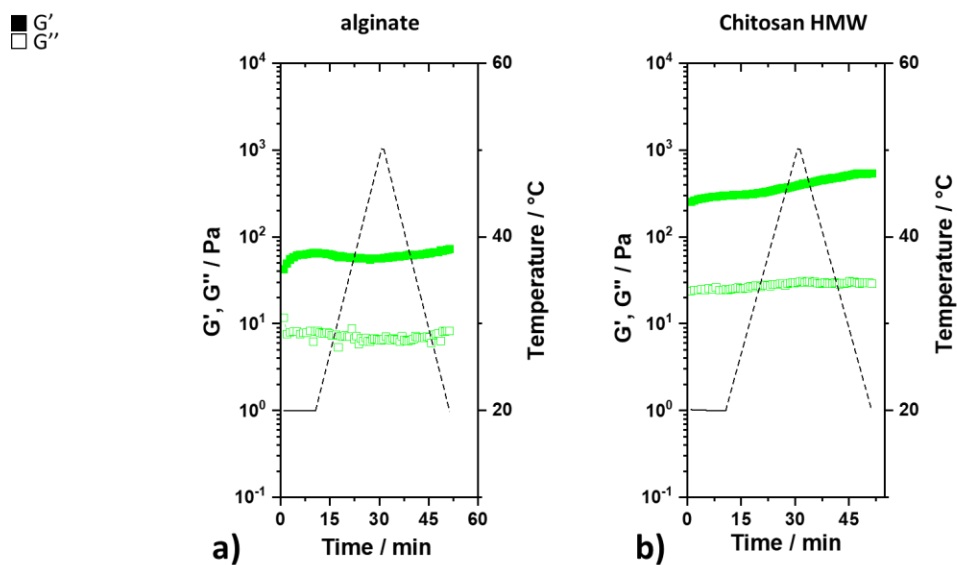


Figure S 2 - Rheological measurements of storage and loss moduli of alginate (a) and chitosan HMW (b) gels at pH 8 in function of temperature

Résumé

Les systèmes polymère-tensioactif ont de nombreuses applications dans la vie de tous les jours, mais leur origine pétrochimique est aujourd'hui controversée. Dans une démarche plus respectueuse de l'environnement, des systèmes biopolymère-biotensioactif seraient une alternative intéressante. Il existe en effet une grande famille de molécules biosourcées, certaines produites par fermentation microbienne, possédant un fort potentiel, cependant aujourd'hui limité, leur comportement en solution n'étant pas encore clairement établi. Le LCMCP a développé une expertise sur ce point, et le but de ces travaux de thèse est dans un premier temps d'étudier en conditions diluées le diagramme de phase de deux biotensioactifs dont l'auto-assemblage dépend du pH en présence de biopolymères. Il en résulte que des coacervats complexes sont formés à pH basique dans les deux cas (biotensioactifs sous forme micellaire), tandis qu'à pH acide l'interaction est soit perturbée quand le biotensioactif se réorganise en fibres, soit maintenue si celui-ci évolue vers une phase vésiculaire, donnant lieu à la formation de structures multilamellaires. Ces dernières se sont avérées prometteuses pour l'encapsulation de molécules modèles, notamment la curcumine, aux nombreuses applications thérapeutiques. Stables en milieu biologique, elles permettent le relargage de la curcumine qui peut exercer son activité, notamment anti-cancéreuse. Dans un deuxième temps, dans des conditions plus concentrées, les effets des différentes phases du biotensioactif sur les propriétés mécaniques de gels de biopolymère ont été étudiés. La phase fibrillaire renforce le gel d'une part, et le gel hybride possède des propriétés modulables en fonction du pH et/ou de la température d'autre part.

Mots-clés: biotensioactif, biopolymère, vésicules multilamellaires, auto-assemblage, stimuli-responsive, hydrogel

Abstract

Polymer-surfactant systems have many applications in everyday life, but their petrochemical origin is currently controversial. In a more environmentally friendly approach, biopolymer-biosurfactant systems would be an interesting alternative. Indeed, there exists a large family of biobased molecules, including ones produced by yeast fermentation, which possess a huge potential, however currently limited as their behavior in solution is not clearly established yet. LCMCP has developed an expertise on this point, and the goal of this work is first to study in dilute conditions the phase diagram of two biosurfactants of which self-assembly depends on pH, in presence of biopolymers. It results that complex coacervates are formed at basic pH in both cases (biosurfactants within their micellar state), while at acidic pH interactions are either disturbed when the biosurfactant reorganizes into fibers, or maintained if this one evolves towards a vesicular phase, forming multilamellar structures. These latter were found promising for the encapsulation of model drug molecules, especially curcumin which has various therapeutic applications. Stable in biological environment, they allow the release of curcumin which can exercise its activity, especially against cancer. Secondly, in more concentrated conditions, the effect of the different biosurfactant's phases on the mechanical properties of biopolymer's hydrogels were studied. The fibrillar phase reinforces the gel on the one hand, and the hybrid gel possesses properties which can be tuned by pH and/or temperature on the other hand.

Keywords: biosurfactant, biopolymer, multilamellar vesicles, self-assembly, stimuli-responsive, hydrogel